Gamma-Ray Bursts

Contents

1. Topics

- The "canonical" GRB: "genuine short" vs long vs "disguised short" GRBs
- "Disguised short" GRB host galaxies: correlation between offset and extended afterglow peak luminosity
- The theoretical explanation of the "Amati relation"
- The "Amati relation" as a tool to identify "disguised short" GRBs
- "Genuine short" GRBs: Possible identifications and selection effects
- A modified spectral energy distribution for highly energetic GRBs
- The observed spectra of the P-GRBs
- GRB prompt emission spectra below 5 keV: challenges for future missions
- Interpretation of the ultra high energy emission from GRBs observed by Fermi and AGILE
- Analysis of different families of progenitors for GRBs with different energetics
- GRBs at redshift $z > 6$
- GRBs originating from a multiple collapse
- Prompt emission and X-ray flares: the clumpiness of CBM
- Microphysical description of the interaction between the fireshell and the CBM
- Theoretical interpretation of the "plateau" phase in the X-ray afterglow
- Possible existence of a "proto-black hole" emission as first Episode of GRBs.
- Emission from newly born neutron stars, or "neo neutron stars".
- Induced Gravitational Collapse process for GRBs associated with supernovae.

- Redshift estimators for GRBs with no measured redshift.

2. Participants

2.1. ICRANet participants

- David Arnett
- Carlo Luciano Bianco
- Massimo Della Valle
- Luca Izzo
- Jorge Armando Rueda Hernandez
- Remo Ruffini
- Gregory Vereshchagin
- She-Sheng Xue

2.2. Past collaborators

- Sabrina Casanova (MPIK, Germany)
- Letizia Caito
- Pascal Chardonnet (Université de Savoie, France)
- Demetrios Christodoulou (ETH Zurich, Switzerland)
- Alessandra Corsi (INAF-IASF Roma, Italy)
- Valeri Chechetkin
- Maria Giovanna Dainotti
- Thibault Damour (IHES, France)
- Walter Ferrara
- Federico Fraschetti (CEA Saclay, France)
- Roberto Guida

- Vahe Gurzadyan (Yerevan Physics Institute, Armenia)
- Massimiliano Lattanzi (Oxford Astrophysics, UK)
- Nino Panagia
- Elena Pian
- Giuliano Preparata (Università di Milano, Italy)
- Jay D. Salmonson (Livermore Lab, USA)
- Jim Wilson (Livermore Lab, USA)

2.3. Ongoing collaborations

- Alexey Aksenov (ITEP, Russia)
- Lorenzo Amati (INAF-IASF Bologna, Italy)
- Maria Grazia Bernardini (OAB, Italy)
- Joao Braga (INPE, Brazil)
- Sandip Kumar Chakrabarti (S.N. Bose National Centre and Indian Centre for Space Physics, India)
- Alessandro Chieffi (INAF-IASF Roma, Italy)
- Guido Chincarini (Universit di Milano “Bicocca”, Italy)
- Stefano Covino (OAB, Italy)
- Filippo Frontera (Universit di Ferrara, Italy)
- Dafne Guetta (OAR, Italy)
- Cristiano Guidorzi (OAB, Italy)
- Stanislav Kelner (MEPhI, Russia, and MPIK, Germany)
- Marco Limongi (OAR, Italy)
- Vanessa Mangano (INAF-IASF Palermo, Italy)
- Barbara Patricelli (Astronomy Institute - UNAM, México))
- Susanna Vergani (Dunsink Observatory, Ireland)
- Francesco Vissani (INFN, Italy)

2.4. Students

- Andrey Baranov (IRAP PhD, Russia)
- Cristina Barbarino (IRAP PhD, Italy)
- Riccardo Belvedere (IRAP PhD, Italy)
- Gustavo de Barros (IRAP PhD, Brazil)
- Maxime Enderli (IRAP PhD, France)
- Wen-Biao Han (IRAP PhD, China)
- Milos Kovacevic (IRAP PhD, Serbia)
- Vincenzo Liccardo (IRAP PhD, Italy)
- Hendrik Ludwig (IRAP PhD, Germany)
- Marco Muccino (IRAP PhD, Italy)
- Ana Virginia Penacchioni (IRAP PhD, Argentina)
- Giovanni Battista Pisani (IRAP PhD, Italy)
- Luis Juracy Rangel Lemos (IRAP PhD, Brazil)
- Ivan Siutsou (IRAP PhD, Belarus)
- Vineeth Valsan (IRAP PhD, India)
- Yu Wang (IRAP PhD, China)

3. Brief description

3.1. The space, time and energetics of GRBs

The new era of GRBs started with the discovery of Beppo-SAX of the existence of the afterglow of GRBs (Costa et al., 1997). This fortunate discovery, as it is well known, led to the optical identification of GRB sources and to the determination of their distances and of their energetics. After that pioneering work a large number of missions including HETE-II, INTEGRAL, KONUS-Wind, Suzaku, Swift have given a wealth of information of GRB sources, giving details of their cosmological redshifts, their energetics and their spectra. It has been then possible to draw a figure (see Fig. 3.1) representing these sources as well as giving a diagram of the number of GRBs at selected redshift value (Fig. 3.2), where there are represented all the 140 GRBs with such characteristics.

3.2. The black hole and GRB uniqueness

It has become evident from the theoretical analysis of these sources that we are witnessing a vast number of progenitors to the GRB phenomena. In particular, we can identify a family of progenitors formed by a binary system of a neutron star and a companion star in the late phase of thermonuclear evolution. These systems lead to the less energetic GRB sources which have the characteristic signature of being associated to a supernovae explosion. A specific model has been studied by our group following the idea of induced gravitational collapse, see section A. The emission of GRB in this case originates from a black hole with the smallest possible mass: the one originating from a neutron star going over to its critical mass. This naturally explains why these sources are the less energetic ones.

There is also evidence for GRBs originating from binary neutron star-white dwarf system, and from neutron star-neutron star binary systems (see e.g. GRB 060614 in section C.2, GRB 071227 in section C.3 and GRB 050509B in section C.4). And there is mounting evidence for a different family of black holes linked to more energetic gravitational collapse of a massive core around 10 $M_\odot$ (see e.g. GRB 080916C and GRB 050904 in section 7 as well as GRB 090423 at $z \sim 8.1$ in section 16, GRB 080916C and GRB 090902B in section 17)).

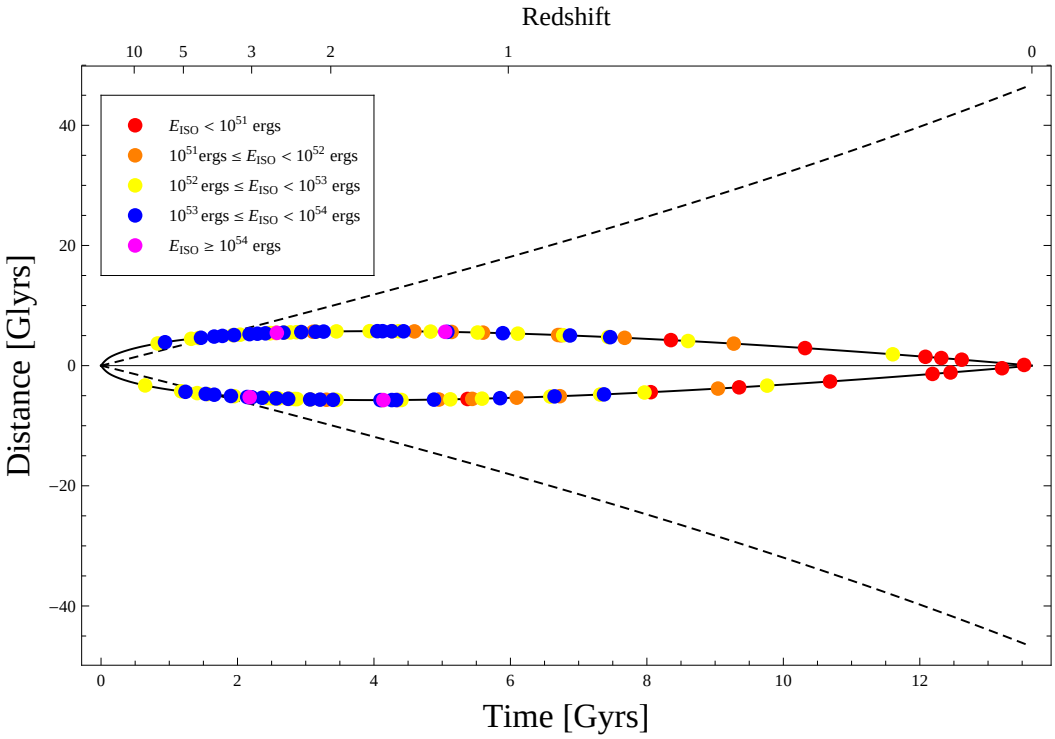

Figure 3.1.: GRB Distribution in distance and in energy.

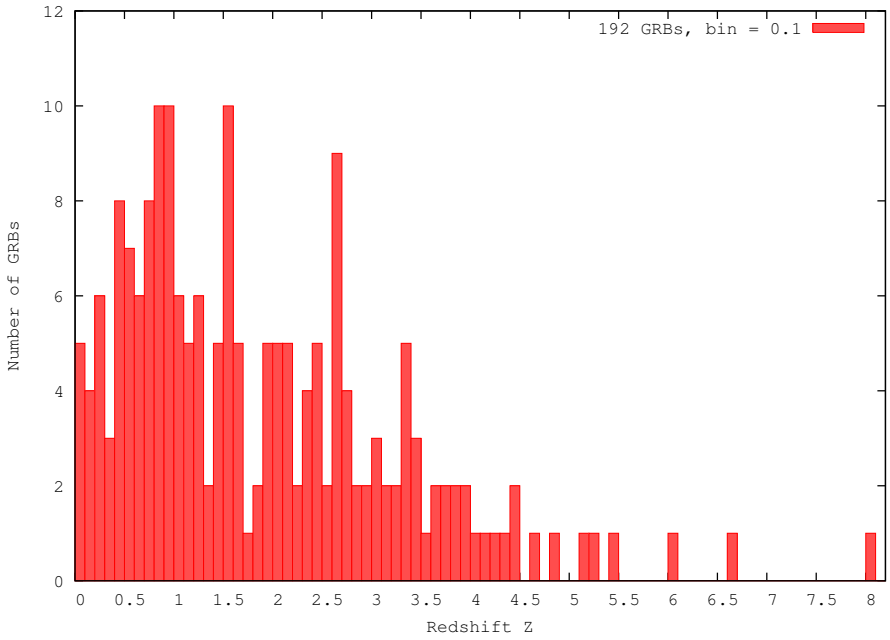

Figure 3.2.: Histogram of GRB redshifts.

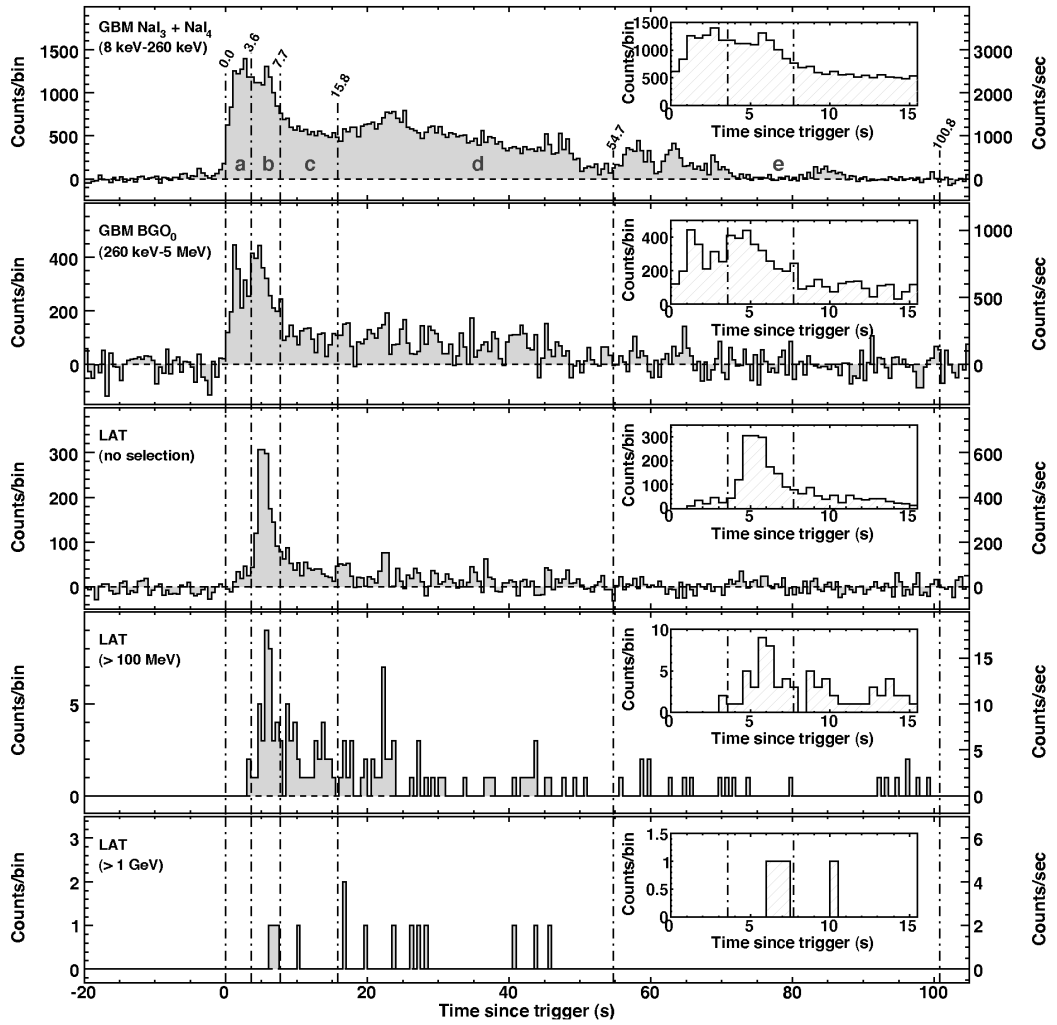

Figure 3.3.: Fermi observations of GRB 080916C

After the pioneering observations of the AGILE satellite and the Fermi mission it appears that there is an additional family of sources, extremely energetic, giving rise not only to emission in the X- and γ-rays, but also in the GeV region (see Fig. 3.3).

One may wonder how such a variety of astrophysical scenarios and of initial conditions may lead to a unified picture of GRBs.

The fundamental point is that all the above mentioned processes (see Fig. 3.4) are leading to the formation of a black hole, characterized uniquely by the three parameters of mass, charge and angular momentum. The emission process of GRBs occurs when this standard final configuration is approached. Therefore, the differences are uniquely in the energetics, but it is clear that the underlying physical process is the same. We report in the following progress in this understanding based on the theoretical analysis of specific sources

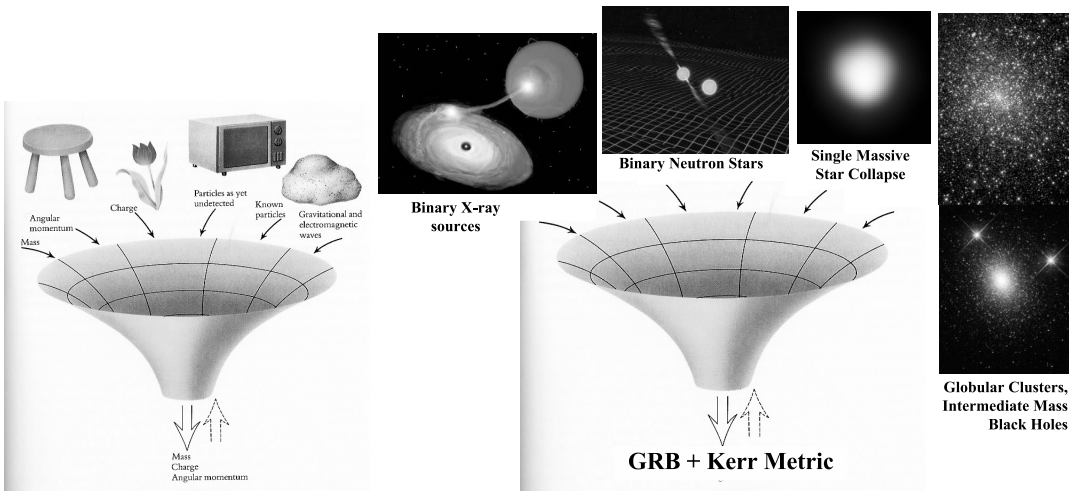

Figure 3.4.: Left: The Black Hole Uniqueness theorem (see e.g. Ref. Ruffini and Wheeler, 1971). **Right:** The GRB uniqueness.

which we have accomplished in this year.

3.3. The blackholic energy

It is now clear that the basic mechanism of acceleration of the GRBs is the electron-positron plasma created in the process of gravitational collapse to a black hole. The latest developments on these topics have been presented in the Reports on pages 559 and 1333, where we have also reported progresses in the understanding of dyadospheres and dyado-torii of black holes. We have also formalized the understanding of the crucial thermalization process of such electron-positron plasma and its interaction with the baryons, see the report on page 1333. We also obtained recent results on the dynamical evolution of such an electron-positron plasma, in presence of selected profiles of baryons (see Fig. 3.5, details in the report on page 1333).

The understanding of all these processes is crucial for describing the extraction of the blackholic energy, see the report on page 1. Similarly important is the use of the electron-positron plasma for the acceleration of baryons up to Lorentz gamma factors $\gamma \sim 10^3 - 10^4$. Far from being academic topic of researches, such concepts find their natural observational consequence in the study of the structure of the signal emitted when the electron-positron-baryon plasma reaches transparency in the emission of the Proper-GRB (see below).

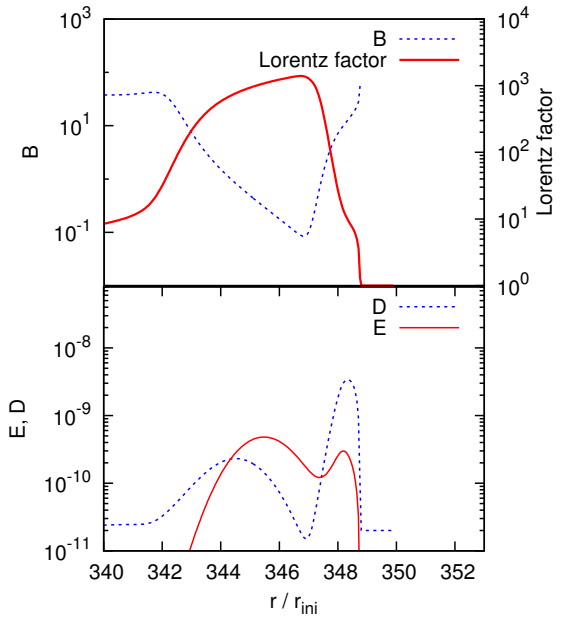

Figure 3.5.: Detailed structure of the spatial distribution of Lorentz factor and baryonic loading (upper panel), energy and matter density (lower panel) is shown for the hybrid case and for the moment $t = 434$. The B parameter changes 8 orders of magnitude in the extension of the shell. B is plotted until the point where Lorentz factor is equal one. Now we can see two shells for both densities E and D. Details in the report on page 1333.

3.4. The limits on the energetics of GRBs

One of the crucial steps which made possible the identification of the first black hole in our Galaxy has been the establishing an upper limits on the neutron star mass on general principles: 1) the validity of General Relativity, 2) the velocity of sound smaller than the speed of light, and 3) the existence of a fiducial density. This is today considered a classic result (see the report on page 1). What we have attempted now (presented in the talk by R. Ruffini at XII Marcel Grossmann Meeting) is to find a similar argument on the upper limit of the energetics of GRBs, quite independent of any details of the process, and uniquely based on the properties of the black holes and of the vacuum polarization process.

In brief, we recall that, in the process of gravitational collapse, a massive object of mass M reaches a minimum dimension R given by

$$R \sim d\frac{GM}{c^2}, \tag{3.4.1}$$

where d is a number of the order of 1-2 for black holes and close to 10 in the case of neutron stars. The gravitational energy at disposal is of the order of

$$E_{grav} \sim \frac{Mc^2}{d}, \tag{3.4.2}$$

and the average density of such an object is given by

$$\langle\rho\rangle \sim 1.86^2 \frac{m_n}{\frac{4}{3}\pi d^3 \left(\frac{\hbar}{m_n c}\right)^3 \left(\frac{M}{M_\odot}\right)^2}. \tag{3.4.3}$$

Since the process of vacuum polarization necessarily occur at nuclear densities, see report on page 429, we have

$$\langle\rho\rangle > \rho_{nucl} \sim \frac{m_n}{\frac{4}{3}\pi d^3 \left(\frac{\hbar}{m_n c}\right)^3}. \tag{3.4.4}$$

And the necessary condition that $\langle\rho\rangle > \rho_{nucl}$ imposes an upper limit on the mass of the collapsing object:

$$\frac{M}{M_\odot} < 1.86 d^{-3/2} \left(\frac{m_n}{m_\pi}\right)^{3/2}. \tag{3.4.5}$$

This implies that the mass of a neutron star should be in the range $0.1 < \frac{M_{NS}}{M_\odot} < 3.2$, while for black holes $M_{BH} < 32.5 d^{3/2} M_\odot = 11.5 M_\odot$. We can then conclude that an absolute upper limit to the energy of GRBs is $E < 1.1 \times 10^{55}$

ergs.

A larger value observed in a GRB would imply either a violation of a very basic physical law, or, more likely, a multiple structure in the gravitational collapse process as proposed by Ruffini and Wheeler in 1971, see Rees et al. (1974) and Fig. 3.6.

3.5. The "canonical" GRB: short vs long GRBs (GRB991216 and GRB 050315 as the prototypes)

As we recall later (see section 6) in our "canonical GRB" scenario there are only two free parameters characterizing the source (Ruffini et al., 2000, 2001b, 2007a):

- the total energy $E^{tot}_{e^\pm}$ of the $e^\pm$ plasma forming the self-accelerating optically thick fireshell
- the fireshell baryon loading $B \equiv M_B c^2 / E^{tot}_{e^\pm}$, where M_B is the total baryons' mass.

These two parameters fully determine the optically thick self-acceleration phase of the fireshell, which lasts until the transparency condition is reached and the Proper-GRB (P-GRB) is emitted. After the transparency point the self-acceleration phase ends and it remains only an optically thin fireshell of baryonic matter ballistically expanding with an initially ultrarelativistic velocity and loosing its kinetic energy via the interaction with the CircumBurst Medium (CBM).

Therefore, we define a "canonical GRB" light curve with two sharply different components (see Fig. 3.7 and Ruffini et al., 2001b, 2007a; Bernardini et al., 2007; Bianco et al., 2008a,b):

- **The P-GRB**, which is emitted when the optically thick fireshell becomes transparent. It depends only on $E^{tot}_{e^\pm}$ and B. It has the imprint of the black hole formation, an harder spectrum and no spectral lag (Bianco et al., 2001; Ruffini et al., 2005d).
- **the extended afterglow**, which is due to the collision between the left-over optically thin fireshell and the CBM (Ruffini et al., 2001b, 2007a; Bianco and Ruffini, 2004, 2005b,a). It depends on $E^{tot}_{e^\pm}$ and B but its temporal structure depends also on the additional parameters describing the effective CBM distribution: its density n_{cbm} and the ratio $\mathcal{R} \equiv A_{eff}/A_{vis}$ between the effective emitting area of the fireshell A_{eff} and its total visible area A_{vis}. It presents a clear hard-to-soft spectral evolution in time and it is composed by a rising part, a peak and a decaying

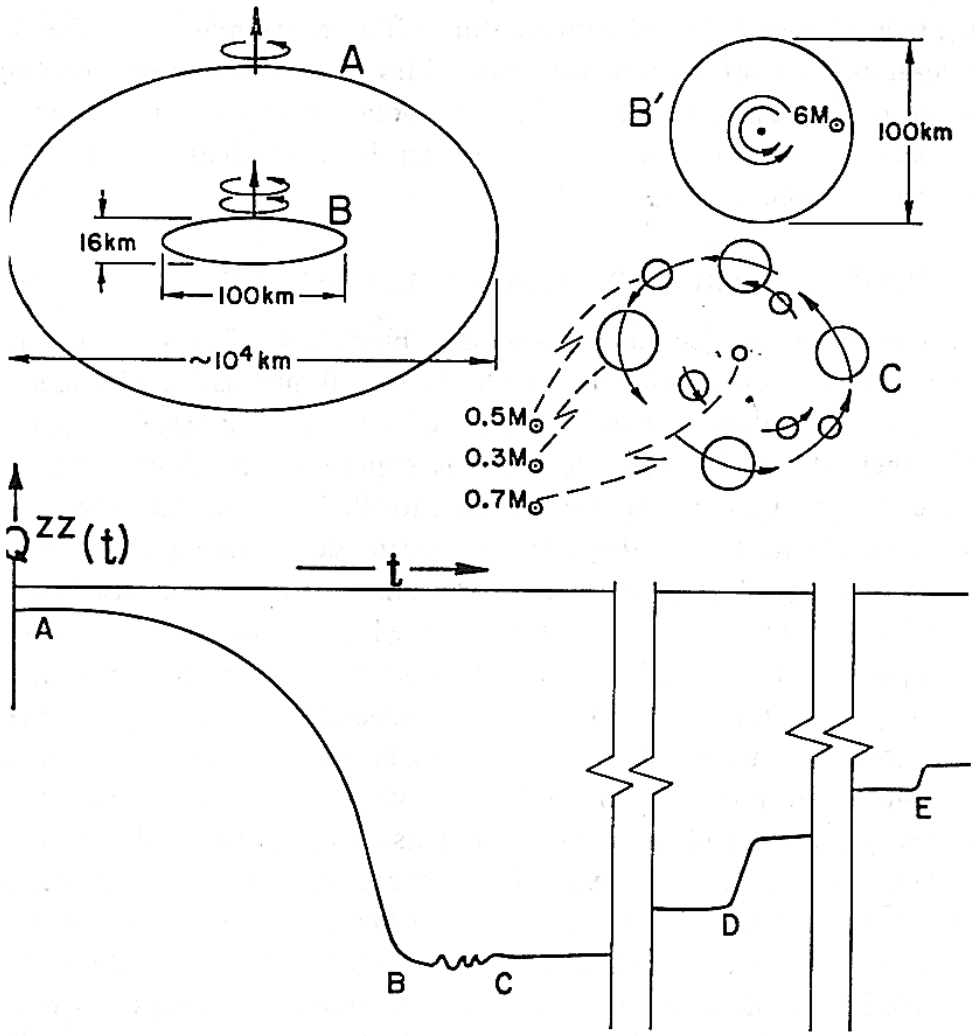

Figure 33 A rotating star with dense core A collapses to a pancake neutron star B; it fragments C; the fragments lose energy in periodic and splash gravitational radiation and recombine. The lower curve gives a schematic representation of the quadrupole moment as a function of time. Between B and C impulse radiation is created in the act of fragmentation not adequately described by the one indicated component of the quadrupole moment tensor. Between C and D multiply periodic radiation is given out until at D two fragments have lost enough angular momentum so that they combine with a splash of gravitational radiation; similarly at *E*, etc.

Figure 3.6.: The Pursuit & Plunge scenario, from Rees et al. (1974).

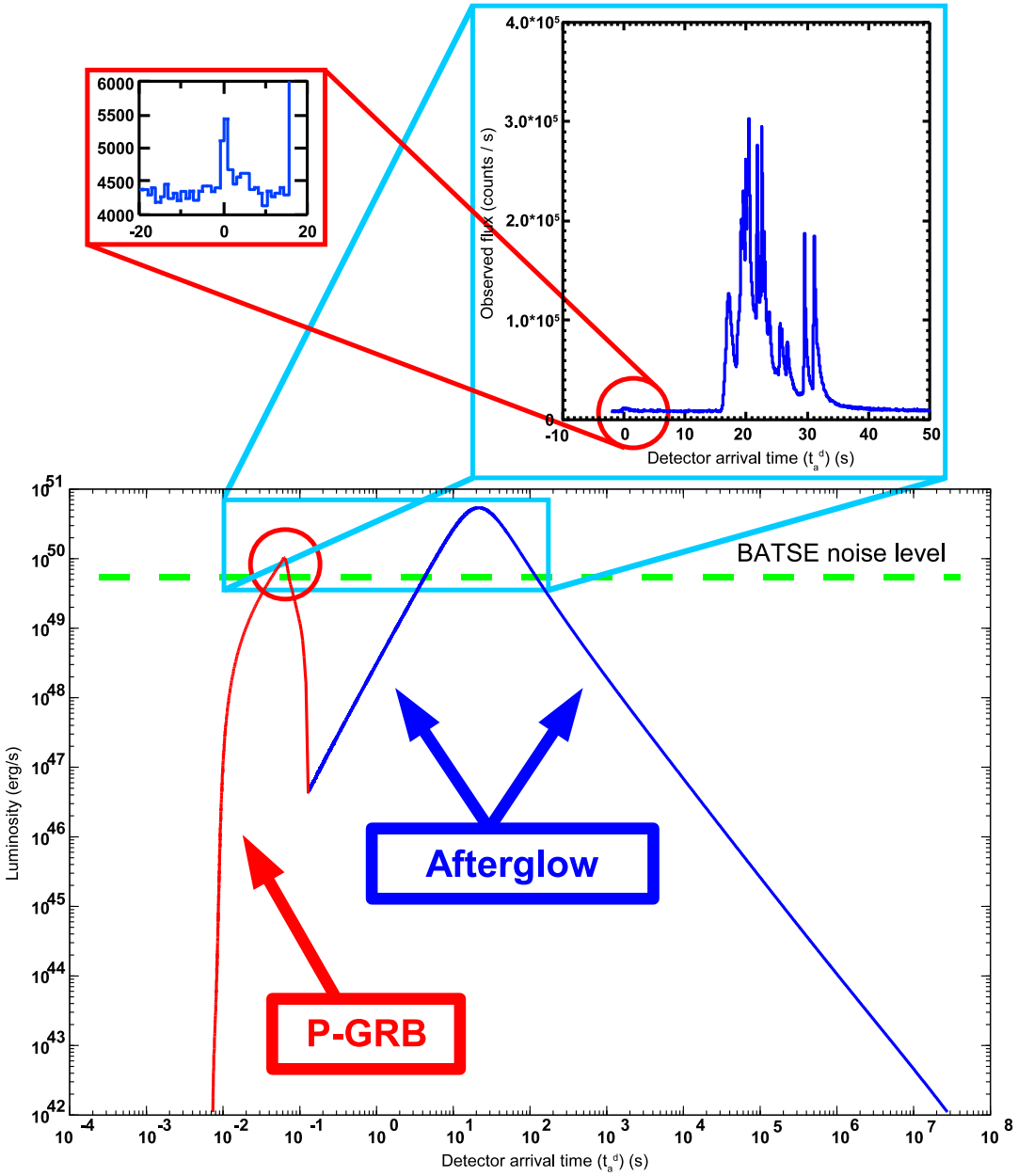

Figure 3.7.: The "canonical GRB" light curve theoretically computed for GRB 991216. The prompt emission observed by BATSE is identified with the peak of the afterglow, while the small precursor is identified with the P-GRB. For this source we have $E^{tot}_{e^\pm} = 4.83 \times 10^{53}$ ergs, $B \simeq 3.0 \times 10^{-3}$ and $\langle n_{cbm} \rangle \sim 1.0$ particles/cm^3. Details in Ruffini et al. (2001b, 2002, 2007a).

tail (Ruffini et al., 2002, 2004b, 2005c; Bernardini et al., 2005a; Ruffini et al., 2006b; Dainotti et al., 2007).

We clarify that what in the literature is called "prompt emission' within our theory is composed by both the P-GRB and the peak of the extended afterglow (see Fig. 3.7).

The ratio between the total time-integrated luminosity of the P-GRB (namely, its total energy) and the corresponding one of the afterglow is the crucial quantity for the identification of GRBs' nature (Ruffini et al., 2001b):

- When $B \leq 10^{-5}$ we have a P-GRB dominated event (in the limit $B \to 0$ the afterglow vanishes).
- In the opposite limit, for $10^{-4} \leq B \leq 10^{-2}$ we have an afterglow dominated GRB, and this is indeed the case of most of the GRBs we have recently examined (see Fig, 3.8).

3.6. Brief summary of recent progresses

Major progresses have been accomplished this year in the following aspects:

- Particularly exciting is the new possibility of having components yet to be observed in GRB sources. In fact, we have shown that it is not possible to interpret GRB 090618 and GRB 101023 within the framework of the traditional single component GRB model. We argue that the observation of the first episode of duration of around 50s could not be a part of a canonical GRB, while the residual emission could be modeled easily with the models existing in literature. This led to the definition of the novel concept of "proto-black hole emission" (see sections 9, 10 and 12).
- Thanks to this new understanding, we studied the X-ray emission shown by GRBs associated to SNe as due to the newly born neutron star, introducing the concept of the "neo neutron stars" and further developing the Induced Gravitational Collapse (IGC) scenario (see sections 8, 9, 10 and 12). This led us on May 2^{nd} to predict, from the observations of the prompt emission of GRB 130427A, the occurrence of an associated supernova between May 10^{th} and May 13^{th}. This prediction has been indeed confirmed by the observations (see section 15).
- We identified the first example of genuine short GRBs (see section 11).
- We identified the new class of GRBs "disguised by excess" (see section 13).

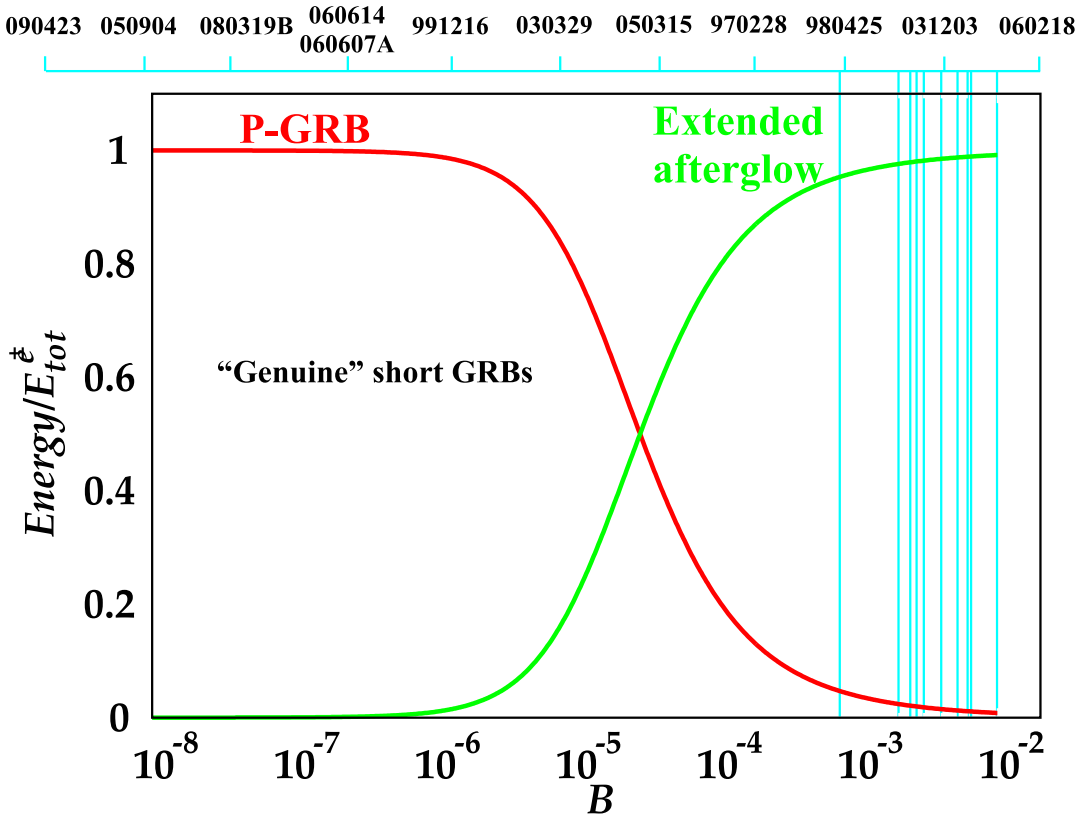

Figure 3.8.: Here the energies emitted in the P-GRB (red line) and in the afterglow (green line), in units of the total energy of the plasma, are plotted as functions of the B parameter. When $B \leq 10^{-5}$, the P-GRB becomes predominant over the afterglow, giving rise to a P-GRB dominated GRB. In the figure are also marked in blue the values of the B parameters corresponding to some GRBs we analyzed.

- The new developments of the IGC scenario led us to explore the possibility to introduce a new redshift estimator for members of the subclass of IGC-GRBs (see sections 10 and 14).

We have reached a new understanding of these family of sources thanks to the knowledge we had acquired previously on GRB 970228, GRB 060614, GRB 071227, GRB 050509b, GRB 011121, GRB 031203, GRB 050315, GRB 060218, GRB 060607A, whose details can be found in appendix C.

4. Selected publications before 2005

4.1. Refereed journals

1. D. Christodoulou, R. Ruffini; "Reversible Transformations of a Charged Black Hole"; Physical Review D, 4, 3552 (1971).

   A formula is derived for the mass of a black hole as a function of its "irreducible mass", its angular momentum, and its charge. It is shown that 50% of the mass of an extreme charged black hole can be converted into energy as contrasted with 29% for an extreme rotating black hole.

2. T. Damour, R. Ruffini; "Quantum electrodynamical effects in Kerr-Newman geometries"; Physical Review Letters, 35, 463 (1975).

   Following the classical approach of Sauter, of Heisenberg and Euler and of Schwinger the process of vacuum polarization in the field of a "bare" Kerr-Newman geometry is studied. The value of the critical strength of the electromagnetic fields is given together with an analysis of the feedback of the discharge on the geometry. The relevance of this analysis for current astrophysical observations is mentioned.

3. G. Preparata, R. Ruffini, S.-S. Xue; "The dyadosphere of black holes and gamma-ray bursts"; Astronomy & Astrophysics, 338, L87 (1999).

   The "dyadosphere" has been defined as the region outside the horizon of a black hole endowed with an electromagnetic field (abbreviated to EMBH for "electromagnetic black hole") where the electromagnetic field exceeds the critical value, predicted by Heisenberg & Euler for $e^{\pm}$ pair production. In a very short time ($\sim O(\hbar/mc^2)$) a very large number of pairs is created there. We here give limits on the EMBH parameters leading to a Dyadosphere for $10M_{\odot}$ and $10^5 M_{\odot}$ EMBH's, and give as well the pair densities as functions of the radial coordinate. We here assume that the pairs reach thermodynamic equilibrium with a photon gas and estimate the average energy per pair as a function of the EMBH mass. These data give the initial conditions for the analysis of an enormous pair-electromagnetic-pulse or "P.E.M. pulse" which naturally leads to relativistic expansion. Basic energy requirements for gamma ray bursts (GRB), including GRB971214 recently observed at z=3.4, can be accounted for by processes occurring in the dyadosphere. In this letter we do not address the prob-

lem of forming either the EMBH or the dyadosphere: we establish some inequalities which must be satisfied during their formation process.

4. R. Ruffini, J.D. Salmonson, J.R. Wilson, S.-S. Xue; "On the pair electromagnetic pulse of a black hole with electromagnetic structure"; Astronomy & Astrophysics, 350, 334 (1999).

   We study the relativistically expanding electron-positron pair plasma formed by the process of vacuum polarization around an electromagnetic black hole (EMBH). Such processes can occur for EMBH's with mass all the way up to $6 \times 10^5 M_\odot$. Beginning with a idealized model of a Reissner-Nordstrom EMBH with charge to mass ratio $\xi = 0.1$, numerical hydrodynamic calculations are made to model the expansion of the pair-electromagnetic pulse (PEM pulse) to the point that the system is transparent to photons. Three idealized special relativistic models have been compared and contrasted with the results of the numerically integrated general relativistic hydrodynamic equations. One of the three models has been validated: a PEM pulse of constant thickness in the laboratory frame is shown to be in excellent agreement with results of the general relativistic hydrodynamic code. It is remarkable that this precise model, starting from the fundamental parameters of the EMBH, leads uniquely to the explicit evaluation of the parameters of the PEM pulse, including the energy spectrum and the astrophysically unprecedented large Lorentz factors (up to 6×10^3 for a $10^3 M_\odot$ EMBH). The observed photon energy at the peak of the photon spectrum at the moment of photon decoupling is shown to range from 0.1 MeV to 4 MeV as a function of the EMBH mass. Correspondingly the total energy in photons is in the range of 10^{52} to 10^{54} ergs, consistent with observed gamma-ray bursts. In these computations we neglect the presence of baryonic matter which will be the subject of forthcoming publications.

5. R. Ruffini, J.D. Salmonson, J.R. Wilson, S.-S. Xue; "On the pair-electro magnetic pulse from an electromagnetic black hole surrounded by a baryonic remnant"; Astronomy & Astrophysics, 359, 855 (2000).

   The interaction of an expanding Pair-Electromagnetic pulse (PEM pulse) with a shell of baryonic matter surrounding a Black Hole with electromagnetic structure (EMBH) is analyzed for selected values of the baryonic mass at selected distances well outside the dyadosphere of an EMBH. The dyadosphere, the region in which a super critical field exists for the creation of e+e- pairs, is here considered in the special case of a Reissner-Nordstrom geometry. The interaction of the PEM pulse with the baryonic matter is described using a simplified model of a slab of constant thickness in the laboratory frame (constant-thickness approximation) as well as performing the integration of the general relativistic hydrodynamical equations. Te validation of the constant-thickness approximation, already presented in a previous paper Ruffini et al. (1999) for a PEM pulse in vacuum, is here generalized to the presence of baryonic matter. It is found that for a baryonic shell of mass-energy less than 1% of the total

energy of the dyadosphere, the constant-thickness approximation is in excellent agreement with full general relativistic computations. The approximation breaks down for larger values of the baryonic shell mass, however such cases are of less interest for observed Gamma Ray Bursts (GRBs). On the basis of numerical computations of the slab model for PEM pulses, we describe (i) the properties of relativistic evolution of a PEM pulse colliding with a baryonic shell; (ii) the details of the expected emission energy and observed temperature of the associated GRBs for a given value of the EMBH mass; $10^3 M_\odot$, and for baryonic mass-energies in the range 10^{-8} to 10^{-2} the total energy of the dyadosphere.

6. C.L. Bianco, R. Ruffini, S.-S. Xue; "The elementary spike produced by a pure e+e- pair-electromagnetic pulse from a Black Hole: The PEM Pulse"; Astronomy & Astrophysics, 368, 377 (2001).

   In the framework of the model that uses black holes endowed with electromagnetic structure (EMBH) as the energy source, we study how an elementary spike appears to the detectors. We consider the simplest possible case of a pulse produced by a pure e^+e^- pair-electro-magnetic plasma, the PEM pulse, in the absence of any baryonic matter. The resulting time profiles show a *Fast-Rise-Exponential-Decay* shape, followed by a power-law tail. This is obtained without any special fitting procedure, but only by fixing the energetics of the process taking place in a given EMBH of selected mass, varying in the range from 10 to 10^3 $M_\odot$ and considering the relativistic effects to be expected in an electron-positron plasma gradually reaching transparency. Special attention is given to the contributions from all regimes with Lorentz γ factor varying from $\gamma = 1$ to $\gamma = 10^4$ in a few hundreds of the PEM pulse travel time. Although the main goal of this paper is to obtain the elementary spike intensity as a function of the arrival time, and its observed duration, some qualitative considerations are also presented regarding the expected spectrum and on its departure from the thermal one. The results of this paper will be comparable, when data will become available, with a subfamily of particularly short GRBs not followed by any afterglow. They can also be propedeutical to the study of longer bursts in presence of baryonic matter currently observed in GRBs.

7. R. Ruffini, C.L. Bianco, P. Chardonnet, F. Fraschetti, S.-S. Xue; "Relative spacetime transformations in Gamma-Ray Bursts"; The Astrophysical Journal, 555, L107 (2001).

   The GRB 991216 and its relevant data acquired from the BATSE experiment and RXTE and Chandra satellites are used as a prototypical case to test the theory linking the origin of gamma ray bursts (GRBs) to the process of vacuum polarization occurring during the formation phase of a black hole endowed with electromagnetic structure (EMBH). The relative space-time transformation paradigm (RSTT paradigm) is presented. It relates the observed signals of GRBs to their past light cones, defining the events on the worldline of the

source essential for the interpretation of the data. Since GRBs present regimes with unprecedently large Lorentz γ factor, also sharply varying with time, particular attention is given to the constitutive equations relating the four time variables: the comoving time, the laboratory time, the arrival time at the detector, duly corrected by the cosmological effects. This paradigm is at the very foundation of any possible interpretation of the data of GRBs.

8. R. Ruffini, C.L. Bianco, P. Chardonnet, F. Fraschetti, S.-S. Xue; "On the interpretation of the burst structure of Gamma-Ray Bursts"; The Astrophysical Journal, 555, L113 (2001).

   Given the very accurate data from the BATSE experiment and RXTE and Chandra satellites, we use the GRB 991216 as a prototypical case to test the EMBH theory linking the origin of the energy of GRBs to the electromagnetic energy of black holes. The fit of the afterglow fixes the only two free parameters of the model and leads to a new paradigm for the interpretation of the burst structure, the IBS paradigm. It leads as well to a reconsideration of the relative roles of the afterglow and burst in GRBs by defining two new phases in this complex phenomenon: a) the injector phase, giving rise to the proper-GRB (P-GRB), and b) the beam-target phase, giving rise to the extended afterglow peak emission (E-APE) and to the afterglow. Such differentiation leads to a natural possible explanation of the bimodal distribution of GRBs observed by BATSE. The agreement with the observational data in regions extending from the horizon of the EMBH all the way out to the distant observer confirms the uniqueness of the model.

9. R. Ruffini, C.L. Bianco, P. Chardonnet, F. Fraschetti, S.-S. Xue; "On a possible Gamma-Ray Burst-Supernova time sequence"; The Astrophysical Journal, 555, L117 (2001).

   The data from the Chandra satellite on the iron emission lines in the afterglow of GRB 991216 are used to give further support for the EMBH theory, which links the origin of the energy of GRBs to the extractable energy of electromagnetic black holes (EMBHs), leading to an interpretation of the GRB-supernova correlation. Following the relative space-time transformation (RSTT) paradigm and the interpretation of the burst structure (IBS) paradigm, we introduce a paradigm for the correlation between GRBs and supernovae. The following sequence of events is shown as kinematically possible and consistent with the available data: a) the GRB-progenitor star P_1 first collapses to an EMBH, b) the proper GRB (P-GRB) and the peak of the afterglow (E-APE) propagate in interstellar space until the impact on a supernova-progenitor star P_2 at a distance $\leq 2.69 \times 10^{17}$ cm, and they induce the supernova explosion, c) the accelerated baryonic matter (ABM) pulse, originating the afterglow, reaches the supernova remnants 18.5 hours after the supernova explosion and gives rise to the iron emission lines. Some considerations on the dynamical implementation of the paradigm are presented. The concept of induced supernova

explosion introduced here specifically for the GRB-supernova correlation may have more general application in relativistic astrophysics.

10. R. Ruffini, C.L. Bianco, P. Chardonnet, F. Fraschetti, S.-S. Xue; "On the physical processes which lie at the bases of time variability of GRBs"; Il Nuovo Cimento B, 116, 99 (2001).

    The relative-space-time-transformation (RSTT) paradigm and the interpretation of the burst-structure (IBS) paradigm are applied to probe the origin of the time variability of GRBs. Again GRB 991216 is used as a prototypical case, thanks to the precise data from the CGRO, RXTE and Chandra satellites. It is found that with the exception of the relatively inconspicuous but scientifically very important signal originating from the initial "proper gamma ray burst" (P-GRB), all the other spikes and time variabilities can be explained by the interaction of the accelerated-baryonic-matter pulse with inhomogeneities in the interstellar matter. This can be demonstrated by using the RSTT paradigm as well as the IBS paradigm, to trace a typical spike observed in arrival time back to the corresponding one in the laboratory time. Using these paradigms, the identification of the physical nature of the time variablity of the GRBs can be made most convincingly. It is made explicit the dependence of a) the intensities of the afterglow, b) the spikes amplitude and c) the actual time structure on the Lorentz gamma factor of the accelerated-baryonic-matter pulse. In principle it is possible to read off from the spike structure the detailed density contrast of the interstellar medium in the host galaxy, even at very high redshift.

11. R. Ruffini, C.L. Bianco, P. Chardonnet, F. Fraschetti, S.-S. Xue; "On the structures in the afterglow peak emission of gamma ray bursts"; The Astrophysical Journal, 581, L19 (2002).

    Using GRB 991216 as a prototype, it is shown that the intensity substructures observed in what is generally called the "prompt emission" in gamma ray bursts (GRBs) do originate in the collision between the accelerated baryonic matter (ABM) pulse with inhomogeneities in the interstellar medium (ISM). The initial phase of such process occurs at a Lorentz factor $\gamma \sim 310$. The crossing of ISM inhomogeneities of sizes $\Delta R \sim 10^{15}$ cm occurs in a detector arrival time interval of ~ 0.4 s implying an apparent superluminal behavior of $\sim 10^5 c$. The long lasting debate between the validity of the external shock model vs. the internal shock model for GRBs is solved in favor of the first.

12. R. Ruffini, C.L. Bianco, P. Chardonnet, F. Fraschetti, S.-S. Xue; "On the structure of the burst and afterglow of Gamma-Ray Bursts I: the radial approximation"; International Journal of Modern Physics D, 12, 173 (2003).

    We have recently proposed three paradigms for the theoretical interpretation of gamma-ray bursts (GRBs). (1) The relative space-time transformation (RSTT) paradigm emphasizes how the knowledge of the entire world-line of the source

from the moment of gravitational collapse is a necessary condition in order to interpret GRB data. (2) The interpretation of the burst structure (IBS) paradigm differentiates in all GRBs between an injector phase and a beam-target phase. (3) The GRB-supernova time sequence (GSTS) paradigm introduces the concept of *induced supernova explosion* in the supernovae-GRB association. In the introduction the RSTT and IBS paradigms are enunciated and illustrated using our theory based on the vacuum polarization process occurring around an electromagnetic black hole (EMBH theory). The results are summarized using figures, diagrams and a complete table with the space-time grid, the fundamental parameters and the corresponding values of the Lorentz gamma factor for GRB 991216 used as a prototype. In the following sections the detailed treatment of the EMBH theory needed to understand the results of the three above letters is presented. We start from the considerations on the dyadosphere formation. We then review the basic hydrodynamic and rate equations, the equations leading to the relative space-time transformations as well as the adopted numerical integration techniques. We then illustrate the five fundamental eras of the EMBH theory: the self acceleration of the e^+e^- pair-electromagnetic plasma (PEM pulse), its interaction with the baryonic remnant of the progenitor star, the further self acceleration of the e^+e^- pair-electroma-gnetic radiation and baryon plasma (PEMB pulse). We then study the approach of the PEMB pulse to transparency, the emission of the proper GRB (P-GRB) and its relation to the "short GRBs". Particular attention is given to the free parameters of the theory and to the values of the thermodynamical quantities at transparency. Finally the three different regimes of the afterglow are described within the fully radiative and radial approximations: the ultrarelativistic, the relativistic and the nonrelativistic regimes. The best fit of the theory leads to an unequivocal identification of the "long GRBs" as extended emission occurring at the afterglow peak (E-APE). The relative intensities, the time separation and the hardness ratio of the P-GRB and the E-APE are used as distinctive observational test of the EMBH theory and the excellent agreement between our theoretical predictions and the observations are documented. The afterglow power-law indexes in the EMBH theory are compared and contrasted with the ones in the literature, and no beaming process is found for GRB 991216. Finally, some preliminary results relating the observed time variability of the E-APE to the inhomogeneities in the interstellar medium are presented, as well as some general considerations on the EMBH formation. The issue of the GSTS paradigm will be the object of a forthcoming publication and the relevance of the iron-lines observed in GRB 991216 is shortly reviewed. The general conclusions are then presented based on the three fundamental parameters of the EMBH theory: the dyadosphere energy, the baryonic mass of the remnant, the interstellar medium density. An in depth discussion and comparison of the EMBH theory with alternative theories is presented as well as indications of further developments beyond the radial approximation, which will be the subject of paper II in this series. Future needs for specific

GRB observations are outlined.

13. R. Ruffini, C.L. Bianco, P. Chardonnet, F. Fraschetti, V. Gurzadyan, S.-S. Xue; "On the instantaneous spectrum of gamma ray bursts"; International Journal of Modern Physics D, 13, 843 (2004).

    A theoretical attempt to identify the physical process responsible for the afterglow emission of Gamma-Ray Bursts (GRBs) is presented, leading to the occurrence of thermal emission in the comoving frame of the shock wave giving rise to the bursts. The determination of the luminosities and spectra involves integration over an infinite number of Planckian spectra, weighted by appropriate relativistic transformations, each one corresponding to a different viewing angle in the past light cone of the observer. The relativistic transformations have been computed using the equations of motion of GRBs within our theory, giving special attention to the determination of the equitemporal surfaces. The only free parameter of the present theory is the "effective emitting area" in the shock wave front. A self consistent model for the observed hard-to-soft transition in GRBs is also presented. When applied to GRB 991216 a precise fit $\left(\chi^2 \simeq 1.078\right)$ of the observed luminosity in the 2–10 keV band is obtained. Similarly, detailed estimates of the observed luminosity in the 50–300 keV and in the 10–50 keV bands are obtained.

4.2. Conference proceedings

1. R. Ruffini; "Beyond the critical mass: The dyadosphere of black holes"; in "Black Holes and High Energy Astrophysics", H. sato, N. Sugiyama, Editors; p. 167; Universal Academy Press (Tokyo, Japan, 1998).

    The "dyadosphere" (from the Greek word "duas-duados" for pairs) is here defined as the region outside the horizon of a black hole endowed with an electromagnetic field (abbreviated to EMBH for "electromagnetic black hole") where the electromagnetic field exceeds the critical value, predicted by Heisenberg and Euler for e^+e^- pair production. In a very short time ($\sim O(\hbar/mc^2)$), a very large number of pairs is created there. I give limits on the EMBH parameters leading to a Dyadosphere for $10M_\odot$ and $10^5M_\odot$ EMBH's, and give as well the pair densities as functions of the radial coordinate. These data give the initial conditions for the analysis of an enormous pair-electromagnetic-pulse or "PEM-pulse" which naturally leads to relativistic expansion. Basic energy requirements for gamma ray bursts (GRB), including GRB971214 recently observed at $z = 3.4$, can be accounted for by processes occurring in the dyadosphere.

2. R. Ruffini, C.L. Bianco, P. Chardonnet, F. Fraschetti, L. Vitagliano, S.-S. Xue; "New perspectives in physics and astrophysics from the theoretical understanding of Gamma-Ray Bursts"; in "COSMOLOGY AND

GRAVITATION: Xth Brazilian School of Cosmology and Gravitation; 25th Anniversary (1977-2002)", Proceedings of the Xth Brazilian School on Cosmology and Gravitation, Mangaratiba, Rio de Janeiro (Brazil), July - August 2002, M. Novello, S.E. Perez Bergliaffa, Editors; AIP Conference Proceedings, 668, 16 (2003).

If due attention is given in formulating the basic equations for the Gamma-Ray Burst (GRB) phenomenon and in performing the corresponding quantitative analysis, GRBs open a main avenue of inquiring on totally new physical and astrophysical regimes. This program is very likely one of the greatest computational efforts in physics and astrophysics and cannot be actuated using shortcuts. A systematic approach is needed which has been highlighted in three basic new paradigms: the relative space-time transformation (RSTT) paradigm, the interpretation of the burst structure (IBS) paradigm, the GRB-supernova time sequence (GSTS) paradigm. From the point of view of fundamental physics new regimes are explored: (1) the process of energy extraction from black holes; (2) the quantum and general relativistic effects of matter-antimatter creation near the black hole horizon; (3) the physics of ultrarelativisitc shock waves with Lorentz gamma factor $\gamma > 100$. From the point of view of astronomy and astrophysics also new regimes are explored: (i) the occurrence of gravitational collapse to a black hole from a critical mass core of mass $M \gtrsim 10 M_{\odot}$, which clearly differs from the values of the critical mass encountered in the study of stars "catalyzed at the endpoint of thermonuclear evolution" (white dwarfs and neutron stars); (ii) the extremely high efficiency of the spherical collapse to a black hole, where almost 99.99% of the core mass collapses leaving negligible remnant; (iii) the necessity of developing a fine tuning in the final phases of thermonuclear evolution of the stars, both for the star collapsing to the black hole and the surrounding ones, in order to explain the possible occurrence of the "induced gravitational collapse". New regimes are as well encountered from the point of view of nature of GRBs: (I) the basic structure of GRBs is uniquely composed by a proper-GRB (P-GRB) and the afterglow; (II) the long bursts are then simply explained as the peak of the afterglow (the E-APE) and their observed time variability is explained in terms of inhomogeneities in the interstellar medium (ISM); (III) the short bursts are identified with the P-GRBs and the crucial information on general relativistic and vacuum polarization effects are encoded in their spectra and intensity time variability. A new class of space missions to acquire information on such extreme new regimes are urgently needed.

3. R. Ruffini, C.L. Bianco, P. Chardonnet, F. Fraschetti, S.-S. Xue; "The EMBH Model in GRB 991216 and GRB 980425"; in Proceedings of "Third Rome Workshop on Gamma-Ray Burst in the Afterglow Era", 17-20 September 2002; M. Feroci, F. Frontera, N. Masetti, L. Piro, Editors; ASP Conference Series, 312, 349 (2004).

This is a summary of the two talks presented at the Rome GRB meeting by C.L. Bianco and R. Ruffini. It is shown that by respecting the Relative Space-Time Transformation (RSTT) paradigm and the Interpretation of the Burst Structure (IBS) paradigm, important inferences are possible: a) in the new physics occurring in the energy sources of GRBs, b) on the structure of the bursts and c) on the composition of the interstellar matter surrounding the source.

4. M.G. Bernardini, C.L. Bianco, P. Chardonnet, F. Fraschetti, R. Ruffini, S.-S. Xue; "A New Astrophysical 'Triptych': GRB030329/SN2003dh/ URCA-2"; in "GAMMA-RAY BURSTS: 30 YEARS OF DISCOVERY", Proceedings of the Los Alamos "Gamma Ray Burst Symposium", Santa Fe, New Mexico, 8 12 September 2003, E.E. Fenimore, M. Galassi, Editors; AIP Conference Proceedings, 727, 312 (2004).

   We analyze the data of the Gamma-Ray Burst/Supernova GRB030329/ SN2003dh system obtained by HETE-2, R-XTE, XMM and VLT within our theory for GRB030329. By fitting the only three free parameters of the EMBH theory, we obtain the luminosity in fixed energy bands for the prompt emission and the afterglow. Since the Gamma-Ray Burst (GRB) analysis is consistent with a spherically symmetric expansion, the energy of GRB030329 is $E = 2.1 \times 10^{52}$ erg, namely $\sim 2 \times 10^3$ times larger than the Supernova energy. We conclude that either the GRB is triggering an induced-supernova event or both the GRB and the Supernova are triggered by the same relativistic process. In no way the GRB can be originated from the supernova. We also evidence that the XMM observations, much like in the system GRB980425/SN1998bw, are not part of the GRB afterglow, as interpreted in the literature, but are associated to the Supernova phenomenon. A dedicated campaign of observations is needed to confirm the nature of this XMM source as a newly born neutron star cooling by generalized URCA processes.

5. F. Fraschetti, M.G. Bernardini, C.L. Bianco, P. Chardonnet, R. Ruffini, S.-S. Xue; "The GRB980425-SN1998bw Association in the EMBH Model"; in "GAMMA-RAY BURSTS: 30 YEARS OF DISCOVERY", Proceedings of the Los Alamos "Gamma Ray Burst Symposium", Santa Fe, New Mexico, 8 12 September 2003, E.E. Fenimore, M. Galassi, Editors; AIP Conference Proceedings, 727, 424 (2004).

   Our GRB theory, previously developed using GRB 991216 as a prototype, is here applied to GRB 980425. We fit the luminosity observed in the 40–700 keV, 2–26 keV and 2–10 keV bands by the BeppoSAX satellite. In addition the supernova SN1998bw is the outcome of an "induced gravitational collapse" triggered by GRB 980425, in agreement with the GRB-Supernova Time Sequence (GSTS) paradigm. A further outcome of this astrophysically exceptional sequence of events is the formation of a young neutron star generated by the SN1998bw event. A coordinated observational activity is recommended to

further enlighten the underlying scenario of this most unique astrophysical system.

6. A. Corsi, M.G. Bernardini, C.L. Bianco, P. Chardonnet, F. Fraschetti, R. Ruffini, S.-S. Xue; "GRB 970228 Within the EMBH Model"; in "GAMMA-RAY BURSTS: 30 YEARS OF DISCOVERY", Proceedings of the Los Alamos "Gamma Ray Burst Symposium", Santa Fe, New Mexico, 8 12 September 2003, E.E. Fenimore, M. Galassi, Editors; AIP Conference Proceedings, 727, 428 (2004).

   We consider the gamma-ray burst of 1997 February 28 (GRB 970228) within the ElectroMagnetic Black Hole (EMBH) model. We first determine the value of the two free parameters that characterize energetically the GRB phenomenon in the EMBH model, that is to say the dyadosphere energy, $E_{dya} = 5.1 \times 10^{52}$ ergs, and the baryonic remnant mass M_B in units of E_{dya}, $B = M_B c^2 / E_{dya} = 3.0 \times 10^{-3}$. Having in this way estimated the energy emitted during the beam-target phase, we evaluate the role of the InterStellar Medium (ISM) number density (n_{ISM}) and of the ratio $\mathcal{R}$ between the effective emitting area and the total surface area of the GRB source, in reproducing the observed profiles of the GRB 970228 prompt emission and X-ray (2-10 keV energy band) afterglow. The importance of the ISM distribution three-dimensional treatment around the central black hole is also stressed in this analysis.

5. Publications (2005–2013)

5.1. Refereed journals

1. R. Ruffini, C.L. Bianco, P. Chardonnet, F. Fraschetti, V. Gurzadyan, S.-S. Xue; "Emergence of a filamentary structure in the fireball from GRB spectra"; International Journal of Modern Physics D, 14, 97 (2005).

   It is shown that the concept of a fireball with a definite filamentary structure naturally emerges from the analysis of the spectra of Gamma-Ray Bursts (GRBs). These results, made possible by the recently obtained analytic expressions of the equitemporal surfaces in the GRB afterglow, depend crucially on the single parameter R describing the effective area of the fireball emitting the X-ray and gamma-ray radiation. The X-ray and gamma-ray components of the afterglow radiation are shown to have a thermal spectrum in the comoving frame of the fireball and originate from a stable shock front described self-consistently by the Rankine-Hugoniot equations. Precise predictions are presented on a correlation between spectral changes and intensity variations in the prompt radiation verifiable, e.g., by the Swift and future missions. The highly variable optical and radio emission depends instead on the parameters of the surrounding medium. The GRB 991216 is used as a prototype for this model.

2. R. Ruffini, M.G. Bernardini, C.L. Bianco, P. Chardonnet, F. Fraschetti, V. Gurzadyan, M. Lattanzi, L. Vitagliano, S.-S. Xue; "Extracting energy from black holes: 'long' and 'short' GRBs and their astrophysical settings"; Il Nuovo Cimento C, 28, 589 (2005).

   The introduction of the three interpretational paradigms for Gamma-Ray Bursts (GRBs) and recent progress in understanding the X- and gamma-ray luminosity in the afterglow allow us to make assessments about the astrophysical settings of GRBs. In particular, we evidence the distinct possibility that some GRBs occur in a binary system. This subclass of GRBs manifests itself in a "tryptich": one component formed by the collapse of a massive star to a black hole, which originates the GRB; a second component by a supernova and a third one by a young neutron star born in the supernova event. Similarly, the understanding of the physics of quantum relativistic processes during the gravitational collapse makes possible precise predictions about the structure of short GRBs.

3. M.G. Bernardini, C.L. Bianco, P. Chardonnet, F. Fraschetti, R. Ruffini, S.-S. Xue; "Theoretical interpretation of luminosity and spectral properties of GRB 031203"; The Astrophysical Journal, 634, L29 (2005).

   The X-ray and gamma-ray observations of the source GRB 031203 by INTEGRAL are interpreted within our theoretical model. In addition to a complete spacetime parameterization of the GRB, we specifically assume that the afterglow emission originates from a thermal spectrum in the comoving frame of the expanding baryonic matter shell. By determining the two free parameters of the model and estimating the density and filamentary structure of the ISM, we reproduce the observed luminosity in the 20-200 keV energy band. As in previous sources, the prompt radiation is shown to coincide with the peak of the afterglow, and the luminosity substructure is shown to originate in the filamentary structure of the ISM. We predict a clear hard-to-soft behavior in the instantaneous spectra. The time-integrated spectrum over 20 s observed by INTEGRAL is well fitted. Despite the fact that this source has been considered "unusual", it appears to us to be a normal low-energy GRB.

4. R. Ruffini, M.G. Bernardini, C.L. Bianco, P. Chardonnet, F. Fraschetti, S.-S. Xue; Evidence for isotropic emission in GRB991216; Advances in Space Research, 38, 1291 (2006).

   The issue of the possible presence or absence of jets in GRBs is here re-examined for GRB991216. We compare and contrast our theoretically predicted afterglow luminosity in the 2–10 keV band for spherically symmetric versus jetted emission. At these wavelengths the jetted emission can be excluded and data analysis confirms spherical symmetry. These theoretical fits are expected to be improved by the forthcoming data of the Swift mission.

5. R. Ruffini, M.G. Bernardini, C.L. Bianco, P. Chardonnet, F. Fraschetti, R. Guida, S.-S. Xue; "GRB 050315: A step toward understanding the uniqueness of the overall GRB structure"; The Astrophysical Journal, 645, L109 (2006).

   Using the Swift data of GRB 050315, we are making progress toward understanding the uniqueness of our theoretically predicted gamma-ray burst (GRB) structure, which is composed of a proper GRB (P-GRB), emitted at the transparency of an electron-positron plasma with suitable baryon loading, and an afterglow comprising the so-called prompt emission due to external shocks. Thanks to the Swift observations, the P-GRB is identified, and for the first time we can theoretically fit detailed light curves for selected energy bands on a continuous timescale ranging over 106 s. The theoretically predicted instantaneous spectral distribution over the entire afterglow is presented, confirming a clear hard-to-soft behavior encompassing, continuously, the "prompt emission" all the way to the latest phases of the afterglow.

6. C.L. Bianco, L. Caito, R. Ruffini; "Theoretical interpretation of GRB 011121"; Il Nuovo Cimento B, 121, 1441 (2006).

   GRB011121 is analyzed as a prototype to understand the "flares" recently observed by Swift in the afterglow of many GRB sources. Detailed theoretical computation of the GRB011121 light curves in selected energy bands are presented and compared and contrasted with observational BeppoSAX data.

7. R. Ruffini, M.G. Bernardini, C.L. Bianco, P. Chardonnet, F. Fraschetti, R. Guida, S.-S. Xue; "GRB 050315: A step toward the uniqueness of the overall GRB structure"; Il Nuovo Cimento B, 121, 1367 (2006).

   Using the *Swift* data of GRB 050315, we progress on the uniqueness of our theoretically predicted Gamma-Ray Burst (GRB) structure as composed by a proper-GRB (P-GRB), emitted at the transparency of an electron-positron plasma with suitable baryon loading, and an afterglow comprising the so called "prompt emission" as due to external shocks. Thanks to the *Swift* observations, we can theoretically fit detailed light curves for selected energy bands on a continuous time scale ranging over 10^6 seconds. The theoretically predicted instantaneous spectral distribution over the entire afterglow confirms a clear hard-to-soft behavior encompassing, continuously, the "prompt emission" all the way to the latest phases of the afterglow. Consequences of the instrumental threshold on the definition of "short" and "long" GRBs are discussed.

8. M.G. Bernardini, C.L. Bianco, L. Caito, P. Chardonnet, A. Corsi, M.G. Dainotti, F. Fraschetti, R. Guida, R. Ruffini, S.-S. Xue; GRB970228 as a prototype for short GRBs with afterglow; Il Nuovo Cimento B, 121, 1439 (2006).

   GRB970228 is analyzed as a prototype to understand the relative role of short GRBs and their associated afterglows, recently observed by Swift and HETE-II. Detailed theoretical computation of the GRB970228 light curves in selected energy bands are presented and compared with observational BeppoSAX data.

9. M.G. Dainotti, M.G. Bernardini, C.L. Bianco, L. Caito, R. Guida, R. Ruffini; "GRB060218 and GRBs associated with Supernovae Ib/c"; Astronomy & Astrophysics, 471, L29 (2007).

   Context: The *Swift* satellite has given continuous data in the range 0.3–150 keV from 0 s to 10^6 s for GRB060218 associated with SN2006aj. This Gamma-Ray Burst (GRB) which has an unusually long duration ($T_{90} \sim 2100$ s) fulfills the Amati relation. These data offer the opportunity to probe theoretical models for GRBs connected with Supernovae (SNe).
   Aims: We plan to fit the complete γ- and X-ray light curves of this long duration GRB, including the prompt emission, in order to clarify the nature of the progenitors and the astrophysical scenario of the class of GRBs associated with SNe Ib/c.

Methods: We apply our "fireshell" model based on the formation of a black hole, giving the relevant references. It is characterized by the precise equations of motion and equitemporal surfaces and by the role of thermal emission.
Results: The initial total energy of the electron-positron plasma $E_{e^\pm}^{tot} = 2.32 \times 10^{50}$ erg has a particularly low value, similar to the other GRBs associated with SNe. For the first time, we observe a baryon loading $B = 10^{-2}$ which coincides with the upper limit for the dynamical stability of the fireshell. The effective CircumBurst Medium (CBM) density shows a radial dependence $n_{cbm} \propto r^{-\alpha}$ with $1.0 \lesssim \alpha \lesssim 1.7$ and monotonically decreases from 1 to 10^{-6} particles/cm^3. This behavior is interpreted as being due to a fragmentation in the fireshell. Analogies with the fragmented density and filling factor characterizing Novae are outlined. The fit presented is particularly significant in view of the complete data set available for GRB060218 and of the fact that it fulfills the Amati relation.
Conclusions: We fit GRB060218, usually considered as an X-Ray Flash (XRF), as a "canonical GRB" within our theoretical model. The smallest possible black hole, formed by the gravitational collapse of a neutron star in a binary system, is consistent with the especially low energetics of the class of GRBs associated with SNe Ib/c. We provide the first evidence for a fragmentation in the fireshell. This fragmentation is crucial in explaining both the unusually large T_{90} and the consequently inferred abnormally low value of the CBM effective density.

10. M.G. Bernardini, C.L. Bianco, L. Caito, M.G. Dainotti, R. Guida, R. Ruffini; "GRB970228 and a class of GRBs with an initial spikelike emission"; Astronomy & Astrophysics, 474, L13 (2007).

Context: The discovery by *Swift* and HETE-2 of an afterglow emission associated possibly with short GRBs opened the new problematic of their nature and classification. This issue has been further enhanced by the observation of GRB060614 and by a new analysis of the BATSE catalog which led to the identification of a new class of GRBs with "an occasional softer extended emission lasting tenths of seconds after an initial spikelike emission".
Aims: We plan a twofold task: a) to fit this new class of "hybrid" sources within our "canonical GRB" scenario, where all GRBs are generated by a "common engine" (i.e. the gravitational collapse to a black hole); b) to propose GRB970228 as the prototype of the above mentioned class, since it shares the same morphology and observational features.
Methods: We analyze *Beppo*SAX data on GRB970228 within the "fireshell" model and we determine the parameters describing the source and the CircumBurst Medium (CBM) needed to reproduce its light curves in the 40–700 keV and 2–26 keV energy bands.
Results: We find that GRB970228 is a "canonical GRB", like e.g. GRB050315, with the main peculiarity of a particularly low average density of the CBM $\langle n_{cbm} \rangle \sim 10^{-3}$ particles/cm^3. We also simulate the light curve corresponding

to a rescaled CBM density profile with $\langle n_{cbm} \rangle = 1$ particle/cm^3. From such a comparison it follows that the total time-integrated luminosity is a faithful indicator of the nature of GRBs, contrary to the peak luminosity which is merely a function of the CBM density.
Conclusions: We call attention on discriminating the short GRBs between the "genuine" and the "fake" ones. The "genuine" ones are intrinsically short, with baryon loading $B \lesssim 10^{-5}$, as stated in our original classification. The "fake" ones, characterized by an initial spikelike emission followed by an extended emission lasting tenths of seconds, have a baryon loading $10^{-4} \lesssim B \leq 10^{-2}$. They are observed as such only due to an underdense CBM consistent with a galactic halo environment which deflates the afterglow intensity.

11. R. Guida, M.G. Bernardini, C.L. Bianco, L. Caito, M.G. Dainotti, R. Ruffini; "The Amati relation in the "fireshell" model"; Astronomy & Astrophysics, 487, L37 (2008).

Context: The cosmological origin of gamma-ray bursts (GRBs) has been firmly established, with redshifts up to $z = 6.29$. They are possible candidates for use as "distance indicators" for testing cosmological models in a redshift range hardly achievable by other cosmological probes. Asserting the validity of the empirical relations among GRB observables is now crucial for their calibration.
Aims: Motivated by the relation proposed by Amati and collaborators, we look within the "fireshell" model for a relation between the peak energy E_p of the νF_ν total time-integrated spectrum of the afterglow and the total energy of the afterglow E_{aft}, which in our model encompasses and extends the prompt emission.
Methods: The fit within the fireshell model, as for the "canonical" GRB050315, uses the complete arrival time coverage given by the Swift satellite. It is performed simultaneously, self-consistently, and recursively in the four BAT energy bands (15–25 keV, 25–50 keV, 50–100 keV, and 100-150 keV), as well as in the XRT one (0.2–10 keV). It uniquely determines the two free parameters characterizing the GRB source, the total energy $E_{tot}^{e^\pm}$ of the $e^\pm$ plasma and its baryon loading B, as well as the effective CircumBurst Medium (CBM) distribution. We can then build two sets of "gedanken" GRBs varying the total energy of the electron-positron plasma $E_{tot}^{e^\pm}$ and keeping the same baryon loading B of GRB050315. The first set assumes the one obtained in the fit of GRB050315 for the effective CBM density. The second set assumes instead a constant CBM density equal to the average value of the GRB050315 prompt phase.
Results: For the first set of "gedanken" GRBs we find a relation $E_p \propto (E_{aft})^a$, with $a = 0.45 \pm 0.01$, whose slope strictly agrees with the Amati one. Such a relation, in the limit $B \to 10^{-2}$, coincides with the Amati one. Instead, no correlation is found in the second set of "gedanken" GRBs.
Conclusions: Our analysis excludes the proper GRB (P-GRB) from the prompt emission, extends all the way to the latest afterglow phases, and is independent of the assumed cosmological model, since all "gedanken" GRBs are at

the same redshift. The Amati relation, on the other hand, includes the P-GRB, focuses only on the prompt emission, being therefore influenced by the instrumental threshold that fixes the end of the prompt emission, and depends on the assumed cosmology. This might explain the intrinsic scatter observed in the Amati relation.

12. L. Caito, M.G. Bernardini, C.L. Bianco, M.G. Dainotti, R. Guida, R. Ruffini; "GRB060614: a "fake" short GRB from a merging binary system"; Astronomy & Astrophysics, 489, 501 (2009).

Context: GRB060614 observations by VLT and by Swift have infringed the traditionally accepted gamma-ray burst (GRB) collapsar scenario that purports the origin of all long duration GRBs from supernovae (SN). GRB060614 is the first nearby long duration GRB clearly not associated with a bright Ib/c SN. Moreover, its duration ($T_{90} \sim 100$ s) makes it hardly classifiable as a short GRB. It presents strong similarities with GRB970228, the prototype of a new class of "fake" short GRBs that appear to originate from the coalescence of binary neutron stars or white dwarfs spiraled out into the galactic halo. *Aims*: Within the "canonical" GRB scenario based on the "fireshell" model, we test if GRB060614 can be a "fake" or "disguised" short GRB. We model the traditionally termed "prompt emission" and discriminate the signal originating from the gravitational collapse leading to the GRB from the process occurring in the circumburst medium (CBM). *Methods*: We fit GRB060614 light curves in Swift's BAT ($15-150$ keV) and XRT ($0.2-10$ keV) energy bands. Within the fireshell model, light curves are formed by two well defined and different components: the proper-GRB (P-GRB), emitted when the fireshell becomes transparent, and the extended afterglow, due to the interaction between the leftover accelerated baryonic and leptonic shell and the CBM. *Results*: We determine the two free parameters describing the GRB source within the fireshell model: the total $e^{\pm}$ plasma energy ($E_{tot}^{e^{\pm}} = 2.94 \times 10^{51}$erg) and baryon loading ($B = 2.8 \times 10^{-3}$). A small average CBM density $\sim 10^{-3}$ particles/cm^3 is inferred, typical of galactic halos. The first spikelike emission is identified with the P-GRB and the following prolonged emission with the extended afterglow peak. We obtain very good agreement in the BAT ($15-150$ keV) energy band, in what is traditionally called "prompt emission", and in the XRT ($0.2-10$ keV) one. *Conclusions*: The *anomalous* GRB060614 finds a natural interpretation within our canonical GRB scenario: it is a "disguised" short GRB. The total time-integrated extended afterglow luminosity is greater than the P-GRB one, but its peak luminosity is smaller since it is deflated by the peculiarly low average CBM density of galactic halos. This result points to an old binary system, likely formed by a white dwarf and a neutron star, as the progenitor of GRB060614 and well justifies the absence of an associated SN Ib/c. Particularly important for further studies of the final merging process are the temporal structures in the P-GRB down to 0.1 s.

13. M.G. Bernardini, C.L. Bianco, L. Caito, M.G. Dainotti, R. Guida, R. Ruffini; "GRB970228 in the "canonical GRB" scenario"; Journal of the Korean Physical Society, 56, 1575 (2010).

    Within the "fireshell" model, we define a "canonical GRB" light curve with two sharply different components: the proper-GRB (P-GRB), emitted when the optically thick fireshell of an electron-positron plasma originating from the phenomenon reaches transparency, and the afterglow, emitted due to the collision between the remaining optically thin fireshell and the circumburst medium (CBM). On the basis of the recent understanding of GRB970228 as the prototype for a new class of GRBs with "an occasional softer extended emission lasting tenths of seconds after an initial spikelike emission", we outline our "canonical GRB" scenario, originating from the gravitational collapse to a black hole, with special emphasis on the discrimination between "genuine" and "fake" short GRBs. Furthermore, we investigate how the GRB970228 analysis provides a theoretical explanation for the apparent absence of such a correlation for the GRBs belonging to this new class.

14. L. Caito, M.G. Bernardini, C.L. Bianco, M.G. Dainotti, R. Guida, R. Ruffini; "GRB060614: a preliminary result"; Journal of the Korean Physical Society, 56, 1579 (2010).

    The explosion of GRB 060614 produced a deep break in the GRB scenario and opened new horizons of investigation because it can't be traced back to any traditional scheme of classification. In fact, it manifests peculiarities both of long bursts and of short bursts, and above all, it is the first case of a long-duration near GRB without any bright Ib/c associated Supernova. We will show that, in our canonical GRB scenario, this "anomalous" situation finds a natural interpretation and allows us to discuss a possible variation in the traditional classification scheme, introducing a distinction between "genuine" and "fake" short bursts.

15. M.G. Dainotti, M.G. Bernardini, C.L. Bianco, L. Caito, R. Guida, R. Ruffini; "The astrophysical trypthic: GRB, SN and URCA can be extended to GRB060218?"; Journal of the Korean Physical Society, 56, 1588 (2010).

    The *Swift* satellite has given continuous data in the range 0.3–150 keV from 0 s to 10^6 s for GRB060218 associated with SN2006aj. This GRB is the fourth GRB spectroscopically associated with SNe after the cases of GRB980425-SN1998bw, GRB031203-SN2003lw, GRB 030329-SN2003dh. It has an unusually long duration ($T_{90} \sim 2100$ s). These data offer the opportunity to probe theoretical models for Gamma-Ray Bursts (GRBs) connected with Supernovae (SNe). We plan to fit the complete γ- and X-ray light curves of this long duration GRB, including the prompt emission, in order to clarify the nature of the progenitors and the astrophysical scenario of the class of GRBs associated to SNe Ib/c. We apply our "fireshell" model based on the formation of a black hole, giving

the relevant references. The initial total energy of the electron-positron plasma $E^{tot}_{e^\pm} = 2.32 \times 10^{50}$ erg has a particularly low value similarly to the other GRBs associated with SNe. For the first time we observe a baryon loading $B = 10^{-2}$ which coincides with the upper limit for the dynamical stability of the fireshell. The effective CircumBurst Medium (CBM) density shows a radial dependence $n_{cbm} \propto r^{-\alpha}$ with $1.0 \lesssim \alpha \lesssim 1.7$ and monotonically decreases from 1 to 10^{-6} particles/cm^3. Such a behavior is interpreted as due to a fragmentation in the fireshell. Such a fragmentation is crucial in explaining both the unusually large T_{90} and the consequently inferred abnormal low value of the CBM effective density. We fit GRB060218, usually considered as an X-Ray Flash (XRF), as a "canonical GRB" within our theoretical model. The smallest possible black hole, formed by the gravitational collapse of a neutron star in a binary system, is consistent with the especially low energetics of the class of GRBs associated with SNe Ib/c. We present the URCA process and the connection between the GRBs associated with SNe extended also to the case of GRB060218.

16. L. Izzo, M.G. Bernardini, C.L. Bianco, L. Caito, B. Patricelli, R. Ruffini; "GRB 090423 at Redshift 8.1: a Theoretical Interpretation"; Journal of the Korean Physical Society, 57, 551 (2010).

    GRB 090423 is the farthest gamma ray burst ever observed, with a redshift of about 8.1. We present within the fireshell scenario a complete analysis of this GRB. We model the prompt emission and the first rapid flux decay of the afterglow emission as being to the canonical emission of the interaction in the interval $0 \leq t \leq 440$ s by using accelerated baryonic matter with the circumburst medium. After the data reduction of the Swift data in the BAT (15 - 150 keV) and XRT (0.2 - 10 keV) energy bands, we interpret the light curves and the spectral distribution in the context of the fireshell scenario. We also confirm in this source the existence of a second component, a plateau phase, as being responsible for the late emission in the X-ray light curve. This extra component originates from the fact that the ejecta have a range of the bulk Lorentz Γ factor, which starts to interact each other ejecta at the start of the plateau phase.

17. L. Caito, L. Amati, M.G. Bernardini, C.L. Bianco, G. De Barros, L. Izzo, B. Patricelli, R. Ruffini; "GRB 071227: an additional case of a disguised short burst"; Astronomy & Astrophysics, 521, A80 (2010).

    Context: Observations of gamma-ray bursts (GRBs) have shown an hybridization between the two classes of long and short bursts. In the context of the fireshell model, the GRB light curves are formed by two different components: the *proper* GRB (P-GRB) and the extended afterglow. Their relative intensity is linked to the fireshell baryon loading B. The GRBs with P-GRB predominance are the short ones, the remainders are long. A new family of *disguised* short bursts has been identified: long bursts with a protracted low instantaneous luminosity due to a low density CircumBurst Medium (CBM). In the 15–150

keV energy band GRB 071227 exhibits a short duration (about 1.8s) spike-like emission followed by a very soft extended tail up to one hundred seconds after the trigger. It is a faint ($E_{iso} = 5.8 \times 10^{50}$) nearby GRB ($z = 0.383$) that does not have an associated type Ib/c bright supernova (SN). For these reasons, GRB 071227 has been classified as a short burst not fulfilling the Amati relation holding for long burst. *Aims:* We check the classification of GRB 071227 provided by the fireshell model. In particular, we test whether this burst is another example of a *disguised* short burst, after GRB 970228 and GRB 060614, and, for this reason, whether it fulfills the Amati relation. *Methods:* We simulate GRB 071227 light curves in the *Swift* BAT 15–50 keV bandpass and in the XRT (0.3–10 keV) energy band within the fireshell model. *Results:* We perform simulations of the tail in the 15–50 keV bandpass, as well as of the first part of the X-ray afterglow. This infers that: $E_{tot}^{e^{\pm}} = 5.04 \times 10^{51}$ erg, $B = 2.0 \times 10^{-4}$, $E_{P-GRB}/E_{aft} \sim 0.25$, and $\langle n_{cbm} \rangle = 3.33\,\mathrm{particles/cm^3}$. These values are consistent with those of "long duration" GRBs. We interpret the observed energy of the first hard emission by identifying it with the P-GRB emission. The remaining long soft tail indeed fulfills the Amati relation. *Conclusions:* Previously classified as a short burst, GRB 071227 on the basis of our analysis performed in the context of the fireshell scenario represents another example of a *disguised* short burst, after GRB 970228 and GRB 060614. Further confirmation of this result is that the soft tail of GRB 071227 fulfills the Amati relation.

18. M.G. Bernardini, C.L. Bianco, L. Caito, L. Izzo, B. Patricelli, R. Ruffini; "Analysis of GRB060607A within the fireshell model: prompt emission, X-ray flares and late afterglow phase"; Astronomy & Astrophysics, submitted to.

    Context: GRB060607A is a very distant ($z = 3.082$) and energetic event ($E_{iso} \sim 10^{53}$ erg). Its main peculiarity is that the peak of the near-infrared (NIR) afterglow has been observed with the REM robotic telescope. This NIR peak has been interpreted as the afterglow onset within the fireball forward shock model, and the initial Lorentz gamma factor of the emitting system has been inferred. *Aims*: We analyze GRB060607A within the fireshell model. We emphasize the central role of the prompt emission in determining the initial Lorentz gamma factor of the extended afterglow and we interpret the X-ray flares as produced by the interaction of the optically thin fireshell with overdense CircumBurst Medium (CBM) clumps. *Methods*: We deal only with the Swift BAT and XRT observations, that are the basic contribution to the GRB emission and that are neglected in the treatment adopted in the current literature. The numerical modeling of the fireshell dynamics allows to calculate all its characteristic quantities, in particular the exact value of the Lorentz gamma factor at the transparency. *Results*: We show that the theoretically computed prompt emission light curves are in good agreement with the observations in all the *Swift* BAT energy bands as well as the spectra integrated over different time intervals. The flares observed in the decaying phase of the X-ray afterglow are

also reproduced by the same mechanism, but in a region in which the typical dimensions of the clumps are smaller than the visible area of the fireshell and most energy lies in the X-ray band due to the hard-to-soft evolution. *Conclusions*: We show that it is possible to obtain flares with $\Delta t/t$ compatible with the observations when the three-dimensional structure of the CBM clumps is duly taken into account. We stop our analysis at the beginning of the X-ray plateau phase, since we suppose this originates from the instabilities developed in the collision between different subshells within a structured fireshell.

19. G. de Barros, M. G. Bernardini, C.L. Bianco, L. Caito, L. Izzo, B. Patricelli, R. Ruffini; "On the nature of GRB 050509b: a disguised short GRB"; Astronomy & Astrophyscs, 529, A130 (2011)

    Context: GRB 050509b, detected by the *Swift* satellite, is the first case where an X-ray afterglow has been observed associated with a short gamma-ray burst (GRB). Within the fireshell model, the canonical GRB light curve presents two different components: the proper-GRB (P-GRB) and the extended afterglow. Their relative intensity is a function of the fireshell baryon loading parameter B and of the CircumBurst Medium (CBM) density (n_{CBM}). In particular, the traditionally called short GRBs can be either "genuine" short GRBs (with $B \lesssim 10^{-5}$, where the P-GRB is energetically predominant) or "disguised" short GRBs (with $B \gtrsim 3.0 \times 10^{-4}$ and $n_{CBM} \ll 1$, where the extended afterglow is energetically predominant). *Aims*: We verify whether GRB 050509b can be classified as a "genuine" short or a "disguised" short GRB, in the fireshell model. *Methods*: We investigate two alternative scenarios. In the first, we start from the assumption that this GRB is a "genuine" short burst. In the second attempt, we assume that this GRB is a "disguised" burst. *Results*: If GRB 050509b were a genuine short GRB, there should initially be very hard emission which is ruled out by the observations. The analysis that assumes that this is a disguised short GRB is compatible with the observations. The theoretical model predicts a value of the extended afterglow energy peak that is consistent with the Amati relation. *Conclusions*: GRB 050509b cannot be classified as a "genuine" short GRB. The observational data are consistent with a "disguised" short GRB classification, i.e., a long burst with a weak extended afterglow "deflated" by the low density of the CBM. We expect that all short GRBs with measured redshifts are disguised short GRBs because of a selection effect: if there is enough energy in the afterglow to measure the redshift, then the proper GRB must be less energetic than the afterglow. The Amati relation is found to be fulfilled only by the extended afterglow excluding the P-GRB.

20. L. Caito, M.G. Bernardini, C.L. Bianco, L. Izzo, B. Patricelli, R. Ruffini; "GRB 071227: another disguised short burst"; International Journal of Modern Physics D, 20, 1931 (2011).

    Observations of Gamma-ray Bursts (GRBs) put forward in the recent years have revealed, with increasing evidence, that the historical classification be-

tween long and short bursts has to be revised. Within the Fireshell scenario, both short and long bursts are canonical bursts, consisting of two different phases. First, a Proper-GRB (P-GRB), that is the emission of photons at the transparency of the fireshell. Then, the Extended Afterglow, multiwavelength emission due to the interacion of the baryonic remnants of the fireshell with the CircumBurst Medium (CBM). We discriminate between long and short bursts by the amount of energy stored in the first phase with respect to the second one. Within the Fireshell scenario, we have introduced a third intermediate class: the disguised GRBs. They appear like short bursts, because their morphology is characterized by a first, short, hard episode and a following deflated tail, but this last part — coincident with the peak of the afterglow — is energetically predominant. The origin of this peculiar kind of sources is inferred to a very low average density of the environment (of the order of 10^{-3}). After GRB 970228 and GRB 060614, we find in GRB 071227 a third example of disguised burst.

21. L. Izzo, M.G. Bernardini, C.L. Bianco, L. Caito, B. Patricelli, L.J. Rangel Lemos, R. Ruffini; "GRB 080916C and the high-energy emission in the fireshell scenario"; International Journal of Modern Physics D, 20, 1949 (2011).

    In this paper we discuss a possible explanation for the high energy emission (up to $\sim$ GeV) seen in GRB 080916C. We propose that the GeV emission is originated by the collision between relativistic baryons in the fireshell after the transparency and the nucleons located in molecular clouds near the burst site. This collision should give rise pion production, whose immediate decay provides high energy photons, neutrinos and leptons. Using a public code (SYBILL) we simulate these relativistic collisions in their simple form, so that we can draw our preliminar results in this paper. We will present moreover our hypothesis that the delayed onset of this emission identifies in a complete way the P-GRB emission.

22. B. Patricelli, M.G. Bernardini, C.L. Bianco, L. Caito, L. Izzo, R. Ruffini, G. Vereshchagin; "A new spectral energy distribution of photons in the fireshell model of GRBs"; International Journal of Modern Physics D, 20, 1983 (2011).

    The analysis of various Gamma-Ray Bursts (GRBs) having a low energetics (an isotropic energy $E_{iso} \lesssim 10^{53}$ ergs) within the fireshell model has shown how the $N(E)$ spectrum of their prompt emission can be reproduced in a satisfactory way by a convolution of thermal spectra. Nevertheless, from the study of very energetic bursts ($E_{iso} \lesssim 10^{54}$ ergs) such as, for example, GRB 080319B, some discrepancies between the numerical simulations and the observational data have been observed. We investigate a different spectrum of photons in the comoving frame of the fireshell in order to better reproduce the spectral properties of GRB prompt emission within the fireshell model. We introduce

a phenomenologically modified thermal spectrum: a thermal spectrum characterized by a different asymptotic power-law index in the low energy region. Such an index depends on a free parameter α, so that the pure thermal spectrum corresponds to the case $\alpha = 0$. We test this spectrum by comparing the numerical simulations with the observed prompt emission spectra of various GRBs. From this analysis it has emerged that the observational data can be correctly reproduced by assuming a modified thermal spectrum with $\alpha = -1.8$.

23. A.V. Penacchioni, R. Ruffini, L. Izzo, M. Muccino, C.L. Bianco, L. Caito, B. Patricelli, L. Amati; "Evidence for a proto-black hole and a double astrophysical component in GRB 101023"; Astronomy & Astrophysics, 538, A58 (2012).

Context: It has been recently shown that GRB 090618, observed by AGILE, Coronas Photon, Fermi, Konus, Suzaku and Swift, is composed of two very different components: episode 1, lasting 50 s, shows a thermal plus power-law spectrum with a characteristic temperature evolving in time as a power law; episode 2 (the remaining 100 s) is a canonical long GRB. We have associated episode 1 to the progenitor of a collapsing bare core leading to the formation of a black hole: what was defined as a "proto black hole". *Aims*: In precise analogy with GRB 090618 we aim to analyze the 89s of the emission of GRB 101023, observed by Fermi, Gemini, Konus and Swift, to see if there are two different episodes: the first one presenting a characteristic black-body temperature evolving in time as a broken power law, and the second one consistent with a canonical GRB. *Methods*: To obtain information on the spectra, we analyzed the data provided by the GBM detector onboard the Fermi satellite, and we used the heasoft package XSPEC and RMFIT to obtain their spectral distribution. We also used the numerical code GRBsim to simulate the emission in the context of the fireshell scenario for episode 2. *Results*: We confirm that the first episode can be well fit by a black body plus power-law spectral model. The temperature changes with time following a broken power law, and the photon index of the power-law component presents a soft-to-hard evolution. We estimate that the radius of this source increases with time with a velocity of $1.5 \times 10^4 km/s$. The second episode appears to be a canonical GRB. By using the Amati and the Atteia relations, we determined the cosmological redshift, $z \sim 0.9 \pm 0.084(stat.) \pm 0.2(sys.)$. The results of GRB 090618 are compared and contrasted with the results of GRB 101023. Particularly striking is the scaling law of the soft X-ray component of the afterglow. *Conclusions*: We identify GRB 090618 and GRB 101023 with a new family of GRBs related to a single core collapse and presenting two astrophysical components: a first one related to the proto-black hole prior to the process of gravitational collapse (episode 1), and a second one, which is the canonical GRB (episode 2) emitted during the formation of the black hole. For the first time we are witnessing the process of a black hole formation from the instants preceding the gravitational collapse up to the GRB emission. This analysis indicates progress towards developing

a GRB distance indicator based on understanding the P-GRB and the prompt emission, as well as the soft X-ray behavior of the late afterglow.

24. R. Negreiros, R. Ruffini, C. L. Bianco, J. A. Rueda; "Cooling of young neutron stars in GRB associated to supernovae"; Astronomy & Astrophysics, 540, A12 (2012).

    Context: The traditional study of neutron star cooling has been generally applied to quite old objects such as the Crab Pulsar (957 years) or the central compact object in Cassiopeia A (330 years) with an observed surface temperature $\sim 10^6$ K. However, recent observations of the late ($t = 10^8$–10^9 s) emission of the supernovae (SNe) associated to GRBs (GRB-SN) show a distinctive emission in the X-ray regime consistent with temperatures $\sim 10^7$–10^8 K. Similar features have been also observed in two Type Ic SNe SN 2002ap and SN 1994I that are not associated to GRBs. *Aims*: We advance the possibility that the late X-ray emission observed in GRB-SN and in isolated SN is associated to a hot neutron star just formed in the SN event, here defined as a neo-neutron star. *Methods*: We discuss the thermal evolution of neo-neutron stars in the age regime that spans from ~ 1 minute (just after the proto-neutron star phase) all the way up to ages < 10–100 yr. We examine critically the key factor governing the neo-neutron star cooling with special emphasis on the neutrino emission. We introduce a phenomenological heating source, as well as new boundary conditions, in order to mimic the high temperature of the atmosphere for young neutron stars. In this way we match the neo-neutron star luminosity to the observed late X-ray emission of the GRB-SN events: URCA-1 in GRB980425-SN1998bw, URCA-2 in GRB030329-SN2003dh, and URCA-3 in GRB031203-SN2003lw. *Results*: We identify the major role played by the neutrino emissivity in the thermal evolution of neo-neutron stars. By calibrating our additional heating source at early times to $\sim 10^{12}$–10^{15} erg/g/s, we find a striking agreement of the luminosity obtained from the cooling of a neo-neutron stars with the prolonged ($t = 10^8$–10^9 s) X-ray emission observed in GRB associated with SN. It is therefore appropriate a revision of the boundary conditions usually used in the thermal cooling theory of neutron stars, to match the proper conditions of the atmosphere at young ages. The traditional thermal processes taking place in the crust might be enhanced by the extreme high-temperature conditions of a neo-neutron star. Additional heating processes that are still not studied within this context, such as e^+e^- pair creation by overcritical fields, nuclear fusion, and fission energy release, might also take place under such conditions and deserve further analysis. *Conclusions*: Observation of GRB-SN has shown the possibility of witnessing the thermal evolution of neo-neutron stars. A new campaign of dedicated observations is recommended both of GRB-SN and of isolated Type Ic SN.

25. L. Izzo, R. Ruffini, A.V. Penacchioni, C.L. Bianco, L. Caito, S.K. Chakrabarti, J.A. Rueda, A. Nandi, B. Patricelli; "A double component in GRB 090618:

a proto-black hole and a genuinely long gamma-ray burst"; Astronomy & Astrophysics, 543, A10 (2012).

Context: The joint X-ray and gamma-ray observations of GRB 090618 by very many satellites offer an unprecedented possibility of testing crucial aspects of theoretical models. In particular, they allow us to test (a) in the process of gravitational collapse, the formation of an optically thick e+e.-baryon plasma self-accelerating to Lorentz factors in the range $200 < \Gamma < 3000$; (b) its transparency condition with the emission of a component of 10^{53-54} baryons in the TeV region and (c) the collision of these baryons with the circumburst medium (CBM) clouds, characterized by dimensions of 10^{15-16} cm. In addition, these observations offer the possibility of testing a new understanding of the thermal and power-law components in the early phase of this GRB. *Aims*: We test the fireshell model of GRBs in one of the closest ($z = 0.54$) and most energetic ($E_{iso} = 2.90 \times 10^{53}$ erg) GRBs, namely GRB 090618. It was observed at ideal conditions by several satellites, namely *Fermi*, *Swift*, Konus-WIND, AGILE, RT-2, and Suzaku, as well as from on-ground optical observatories. *Methods*: We analyzed the emission from GRB 090618 using several spectral models, with special attention to the thermal and power-law components. We determined the fundamental parameters of a canonical GRB within the context of the fireshell model, including the identification of the total energy of the e^+e^- plasma, $E_{tot}^{e^+e^-}$, the proper GRB (P-GRB), the baryon load, the density and structure of the CBM. *Results*: We find evidence of the existence of two different episodes in GRB 090618. The first episode lasts 50 s and is characterized by a spectrum consisting of a thermal component, which evolves between $kT = 54$ keV and $kT = 12$ keV, and a power law with an average index $\gamma = 1.75 \pm 0.04$. The second episode, which lasts for ~ 100 s, behaves as a canonical long GRB with a Lorentz gamma factor at transparency of $\Gamma = 495$, a temperature at transparency of 29.22 keV and with a characteristic size of the surrounding clouds of $R_{cl} \sim 10^{15-16}$ cm and masses of $\sim 10^{22-24}$ g. *Conclusions*: We support the recently proposed two-component nature of GRB 090618, namely, episode 1 and episode 2, with a specific theoretical analysis.We furthermore illustrate that episode 1 cannot be considered to be either a GRB or a part of a GRB event, but it appears to be related to the progenitor of the collapsing bare core, leading to the formation of the black hole, which we call a "proto-black hole". Thus, for the first time, we are witnessing the process of formation of a black hole from the phases just preceding the gravitational collapse all the way up to the GRB emission.

26. B. Patricelli, M.G. Bernardini, C.L. Bianco, L. Caito, G. De Barros, L. Izzo, R. Ruffini, G.V. Vereshchagin; "Analysis of GRB 080319B and GRB 050904 within the Fireshell Model: Evidence for a Broader Spectral Energy Distribution"; The Astrophysical Journal, 756, 16 (2012).

The observation of GRB 080319B, with an isotropic energy $E_{iso} = 1.32 \times 10^{54}$

erg, and GRB 050904, with $E_{iso} = 1.04 \times 10^{54}$ erg, offers the possibility of studying the spectral properties of the prompt radiation of two of the most energetic Gamma Ray Bursts (GRBs). This allows us to probe the validity of the fireshell model for GRBs beyond 10^{54} erg, well outside the energy range where it has been successfully tested up to now (10^{49}–10^{53} erg). We find that in the low energy region, the prompt emission spectra observed by *Swift* BAT reveals more power than theoretically predicted. The opportunities offered by these observations to improve the fireshell model are outlined in this paper. One of the distinguishing features of the fireshell model is that it relates the observed GRB spectra to the spectrum in the comoving frame of the fireshell. Originally, a fully radiative condition and a comoving thermal spectrum were adopted. An additional power-law in the comoving thermal spectrum is required due to the discrepancy of the theoretical and observed light curves and spectra in the fireshell model for GRBs 080319B and 050904. A new phenomenological parameter α is correspondingly introduced in the model. We perform numerical simulations of the prompt emission in the *Swift* BAT bandpass by assuming different values of α within the fireshell model. We compare them with the GRB 080319B and GRB 050904 observed time-resolved spectra, as well as with their time-integrated spectra and light curves. Although GRB 080319B and GRB 050904 are at very different redshifts (z=0.937 and z=6.29 respectively), a value of $\alpha = -1.8$ leads for both of them to a good agreement between the numerical simulations and the observed BAT light curves, time-resolved and time-integrated spectra. Such a modified spectrum is also consistent with the observations of previously analyzed less energetic GRBs and reasons for this additional agreement are given. Perspectives for future low energy missions are outlined.

27. M. Muccino, R. Ruffini, C.L. Bianco, L. Izzo, A.V. Penacchioni; "GRB 090227B: The missing link between the genuine short and long GRBs"; The Astrophysical Journal, 763, 125 (2013).

    The time-resolved spectral analysis of GRB 090227B, made possible by the *Fermi*-GBM data, allows to identify in this source the missing link between the genuine short and long GRBs. Within the Fireshell model of the Gamma-Ray Bursts (GRBs) we predict genuine short GRBs: bursts with the same inner engine of the long bursts but endowed with a severely low value of the Baryon load, $B \lesssim 5 \times 10^{-5}$. A first energetically predominant emission occurs at the transparency of the e^+e^- plasma, the Proper-GRB (P-GRB), followed by a softer emission, the extended afterglow. The typical separation between the two emissions is expected to be of the order of 10^{-3} – 10^{-2} s. We identify the P-GRB of GRB 090227B in the first 96 ms of emission, where a thermal component with the temperature $kT = (517 \pm 28)$ keV and a flux comparable with the non thermal part of the spectrum is observed. This non thermal component as well as the subsequent emission, where there is no evidence for a thermal spectrum, is identified with the extended afterglow. We deduce a the-

oretical cosmological redshift $z = 1.61 \pm 0.14$. We then derive the total energy $E^{tot}_{e^+e^-} = (2.83 \pm 0.15) \times 10^{53}$ ergs, the Baryon load $B = (4.13 \pm 0.05) \times 10^{-5}$, the Lorentz Γ factor at transparency $\Gamma_{tr} = (1.44 \pm 0.01) \times 10^4$, and the intrinsic duration $\Delta t' \sim 0.35$ s. We also determine the average density of the CircumBurst Medium (CBM), $\langle n_{CBM} \rangle = (1.90 \pm 0.20) \times 10^{-5}$ particles/cm^3. There is no evidence of beaming in the system. In view of the energetics and of the Baryon load of the source, as well as of the low interstellar medium and of the intrinsic time scale of the signal, we identify the GRB progenitor as a binary neutron star. From the recent progress in the theory of neutron stars, we obtain masses of the stars $m_1 = m_2 = 1.34 M_\odot$ and their corresponding radii $R_1 = R_2 = 12.24$ km and thickness of their crusts ~ 0.47 km, consistent with the above values of the Baryon load, of the energetics and of the time duration of the event.

28. A.V. Penacchioni, R. Ruffini, C.L. Bianco, L. Izzo, M. Muccino, G.B. Pisani, J.A. Rueda; "GRB 110709B in the induced gravitational collapse paradigm"; Astronomy & Astrophysics, 551, A133 (2013).

Context: GRB 110709B is the first source for which *Swift* BAT triggered twice, with a time separation of ~ 10 minutes. The first emission (called here Episode 1) goes from 40 s before the first trigger up to 60 s after it. The second emission (hereafter Episode 2) goes from 35 s before the second trigger to 100 s after it. These features reproduce the ones of GRB 090618, which has been recently interpreted within the Induced Gravitational Collapse paradigm (IGC). In line with this paradigm we assume the progenitor to be a close binary system composed of a core of an evolved star and a Neutron Star (NS). The evolved star explodes as a Supernova (SN) and ejects material that is partially accreted by the NS. We identify this process with Episode 1. The accretion process brings the NS over its critical mass, thus gravitationally collapsing to a BH. This process leads to the GRB emission, Episode 2. The double trigger has given for the first time the possibility to have a coverage of the X-ray emission observed by XRT both prior to and during the prompt phase of GRB 110709B. *Aims*: We analyze the spectra and time variability of Episode 1 and 2 and compute the relevant parameters of the binary progenitor, as well as the astrophysical parameters both in the SN and the GRB phase in the IGC paradigm. *Methods*: We perform a time-resolved spectral analysis of Episode 1 by fitting the spectrum with a blackbody (BB) plus a power-law (PL) spectral model. From the BB fluxes and temperatures of Episode 1 and the luminosity distance d_L, we evaluate the evolution with time of the radius of the BB emitter, associated here to the evolution of the SN ejecta. We analyze Episode 2 within the Fireshell model, identifying the Proper-GRB (P-GRB) and simulating the light curve and spectrum. We establish the redshift to be $z = 0.75$, following the phenomenological methods by Amati, by Yonetoku and by Grupe, and our analysis of the late X-ray afterglow. It is most remarkable that the determination of the cosmological redshift on the ground of the scaling of the late X-ray afterglow, already verified in GRB 090618 and GRB 101023, is again verified

by this analysis. *Results*: We find for Episode 1 a temperature of the BB component that evolves with time following a broken PL, with the slope of the PL at early times $\alpha = 0$ (constant function) and the slope of the PL at late times $\beta = -4 \pm 2$. The break occurs at $t = 41.21$ s. The total energy of Episode 1 is $E_{iso}^{(1)} = 1.42 \times 10^{53}$ erg. The total energy of Episode 2 is $E_{iso}^{(2)} = 2.43 \times 10^{52}$ erg. We find at transparency a Lorentz factor $\Gamma \sim 1.73 \times 10^2$, laboratory radius of 6.04×10^{13} cm, P-GRB observed temperature $kT_{P-GRB} = 12.36$ keV, baryon load $B = 5.7 \times 10^{-3}$ and P-GRB energy of $E_{P-GRB} = 3.44 \times 10^{50}$ erg. We find a remarkable coincidence of the cosmological redshift by the scaling of the XRT data and with three other phenomenological methods. *Conclusions*: We interpret GRB 110709B as a member of the IGC sources, together with GRB 970828, GRB 090618 and GRB 101023. The existence of the XRT data during the prompt phase of the emission of GRB 110709B (Episode 2) offers an unprecedented tool for improving the diagnostic of GRBs emission.

29. G.B. Pisani, L. Izzo, R. Ruffini, C.L. Bianco, M. Muccino, A.V. Penacchioni, J.A. Rueda, Y. Wang; "Novel distance indicator for gamma-ray bursts associated with supernovae"; Astronomy & Astrophysics, 552, L5 (2013).

    Context: In recent years it has been proposed that the temporal coincidence of a Gamma Ray Burst (GRB) and a type Ib/c supernova (SN) can be explained by the concept of Induced Gravitational Collapse (IGC) of a Neutron Star (NS) to a Black Hole (BH) by accretion of matter ejected by a SN Ib/c. This scenario reveals a possible common behavior in the late time X-ray emission of this subclass of GRBs. *Aims*: We want to test if such a common behavior can actually be present in the sources belonging to this GRB sub-class and if this may lead to a redshift estimator for these sources. *Methods*: We build a sample of GRBs belonging to this sub-class, and we rescale the X-ray light curves of all of them both in time and in flux to a common cosmological redshift. *Results*: We found that the X-ray light curves of all the GRBs of the sample with a measured redshift present a common late time behavior when rescaled to a common redshift $z = 1$. We then use this result to estimate the redshift of the GRBs of the sample with no measured redshift. *Conclusions*: The common behavior in the late decay of the X-ray light curves of the GRBs of the sample points to a common physical mechanism in this particular phase of the GRB emission, possibly related to the SN process. This scenario may represent an invaluable tool to estimate the redshift of GRBs belonging to this sub-class of events. More GRBs are therefore needed in order to enlarge the subclass and to make more stringent constraints on the redshift estimates performed with this method for GRBs pertaining to this class.

30. C.L. Bianco, M. G. Bernardini, L. Caito, G. De Barros, L. Izzo, M. Muccino, B. Patricelli, A.V. Penacchioni, G.B. Pisani, R. Ruffini; "The canonical GRB scenario"; Il Nuovo Cimento C, 36 s01, 21 (2013).

The canonical GRB scenario implied by the fireshell model is briefly summarized.

31. A.V. Penacchioni, R. Ruffini, L. Izzo, M. Muccino, C.L. Bianco, L. Caito, B. Patricelli; "Evidences for a double component in the emission of GRB 101023"; Il Nuovo Cimento C, 36 s01, 117 (2013).

    In this work we present the results of the analysis of GRB 101023 in the fireshell scenario. Its redshift is not known, so we attempted to infer it from the Amati Relation, obtaining $z = 0.9$. Its light curve presents a double emission, which makes it very similar to the already studied GRB 090618. We called each part Episode 1 and Episode 2. We performed a time-resolved spectral analysis with RMFIT using different spectral models, and fitted the light curve with a numerical code integrating the fireshell equations of motion. We used Fermi GBM data to build the light curve, in particular the second NaI detector, in the range (8.5–1000 keV). We considered different hypotheses regarding which part of the light curve could be the GRB and performed the analysis of all of them. We noticed a great variation of the temperature with time in the first episode, as well as almost no variation of the progenitor radius. We found that the first emission does not match the requirements for a GRB, while the second part perfectly agrees with being a canonical GRB, with a P-GRB lasting 4 s.

32. M. Muccino, R. Ruffini, C.L. Bianco, L. Izzo, A.V. Penacchioni, G.B. Pisani; "GRB 090510: A Disguised Short Gamma-Ray Burst with the Highest Lorentz Factor and Circumburst Medium"; The Astrophysical Journal, 772, 62 (2013).

    GRB 090510, observed both by Fermi and AGILE satellites, is the first bright short-hard Gamma-Ray Burst (GRB) with an emission from the keV up to the GeV energy range. Within the Fireshell model, we interpret the faint precursor in the light curve as the emission at the transparency of the expanding e^+e^- plasma: the Proper-GRB (P-GRB). From the observed isotropic energy we assume a total plasma energy $E^{tot}_{e^+e^-} = (1.10 \pm 0.06) \times 10^{53}$erg and derive a Baryon load $B = (1.45 \pm 0.28) \times 10^{-3}$ and a Lorentz factor at transparency $\Gamma_{tr} = (6.7 \pm 1.6) \times 10^2$. The main emission $\sim$ 0.4s after the initial spike is interpreted as the extended afterglow, due to the interaction of the ultrarelativistic baryons with the CircumBurst Medium (CBM). Using the condition of fully radiative regime, we infer a CBM average spherically symmetric density of $\langle n_{CBM} \rangle = (1.85 \pm 0.14) \times 10^3$ particles/cm^3, one of the highest found in the Fireshell model. The value of the filling factor, $1.5 \times 10^{-10} \leq \mathcal{R} \leq 3.8 \times 10^{-8}$, leads to the estimate of filaments with densities $n_{fil} = n_{CBM}/\mathcal{R} \approx (10^6 - 10^{14})$ particles/cm^3. The sub-MeV and the MeV emissions are well reproduced. When compared to the canonical GRBs with $\langle n_{CBM} \rangle \approx 1$ particles/cm^3 and to the disguised short GRBs with $\langle n_{CBM} \rangle \approx 10^{-3}$ particles/cm^3, the case of GRB 090510 leads to the existence of a new family of bursts exploding in an

over-dense galactic region with $\langle n_{CBM} \rangle \approx 10^3$ particles/cm^3. The joint effect of the high Γ_{tr} and the high density compresses in time and "inflates" in intensity the extended afterglow, making it appear as a short burst, which we here define as "disguised short GRB by excess". The determination of the above parameters values may represent an important step towards the explanation of the GeV emission.

5.2. Conference proceedings

1. R. Ruffini, M.G. Bernardini, C.L. Bianco, P. Chardonnet, F. Fraschetti, V. Gurzadyan, L. Vitagliano, S.-S. Xue; "The Blackholic energy: long and short Gamma-Ray Bursts (New perspectives in physics and astrophysics from the theoretical understanding of Gamma-Ray Bursts, II)"; in Proceedings of the XIth Brazilian School on Cosmology and Gravitation, Mangaratiba, Rio de Janeiro (Brazil), July August 2004, M. Novello, S.E. Perez Bergliaffa, Editors; AIP Conference Proceedings, 782, 42 (2005).

   We outline the confluence of three novel theoretical fields in our modeling of Gamma-Ray Bursts (GRBs): 1) the ultrarelativistic regime of a shock front expanding with a Lorentz gamma factor $\sim$ 300; 2) the quantum vacuum polarization process leading to an electron-positron plasma originating the shock front; and 3) the general relativistic process of energy extraction from a black hole originating the vacuum polarization process. There are two different classes of GRBs: the long GRBs and the short GRBs. We here address the issue of the long GRBs. The theoretical understanding of the long GRBs has led to the detailed description of their luminosities in fixed energy bands, of their spectral features and made also possible to probe the astrophysical scenario in which they originate. We are specially interested, in this report, to a subclass of long GRBs which appear to be accompanied by a supernova explosion. We are considering two specific examples: GRB980425/SN1998bw and GRB030329/SN2003dh. While these supernovae appear to have a standard energetics of 10^{49} ergs, the GRBs are highly variable and can have energetics 10^4 – 10^5 times larger than the ones of the supernovae. Moreover, many long GRBs occurs without the presence of a supernova. It is concluded that in no way a GRB can originate from a supernova. The precise theoretical understanding of the GRB luminosity we present evidence, in both these systems, the existence of an independent component in the X-ray emission, usually interpreted in the current literature as part of the GRB afterglow. This component has been observed by Chandra and XMM to have a strong decay on scale of months. We have named here these two sources respectively URCA-1 and URCA-2, in honor of the work that George Gamow and Mario Shoenberg did in 1939 in this town of Urca identifying the basic mechanism, the Urca processes, leading to the process of gravitational collapse and the formation of

a neutron star and a supernova. The further hypothesis is considered to relate this X-ray source to a neutron star, newly born in the Supernova. This hypothesis should be submitted to further theoretical and observational investigation. Some theoretical developments to clarify the astrophysical origin of this new scenario are outlined. We turn then to the theoretical developments in the short GRBs: we first report some progress in the understanding the dynamical phase of collapse, the mass-energy formula and the extraction of blackholic energy which have been motivated by the analysis of the short GRBs. In this context progress has also been accomplished on establishing an absolute lower limit to the irreducible mass of the black hole as well as on some critical considerations about the relations of general relativity and the second law of thermodynamics. We recall how this last issue has been one of the most debated in theoretical physics in the past thirty years due to the work of Bekenstein and Hawking. Following these conceptual progresses we analyze the vacuum polarization process around an overcritical collapsing shell. We evidence the existence of a separatrix and a dyadosphere trapping surface in the dynamics of the electron-positron plasma generated during the process of gravitational collapse. We then analyze, using recent progress in the solution of the Vlasov-Boltzmann-Maxwell system, the oscillation regime in the created electron-positron plasma and their rapid convergence to a thermalized spectrum. We conclude by making precise predictions for the spectra, the energy fluxes and characteristic time-scales of the radiation for short-bursts. If the precise luminosity variation and spectral hardening of the radiation we have predicted will be confirmed by observations of short-bursts, these systems will play a major role as standard candles in cosmology. These considerations will also be relevant for the analysis of the long-bursts when the baryonic matter contribution will be taken into account.

2. R. Ruffini, M.G. Bernardini, C.L. Bianco, P. Chardonnet, F. Fraschetti, V. Gurzadyan, L. Vitagliano, S.-S. Xue; "Black hole physics and astrophysics: The GRB-Supernova connection and URCA-1 URCA-2"; in Proceedings of the Tenth Marcel Grossmann Meeting on General Relativity, Rio de Janeiro, Brazil, July 2003, M. Novello, S.E. Perez-Bergliaffa, Editors; p. 369; World Scientific, (Singapore, 2006).

   We outline the confluence of three novel theoretical fields in our modeling of Gamma-Ray Bursts (GRBs): 1) the ultrarelativistic regime of a shock front expanding with a Lorentz gamma factor ~ 300; 2) the quantum vacuum polarization process leading to an electron-positron plasma originating the shock front; and 3) the general relativistic process of energy extraction from a black hole originating the vacuum polarization process. There are two different classes of GRBs: the long GRBs and the short GRBs. We here address the issue of the long GRBs. The theoretical understanding of the long GRBs has led to the detailed description of their luminosities in fixed energy bands, of their spectral features and made also possible to probe the astrophysical sce-

nario in which they originate. We are specially interested, in this report, to a subclass of long GRBs which appear to be accompanied by a supernova explosion. We are considering two specific examples: GRB980425/SN1998bw and GRB030329/SN2003dh. While these supernovae appear to have a standard energetics of 10^{49} ergs, the GRBs are highly variable and can have energetics 10^4 – 10^5 times larger than the ones of the supernovae. Moreover, many long GRBs occurs without the presence of a supernova. It is concluded that in no way a GRB can originate from a supernova. The precise theoretical understanding of the GRB luminosity we present evidence, in both these systems, the existence of an independent component in the X-ray emission, usually interpreted in the current literature as part of the GRB afterglow. This component has been observed by Chandra and XMM to have a strong decay on scale of months. We have named here these two sources respectively URCA-1 and URCA-2, in honor of the work that George Gamow and Mario Shoenberg did in 1939 in this town of Urca identifying the basic mechanism, the Urca processes, leading to the process of gravitational collapse and the formation of a neutron star and a supernova. The further hypothesis is considered to relate this X-ray source to a neutron star, newly born in the Supernova. This hypothesis should be submitted to further theoretical and observational investigation. Some theoretical developments to clarify the astrophysical origin of this new scenario are outlined.

3. M.G. Bernardini, C.L. Bianco, P. Chardonnet, F. Fraschetti, R. Ruffini, S.-S. Xue; "General features of GRB 030329 in the EMBH model"; in Proceedings of the Tenth Marcel Grossmann Meeting on General Relativity, Rio de Janeiro, Brazil, July 2003, M. Novello, S.E. Perez-Bergliaffa, Editors; p. 2459; World Scientific, (Singapore, 2006).

   GRB 030329 is considered within the EMBH model. We determine the three free parameters and deduce its luminosity in given energy bands comparing it with the observations. The observed substructures are compared with the predictions of the model: by applying the result that substructures observed in the extended afterglow peak emission (E-APE) do indeed originate in the collision of the accelerated baryonic matter (ABM) pulse with the inhomogeneities in the interstellar medium around the black-hole, masks of density inhomogeneities are considered in order to reproduce the observed temporal substructures. The induced supernova concept is applied to this system and the general consequences that we are witnessing are the formation of a cosmological thriptych of a black hole originating the GRB 030329, the supernova SN2003dh and a young neutron star. Analogies to the system GRB 980425–SN1998bw are outlined.

4. R. Ruffini, M.G. Bernardini, C.L. Bianco, P. Chardonnet, A. Corsi, F. Fraschetti, S.-S. Xue; "GRB 970228 and its associated Supernova in the EMBH model"; in Proceedings of the Tenth Marcel Grossmann Meeting

on General Relativity, Rio de Janeiro, Brazil, July 2003, M. Novello, S.E. Perez-Bergliaffa, Editors; p. 2465; World Scientific, (Singapore, 2006).

The γ-ray burst of 1997 February 28 is analyzed within the Electromagnetic Black Hole model. We first estimate the value of the total energy deposited in the dyadosphere, E_{dya}, and the amount of baryonic matter left over by the EMBH progenitor star, $B = M_B c^2 / E_{dya}$. We then consider the role of the interstellar medium number density n_{ISM} and of the ratio R between the effective emitting area and the total surface area of the γ-ray burst source, in reproducing the prompt emission and the X-ray afterglow of this burst. Some considerations are also done concerning the possibility of explaining, within the theory, the observed evidence for a supernova in the optical afterglow.

5. F. Fraschetti, M.G. Bernardini, C.L. Bianco, P. Chardonnet, R. Ruffini, S.-S. Xue; "Inferences on the ISM structure around GRB980425 and GRB980425-SN1998bw association in the EMBH Model"; in Proceedings of the Tenth Marcel Grossmann Meeting on General Relativity, Rio de Janeiro, Brazil, July 2003, M. Novello, S.E. Perez-Bergliaffa, Editors; p. 2451; World Scientific, (Singapore, 2006).

   We determine the four free parameters within the EMBH model for GRB 980425 and deduce its luminosity in given energy bands, its spectra and its time variability in the prompt radiation. We compute the basic kinematical parameters of GRB 980425. In the extended afterglow peak emission the Lorentz γ factor is lower than the critical value 150 which has been found in Ruffini et al. (2002) to be necessary in order to perform the tomography of the ISM surrounding the GRB as suggested by Dermer & Mitman (1999). The detailed structure of the density inhomogeneities as well as the effects of radial apparent superluminal effects are evaluated within the EMBH model. Under the assumption that the energy distribution of emitted radiation is thermal in the comoving frame, time integrated spectra of EMBH model for prompt emission are computed. The induced supernova concept is applied to this system and general consequences on the astrophysical and cosmological scenario are derived.

6. R. Ruffini, M.G. Bernardini, C.L. Bianco, P. Chardonnet, F. Fraschetti, R. Guida, S.-S. Xue; "GRB 050315: A step in the proof of the uniqueness of the overall GRB structure"; in "GAMMA-RAY BURSTS IN THE SWIFT ERA: Sixteenth Maryland Astrophysics Conference", Washington, DC, USA, November 29th December 2nd 2005, Stephen S. Holt, Neil Gehrels, John A. Nousek, Editors; AIP Conference Proceedings, 836, 103 (2006).

   Using the Swift data of GRB 050315, we progress in proving the uniqueness of our theoretically predicted Gamma-Ray Burst (GRB) structure as composed by a proper-GRB, emitted at the transparency of an electron-positron plasma with suitable baryon loading, and an afterglow comprising the "prompt radiation" as due to external shocks. Detailed light curves for selected energy bands

are theoretically fitted in the entire temporal region of the Swift observations ranging over 10^6 seconds.

7. R. Ruffini, M.G. Bernardini, C.L. Bianco, P. Chardonnet, F. Fraschetti, S.-S. Xue; "Theoretical Interpretation of GRB 031203 and URCA-3"; in "Relativistic Astrophysics and Cosmology - Einsteins Legacy", B. Aschenbach, V. Burwitz, G. Hasinger, B. Leibundgut, Editors; Springer-Verlag (2007).

8. R. Ruffini, M.G. Bernardini, C.L. Bianco, L. Caito, P. Chardonnet, M.G. Dainotti, F. Fraschetti, R. Guida, M. Rotondo, G. Vereshchagin, L. Vita-gliano, S.-S. Xue; "The Blackholic energy and the canonical Gamma-Ray Burst"; in Proceedings of the XIIth Brazilian School on Cosmology and Gravitation, Mangaratiba, Rio de Janeiro (Brazil), September 2006, M. Novello, S.E. Perez Bergliaffa, Editors; AIP Conference Proceedings, 910, 55 (2007).

   Gamma-Ray Bursts (GRBs) represent very likely "the" most extensive computational, theoretical and observational effort ever carried out successfully in physics and astrophysics. The extensive campaign of observation from space based X-ray and γ-ray observatory, such as the *Vela*, CGRO, BeppoSAX, HETE-II, INTEGRAL, *Swift*, R-XTE, *Chandra*, XMM satellites, have been matched by complementary observations in the radio wavelength (e.g. by the VLA) and in the optical band (e.g. by VLT, Keck, ROSAT). The net result is unprecedented accuracy in the received data allowing the determination of the energetics, the time variability and the spectral properties of these GRB sources. The very fortunate situation occurs that these data can be confronted with a mature theoretical development. Theoretical interpretation of the above data allows progress in three different frontiers of knowledge: **a)** the ultrarelativistic regimes of a macroscopic source moving at Lorentz gamma factors up to ~ 400; **b)** the occurrence of vacuum polarization process verifying some of the yet untested regimes of ultrarelativistic quantum field theories; and **c)** the first evidence for extracting, during the process of gravitational collapse leading to the formation of a black hole, amounts of energies up to 10^{55} ergs of blackholic energy — a new form of energy in physics and astrophysics. We outline how this progress leads to the confirmation of three interpretation paradigms for GRBs proposed in July 2001. Thanks mainly to the observations by *Swift* and the optical observations by VLT, the outcome of this analysis points to the existence of a "canonical" GRB, originating from a variety of different initial astrophysical scenarios. The communality of these GRBs appears to be that they all are emitted in the process of formation of a black hole with a negligible value of its angular momentum. The following sequence of events appears to be canonical: the vacuum polarization process in the dyadosphere with the creation of the optically thick self accelerating electron-positron plasma; the engulfment of baryonic mass during the plasma expansion; adiabatic expan-

sion of the optically thick "fireshell" of electron-positron-baryon plasma up to the transparency; the interaction of the accelerated baryonic matter with the interstellar medium (ISM). This leads to the canonical GRB composed of a proper GRB (P-GRB), emitted at the moment of transparency, followed by an extended afterglow. The sole parameters in this scenario are the total energy of the dyadosphere E_{dya}, the fireshell baryon loading M_B defined by the dimensionless parameter $B \equiv M_B c^2 / E_{dya}$, and the ISM filamentary distribution around the source. In the limit $B \to 0$ the total energy is radiated in the P-GRB with a vanishing contribution in the afterglow. In this limit, the canonical GRBs explain as well the short GRBs. In these lecture notes we systematically outline the main results of our model comparing and contrasting them with the ones in the current literature. In both cases, we have limited ourselves to review already published results in refereed publications. We emphasize as well the role of GRBs in testing yet unexplored grounds in the foundations of general relativity and relativistic field theories.

9. R. Ruffini, M.G. Bernardini, C.L. Bianco, L. Caito, P. Chardonnet, M.G. Dainotti, F. Fraschetti, R. Guida, G. Vereshchagin, S.-S. Xue; "The role of GRB 031203 in clarifying the astrophysical GRB scenario"; in Proceedings of the 6^{th} Integral Workshop - The Obscured Universe, Moscow, (Russia), July 2006, S. Grebenev, R. Sunyaev, C. Winkler, A. Parmar, L. Ouwehand, Editors; ESA Special Publication, SP-622, 561 (2007).

   The luminosity and the spectral distribution of the afterglow of GRB 031203 have been presented within our theoretical framework, which envisages the GRB structure as composed by a proper-GRB, emitted at the transparency of an electron-positron plasma with suitable baryon loading, and an afterglow comprising the "prompt emission" as due to external shocks. In addition to the GRB emission, there appears to be a prolonged soft X-Ray emission lasting for 10^6–10^7 seconds followed by an exponential decay. This additional source has been called by us URCA-3. It is urgent to establish if this component is related to the GRB or to the Supernova (SN). In this second case, there are two possibilities: either the interaction of the SN ejecta with the interstellar medium or, possibly, the cooling of a young neutron star formed in the SN 2003lw process. The analogies and the differences between this triptych GRB 031203 / SN 2003lw / URCA-3 and the corresponding ones GRB 980425 / SN 1998bw / URCA-1 and GRB 030329 / SN 2003dh / URCA-2, as well as GRB 060218 / SN 2006aj are discussed.

10. M.G. Bernardini, C.L. Bianco, L. Caito, M.G. Dainotti, R. Guida, R. Ruffini; "GRB970228 and the class of GRBs with an initial spikelike emission: do they follow the Amati relation?"; in Relativistic Astrophysics Proceedings of the 4^{th} Italian-Sino Workshop, Pescara (Italy), July 2007, C.L. Bianco, S.-S. Xue, Editors; AIP Conference Proceedings, 966, 7 (2008).

    On the basis of the recent understanding of GRB050315 and GRB060218, we

return to GRB970228, the first Gamma-Ray Burst (GRB) with detected afterglow. We proposed it as the prototype for a new class of GRBs with "an occasional softer extended emission lasting tenths of seconds after an initial spikelike emission". Detailed theoretical computation of the GRB970228 light curves in selected energy bands for the prompt emission are presented and compared with observational *Beppo*SAX data. From our analysis we conclude that GRB970228 and likely the ones of the above mentioned new class of GRBs are "canonical GRBs" have only one peculiarity: they exploded in a galactic environment, possibly the halo, with a very low value of CBM density. Here we investigate how GRB970228 unveils another peculiarity of this class of GRBs: they do not fulfill the "Amati relation". We provide a theoretical explanation within the fireshell model for the apparent absence of such correlation for the GRBs belonging to this new class.

11. C.L. Bianco, M.G. Bernardini, L. Caito, M.G. Dainotti, R. Guida, R. Ruffini; "The "Fireshell" Model and the "Canonical" GRB Scenario; in Relativistic Astrophysics Proceedings of the 4^{th} Italian-Sino Workshop, Pescara (Italy), July 2007, C.L. Bianco, S.-S. Xue, Editors; AIP Conference Proceedings, 966, 12 (2008).

    In the "fireshell" model we define a "canonical GRB" light curve with two sharply different components: the Proper-GRB (P-GRB), emitted when the optically thick fireshell of electron-positron plasma originating the phenomenon reaches transparency, and the afterglow, emitted due to the collision between the remaining optically thin fireshell and the CircumBurst Medium (CBM). We outline our "canonical GRB" scenario, originating from the gravitational collapse to a black hole, with a special emphasis on the discrimination between "genuine" and "fake" short GRBs.

12. L. Caito, M.G. Bernardini, C.L. Bianco, M.G. Dainotti, R. Guida, R. Ruffini; "GRB 060614: A Progress Report"; in Relativistic Astrophysics Proceedings of the 4^{th} Italian-Sino Workshop, Pescara (Italy), July 2007, C.L. Bianco, S.-S. Xue, Editors; AIP Conference Proceedings, 966, 16 (2008).

    The explosion of GRB 060614, detected by the Swift satellite, produced a deep break in the GRB scenario opening new horizons of investigation, because it can't be traced back to any traditional scheme of classification. In fact, it manifests peculiarities both of long bursts and of short bursts. Above all, it is the first case of long duration near GRB without any bright Ib/c associated Supernova. We will show that, in our canonical GRB scenario, this "anomalous" situation finds a natural interpretation and allows us to discuss a possible variation to the traditional classification scheme, introducing the distinction between "genuine" and "fake" short bursts.

13. M.G. Dainotti, M.G. Bernardini, C.L. Bianco, L. Caito, R. Guida, R. Ruffini; "GRB 060218 and the Binaries as Progenitors of GRB-SN Systems"; in

Relativistic Astrophysics Proceedings of the 4^{th} Italian-Sino Workshop, Pescara (Italy), July 2007, C.L. Bianco, S.-S. Xue, Editors; AIP Conference Proceedings, 966, 25 (2008).

We study the Gamma-Ray Burst (GRB) 060218: a particularly close source at $z = 0.033$ with an extremely long duration, namely $T_{90} \sim 2000$ s, related to SN 2006aj. This source appears to be a very soft burst, with a peak in the spectrum at 4.9 keV, therefore interpreted as an X-Ray Flash (XRF). It fullfills the Amati relation. I present the fitting procedure, which is time consuming. In order to show its sensitivity I also present two examples of fits with the same value of B and different value of $E^{tot}_{e^\pm}$. We fit the X- and γ-ray observations by *Swift* of GRB 060218 in the 0.1–150 keV energy band during the entire time of observations from 0 all the way to 10^6 s within a unified theoretical model. The free parameters of our theory are only three, namely the total energy $E^{tot}_{e^\pm}$ of the $e^\pm$ plasma, its baryon loading $B \equiv M_B c^2 / E^{tot}_{e^\pm}$, as well as the CircumBurst Medium (CBM) distribution. We justify the extremely long duration of this GRB by a total energy $E^{tot}_{e^\pm} = 2.32 \times 10^{50}$ erg, a very high value of the baryon loading $B = 1.0 \times 10^{-2}$ and the effective CircumBurst Medium (CBM) density which shows a radial dependence $n_{cbm} \propto r^{-\alpha}$ with $1.0 \leq \alpha \leq 1.7$ and monotonically decreases from 1 to 10^{-6} particles/cm^3. We recall that this value of the B parameter is the highest among the sources we have analyzed and it is very close to its absolute upper limit expected. By our fit we show that there is no basic differences between XRFs and more general GRBs. They all originate from the collapse process to a black hole and their difference is due to the variability of the three basic parameters within the range of full applicability of the theory. We also think that the smallest possible black hole, formed by the gravitational collapse of a neutron star in a binary system, is consistent with the especially low energetics of the class of GRBs associated with SNe Ib/c.

14. R. Guida, M.G. Bernardini, C.L. Bianco, L. Caito, M.G. Dainotti, R. Ruffini; "The Amati Relation within the Fireshell Model"; in Relativistic Astrophysics Proceedings of the 4^{th} Italian-Sino Workshop, Pescara (Italy), July 2007, C.L. Bianco, S.-S. Xue, Editors; AIP Conference Proceedings, 966, 46 (2008).

In this work we show the existence of a spectral-energy correlation within our "fireshell" model for GRBs. The free parameters of the model are the total energy $E^{e\pm}_{tot}$ of the $e^\pm$ plasma and its baryon loading $B \equiv M_B\, c^2 / E^{e\pm}_{tot}$, characterizing the source, and the parameters describing the effective CircumBurst medium (CBM) distribution, namely its particle number density ρ and its effective emitting area R. We build a sample of pseudo-GRBs, i.e. a set of theoretically simulated light curves, varying the total energy of the electron-positron plasma $E^{e\pm}_{tot}$ and keeping the same baryon loading; the parametrization used to describe the distribution of the CircumBurst medium is the same as well for all the pseudo-GRBs. The values of these parameters (B, ρ and R) used in this

work are equal to the ones assumed to fit GRB050315, a *Swift* burst representing a good example of what in the literature has been addressed as "canonical light curve". For each GRB of the sample we calculate the νF_ν spectrum integrating the theoretically computed light curve over the total time, namely from our T_0, the end of the Proper-GRB (P-GRB), up to the end of our afterglow phase, when the fireshell Lorentz gamma factor is close to unity; we exclude the P-GRB from this spectral computation because, following our "canonical" GRB scenario, this component of the GRB emission is physically different from the other component, that is our afterglow component, so one should take care in no mixing them. We find that the maximum of this spectrum, that is the observed peak energy $E_{p,tot}$, correlates with the initial electron-positron plasma energy $E^{e\pm}_{tot}$ in a way very similar to the Amati one: $E_{p,tot} \propto (E^{e\pm}_{tot})^{0.5}$.

15. R. Guida, M.G. Bernardini, C.L. Bianco, L. Caito, M.G. Dainotti, R. Ruffini; "Theoretical interpretation of the Amati relation within the fireshell model"; in GAMMA-RAY BURSTS 2007: Proceedings of the Santa Fe Conference, Santa Fe (NM, USA), November 2007, M. Galassi, D. Palmer, E. Fenimore, Editors; AIP Conference Proceedings, 1000, 60 (2008).

    We discuss within our theoretical "fireshell" model for Gamma-Ray Bursts (GRBs) the theoretical interpretation of the phenomenological correlation between the isotropic-equivalent radiated energy of the prompt emission E_{iso} and the cosmological rest-frame νF_ν spectrum peak energy E_p observed by Amati and collaborators. Possible reasons for some of the outliers of this relation are given.

16. L. Caito, M.G. Bernardini, C.L. Bianco, M.G. Dainotti, R. Guida, R. Ruffini; "GRB 060614: a Fake Short Gamma-Ray Burst"; in GAMMA-RAY BURSTS 2007: Proceedings of the Santa Fe Conference, Santa Fe (NM, USA), November 2007, M. Galassi, D. Palmer, E. Fenimore, Editors; AIP Conference Proceedings, 1000, 301 (2008).

    The explosion of GRB 060614 produced a deep break in the GRB scenario and opened new horizons of investigation because it can't be traced back to any traditional scheme of classification. In fact, it manifests peculiarities both of long bursts and of short bursts and, above all, it is the first case of long duration near GRB without any bright Ib/c associated Supernova. We will show that, in our canonical GRB scenario, this "anomalous" situation finds a natural interpretation and allows us to discuss a possible variation to the traditional classification scheme, introducing the distinction between "genuine" and "fake" short bursts.

17. C.L. Bianco, M.G. Bernardini, L. Caito, M.G. Dainotti, R. Guida, R. Ruffini; "Short and canonical GRBs"; in GAMMA-RAY BURSTS 2007: Proceedings of the Santa Fe Conference, Santa Fe (NM, USA), November 2007,

M. Galassi, D. Palmer, E. Fenimore, Editors; AIP Conference Proceedings, 1000, 305 (2008).

Within the "fireshell" model for the Gamma-Ray Bursts (GRBs) we define a "canonical GRB" light curve with two sharply different components: the Proper-GRB (P-GRB), emitted when the optically thick fireshell of electron-positron plasma originating the phenomenon reaches transparency, and the afterglow, emitted due to the collision between the remaining optically thin fireshell and the CircumBurst Medium (CBM). We outline our "canonical GRB" scenario, with a special emphasis on the discrimination between "genuine" and "fake" short GRBs.

18. C.L. Bianco, M.G. Bernardini, L. Caito, M.G. Dainotti, R. Guida, R. Ruffini, G. Vereshchagin, S.-S. Xue; "The Equations of motion of the "fireshell""; in OBSERVATIONAL EVIDENCE FOR BLACK HOLES IN THE UNIVERSE: Proceedings of the 2^{nd} Kolkata Conference, Kolkata (India), February 2008, S.K. Chakrabarti, A.S. Majumdar, Editors; AIP Conference Proceedings, 1053, 259 (2008).

    The Fireshell originating a Gamma-Ray Burst (GRB) encompasses an optically thick regime followed by an optically thin one. In the first one the fireshell self-accelerates from a Lorentz gamma factor equal to 1 all the way to 200-300. The physics of this system is based on the continuous annihilation of electron-positron pairs in an optically thick e^+e^- plasma with a small baryon loading. In the following regime, the optically thin fireshell, composed by the baryons left over after the transparency point, ballistically expands into the CircumBurst Medium (CBM). The dynamics of the fireshell during both regimes will be analyzed. In particular we will re-examine the validity of the constant-index power-law relation between the fireshell Lorentz gamma factor and its radial coordinate, usually adopted in the current literature on the grounds of an "ultrarelativistic" approximation. Such expressions are found to be mathematically correct but only approximately valid in a very limited range of the physical and astrophysical parameters and in an asymptotic regime which is reached only for a very short time, if any.

19. M.G. Bernardini, C.L. Bianco, L. Caito, M.G. Dainotti, R. Guida, R. Ruffini; "The "Canonical" GRBs within the fireshell model"; in OBSERVATIONAL EVIDENCE FOR BLACK HOLES IN THE UNIVERSE: Proceedings of the 2^{nd} Kolkata Conference, Kolkata (India), February 2008, S.K. Chakrabarti, A.S. Majumdar, Editors; AIP Conference Proceedings, 1053, 267 (2008).

    Within the fireshell model we define a "canonical" GRB light curve with two sharply different components: the Proper-GRB (P-GRB), emitted when the optically thick fireshell of electron-positron plasma originating the phenomenon reaches transparency, and the afterglow, emitted due to the collision between the remaining optically thin fireshell and the CircumBurst Medium (CBM). On

the basis of the recent understanding of GRB970228 as the prototype for a new class of GRBs with "an occasional softer extended emission lasting tenths of seconds after an initial spikelike emission" we outline our "canonical" GRB scenario, originating from the gravitational collapse to a black hole, with a special emphasis on the discrimination between short GRBs and the ones appearing as such due to their peculiar astrophysical setting.

20. M.G. Dainotti, M.G. Bernardini, C.L. Bianco, L. Caito, R. Guida, R. Ruffini; "GRB 060218: the density mask and its peculiarity compared to the other sources"; in OBSERVATIONAL EVIDENCE FOR BLACK HOLES IN THE UNIVERSE: Proceedings of the 2^{nd} Kolkata Conference, Kolkata (India), February 2008, S.K. Chakrabarti, A.S. Majumdar, Editors; AIP Conference Proceedings, 1053, 283 (2008).

    The Swift satellite has given continuous data in the range 0.3150 keV from 0 s to 106 s for GRB060218 associated with SN2006aj. It has an unusually long duration ($T_{90} \sim 2100$ s). We plan to fit the complete γ- and X-ray light curves of this long duration GRB, including the prompt emission and we give peculiar attention to the afterglow lightcurve in order to better constrain the density mask. We apply our "fireshell" model based on the formation of a black hole, giving the relevant references. The initial total energy of the electron-positron plasma $E^{tot}_{e^{\pm}} == 2.32 \times 10^{50}$ erg has a particularly low value similarly to the other GRBs associated with SNe. For the first time we observe a baryon loading $B = 10^{-2}$ which coincides with the upper limit for the dynamical stability of the fireshell. The effective CircumBurst Medium (CBM) density shows a radial dependence $n_{cbm} \propto r^{-a}$ with $1.0 \leq a \leq 1.7$ and monotonically decreases from 1 to 10^{-6} particles/cm^3. Such a behavior is interpreted as due to a fragmentation in the fireshell. Such a fragmentation is crucial in explaining both the unusually large T_{90} and the consequently inferred abnormal low value of the CBM effective density. We present the comparison between the density mask of this source and the ones of a normal GRB 050315 and a fake short, GRB 970228, making some assumptions on the CBM behaviour in the surrounding of the Black hole.

21. L. Caito, M.G. Bernardini, C.L. Bianco, M.G. Dainotti, R. Guida, R. Ruffini; "GRB 060614 in the canonical fireshell model"; in OBSERVATIONAL EVIDENCE FOR BLACK HOLES IN THE UNIVERSE: Proceedings of the 2^{nd} Kolkata Conference, Kolkata (India), February 2008, S.K. Chakrabarti, A.S. Majumdar, Editors; AIP Conference Proceedings, 1053, 291 (2008).

    Gamma-Ray Burst (GRB) 060614 is the first nearby long duration GRB clearly not associated to any bright Ib/c Supernova. The explosion of this burst undermines one of the fundamental assumptions of the standard scenario and opens new horizons and hints of investigation. GRB 060614, hardly classifiable as a short GRB, is not either a "typical" long GRB since it occurs in a low star forming region. Moreover, it presents deep similarities with GRB 970228,

which is the prototype of the "fake" short bursts, or better canonical GRBs disguised as short ones. Within the "fireshell" model, we test if this "anomalous" source can be a disguised short GRB.

22. L.J. Rangel Lemos, S. Casanova, R. Ruffini, S.S. Xue; "Fermis approach to the study of pp interactions"; in OBSERVATIONAL EVIDENCE FOR BLACK HOLES IN THE UNIVERSE: Proceedings of the 2^{nd} Kolkata Conference, Kolkata (India), February 2008, S.K. Chakrabarti, A.S. Majumdar, Editors; AIP Conference Proceedings, 1053, 275 (2008).

    The physics of hadronic interactions found much difficulties for explain the experimental data. In this work we study the approach of Fermi (1950) about the multiplicity of pions emitted in pp interactions and in follow we compare with the modern approach

23. R. Ruffini, A.G. Aksenov, M.G. Bernardini, C.L. Bianco, L. Caito, M.G. Dainotti, G. De Barros, R. Guida, G.V. Vereshchagin, S.-S. Xue; "The canonical Gamma-Ray Bursts and their 'precursors"'; in 2008 NANJING GAMMA-RAY BURST CONFERENCE, Proceedings of the 2008 Nanjing Gamma-Ray Burst Conference, Nanjing (China), June 2008, Y.-F. Huang, Z.-G. Dai, B. Zhang, Editors; AIP Conference Proceedings, 1065, 219 (2008).

    The fireshell model for Gamma-Ray Bursts (GRBs) naturally leads to a canonical GRB composed of a proper-GRB (P-GRB) and an afterglow. P-GRBs, introduced by us in 2001, are sometimes considered "precursors" of the main GRB event in the current literature. We show in this paper how the fireshell model leads to the understanding of the structure of GRBs, with precise estimates of the time sequence and intensities of the P-GRB and the of the afterglow. It leads as well to a natural classification of the canonical GRBs which overcomes the traditional one in short and long GRBs.

24. M.G. Bernardini, C.L. Bianco, L. Caito, M.G. Dainotti, R. Guida, R. Ruffini; "Preliminary analysis of GRB060607A within the fireshell model"; in 2008 NANJING GAMMA-RAY BURST CONFERENCE; Proceedings of the 2008 Nanjing Gamma-Ray Burst Conference, Nanjing (China), June 2008, Y.-F. Huang, Z.-G. Dai, B. Zhang, Editors; AIP Conference Proceedings, 1065, 227 (2008).

    GRB060607A is a very distant ($z = 3.082$) and energetic event ($E_{iso} \sim 10^{53}$ erg). Its main peculiarity is that the peak of the near-infrared afterglow has been observed with the REM robotic telescope, allowing to infer the initial Lorentz gamma factor of the emitting system. We present a preliminary analysis of the spectra and light curves of GRB060607A prompt emission within the fireshell model. We show that the N(E) spectrum of the prompt emission, whose behavior is usually described as "simple power-law", can also be fitted in a satisfactory way by a convolution of thermal spectra as predicted by

the model we applied. The theoretical time-integrated spectrum of the prompt emission as well as the light curves in the BAT and XRT energy band are in good agreement with the observations, enforcing the plausibility of our approach. Furthermore, the initial value of Lorentz gamma factor we predict is compatible with the one deduced from the REM observations.

25. C.L. Bianco, M.G. Bernardini, L. Caito, M.G. Dainotti, R. Guida, R. Ruffini; "The "fireshell" model and the "canonical GRB" scenario"; in 2008 NANJING GAMMA-RAY BURST CONFERENCE; Proceedings of the 2008 Nanjing Gamma-Ray Burst Conference, Nanjing (China), June 2008, Y.-F. Huang, Z.-G. Dai, B. Zhang, Editors; AIP Conference Proceedings, 1065, 223 (2008).

    The Swift observation of GRB 060614, as well as the catalog analysis by Norris and Bonnell (2006), opened the door "on a new Gamma-Ray Bursts (GRBs) classification scheme that straddles both long and short bursts" (Gehrels et al., 2006). Within the "fireshell" model for the Gamma-Ray Bursts (GRBs) we define a "canonical GRB" light curve with two sharply different components: the Proper-GRB (P-GRB), emitted when the optically thick fireshell of electron-positron plasma originating the phenomenon reaches transparency, and the afterglow, emitted due to the collision between the remaining optically thin fireshell and the CircumBurst Medium (CBM). We here outline our "canonical GRB" scenario, which implies three different GRB classes: the "genuine" short GRBs, the "fake" or "disguised" short GRBs and the other (so-called "long") GRBs. We also outline some implications for the theoretical interpretation of the Amati relation.

26. G. De Barros, M.G. Bernardini, C.L. Bianco, L. Caito, M.G. Dainotti, R. Guida, R. Ruffini; "Is GRB 050509b a genuine short GRB?"; in 2008 NANJING GAMMA-RAY BURST CONFERENCE; Proceedings of the 2008 Nanjing Gamma-Ray Burst Conference, Nanjing (China), June 2008, Y.-F. Huang, Z.-G. Dai, B. Zhang, Editors; AIP Conference Proceedings, 1065, 231 (2008).

    Within our "fireshell" model we introduced a "canonical" GRB scenario which differentiates physically the "proper GRB" (P-GRB) emission when photons decouple, and the afterglow emission due to interaction of the accelerated baryons with the CircumBurst Medium (CBM). The ratio between energetics of the two components is ruled by the baryon loading of the fireshell. We here analyse the possibility that GRB050509b is the first case of a "genuine" short GRB the ones with smaller baryon loading. In such a case, the GRB050509b "prompt emission" would be dominated by the "proper GRB" and, moreover, the P-GRB total energy would be greater than the afterglow one. Our fit of the afterglow data and of the P-GRB energetics indicates that this source present the smallest baryon loading we ever encountered so far, being on the order of 10^{-4}.

27. G. De Barros, A.G. Aksenov, C.L. Bianco, R. Ruffini, G.V. Vereshchagin; "Fireshell versus Fireball scenarios"; in 2008 NANJING GAMMA-RAY BURST CONFERENCE; Proceedings of the 2008 Nanjing Gamma-Ray Burst Conference, Nanjing (China), June 2008, Y.-F. Huang, Z.-G. Dai, B. Zhang, Editors; AIP Conference Proceedings, 1065, 234 (2008).

    We revisit Cavallo and Rees classification based on the analysis of initial conditions in electron-positron-photon plasma which appears suddenly around compact astrophysical objects and gives origin to GRBs. These initial conditions were recently studied in [1,2] by numerical integration of relativistic Boltzmann equations with collision integrals, including binary and triple interactions between particles. The main conclusion is that the pair plasma in GRB sources quickly reaches thermal equilibrium well before its expansion starts. In light of this work we comment on each of the four scenarios proposed by Cavallo and Rees and discuss their applicability to describe evolution of GRB sources.

28. M.G. Bernardini, C.L. Bianco, L. Caito, M.G. Dainotti, R. Guida, R. Ruffini; "GRB970228 as a prototype for the class of GRBs with an initial spikelike emission"; in Proceedings of the Eleventh Marcel Grossmann Meeting on General Relativity, Berlin, Germany, July 2006, H. Kleinert, R.T. Jantzen, Editors; World Scientific, (Singapore, 2008).

    We interpret GRB970228 prompt emission within our "canonical" GRB scenario, identifying the initial spikelike emission with the Proper-GRB (P-GRB) and the following bumps with the afterglow peak emission. Furthermore, we emphasize the necessity to consider the "canonical" GRB as a whole due to the highly non-linear nature of the model we applied.

29. M.G. Bernardini, C.L. Bianco, L. Caito, M.G. Dainotti, R. Guida, R. Ruffini; "GRB980425 and the puzzling URCA1 emission"; in Proceedings of the Eleventh Marcel Grossmann Meeting on General Relativity, Berlin, Germany, July 2006, H. Kleinert, R.T. Jantzen, Editors; World Scientific, (Singapore, 2008).

    We applied our "fireshell" model to GRB980425 observational data, reproducing very satisfactory its prompt emission. We use the results of our analysis to provide a possible interpretation for the X-ray emission of the source S1. The effect on the GRB analysis of the lack of data in the pre-Swift observations is also outlined.

30. C.L. Bianco, M.G. Bernardini, L. Caito, P. Chardonnet, M.G. Dainotti, F. Fraschetti, R. Guida, R. Ruffini, S.-S. Xue; "Theoretical interpretation of 'long' and 'short' GRBs"; in Proceedings of the Eleventh Marcel Grossmann Meeting on General Relativity, Berlin, Germany, July 2006, H. Kleinert, R.T. Jantzen, Editors; World Scientific, (Singapore, 2008).

Within the "fireshell" model we define a "canonical GRB" light curve with two sharply different components: the Proper-GRB (P-GRB), emitted when the optically thick fireshell of electron-positron plasma originating the phenomenon reaches transparency, and the afterglow, emitted due to the collision between the remaining optically thin fireshell and the CircumBurst Medium (CBM). We here present the consequences of such a scenario on the theoretical interpretation of the nature of "long" and "short" GRBs.

31. C.L. Bianco, M.G. Bernardini, P. Chardonnet, F. Fraschetti, R. Ruffini, S.-S. Xue; "Theoretical interpretation of luminosity and spectral properties of GRB 031203"; in Proceedings of the Eleventh Marcel Grossmann Meeting on General Relativity, Berlin, Germany, July 2006, H. Kleinert, R.T. Jantzen, Editors; World Scientific, (Singapore, 2008).

    We show how an emission endowed with an instantaneous thermal spectrum in the co-moving frame of the expanding fireshell can reproduce the time-integrated GRB observed non-thermal spectrum. An explicit example in the case of GRB 031203 is presented.

32. C.L. Bianco, R. Ruffini; "The 'Fireshell' model in the Swift era"; in Proceedings of the Eleventh Marcel Grossmann Meeting on General Relativity, Berlin, Germany, July 2006, H. Kleinert, R.T. Jantzen, Editors; World Scientific, (Singapore, 2008).

    We here re-examine the validity of the constant-index power-law relation between the fireshell Lorentz gamma factor and its radial coordinate, usually adopted in the current Gamma-Ray Burst (GRB) literature on the grounds of an "ultrarelativistic" approximation. Such expressions are found to be mathematically correct but only approximately valid in a very limited range of the physical and astrophysical parameters and in an asymptotic regime which is reached only for a very short time, if any.

33. L. Caito, M.G. Bernardini, C.L. Bianco, M.G. Dainotti, R. Guida, R. Ruffini; "Theoretical interpretation of GRB011121"; in Proceedings of the Eleventh Marcel Grossmann Meeting on General Relativity, Berlin, Germany, July 2006, H. Kleinert, R.T. Jantzen, Editors; World Scientific, (Singapore, 2008).

    GRB 011121, detected by the BeppoSAX satellite, is studied as a prototype to understand the presence of flares observed by Swift in the afterglow of many GRB sources. Detailed theoretical analysis of the GRB 011121 light curves in selected energy bands are presented and compared with observational data. An interpretation of the flare of this source is provided by the introduction of the three-dimensional structure of the CircumBurst Medium(CBM).

34. M.G. Dainotti, M.G. Bernardini, C.L. Bianco, L. Caito, R. Guida, R. Ruffini; "On GRB 060218 and the GRBs related to Supernovae Ib/c"; in Proceed-

ings of the Eleventh Marcel Grossmann Meeting on General Relativity, Berlin, Germany, July 2006, H. Kleinert, R.T. Jantzen, Editors; World Scientific, (Singapore, 2008).

We study the Gamma-Ray Burst (GRB) 060218: a particularly close source at $z = 0.033$ with an extremely long duration, namely $T_{90} \sim 2000$ s, related to SN 2006aj. This source appears to be a very soft burst, with a peak in the spectrum at 4.9 keV, therefore interpreted as an X-Ray Flash (XRF) and it obeys to the Amati relation. We fit the X- and γ-ray observations by Swift of GRB 060218 in the 0.1150 keV energy band during the entire time of observations from 0 all the way to 106 s within a unified theoretical model. The details of our theoretical analysis have been recently published in a series of articles. The free parameters of the theory are only three, namely the total energy $E^{tot}_{e^\pm}$ of the $e^\pm$ plasma, its baryon loading $B = M_B c^2 / E^{tot}_{e^\pm}$, as well as the CircumBurst Medium (CBM) distribution. We fit the entire light curve, including the prompt emission as an essential part of the afterglow. We recall that this value of the B parameter is the highest among the sources we have analyzed and it is very close to its absolute upper limit expected. We successfully make definite predictions about the spectral distribution in the early part of the light curve, exactly we derive the instantaneous photon number spectrum N(E) and we show that although the spectrum in the co-moving frame of the expanding pulse is thermal, the shape of the final spectrum in the laboratory frame is clearly non thermal. In fact each single instantaneous spectrum is the result of an integration of thousands of thermal spectra over the corresponding EQuiTemporal Surfaces (EQTS). By our fit we show that there is no basic differences between XRFs and more general GRBs. They all originate from the collapse process to a black hole and their difference is due to the variability of the three basic parameters within the range of full applicability of the theory.

35. R. Guida, M.G. Bernardini, C.L. Bianco, L. Caito, M.G. Dainotti, R. Ruffini; "Theoretical interpretation of GRB060124"; in Proceedings of the Eleventh Marcel Grossmann Meeting on General Relativity, Berlin, Germany, July 2006, H. Kleinert, R.T. Jantzen, Editors; World Scientific, (Singapore, 2008).

We show the preliminary results of the application of our "fireshell" model to GRB060124. This source is very peculiar because it is the first event for which both the prompt and the afterglow emission were observed simultaneously by the three Swift instruments: BAT (15 - 350 keV), XRT (0,2 - 10 keV) and UVOT (170 - 650 nm), due to the presence of a precursor ~ 570 s before the main burst. We analyze GRB060124 within our "canonical" GRB scenario, identifying the precursor with the P-GRB and the prompt emission with the afterglow peak emission. In this way we reproduce correctly the energetics of both these two components. We reproduce also the observed time delay between the precursor (P-GRB) and the main burst. The effect of such a time delay in our model

will be discussed.

36. R. Ruffini, M.G. Bernardini, C.L. Bianco, L. Caito, P. Chardonnet, C. Cherubini, M.G. Dainotti, F. fraschetti, A. Geralico, R. Guida, B. Patricelli, M. Rotondo, J. Rueda Hernandez, G. Vereshchagin, S.-S. Xue; "Gamma-Ray Bursts"; in Proceedings of the Eleventh Marcel Grossmann Meeting on General Relativity, Berlin, Germany, July 2006, H. Kleinert, R.T. Jantzen, Editors; World Scientific, (Singapore, 2008).

    We show by example how the uncoding of Gamma-Ray Bursts (GRBs) offers unprecedented possibilities to foster new knowledge in fundamental physics and in astrophysics. After recalling some of the classic work on vacuum polarization in uniform electric fields by Klein, Sauter, Heisenberg, Euler and Schwinger, we summarize some of the efforts to observe these effects in heavy ions and high energy ion collisions. We then turn to the theory of vacuum polarization around a Kerr-Newman black hole, leading to the extraction of the blackholic energy, to the concept of dyadosphere and dyadotorus, and to the creation of an electron-positron-photon plasma. We then present a new theoretical approach encompassing the physics of neutron stars and heavy nuclei. It is shown that configurations of nuclear matter in bulk with global charge neutrality can exist on macroscopic scales and with electric fields close to the critical value near their surfaces. These configurations may represent an initial condition for the process of gravitational collapse, leading to the creation of an electron-positron-photon plasma: the basic self-accelerating system explaining both the energetics and the high energy Lorentz factor observed in GRBs. We then turn to recall the two basic interpretational paradigms of our GRB model: 1) the Relative Space-Time Transformation (RSTT) paradigm and 2) the Interpretation of the Burst Structure (IBS) paradigm. These paradigms lead to a "canonical" GRB light curve formed from two different components: a Proper-GRB (P-GRB) and an extended afterglow comprising a raising part, a peak, and a decaying tail. When the P-GRB is energetically predominant we have a "genuine" short GRB, while when the afterglow is energetically predominant we have a so-called long GRB or a "fake" short GRB. We compare and contrast the description of the relativistic expansion of the electron-positron plasma within our approach and within the other ones in the current literature. We then turn to the special role of the baryon loading in discriminating between "genuine" short and long or "fake" short GRBs and to the special role of GRB 991216 to illustrate for the first time the "canonical" GRB bolometric light curve. We then propose a spectral analysis of GRBs, and proceed to some applications: GRB 031203, the first spectral analysis, GRB 050315, the first complete light curve fitting, GRB 060218, the first evidence for a critical value of the baryon loading, GRB 970228, the appearance of "fake" short GRBs. We finally turn to the GRB-Supernova Time Sequence (GSTS) paradigm: the concept of induced gravitational collapse. We illustrate this paradigm by the systems GRB 980425 / SN 1998bw, GRB 030329 / SN 2003dh, GRB 031203 /

SN 2003lw, GRB 060218 / SN 2006aj, and we present the enigma of the URCA sources. We then present some general conclusions.

37. R. Ruffini, A.G. Aksenov, M.G. Bernardini, C.L. Bianco, L. Caito, M.G. Dainotti, G. De Barros, R. Guida, G. Vereshchagin, S.-S. Xue; "The canonical Gamma-Ray Bursts: long, 'fake'-'disguised' and 'genuine' short bursts; in PROBING STELLAR POPULATIONS OUT TO THE DISTANT UNIVERSE: CEFALU 2008, Proceedings of the International Conference; Cefal (Italy), September 2008, G. Giobbi, A. Tornambe, G. Raimondo, M. Limongi, L. A. Antonelli, N. Menci, E. Brocato, Editors; AIP Conference Proceedings, 1111, 325 (2009).

    The Gamma-Ray Bursts (GRBs) offer the unprecedented opportunity to observe for the first time the blackholic energy extracted by the vacuum polarization during the process of gravitational collapse to a black hole leading to the formation of an electron-positron plasma. The uniqueness of the Kerr-Newman black hole implies that very different processes originating from the gravitational collapse a) of a single star in a binary system induced by the companion, or b) of two neutron stars, or c) of a neutron star and a white dwarf, do lead to the same structure for the observed GRB. The recent progress of the numerical integration of the relativistic Boltzmann equations with collision integrals including 2-body and 3-body interactions between the particles offer a powerful conceptual tool in order to differentiate the traditional "fireball" picture, an expanding hot cavity considered by Cavallo and Rees, as opposed to the "fireshell" model, composed of an internally cold shell of relativistically expanding electron-positron-baryon plasma. The analysis of the fireshell naturally leads to a canonical GRB composed of a proper-GRB and an extended afterglow. By recalling the three interpretational paradigms for GRBs we show how the fireshell model leads to an understanding of the GRB structure and to an alternative classification of short and long GRBs.

38. M.G. Bernardini, M.G. Dainotti, C.L. Bianco, L. Caito, R. Guida, R. Ruffini; "Prompt emission and X-ray flares: the case of GRB 060607 A"; in PROBING STELLAR POPULATIONS OUT TO THE DISTANT UNIVERSE: CEFALU 2008, Proceedings of the International Conference; Cefal (Italy), September 2008, G. Giobbi, A. Tornambe, G. Raimondo, M. Limongi, L. A. Antonelli, N. Menci, E. Brocato, Editors; AIP Conference Proceedings, 1111, 383 (2009).

    GRB 060607A is a very distant and energetic event. Its main peculiarity is that the peak of the near-infrared (NIR) afterglow has been observed with the REM robotic telescope, allowing to estimate the initial Lorentz gamma factor within the fireball forward shock model. We analyze GRB 060607A within the fireshell model. The initial Lorentz gamma factor of the fireshell can be obtained adopting the exact solutions of its equations of motion, dealing only

with the BAT and XRT observations, that are the basic contribution to the afterglow emission, up to a distance from the progenitor $r \sim 10^{18}$ cm. According to the "canonical GRB" scenario we interpret the whole prompt emission as the peak of the afterglow emission, and we show that the observed temporal variability of the prompt emission can be produced by the interaction of the fireshell with overdense CircumBurst Medium (CBM) clumps. This is indeed the case also of the X-ray flares which are present in the early phases of the afterglow light curve.

39. C.L. Bianco, M.G. Bernardini, L. Caito, M.G. Dainotti, R. Guida, R. Ruffini; "The 'fireshell' model and the 'canonical GRB' scenario. Implications for the Amati relation"; in PROBING STELLAR POPULATIONS OUT TO THE DISTANT UNIVERSE: CEFALU 2008, Proceedings of the International Conference; Cefal (Italy), September 2008, G. Giobbi, A. Tornambe, G. Raimondo, M. Limongi, L. A. Antonelli, N. Menci, E. Brocato, Editors; AIP Conference Proceedings, 1111, 587 (2009).

    Within the "fireshell" model for GRBs we define a "canonical GRB" light curve with two sharply different components: the Proper-GRB (P-GRB), emitted when the optically thick fireshell reaches transparency, and the extended afterglow, emitted due to the collision between the remaining optically thin fireshell and the CircumBurst Medium (CBM). We here outline our "canonical GRB" scenario, which implies three different GRB classes: the "genuine" short GRBs, the "fake" or "disguised" short GRBs and the other (so-called "long") GRBs. We will also outline the corresponding implications for the Amati relation, which are opening its use for cosmology.

40. R. Ruffini, A.G. Aksenov, M.G. Bernardini, C.L. Bianco, L. Caito, P. Chardonnet, M.G. Dainotti, G. De Barros, R. Guida, L. Izzo, B. Patricelli, L.J. Rangel Lemos, M. Rotondo, J.A. Rueda Hernandez, G. Vereshchagin, S.-S. Xue; "The Blackholic energy and the canonical Gamma-Ray Burst IV: the 'long', 'genuine short' and 'fake disguised short' GRBs"; in Proceedings of the XIIIth Brazilian School on Cosmology and Gravitation, Mangaratiba, Rio de Janeiro (Brazil), July-August 2008, M. Novello, S.E. Perez Bergliaffa, Editors; AIP Conference Proceedings, 1132, 199 (2009).

    We report some recent developments in the understanding of GRBs based on the theoretical framework of the "fireshell" model, already presented in the last three editions of the "Brazilian School of Cosmology and Gravitation". After recalling the basic features of the "fireshell model", we emphasize the following novel results: 1) the interpretation of the X-ray flares in GRB afterglows as due to the interaction of the optically thin fireshell with isolated clouds in the CircumBurst Medium (CBM); 2) an interpretation as "fake - disguised" short GRBs of the GRBs belonging to the class identified by Norris & Bonnell; we present two prototypes, GRB 970228 and GRB 060614; both these cases are

consistent with an origin from the final coalescence of a binary system in the halo of their host galaxies with particularly low CBM density $n_{cbm} \sim 10^{-3}$ particles/cm^3; 3) the first attempt to study a genuine short GRB with the analysis of GRB 050509B, that reveals indeed still an open question; 4) the interpretation of the GRB-SN association in the case of GRB 060218 via the "induced gravitational collapse" process; 5) a first attempt to understand the nature of the "Amati relation", a phenomenological correlation between the isotropic-equivalent radiated energy of the prompt emission E_{iso} with the cosmological rest-frame νF_ν spectrum peak energy $E_{p,i}$. In addition, recent progress on the thermalization of the electron-positron plasma close to their formation phase, as well as the structure of the electrodynamics of Kerr-Newman Black Holes are presented. An outlook for possible explanation of high-energy phenomena in GRBs to be expected from the AGILE and the Fermi satellites are discussed. As an example of high energy process, the work by Enrico Fermi dealing with ultrarelativistic collisions is examined. It is clear that all the GRB physics points to the existence of overcritical electrodynamical fields. In this sense we present some progresses on a unified approach to heavy nuclei and neutron stars cores, which leads to the existence of overcritical fields under the neutron star crust.

41. A.G. Aksenov, M.G. Bernardini, C.L. Bianco, L. Caito, C. Cherubini, G. De Barros, A. Geralico, L. Izzo, F.A. Massucci, B. Patricelli, M. Rotondo, J.A. Rueda Hernandez, R. Ruffini, G. Vereshchagin, S.-S. Xue; "The fireshell model for Gamma-Ray Bursts"; in The Shocking Universe, Proceedings of the conference held in Venice (Italy), September 2009, G. Chincarini, P. DAvanzo, R. Margutti, R. Salvaterra, Editors; SIF Conference Proceedings, 102, 451 (2010).

    The fireshell model for GRBs is briefly outlined, and the currently ongoing developments are summarized.

42. M.G. Bernardini, C.L. Bianco, L. Caito, L. Izzo, B. Patricelli, R. Ruffini; "The end of the prompt emission within the fireshell model"; in The Shocking Universe, Proceedings of the conference held in Venice (Italy), September 2009, G. Chincarini, P. DAvanzo, R. Margutti, R. Salvaterra, Editors; SIF Conference Proceedings, 102, 489 (2010)

    The shallow decay emission, revealed by the Swift satellite in the X-ray afterglow of a good sample of bursts, is a puzzle. Within the fireshell model it has been recently proposed an alternative explanation: if we assume that after the prompt phase the system has a range of Lorentz factors, the plateau phase is simply the product of the injection of slower material into the fireshell. This injection produces a modification both in the dynamics of the fireshell and in the spectrum of the emitted radiation. We postulate that this spread in the fireshell Lorentz factor occurs when the fireshell becomes transparent and do not depend on a prolonged activity of the central engine. The aim of this paper

is to characterize dynamically the system in order to understand the nature of that material.

43. L. Izzo, M.G. Bernardini, C.L. Bianco, L. Caito, B. Patricelli, R. Ruffini; "GRB 090423 in the fireshell scenario"; in The Shocking Universe, Proceedings of the conference held in Venice (Italy), September 2009, G. Chincarini, P. DAvanzo, R. Margutti, R. Salvaterra, Editors; SIF Conference Proceedings, 102, 537 (2010).

44. B. Patricelli, M.G. Bernardini, C.L. Bianco, L. Caito, L. Izzo, R. Ruffini, G. Vereshchagin; "A new spectral energy distribution of photons in the fireshell model of GRBs"; in The Shocking Universe, Proceedings of the conference held in Venice (Italy), September 2009, G. Chincarini, P. DAvanzo, R. Margutti, R. Salvaterra, Editors; SIF Conference Proceedings, 102, 559 (2010).

    The fireshell model of Gamma Ray Bursts (GRBs) postulates that the emission process is thermal in the comoving frame of the fireshell, but this is just a first approximation. We investigate a different spectrum of photons in the comoving frame in order to better reproduce the observed spectral properties of GRB prompt emission. We introduce a modified thermal spectrum whose low energy slope depends on an index α, left as a free parameter. We test it by comparing the numerical simulations with observed BAT spectra integrated over different intervals of time. We find that the observational data can be correctly reproduced by assuming $\alpha = -1.8$.

45. C.L. Bianco, M.G. Bernardini, L. Caito, G. De Barros, L. Izzo, B. Patricelli, R. Ruffini; "Disguised Short Bursts and the Amati Relation"; in Deciphering the ancient universe with Gamma-Ray Bursts, Proceedings of the conference held in Kyoto (Japan), April 2010, N. Kawai, S. Nagataki, Editors; AIP Conference Proceedings, 1279, 299 (2010).

    The class of "Disguised short" GRBs implied by the fireshell scenario is presented, with special emphasis on the implications for the Amati relation.

46. L. Izzo, M.G. Bernardini, C.L. Bianco, L. Caito, B. Patricelli, L.J. Rangel Lemos, R. Ruffini; "On GRB 080916C and GRB 090902B observed by the Fermi satellite"; in Deciphering the ancient universe with Gamma-Ray Bursts, Proceedings of the conference held in Kyoto (Japan), April 2010, N. Kawai, S. Nagataki, Editors; AIP Conference Proceedings, 1279, 343 (2010).

    We propose a possible explanation, in the context of the Fireshell scenario, for the high-energy emission observed in GRB 080916C and GRB 090902B. The physical process underlying this emission consists mainly in the interaction of the baryon in the Fireshell with some high-density region around the burst

site. Moreover we associate the observed delay of the onset of the high-energy emission as due to the P-GRB emission.

47. B. Patricelli, M.G. Bernardini, C.L. Bianco, L. Caito, G. De Barros, L. Izzo, R. Ruffini; "Black Holes in Gamma Ray Bursts"; in Deciphering the ancient universe with Gamma-Ray Bursts, Proceedings of the conference held in Kyoto (Japan), April 2010, N. Kawai, S. Nagataki, Editors; AIP Conference Proceedings, 1279, 406 (2010).

    Within the fireshell model, Gamma Ray Bursts (GRBs) originate from an optically thick $e^{\pm}$ plasma created by vacuum polarization process during the formation of a Black Hole (BH). Here we briefly recall the basic features of this model, then we show how it is possible to interpret GRB observational properties within it. In particular we present, as a specific example, the analysis of GRB 050904 observations of the prompt emission light curve and spectrum in the Swift BAT energy band (15-150 keV).

48. M.G. Bernardini, C.L. Bianco, L. Caito, M.G. Dainotti, R. Guida, R. Ruffini; "The GRB classification within the "fireshell" model: short, long and "fake" short GRBs"; in Proceedings of the 3rd Stueckelberg Workshop on Relativistic Field Theories, Pescara, Italy, July 2008, N. Carlevaro, R. Ruffini, G.V. Vereshchagin, Editors; Cambridge Scientific Publishers, (UK, 2011).

49. C.L. Bianco, M.G. Bernardini, L. Caito, M.G. Dainotti, R. Guida, R. Ruffini, G.V. Vereshchagin, S.-S. Xue; "Equations of motion of the "fireshell""; in Proceedings of the 3rd Stueckelberg Workshop on Relativistic Field Theories, Pescara, Italy, July 2008, N. Carlevaro, R. Ruffini, G.V. Vereshchagin, Editors; Cambridge Scientific Publishers, (UK, 2011).

50. L. Caito, M.G. Bernardini, C.L. Bianco, M.G. Dainotti, R. Guida, R. Ruffini; "GRB 060614: another example of "fake" short burst from a merging binary system"; in Proceedings of the 3rd Stueckelberg Workshop on Relativistic Field Theories, Pescara, Italy, July 2008, N. Carlevaro, R. Ruffini, G.V. Vereshchagin, Editors; Cambridge Scientific Publishers, (UK, 2011).

51. G. De Barros, M.G. Bernardini, C.L. Bianco, L. Caito, R. Guida, R. Ruffini; "Analysis of GRB 050509b"; in Proceedings of the 3rd Stueckelberg Workshop on Relativistic Field Theories, Pescara, Italy, July 2008, N. Carlevaro, R. Ruffini, G.V. Vereshchagin, Editors; Cambridge Scientific Publishers, (UK, 2011).

52. R. Ruffini, L. Izzo, A.V. Penacchioni, C.L. Bianco, L. Caito, S.K. Chakrabarti, A. Nandi; "GRB 090618: a possible case of multiple GRB?"; in Proceedings of the 25th Texas Symposium on Relativistic Astrophysics, held in

Heidelberg (Germany), December 2010, F.M. Rieger, C. van Eldik, W. Hofmann, Editors; PoS(Texas2010), 101.

53. L.J. Rangel Lemos, C.L. Bianco, H.J. Mosquera Cuesta, J.A. Rueda, R. Ruffini; "Luminosity function of BATSE GRBs dominated by extended afterglow"; in Proceedings of the 25th Texas Symposium on Relativistic Astrophysics, held in Heidelberg (Germany), December 2010, F.M. Rieger, C. van Eldik, W. Hofmann, Editors; PoS(Texas2010), 204.

54. R. Ruffini, A.G. Aksenov, M.G. Bernardini, C.L. Bianco, L. Caito, P. Chardonnet, M.G. Dainotti, G. De Barros, R. Guida, L. Izzo, B. Patricelli, L.J. Rangel Lemos, M. Rotondo, J.A. Rueda Hernandez, G. Vereshchagin, She-Sheng Xue; "Black Holes Energetics and GRBs"; in The Sun, the Stars, the Universe and General Relativity: Proceedings of Sobral 2009; S.E. Perez Bergliaffa, M. Novello , R. Ruffini, Editors; Cambridge Scientific Publishers (UK, 2011).

55. C.L. Bianco, L. Amati, M.G. Bernardini, L. Caito, G. De Barros, L. Izzo, B. Patricelli, R. Ruffini; "The class of 'disguised' short GRBs and its implications for the Amati relation"; in GRBs as probes - from the progenitors environment to the high redshift Universe, Proceedings of the conference held in Como (Italy), May 2011, S. Campana, P. DAvanzo, A. Melandri, Editors; Mem. S.A.It. Suppl., 21, 139 (2012).

56. A.V. Penacchioni, R. Ruffini, L. Izzo, M. Muccino, C.L. Bianco, L. Caito, B. Patricelli; "Evidences for a double component in the emission of GRB 101023"; in GRBs as probes - from the progenitors environment to the high redshift Universe, Proceedings of the conference held in Como (Italy), May 2011, S. Campana, P. DAvanzo, A. Melandri, Editors; Mem. S.A.It. Suppl., 21, 230 (2012).

57. M.G. Bernardini, C.L. Bianco, L. Caito, L. Izzo, B. Patricelli, R. Ruffini; "The X-Ray Flares of GRB 060607A within the Fireshell Model"; in Proceedings of the Twelfth Marcel Grossmann Meeting on General Relativity, Paris, France, July 2009, T. Damour, R.T. Jantzen, R. Ruffini, Editors; World Scientific, (Singapore, 2012).

58. L. Izzo, M.G. Bernardini, C.L. Bianco, L. Caito, B. Patricelli, R. Ruffini; "GRB 090423 in the Fireshell Scenario: A Canonical GRB at Redshift 8.2"; in Proceedings of the Twelfth Marcel Grossmann Meeting on General Relativity, Paris, France, July 2009, T. Damour, R.T. Jantzen, R. Ruffini, Editors; World Scientific, (Singapore, 2012).

59. B. Patricelli, M.G. Bernardini, C.L. Bianco, L. Caito, L. Izzo, R. Ruffini, G.V. Vereshchagin; "A New Spectral Energy Distribution of Photons in the Fireshell Model of GRBs"; in Proceedings of the Twelfth Marcel

Grossmann Meeting on General Relativity, Paris, France, July 2009, T. Damour, R.T. Jantzen, R. Ruffini, Editors; World Scientific, (Singapore, 2012).

60. C.L. Bianco, M.G. Bernardini, L. Caito, G. De Barros, L. Izzo, M. Muccino, B. Patricelli, A.V. Penacchioni, G.B. Pisani, R. Ruffini; "Needs for a new GRB classification following the fireshell model: genuine short, disguised short and long GRBs"; in Proceedings of the Gamma-Ray Bursts 2012 Conference, held in Munich (Germany), May 2012, A. Rau, J. Greiner, Editors; PoS(GRB 2012), 043.

61. A.V. Penacchioni, G.B. Pisani, R. Ruffini, C.L. Bianco, L. Izzo, M. Muccino; "The proto-black hole concept in GRB 101023 and its possible extension to GRB 110709B"; in Proceedings of the Gamma-Ray Bursts 2012 Conference, held in Munich (Germany), May 2012, A. Rau, J. Greiner, Editors; PoS(GRB 2012), 042.

62. B. Patricelli, M.G. Bernardini, C.L. Bianco, L. Caito, L. Izzo, R. Ruffini; "GRB 050904: The study of a high redshift GRB within the Fireshell Model"; in Proceedings of the Twelfth Marcel Grossmann Meeting on General Relativity, Paris, France, July 2009, T. Damour, R.T. Jantzen, R. Ruffini, Editors; World Scientific, (Singapore, 2012).

63. L. Izzo, G.B. Pisani, M. Muccino, J.A. Rueda, Y.Wang, C.L. Bianco, A.V. Penacchioni, R. Ruffini; "A common behavior in the late X-ray afterglow of energetic GRB-SN systems"; EAS Publications Series, Volume 61, 595-597 (2013).

6. Brief reminder of the fireshell model

The black hole uniqueness theorem (see Left panel in Fig. 3.4 and e.g. Ref. Ruffini and Wheeler, 1971) is at the very ground of the fact that it is possible to explain the different Gamma-Ray Burst (GRB) features with a single theoretical model, over a range of energies spanning over 6 orders of magnitude. The fundamental point is that, independently of the fact that the progenitor of the gravitational collapse is represented by merging binaries composed by neutron stars and white dwarfs in all possible combinations, or by a single process of gravitational collapse, or by the process of "induced" gravitational collapse, the formed black hole is totally independent from the initial conditions and reaches the standard configuration of a Kerr-Newman black hole (see Right panel in Fig. 3.4). It is well known that pair creation by vacuum polarization process can occur in a Kerr-Newman black hole (Damour and Ruffini, 1975; Ruffini et al., 2010d).

We consequently assume, within the fireshell model, that all GRBs originate from an optically thick $e^{\pm}$ plasma with total energy $E_{tot}^{e^{\pm}}$ in the range 10^{49}–10^{54} ergs and a temperature T in the range 1–4 MeV (Preparata et al., 1998). Such an $e^{\pm}$ plasma has been widely adopted in the current literature (see e.g. Refs. Piran, 2005; Meszaros, 2006, and references therein). After an early expansion, the $e^{\pm}$-photon plasma reaches thermal equilibrium with the engulfed baryonic matter M_B described by the dimensionless parameter $B = M_B c^2 / E_{tot}^{e^{\pm}}$, that must be $B < 10^{-2}$ (Ruffini et al., 1999b, 2000). As the optically thick fireshell composed by $e^{\pm}$-photon-baryon plasma self-accelerate to ultrarelativistic velocities, it finally reaches the transparency condition. A flash of radiation is then emitted. This is the P-GRB (Ruffini et al., 2001b). Different current theoretical treatments of these early expansion phases of GRBs are compared and contrasted in Bianco et al. (2006c) and Ruffini et al. (2008a). The amount of energy radiated in the P-GRB is only a fraction of the initial energy $E_{tot}^{e^{\pm}}$. The remaining energy is stored in the kinetic energy of the optically thin baryonic and leptonic matter fireshell that, by inelastic collisions with the CBM, gives rise to a multi-wavelength emission. This is the extended afterglow. It presents three different regimes: a rising part, a peak and a decaying tail. We therefore define a "canonical GRB" light curve with two sharply different components (see Fig. 6.1) (Ruffini et al., 2001b, 2007a; Bernardini et al., 2007; Bianco et al., 2008a,b): 1) the P-GRB and 2) the extended afterglow.

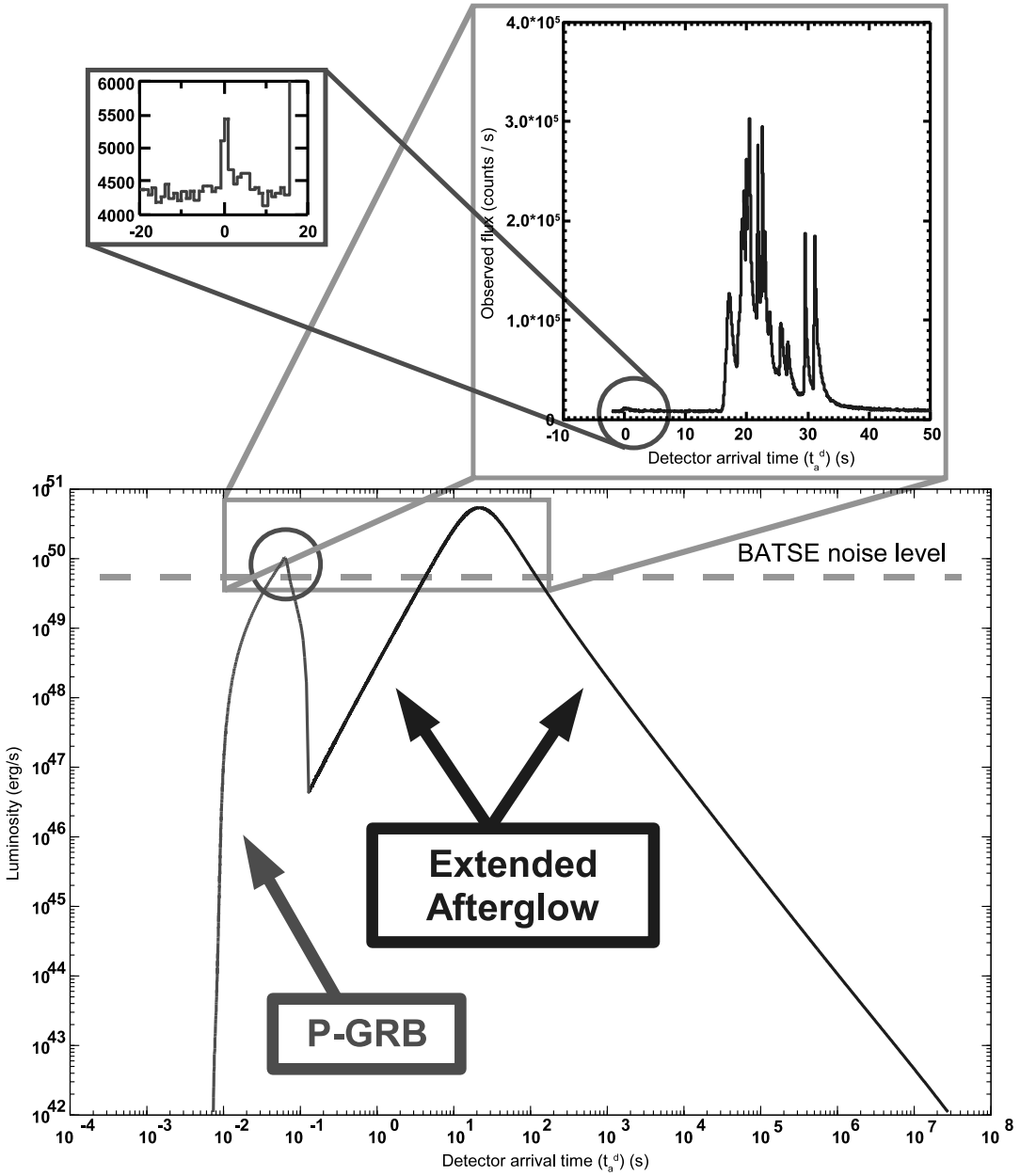

Figure 6.1.: The "canonical GRB" light curve theoretically computed for GRB 991216. The prompt emission observed by BATSE is identified with the peak of the extended afterglow, while the small precursor is identified with the P-GRB. For this source we have $E^{tot}_{e^\pm} = 4.83 \times 10^{53}$ ergs, $B \simeq 3.0 \times 10^{-3}$ and $\langle n_{cbm} \rangle \sim 1.0$ particles/cm^3. Details in Ruffini et al. (2001b, 2002, 2007a).

What is usually called "Prompt emission" in the current literature mixes the P-GRB with the raising part and the peak of the extended afterglow. Such an unjustified mixing of these components, originating from different physical processes, leads to difficulties in the current models of GRBs, and can as well be responsible for some of the intrinsic scatter observed in the Amati relation (Amati, 2006; Guida et al., 2008b, , see also below, section *Theoretical background for GRBs' empirical correlations*).

6.1. The optically thick phase

In Fig. 6.2 we present the evolution of the optically thick fireshell Lorentz γ factor as a function of the external radius for 7 different values of the fireshell baryon loading B and two selected limiting values of the total energy $E^{tot}_{e^\pm}$ of the $e^\pm$ plasma. We can identify three different eras:

1. **Era I:** The fireshell is made only of electrons, positrons and photons in thermodynamical equilibrium (the "pair-electromagnetic pulse", or PEM pulse for short). It self-accelerate and begins its expansion into vacuum, because the environment has been cleared by the black hole collapse. The Lorentz γ factor increases with radius and the dynamics can be described by the energy conservation and the condition of adiabatic expansion (Ruffini et al., 1999b; Bianco et al., 2006c):

$$T^{0\nu}{}_{,\nu} = 0 \tag{6.1.1}$$

$$\frac{\epsilon_\circ}{\epsilon} = \left(\frac{V}{V_\circ}\right)^\Gamma = \left(\frac{\mathcal{V}\gamma}{\mathcal{V}_\circ\gamma_\circ}\right)^\Gamma \tag{6.1.2}$$

   where $T^{\mu\nu}$ is the energy-momentum tensor of the e^+e^- plasma (assumed to be a perfect fluid), ϵ is its internal energy density, V and $\mathcal{V}$ are its volumes in the co-moving and laboratory frames respectively, Γ is the thermal index and the quantities with and without the $\circ$ subscript are measured at two different times during the expansion.

2. **Era II:** The fireshell impacts with the non-collapsed bayonic remnants and engulfs them. The Lorentz γ factor drops. The dynamics of this era can be described by imposing energy and momentum conservation during the fully inelastic collision between the fireshell and the baryonic remnant. For the fireshell solution to be still valid, it must be $B \lesssim 10^{-2}$ (Ruffini et al., 2000).

3. **Era III:** The fireshell is now made of electrons, positrons, baryons and photons in thermodynamical equilibrium (the "pair-electromagnetic-

baryonic pulse", or PEMB pulse for short). It self-accelerate again and the Lorentz γ factor increases again with radius up to when the transparency condition is reached, going to an asymptotic value $\gamma_{asym} = 1/B$. If $B \sim 10^{-2}$ the transparency condition is reached when $\gamma \sim \gamma_{asym}$. On the other hand, when $B < 10^{-2}$, the transparency condition is reached much before γ reaches its asymptotic value (Ruffini et al., 2000, 2001b, , see next section for details). In this era the dynamical equations are the same of the first one, together with the baryon number conservation:

$$T^{0\nu}{}_{,\nu} = 0 \tag{6.1.3}$$

$$\frac{\epsilon_\circ}{\epsilon} = \left(\frac{V}{V_\circ}\right)^\Gamma = \left(\frac{\mathcal{V}\gamma}{\mathcal{V}_\circ\gamma_\circ}\right)^\Gamma \tag{6.1.4}$$

$$\frac{n_B^\circ}{n_B} = \frac{V}{V_\circ} = \frac{\mathcal{V}\gamma}{\mathcal{V}_\circ\gamma_\circ} \tag{6.1.5}$$

where n_B is the baryon number density in the fireshell. In this era it starts to be crucial the contribution of the rate equation to describe the annihilation of the e^+e^- pairs:

$$\frac{\partial}{\partial t}N_{e^\pm} = -N_{e^\pm}\frac{1}{\mathcal{V}}\frac{\partial\mathcal{V}}{\partial t} + \overline{\sigma v}\frac{1}{\gamma^2}\left(N_{e^\pm}^2(T) - N_{e^\pm}^2\right) \tag{6.1.6}$$

where $N_{e^\pm}$ is the number of e^+e^- pairs and $N_{e^\pm}(T)$ is the number of e^+e^- pairs at thermal equilibrium at temperature T (Ruffini et al., 2000; Bianco et al., 2006c).

In the "fireball" model in the current literature the baryons are usually considered present in the plasma since the beginning. In other words, in the fireball dynamics there is only one era corresponding to the Era III above (Meszaros et al., 1993; Shemi and Piran, 1990; Piran et al., 1993; Bianco et al., 2006c). Moreover, the rate equation is usually neglected, and this affects the reaching of the transparency condition. A detailed comparison between the different approaches is reported in Bianco et al. (2006c).

6.2. The transparency point

At the transparency point, the value of the B parameter rules the ratio between the energetics of the P-GRB and the kinetic energy of the baryonic and leptonic matter giving rise to the extended afterglow. It rules as well the time separation between the corresponding peaks (Ruffini et al., 2001b, 2008a).

We have recently shown (Aksenov et al., 2009) that a thermal spectrum still occurs in presence of $e^\pm$ pairs and baryons. By solving the rate equation we

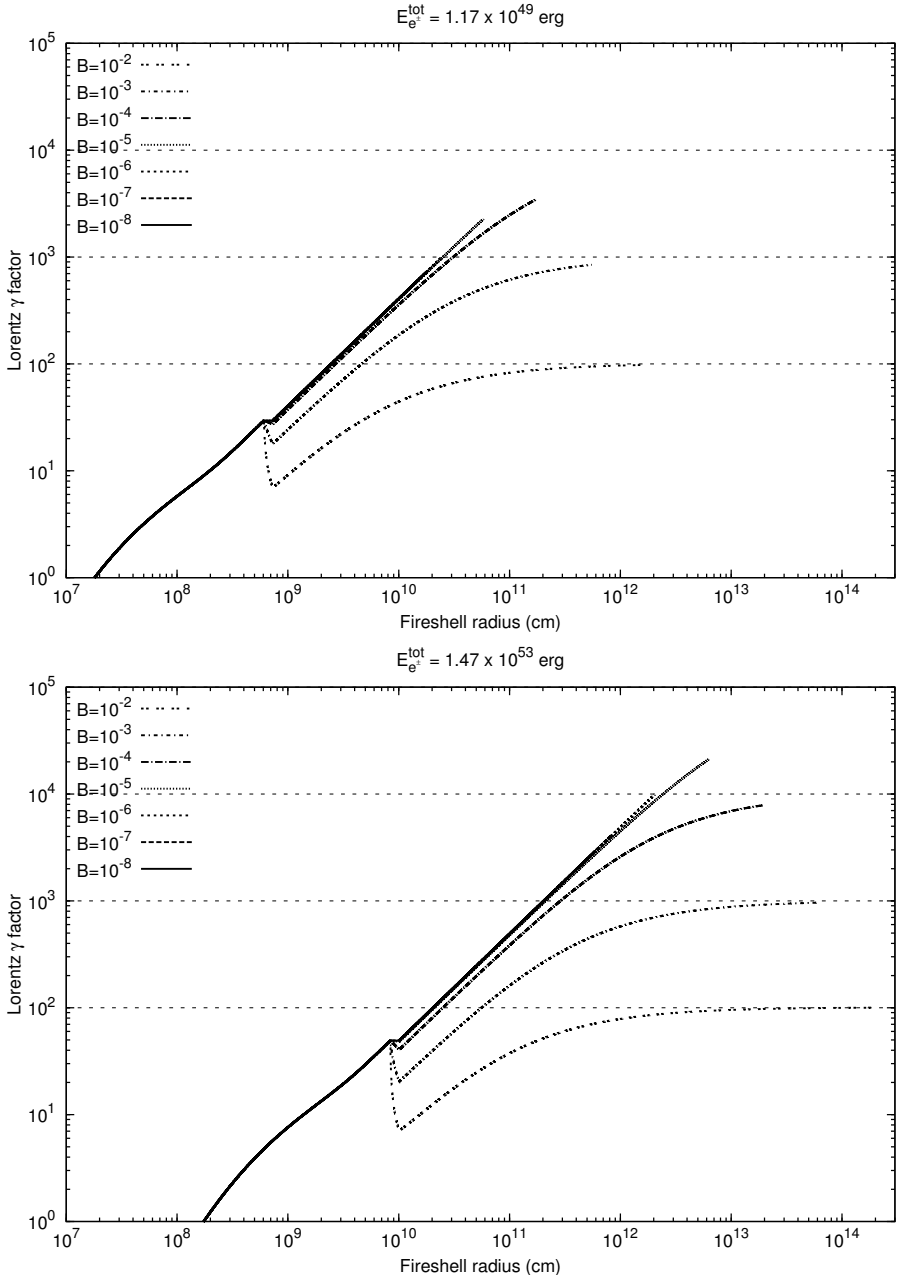

Figure 6.2.: The Lorentz γ factor of the expanding fireshell is plotted as a function of its external radius for 7 different values of the fireshell baryon loading B, ranging from $B = 10^{-8}$ and $B = 10^{-2}$, and two selected limiting values of the total energy $E^{tot}_{e^\pm}$ of the $e^\pm$ plasma: $E^{tot}_{e^\pm} = 1.17 \times 10^{49}$ ergs (upper panel) and $E^{tot}_{e^\pm} = 1.47 \times 10^{53}$ ergs (lower panel). The asymptotic values $\gamma \rightarrow 1/B$ are also plotted (dashed horizontal lines). The lines are plotted up to when the fireshell transparency is reached.

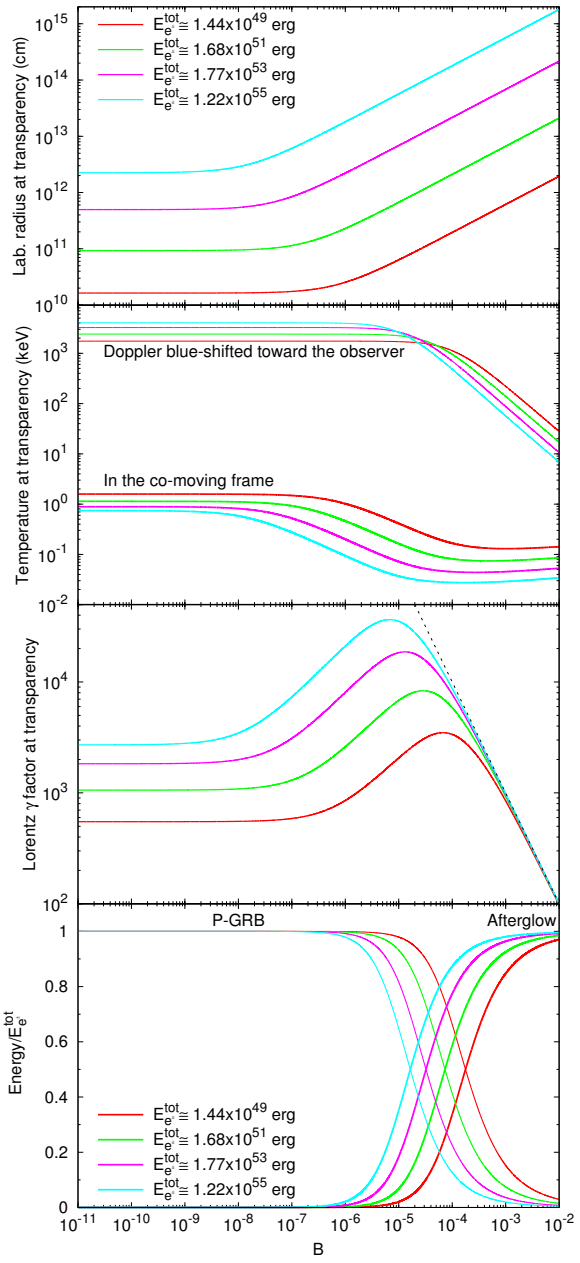

Figure 6.3.: At the fireshell transparency point, for 4 different values of $E^{tot}_{e^\pm}$, we plot as a function of B, from top panel to bottom one: The fireshell radius in the laboratory frame; the fireshell temperature in the co-moving frame $T^{com}_\circ$ (thicker lines) and the one Doppler blue-shifted along the line of sight toward the observer in the source cosmological rest frame $T^{obs}_\circ$ (thinner lines); The fireshell Lorentz gamma factor $\gamma_\circ$ together with the asymptotic value $\gamma_\circ = 1/B$; The energy radiated in the P-GRB (thinner lines, rising when B decreases) and the one converted into baryonic kinetic energy and later emitted in the extended afterglow (thicker lines, rising when B increases), in units of $E^{tot}_{e^\pm}$.

have evaluated the evolution of the temperature during the fireshell expansion, all the way up to when the transparency condition is reached (Ruffini et al., 1999b, 2000). In the first panel of Fig. 6.3 we plot, as a function of B, the fireshell radius at the transparency point. The plot is drawn for four different values of $E_{e^\pm}^{tot}$ in the interval $[10^{49}, 10^{55}]$ ergs, well encompassing GRBs' observed isotropic energies.

In the second panel of Fig. 6.3 we plot, as a function of B, the fireshell temperature $T_\circ$ at the transparency point, i.e. the temperature of the P-GRB radiation. The plot is drawn for the same four different values of $E_{e^\pm}^{tot}$ of the upper panel. We plot both the value in the co-moving frame $T_\circ^{com}$ and the one Doppler blue-shifted toward the observed $T_\circ^{obs} = (1+\beta_\circ)\gamma_\circ T_\circ^{com}$, where $\beta_\circ$ is the fireshell speed at the transparency point in units of c (Ruffini et al., 2000).

In the middle panel of Fig. 6.3 we plot, as a function of B, the fireshell Lorentz gamma factor at the transparency point $\gamma_\circ$. The plot is drawn for the same four different values of $E_{e^\pm}^{tot}$ of the upper panel. Also plotted is the asymptotic value $\gamma_\circ = 1/B$, which corresponds to the condition when the entire initial internal energy of the plasma $E_{e^\pm}^{tot}$ has been converted into kinetic energy of the baryons (Ruffini et al., 2000). We see that such an asymptotic value is approached for $B \to 10^{-2}$. We see also that, if $E_{e^\pm}^{tot}$ increases, the maximum values of $\gamma_\circ$ are higher and they are reached for lower values of B.

In the lower panel of Fig. 6.3 we plot, as a function of B, the total energy radiated at the transparency point in the P-GRB and the one converted into baryonic and leptonic kinetic energy and later emitted in the extended afterglow. The plot is drawn for the same four different values of $E_{e^\pm}^{tot}$ of the upper panel and middle panels. We see that for $B \lesssim 10^{-5}$ the total energy emitted in the P-GRB is always larger than the one emitted in the extended afterglow. In the limit $B \to 0$ it gives rise to a "genuine" short GRB (see also Fig. 6.4). On the other hand, for $3.0 \times 10^{-4} \lesssim B < 10^{-2}$ the total energy emitted in the P-GRB is always smaller than the one emitted in the extended afterglow. If it is not below the instrumental threshold and if $n_{cbm} \sim 1$ particle/cm^3, the P-GRB can be observed in this case as a small pulse preceding the main GRB event (which coincides with the peak of the extended afterglow), i.e. as a GRB "precursor" (Ruffini et al., 2001b, 2003a; Bianco et al., 2008b; Ruffini et al., 2008a; Bernardini et al., 2007; Bianco et al., 2008c).

Particularly relevant for the new era of the *Agile* and *GLAST* satellites is that for $B < 10^{-3}$ the P-GRB emission has an observed temperature up to 10^3 keV or higher. This high-energy emission has been unobservable by the *Swift* satellite.

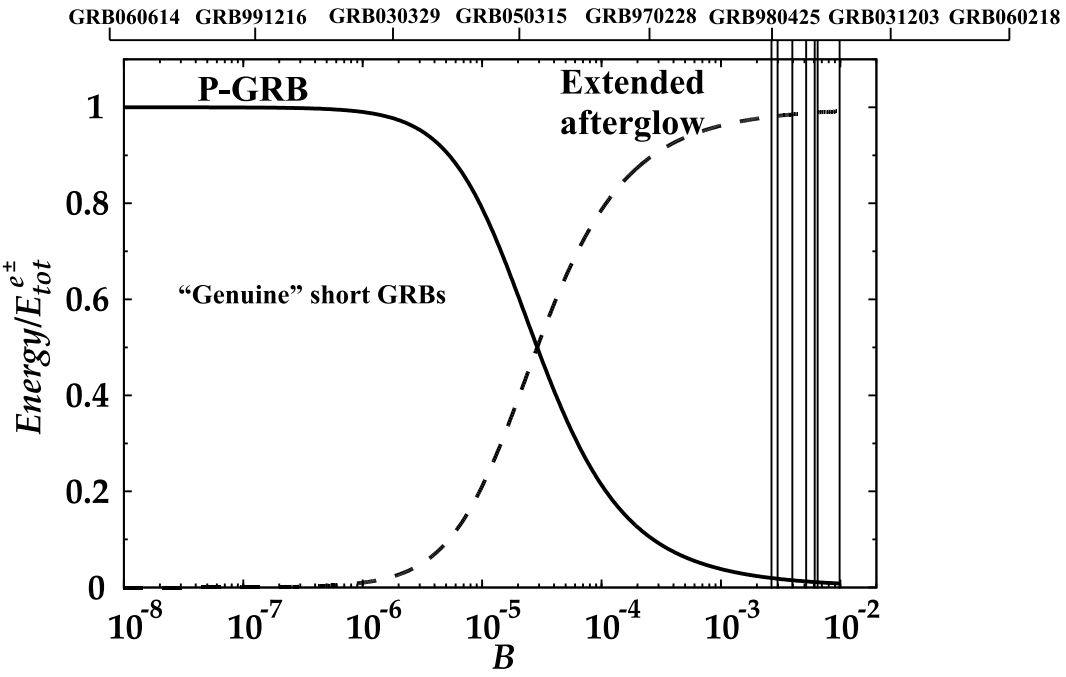

Figure 6.4.: Here the energies emitted in the P-GRB (solid line) and in the extended afterglow (dashed line), in units of the total energy of the plasma, are plotted as functions of the B parameter for a typical value of $E_{e^\pm}^{tot} \sim 10^{53}$ erg (see lower panel of Fig. 6.3). When $B \lesssim 10^{-5}$, the P-GRB becomes predominant over the extended afterglow, giving rise to a "genuine" short GRB. In the figure are also marked the values of the B parameters corresponding to some GRBs we analyzed, all belonging to the class of long GRBs.

6.3. The optically thin phase

The dynamics of the optically thin fireshell of baryonic matter propagating in the CBM can be obtained from the relativistic conservation laws of energy and momentum (see e.g. Ref. Bianco and Ruffini, 2005b):

$$\begin{cases} dE_{\rm int} = (\gamma - 1)\, dM_{\rm cbm} c^2 \\ d\gamma = -\dfrac{\gamma^2 - 1}{M} dM_{\rm cbm} \\ dM = \dfrac{1-\varepsilon}{c^2} dE_{\rm int} + dM_{\rm cbm} \\ dM_{\rm cbm} = 4\pi m_p n_{\rm cbm} r^2 dr \end{cases} \tag{6.3.1}$$

where γ, $E_{\rm int}$ and M are the pulse Lorentz gamma factor, internal energy and mass-energy respectively, $n_{\rm cbm}$ is the CBM number density, m_p is the proton mass, ε is the emitted fraction of the energy developed in the collision with the CBM and $M_{\rm cbm}$ is the amount of CBM mass swept up within the radius r: $M_{\rm cbm} = m_p n_{\rm cbm} (4\pi/3)(r^3 - {r_\circ}^3)$, where $r_\circ$ is the starting radius of the shock front.

In both our approach and in the other ones in the current literature (see e.g. Refs. Piran, 1999; Chiang and Dermer, 1999; Bianco and Ruffini, 2005b,a; Ruffini et al., 2007a) such conservations laws are used. The main difference is that in the current literature an ultra-relativistic approximation, following the Blandford and McKee (1976) self-similar solution, is widely adopted, leading to a simple constant-index power-law relations between the Lorentz γ factor of the optically thin "fireshell" and its radius:

$$\gamma \propto r^{-a}\,, \tag{6.3.2}$$

with $a = 3$ in the fully radiative case and $a = 3/2$ in the adiabatic case (Piran, 1999; Bianco and Ruffini, 2005a). On the contrary, we use the exact solutions of the equations of motion of the fireshell (Bianco and Ruffini, 2004, 2005b,a, 2006; Ruffini et al., 2007a). In the adiabatic regime ($\varepsilon = 0$) we get:

$$\gamma^2 = \frac{\gamma_\circ^2 + 2\gamma_\circ \left(M_{\rm cbm}/M_B\right) + \left(M_{\rm cbm}/M_B\right)^2}{1 + 2\gamma_\circ \left(M_{\rm cbm}/M_B\right) + \left(M_{\rm cbm}/M_B\right)^2}\,, \tag{6.3.3}$$

where $\gamma_\circ$ and M_B are respectively the values of the Lorentz gamma factor and of the mass of the accelerated baryons at the beginning of the afterglow phase. In the fully radiative regime ($\varepsilon = 1$), instead, we have:

$$\gamma = \frac{1 + \left(M_{\rm cbm}/M_B\right)\left(1 + \gamma_\circ^{-1}\right)\left[1 + (1/2)\left(M_{\rm cbm}/M_B\right)\right]}{\gamma_\circ^{-1} + \left(M_{\rm cbm}/M_B\right)\left(1 + \gamma_\circ^{-1}\right)\left[1 + (1/2)\left(M_{\rm cbm}/M_B\right)\right]}\,. \tag{6.3.4}$$

A detailed comparison between the equations used in the two approaches has been presented by Bianco and Ruffini (2004, 2005b,a, 2006). In particular, Bianco and Ruffini (2005a) show that the regime represented in Eq.(6.3.2) is reached only asymptotically when $\gamma_\circ \gg \gamma \gg 1$ in the fully radiative regime and $\gamma_\circ^2 \gg \gamma^2 \gg 1$ in the adiabatic regime, where $\gamma_\circ$ the initial Lorentz gamma factor of the optically thin fireshell.

In Fig. 6.5 we show the differences between the two approaches. In the upper panel there are plotted the exact solutions for the fireshell dynamics in the fully radiative and adiabatic cases. In the lower panel we plot the corresponding "effective" power-law index a_{eff}, defined as the index of the power-law tangent to the exact solution (Bianco and Ruffini, 2005a):

$$a_{eff} = -\frac{d\ln\gamma}{d\ln r}\,. \tag{6.3.5}$$

Such an "effective" power-law index of the exact solution smoothly varies from 0 to a maximum value which is always smaller than 3 or 3/2, in the fully radiative and adiabatic cases respectively, and finally decreases back to 0 (see Fig. 6.5).

6.4. Extended afterglow luminosity and spectrum

The extended afterglow luminosity in the different energy bands is governed by two quantities associated to the environment. Within the fireshell model, these are the effective CBM density profile, n_{cbm}, and the ratio between the effective emitting area A_{eff} and the total area A_{tot} of the expanding baryonic and leptonic shell, $\mathcal{R} = A_{eff}/A_{tot}$. This last parameter takes into account the CBM filamentary structure (Ruffini et al., 2004b, 2005c) and the possible occurrence of a fragmentation in the shell (Dainotti et al., 2007).

Within the "fireshell" model, in addition to the determination of the baryon loading, it is therefore possible to infer a detailed description of the CBM, its average density and its porosity and filamentary structure, all the way from the black hole horizon to distance $r \lesssim 10^{17}$ cm. This corresponds to the prompt emission. This description is lacking in the traditional model based on the synchrotron emission. The attempt to use the internal shock model for the prompt emission (see e.g. Refs. Rees and Meszaros, 1994; Piran, 2005; Meszaros, 2006, and references therein) only applies to regions where $r > 10^{17}$ cm (Kumar and McMahon, 2008).

In our hypothesis, the emission from the baryonic and leptonic matter shell is spherically symmetric. This allows us to assume, in a first approximation, a modeling of thin spherical shells for the CBM distribution and consequently to consider just its radial dependence (Ruffini et al., 2002). For simplicity, and in order to have an estimate of the energetics, the emission process is

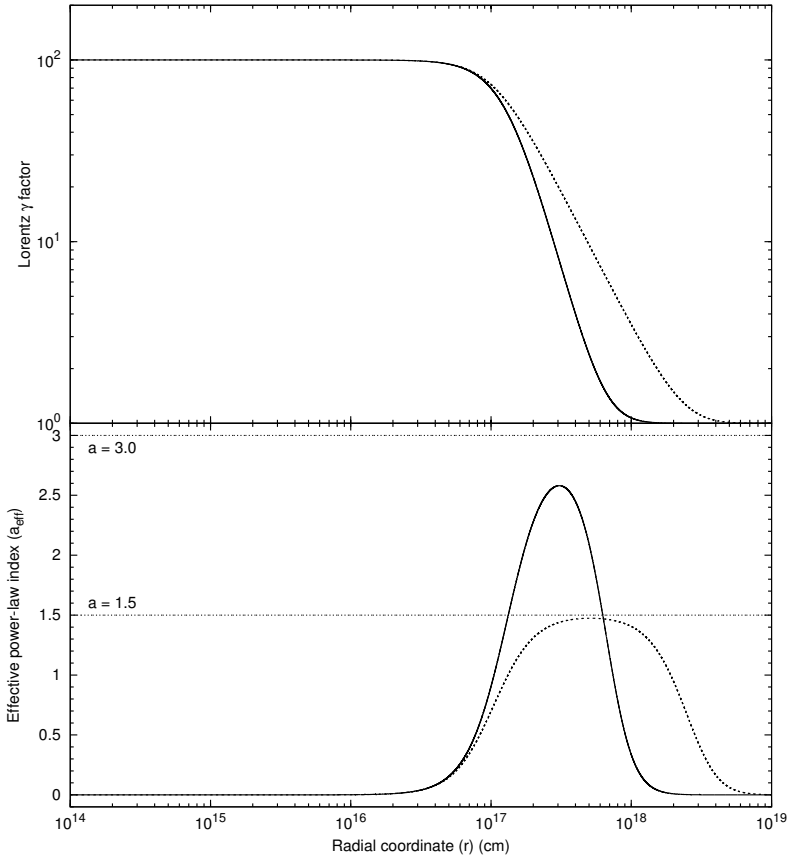

Figure 6.5.: In the upper panel, the analytic behavior of the Lorentz γ factor during the afterglow era is plotted versus the radial coordinate of the expanding optically thin fireshell in the fully radiative case (solid line) and in the adiabatic case (dotted line) starting from $\gamma_\circ = 10^2$ and the same initial conditions as GRB 991216 (Bianco and Ruffini, 2005a). In the lower panel are plotted the corresponding values of the "effective" power-law index a_{eff} (see Eq.(6.3.5)), which is clearly not constant, is highly varying and systematically lower than the constant values 3 and 3/2 purported in the current literature (horizontal thin dotted lines).

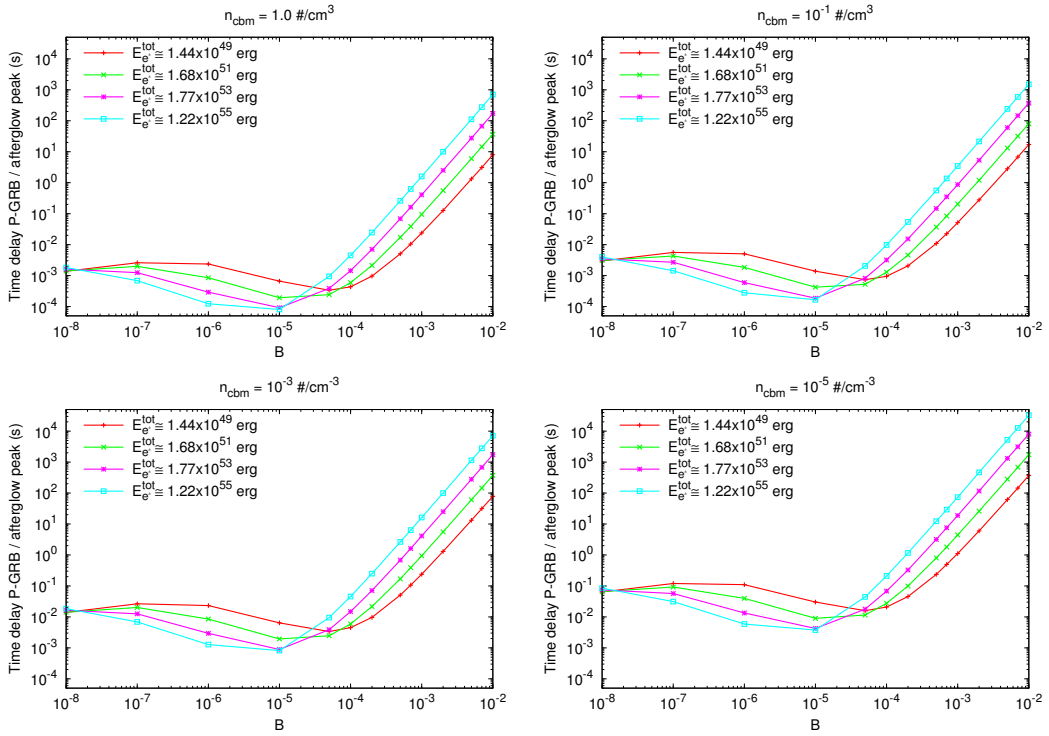

Figure 6.6.: For 4 different values of $E_{e^\pm}^{tot}$, we plot as a function of B the arrival time separation Δt_a between the P-GRB and the peak of the extended afterglow (i.e. the "quiescent time between the "precursor" and the main GRB event), measured in the source cosmological rest frame. The computation has been performed assuming a constant value of the CBM density in four different cases: $n_{cbm} = 1.0$ particles/cm^3, $n_{cbm} = 1.0 \times 10^{-3}$ particles/cm^3, $n_{cbm} = 1.0 \times 10^{-5}$ particles/cm^3, $n_{cbm} = 1.0 \times 10^{-7}$ particles/cm^3. The points represents the actually numerically computed values, connected by straight line segments.

postulated to be thermal in the co-moving frame of the shell (Ruffini et al., 2004b). We are currently examining a departure from this basic mechanism by taking into account inverse Compton effects due to the electron collisions with the thermal photons. The observed GRB non-thermal spectral shape is due to the convolution of an infinite number of thermal spectra with different temperatures and different Lorentz and Doppler factors. Such a convolution is to be performed over the surfaces of constant arrival time of the photons at the detector (EQuiTemporal Surfaces, EQTSs; see e.g. Ref. Bianco and Ruffini, 2005b) encompassing the whole observation time (Bernardini et al., 2005a).

In Fig. 6.6 we plot, as a function of B, the arrival time separation Δt_a between the P-GRB and the peak of the extended afterglow measured in the cosmological rest frame of the source. Such a time separation Δt_a is the "quiescent time" between the precursor (i.e. the P-GRB) and the main GRB event

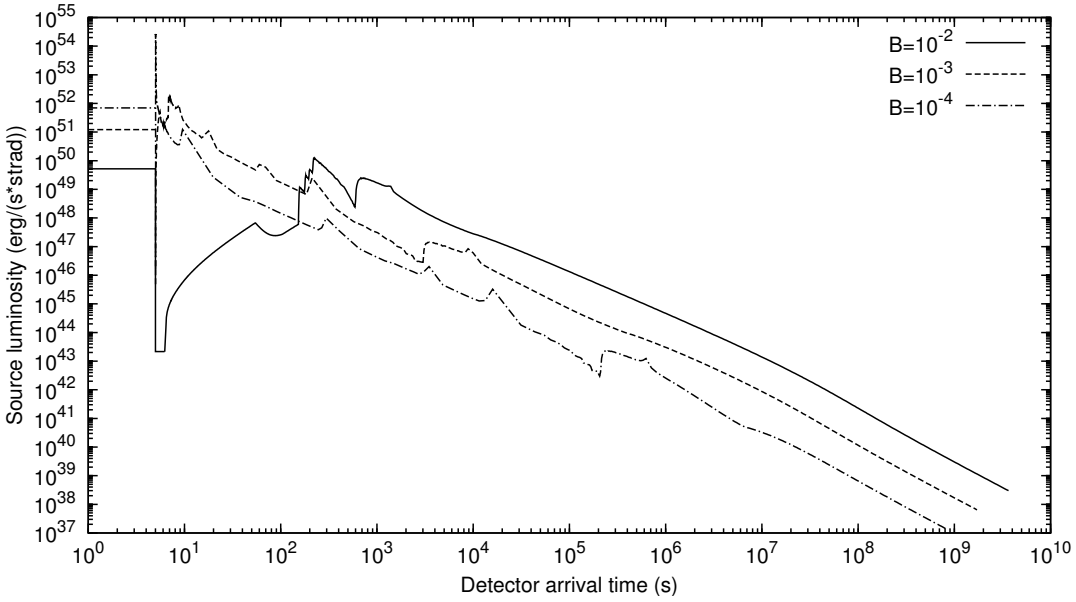

Figure 6.7.: We plot three theoretical extended afterglow bolometric light curves together with the corresponding P-GRB peak luminosities (the horizontal segments). The computations have been performed assuming the same $E^{tot}_{e^\pm}$ and CBM structure of GRB 991216 and three different values of B. The P-GRBs have been assumed to have the same duration in the three cases, i.e. 5 s. For B decreasing, the extended afterglow light curve squeezes itself on the P-GRB.

(i.e. the peak of the extended afterglow). The plot is drawn for the same four different values of $E^{tot}_{e^\pm}$ of Fig. 6.3. The arrival time of the peak of the extended afterglow emission depends on the detailed profile of the CBM density. In this plot it has been assumed a constant CBM density in four different cases: $n_{cbm} = 1.0$ particles/cm^3, $n_{cbm} = 1.0 \times 10^{-3}$ particles/cm^3, $n_{cbm} = 1.0 \times 10^{-5}$ particles/cm^3, $n_{cbm} = 1.0 \times 10^{-7}$ particles/cm^3. We can see that, for $3.0 \times 10^{-4} \lesssim B < 10^{-2}$, which is the condition for P-GRBs to be "precursors" (see above), Δt_a increases both with B and with $E^{tot}_{e^\pm}$. We can have $\Delta t_a > 10^2$ s and, in some extreme cases even $\Delta t_a \sim 10^3$ s. For $B \lesssim 3.0 \times 10^{-4}$, instead, Δt_a presents a behavior which qualitatively follows the opposite of $\gamma_\circ$ (see middle panel of Fig. 6.3).

Finally, in Fig. 6.7 we present three theoretical extended afterglow bolometric light curves together with the corresponding P-GRB peak luminosities for three different values of B. The duration of the P-GRBs has been assumed to be the same in the three cases (i.e. 5 s). The computations have been performed assuming the same $E^{tot}_{e^\pm}$ and the same detailed CBM density profile of GRB 991216 (Ruffini et al., 2003a). In this picture we clearly see how, for B decreasing, the extended afterglow light curve "squeezes" itself on the P-GRB and the P-GRB peak luminosity increases.

The "prompt emission" light curves of many GRBs present a small pulse preceding the main GRB event, with a lower peak flux and separated by this last one by a quiescent time. The nature of such GRB "precursors" is one of the most debated issues in the current literature (see e.g. Refs. Burlon et al., 2008; Ruffini et al., 2008a). Already in 2001 (Ruffini et al., 2001b), within the "fireshell" model, we proposed that GRB "precursors" are the P-GRBs emitted when the fireshell becomes transparent, and we gave precise estimates of the time sequence and intensities of the P-GRB and of the extended afterglow, recalled above.

The radiation viewed in the co-moving frame of the accelerated baryonic matter is assumed to have a thermal spectrum and to be produced by the interaction of the CBM with the front of the expanding baryonic shell (Ruffini et al., 2004b). In Bernardini et al. (2005a) it is shown that, although the instantaneous spectrum in the co-moving frame of the optically thin fireshell is thermal, the shape of the final instantaneous spectrum in the laboratory frame is non-thermal. In fact, as explained in Ruffini et al. (2004b), the temperature of the fireshell is evolving with the co-moving time and, therefore, each single instantaneous spectrum is the result of an integration of hundreds of thermal spectra with different temperature over the corresponding EQTS. This calculation produces a non thermal instantaneous spectrum in the observer frame (Bernardini et al., 2005a). Another distinguishing feature of the GRBs spectra which is also present in these instantaneous spectra is the hard to soft transition during the evolution of the event (Crider et al., 1997; Piran, 1999; Frontera et al., 2000; Ghirlanda et al., 2002). In fact the peak of the energy distributions E_p drift monotonically to softer frequencies with time (Bernardini et al., 2005a). This feature explains the change in the power-law low energy spectral index (Band et al., 1993) α which at the beginning of the prompt emission of the burst ($t_a^d = 2$ s) is $\alpha = 0.75$, and progressively decreases for later times (Bernardini et al., 2005a). In this way the link between E_p and α identified in Crider et al. (1997) is explicitly shown.

The time-integrated observed GRB spectra show a clear power-law behavior. Within a different framework (see e.g. Ref. Pozdniakov et al., 1983, and references therein) it has been argued that it is possible to obtain such power-law spectra from a convolution of many non power-law instantaneous spectra monotonically evolving in time. This result was recalled and applied to GRBs (Blinnikov et al., 1999) assuming for the instantaneous spectra a thermal shape with a temperature changing with time. It was shown that the integration of such energy distributions over the observation time gives a typical power-law shape possibly consistent with GRB spectra.

Our specific quantitative model is more complicated than the one considered by Blinnikov et al. (1999): the instantaneous spectrum here is not a black body. Each instantaneous spectrum is obtained by an integration over the corresponding EQTS: (Bianco and Ruffini, 2004, 2005b) it is itself a convolution, weighted by appropriate Lorentz and Doppler factors, of $\sim 10^6$ thermal

spectra with variable temperature. Therefore, the time-integrated spectra are not plain convolutions of thermal spectra: they are convolutions of convolutions of thermal spectra (Ruffini et al., 2004b; Bernardini et al., 2005a). In Fig. 6.8 we present the photon number spectrum $N(E)$ time-integrated over the 20 s of the whole duration of the prompt event of GRB 031203 observed by INTEGRAL (Sazonov et al., 2004a): in this way we obtain a typical non-thermal power-law spectrum which results to be in good agreement with the INTEGRAL data (Sazonov et al., 2004a; Bernardini et al., 2005a) and gives a clear evidence of the possibility that the observed GRBs spectra are originated from a thermal emission (Bernardini et al., 2005a)

Before closing, we like to mention that, using the diagrams represented in Figs. 6.3-6.6, in principle one can compute the two free parameters of the fireshell model, namely $E^{tot}_{e^\pm}$ and B, from the ratio between the total energies of the P-GRB and of the extended afterglow and from the temporal separation between the peaks of the corresponding bolometric light curves. None of these quantities depends on the cosmological model. Therefore, one can in principle use this method to compute the GRBs' intrinsic luminosity and make GRBs the best cosmological distance indicators available today. The increase of the number of observed sources, as well as the more accurate knowledge of their CBM density profiles, will possibly make viable this procedure to test cosmological parameters, in addition to the Amati relation (Amati et al., 2008; Guida et al., 2008b).

6.5. The new class of "disguised" short GRBs

In the context of the fireshell model, we considered a new class of GRBs, pioneered by Norris and Bonnell (2006). This class is characterized by an occasional softer extended emission after an initial spike-like emission. The softer extended emission has a peak luminosity lower than the one of the initial spike-like emission. As shown in the prototypical case of GRB 970228 (Bernardini et al., 2007) and then in GRB 060614 (Caito et al., 2009), we can identify the initial spike-like emission with the P-GRB and the softer extended emission with the peak of the extended afterglow. That the time-integrated extended afterglow luminosity is much larger than the P-GRB one is crucial. This unquestionably identifies GRB 970228 and GRB 060614 as canonical GRBs with $B > 10^{-4}$. The consistent application of the fireshell model allows us to infer the CBM filamentary structure and average density, which, in that specific case, is $n_{cbm} \sim 10^{-3}$ particles/cm^3 (Bernardini et al., 2007). This low CBM density value explains the peculiarity of the low extended afterglow peak luminosity and its more protracted time evolution. These features are not intrinsic to the progenitor, but depend uniquely on the peculiarly low value of the CBM density. This led us to expand the traditional classification of GRBs to three classes: "genuine" short GRBs, "fake" or

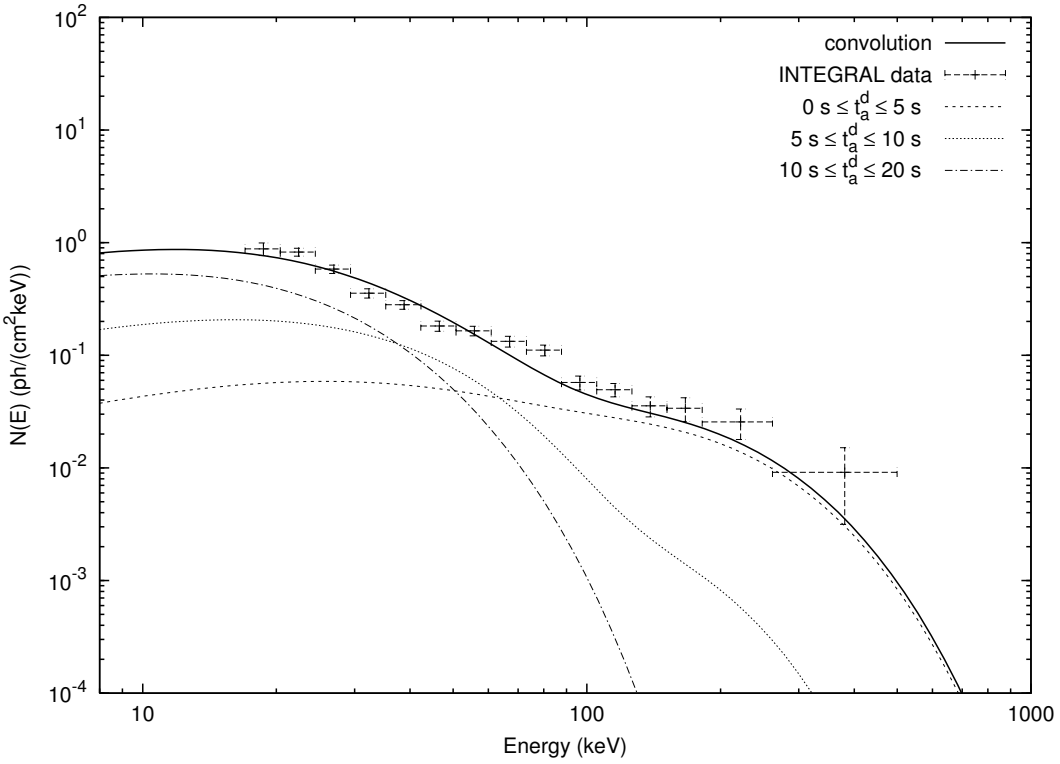

Figure 6.8.: Three theoretically predicted time-integrated photon number spectra $N(E)$, computed for GRB 031203 (Bernardini et al., 2005a), are here represented for $0 \leq t_a^d \leq 5$ s, $5 \leq t_a^d \leq 10$ s and $10 \leq t_a^d \leq 20$ s (dashed and dotted curves), where t_a^d is the photon arrival time at the detector (Ruffini et al., 2001c; Bernardini et al., 2005a). The hard to soft behavior is confirmed. Moreover, the theoretically predicted time-integrated photon number spectrum $N(E)$ corresponding to the first 20 s of the "prompt emission" (black bold curve) is compared with the data observed by INTEGRAL (Sazonov et al., 2004a). This curve is obtained as a convolution of 108 instantaneous spectra, which are enough to get a good agreement with the observed data. Details in Bernardini et al. (2005a).

"disguised" short GRBs, and the remaining "long duration" ones.

A CBM density $n_{cbm} \sim 10^{-3}$ particles/cm^3 is typical of a galactic halo environment, and GRB 970228 was indeed found to be in the halo of its host galaxy (Sahu et al., 1997; van Paradijs et al., 1997). We therefore proposed that the progenitors of this new class of "disguised" short GRBs are merging binary systems, formed by neutron stars and/or white dwarfs in all possible combinations, which spiraled out from their birth place into the halo (see Bernardini et al., 2007; Caito et al., 2009; Kramer, 2008). This hypothesis can also be supported by other observations. Assuming that the soft tail peak luminosity is directly related to the CBM density, GRBs displaying a prolonged soft tail should have a systematically smaller offset from the center of their host galaxy. Some observational evidence was found in this sense (Troja et al., 2008). However, the present sample of observations does not enable us to derive any firm conclusion that short GRBs with extended emission have smaller physical offsets than those without extended emission (Fong et al., 2010; Berger, 2010).

6.6. The "fireshell" model and GRB progenitors

We have recalled in the introduction that "long" GRBs are traditionally related in the current literature to the idea of a single progenitor, identified as a "collapsar" (Woosley, 1993). Similarly, short GRBs are assumed to originate from binary mergers formed by white dwarfs, neutron stars, and black holes in all possible combinations. It also has been suggested that short and long GRBs originate from different galaxy types. In particular, short GRBs are proposed to be associated with galaxies with low specific star forming rate (see e.g. Berger, 2009). Some evidence against such a scenario have been advanced, due to the small sample size and the different estimates of the star forming rates (see e.g. Savaglio et al., 2009). However, the understanding of GRB structure and of its relation to the CBM distribution, within the fireshell model, leads to a more complex and interesting perspective than the one in the current literature.

The first general conclusion of the "fireshell" model (Ruffini et al., 2001b) is that, while the time scale of "short" GRBs is indeed intrinsic to the source, this does not happen for the "long" GRBs: their time scale is clearly only a function of the instrumental noise threshold. This has been dramatically confirmed by the observations of the Swift satellite (Ruffini et al., 2006a). Among the traditional classification of "long" GRBs we distinguish two different subclasses of events, neither of which originates from collapsars.

The first sub-class contains "long" GRBs that are particularly weak ($E_{iso} \sim 10^{50}$ erg) and associated with SN Ib/c. In fact, it has been often proposed that such GRBs, only observed at smaller redshift $0.0085 < z < 0.168$, form a different class, less luminous and possibly much more numerous than the high

luminosity GRBs at higher redshift (Pian et al., 2006; Soderberg et al., 2004; Maeda et al., 2007; Della Valle, 2006). Therefore in the current literature they have been proposed to originate from a separate class of progenitors (Liang et al., 2007; Cobb et al., 2006). Within our "fireshell" model, they originate in a binary system formed by a neutron star, close to its critical mass, and a companion star, evolved out of the main sequence. They produce GRBs associated with SNe Ib/c, via the "induced gravitational collapse" process (Ruffini et al., 2001a). The low luminosity of these sources is explained by the formation of a black hole with the smallest possible mass: the one formed by the collapse of a just overcritical neutron star (Ruffini et al., 2007b; Dainotti et al., 2007).

A second sub-class of "long" GRBs originates from merging binary systems, formed either by two neutron stars or a neutron star and a white dwarf. A prototypical example of such systems is GRB970228. The binary nature of the source is inferred by its migration from its birth location in a star forming region to a low density region within the galactic halo, where the final merging occurs (Bernardini et al., 2007). The location of such a merging event in the galactic halo is indeed confirmed by optical observations of the GRB970228 afterglow (Sahu et al., 1997; van Paradijs et al., 1997). The crucial point is that, as recalled above, GRB970228, GRB060614, GRB071227 and GRB050509b are "canonical" GRBs with $B > 10^{-4}$ "disguised" as short GRBs.

If the binary merging would occur in a region close to its birth place, with an average density of 1 particle/cm^3, the GRB would appear as a traditional high-luminosity "long" GRB, of the kind currently observed at higher redshifts (see Fig. C.3), similar to, e.g., GRB050315 (Ruffini et al., 2006b).

Within our approach, therefore, there is the distinct possibility that all GRB progenitors are formed by binary systems, composed of neutron stars, white dwarfs, or stars evolved out of the main sequence, in different combinations.

The case of the "genuine" short GRBs is currently being examined within the "fireshell" model.

7. Evidence for broadening of the spectral energy distribution of GRBs within the fireshell model: analysis of GRB 080319B and GRB 050904

7.1. Introduction

Out of the hundreds of Gamma Ray Bursts (GRBs) so far observed with known redshifts, there are approximately ten GRBs with an isotropic energy $E_{iso} \gtrsim 10^{54}$ erg: GRB 990123, GRB 990506, GRB 000131, GRB 050820A, GRB 050904, GRB 080319B, GRB 080607, GRB 080721, GRB 080916C, GRB 090323, GRB 090926A (see e.g. Amati et al., 2008, 2009; Kann et al., 2010), GRB 090902B (see Abdo et al., 2009a) and GRB 110918A (Frederiks and Pal'Shin, 2011). We will analyse two of these sources to probe the fireshell model, which has been successfully applied to GRBs with E_{iso} up to 10^{53} erg. The two candidates are GRB 080319B and GRB 050904, having an isotropic γ-ray energy release respectively of $E_{iso} = 1.32 \times 10^{54}$ erg (20 keV – 7 MeV, see Golenetskii et al., 2008) and $E_{iso} = 1.04^{+0.25}_{-0.17} \times 10^{54}$ erg (15 keV – 5 MeV, see Sugita et al., 2009).

Much of the progress made in observing GRBs in recent years has been due to the coordinated efforts of a large number of satellites including *Konus*-WIND (Aptekar et al., 1995), *Swift* (Gehrels et al., 2004), *Suzaku*-WAM (Yamaoka et al., 2009), AGILE (Tavani et al., 2009) and *Fermi* (Atwood et al., 2009; Meegan et al., 2009). These satellites allow an overall energy coverage from 0.2 keV to 300 GeV.

GRB 080319B and GRB 050904 have been triggered by *Swift*. What is relevant here is that, in both these sources with unusually high E_{iso}, the observed peak energy E^{obs}_{peak} occurs well above the *Swift* BAT bandpass (see Tab. 7.3 in Sec. 7.6): for GRB 050904 we have $E^{obs}_{peak} = 314^{+173}_{-89}$ keV Sugita et al. (2009); for GRB 080319B we have $E^{obs}_{peak} = 675 \pm 22$ keV. This, in turn, through the *Swift* observations, for the first time allows the exploration of GRB spectra at $E \lesssim 0.1 E_{peak}$ (see Fig. 7.1). This is at variance with the previous obser-

vations of lower energetics GRBs where E_{peak} falls within the instrumental bandpass (see Fig. 7.1). The observation of GRB 080319B has occurred prior to the launch of *Fermi* and after the one of AGILE, but AGILE has been occulted by Earth during the burst detection. The high energy photons have been detected by *Konus*-WIND (Racusin et al., 2008). The observation of GRB 050904 occurred prior to the launch of both AGILE and *Fermi*. The high energy photons were detected by *Suzaku*-WAM and *Konus*-WIND (Sugita et al., 2009).

GRB 080319B was discovered by BAT on March 19, 2008 (Racusin et al., 2008). It has a redshift $z = 0.937$ (Vreeswijk et al., 2008) and is characterized by an extraordinarily bright optical emission accompanying its γ-ray emission, that makes it the brightest optical burst ever observed: with a peak visual magnitude of 5.3, it could have been seen with the naked eye by an observer in a dark location (Racusin et al., 2008). It is also one of the brightest GRBs in γ and X rays.

This extremely bright optical flash has promoted an intense theoretical analysis on the role of synchrotron self-Compton (SSC, see Sec. 7.2) radiation and this scenario has been investigated by several authors, including e.g. Racusin et al. (2008) and Kumar and Panaitescu (2008).

There has been also interest in examining the possible existence of beaming in order to reduce the energetics of this source. Racusin et al. (2008) proposed a two-component jet model: a narrow jet, with a half-opening angle $\theta_{jet} \sim 0.2^\circ$, dominating the early emission, surrounded by a wider jet, with $\theta_{jet} \sim 4^\circ$, dominating the emission at intermediate and late times. This two-jet model would reduce the total energy budget to $\sim 4 \times 10^{50}$ erg. However, the narrow jet should produce a jet break ~ 1 hr post-burst, which has not been observed. Racusin et al. (2008) suggested that this could be explained if the optical flux of the narrow jet is fainter than that of the wider jet. The wider jet should give rise to a break at $\sim 10^6$ s. Tanvir et al. (2010) reported the observation of a jet break at ~ 11 days with an "approximately achromatic behaviour", recalling that, in the *Swift* era, the expected "achromatic behaviour of breaks in X-ray and optical light curves has been rarely seen (Curran et al., 2008)". An alternative single jet model has been considered by Kumar and Panaitescu (2008): taking into account the lack of an optical jet break during the first ten days of emission, they find a lower limit $\theta_{jet} \gtrsim 2^\circ$. The energy of the GRB could in this case be $\gtrsim 10^{52.3}$ erg (twice larger for a double-sided jet).

GRB 050904 was discovered by BAT on September 4, 2005 (Cummings et al., 2005). It is one of the farthest GRBs ever observed, with $z = 6.29$ (Kawai et al., 2005). Also this burst is characterized by an intense optical emission: a bright optical flare was in fact detected by TAROT near the end of the prompt phase, in temporal coincidence with an X-ray flare (Boër et al., 2006; Gendre et al., 2007).

Tagliaferri et al. (2005) found a "steepening" in the *J*-band light curve at 2.6

$\pm$ 1.0 days and proposed that "it may be due to a jet break". In this case a jet opening angle $\theta_{jet} \sim 3^\circ$ could be inferred. This analysis was refined by Kann et al. (2007), who put the steepening at 2.63 ± 0.37 days, corresponding to $\theta_{jet} \sim 3.30^\circ$. In this case the beaming-corrected energy is 1.73×10^{51} erg (Sugita et al., 2009).

In this paper we limit the analysis of these two sources to the γ-ray emission of the prompt phase, which is energetically predominant with respect to the optical emission: the optical isotropic energy is $\sim 0.1\%$ of E_{iso} (Bartolini et al., 2009) for GRB 080319B and is even less for GRB 050904 (Boër et al., 2006; Gendre et al., 2007).

Also in view of the absence of achromatic breaks required by the jetted emission model, for GRB 080319B and GRB 050904 we assume spherical symmetry, which is one of the main features of the fireshell model.

We recall that a satisfactory agreement between the theoretical predictions of the fireshell model and the observed light curves and spectra of GRBs with E_{iso} up to 10^{53} erg has been previously obtained (see e.g. Bernardini et al., 2005a; Ruffini et al., 2006b; Dainotti et al., 2007; Bernardini et al., 2007; Caito et al., 2009, 2010; de Barros et al., 2011). What is really new in the analysis of these two sources is: 1) the very large value of E^{obs}_{peak}, well above the *Swift* BAT bandpass (see Fig. 7.1 and Tab. 7.3); 2) the fact that for both sources the *Swift* BAT bandpass covers the low energy part of the spectrum, that could then be investigated; 3) in the case of lower energetic sources, the energy region near the peak has been observed by BAT, while the low energy spectral component has been missed (see Fig. 7.1) and will possibly be the object of future specific space missions.

In both GRB 080319B and GRB 050904, *Swift* BAT data show more power in the low energy region than the theoretical predictions of the fireshell model (see Sec. 7.4). We then introduce a new phenomenological spectrum in the comoving frame of the fireshell: the "modified" thermal spectrum (see Sec. 7.3.3), characterized by a phenomenological parameter α. The new comoving spectrum: 1) allows the correct reproduction of the observed prompt γ-ray emission light curves and spectra of both GRBs (see Secs. 7.4 and 7.5); 2) clearly, as shown by Fig. 7.1, does not modify significantly the considerations on the less energetic GRBs previously discussed within the fireshell model, since in that case only the region encompassing the peak is inside the instrument bandpass and is not significantly affected by the value of α; 3) predicts a possible broader emission in the low energy spectral component of the lower energetics GRBs which will possibly be tested by future missions below 10 keV such as, e.g., LOFT (Feroci and The LOFT Consortium, 2011) and MIRAX (Amati et al., 2011). These observations will determine the possible general validity of the comoving spectrum introduced here. It will also be important to verify if an analogous phenomenological correction in the Wien part of the comoving blackbody spectrum will allow the interpretation of the high energy data

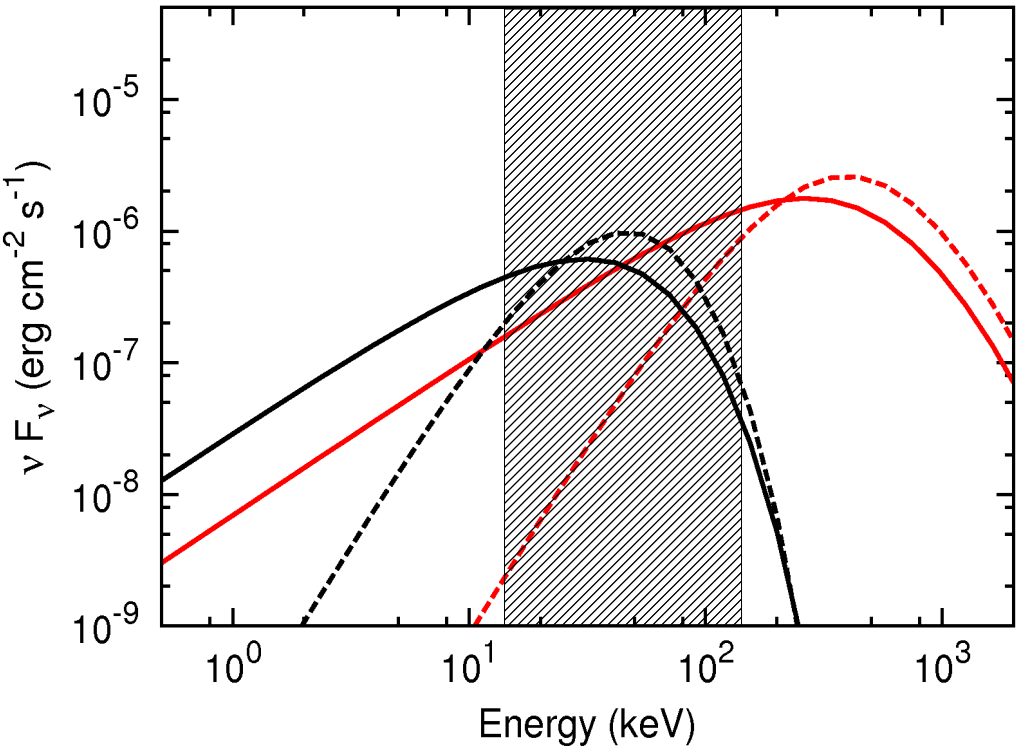

Figure 7.1.: Theoretically simulated spectra obtained by assuming two different values of E_{iso}: 10^{54} erg (in red) and 2.5×10^{53} erg (in black). Solid lines refer to the case $\alpha = -1.8$. Dotted lines refer to the case $\alpha = 0.0$, corresponding to the pure thermal comoving spectrum (see Sec. 7.3.3). The box marks the energy band covered by *Swift* BAT (15 keV – 150 keV). The behaviour of the spectra around the peak energy is not significantly affected by the value of α (see Sec. 7.3.3). For the higher energetic sources, the low energy component of the spectra falls inside the energy band covered by BAT; this is not the case for the lower energetic sources, for which only the region around the peak can be investigated.

(above hundreds of MeV) later observed in equally energetic GRBs by AGILE and *Fermi*. In this respect, it must be noted that an extra high-energy power-law component has been actually invoked in the current literature to explain the emission above hundreds MeV observed in e.g. GRB 090902B (Abdo et al., 2009a), GRB 090510 (Ackermann et al., 2010) and GRB 090926A (Ackermann et al., 2011). However, the phenomenological extra power-law component characterizing the low energy tail of the new comoving spectrum introduced here is not necessarily related to the low energy extrapolation of such a high-energy component. In fact it is also present in sources which show no evidence of high energy emission, like e.g. GRB 090618 (Izzo et al., 2012c) and GRB 101023 (Penacchioni et al., 2012).

The work is organized as follows. In Sec. 7.2 we describe the phenomenological and theoretical interpretation of GRB prompt emission. In Sec. 7.3 we briefly outline the fireshell model, we introduce the "modified" thermal spectrum and explain how we perform the numerical simulations to be compared with the observational data. In secs. 7.4 and 7.5 we present, as specific examples, the analysis of GRB 080319B and GRB 050904 observations of the prompt γ-ray emission. In Sec. 7.6 we discuss the possible explanation for the need to introduce the "modified" thermal spectrum and in Sec. 7.7 we present our conclusions.

7.2. The spectral energy distribution of GRB prompt emission

The study of the GRB prompt emission is often performed by means of phenomenological approaches consisting, for example, in modeling the burst spectra with empirical functions whose parameters are fixed by the χ^2 minimization procedure of the spectral data (see, e.g., Preece et al., 1998, 2000; Ghirlanda et al., 2002; Kaneko et al., 2006, 2008; Guidorzi et al., 2011). The explanation of the results obtained from such phenomenological approaches are a main goal of the theoretical models of GRBs.

7.2.1. Phenomenological approaches to GRB prompt emission

The photon number spectrum time-integrated over the GRB prompt emission duration is typically best fit by two power-laws joined smoothly at a given break energy (the "Band function", Band et al., 1993), whose low energy and high energy photon indices, α and β, have median values of -1 and -2.3 respectively (Preece et al., 2000; Kaneko et al., 2006).

Another example of phenomenological analysis is the correlation between the rest-frame value of the peak energy E^i_{peak} and the isotropic equivalent

radiated γ-ray energy E_{iso}, which leads to a power-law dependece: $E^i_{peak} \propto E^\lambda_{iso}$, with $\lambda \sim 0.57$ (Amati, 2006; Amati et al., 2002, 2009).

There is also an additional phenomenological relation which has manifested itself in recent years, attracting attention: the possibility of fitting the observed spectra, integrated over selected time intervals, by a blackbody plus power-law (BB+PL). There are cases in which the GRB spectrum, again integrated over selected time intervals, is statistically indistinguishable between fits with a Band function and a BB+PL; there are other cases in which the BB+PL model is even preferred over the Band function and finally there are sources for which the data fulfill the Band function but not the BB+PL (Ryde, 2004, 2005; Ryde and Pe'er, 2009; Ryde et al., 2010, 2011).

Generally, the additional blackbody component occurs in the early part of the prompt emission (see e.g. Ryde et al., 2010). There are bursts for which it is dominant with respect to the power-law, but opposite cases also exist, in which the power-law component is predominant with respect to the thermal one; the relative intensity of the two components can vary with time (Ryde, 2004, 2005).

In some interesting cases the blackbody component shows a characteristic evolution in time, with both its observed temperature and flux having a dependence from the arrival time well described by a broken power-law with indexes a_T, b_T, a_F and b_F (Ryde, 2004, 2005; Ryde and Pe'er, 2009). It is appropriate to emphasize that the correspondence between different spectral models cannot, in general, be applied to the entire GRB light curve. There is then the necessity of identifying the specific time interval over which the different spectral features are identified, also possibly in order to recover their physical origin (see e.g. Ruffini et al., 2010b, 2011a).

Specifically, for GRB 080319B and GRB 050904 both time-resolved and time-integrated BAT spectra, including the Proper-GRB (P-GRB, see below Sec. 7.3.1) spectrum of GRB 080319B, are best fit by a simple power-law (see Sec. 7.4 and 7.5; see also Racusin et al., 2008; Stamatikos et al., 2009 and Cusumano et al., 2007); alternative models, such as a Band function or a BB+PL, cannot be constrained by the BAT data. No concluding statements on the presence of a blackbody component in the P-GRB of GRB 080319B can be made due to the limited bandpass of the instruments (see Sec. 7.4). The analysis of *Konus*-WIND data from GRB 080319B has shown a best fit with a Band function (Racusin et al., 2008). For GRB 050904 Sugita et al. (2009) performed a joint spectral analysis among *Swift* BAT, *Suzaku*-WAM and *Konus*-WIND, finding a good fit with both a power-law with exponential cutoff and the Band function. A blackbody component has not been observed in either of these two sources. It is not clear at this stage if different conclusions could have been reached if these sources would have been observed by *Fermi* or AGILE.

7.2.2. Theoretical models of GRB prompt emission

Many different models have been developed to theoretically explain the observational properties of GRBs. One of the most quoted ones is the fireball model (see Piran, 2004 for a review). An alternative one, originating in the electrodynamical processes around a Kerr-Newmann black hole (Damour and Ruffini, 1975), is the fireshell model.

The fireball model was first proposed by Cavallo and Rees (1978), Goodman (1986) and Paczynski (1986), who have shown that the release of a large quantity of γ-ray photons into a compact region can lead to an optically thick photon-lepton "fireball" through the production of $e^{\pm}$ pairs. The term "fireball" refers to an opaque plasma whose initial energy is significantly greater than its rest mass (Piran, 1999).

The fireshell model also starts from an optically thick $e^{\pm}$ plasma whose evolution has been followed in a sequence of states of thermal equilibrium, taking properly into account the ultrarelativistic expansion and the detailed computation of the rate equation for the $e^{\pm}$ annihilation (see Sec. 7.3.1 and Ruffini et al., 1999b, 2000).

In the fireball model, the prompt emission, including the sharp luminosity variations (Ramirez-Ruiz and Fenimore, 2000), are due to the prolonged and variable activity of the "inner engine" (Rees and Meszaros, 1994; Piran, 2004). The conversion of the fireball energy to radiation occurs via shocks, either internal (when faster moving matter overtakes a slower moving shell, see Rees and Meszaros, 1994) or external (when the moving matter is slowed down by the external medium surrounding the burst, see Rees and Meszaros, 1992). Specifically, for GRB 080319B internal shocks have been considered responsible for the prompt emission (Racusin et al., 2008; see, however, Kumar and Narayan, 2009) and external shocks are then considered responsible for the afterglow (see also, however, Kumar, 1999 and references therein). For GRB 050904 Cusumano et al. (2007) proposed that internal shocks are responsible for both the prompt and the afterglow emission (see, however, Gendre et al., 2007 for a detailed description of limits and advantages of both the internal and the external shock scenario).

Much attention has been given to synchrotron emission from relativistic electrons, possibly accompanied by SSC emission to explain the observed GRB spectrum. These processes were found to be consistent with the observational data of many GRBs (see e.g. Tavani, 1996; Frontera et al., 2000; Schaefer et al., 1998). However, several limitations have been evidenced in relation with the low energy spectral slopes of time-integrated spectra (see Crider et al., 1997, Preece et al., 2002, Ghirlanda et al., 2002 and Ghirlanda et al., 2003; see also, however, Daigne et al., 2009) and time-resolved spectra (see Crider et al., 1998 and Ghirlanda et al., 2003); additional limitations on SSC have also been pointed out by Kumar and McMahon (2008) and Piran et al. (2009).

In all the above considerations, the equations of motion of the fireball are evaluated under the ultrarelativistic approximation, leading to the Blandford and McKee (1976) self-similar power-law solution (see Sec. 7.3.1). The maximum Lorentz factor of the fireball is estimated from the temporal occurrence of the peak of the optical emission, which is identified with the peak of the forward external shock emission (Molinari et al., 2007; Rykoff et al., 2009) in the thin shell approximation (Sari and Piran, 1999). It was also proposed to put an upper limit on the maximum fireball Lorentz gamma factor from the upper limit on the intensity of a possible smooth background signal in the hard X-rays to soft gamma rays during the prompt emission, which is identified with the contribution of the forward external shock emission to the prompt phase (Zou and Piran, 2010). Another proposal was advanced to use compactness arguments within a scenario with two separate emitting regions for the MeV and the GeV emissions (Zou et al., 2011).

Partly alternative and/or complementary scenarios to the fireball model have been developed, e.g. the ones based on: quasi-thermal Comptonization (Ghisellini and Celotti, 1999), Compton drag emission (Zdziarski et al., 1991; Shemi, 1994; Lazzati et al., 2000), synchrotron emission from a decaying magnetic field (Pe'er and Zhang, 2006), jitter radiation (Medvedev, 2000), Compton scattering of synchrotron self-absorbed photons (Panaitescu and Mészáros, 2000; Stern and Poutanen, 2004), photospheric emission (Eichler and Levinson, 2000; Mészáros and Rees, 2000; Mészáros et al., 2002; Daigne and Mochkovitch, 2002; Giannios, 2006; Ryde and Pe'er, 2009; Lazzati and Begelman, 2010). In particular, Ryde and Pe'er (2009) pointed out that photospheric emission overcomes some of the difficulties of pure non-thermal emission models.

In this paper we focus on the fireshell model. The characteristic parameters of the model are the total energy $E_{tot}^{e^\pm}$, the baryon loading B and the CircumBurst Medium (CBM) density n_{cbm} (see Secs. 7.3.1 and 7.3.4). The Lorentz γ factor, directly linked to B and $E_{tot}^{e^\pm}$, is explicitly computed from the description of all the phases starting from the moment of gravitational collapse. The fireshell radial coordinate is explicitly evaluated as a function of the laboratory time, the comoving time and the arrival time at the detector (see Sec. 7.3.1). The optically thick $e^\pm$ plasma, endowed with baryon loading, is followed all the way to transparency. The collision with the CBM of the emerging relativistic expanding shell of baryons gives rise to the extended afterglow, which comprises both the prompt emission and the traditional decaying afterglow phases (see Sec. 7.3.1). Relativistic effects are taken into account in the computation of the equations of motion of the shell and of the EQuiTemporal Surfaces (EQTS, Bianco and Ruffini, 2004, 2005b, see Sec. 7.3.3). Taking into proper account these relativistic effects, it is possible to deduce the spectrum of the collision process between the baryons and the CBM in the comoving frame of the shell. For simplicity it was initially as-

sumed that such collisions occur in a fully radiative regime and give rise to a pure thermal spectrum in the comoving frame (see Sec. 7.3.3). The observed spectrum is then obtained as a double convolution of thousands of thermal spectra, each one with a different temperature and weighted by the appropriate Lorentz and Doppler factors, following the solution of the equations of motion of the fireshell, both over the EQTS and over the observation time (Ruffini et al., 2004b; Bernardini et al., 2005a)[1].

As we recalled in the Introduction, this ansatz of a pure black body spectrum in the fireshell comoving frame, in spite of its simplicity, led to a successful interpretation of many different sources with an E^{obs}_{peak} inside the instrumental bandpass (see e.g. Bernardini et al., 2005a; Ruffini et al., 2006b; Dainotti et al., 2007; Bernardini et al., 2007; Caito et al., 2009, 2010; de Barros et al., 2011). We were then quite confident that we could obtain any observed power-law by an adequate convolution of thermal spectra duly weighted by the relativistic Doppler factors. The impossibility of obtaining the correct power-law indexes observed in both the sources treated in this paper, which have an E^{obs}_{peak} above the instrumental bandpass, using solely thermal spectra in the fireshell comoving frame, was quite unexpected. This impossibility stems from the fact that neither the distribution of the temperature in the comoving frame, nor the Doppler factors used in the thousands of convolution processes, can be arbitrarily given. Both of them are constrained by the equations of motion of the fireshell and by the consequent release of kinetic energy in the collision. A priori, a convolution of thermal spectra with arbitrary temperatures and Doppler factors can always fit any observed power-law. There is, however, no way to fit by convolutions of thermal spectra the observed power-laws consistently with the fireshell equations of motion in these two sources with E^{obs}_{peak} above the instrumental bandpass.

What is particularly interesting, however, is the fact that this difficulty can be overcome simply by adding an extra power-law component to the pure black body spectrum. As we will see, the application of the fireshell model to GRB 080319B and GRB 050904 leads in fact to the introduction of an additional phenomenological parameter α, which characterizes the departure of the slope of the low energy part of the comoving spectrum from a pure thermal one (see Sec. 7.3.3).

This new result is consistent also with all the previously analyzed GRBs, and reasons for this are given in Fig. 7.1. The success of this approach is not trivial, since there is no direct analytic relation between the index of the power-law introduced in the spectrum in the fireshell comoving frame and the observed one. It is quite significant that the introduction of a single power-law makes the fireshell model consistent with all observed GRB spectra.

[1]Typically, a resolution of $\sim 5 \times 10^4$ thermal spectra for each second of observation has been used.

The physical explanation for α has not yet been found. Analogously, no physical explanation has yet been found for the above described (Sec. 7.2.1) phenomenological parameters of the Band function and of the Amati relation, and in this sense for the ones described by Ryde (2004, 2005) and Ryde and Pe'er (2009) as well. All these phenomenological parameters lead to a better quantitative description of GRBs; they are the object of active theoretical studies and are an important step toward reaching the future identification of the underlying physical processes characterizing the GRBs.

We now proceed to a detailed description of the fireshell model (Sec. 7.3).

7.3. The fireshell model: the GRB luminosity and spectrum

The fireshell model, avoiding a piecewise fit of the observed GRB data, proposes a unified picture starting from the initial process of gravitational collapse to a black hole through all successive stages. It gives a theoretical treatment of each stage, identifying the parameters intrinsic to the source, essential to describing the evolution of the system, as well as its interaction with the CBM. The corresponding equations of motion are treated accordingly. Regimes of Lorentz gamma factors in the range 100–1000 are encountered, implying the necessity of a fully relativistic approach. The model is intrinsically endowed with highly nonlinear effects: each prediction of the theoretical model at a given instant of the observation time is influenced by the entire history of the source. Consequently, any solution of the model in agreement with the observations necessarily implies a high level of self-consistency.

7.3.1. The canonical GRB

Within the fireshell model, all GRBs originate from an optically thick electron–positron plasma in thermal equilibrium, having total energy $E_{tot}^{e^\pm}$ and formed in the gravitational collapse to a black hole (Ruffini et al., 2010e). The condition of thermal equilibrium assumed in our model and proved by Aksenov et al. (2007) distinguishes our model from alternative approaches (e.g. the one by Cavallo and Rees, 1978), where the total annihilation of the $e^\pm$ plasma was assumed, leading to a vast release of energy pushing on the CBM (the concept of a "fireball"). In our case the annihilation of the $e^\pm$ pairs occurs gradually and is confined within an expanding shell: the "fireshell". The rate equation for the $e^\pm$ pairs and their dynamics (the pair-electromagnetic pulse or PEM pulse for short) has been given by Ruffini et al. (1999b). This plasma engulfs the baryonic material left over in the process of gravitational collapse having mass M_B, still keeping thermal equilibrium between electrons, positrons and baryons. The baryon loading is measured by the dimen-

sionless parameter $B = M_B c^2 / E_{tot}^{e^\pm}$. It was shown (see Ruffini et al., 2000) that no relativistic expansion of the plasma can be found for $B > 10^{-2}$. The fireshell is still optically thick and self-accelerates to ultrarelativistic velocities (the pair-electromagnetic-baryonic pulse or PEMB pulse for short, Ruffini et al., 2000). Then the fireshell becomes transparent and the P-GRB is emitted (Ruffini et al., 2001b). The amount of energy radiated in the P-GRB is only a fraction of $E_{tot}^{e^\pm}$. The remaining energy is stored in the kinetic energy of the optically thin baryonic and leptonic matter fireshell. The final Lorentz γ factor at transparency, γ_0, can vary in a vast range between 10^2 and 10^3 as a function of $E_{tot}^{e^\pm}$ and B (Ruffini et al., 2000).

After transparency, the remaining accelerated baryonic matter still expands ballistically and starts to slow down by the collisions with the CBM, having average density n_{cbm}. During this phase, the extended afterglow emission occurs (Ruffini et al., 2001b). In common with the majority of existing models, we describe the motion of the baryons as an expanding thin shell enforcing energy and momentum conservation in the collision with the CBM. The condition of a fully radiative regime is assumed (Ruffini et al., 2003a). It is appropriate to recall a further difference between our treatment and the ones in the current literature. The complete analytic solution of the equations of motion of the baryonic shell has been developed (Bianco and Ruffini, 2004, 2005b), while in the current literature usually the Blandford and McKee (1976) self-similar solution has been uncritically adopted (e.g. Meszaros et al., 1993; Sari, 1997, 1998; Waxman, 1997; Rees and Meszaros, 1998; Granot et al., 1999; Panaitescu and Meszaros, 1998; Piran, 1999; Gruzinov and Waxman, 1999; van Paradijs et al., 2000; Mészáros, 2002). The similarities and differences between the two approaches have been explicitly pointed out in Bianco and Ruffini (2005a).

From this general approach, a canonical GRB bolometric light curve is defined which is composed of two different parts: the P-GRB and the extended afterglow. The relative energetics of these two components, as well as the observed temporal separation between the corresponding peaks, is a function of the above three parameters $E_{tot}^{e^\pm}$, B, and n_{cbm}; the first two parameters are inherent to the accelerator characterizing the GRB, i.e., the optically thick phase, while the third one is inherent to the GRB surrounding environment which gives rise to the extended afterglow. What is usually called the GRB "prompt emission" in the literature is actually composed of both the P-GRB and the initial part of the extended afterglow encompassing its peak. As we proposed in Ruffini et al. (2001b), both the so-called "short" and "long" GRBs fit into this canonical GRB scenario. In particular, for baryon loading $B \lesssim 10^{-5}$, the P-GRB component is energetically dominant over the extended afterglow. In the limit $B \to 0$ it gives rise to a "genuine short" GRB. Otherwise, when $3.0 \times 10^{-4} \lesssim B \leq 10^{-2}$, the kinetic energy of the baryonic and leptonic matter, and consequently the extended afterglow emission, predominates with

respect to the P-GRB, giving rise to the "long" GRBs or the "disguised short" GRBs depending on the average CBM density and the astrophysical scenario (Ruffini et al., 2001b, 2002; Bernardini et al., 2007; Caito et al., 2009, 2010; de Barros et al., 2011). Since the "critical" value of B (i.e. the value of B for which both the P-GRB and the extended afterglow have the same energy) is a slowly varying function of $E_{tot}^{e^\pm}$, for $10^{-5} \lesssim B \lesssim 3.0 \times 10^{-4}$ the ratio of the total energies of the P-GRB and of the extended afterglow is also a function of $E_{tot}^{e^\pm}$ (Ruffini et al., 2009).

If one goes to the observational properties of this model of a relativistic expanding shell, a crucial concept has been the introduction of the EQTS. In this topic, also, our model is distinguished from those in the literature for deriving analytic expressions for the EQTS from the analytic solutions of the equations of motion (Bianco and Ruffini, 2005b).

The observed temporal variability of the extended afterglow is produced in our model by the interaction of the fireshell with CBM "clumps" (Ruffini et al., 2002, see also Sec. 7.3.4). The issue of time variability in GRB light curves has been longly debated. Several authors, e.g. Zhang et al. (2006); Nakar and Granot (2007), found that CBM inhomogeneities are not able to produce the short-timescale variability in GRB prompt and afterglow emission light curves, mainly because photons emitted at the same instant of time from different parts of the emitting regions have different arrival times: this tends to smoothen the light curve significantly.

Within the fireshell model, also on this point there are some differences with the other models. It is emphasized that, from the correct computations of the equations of motion of the shell and of the Lorentz γ factor, the short time scale variability of GRB light curves occurs in regimes with the largest values of the Lorentz gamma factor, when the total visible area of the emission region is very small and the "dispersion" in arrival time of the luminosity peaks is negligible. Therefore, under this condition the short-timescale variability of GRB light curves can be produced by inhomogeneities in the CBM, as found also by Dermer and Mitman (1999) and Dermer (2006, 2008). The application of the fireshell model leads to a direct evaluation of the filamentary and clumpy structure of the CBM, which was already predicted in pioneering works by Enrico Fermi in the theoretical study of Interstellar Matter (ISM) in our galaxy (Fermi, 1949, 1954), and is much on line with the knowledge obtained from various studies of the ISM in galaxies (see, for example, Kim et al., 1998; Lockman, 2002; Finkelstein et al., 2009).

Clearly, the fact that the short time scale variability is observed only in the prompt emission, while the X-ray afterglow light curves are usually smooth, does not mean that the CBM is inhomogeneous only up to a given radius, beyond which it becomes homogeneous. Inhomogeneities are everywhere in the CBM, but beyond a given distance from the source, corresponding approximately to the end of the prompt emission phase, they do not produce

observable effects on the light curve since they are indeed smeared out by the curvature effect and the relativistic effects between the time in the fireshell comoving frame and the photon arrival time at the detector (Ruffini et al., 2002, 2006b). The early X-ray afterglow originates in fact from the same kind of interaction of the fireshell with a clumpy CBM. The absence of spiky emission is simply a consequence of these effects. In other words, it is true that the fireshell model predicts that the same clumps at larger radii would produce longer spikes (Ruffini et al., 2001d). However, at such large radii where the effect would be measurable, the smearing dominates and prevents the effect to be observed (Ruffini et al., 2002, 2006b). Vice versa, the prompt emission, where the effect of the CBM clumps are observable, occurs encompassing too limited a range of radial distances to make this effect noticeable in all sources. The only exception may occur in the case of isolated high density clumps along the line of sight at late time of emission where indeed this effect is observable (Bianco et al., 2006a; Bernardini et al., 2008d, 2009; Ruffini et al., 2009; Izzo et al., 2010). We are currently verifying if this aspect of the fireshell model may also explain some specific properties of the X-ray flares recently evidenced in the afterglow phase (see e.g. Margutti et al., 2011a,b, and references therein). The drop in energy of 2–4 orders of magnitude from the prompt γ-ray phase to the early X-ray afterglow is perfectly in line with the decrease of the Lorentz gamma factor in the expansion of the fireshell. The fact that the prompt emission in γ-rays stops at some time is related to the well known hard-to-soft evolution of the emission process, which is perfectly explained within the fireshell model (see Sec. 7.3.3) and it is related to the solution of the equations of motion of the system, implying the decrease of the Lorentz gamma factor as well as the amount of energy release in the collision between the fireshell baryonic matter and the CBM (Ruffini et al., 2004b; Bernardini et al., 2005a).

7.3.2. The P-GRB spectral properties

The spectrum at transparency has been given in Ruffini et al. (2000) with a temperature computed consistently with the local thermodynamics of the $e^{\pm}$-baryon plasma and the Lorentz gamma factor. Details are given in Ruffini et al. (2009). It is appropriate to stress that in the emission of the P-GRB there are two different contributions: one corresponding to the emission of the photons due to the reach of the transparency, and the second originating from the interaction of the protons and electrons with the CBM. A spectral energy distribution with a thermal component and a non-thermal one should be expected to occur.

7.3.3. The extended afterglow spectral properties

The majority of work in the current literature has addressed the analysis of the prompt emission as originating from various combinations of synchrotron and inverse Compton processes (Piran, 2004). It appears clear, however, that this interpretation is not satisfactory (see Sec. 7.1; see also Ghirlanda et al., 2003; Kumar and McMahon, 2008; Piran et al., 2009). Furthermore, in the description of an ultrarelativistic collision between protons and electrons and the CBM new collective processes of ultrarelativistic plasma physics occur, not yet fully explored and understood (e.g. Weibel instability, see Medvedev and Loeb, 1999). Most promising results along this line have been already obtained by Spitkovsky (2008a); Medvedev and Spitkovsky (2009).

Without waiting for the developments of these investigations, we have adopted a very pragmatic approach in the fireshell model by making full use of the knowledge of the equations of motion, of all the EQTS formulations as well as of the correct relativistic transformations between the comoving frame of the fireshell and the observer frame. In this respect, we have adopted a fundamental procedure: to make an ansatz on the spectral properties of emission of the collisions between the baryons and the CBM in the comoving frame, and then evaluate all the observational properties in the observer frame. In order to take into proper account the filamentary, clumpy and porosity structure of the CBM, we have introduced an additional parameter $\mathcal{R}$, which describes the fireshell surface filling factor. It is defined as the ratio between the effective emitting area of the fireshell A_{eff} and its total visible area A_{vis} (Ruffini et al., 2002, 2004b, 2005c).

It must be emphasized that the fact that only a fraction $\mathcal{R}$ of the shell surface is emitting does not mean that only a fraction $\mathcal{R}$ of the total shell energy is emitted. We must in fact distinguish between an instantaneous interaction of the fireshell with a single filament and its overall interaction with all the filaments of the entire cloud giving rise to the spiky structure of the light curve. This global interaction is clearly the superposition of randomly distributed instantaneous events. The different filaments inside the cloud interact with different parts of the fireshell and the entire cloud reduces the kinetic energy of the entire fireshell. The key point is that, during the prompt emission, the cloud, typically with a mass of the order of $10^{-8} - 10^{-11}$ solar masses, covers the entire visible area of the fireshell (typically with a radius between 10^{13} cm and 10^{15} cm for the sources analyzed in the present paper, see Tables 7.1 and 7.2). Consequently, at any given instant of time, each filament of the cloud covers only a small fraction of the fireshell surface. However, when we integrate over the cloud crossing time, the coverage of the cloud as a whole is equal to unity.

As a first ansatz, we have assumed that the extended afterglow radiation has a thermal spectrum in the comoving frame of the fireshell (Ruffini et al., 2004b). The observed GRB spectrum is given by the convolution of hun-

dreds of thermal spectra with different temperatures and different Lorentz and Doppler factors. Such a convolution is to be performed over the EQTSs (Bianco and Ruffini, 2004, 2005b), which are the surfaces of constant arrival time of the photons at the detector, and over the observation time (Bernardini et al., 2005a).

The hard-to-soft transition of GRB time-integrated and time-resolved spectra, that was first observed in BATSE GRBs (Crider et al., 1997), within the fireshell model comes out naturally from: 1) the evolution of the comoving temperature; 2) the decrease of the bulk γ factor; 3) the curvature effect (Bianco and Ruffini, 2004; Ruffini et al., 2004b; Bernardini et al., 2005a).

Within the fireshell model, the extended afterglow luminosity at the detector arrival time t_a^d per unit of solid angle $d\Omega$ and in the energy band $[\nu_1, \nu_2]$ is given by (Ruffini et al., 2004b)

$$\frac{dE^{[\nu_1,\nu_2]}}{dt_a^d d\Omega} = \int_{EQTS} \frac{\Delta\epsilon}{4\pi} v \cos\theta \Lambda^4 \frac{dt}{dt_a^d} W(\nu_1, \nu_2, T_{arr}) d\Sigma, \tag{7.3.1}$$

where $\Delta\epsilon = \Delta E_{int}/V$ is the emitted energy density released in the interaction of the accelerated baryons with the CBM measured in the comoving frame, $\Lambda = \{\gamma[1-(v/c)cos\theta]\}^{-1}$ is the Doppler factor, W(ν_1,ν_2,T_{arr}) is an "effective weight" required to evaluate only the contributions in the energy band $[\nu_1, \nu_2]$, $d\Sigma$ is the surface element of the EQTS at detector arrival time t_a^d on which the integration is performed and T_{arr} is the observed temperature of the radiation emitted from $d\Sigma$. The "effective weight" W(ν_1,ν_2,T_{arr}) is defined as the ratio between the energy density emitted in a given energy band $[\nu_1, \nu_2]$ and the bolometric energy density:

$$W(\nu_1, \nu_2, T_{arr}) = \frac{\int_{\epsilon_1}^{\epsilon_2} \left(\frac{dN_\gamma}{dVd\epsilon}\right) \epsilon d\epsilon}{\int_0^{\infty} \left(\frac{dN_\gamma}{dVd\epsilon}\right) \epsilon d\epsilon}, \tag{7.3.2}$$

where $\frac{dN_\gamma}{dVd\epsilon}$ is the number density of the photons per unit of energy in the comoving frame of the fireshell.

Thermal case

With the assumption of a thermal spectrum in the comoving frame of the fireshell

$$\frac{dN_\gamma}{dVd\epsilon} = \left(\frac{8\pi}{h^3c^3}\right) \frac{\epsilon^2}{\exp\left(\frac{\epsilon}{k_B T}\right) - 1}, \tag{7.3.3}$$

(h is the Planck constant, c is the speed of light and k_B is the Boltzmann constant) we have

$$W(\nu_1, \nu_2, T_{arr}) = \frac{\int_{\epsilon_1}^{\epsilon_2} \left(\frac{dN_\gamma}{dVd\epsilon}\right) \epsilon d\epsilon}{aT^4}, \tag{7.3.4}$$

where a is the radiation constant and T is the temperature in the comoving frame.

In general, the temperature in the comoving frame can be evaluated starting from the following relation:

$$\frac{\Delta E_{int}}{\Delta\tau} = \pi r^2 c\, \mathcal{R} \int_0^\infty \left(\frac{dN_\gamma}{dVd\epsilon}\right) \epsilon d\epsilon, \tag{7.3.5}$$

where $\Delta\tau$ is the time interval in which the energy ΔE_{int} is developed. By inserting Eq. (7.3.3) into Eq. (7.3.5) we obtain

$$T = \left(\frac{\Delta E_{int}}{4\pi r^2 \sigma \mathcal{R} \Delta\tau}\right)^{1/4}, \tag{7.3.6}$$

with σ the Stefan-Boltzmann constant.

The "modified" thermal spectrum

The new SED for the radiation emitted in the comoving frame of the fireshell is a "modified" thermal spectrum: a spectrum characterized by a different asymptotic power-law index in the low energy region with respect to the thermal one. This index is represented by a free parameter α, so that the pure thermal spectrum corresponds to the case $\alpha = 0$:

$$\frac{dN_\gamma}{dVd\epsilon} = \left(\frac{8\pi}{h^3c^3}\right) \left(\frac{\epsilon}{k_B T}\right)^\alpha \frac{\epsilon^2}{\exp\left(\frac{\epsilon}{k_B T}\right) - 1}. \tag{7.3.7}$$

α is a phenomenological parameter defined in the comoving frame of the fireshell. This phenomenological approach can be relevant in identifying the true physical mechanisms occurring in the collisions in the comoving frame, and uniquely separates them from the relativistic contributions coming from relativistic transformations and convolutions over the EQTS leading to the observed spectrum.

By using the Eq. (7.3.7) and introducing the variable $y = \epsilon/(k_B T)$, we obtain the following expression for the "effective weight":

$$W(\nu_1, \nu_2, T_{arr}) = \frac{\int_{y_1}^{y_2} \frac{y^{\alpha+3}}{\exp(y)-1} dy}{\Gamma(4+\alpha)\, Li_{4+\alpha}(1)} \tag{7.3.8}$$

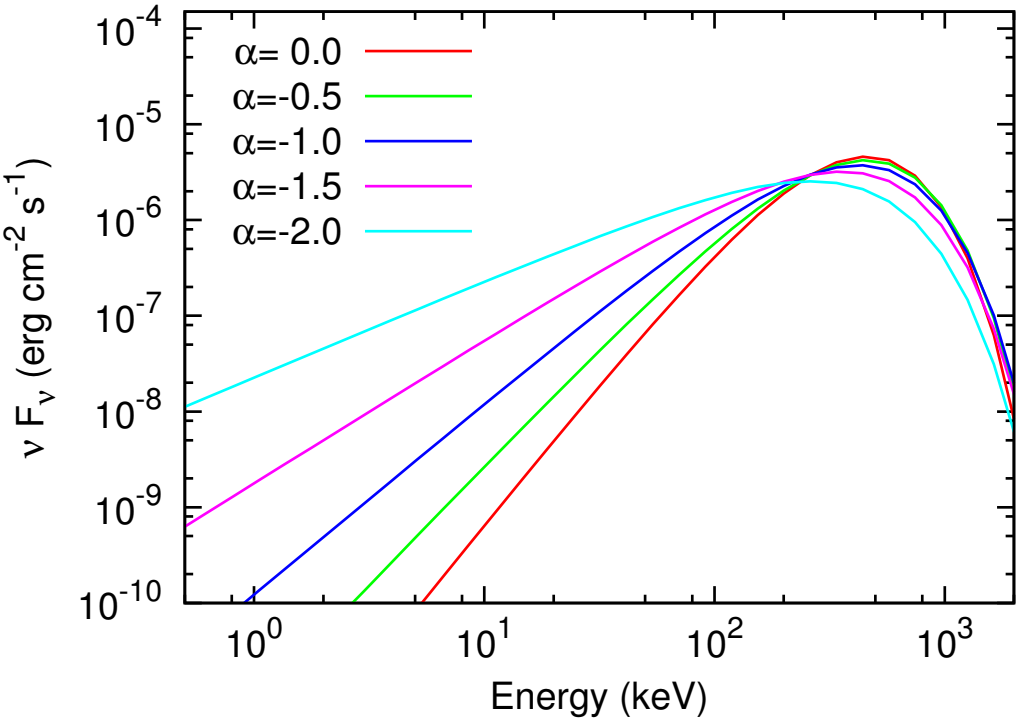

Figure 7.2.: Theoretically simulated instantaneous spectra obtained by assuming $E^{tot}_{e^+e^-} = 1.0 \times 10^{54}$ erg, $B = 2.5 \times 10^{-3}$, $n_{cbm} = 1$ part cm^{-3} and different values of the index α. The curve with $\alpha = 0.0$ corresponds to the pure thermal spectrum case.

where $\Gamma(z) = \int_0^\infty t^{z-1}e^{-t}dt$ is the Gamma function and $Li_n(z) = \sum_{k=1}^\infty z^k/k^n$ is Jonquière's function.

In analogy with the thermal case, we can define an "effective temperature" for the "modified" thermal spectrum; by inserting Eq. (7.3.7) in Eq. (7.3.5) we obtain:

$$T = \left[\left(\frac{\Delta E_{int}}{\Delta \tau} \right) \frac{h^3 c^2}{(4\pi r^2)\, 2\pi \mathcal{R}\, k_B^4\, \Gamma(4+\alpha)\, Li_{4+\alpha}(1)} \right]^{1/4} . \tag{7.3.9}$$

It can be easily seen that, for $\alpha = 0$, we obtain Eq. (7.3.6).

In Fig. 7.2 are shown several theoretically predicted instantaneous spectra characterized by the same temperature and different values of the free parameter α. It can be seen that the main effect of varying the value of α is a change in the low energy slope of the spectral energy distribution. In particular, by decreasing α the low energy emission increases. Around the peak energy the spectrum is instead only weakly dependent on the value of α.

In the present paper we test the comoving modified thermal spectrum by comparing the numerical simulations with the observed prompt emission

spectra and light curves of highly energetic GRBs. In particular we present, as specific examples, the analysis of the observational BAT data (in the 15–150 keV bandpass) of GRB 080319B ($E_{iso} = 1.34 \times 10^{54}$ erg, Golenetskii et al., 2008) and GRB 050904 ($E_{iso} = 1.04^{+0.25}_{-0.17} \times 10^{54}$ erg, Sugita et al., 2009) in Secs. 7.4 and 7.5, respectively.

7.3.4. The numerical simulation of GRB light curves and spectra

To best reproduce the observational data within the fireshell model, we need to determine the following five parameters: $E^{e^\pm}_{tot}$, B, α, n_{cbm} and $\mathcal{R}$.

The procedure assumes a specific value of $E^{e^\pm}_{tot}$ and B. It is clear that $E^{e^\pm}_{tot}$ has to be larger or equal to the observed isotropic equivalent energy E_{iso} of the GRB. $E^{e^\pm}_{tot}$ can be actually quite larger than E_{iso} since, in many sources, we are limited by the threshold and the bandpass of the detectors. The value of B is determined by the ratio between the energetics of the P-GRB and of the extended afterglow, as well as by the time separation between the corresponding peaks (Ruffini et al., 2001b, 2008a; Aksenov et al., 2010).

The determination of the three remaining parameters depends on the detailed "fitting" of the shape of the extended afterglow light curves and spectra. In particular, the parameter $\mathcal{R}$ determines the effective temperature in the comoving frame and the corresponding peak energy of the spectrum, α determines the low energy slope of the comoving spectrum and n_{cbm} determines the temporal behavior of the light curve. It is found that the CBM is typically formed of "clumps" of width $\sim 10^{15} - 10^{16}$ cm and density contrast $10^{-1} \lesssim \delta n/n \lesssim 10$. Particularly important is the determination of the average value of n_{cbm}. Values of the order of 0.1–10 particles/cm^3 have been found for GRBs exploding inside star forming region galaxies, while values of the order of 10^{-3} particles/cm^3 have been found for GRBs exploding in galactic halos (i.e. the "disguised" GRBs, see Bernardini et al., 2007; Caito et al., 2009, 2010; de Barros et al., 2011).

Of course, "fitting" a GRB within the fireshell model is much more complex than simply fitting the $N(E)$ spectrum with phenomenological analytic formulas for a finite temporal range of the data. It is a consistent picture, which has to "fit" the intrinsic parameters of the source, as well as its spectrum and its light curve temporal structure. Concerning the theoretical spectrum to be compared with the observational data, it is obtained by an averaging procedure of instantaneous spectra. In turn, each instantaneous spectrum is linked to the fit of the observed multiband light curves in the chosen time interval. Therefore, both the "fit" of the spectrum and of the observed multiband light curves have to be performed together and jointly optimized. Moreover, the parameters used in the numerical simulations are not independent. In fact, they have to be computed self-consistently through the entire dynam-

ical evolution of the system and not separately at each time step. For each spike in the light curve the parameters of the corresponding CBM clumps must be computed, taking into proper account all the thousands of convolutions of comoving spectra over each EQTS leading to the observed spectrum. It is clear then that since the EQTS encompass emission processes occurring at different comoving times, weighted by their Lorentz and Doppler factors, the "fitting" of a single spike of the light curve is not only a function of the properties of the specific CBM clump but of the entire previous history of the source. Any step of the "fitting" process affects the entire following evolution and, viceversa, at any step a "fit" must be made consistently with all the previous and subsequent history: due to the non linearity of the system and to the EQTS, any change in the "fit" produces observable effects up to a much later time. This implies that the "fitting" process cannot proceed for successive temporal steps: the complete analysis must be applied to the entire GRB as a whole, to avoid possible systematic error propagation from a temporal step to the following ones. This leads to an extremely complex trial and error procedure in the fitting of the data in which the uniqueness of the parameters defining the source are further and further narrowed down. Of course, we cannot expect the latest parts of the fit to be very accurate, since some of the basic hypotheses on the equations of motion, and the possible fragmentation of the shell (Dainotti et al., 2007), can affect the fitting procedure.

7.4. GRB 080319B

We analyzed the GRB 080319B prompt emission light curve and spectrum observed by BAT within the fireshell model. As we already mentioned in the introduction, for GRB 080319B we have $E^{obs}_{peak} = 675 \pm 22$ keV, although there is a hard-to-soft spectral evolution going from with $E^{obs}_{peak} = (748 \pm 26)$ keV at 22 s after the BAT trigger to $E^{obs}_{peak} = (528 \pm 28)$ keV at 24 s after the BAT trigger, and the BAT spectral index reduces from ~ 1.0 to ~ 2.1 at 53 seconds after the BAT trigger (Racusin et al., 2008).

Several authors found some evidence of the possibility to separate the prompt emission of this source into two main episodes, partitioned at about 28 s after the BAT trigger time. Margutti et al. (2008) analyzed the variability time-scale t_{var} of the γ-ray prompt emission, finding that the first part of the light curve (up to ~ 28 s) is dominated by $t_{var} \sim 0.1$ s, while the last part shows a much longer characteristic time-scale ($t_{var} \sim 0.7$ s). Stamatikos et al. (2009) found that the arrival offset between the Swift-BAT 15-25 keV and 50-100 keV energy band (γ-ray spectral lag) is maximum at t $\gtrsim 28$ s and it appears to be anti-correlated with the arrival offset between prompt 15-350 keV γ-rays and the optical emission observed by TORTORA (optical/γ-ray spectral lag), maximum at t $\lesssim 28$ s.

Concerning the first episode, we identify the first 7 s of emission (from -5 s up to 2 s after the BAT trigger time) with the P-GRB; the theoretically estimated total isotropic energy emitted in the P-GRB and the observed temperature are $E^{iso}_{P-GRB} = 1.85 \times 10^{52}$ erg and $T^{obs}_{P-GRB} \sim 16$ keV respectively. There are three main reasons that supports this interpretation:

1. First, we performed the analysis of BAT spectra integrated over subintervals of time encompassing the whole prompt emission by using the standard FTOOLS package (Heasoft, version 6.10). We found that all these spectra are best modeled with power-laws and a discontinuity in the hard-to-soft evolution came out a few seconds after the BAT trigger time, as shown in Fig. 7.3 (see also Stamatikos et al., 2009). In particular, there is a clear soft-to-hard evolution up to ~ 1 s after the BAT trigger time, while a typical hard-to-soft transition starts at about 8 s after BAT trigger time. It is difficult to evaluate at what time exactly the discontinuity occurs: in fact, in the region between ~ 1 s and ~ 8 s, the photon index first appears to reach an asymptotic value of ~ 0.76, then further decreases up to ~ 0.7: this behaviour could be due to the partial superimposition of the contributions of both the P-GRB and the extended afterglow.

2. The second reason suggesting the interpretation of the first seconds of emission as the P-GRB is that the optical emission starts at t ~ 9 s after the BAT trigger time (see Fig. 7.4): in fact, within the fireshell model the optical radiation is expected in the extended afterglow, but not in the P-GRB.

3. It is important to point out that, besides the two above observational considerations, the identification of the first 7 s of emission as the P-GRB is the only interpretation that allow us to constrain the values of $E^{e^{\pm}}_{tot}$ and B in such a way as to make a consistent fit of both the P-GRB and the extended afterglow.

Of course, none of these three arguments separately would give support to our interpretation: e.g., the optical component could have also been present before ~ 9 s but unobserved due to the instrumental constraints. However, the redundant occurrence of all three arguments implies that our interpretation of the first 7 s as the P-GRB component is fully compatible both with our theoretical framework and with the observed data. The P-GRB spectrum is expected to be composed of a thermal plus a non-thermal component (see Sec. 7.3.2). We found that the BAT spectrum of the first 7 s of the prompt emission is best fit by a power-law with photon index γ=0.84 $\pm$ 0.04, with a chi square value of $\chi^2 = 48.26$ for 60 degrees of freedom. The presence of the expected additional thermal component cannot be constrained by the data (C. Guidorzi, private communication). A possibility is that thermal flux

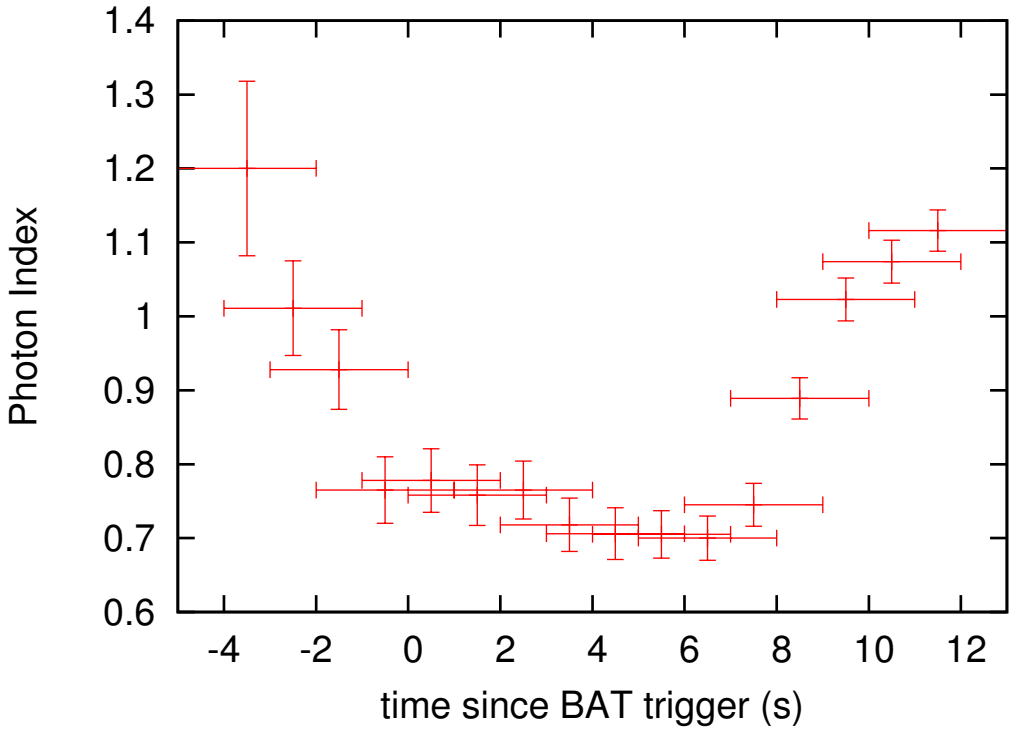

Figure 7.3.: Time evolution of the photon index for power-law fit to 15-150 keV Swift BAT spectra integrated over time intervals of 3 s. A clear soft-to-hard evolution up to $\sim$ 1 s after the BAT trigger time, while a typical hard-to-soft transition starts at about 8 s after the BAT trigger time. In the region between $\sim$ 1 s and $\sim$ 8 s, the photon index first appears to reach an asymptotic value of $\sim$ 0.76, then further decreases up to $\sim$ 0.7.

is much lower than the non-thermal one and then it is negligible. Another alternative and/or complementary possibility is that the thermal component has been missed due to the limited bandpass of the instruments. It can be only matter of speculation if observations by *Fermi* and AGILE would have led to a different conclusion.

The remaining part of the first episode (from $\sim$ 7 s up to about 28 s) is interpreted as the peak of the extended afterglow, whose temporal variability is produced by the interaction with the CBM. The numerical simulation that best reproduces the light curve (Fig. 7.5) and the time-integrated spectrum (Fig. 7.7) of this first episode ($3s \leq t_a^d \leq 28s$) is obtained with the following parameters: $E_{tot}^{e^\pm} = 1.32 \times 10^{54}$ erg, $B = 2.3 \times 10^{-3}$ and $\alpha = -1.8$; the Lorentz gamma factor at the transparency point, occurring at $r_0 = 2.8 \times 10^{14}$ cm, is $\gamma_0 = 428$. We consider an average number density $\langle n_{cbm} \rangle \sim 6$ particles cm^{-3} and $\mathcal{R} = 3.5 \times 10^{-10}$. The structure of the CBM adopted is presented in Fig. 7.6 and the adopted density contrast with respect to the average density is reported in Tab. 7.1. The distribution of the CBM is just an approxima-

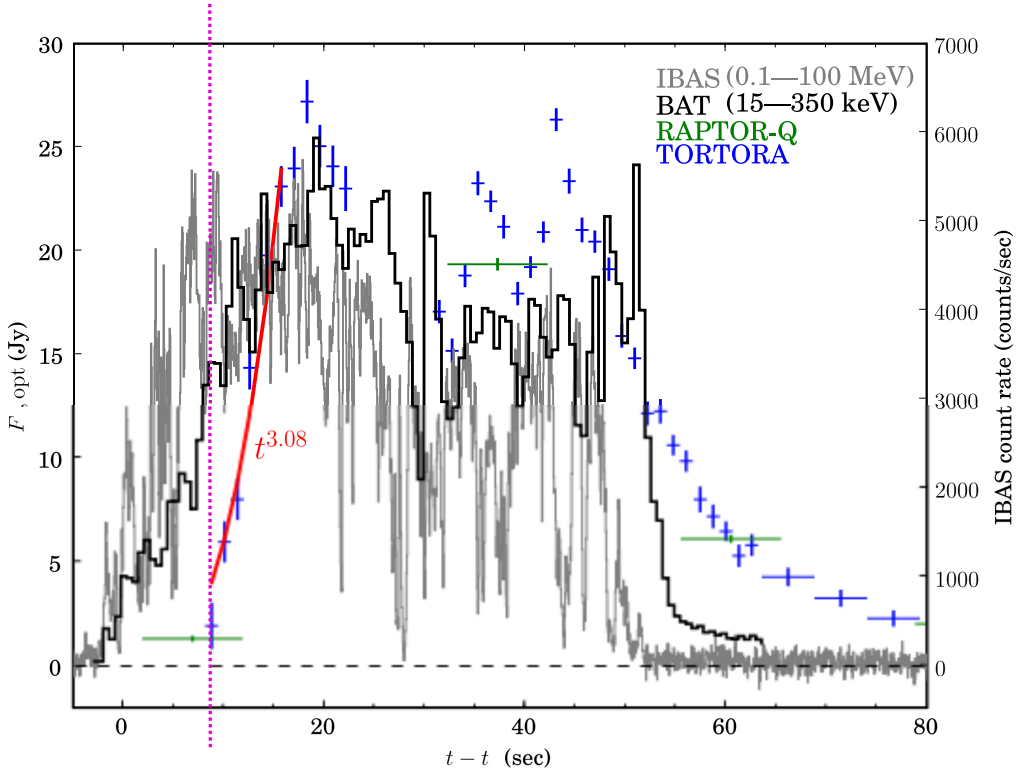

Figure 7.4.: Comparison of the prompt optical light curve (TORTORA, blue points; RAPTOR-Q, green points; Pi of the Sky, blue points) and the hard X-ray to γ-ray light curve (IBAS, grey points; BAT, black points) of GRB 080319B; the pink dotted line marks the begin of the optical emission detected by TORTORA (t $\sim$ 9 s after the BAT trigger time), whose onset is very rapid ($\sim t^{3.08}$). Reproduced from Woźniak et al. (2009) with kind permission of P.R. Woźniak and of AAS.

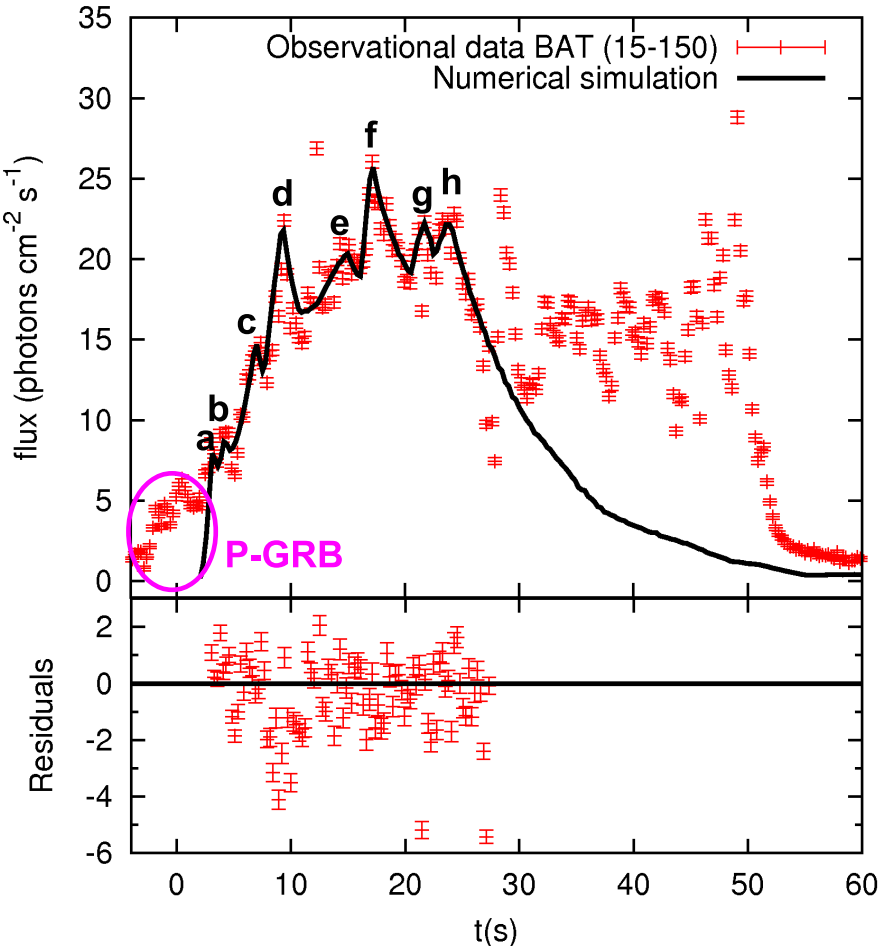

Figure 7.5.: Theoretically simulated light curve of GRB 080319B prompt emission in the 15-150 keV energy band (black solid curve) is compared with the data observed by BAT (red points); the P-GRB is marked with a magenta circle. The vertical dotted line marks the begin of the second part of the prompt emission (t $\sim$ 28 s). The labels "a", "b", "c", "d", "e", "f", "g" and "h" identify the peaks (see Fig. 7.6 and Tab. 7.1).

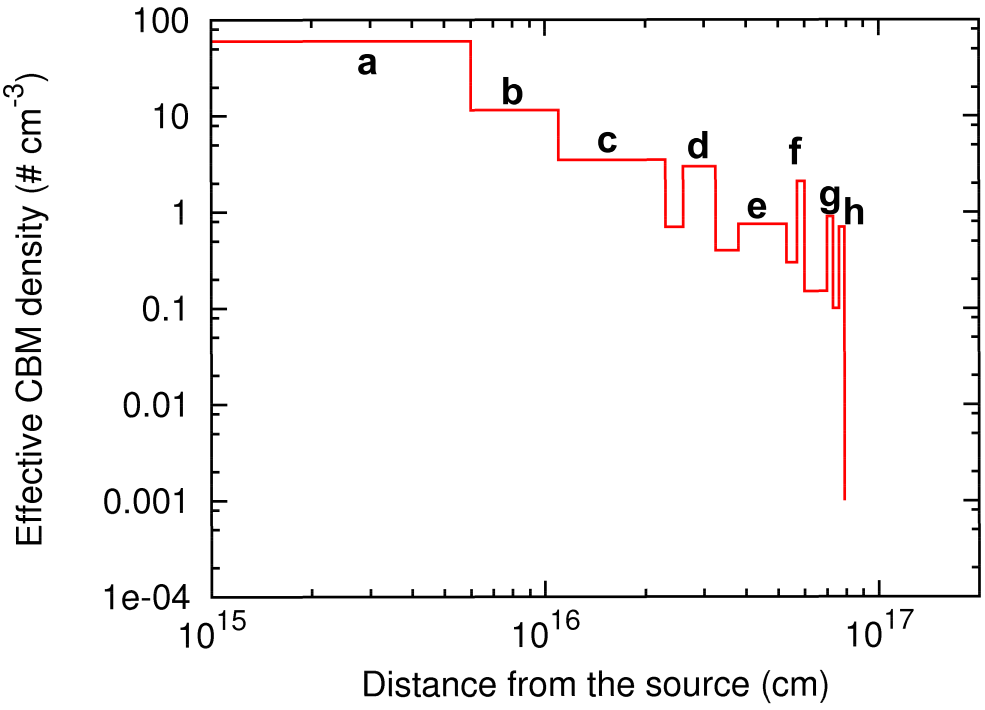

Figure 7.6.: Structure of the CBM adopted for GRB 080319B. The labels "a", "b", "c", "d", "e", "f", "g" and "h" indicate the values corresponding to the peaks in the BAT light curve (see Fig. 7.5 and Tab. 7.1).

peak	r (cm)	Δr (cm)	$\delta n/n$	$M_{cloud}(M_\odot)$	$A_{vis}(cm)$
a	0.0	6.0×10^{15}	9.37	5.7×10^{-9}	-
b	6.0×10^{15}	5.0×10^{15}	1.80	6.3×10^{-10}	3.1×10^{13}
c	1.1×10^{16}	1.2×10^{16}	0.55	2.7×10^{-9}	5.7×10^{13}
d	2.6×10^{16}	6.5×10^{15}	0.47	3.6×10^{-10}	1.4×10^{14}
e	3.8×10^{16}	1.5×10^{16}	0.12	1.1×10^{-9}	2.2×10^{14}
f	5.7×10^{16}	3.0×10^{15}	0.33	2.5×10^{-11}	3.5×10^{14}
g	7.0×10^{16}	3.0×10^{16}	0.14	1.1×10^{-11}	4.6×10^{14}
h	7.6×10^{16}	3.0×10^{16}	0.11	8.3×10^{-12}	5.2×10^{14}

Table 7.1.: Properties of the CBM structure adopted for GRB 080319B: distance from the center of the explosion, thickness, normalized density and mass of the clumps; for each distance the transverse dimension of the visible area is also reported.

tion of the real one, where the CBM density shows some smooth fluctuations around its trend during the fireshell evolution. Nevertheless, it is sufficient to account for the observed variability in the luminosity. We must note that there is a sharp and short spike in the light curve 12.4 s after the BAT trigger time (see e.g. Stamatikos et al., 2009) which we are unable to reproduce within our model, based on a spherically symmetric approximate dynamics. For this spike to be interpreted, a fully three-dimensional description of the CBM is needed. However, we expect that this more detailed description will not modify the overall dynamics of the system. In fact, the fluence of this spike is $\sim$ 4.9% of the fluence observed in the first episode (between 2 s and 28 s) and $\sim$ 2.5% of the fluence of the entire prompt emission (between 2 s and 57 s). Therefore, the error introduced by the omission of this spike from the numerical simulation is much smaller than the difference between the co-moving pure thermal spectrum and the modified one discussed in this paper. We can then omit the spike from our analysis, without hampering qualitatively the conclusions of our paper.

With the above described set of parameters it is possible to interpret also successfully the spectra integrated over smaller intervals of time. Fig 7.8 shows, as an example, the spectrum for $3s \leq t_a^d \leq 13s$: it can be seen that with the modified thermal spectrum we can correctly reproduce also this spectrum; on the contrary, by assuming a comoving thermal spectrum there are several discrepancies between the theoretical prediction and the observational data, especially at the lower energies. This is an important check to be made each time. In fact, changing the spectrum integration time means changing the number of different co-moving spectra which are convolved to

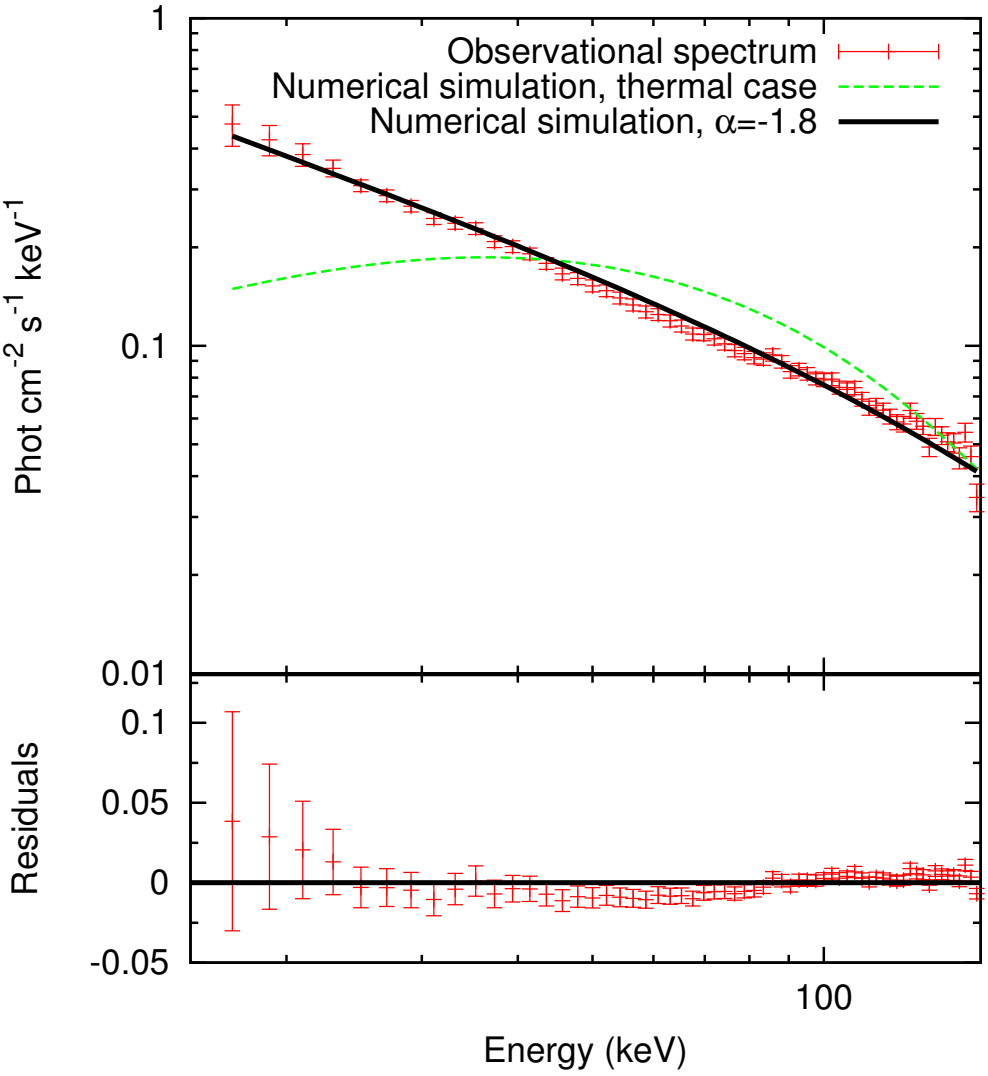

Figure 7.7.: Theoretically simulated spectra of GRB 080319B integrated over the time interval $3s \leq t_a^d \leq 28s$ with $\alpha = -1.8$ (black solid line) and $\alpha = 0.0$ (pure thermal case, green dashed line) are compared with the data observed by BAT (red points). It can be seen that with the "modified" thermal spectrum we can correctly reproduce the observed spectrum, contrary to what happens with the pure thermal spectrum. In the residual plot the pure thermal case is omitted.

get the observed one. The fact that the model is able to reproduce the observed spectrum regardless of the time scale over which it is integrated is therefore a clear support of the correctness of the assumed co-moving spectral shape.

To have an estimate of the sensitivity of the determination of these parameters of the model, we can proceed as follows. We fix $E^{e^\pm}_{tot}$ to the observed value of 1.32×10^{54} erg (Golenetskii et al., 2008). From the observational data we have that the fluence of the first 7 seconds, which correspond to the fluence of the P-GRB, $f_{P\text{-}GRB}$, is $2.19 \times 10^{-6} \leq f_{P\text{-}GRB} \lesssim 2.29 \times 10^{-6}$ erg/cm^2. This fixes a range of values for B: $2.19 \times 10^{-3} \lesssim B \leq 2.33 \times 10^{-3}$. Correspondingly, we must have $1.5 \times 10^{-10} \leq \mathcal{R} \leq 6.0 \times 10^{-10}$ and $4.1 \leq \langle n_{cbm} \rangle \leq 8.2$ particles/cm^3 to reproduce the observed light curves and spectra. It must be noted that the upper limit on $f_{P\text{-}GRB}$, and therefore the lower limit on B, is less stringent since we cannot exclude that more energy has been emitted in the P-GRB outside of the instrumental bandpass.

Concerning the second episode, lasting from 28 s to the end of the prompt emission, we performed numerical simulations with different sets of parameters, but we encountered several difficulties. In particular, while we can obtain a theoretical spectrum compatible with the observed one, it is not possible to correctly reproduce the time variability of the light curve, even when a bi-dimensional model for the CBM is adopted (Bianco et al., 2006a; Bernardini et al., 2009). This is consistent with the results presented by other authors: the time-resolved prompt emission spectra are best fit with power-laws and no change in the photon index is observed between the first and the second component (Stamatikos et al., 2009); on the contrary, a variation of the time-variability is found (Margutti et al., 2008). A possible explanation for this problem is that a fully three-dimensional modeling of the CBM is needed.

7.5. GRB 050904

We analyzed the prompt emission light curve (Fig. 7.9) and spectrum (Fig. 7.11) of GRB 050904 observed by BAT. As we already mentioned in the Introduction, for GRB 050904 we have $E^{obs}_{peak} = 314^{+173}_{-89}$ keV (Sugita et al., 2009). The data have been obtained by using the standard FTOOLS package (Heasoft, version 6.10); the BAT spectrum integrated over the T_{90} of the source ($T_{90} = 225 \pm 10$ s, see Sakamoto et al., 2005) is best modeled with a power-law with photon index γ=1.25 $\pm$ 0.07, with a chi square value of $\chi^2 = 64.09$ for 60 degrees of freedom. Within the fireshell model, we identify the prompt emission with the peak of the extended afterglow. In this case the P-GRB has not been observed. In fact, we have estimated $E^{iso}_{P\text{-}GRB} = 1.99 \times 10^{52}$ erg, that for $z = 6.29$ corresponds to a fluence of $\sim 6.3 \times 10^{-9}$ erg cm^{-2}. If we as-

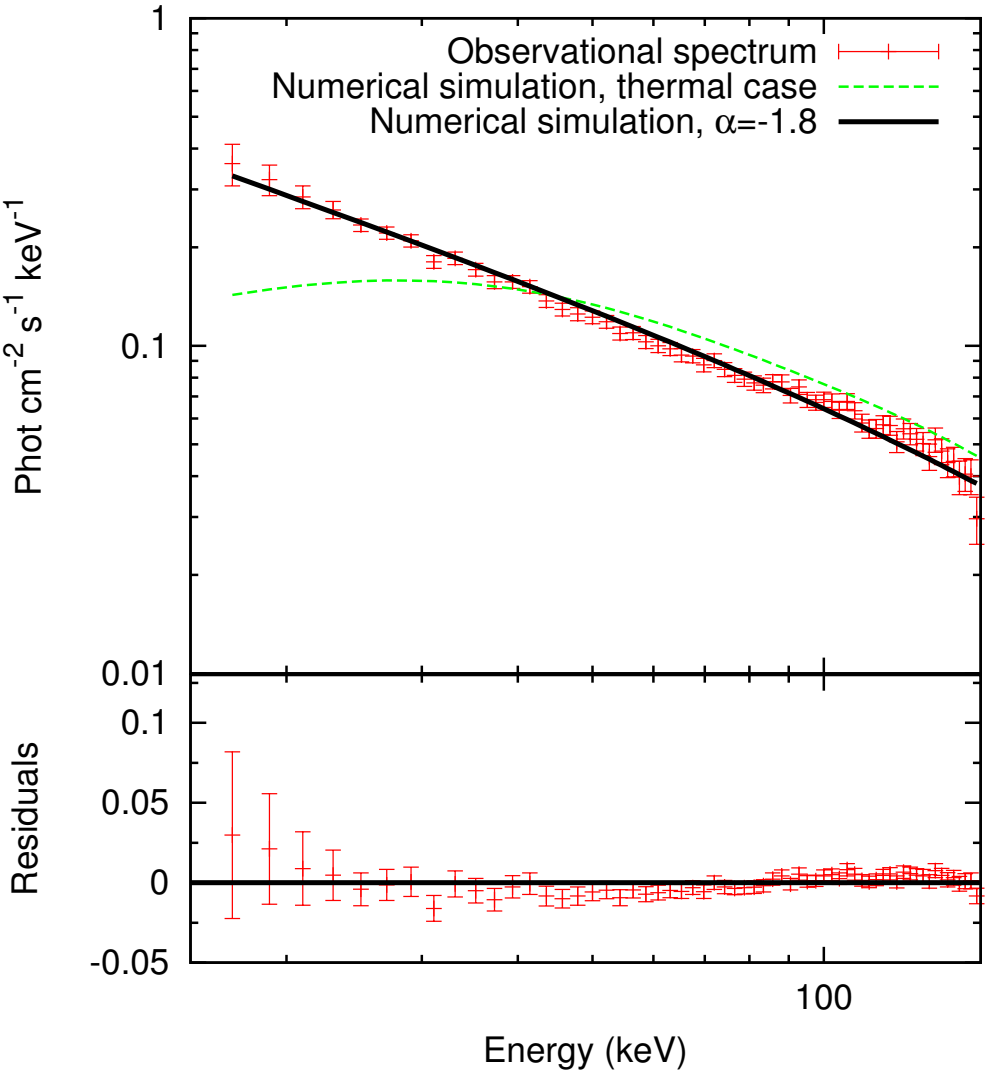

Figure 7.8.: Theoretically simulated spectra of GRB 080319B integrated over the time interval $3s \leq t_a^d \leq 13s$ with $\alpha = -1.8$ (black solid line) and $\alpha = 0.0$ (pure thermal case, green dashed line) are compared with the data observed by BAT (red points). It can be seen that with the "modified" thermal spectrum we can correctly reproduce the observed spectrum, contrary to what happens with the pure thermal spectrum. In the residual plot the pure thermal case is omitted.

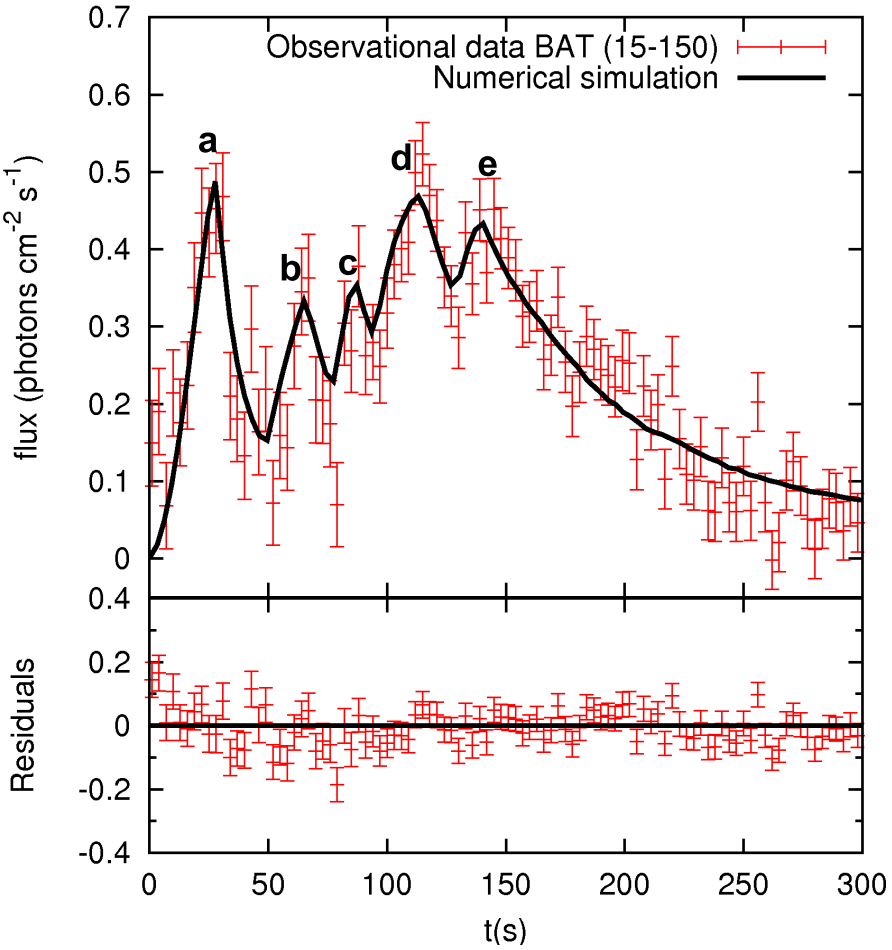

Figure 7.9.: Theoretically simulated light curve of GRB 050904 prompt emission in the 15-150 keV energy band (black solid curve) is compared with data observed by BAT (red points). The labels "a", "b","c","d" and "e" identify the peaks (see Fig. 7.10 and Tab. 7.2).

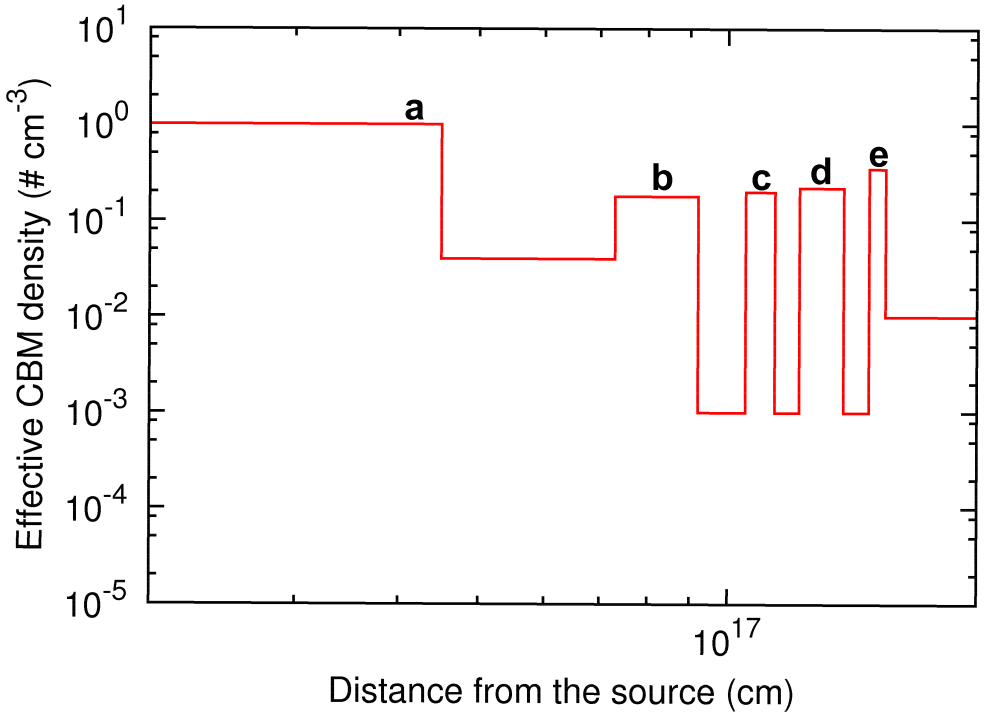

Figure 7.10.: Structure of the CBM adopted for GRB 050904. The labels "a", "b","c","d" and "e" indicate the values corresponding to the peaks in the BAT light curve (see Fig. 7.9 and Tab. 7.2).

peak	r (cm)	Δr (cm)	$\delta n/n$	$M_{cloud}(M_\odot)$	$A_{vis}(cm)$
a	0.0	4.5×10^{16}	4.3	4.0×10^{-8}	-
b	7.3×10^{16}	1.9×10^{16}	0.8	5.4×10^{-10}	3.7×10^{14}
c	1.05×10^{17}	9.0×10^{15}	0.9	6.4×10^{-11}	5.7×10^{14}
d	1.22×10^{17}	1.6×10^{16}	1.0	4.0×10^{-10}	7.1×10^{14}
e	1.48×10^{17}	7.0×10^{15}	1.5	5.3×10^{-11}	1.0×10^{15}

Table 7.2.: Properties of the CBM structure adopted for GRB 050904: distance from the center of the explosion, thickness, normalized density and mass of the clumps; for each distance the transverse dimension of the visible area is also reported.

sume an observed duration $\Delta t_{P\text{-}GRB} \gtrsim 1$ s, the P-GRB flux is under the BAT threshold. The numerical simulation that best reproduce the observational data is obtained with similar values of $E_{tot}^{e^\pm}$ and B found for GRB 080319B: $E_{tot}^{e^\pm} = 1.0 \times 10^{54}$ erg and $B = 2.2 \times 10^{-3}$, with a Lorentz gamma factor at the transparency point $\gamma_0 = 446$. This could be an indication of a similar progenitor for the two sources. Concerning the other model parameters, we found an average number density $\langle n_{cbm} \rangle \sim 0.2$ particles cm^{-3} and $\mathcal{R} = 2 \times 10^{-11}$; these values are different from the ones obtained for GRB 080319B and this could be an indication of the fact that the two bursts occurred in different environments. The structure of the CBM adopted is shown in Fig. 7.10 and the adopted density contrast with respect to the mean density is reported in Tab. 7.2.

Also in this case the numerical simulation that best reproduces the observational data has been obtained assuming the value -1.8 for the free parameter α; in this way we can also correctly reproduce spectra integrated over intervals of time much less than the T_{90} of the source (in Fig. 7.12 is shown, as an example, the BAT spectrum integrated over the first 50 s). Once again, the fact that the model is able to reproduce the observed spectrum regardless of the time scale over which it is integrated is a clear support of the correctness of the assumed co-moving spectral shape.

Estimating the sensitivity of the determination of these parameters of the model in this case of GRB 050904 is more difficult than in the previous case of GRB 080319B. In fact, in this case the P-GRB is not observed and therefore we may have only a lower limit on the value of B. However, we can proceed as follows. We fix $E_{tot}^{e^\pm}$ to the observed value of $E_{iso} = 1.04^{+0.25}_{-0.17} \times 10^{54}$ erg (Sugita et al., 2009), i.e. $8.7 \times 10^{53} \leq E_{tot}^{e^\pm} \leq 1.29 \times 10^{54}$ erg. We can then make an educated guess about the average value of n_{cbm}, i.e. we can assume that $0.1 \lesssim \langle n_{cbm} \rangle \lesssim 10$ particles/cm^3 (see Sec. 7.3.4). With this choice, we obtain $1.9 \times 10^{-3} \lesssim B \lesssim 3.4 \times 10^{-3}$ and $1.5 \times 10^{-11} \lesssim \mathcal{R} \lesssim 8.0 \times 10^{-11}$ to reproduce the observed light curves and spectra.

7.6. Discussion on the comoving spectrum

We have mentioned in Sec. 7.1 that GRBs with E_{iso} up to 10^{53} erg have been successfully interpreted within the traditional fireshell model by assuming a pure comoving thermal spectrum. In the previous sections we have also shown that a modification of the comoving spectrum (see Eq. 7.3.7) is needed to correctly reproduce the observational data of two of the most energetic GRBs, GRB 080319B and GRB 050904, within the fireshell model: the difficulty in interpreting the BAT data by assuming a pure comoving thermal spectrum for these sources has been clearly shown in Fig. 7.8.

The reasons of this result can be summarized as follows (see also Sec. 7.1):

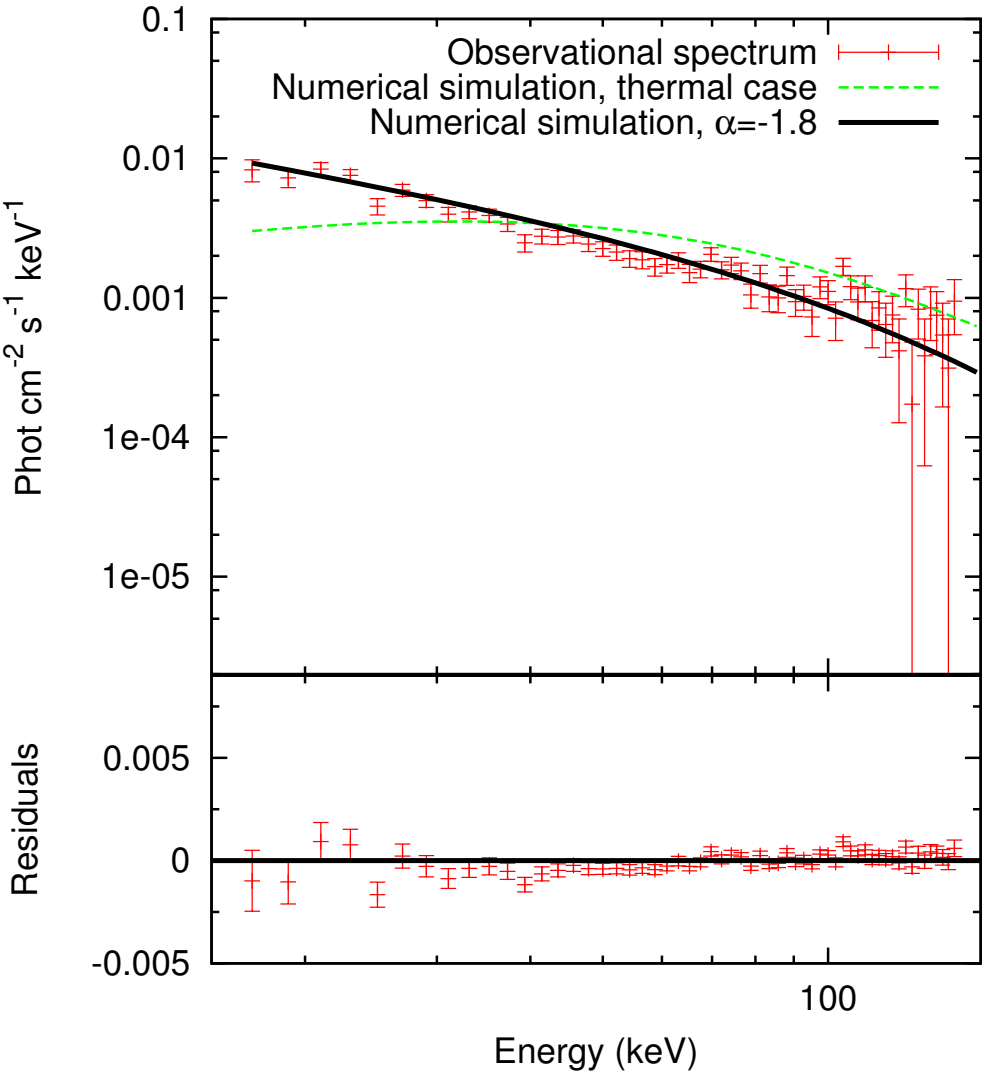

Figure 7.11.: Theoretically simulated time integrated spectra of GRB 050904 for $0 \leq t_a^d \leq 225s$ with $\alpha = -1.8$ (black solid line) and $\alpha = 0.0$ (pure thermal case, green dashed line) are compared with the data observed by BAT (red points). It can be seen that with the "modified" thermal spectrum we can correctly reproduce the observed spectrum, contrary to what happens with the pure thermal spectrum. In the residual plot the pure thermal case is omitted. The range of vertical axes in the residual plot has been chosen to be the same of Fig. 7.12.

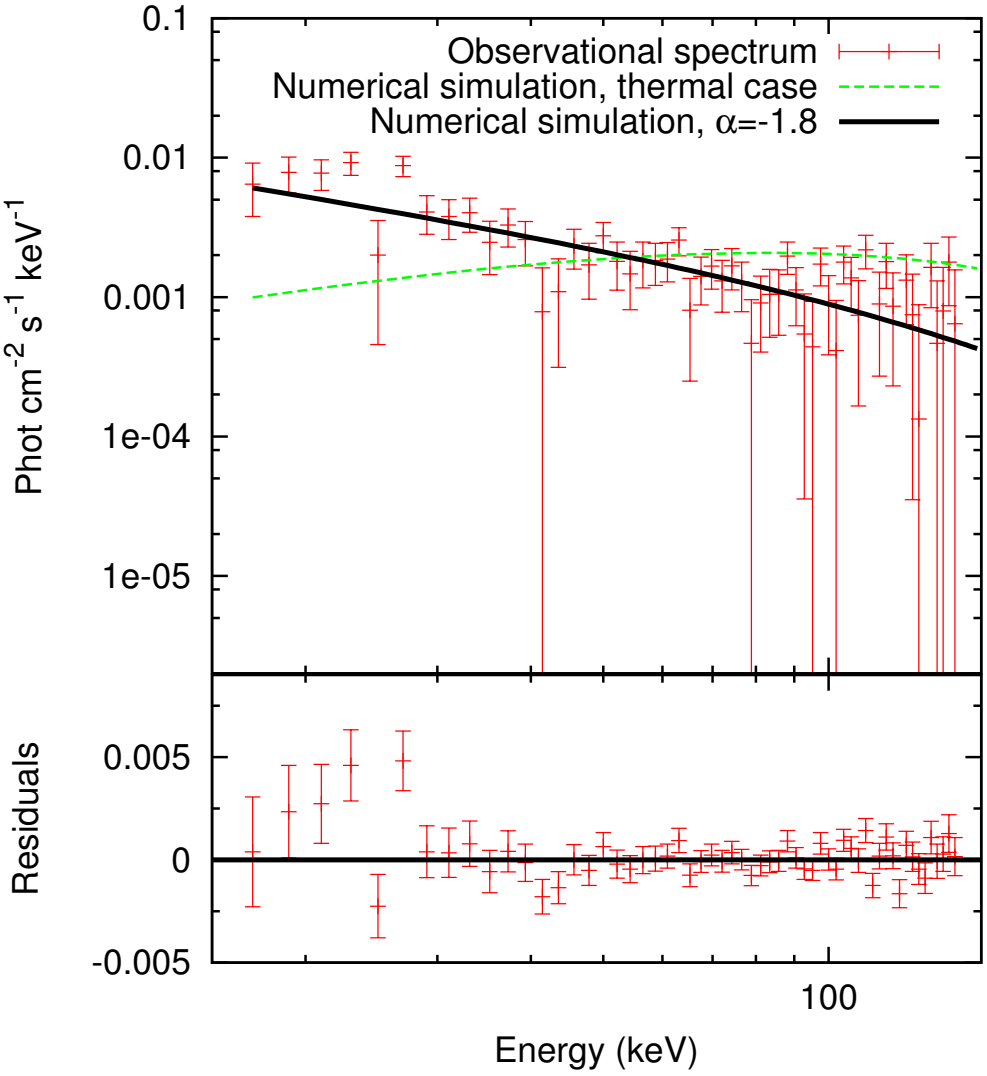

Figure 7.12.: Theoretically simulated time integrated spectra of GRB 050904 for $0 \leq t_a^d \leq 50s$ with $\alpha = -1.8$ (black solid line) and $\alpha = 0.0$ (pure thermal case, green dashed line) are compared with the data observed by BAT (red points). It can be seen that with the "modified" thermal spectrum we can correctly reproduce the observed spectrum, contrary to what happens with the pure thermal spectrum. In the residual plot the pure thermal case is omitted.

GRB	031203 (a)	060607A (b)	080319B (c)	050904 (d)
z	0.106	3.082	0.937	6.29
E_{iso} (erg)	10^{50}	1.1×10^{53}	1.34×10^{54}	1.04×10^{54}
E^{i}_{peak} (keV)	158 ± 51	478^{+314}_{-69}	1261 ± 65	2291^{+1263}_{-634}
E^{obs}_{peak} (keV)	144 ± 46	117^{+77}_{-17}	675 ± 22	314^{+173}_{-89}
Satellite	INTEGRAL	*Swift*	*Swift*	*Swift*
Instrument	IBIS/ISGRI	BAT	BAT	BAT
ΔE (keV)	17 – 500	15 – 150	15 – 150	15 – 150

Table 7.3.: Redshift (z), isotropic energy (E_{iso}), intrinsic and observed peak energy (E^{i}_{peak} and E^{obs}_{peak} respectively) of GRB spectra analysed within the fireshell model. The instruments by which the observational data interpreted within the fireshell model have been taken, together with the energy range they cover (ΔE), are also reported. References for z: (a) Prochaska et al. (2004); (b) Ledoux et al. (2006); (c) Vreeswijk et al. (2008); (d) Kawai et al. (2005). References for E_{iso}: (a) Amati (2006); (b) L. Amati, private communication; (c) Golenetskii et al. (2008) ; (d) Sugita et al. (2009). References for E^{i}_{peak}: (a) Amati (2006); (b) L. Amati, private communication; (c) Golenetskii et al. (2008) ; (d) Sugita et al. (2009). References for E^{obs}_{peak}: (a) Ulanov et al. (2005) ; (b) L. Amati, private communication; (c) Racusin et al. (2008); (d) Sugita et al. (2009).

1. The modification of the spectral energy distribution given in Eq. 7.3.7 does not affect the spectrum near the peak, but it affects the low energy Rayleigh-Jeans tail of the distribution (see Figs. 7.1 and 7.2).

2. For the sources with $E_{iso} \lesssim 10^{53}$ erg previously analysed within the fireshell model, only the spectral region around the peak contributes to the emission in the instrument bandpasses. We give two explicit examples in Tab. 7.3: the INTEGRAL and *Swift* BAT observations of GRB 031203 and GRB 060607A only cover the region around the peak.

3. In the case of the most energetic sources, like GRB 080319B and GRB 050904, E^{obs}_{peak} is outside the *Swift* BAT bandpass (see Tab. 7.3). Conversely, the *Swift* BAT data cover precisely the low energy component of the spectrum, where the effect of the new parametrization of the spectrum is maximised (see Tab. 7.3).

The issue if the modification of the comoving spectrum given in Eq. 7.3.7 is really universal and applies as well to lower energetic sources is still open. It could only be settled by future space missions dedicated to the observation of the prompt emission below 10 keV such as LOFT (Feroci and The LOFT Consortium, 2011) and MIRAX (Amati et al., 2011).

As correctly pointed out to us by an anonymous referee, a critical test for the modified comoving thermal spectrum can also come from GRB 061121

(Page et al., 2007). In this special case, a soft precursor pulse triggered BAT, which allowed Swift to slew in time for BAT, XRT (Page et al., 2006b) and UVOT to simultaneously observe the prompt emission. Furthermore, Konus-Wind (Golenetskii et al., 2006a) also observed this burst, which resulted in an $E^{obs}_{peak} \sim 606 + 90/-72$ keV (well above the BAT bandpass) and $E_{iso} \sim 2.5 \times 10^{53}$ erg, given a redshift of $z = 1.314$ (Bloom et al., 2006a). This source presents many other interesting and challenging observational features, and a complete analysis is going to be presented in a separate paper. However, we like to emphasize that the photon index of the XRT data during the main event of the prompt emission is $0.6 \lesssim \Gamma \lesssim 0.8$ [2], in very good agreement with the expected value from the modified thermal spectrum assuming $\alpha = -1.8$, which is indeed ~ 0.8.

7.7. Conclusions

GRB 050904 was discovered in the pre-*Fermi* and pre-AGILE era, while GRB 080319B was discovered in the pre-*Fermi* era and was unobservable by AGILE due to Earth occultation. With the exception of the data from *Konus*-WIND and *Suzaku*-WAM, no observations on the high energy component of these two sources are available. The high quality data from the BAT instrument on board the *Swift* satellite, nevertheless, have allowed us to reach a quite firm conclusion on the low energy component of the spectra of these sources.

Thanks to these most energetic sources we have been able, for the first time, to explore the Rayleigh-Jeans tail of the comoving blackbody spectral energy distribution and to conclude that it must be modified with an additional component. We recall, in fact, that in the original proposal the thermal nature of the spectrum in the comoving frame was adopted only for simplicity, inspired by a similar approach followed by Enrico Fermi in the different context of ultra high-energy collisions. Notice that even photospheric emission in ultrarelativistically expanding sources does not produce pure thermal spectra (Ruffini et al., 2011b; see also Pe'er and Ryde, 2011). The successful interpretation of many sources (see e.g. Bernardini et al., 2005a; Ruffini et al., 2006b; Dainotti et al., 2007; Bernardini et al., 2007; Caito et al., 2009, 2010; de Barros et al., 2011) showed the viability of this ansatz (Ruffini et al., 2004b). In the intervening years, thanks to the data analysis by Felix Ryde and collaborators (see e.g. Ryde, 2004; Ryde and Pe'er, 2009), it has become clear that the existence of a pure black body spectra in any GRB observation is more an exception than the rule (see Sec. 7.2.1). In the present work we show that this is also the case for the comoving spectrum of the extended afterglow. The most interesting aspect is that it is possible to generalize the previous ansatz by the addition of a single power-law component in order to recover a con-

[2] see e.g. data at `http://www.swift.ac.uk/burst_analyser/00239899/`.

GRB	GRB 080319B	GRB 050904
$E_{tot}^{e^{\pm}}$ (erg)	1.32×10^{54}	1.0×10^{54}
B	2.3×10^{-3}	2.2×10^{-3}
α	-1.8	-1.8
$\langle n_{cbm} \rangle$ (#/cm^3)	~ 6	~ 0.2
$\mathcal{R}$	3.5×10^{-10}	2×10^{-11}

Table 7.4.: Summary of parameters characterizing GRB 080319B and GRB 050904.

sistent interpretation of all previous results and of the ones corresponding to the present more energetic sources. We have introduced a new phenomenological parameter α describing such an additional component. The choice of $\alpha = -1.8$ leads to a coherent description of both sources, not contradictory with the previous results on the less energetic sources. The main goal of our work in this paper is to maximize the knowledge acquirable for these very energetic sources ($E_{iso} \sim 10^{54}$ erg), which have a peak of emission at energies much higher than the less energetic ones ($E_{p,i} > 1$ MeV), and therefore to explore the low energy part of the spectrum of the prompt emission. A strong and promising theoretical activity is currently devoted to ascertain a possible role of collisionless shocks in generating power law components in the high energy part of the photon spectrum (Spitkovsky, 2008b). Also, the synchrotron "line of death" appears to be problematic for such models (Sironi and Spitkovsky, 2009). The knowledge of the spectrum in the comoving frame is certainly an important step toward the identification of the physical process occurring in the interaction of the accelerated baryons with the CBM, which is yet largely unknown.

As an additional result, the analysis of GRB light curves and spectra within the fireshell model allows us to infer the filamentary, clumpy and porosity structure of the CBM. Specifically, we determined $\langle n_{cbm} \rangle = 6$ particles cm^{-3} and $\mathcal{R} = 3.5 \times 10^{-10}$ for GRB 080319B, $\langle n_{cbm} \rangle$= 0.2 particles cm^{-3} and $\mathcal{R} = 2.0 \times 10^{-11}$ for GRB 050904 (see also Tab. 7.4).

We can correctly reproduce the whole BAT prompt emission data of GRB 050904. For GRB 080319B only the first ~ 28 s have been satisfactorily interpreted within the fireshell model with a mono-dimensional CBM description. Concerning the remaining part of the prompt emission, it occurs at a distance $r > 10^{17}$ cm, where the transverse dimension of the visible area is much larger than the typical size of the CBM clumps ($5.0 \times 10^{15} \lesssim \Delta r \lesssim 1.7 \times 10^{16}$ cm, see Tab. 7.1). Therefore, a fully three-dimensional modeling of the CBM is needed at such a distance.

We have mentioned in Sec. 7.2 the central role of the phenomenological parameterizations in the description of GRBs. In addition to the α parameter here defined, we have recalled the Band et al. (1993) formula, the Am-

ati et al. (2002) relation and the coefficients described by Ryde (2004, 2005) and Ryde and Pe'er (2009). Although no physical explanation for these parameters have been reached, they represent certainly a fundamental step in reaching a quantitative and qualitative description of the source and help to understand the underlying physical process of GRBs.

In the fireshell model the radiation observed in the BAT data comes from an integration which takes into account the CBM filamentary structure and applies a double convolution, over the EQTS and the observation time, of a mixing of the co-moving thermal and power-law components given by Eq.(7.3.7). In the BAT energy range the cutoffs of the thermal components give a fundamental contribution. It was therefore unexpected that the theoretically computed spectrum would have given rise to a power-law so closely resembling the observed one. There is no simple relation between the power-law index of the observed BAT spectrum and the one of the power-law component in the co-moving spectrum given in Eq.(7.3.7). When the co-moving thermal component becomes negligible at low enough energy, the co-moving spectrum is described by just the power-law component. The convolution of power-laws with the same index results in a power-law of that index. Observations by XRT in the prompt emission of a highly energetic source, if available, may then give direct and independent information about the existence of the power-law component in Eq.(7.3.7) and on its index. If so confirmed, this power-law component would not be just a mere phenomenological optimization of the agreement between our theory and the observed BAT spectra. It would be an independent physical component of the co-moving spectrum, whose index can be directly read from the observational data. This would give an additional strong confirmation of our model.

8. Cooling of young neutron stars in GRB associated to supernovae

8.1. Introduction

The investigation of the thermal evolution of neutron stars is a powerful tool for probing the inner composition of these objects. The cooling of neutron stars has been investigated by many authors, where many different microscopic models were assumed (see Schaab et al., 1996; Page et al., 2004, 2006, 2009; Blaschke et al., 2000; Grigorian et al., 2005; Blaschke et al., 2006; Negreiros et al., 2010). Most of the research on the thermal evolution of compact stars focus on objects older than 10 to 100 years, which is comprehensible if one considers that the thermal data currently available to us is for pulsars with estimated ages the same as or greater than 330 years (Page et al., 2004, 2009). We discuss the thermal evolution of young neutron stars, in the little explored time window that spans ages greater than 1 minute (just after the proto-neutron star regime (Prakash et al., 2001)) to ages $\leq$ 10–100 years, when the neutron star becomes isothermal (see Gnedin et al., 2001, for details).

We discuss the possibility that the late X-ray emission (URCA hereafter [1]) following a few GRBs associated with supernovae (SNe); e.g. URCA-1 in GRB980425-SN1998bw (Ruffini et al., 2004a; Fraschetti et al., 2005; Bernardini et al., 2008c), URCA-2 in GRB030329-SN2003dh (Bernardini et al., 2004, 2005b), and URCA-3 in GRB031203-SN2003lw (Bernardini et al., 2005a; Ruffini et al., 2007c, 2008c) (see Fig. 8.3 for details), might actually be created from young ($t \sim$ 1 minute–(10–100) years), hot ($T \sim 10^7$–10^8 K) neutron stars that are remnants of the SN (Ruffini et al., 2007c) and which we here call neo-neutron stars. Relevant also are the observations of the isolated Type Ic supernova SN 1994I (Immler et al., 2002) and SN 2002ap (Soria et al., 2004), which present late emissions similar to the ones observed in URCA-1, URCA-

[1] The names URCA-1 and URCA-2 mentioned here were given to these sources when presented for the first time at the MG10 meeting held in Rio de Janeiro in the town of Urca. The location of the MG10 meeting was very close to the "Cassino da Urca" where George Gamow and Mario Schoenberg conceived the process of neutrino emission for the cooling process of neutron stars, which also took the name from the town of Urca, the Urca process (see e.g detailed history in Ruffini et al., 2005b; Gamow, 1970b)

2, and URCA-3.

Here we propose a revision of the boundary conditions usually employed in the thermal cooling theory of neutron stars, in order to match the proper conditions of the atmosphere at young ages. We also discuss the importance of the thermal processes taking place in the crust, which also have strong effects on the initial stages of thermal evolution. We stress that we are not calling the validity of the current treatment of the atmosphere of compact stars into question but, instead, we point out the need of extending them to appropriately describe the conditions of neo-neutron stars.

8.2. Cooling of young, hot neutron stars

There are three important ingredients that govern the thermal evolution of a compact star: 1) the microscopic input, which accounts for the neutrino emissivities, specific heat, and thermal conductivity; 2) the macroscopic structure of the star, namely its mass, radius, pressure profile, crust size, etc.; and 3) the boundary condition on the surface of the star, which provides a relationship between the mantle temperature and that of the atmosphere, the latter being what we ultimately observe. These ingredients have been studied extensively, and a comprehensive review can be found in Page et al. (2006). As discussed in Gnedin et al. (2001), during the initial stages of thermal evolution (ages $\leq 10 - 100$ years), the core and the crust of the neutron star are thermally decoupled. This is because the high-density core is emitting neutrinos at a much higher rate than the crust, which causes it to cool down more quickly. This effectively means that, initially, the neutron star is cooling "inside out", with the core colder than the outer layers. This scenario is schematically depicted in Figure 8.1.

The dominant neutrino emission processes in the crust are given by the Bremsstrahlung, plasmon decay, and electron-positron annihilation processes. Following the footsteps of Gnedin et al. (2001), we calculate the thermal evolution of neutron stars, by artificially adding a phenomenological source of heat (see details in Sec. 8.4). This allow us to estimate how much heat is needed, so that the thermal evolution of a neo-neutron star matches the X-ray light curve of late emission of GRB-SN.

After this initial core-crust decoupled state, the "cooling wave" originated in the core reaches the crust, and the object becomes isothermal. The time scale of this process is between 10 and 100 years, depending on the properties of the crust (Gnedin et al., 2001). This means that the crust shields the core during the initial stages of thermal evolution, and all the information we might obtain at this stage refers only to the crust and to the atmosphere of the star. This raises another issue about the atmosphere of the star. The thermal connection between the mantle and the atmosphere is what defines the photon luminosity, which is what we observe. Therefore, the appropriate

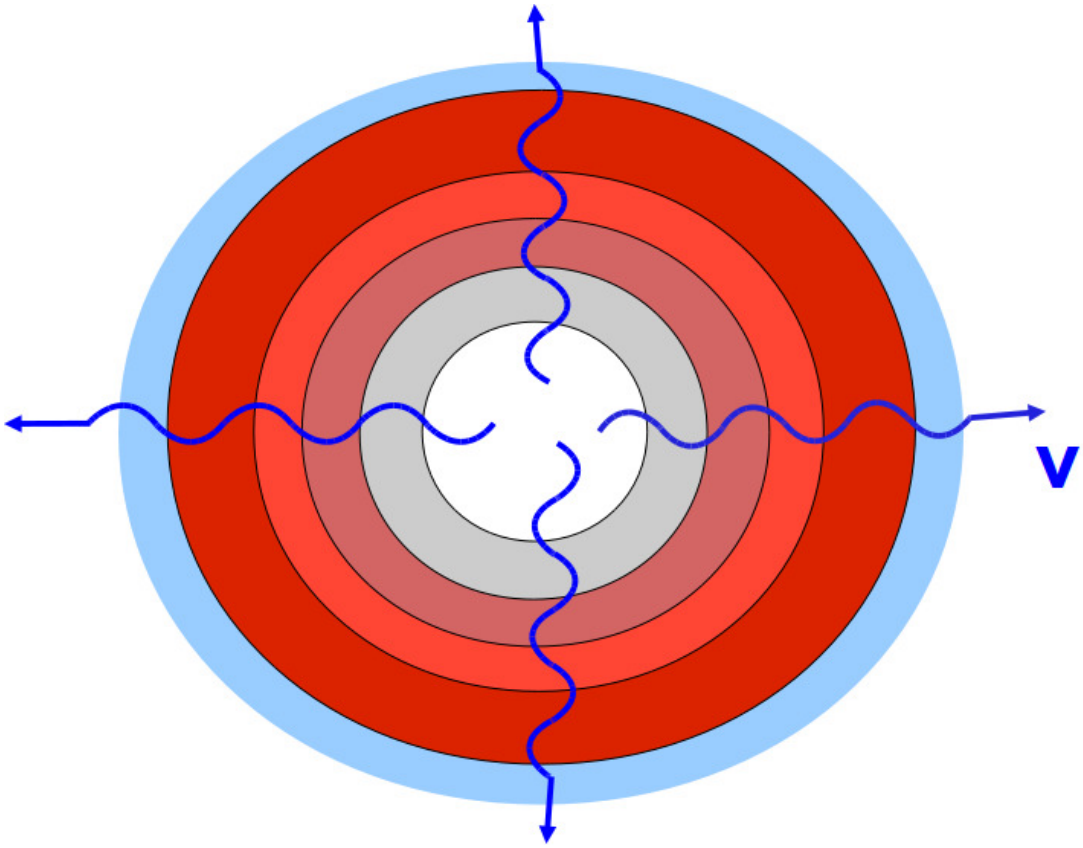

Figure 8.1.: Schematic representation of the cooling of a young neutron star. Due to stronger neutrino emissivities, the core of the star cools down more quickly than the crust, causing the star to cool inside out. Darker and lighter areas represent higher and lower temperatures, respectively.

description of the atmosphere is key to correctly understanding the thermal evolution of neutron stars. In the usual approach, the thermal relaxation time of the atmosphere is assumed to be much shorter than that of the neutron star; furthermore, neutrino emissions from the atmosphere are also considered to be negligible (see Gudmundsson et al., 1983). Under these assumptions, and assuming a plane-parallel approximation (which is reasonable since the atmosphere is ~ 100 m thick), one can get a relationship between the temperature of the mantle T_b and the temperature of atmosphere T_e or, equivalently, the luminosity L_e. Gudmundsson et al. (1983) originally found a T_b-T_e relationship that depends on the surface gravity of the neutron star. This relationship was developed further by Potekhin et al. (1997) to account for the possibility of mass accreted in the initial stages and of magnetic fields effects. As pointed out by Gudmundsson et al. (1983), such assumptions for the atmosphere of the star are only valid for objects older than a few tens of years, when the temperature has dropped below 10^9K for densities below 10^{10} g/cm^3. In fact, we see that the current boundary conditions yields temperatures $\sim 10^7$ K ($L \sim 10^{37}$ erg/s, equivalently) for young neutron stars (age $<$ 1–10 years). This should raise some suspicion since proto-neutron stars studies (see Prakash et al., 2001, and references therein) indicate that neutron stars just after this regime have temperatures $\sim 10^{10}$–10^{11} K.

The properties of the atmosphere of a sufficiently hot, nascent neutron star should differ significantly from those considered in Gudmundsson et al. (1983) and Potekhin et al. (1997), especially since at hot temperatures ($T \gtrsim 10^9$ K) the atmosphere might not be transparent to neutrinos, and thus the neutrino transport equations have to be considered. The coupled equations of neutrino and photon transport, in the atmosphere of a neutron star, were solved by Salpeter and Shapiro (1981), and Duncan et al. (1986). In these works the authors performed detailed calculations of the atmosphere properties of hot neutron stars. They found the following photon luminosity, as observed at infinity,

$$L_\infty = 50 \times t^{-7/12} \times (T_{10})^{7/4} \times (R_{10})^{17/9} \times \left(\frac{M}{M_\odot}\right)^{-1} \times L_E, \qquad (8.2.1)$$

where t is time in seconds, T_{10} is the initial temperature in units of 10 MeV, R_{10} the neutron star radius in units of 10 km, M the neutron star mass, and $L_E \sim 2.0 \times 10^{38}$ erg/s is the Eddington luminosity. Duncan et al. (1986) found that the above expression should be valid for at least the initial 100 s. In Fig. 8.2 we can see how the luminosity of the star changes for the first 100 s, for stars with different initial temperatures.

According to these results, during the initial 100 s, the photon luminosity emerging from the atmosphere will be higher than the Eddington luminosity. This implies that there will be mass loss, owing to neutrino-driven winds from the young atmosphere. As shown by Duncan et al. (1986), the total

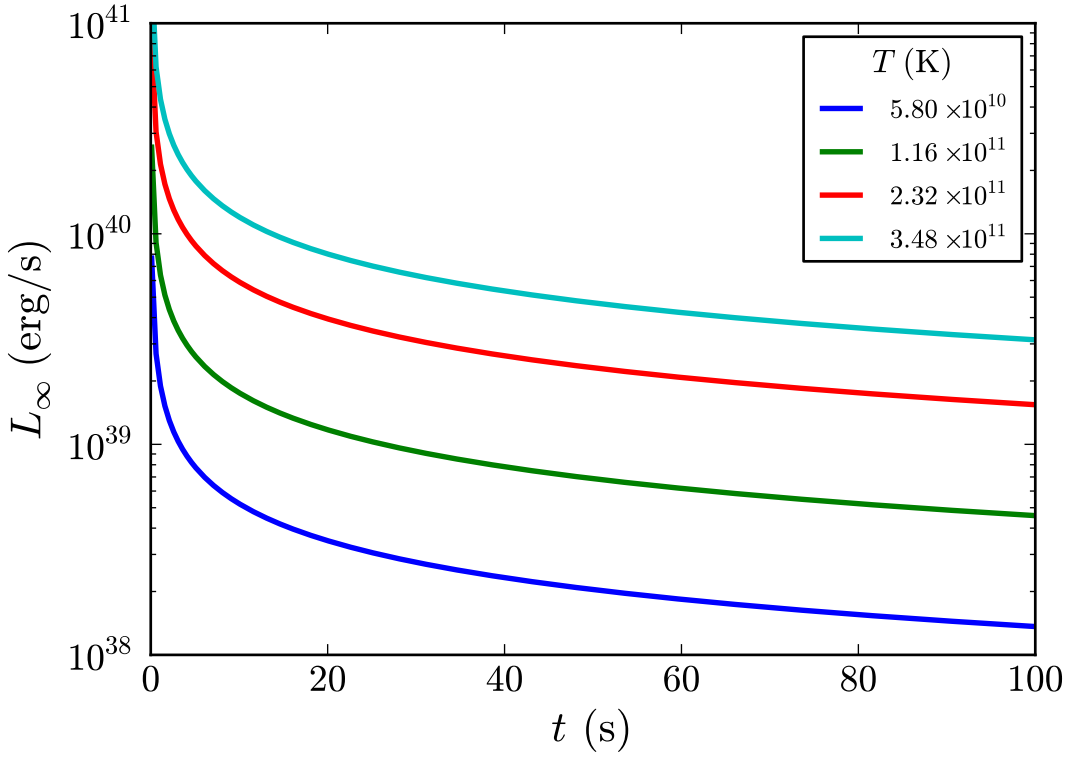

Figure 8.2.: Luminosity of a hot nascent neutron star as observed at infinity given by Eq. (8.2.1) during the initial 100 s (Duncan et al., 1986), with the initial temperatures indicated. The neutron star is assumed to have a mass of $1.4M_\odot$ and a radius of 13 km.

mass loss only becomes appreciable for neutron stars with large radii and high initial temperatures. For a typical neutron star with the canonical mass of $1.4M_{\odot}$, a radius of 13 km and initial temperature of $\sim 10^{11}$ K, the total mass loss was estimated to be $\sim 6.2 \times 10^{-6} M_{\odot}$.

In addition to the high luminosities associated to the atmosphere of young neutron stars, one also needs to consider fallback onto the surface of the neutron star. Potekhin et al. (1997) discuss how fallback, at earlier stages of evolution, would modify the properties of the atmosphere, hence of the boundary conditions. Once more in this investigation, however, such a fallback is assumed to have happened at early times, and the modified boundary conditions are only valid if the fallback has already ceased. Chevalier (1989) studied the fallback onto young neutron stars and found that, while there is an envelope, a luminosity near the Eddington limit should be present. Furthermore, the authors have found that in this case the energy from the envelope can be radiated away in about one year. This timescale, however, might be lengthened if rotation effects are accounted for during the fallback. In addition to that, Turolla et al. (1994) discuss the possibility of "hot solutions" for the atmosphere of neutron stars undergoing spherical accretion. It is shown that for $L \geq 10^{-2} L_E$ the temperature at the atmosphere of a neutron star might be $\sim 10^9$–10^{11} K.

8.3. Late X-ray emission in GRBs associated to supernovae: URCAs

It seems clear to us that, after the analysis of the scenario described above, we must extend the current model for the boundary conditions used in cooling calculations, to include the effects of a high-temperature atmosphere, possibly with super-Eddington luminosity. Up until this point, however, little attention has been given to the thermal evolution of young neutron stars, mainly due to the absence of observational data of neutron stars with ages < 330 years. It has been recently proposed (see Ruffini et al., 2007c, for details) that the long-lasting X-ray emission called URCA there (see Fig. 8.3) of a few GRBs associated to SNe; URCA-1 in GRB980425-SN1998bw (Ruffini et al., 2004a; Fraschetti et al., 2005; Bernardini et al., 2008c), URCA-2 in GRB030329-SN2003dh (Bernardini et al., 2004, 2005b), and URCA-3 in GRB031203-SN2003lw (Bernardini et al., 2005a; Ruffini et al., 2007c, 2008c), might actually originate in the compact star remnant of the SN: a neo-neutron star. In this scenario the GRB is described as the core collapse of a massive star, whose remnant is a black hole. This massive star is supposed to be in a binary system, whose companion is on the verge of becoming an SN. The GRB triggers the SN explosion in the companion star, which in turns leaves behind a neutron star (Ruffini et al., 2001a). An alternative scenario has been recently suggested in

Table 8.1.: GRBs associated to SNe and URCAs. a) see Kaneko et al. (2007); b) Mazzali, P., private communication at MG11 meeting in Berlin, July 2006, Iwamoto et al. (1998); c) evaluated fitting the URCAs with a power law followed by an exponentially decaying part; d) evaluated assuming a mass of the neutron star $M = 1.5 M_\odot$ and $T \sim$ 5–7 keV in the source rest frame; e) see Galama et al. (1998); Greiner et al. (2003b); Prochaska et al. (2004); Mirabal et al. (2006). Here $E^{tot}_{e^\pm}$ is the total energy of GRB, E^{bolom}_{SN} and E^{kin}_{SN} are the bolometric and the kinetic energy of the SN, E_{URCA} is the energy of the late X-ray emission URCA (see Fig. 8.3), R_{NS} is the radius of the neutron star, and z is the redshift of the event.

GRB	$E^{tot}_{e^\pm}$ (erg)	E^{bolom}_{SN} (erg)[a]	E^{kin}_{SN} (erg)[b]	E_{URCA} (erg)[c]	$\frac{E^{tot}_{e^\pm}}{E_{URCA}}$	$\frac{E^{kin}_{SN}}{E_{URCA}}$	R_{NS} (km)[d]	z^e
980425	1.2×10^{48}	2.3×10^{49}	1.0×10^{52}	3×10^{48}	0.4	1.7×10^4	8	0.0085
030329	2.1×10^{52}	1.8×10^{49}	8.0×10^{51}	3×10^{49}	6×10^2	1.2×10^3	14	0.1685
031203	1.8×10^{50}	3.1×10^{49}	1.5×10^{52}	2×10^{49}	8.2	3.0×10^3	20	0.105
060218	1.8×10^{50}	9.2×10^{48}	2.0×10^{51}	?	?	?	?	0.033

which the so-called GRB is actually not a GRB but the observed X-ray emission stems from a collapsing core: a proto-neutron star leading directly to a SN explosion (Ruffini, 2011a). Such a process, if confirmed, will naturally explain the observations of the X-ray outburst 080109/SN 2008D (Soderberg et al., 2008). This concept is very similar to the one of a proto-black hole as introduced in Ruffini et al. (2011a, 2010b); Izzo et al. (2012d); Penacchioni et al. (2012), where the emission from the collapsing core is clearly distinguished from the GRB. In that case, the collapsing core leads to the formation of the black hole, while in the present case it forms a neutron star.

Both scenarios form a neo-neutron star, and they are supported by the observation of supernova 1979C (Patnaude et al., 2011), where a similar X-ray light curve also followed the SN. In Fig. 8.3 we show the X-ray light curve associated with the URCAs.

From Fig. 8.3 we can see that the X-ray luminosities of these sources are of the same magnitude as what is expected for neo-neutron stars, as discussed above. In Table 8.1 we summarize the representative parameters of the four GRB-SN systems, including the very high kinetic energy observed in all SNe (Mazzali, 2006). We have also included the association GRB060218-SN2006aj (see Dainotti et al., 2007, 2010, for details). It must be noted that similar prolonged X-ray emission has also been observed in connection with other Type Ic SN not associated with GRBs, such as SN1994I (Immler et al., 2002) and SN2002ap (Soria et al., 2004) (see Fig. 8.4 for details).

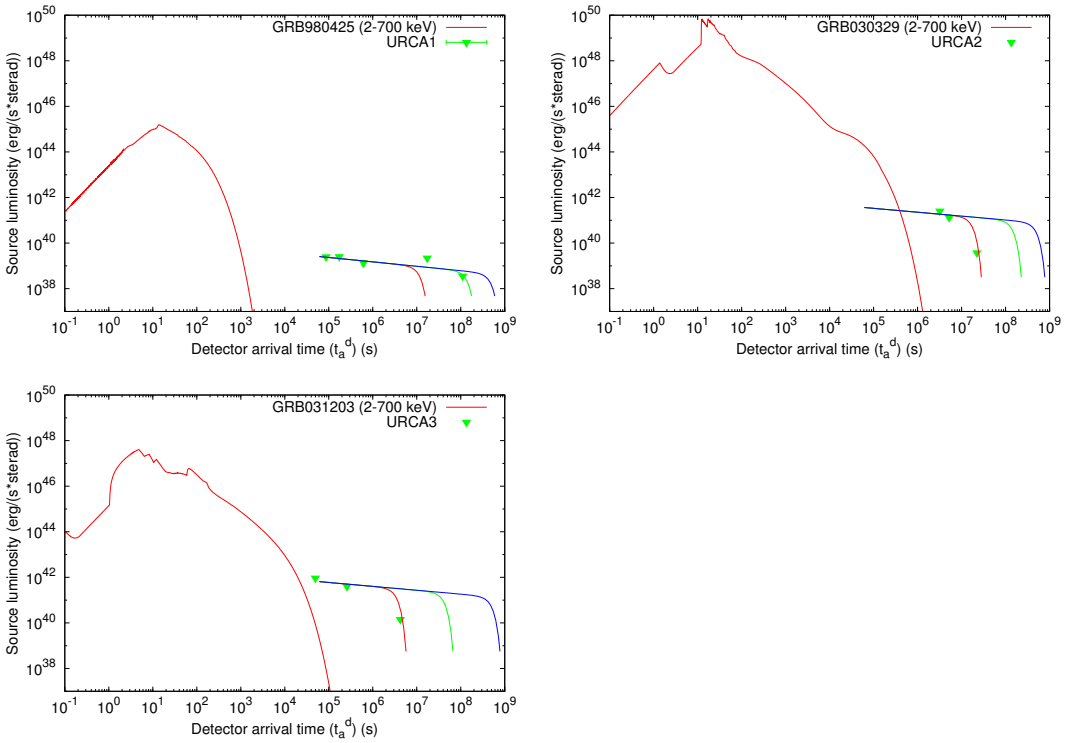

Figure 8.3.: Synthetic light curves of GRB980425 (A) (Ruffini et al., 2004a; Fraschetti et al., 2005; Bernardini et al., 2008c) , GRB030329 (B) (Bernardini et al., 2004, 2005b) and GRB031203 (C) (Bernardini et al., 2005a; Ruffini et al., 2007c, 2008c) . The solid curves represent the hard X-ray emission (10-200 keV range) and the triangles are 2-10 keV flux points. The optical luminosities of the SNe accompanying these GRBs are also reported with crosses (see Ruffini et al., 2007c, for details). The curves fitting the late X-ray luminosity (URCAs) are qualitative cooling curves based on Canuto (1978); see also Ruffini et al. (2004a, 2007c, 2008c), Bernardini et al. (2004, 2005a,b, 2008c), and Fraschetti et al. (2005) for details.

8.4. Neo-neutron star luminosity and the URCAs

Another important ingredient for the cooling of young neutron stars are the crust properties. As illustrated in Fig. 8.1, due to the stronger neutrino emission from the core, the core and crust are thermally decoupled during the initial stages. For that reason, the initial stages of the thermal evolution reflect the properties of the crust, while the core remains invisible. Thus the proper description of the crust structure and composition is also fundamental for understanding the initial thermal stages in the evolution of a neutron star. We now briefly discuss the current understanding of the crustal processes and how it might be related to the data available from the URCAs.

There are several active emission mechanisms in the neutron star crust,

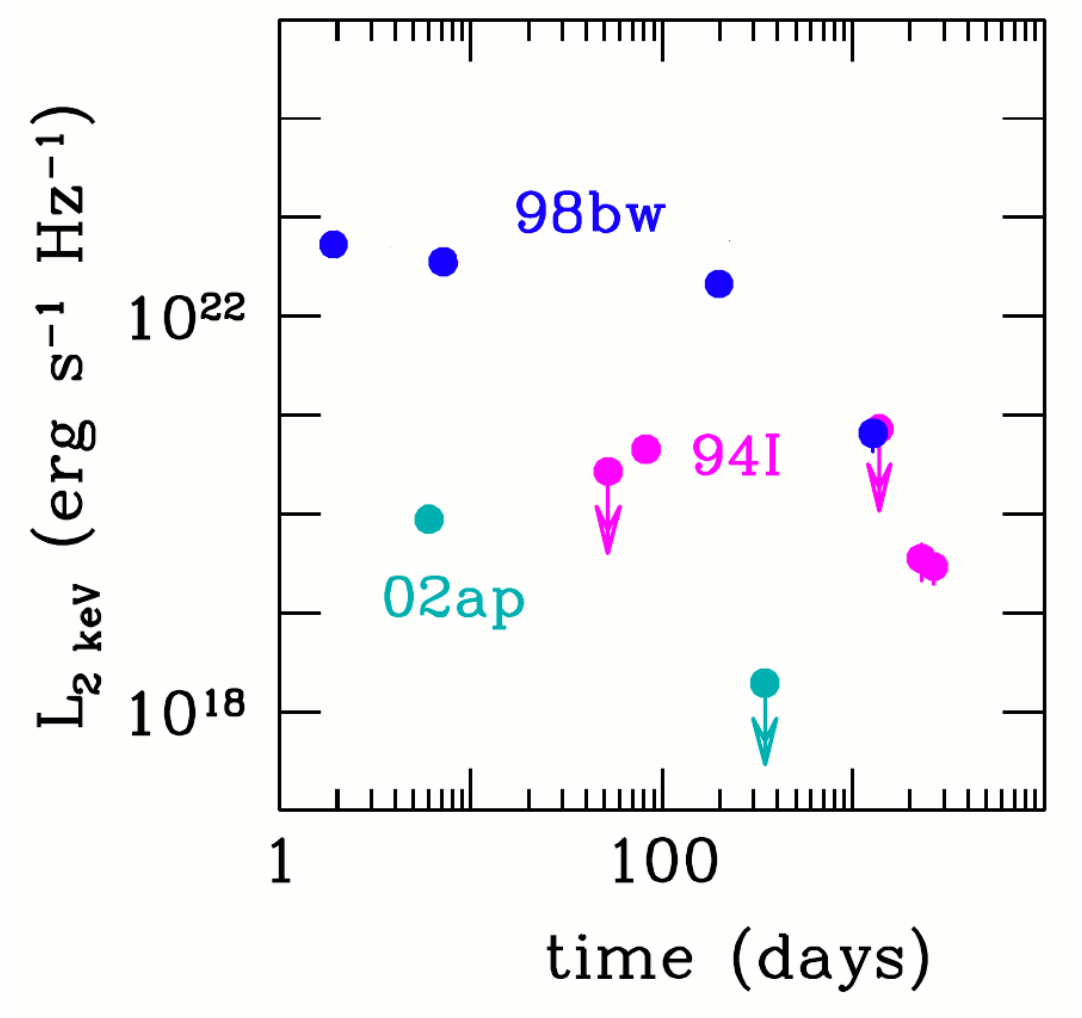

Figure 8.4.: X-ray light curves of the counterparts of GRB980425-SN1998bw and of two Type Ic SNe not accompanied by GRBs: SN1994I ("normal") and SN2002ap (broad-lined). The data are from Pian et al. (2000), Immler et al. (2002), Kouveliotou et al. (2004), and Soria et al. (2004).

e.g. *e*-ion Bremsstrahlung, plasmon decay, e^+-e^- annihilation, *e*-*e* and *n*-*n* Bremsstrahlung, synchrotron emission, as well as Cooper pair processes for temperatures below the critical temperature for superfluidity $T_{\rm crit}$. However, as shown by Yakovlev et al. (2001), the first three processes are the dominant ones for temperatures above 10^8 K, which is the regime we are interested in. For instance, synchrotron emission channels might become slightly relevant, but only for $T < 10^8$ K and for very high magnetic fields $> 10^{14}$ G. The Cooper pair mechanism, possibly important for objects a few hundred years old like Cas A (see e.g. Page et al., 2011a; Shternin et al., 2011, for details), is irrelevant in the present case since we are dealing with neutron star ages below ten years and thus temperatures well above $T_{\rm crit}$.

At temperatures $T \sim 3 \times 10^9$ K, we can write for the most important emission processes in the crust,

$$\epsilon_B \sim 10^{21} \mathrm{erg\ s^{-1} cm^{-3}}, \tag{8.4.1}$$

$$\epsilon_P \sim 10^{22} \mathrm{erg\ s^{-1} cm^{-3}}, \tag{8.4.2}$$

$$\epsilon_{ep} \sim 10^{19} \mathrm{erg\ s^{-1} cm^{-3}}, \tag{8.4.3}$$

where ϵ_i denotes the emissivity, and the indexes B, P, ep denote the Bremsstrahlung, plasmon decay, and pair annihilation processes, respectively.

To estimate the amount of heat needed to match the theoretical thermal evolution of a neo-neutron star to the light curve of the URCAs, we added a phenomenological source of heat parametrized by

$$H = H_0\, e^{-t/\tau_S}\,, \tag{8.4.4}$$

with H_0 the magnitude of the heat source, and τ_S the time scale in which it is active. For our calculations we set $\tau_S = 1$ year.

In addition, we introduced a phenomenological boundary condition for the early stages of evolution of the surface temperature T_s that follows the form $T_s = T_x\, gs_{14}^{1/4} T_8^{0.55}$ K, where $T_x = 0.87 \times 10^6 + (T_0 - 0.87x10^6)\, e^{-t/\tau_S}$ K, T_8 is the mantle temperature T_b in units of 10^8 K, T_0 is the initial temperature of the atmosphere, and gs_{14} is the surface acceleration of gravity in units of 10^{14} cm/s^2. With this new boundary condition, we can mimic the high temperature of the atmosphere for young neutron stars by setting the temperature at early times to a higher value and, for times greater than τ_S, it asymptotically goes to its traditional value $\sim 0.87 \times 10^6$ K.

In Fig. 8.5 we show the cooling curves of neo-neutron stars resulting from the presence of the heating source given by Eq. (8.4.4), in addition to the traditional cooling processes of neutron stars. The cooling curves are obtained self-consistently by exactly solving the full, general relativistic energy transport and balance equations as described in Schaab et al. (1996), Page et al. (2006) and Negreiros et al. (2010). We also show the observed data for the

X-ray light curve associated with the URCAs. This allows us to identify the key factor leading to the matching of the neo-neutron star luminosity with the X-ray emission of the URCAs.

8.5. Discussion and conclusions

The major role played by the neutrino emissions from the crust of a neo-neutron star in its initial stages of the object is illustrated in Fig. 8.5. In addition, by calibrating our additional heating source at early times to $H_0 \sim 10^{12}$–10^{15} erg/g/s, we find striking agreement of the luminosity obtained from the cooling of a neo-neutron stars with the prolonged ($t = 10^8$–10^9 s) X-ray emission observed in GRB associated with an SN (see Fig. 8.5 for details). This could indicate that something might be missing in our current understanding of the crust of neutron stars. It might be that, as is the case for the atmosphere, we need to develop our current models for the crust further, so as to describe properly the properties of neo-neutron stars. The traditional thermal processes taking place in the crust might be enhanced by the extremely high temperature conditions of neo-neutron star and, additional heating processes not yet studied within this context could also take place under such conditions and deserve further analysis.

Particularly interesting in this respect are the processes of e^+e^- pair creation expected to occur in the interphase between the core and the crust during the neutron star formation leading to the appearance of critical fields (see Ruffini et al., 2007d; Ruffini, 2008; Rueda et al., 2010a,b; Popov, 2010; Ruffini et al., 2010e; Rotondo et al., 2011b,c; Rueda et al., 2011a; Rotondo et al., 2011d,a; Rueda et al., 2011b, for details)

It is also worth mentioning that the additional heating source needed at early times, $H_0 \sim 10^{12}$–10^{15} erg/g/s (or $H_0 \sim 10^{-6}$–10^{-3} MeV/Nucleon/s), is in striking agreement with the heat released from nuclear fusion reactions, radiative neutron captures, and photodisintegrations in the early stages of neutron star mergers found by Goriely et al. (2011a,b). Both fission and β-decays have also been included there: i.e neutron-induced fission, spontaneous fission, β-delayed fission, photofission, and β-delayed neutron emission.

All this suggests the exciting possibility that we are, for the first time, observing a nascent hot neutron star. This possibility alone warrants further study of this subject, so we might obtain a more concrete picture of the thermal evolution of neo-neutron stars. A proposal has been recently submitted by E. Pian et al. to the Chandra satellite to observe whether a similar prolonged X-ray emission also exists in GRB100316D that is associated with SN2010bh (Pian et al., 2011). We also encourage dedicated observations of isolated SNe in view of the similarities between URCA-1–URCA-3 and the Type Ic supernova SN 1994I (Immler et al., 2002) and SN 2002ap (Soria et al.,

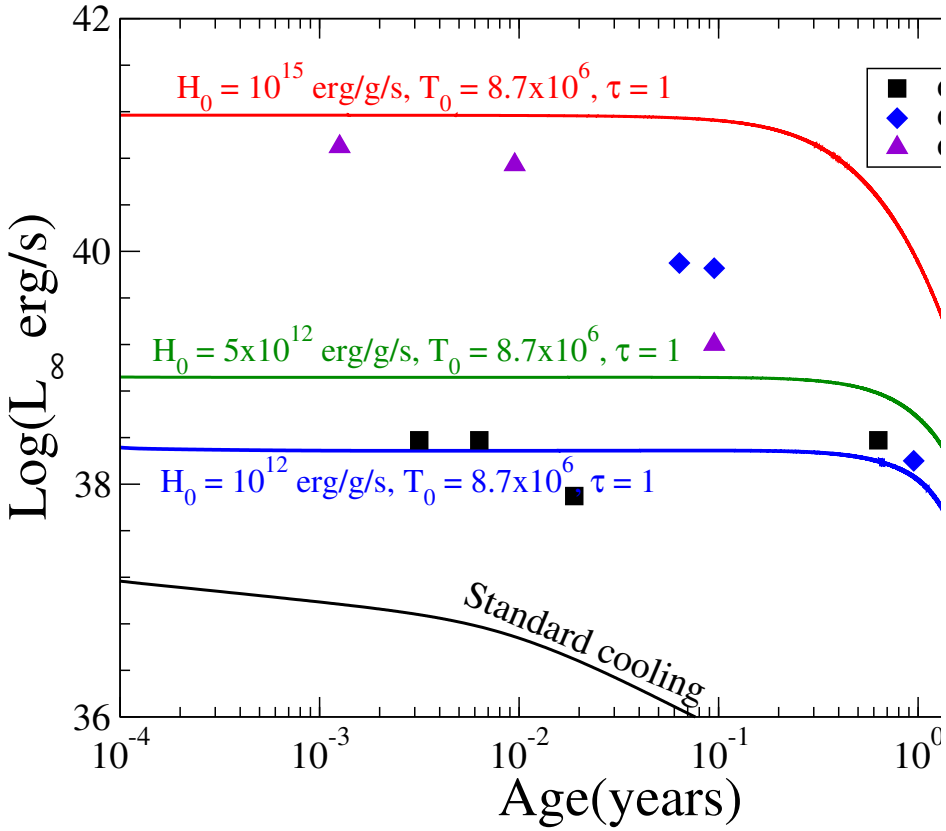

Figure 8.5.: Thermal evolution of neo-neutron stars for selected values of the heating source $H_0 = [10^{12}, 5 \times 10^{12}, 10^{15}]$ erg/g/s and for an initial temperature of the atmosphere $T_0 = 8.7 \times 10^6$ K. The observed data represents the X-ray light curve associated with the URCAs.

2004).

9. A double component in GRB 090618: a proto-black hole and a genuinely long GRB

9.1. Introduction

After the discovery of the Gamma Ray Bursts (GRBs) by the Vela satellites (Klebesadel et al., 1973; Strong and Klebesadel, 1974; Strong et al., 1974; Strong, 1975), the first systematic analysis on a large sample of GRBs was possible thanks to the observations of the BATSE instrument on board the Compton Gamma-Ray Observer (CGRO) satellite (Meegan et al., 1992). The 4BATSE catalog (Meegan, 1997; Paciesas et al., 1999; Kaneko et al., 2006) consists of 2704 confirmed GRBs, and it is widely used by the science community as a reference for spectral and timing analyses on GRBs. One of the outcomes of this early analysis of GRBs led to the classification of GRBs as a function of their observed time duration. T_{90} was defined as the time interval over which the 90% of the total BATSE background-subtracted counts are observed. The distribution of the T_{90} duration was bi-modal: the GRBs with T_{90} less than 2s were classified as "short" while those with T_{90} longer than 2s were classified as "long" (Klebesadel, 1992; Dezalay et al., 1992; Kouveliotou et al., 1993; Tavani, 1998).

After the success of BATSE, a very many of space missions dedicated to GRB observations were launched. Particularly significant was the discovery of an additional prolonged soft X-ray emission by Beppo-SAX (Costa et al., 1997), following the usual hard X-ray emission observed by BATSE. The Beppo-SAX observed emission was named "afterglow", while the BATSE one was called "prompt" radiation. The afterglow allowed pinpointing the GRB position in the sky more accurately and permitted identifying its optical counterpart by space- and ground-based telescopes. The measurement of the cosmological redshift for GRBs became possible and their cosmological nature was firmly established (van Paradijs et al., 1997).

The Beppo-SAX and related results enabled ruling out literally hundreds of theoretical models of GRBs (see for a review Ruffini, 2001). Among the handful of surviving models was the one by Damour and Ruffini (1975), which is based on the mass-energy formula of black holes. This model can naturally explain the energetics up to 10^{54-55} erg, as requested by the cosmological

nature of GRBs, through the creation of an e^+e^--plasma by vacuum polarization processes in the Kerr-Newman geometry (for a recent review see Ruffini et al., 2010d). This model was proposed a few months after the presentation of the discovery of GRBs by Strong (Strong, 1975) at the AAAS meeting in San Francisco.

It soon became clear that, as suggested by Goodman and Paczynski (Goodman, 1986; Paczynski, 1986), a Lorentz gamma factor larger than 100 could overcome the problem of opacity of the e^+e^--plasma and justify the γ-ray emission of GRBs at cosmological distances (see e.g. Piran, 2004). That the dynamics of an e^+e^--plasma with a baryon load with mass M_B would naturally lead to Lorentz gamma factor in the range (10^2- 10^3) was demonstrated by Shemi and Piran (1990), Piran et al. (1993) and Meszaros et al. (1993). The general solution for a baryon load $B = M_B c^2 / E_{tot}^{e^+e^-}$ between 0 and 10^{-2} was obtained in Ruffini et al. (2000). The interaction between the accelerated baryons with the CBM, indicated by Meszaros and Rees (1993), was advocated to explain the nature of the afterglow (see e.g. Piran, 1999, and references therein).

The unprecedented existence of such large Lorentz gamma factors led to the relativistic space-time transformations paradigm for GRBs (Ruffini et al., 2001c). This paradigm made it a necessity to have a global, instead of a piecewise, description of the GRB phenomenon (Ruffini et al., 2001c). This global description led to the conclusion that the emission by the accelerated baryons interacting with the CBM indeed occurs already in the prompt emission phase in a fully radiative regime. A new interpretation of the burst structure paradigm was then introduced (Ruffini et al., 2001b): the existence of a characteristic emission at the transparency of an e^+e^--plasma, the proper-GRB, followed by an extended-afterglow emission. The relative intensity of these two components is a function of the baryon load. It was proposed that $B < 10^{-5}$ corresponds to the short GRBs, while $B > 3 \times 10^{-4}$ corresponds to the long GRBs.

This different parametrization of the prompt – afterglow versus that of the P-GRB – extended-afterglow could have originated years of academic discussions. However, a clear-cut observational evidence came from the Swift satellite, in favor of the second parametrization. The Norris-Bonnell sources, characterized by an initial short spike-like emission in the hard X-rays followed by a softer extended emission, had been indicated in the literature as short bursts. There is clear evidence that they belong to a new class of "disguised" short GRBs, (Bernardini et al., 2007; Caito et al., 2009, 2010; de Barros et al., 2011), where the initial spike is identified as the P-GRB while the prolonged soft emission occurring from the extended-afterglow emission in a CBM typically of the galatic halo. These sources have a baryon load $10^{-4} < B < 7 \times 10^{-4}$: they are just long GRBs exploding in a particularly low-density CBM of the order of 10^{-3} particles/cm^3. This class of sources has

given the first evidence of GRBs originating from binary mergers, which is also strongly supported from direct optical observations (Bloom et al., 2006b; Fong et al., 2010).

It is interesting that independent of the development of new missions, the BATSE data continue to attract full scientific interests, even after the end of the mission in the 2000. Important inferences, based on the BATSE data, on the spectra of the early emission of the GRB have been made by Ryde (2004) and Ryde et al. (2006). These authors have convincingly demonstrated that the spectral feature composed of a blackbody and a power-law plays an important role in selected episodes in the early part of the GRB emission, Zhang et al. (but see also 2011, for further comments on the origin of this blackbody and power-law behavior). They have also shown, in some cases, a power-law variation of the thermal component as a function of time, following a broken power-law behavior, see Fig. 9.17.

The arrival of the Fermi and other satellites allowed further progresses in the understanding of the GRB phenomenon in a much wider energy range. Thanks to the Gamma-Ray Burst Monitor (GBM) (Meegan et al., 2009) and the Large Area Telescope (LAT) (Atwood et al., 2009), additional data are obtained in the 8 keV - 40 MeV and 100 MeV - 300 GeV energy range. This allowed, among others, this first evidence of a GRB originating from the collapse of a core in the late evolution of a massive star, which we called the proto black hole (Ruffini, 2011b; Penacchioni et al., 2012).

In the specific case of GRB 090618, it has been possible to obtain a complete temporal coverage of the emission in gamma and X-rays, thanks to the joint observations by the Swift, Fermi, AGILE, RT-2/Coronas-PHOTON, Konus-WIND, and Suzaku-WAM telescopes. A full coverage in the optical bands, up to 100 days from the burst trigger, has been obtained. This has allowed determining the redshift, $z = 0.54$, of the source from spectroscopical identification of absorption lines (Cenko et al., 2009) and a recent claim of a possible supernova emission ~ 10 days after the GRB trigger. This GRB lasts for ~ 150 s in hard X-rays, and it is characterized by four prominent pulses. In the soft X-rays there are observations up to 30 days from the burst trigger.

We have pointed out in Ruffini et al. (2010b) that two different episodes are present in GRB 090618. We have also showed that while the second episode may fit a canonical GRB, the first episode is not expected to be either a part of a GRB or an independent GRB (Ruffini et al., 2011a).

In the present paper we discuss the nature of these two episodes. In particular:

- in Section 2, we describe the observations, data reduction and analysis. We obtain the Fermi GBM (8 keV - 1 MeV and 260 keV - 40 MeV) flux light curves, shown in Fig. 9.2, following the standard data reduction procedure, and make a detailed spectral analysis of the main emission features, using a Band model and a power-law with exponential high-

energy cut-off spectral models.

- in Section 3, after discussing about the most often quoted GRB model, the fireball, we recall the main features of the fireshell scenario, focusing on the reaching of transparency at the end of the initial optically thick phase, with the emission of the proper-GRB (P-GRB). In Fig. 9.3 we give the theoretical evolution of the Lorentz Γ factor as a function of the radius for selected values of the baryon load, corresponding to fixed values of the total energy $E_{tot}^{e^+e^-}$. The identification of the P-GRB is crucial in determining the main fireshell parameters, which describe the canonical GRB emission. The P-GRB emission is indeed characterized by the temperature, the radius, and the Lorentz Γ factor at the transparency, which are related with the $E_{tot}^{e^+e^-}$ energy and the baryon load, see Fig. 9.4. We then recall the theoretical treatment, the simulation of the light curve and spectrum of the extended-afterglow and, in particular, the determination of the equations of motion, the role of the EQui-Temporal Surfaces (EQTS) (Bianco and Ruffini, 2004, 2005a), as well as the ansatz of the spectral energy distribution in the fireshell comoving frame, (see Patricelli et al., 2011, and references therein).

  The temporal variability of a GRB light curve has been interpreted in some current models as caused by internal shock (Rees and Meszaros, 1994). In the fireshell model this temporal variability is instead produced by the interaction of the ultra-relativistic baryons colliding with the inhomogeneities of the circumburst medium (CBM). This allows one to perform a tomography of the CBM medium around the location of the black hole formation, see Fig. 9.10, gaining important information on its structure. These collisions are described by three parameters: the n_{CBM} average density, the filling factor $\mathcal{R}$, the clumpiness on scales of 10^{15-16} cm, and average density contrast $10^{-1} \lesssim \langle \delta n/n \rangle \lesssim 10$. We then refer also to the explanation of the observed hard-to-soft behavior due to the drop of the Lorentz Γ factor and the curvature effect of the EQTS. We then recall the determination of the instantaneous spectra and the simulations of the observed multi-band light curves in the chosen time interval, taking into account all the thousands of convolutions of comoving spectra over each EQTS leading to the observed spectrum. We also emphasize that these simulations have to be performed together and that they need to be optimized.

- in Section 4, we perform a spectral analysis of GRB 090618. We divided the total GRB emission into six time intervals, see Table 9.1, each one identifying a significant feature in the emission process, see also Rao et al. (2011). We considered two different spectral models in the data fitting procedure: a Band model (Band et al., 1993) and one by a blackbody plus a power-law component, following e.g. Ryde (2004). We find

that the first 50s of emission are well-fitted by both models, equally the following 9s, from 50 to 59s. The remaining part, from 59 to 151 s, is fitted satisfactorily only with the Band model, see Table 9.1.

- in Section 5, we proceed to the analysis of GRB 090618 in the fireshell scenario. In Section 5.1, we attempt our first interpretation of GRB 090618 assuming it to be a single GRB. We recall that the blackbody is an expected feature in the theory of P-GRB. From the spectral analysis of the first 50 s, we find a spectral distribution consistent with a blackbody plus a power-law component. We first attempted a fit of the source identifying these first 50s as the P-GRB, see Fig. 9.6. We confirm the conclusion reached in Ruffini et al. (2010b) that this interpretation is not sustainable for three different reasons, based on 1) the energetics of the source, 2) the time duration, and 3) the theoretical expected temperature for the P-GRB. We then proceed, in sub-section 5.2, to an interpretation of GRB 090618 as a multi-component system, following the procedure outlined in Ruffini et al. (2011a), in which we outlined the possibility that the second episode between 50 and 151s is an independent GRB.

  We identify the P-GRB of this second episode as the first 4s of emission. We find that the spectrum in this initial emission can be fitted by a blackbody plus a power-law component, see Fig. 9.8. Since this extra power-law component can be generated by to the early onset of the extended afterglow, we took this into account to perform a fireshell simulation, which is shown in Fig. 9.8, with an energy $E_{tot}^{e^+e^-} = 2.49 \times 10^{53}$ erg and a baryon load $B = 1.98 \pm 0.15 \times 10^{-3}$. In Figs. 9.10,9.11 and 9.12 we report the results of our simulations, summarized in Table 9.3. We notice, in particular, the presence of a strong time lag in this GRB. A detailed analysis, see Rao et al. (2011), of the time lags in the mean energy ranges of 35 keV, 68 keV and 125 keV, reports quite a long lag , ~ 7 s, in the first 50s of the emission, which is unusual for GRBs, while in the following emission, from 51 to 151 s, the observed lags are quite normal, ~ 1 s.

- in Section 6, we perform a spectral analysis of the first 50s, where we find a strong spectral variation with time, as reported in Table 9.5 and in Figs. 9.16,9.17, with a chacteristic power-law time variation similar to those identified by Ryde and Pe'er (2009) in a sample of 49 BATSE GRBs.

- in Section 7, we estimate the variability of the radius emitter, Fig. 9.18, and proceed to an estimate of the early expansion velocity. We interpret these data as originating in the expansion process occurring previous to the collapse of the core of a massive star to a black hole, see e.g. Arnett

and Meakin (2011): these early 50s of the emission are then defined as the proto-black hole phenomenon.

- In Section 8 we conclude.

9.2. Observations

On 18 June 2009, the Burst Alert Telescope (BAT) on board the Swift satellite (Gehrels et al., 2009) observed GRB 090618 (Schady et al., 2009). After 120 s the X-Ray Telescope (XRT) (Burrows et al., 2005a) and the UltraViolet Optical Telescope (UVOT) (Roming et al., 2005) on board the same satellite started the observations of the afterglow of GRB 090618. UVOT found a very bright optical counterpart, with a white filter magnitude of 14.27 $\pm$ 0.01 (Schady, 2009) not corrected for the extinction, at the coordinates RA(J2000) = 19:35:58.69 = 293.99456, DEC(J2000) = +78:21:24.3 = 78.35676. The BAT light curve shows a multi-peak structure, whose total estimated duration is $\sim$ 320 s, whose T_{90} duration in the (15-350) keV range was 113 s (Baumgartner et al., 2009). The first 50 s of the light curve present a smooth decay trend, followed by a spiky emission, with three prominent peaks at 62, 80, and 112 seconds after the trigger time, respectively, and each have the typical appearance of the FRED pulse (see e.g. Fishman et al., 1994), see Fig. 9.2. The time-integrated spectrum, (t_0 - 4.4, t_0 + 213.6) s in the (15-150)keV range, was found to agree with a power-law spectral model with an exponential cut-off, whose photon index was γ = 1.42 $\pm$ 0.08 and a cut-off energy E_{peak} = 134 $\pm$ 19 keV (Sakamoto et al., 2009). The XRT observations started 125 s after the BAT trigger time and lasted $\sim$ 25.6 ks (Beardmore and Schady, 2009) and reported an initially bright uncataloged source, identified as the afterglow of GRB 090618. Its early decay was very steep, ending at 310 s after the trigger time, when it starts a shallower phase, the plateau. Then the light curve breaks into a more steep last phase.

GRB 090618 was observed also by the Gamma-ray Burst Monitor (GBM) on board the Fermi satellite (Meegan et al., 2009). From a first analysis, the time-integrated spectrum, (t_0, t_0 + 140) s in the (8-1000)keV range, was fitted by a Band (Band et al., 1993) spectral model, with a peak energy E_{peak} = 155.5 keV, $\alpha = -1.26$ and $\beta = -2.50$ (McBreen, 2009), but with strong spectral variations within the considered time interval.

It is appropriate to compare and contrast the considerations of the time-integrated spectral analysis, often adopted in the current literature of GRBs, with the information from the time-resolved spectral analysis, as presented e.g. in this article, Zhang et al. (but see also 2011). For a traditional astrophysical source, steady during the observation time, the time-integrated and time-resolved spectral analysis usually coincide. In the case of GRBs, although the duration is only a few seconds, each instantaneous observation

corresponds to a very different physical process and the two approaches have an extremely different physical and astrophysical content.

The redshift of the source is $z = 0.54$ and it was determined thanks to the identification of the MgII, Mg I, and FeII absorption lines, using the KAST spectrograph mounted at the 3-m Shane telescope at the Lick observatory (Cenko et al., 2009). Given the redshift and the distance of the source, we computed the emitted isotropic energy in the 8 - 10000 keV energy range, with the Schaefer formula (Schaefer, 2007): using the fluence in the (8-1000 keV) as observed by Fermi-GBM, $S_{obs} = 2.7 \times 10^{-4}$ (McBreen, 2009), and the ΛCDM cosmological standard model $H_0 = 70$ km/s/Mpc, $\Omega_m = 0.27$, $\Omega_\Lambda = 0.73$, we obtain for the emitted isotropic energy the value of $E_{iso} = 2.90 \times 10^{53}$ erg.

This GRB was observed also by Konus-WIND (Golenetskii et al., 2009a), Suzaku-WAM (Kono et al., 2009), and by the AGILE satellite (Longo et al., 2009b), which detected emission in the (18-60) keV and in the MCAL instrument, operating at energies greater than 350 keV, but it did not observe high-energy photons above 30 MeV. GRB 090618 was the first GRB observed by the Indian payloads RT-2 on board the Russian Satellite CORONAS-PHOTON (Kotov et al., 2008; Nandi et al., 2009; Rao et al., 2011). Two detectors, namely, RT-2/S and RT-2/G, consist of NaI(Tl)/CsI(Na) scintillators in phoswich assembly viewed by a photomultiplier tube (PMT). RT-2/S has a viewing angle of $4^\circ \times 4^\circ$ and covers an energy range of 15 keV to 1 MeV, whereas RT-2/G has an Al filter that sets the lower energy to $\sim$ 20keV. The mission was launched from Plesetsk Cosmodrom, Russia on 30 January 2009. During the event the RT-2 payload was in the SHADOW mode (away from the Sun) during 08:16:10.207 UT and ended at 08:37:35.465 UT and the GRB 090618 was detected at 77° off-axis angle. During this period, the spectrum was accumulated every 100s, while the eight channel count rates for each detector were accumulated every second. The entire episode was observed for a duration of more than 200 seconds. A closer examination of the data in the accumulated channels 1:15-102 keV, 2:95-250 keV and 3:250-1000 keV indicates that the most significant counts is in channel 2 with a clear evidence of the following: (a) the emission in the first 50 s is prominent and broader in the lower channels, see Fig. 9.1, (b) after the first 50 s, there is evidence of a precursor of about 6 seconds duration before the main pulse (c) a break up into two peaks of the main pulse at intermediate energies (35-200 keV), while at higher energies (250-1000 keV) only the first peak of the main pulse survives, see Rao et al. (2011) and also Fig. 9.2 here.

Thanks to the complete data coverage of the optical afterglow of GRB 090618, the possible presence of a supernova underlying the emission of the GRB 090618 optical afterglow (Cano et al., 2011) was reported. The evidence of a supernova emission came from the presence of several bumps in the light curve and by the change in R_c - i color index over time: in the early phases, the blue color is dominant, typical of the GRB afterglow, but then the color

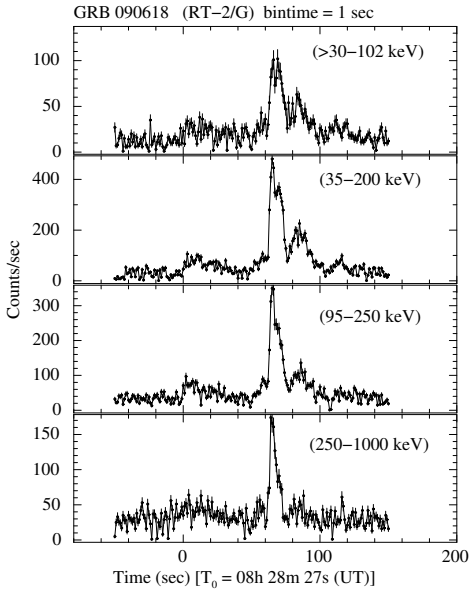

Figure 9.1.: RT2 light curves of GRB 090618.

index increases, suggesting a core-collapse SN. At late times, the contribution from the host galaxy was dominant.

9.2.1. Data analysis

We considered the BAT and XRT data of the Swift satellite together with the Fermi-GBM and RT2 data of the Coronas-PHOTON satellite. The data reduction was made with the Heasoft v6.10 packages[1] for BAT and XRT, and the Fermi-Science tools for GBM.

We obtained the BAT light curve and spectra using the standard `headas` procedure. After the data download from the `gsfc` website[2], we made a detector quality map and corrected the event data for the known errors of the detector and the hot pixels. We subtracted the background from the data, corrected for the improved position, using the tool `batmaskwtevt` and obtained the 1-s binned light curves and spectra in the main BAT energy band 15 - 150 keV and its subranges, using the tool `batbinevt`. After the systematic corrections to the spectrum, we created the response matrices and obtained the final spectra.

For the XRT data, we obtained a total dataset using the standard pipeline, while for a time-resolved analysis we considered the on-line recipe, which is

[1] http://heasarc.gsfc.nasa.gov/lheasoft/
[2] ftp://legacy.gsfc.nasa.gov/swift/data/obs/

well described in literature, see Evans et al. (2007, 2009). The GBM data[3], in particular the fourth NaI detector in the (8 - 440 keV) and the b0 BGO detector (260 keV - 40 MeV), were analyzed using the `gtbindef` tool to obtain a GTI file for the energy distribution and the `gtbin` for the light curves and final spectra. To obtain an energy flux lightcurve, we made a time-resolved spectral analysis dividing the count lightcurve into six time intervals, each of them corresponding to a particular pulse, as described in the work of Rao et al. (2011). All time-resolved spectra were fitted using the XSPEC data analysis software (Arnaud, 1996) version 12.6.0q, included in the Heasoft data package, and considering for each spectrum a classical Band spectral model (Band et al., 1993) and a power-law model with an exponential energy cut-off, folded through the detector response matrix. After subtracting the background, we fitted the spectrum by minimizing the χ^2 between the spectral models described above and the observed data, obtaining the best-fit spectral parameters and the respective model normalization. In Table 9.1 we give the results of our spectral analysis. The time reported in the first column corresponds to the time after the GBM trigger time t_{trig} = 267006508 s, where the β parameter was not constrained, we used its averaged value, as delineated in Guetta et al. (2011) β = -2.3 $\pm$ 0.10. We considered the chi-square statistic for testing our data fitting procedure. The reduced chi-square $\tilde{\chi}^2 = \chi^2/N$, where N is the number of degrees of freedom (dof), which is $N = 82$ for the NaI dataset and $N = 121$ for that of BGO.

For the last pulse of the second episode, the Band model is not very precise ($\tilde{\chi}^2$ = 2.24), but a slightly better approximation is given by the power-law with an exponential cut-off, whose fit results are shown for the same intervals in the last two columns. From these values, we built the flux light curves for both detectors, which are shown in Fig. 9.2.

We turn now to the XRT, which started to observe GRB 090618 $\sim$ 120 s after the BAT trigger. Its early data show a continued activity of the prompt emission, fading away $\sim$ 200 s after the BAT trigger time. Then the light curve is well approximated with a power-law decay. In view of the lack of soft X-ray data before the onset of the XRT, we cannot exclude a previous pulse in the X-ray light curve emission of GRB 090618. The following shallow and late decay phases, well-known in literature (Sari et al., 1999; Nousek et al., 2006), will not be analyzed in this paper since we focus on the first 200 s of the GRB emission.

[3] ftp://legacy.gsfc.nasa.gov/fermi/data/gbm/

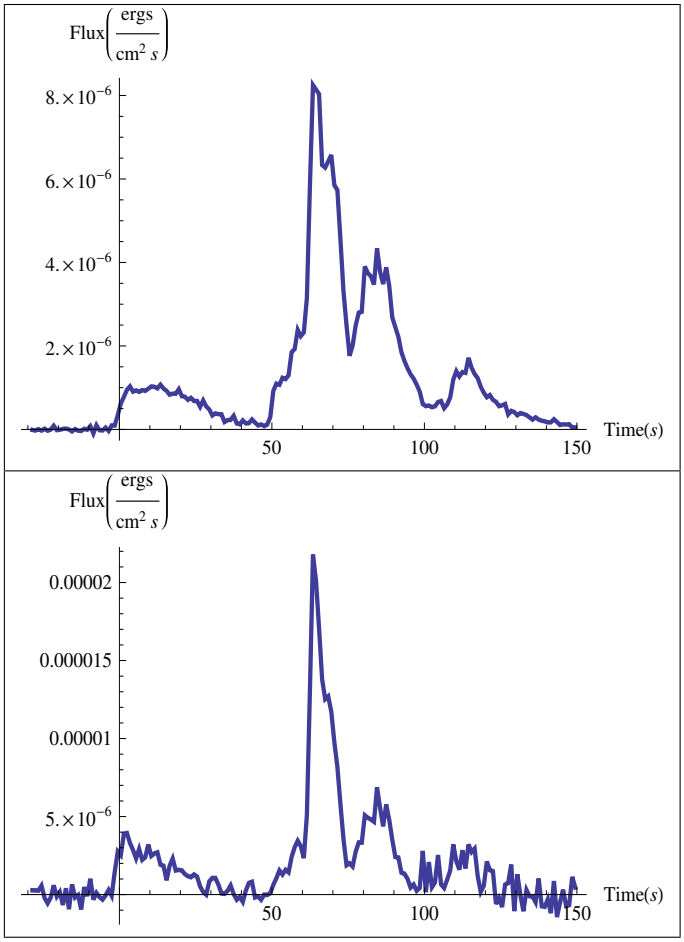

Figure 9.2.: Fermi-GBM flux light curve of GRB 090618 referring to the NaI (8-440 keV, *upper panel*) and BGO (260 keV - 40 MeV, *lower panel*) detectors.

Table 9.1.: Time-resolved spectral analysis of GRB 090618. We considered six time intervals, each one corresponding to a particular emission feature in the light curve. We fitted the GBM (8 keV - 10 MeV) observed emission with a Band model (Band et al., 1993) and a power-law function with an exponential cut-off. In columns 2-4 we list the Band model low-energy index α, the high-energy β and the break energy E_0^{BAND}, with the reduced chi-square value in the 6^{th} column. In the last three columns are listed the power-law index γ, the cut-off energy E_0^{cut} and the reduced chi-square value respectively, as obtained from the spectral fit with the cut-off power-law spectral function.

Time Interval	α	β	E_0^{BAND} (keV)	$\tilde{\chi}^2_{BAND}$	γ	E_0^{cut} (keV)	$\tilde{\chi}^2_{cut}$
0 - 50	$-0.77^{+0.38}_{-0.28}$	$-2.33^{+0.33}_{-0.28}$	$128.12^{+109.4}_{-56.2}$	1.11	$0.91^{+0.18}_{-0.21}$	$180.9^{+93.1}_{-54.2}$	1.13
50 - 57	$-0.93^{+0.48}_{-0.37}$	-2.30 ± 0.10	$104.98^{+142.3}_{-51.7}$	1.22	$1.11^{+0.25}_{-0.30}$	$168.3^{+158.6}_{-70.2}$	1.22
57 - 68	$-0.93^{+0.09}_{-0.08}$	$-2.43^{+0.21}_{-0.67}$	$264.0^{+75.8}_{-54.4}$	1.85	$1.01^{+0.06}_{-0.06}$	$340.5^{+56.0}_{-45.4}$	1.93
68 - 76	$-1.05^{+0.08}_{-0.07}$	$-2.49^{+0.21}_{-0.49}$	$243.9^{+57.1}_{-53.0}$	1.88	$1.12^{+0.04}_{-0.04}$	$311.0^{+38.6}_{-32.9}$	1.90
76 - 103	$-1.06^{+0.08}_{-0.08}$	$-2.65^{+0.19}_{-0.34}$	$125.7^{+23.27}_{-19.26}$	1.23	$1.15^{+0.06}_{-0.06}$	$157.7^{+22.2}_{-18.6}$	1.39
103 - 150	$-1.50^{+0.20}_{-0.18}$	-2.30 ± 0.10	$101.1^{+58.3}_{-30.5}$	1.07	$1.50^{+0.18}_{-0.20}$	$102.8^{+56.8}_{-30.4}$	1.06

9.3. A brief review of the fireshell and alternative models

9.3.1. The GRB prompt emission in the fireball scenario

A variety of models have been developed to theoretically explain the observational properties of GRBs. One of the most quoted is the fireball model (see for a review Piran, 2004). The model was first proposed by Cavallo and Rees (1978), Goodman (1986) and Paczynski (1986), who have shown that the sudden release of a large quantity of energy in a compact region can lead to an optically thick photon-lepton plasma and to the production of e^+e^- pairs. The total annihilation of the e^+e^- plasma was assumed, leading to a vast release of energy pushing on the CBM: the "fireball".

An alternative approach, originating in the gravitational collapse to a black hole, is the fireshell model (see for a review Ruffini et al. (2010d) and (Ruffini, 2011b)). There the GRBs originate from an optically thick electron–positron plasma in thermal equilibrium, with a total energy of $E_{tot}^{e^\pm}$. This plasma is initially confined between the radius of a black hole r_h and the dyadosphere radius

$$r_{ds} = r_h \left[2\alpha \frac{E_{tot}^{e^+e^-}}{m_e c^2} \left(\frac{\hbar / m_e c}{r_h} \right)^3 \right]^{1/4}, \tag{9.3.1}$$

where α is the usual fine structure constant, $\hbar$ and c the Planck constant and the speed of light, and m_e the mass of the electron. The lower limit of $E_{tot}^{e^\pm}$ coincides with E_{iso}. The condition of thermal equilibrium assumed in this

model as shown by Aksenov et al. (2007), differentiates this approach from the alternative ones (e.g. the one by Cavallo and Rees, 1978), see Section 3.2.

In the fireball model, the prompt emission, including the sharp luminosity variations (Ramirez-Ruiz and Fenimore, 2000) are caused by the prolonged and variable activity of the "inner engine" (Rees and Meszaros, 1994; Piran, 2004). The conversion of the fireball energy to radiation originates in shocks, either internal (when faster moving matter takes over a slower moving shell, (see Rees and Meszaros, 1994)) or external (when the moving matter is slowed down by the external medium surrounding the burst, (see Rees and Meszaros, 1992)). Much attention has been given to the synchrotron emission from relativistic electrons, possibly accompanied by SSC emission to explain the observed GRB spectrum. These processes were found to be consistent with the observational data of many GRBs (Tavani, 1996; Frontera et al., 2000). However, several limitations have been reported in relation with the low-energy spectral slopes of time-integrated spectra (Crider et al., 1997; Preece et al., 2002; Ghirlanda et al., 2002, 2003; Daigne et al., 2009) and time-resolved spectra (Ghirlanda et al., 2003). Additional limitations on SSC have also been pointed out by Kumar and McMahon (2008) and Piran et al. (2009).

The latest phases of the afterglow are described in the fireball model by assuming an equation of motion given by the Blandford-McKee self-similar power-law solution (Blandford and McKee, 1976). The maximum Lorentz factor of the fireball is estimated from the temporal occurrence of the peak of the optical emission, which is identified with the peak of the forward external shock emission (Molinari et al., 2007; Rykoff et al., 2009) in the thin shell approximation (Sari and Piran, 1999). Several partly alternative and/or complementary scenarios have been developed to the fireball model, e.g. based on quasi-thermal Comptonization (Ghisellini and Celotti, 1999), Compton drag emission (Zdziarski et al., 1991; Shemi, 1994), synchrotron emission from a decaying magnetic field (Pe'er and Zhang, 2006), jitter radiation (Medvedev, 2000), Compton scattering of synchrotron self-absorbed photons (Panaitescu and Mészáros, 2000; Stern and Poutanen, 2004), photospheric emission (Eichler and Levinson, 2000; Mészáros and Rees, 2000; Mészáros, 2002; Daigne and Mochkovitch, 2002; Giannios, 2006; Ryde and Pe'er, 2009; Lazzati and Begelman, 2010). In particular, Ryde and Pe'er (2009) pointed out that the photospheric emission overcomes some of the difficulties of pure non-thermal emission models.

9.3.2. The fireshell scenario

In the fireshell model, the rate equation for the e^+e^- pairs and its dynamics have been given by Ruffini et al. (2000) (the pair-electromagnetic pulse or PEM pulse for short). This plasma engulfs the baryonic material left over in the process of gravitational collapse having mass M_B, still keeping thermal

equilibrium between electrons, positrons, and baryons. The baryon load is measured by the dimensionless parameter $B = M_B c^2 / E_{tot}^{e^+e^-}$. It was shown (Ruffini, 1999) that no relativistic expansion of the plasma can be found for $B > 10^{-2}$. The fireshell is still optically thick and self-accelerates to ultrarelativistic velocities (the pair-electromagnetic-baryonic pulse or PEMB pulse for short, Ruffini, 1999). Then the fireshell becomes transparent and the proper - GRB (P-GRB) is emitted (Ruffini et al., 2001b). The final Lorentz gamma factor at transparency can vary in a vast range between 10^2 and 10^3 as a function of $E_{tot}^{e^+e^-}$ and B, see Fig. 9.3. For the final determination it is necessary to explicitly integrate the rate equation of the e^+e^- annihilation process and evaluate, for a given black hole mass and a given e^+e^- plasma radius, the reaching of the transparency condition, Ruffini et al. (2000), see Fig. 9.4.

The fireshell scenario does not require any prolonged activity of the inner engine. After transparency, the remaining accelerated baryonic matter still expands ballistically and starts to slow down by the collisions with the CBM, having average density n_{cbm}. In the standard fireball scenario (Meszaros, 2006), the spiky light curve is assumed to be caused by internal shocks. In the fireshell model the entire extended-afterglow emission is assumed to originate from an expanding thin shell, which enforces energy and momentum conservation in the collision with the CBM. The condition of a fully radiative regime is assumed (Ruffini et al., 2001b). This, in turn, allows one to estimate the characteristic inhomogeneities of the CBM, as well as its average value.

It is appropriate to recall another difference between our treatment and those in the current literature. The complete analytic solution of the equations of motion of the baryonic shell has been developed (Bianco and Ruffini, 2004, 2005b), while in the current literature usually the Blandford - McKee (Blandford and McKee, 1976) self-similar solution has been uncritically adopted (e.g. Meszaros et al., 1993; Sari, 1997, 1998; Waxman, 1997; Rees and Meszaros, 1998; Granot et al., 1999; Panaitescu and Meszaros, 1998; Gruzinov and Waxman, 1999; van Paradijs et al., 2000; Mészáros, 2002). The analogies and differences between the two approaches have been explicitly pointed out in Bianco and Ruffini (2005a).

From this general approach, a canonical GRB bolometric light curve composed of two different parts is defined: the P-GRB and the extended afterglow. The relative energetics of these two components, the observed temporal separation between the corresponding peaks, is a function of the above three parameters $E_{tot}^{e^+e^-}$, B, and the average value of the n_{cbm}; the first two parameters are inherent to the accelerator characterizing the GRB, i.e., the optically thick phase, while the third one is inherent to the GRB surrounding environment, which gives rise to the extended-afterglow. Regarding the observational properties of this model of a relativistic expanding shell, a crucial concept has been the introduction of the EQTS. In this topic, also, our model differs from those in the literature for deriving the analytic expression

of the EQTS from the analytic solutions of the equations of motion (Bianco and Ruffini, 2005a).

We assumed $E_{tot}^{e^+e^-} = E_{iso}$. This assumption is based on the very accurate information we have on the luminosity and the spectral properties of the source. In other GRBs, we have assumed $E_{tot}^{e^+e^-} > E_{iso}$ to take into account the observational limitations, owing to detector thresholds, distance effects, and lack of data.

9.3.3. The emission of the P-GRB

The lower limit of $E_{tot}^{e^+e^-}$ is given by the observed isotropic energy emitted in the GRB, E_{iso}. The identification of the energy of the afterglow and of the P-GRB determines the baryon load B and, from these, it is possible to determine the value of the Lorentz Γ factor at transparency, the observed temperature as well as the temperature in the comoving frame and the laboratory radius at transparency, see Fig. 9.4. We can indeed determine from the spectral analysis of the P-GRB candidate the temperature kT_{obs} and the energy emitted in the transparency E_{PGRB}. The relation between these parameters cannot be expressed by an analytical formulation: they can be only obtained by a numerical integration of the entire fireshell equations of motion. In practice we need to perform a trial-and-error procedure to find the set of values that fits the observations.

As we will see in the case of GRB 090618, the direct measure of the temperature of the thermal component at the transparency offers a very important new information on the determination of the GRB parameters. In the emission of the P-GRB two different phases are present: one corresponding to the emission of the photons when the transparency is reached, and the second is the early interaction of the ultra-relativistic protons and electrons with the CBM. A spectral energy distribution with a thermal component and a non-thermal one should be expected to occur.

9.3.4. The extended afterglow

The majority of works in the current literature has addressed the analysis of the afterglow emission as due to various combinations of synchrotron and inverse Compton processes, see e.g. Piran (2004). It appears, however, that this description is not fully satisfactory (see e.g. Ghirlanda et al., 2003; Kumar and McMahon, 2008; Piran et al., 2009).

We adopted in the fireshell model a pragmatic approach by making full use of the knowledge of the equations of motion, of the EQTS formulations (Bianco and Ruffini, 2005b) and of the correct relativistic transformations between the comoving frame of the fireshell and the observer frame. These equations, which relate the four time variables, are necessary for interpret-

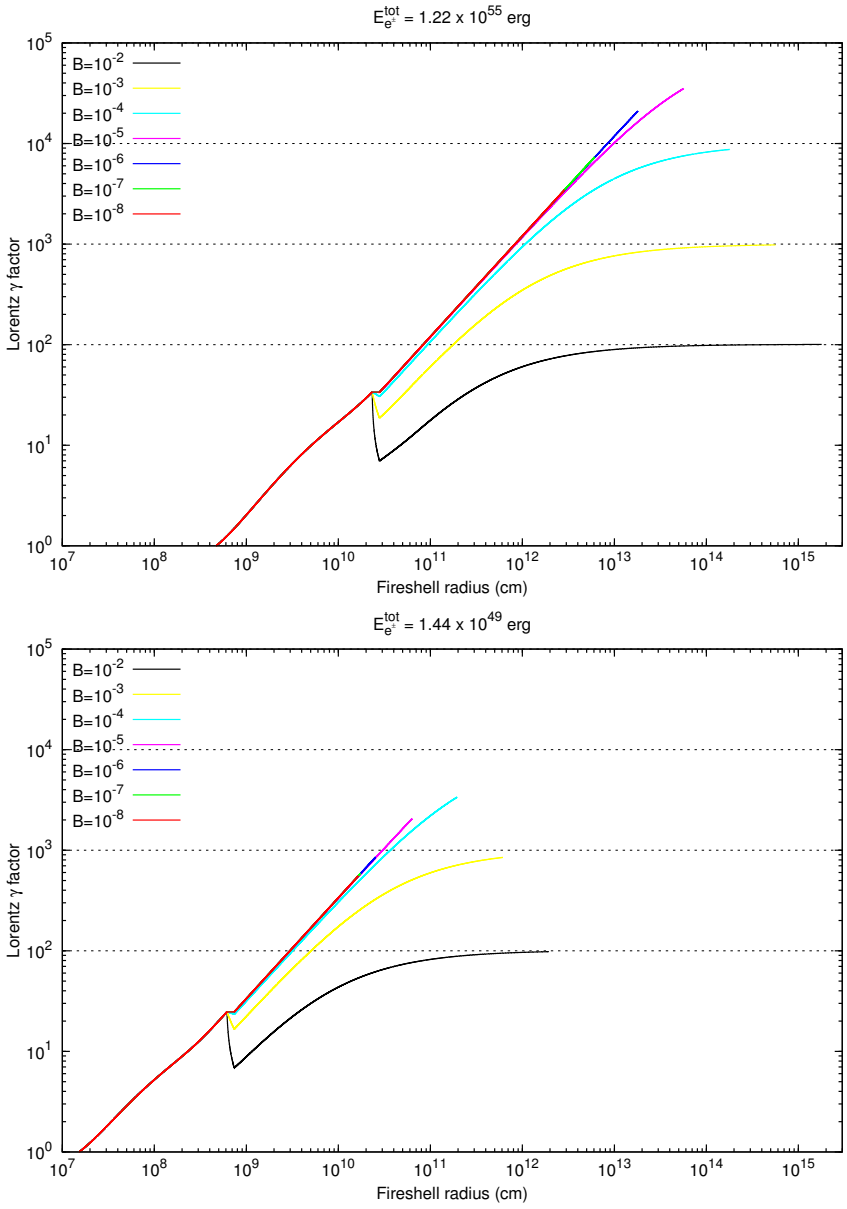

Figure 9.3.: Evolution of the Lorentz Γ factor until the transparency emission for a GRB of a fixed $E_{tot}^{e^+e^-} = 1.22 \times 10^{55}$ (upper panel),and $E_{tot}^{e^+e^-} = 1.44 \times 10^{49}$, for different values of the baryon load B. This computation refers to a mass of the black hole of 10 $M_\odot$ and a $\tau = \int_R dr(n_{e^\pm} + n_{e^-}^b)\sigma_T = 0.67$, where σ_T is the Thomson cross-section and the integration is over the thickness of the fireshell (Ruffini, 1999).

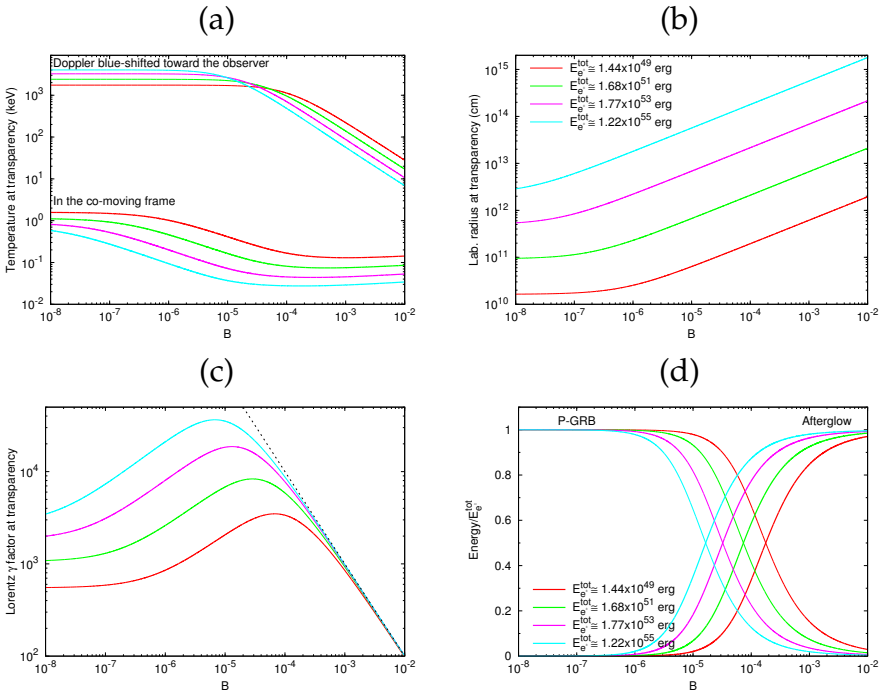

Figure 9.4.: Fireshell temperature in the comoving and observer frame and the laboratory radius at the transparency emission (panels (a) and (b)), the Lorentz Γ factor at the transparency (panel (c)) and the energy radiated in the P-GRB and in the afterglow in units of $E_{tot}^{e^+e^-}$ (panel (d)) as a function of the baryon load B for four different values of $E_{tot}^{e^+e^-}$.

ing the GRB data. They are: a) the comoving time, b) the laboratory time, c) the arrival time, and d) the arrival time at the detector corrected for cosmological effects. This is the content of the relative space-time transformations paradigm, essential for the interpretation of GRBs data (Ruffini et al., 2001c). This paradigm required a global, instead of a piecewise, description of the GRB phenomenon (Ruffini et al., 2001c). This global description led to a new interpretation of the burst structure paradigm (Ruffini et al., 2001b). As recalled in the introduction, a new conclusion, arising from the burst structure paradigm, has been that the emission by the accelerated baryons interacting with the CBM is indeed occurring already in the prompt emission phase, just after the P-GRB emission. This is the extended-afterglow emission, which presents in its "light curve" a rising part, a peak, and a decaying tail. Following this paradigm, the prompt emission phase consists therefore of the P-GRB emission and the peak of the extended afterglow.

To evaluate the extended-afterglow spectral properties, we adopted an ansatz on the spectral properties of the emission in the collisions between the baryons and the CBM in the comoving frame. We then evaluated all observational properties in the observer frame by integrating on the EQTS. The initial ansatz of thermal spectrum (Ruffini et al., 2001b), has recently been modified to

$$\frac{dN_\gamma}{dVd\epsilon} = \left(\frac{8\pi}{h^3c^3}\right)\left(\frac{\epsilon}{k_BT}\right)^{\alpha}\frac{\epsilon^2}{exp\left(\frac{\epsilon}{k_BT}\right)-1}, \tag{9.3.2}$$

where α is a phenomenological parameter defined in the comoving frame of the fireshell (Patricelli et al., 2011), determined by the optimization of the simulation of the observed data. It is well known that in the ultrarelativistic collision of protons and electrons with the CBM, collective processes of ultrarelativistic plasma physics are expected, which are not yet fully explored and understood (e.g. Weibel instability, (see Medvedev and Loeb, 1999)). Promising results along this line have already been obtained by Spitkovsky (2008a) and Medvedev and Spitkovsky (2009), and may lead to the understanding of the physycal origin of the α parameter in Eq. 9.3.2.

To take into due account the filamentary, clumpy and porous structure of the CBM, we introduced the additional parameter $\mathcal{R}$, which describes the fireshell surface filling factor. It is defined as the ratio between the effective emitting area of the fireshell A_{eff} and its total visible area A_{vis} (Ruffini et al., 2002, 2005a).

One of the main features of the GRB afterglow has been the observation of hard-to-soft spectral variation, which is generally absent in the first spike-like emission, which we have identified as the P-GRB, Bernardini et al. (2007); Caito et al. (2009, 2010); de Barros et al. (2011). An explanation of the hard-to-soft spectral variation has been advanced on the grounds of two different contributions: the curvature effect and the intrinsic spectral evolution. In par-

ticular, in the work of Peng et al. (2011) the authors used the model developed in Qin (2002) for the spectral lag analysis, taking into account an intrinsic Band model for the GRBs and a Gaussian profile for the GRB pulses to take into account the angular effects, and they found that both causes provide a very good explanation for the observed time lags. Within the fireshell model we can indeed explain a hard-to-soft spectral variation very naturally, in the extended-afterglow emission. Since the Lorentz Γ factor decreases with time, the observed effective temperature of the fireshell will drop as the emission goes on, consequently the peak of the emission will occur at lower energies. This effect is amplified by the curvature effect, which originates in the EQTS concept. Both these observed features are considered as responsible for the time lag observed in GRBs.

9.3.5. The simulation of a GRB light curve and spectra of the extended afterglow

The simulation of a GRB light curve and the respective spectrum also requires the determination of the filling factor $\mathcal{R}$ and of the CBM density n_{CBM}. These extra parameters are extrinsic and they are just functions of the radial coordinate from the source. The parameter $\mathcal{R}$, in particular, determines the effective temperature in the comoving frame and the corresponding peak energy of the spectrum, while n_{cbm} determines the temporal behavior of the light curve. It is found that the CBM is typically formed of "clumps" of width $\sim 10^{15-16}$ cm and average density contrast $10^{-1} \lesssim \langle \delta n/n \rangle \lesssim 10$ centered on the value of four $particles/cm^3$, see Fig. 9.10, and clumps of masses $M_{clump} \approx 10^{22-24}$ g. Particularly important is the determination of the average value of n_{cbm}. Values on the order of 0.1-10 particles/cm^3 have been found for GRBs exploding inside star-forming region galaxies, while values on the order of 10^{-3} particles/cm^3 have been found for GRBs exploding in galactic halos (Bernardini et al., 2007; Caito et al., 2009; de Barros et al., 2011). This clumpy medium, already predicted in pioneering works of Fermi in the theoretical study of interstellar matter in our galaxy (Fermi, 1949, 1954), is by now well-established both from the GRB observations and by additional astrophysical observations, see e.g. the circum-burst medium observed in novae (Shara et al., 1997), or by theoretical considerations on supergiant, massive stars, clumpy wind (Ducci et al., 2009). Interesting are the considerations by Arnett and Meakin (Arnett and Meakin, 2011), who have shown how realistic 2D simulations of the late evolution of a core collapse show processes of violent emission of clouds: there the 2D simulations differ from those in 1D, which show a much more regular and wind behavior around the collapsing core. Consequently, attention should be given also to instabilities prior to the latest phases of the evolution of the core, possibly giving rise to the cloud pattern observed in the CBM of GRB phenomenon (D.Arnett private communication).

The determination of the $\mathcal{R}$ and n_{CBM} parameters depends essentially on the reproduction of the shape of the extended-afterglow and of the respective spectral emission, in a fixed energy range. Clearly, the simulation of a source within the fireshell model is much more complex than simply fitting the $N(E)$ spectrum with phenomenological analytic formulas for a finite temporal range of the data. It is a consistent picture, which has to find the best value for the parameters of the source, the P-GRB (Ruffini et al., 2001b), its spectrum, its temporal structure, as well as its energetics. For each spike in the light curve the parameters of the corresponding CBM clumps are computed, taking into account all the thousands of convolutions of comoving spectra over each EQTS that lead to the observed spectrum (Bianco and Ruffini, 2005b,a). It is clear that, since the EQTS encompass emission processes occurring at different comoving times weighted by their Lorentz and Doppler factors, the "fitting" of a single spike is not only a function of the properties of the specific CBM clump but of the entire previous history of the source. Any mistake at any step of the simulation process affects the entire evolution that follows and, conversely, at any step a fit must be made consistently with the entire previous history: because of the non-linearity of the system and the EQTS, any change in the simulation produces observable effects up to a much later time. This leads to an extremely complex procedure by trial and error in the data simulation, in which the variation of the parameters defining the source are increasingly narrowed down, reaching the uniqueness very quickly. Of course, we cannot expect the latest parts of the simulation to be very accurate, since some of the basic hypothesis on the equations of motion, and possible fragmentation of the shell, can affect the procedure.

In particular, the theoretical photon number spectrum to be compared with the observational data is obtained by an averaging procedure of instantaneous spectra. In turn, each instantaneous spectrum is linked to the simulation of the observed multiband light curves in the chosen time interval. Therefore, the simulation of the spectrum and of the observed multiband light curves have to be performed together and have optimized simultaneously.

9.4. Spectral analysis of GRB 090618

We proceed now to the detailed spectral analysis of GRB 090618. We divide the emission in six time intervals, shown in Table 9.1, each one identifying a significant feature in the emission process. We then fit for each time interval the spectra by a Band model and a blackbody with an extra power-law component, following Ryde (2004). In particular, we are interested in estimating the temperature kT and the observed energy flux ϕ_{obs} of the blackbody component. The specific intensity of emission of a thermal spectrum at energy E

in energy range dE into solid angle $\Delta\Omega$ is

$$I(E)dE = \frac{2}{h^3c^2}\frac{E^3}{\exp(E/kT)-1}\Delta\Omega dE. \tag{9.4.1}$$

The source of radius R is seen within a solid angle $\Delta\Omega = \pi R^2/D^2$, and its full luminosity is $L = 4\pi R^2\sigma T^4$. What we are fitting, however, is the background-subtracted photon spectra $A(E)$, which is obtained by dividing the specific intensity $I(E)$ by the energy E:

$$\begin{aligned} A(E)dE \equiv \frac{I(E)}{E}dE &= \frac{k^4 L}{2\sigma(kT)^4 D^2 h^3 c^2}\frac{E^2 dE}{\exp(E/kT)-1} \\ &= \frac{15\phi_{obs}}{\pi^4(kT)^4}\frac{E^2 dE}{\exp(E/kT)-1}, \end{aligned} \tag{9.4.2}$$

where h, k and σ are the Planck, the Boltzmann, and the Stefan-Boltzmann constants respectively , c is the speed of light and $\phi_{obs} = L/(4\pi D^2)$ is the observed energy flux of the blackbody emitter. The great advantage of Eq. (9.4.2) is that it is written in terms of the observables ϕ_{obs} and T, so from a spectral fitting procedure we can obtain the values of these quantities for each time interval considered. To determine these parameters, we must perform an integration of the actual photon spectrum $A(E)$ over the instrumental response $R(i,E)$ of the detector that observes the source, where i denotes the different instrument energy channels. The result is a predicted count spectrum

$$C_p(i) = \int_{E_{min}(i)}^{E_{max}(i)} A(E)R(i,E)dE, \tag{9.4.3}$$

where $E_{min}(i)$ and $E_{max}(i)$ are the boundaries of the i-th energy channel of the instrument. Eq. (9.4.3) must be compared with the observed data by a fit statistic.

The main parameters obtained from the fitting procedure are shown in Table 9.2. We divide the entire GRB in two main episodes, as advanced in Ruffini et al. (2011a): one lasting the first 50 s and the other from 50 to 151 s after the GRB trigger time, see Fig. 9.5. Clearly, the first 50 s of emission, corresponding to the first episode, are well-fitted by a Band model as well as a blackbody with an extra power-law model, Fig. 9.6. The same happens for the first 9 s of the second episode (from 50 to 59 s after the trigger time), Fig. 9.7. For the subsequent three intervals corresponding to the main peaks in the light curve, the blackbody plus a power-law model does not provide a satisfactory fit. Only the Band model fits the spectrum with good accuracy, with the exception of the first main spike (compare the values of χ^2 in the table). We find also that the last peak can be fitted by a simple power-law model with a photon index $\gamma = 2.20 \pm 0.03$, better than by a Band model.

Table 9.2.: Time-resolved spectral analysis (8 keV - 10 MeV) of the second episode in GRB 090618.

	Time Interval (s)	α	β	$E_0(keV)$	$\tilde{\chi}^2_{BAND}$	$kT(keV)$	γ	$\tilde{\chi}^2_{BB+po}$
A	0 - 50	-0.74 $\pm$ 0.10	-2.32 $\pm$ 0.16	118.99 $\pm$ 21.71	1.12	32.07 $\pm$ 1.85	1.75 $\pm$ 0.04	1.21
B	50 - 59	-1.07 $\pm$ 0.06	-3.18 $\pm$ 0.97	195.01 $\pm$ 30.94	1.23	31.22 $\pm$ 1.49	1.78 $\pm$ 0.03	1.52
C	59 - 69	-0.99 $\pm$ 0.02	-2.60 $\pm$ 0.09	321.74 $\pm$ 14.60	2.09	47.29 $\pm$ 0.68	1.67 $\pm$ 0.08	7.05
D	69 - 78	-1.04 $\pm$ 0.03	-2.42 $\pm$ 0.06	161.53 $\pm$ 11.64	1.55	29.29 $\pm$ 0.57	1.78 $\pm$ 0.01	3.05
E	78 - 105	-1.06 $\pm$ 0.03	-2.62 $\pm$ 0.09	124.51 $\pm$ 7.93	1.20	24.42 $\pm$ 0.43	1.86 $\pm$ 0.01	2.28
F	105 - 151	-2.63 $\pm$ -1	-2.06 $\pm$ 0.02	unconstrained	1.74	16.24 $\pm$ 0.84	2.23 $\pm$ 0.05	1.15

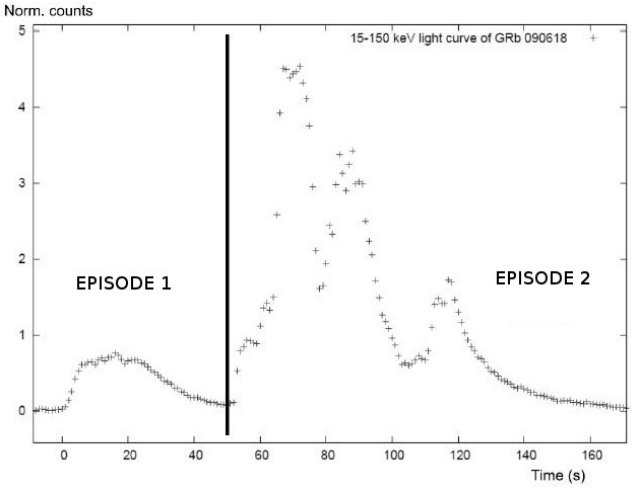

Figure 9.5.: Two episode nature of GRB 090618.

The result of this analysis points to a different emission mechanism in the first 50 s of GRB 090618 and in the following 9 s. A sequence of very strong pulses follows, whose spectral energy distribution is not attributable either to a blackbody or a blackbody and an extra power-law component. The evidence for the transition is well represented by the test of the data fitting, whose indicator is given by the changing of the $\tilde{\chi^2}$ ($N_{dof} = 169$) for the blackbody plus a power-law model for the different time intervals, see Table 9.2. Although the Band spectral model is an empirical model without a clear physical origin, we checked its validity in all time-detailed spectra with the sole exception of the first main pulse of the second episode. The χ^2 corresponding to the Band model for this main pulse, although better than that corresponding to the blackbody and power-law case, is unsatisfactory. We now directly apply the fireshell model to make the above conclusions more stringent and reach a better understanding of the source.

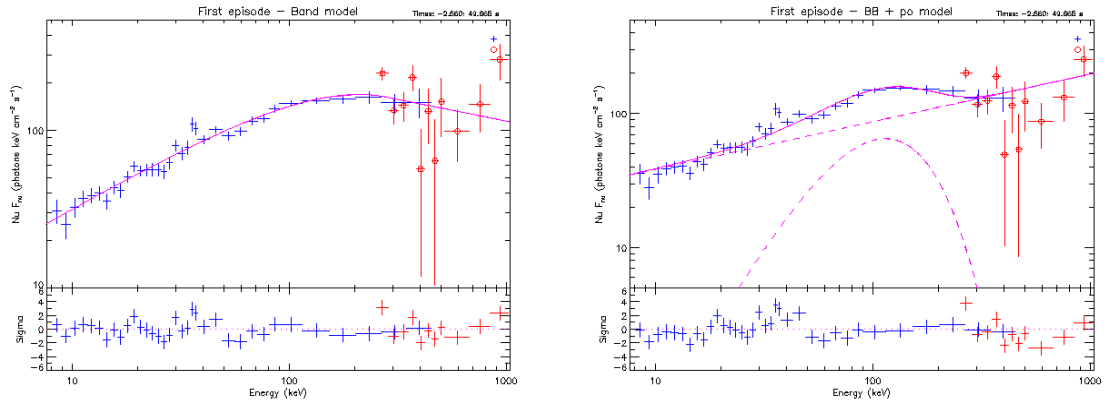

Figure 9.6.: Time-integrated spectra for the first episode (from 0 to 50 s) of GRB 090618 fitted with the Band, $\tilde{\chi}^2$ = 1.12 (left) and blackbody + power-law (right) models, $\tilde{\chi}^2$ = 1.28. In the following we will consider the case of a blackbody + power-law model and infer some physical consequences. The corresponding considerations for the Band model are currently being considered and will be published elsewhere.

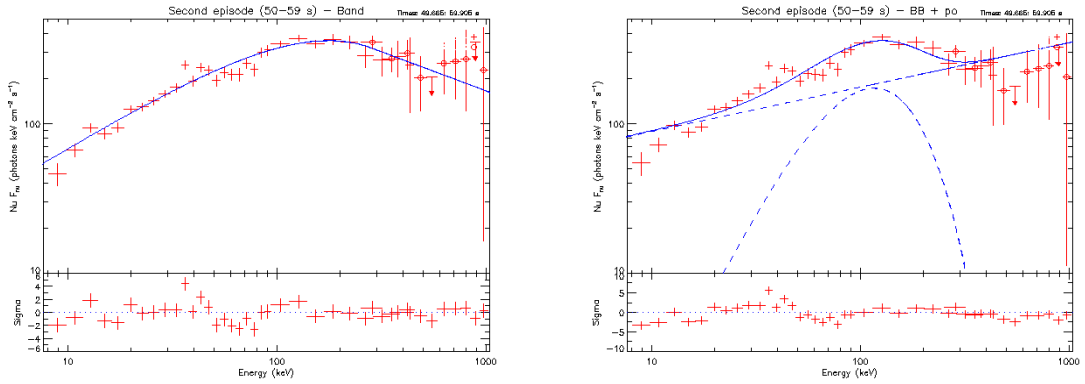

Figure 9.7.: Time-integrated spectra for the first 9 s of the second episode (from 50 to 59 s after the trigger time) of GRB 090618 fitted with the Band, $\tilde{\chi}^2$ = 1.23 (left) and blackbody + power-law (right) models, $\tilde{\chi}^2$ = 1.52.

9.5. Analysis of GRB 090618 in the fireshell scenario: from a single GRB to a multi-component GRB

9.5.1. Attempt for a single GRB scenario: the role of the first episode

We first approach the analysis of GRB 090618 by assuming that we observe a single GRB and attempt to identify its components in a canonical GRB scenario, based on the fireshell model. We first attempt the identification of the P-GRB emission. We have already seen that the integrated first 50 s can be well-fitted with a blackbody at a temperature kT = 32.07 $\pm$ 1.85 keV and an extra power-law component with the photon index γ = -1.75 $\pm$ 0.04, see panel A in Fig. 9.7 and Table 9.2. Because a blackbody component is the distinctive feature of the P-GRB, we first attempted an interpretation of GRB 090618 as a single GRB with the first 50 s as the P-GRB, Ruffini et al. (2010b). We first proceeded to evaluate if the energetics of the emission in the first 50 s can be interpreted as caused by a P-GRB. The energy emitted by the sole blackbody is $E_{BB} = 8.35^{+0.27}_{-0.36} \times 10^{51}$ ergs. Recalling that the isotropic energy of the entire GRB 090618 is $E_{iso} = (2.90 \pm 0.02) \times 10^{53}$ ergs, this means that the blackbody component would be $\sim$ 2.9 % of the total energy emitted in the burst. This would imply, see lower panel in Fig. 9.4, a baryon load $B \sim 10^{-3}$ with a corresponding Lorentz Γ factor of $\sim$ 800 and a temperature of $\sim$ 52 keV. This value disagrees with the observed temperature kT_{obs} = 32.07 keV.

One may attempt to reconcile the value of the theoretically predicted GRB temperature with the observed one by increasing $E_{tot}^{e^+e^-}$. This would lead to an $E_{tot}^{e^+e^-} = 4 \times 10^{54}$ ergs and a corresponding baryon load of $B \approx 10^{-4}$. This would imply three major discrepancies: a) there would be an unjustified complementary unobserved energy; b) in view of the value of the baryon load, and the corresponding Lorentz Γ factor, the duration of the extended-afterglow emission would be more than an order of magnitude lower than the observed 100 s (Bianco et al., 2008c); c) the duration of the first 50 s is much longer than the one typically expected for all P-GRBs identified in other GRBs (Ruffini et al., 2007c), which is at maximum on the order of $\sim$ 10 s. We have therefore considered this approach to be hopeless and proceeded to a different one looking for multiple components.

9.5.2. The multi-component scenario: the second episode as an independent GRB

The identification of the P-GRB of the second episode

We now proceed to the analysis of the data between 50 and 150 s after the trigger time as a canonical GRB in the fireshell scenario, namely the second episode, see Fig. 9.5 (Ruffini et al., 2011a). We proceed to identify the P-GRB within the emission between 50 and 59 s, since we find a blackbody signature in this early second-episode emission. Considerations based on the time variability of the thermal component bring us to consider the first 4 s of this time interval as caused by the P-GRB emission. The corresponding spectrum (8-440 keV) is well fitted ($\tilde{\chi}^2 = 1.15$) with a blackbody of a temperature $kT = 29.22 \pm 2.21$ keV (norm = 3.51 ± 0.49), and an extra power-law component with photon index $\gamma = 1.85 \pm 0.06$, (norm = 46.25 ± 10.21), see Fig. 9.8. The fit with the Band model is also acceptable ($\tilde{\chi}^2 = 1.25$). The fit gives a low-energy power-law index $\alpha = -1.22 \pm 0.08$, a high-energy index $\beta = -2.32 \pm 0.21$ and a break energy $E_0 = 193.2 \pm 50.8$, see Fig. 9.8. In view of the theoretical understanding of the thermal component in the P-GRB, see Section 3.2, we focus below on the blackbody + power-law spectral model.

The isotropic energy of the second episode is $E_{iso} = (2.49 \pm 0.02) \times 10^{53}$ ergs. The simulation within the fireshell scenario is made assuming $E_{tot}^{e^+e^-} \equiv E_{iso}$. From the upper panel in Fig. 9.4 and the observed temperature, we can then derive the corresponding value of the baryon load. The observed temperature of the blackbody component is $kT = 29.22 \pm 2.21$, so that we can determine a value of the baryon load of $B = 1.98 \pm 0.15 \times 10^{-3}$, and deduce the energy of the P-GRB as a fraction of the total $E_{tot}^{e^+e^-}$. We therefore obtain a value of the P-GRB energy of $4.33^{+0.25}_{-0.28} \times 10^{51}$ erg.

Now, from the second panel in Fig. 9.4 we can derive the radius of the transparency condition, to occur at $r_{tr} = 1.46 \times 10^{14}$ cm. From the third panel we derive the bulk Lorentz factor of $\Gamma_{th} = 495$. We compare this value with the energy measured in the sole blackbody component of $E_{BB} = 9.24^{+0.50}_{-0.58} \times 10^{50}$ erg, and with the energy in the blackbody plus the power-law component of $E_{BB+po} = 5.43^{+0.07}_{-0.11} \times 10^{51}$ erg, and verify that the theoretical value is in between these observed energies. We have found this result quite satisfactory: it represents the first attempt to relate the GRB properties to the details of the black hole responsible for the overall GRB energetics. The above theoretical estimates were based on a non rotating black hole of 10 $M_\odot$, a total energy of $E_{tot}^{e^+e^-} = 2.49 \times 10^{53}$ erg and a mean temperature of the initial plasma of e^+e^- of 2.4 MeV, derived from the expression of the dyadosphere radius, Eq. 9.3.1. Any refinement of the direct comparison between theory and observations will have to address a variety of fundamental problems such as 1) the possible effect of rotation of the black hole, leading to a more complex dyadotorus structure; 2) a more detailed analysis of the trans-

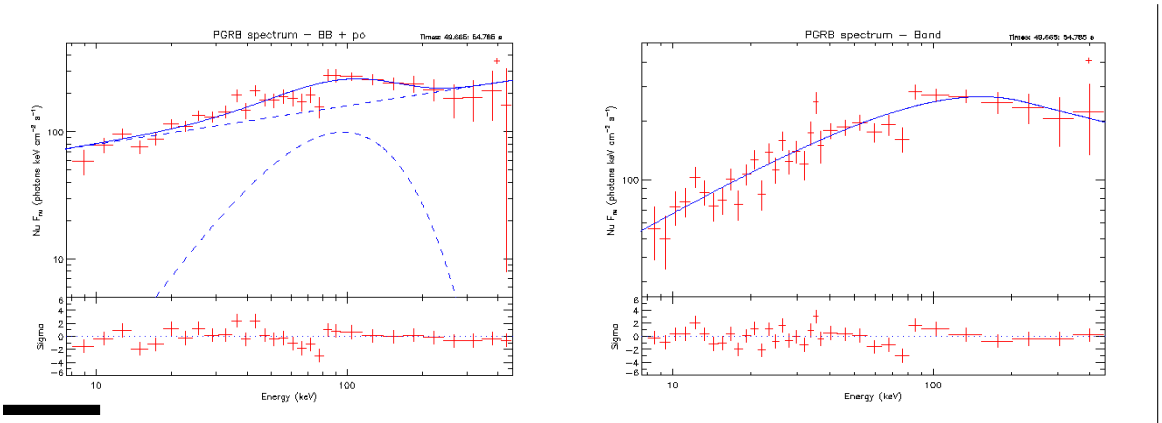

Figure 9.8.: Left panel, the time-integrated spectrum (8-440 keV) for the P-GRB emission episode (from 50 to 54 s after the trigger time) of GRB 090618 fitted with the blackbody + power-law models, $\tilde{\chi}^2$ = 1.15, while the right panel shows the fit with a Band model, $\tilde{\chi}^2$ = 1.25.

parency condition of the e^+e^- plasma, simply derived from the condition $\tau = \int_R dr(n_{e^\pm} + n^b_{e^-})\sigma_T = 0.67$ (Ruffini, 1999); 3) an analysis of the general relativistic, electrodynamical, strong interactions descriptions of the gravitational collapse core leading to a black hole formation, (Cherubini et al., 2009; Ruffini et al., 2003a; Ruffini, 1999).

The analysis of the extended afterglow of the second episode

The extended afterglow starts at the above given radius of the transparency, with an initial value of the Lorentz Γ factor of Γ_0 = 495. To simulate the extended-afterglow emission, we need to determine the radial distribution of the CBM around the burst site, which we assume for simplicity to be spherically symmetric, we infer a characteristic size of $\Delta R = 10^{15-16}$ cm. We already recalled how the simulation of the spectra and of the observed multi-band light curves have to be performed together and need to be jointly optimized, leading to the determination of the fundamental parameters characterizing the CBM medium (Ruffini et al., 2007c). This radial distribution is shown in Fig. 9.10, and is characterized by a mean value of $< n >$ = 0.6 part/cm^3 and an average density contrast with a $< \delta n/n > \approx 2$, see Fig. 9.10 and Table 9.4. The data up to 8.5×10^{16} cm are simulated with a value for the filling factor $\mathcal{R} = 3 \times 10^{-9}$, while the data from this value on with $\mathcal{R} = 9 \times 10^{-9}$. From the radial distribution of the CBM density, and considering the $1/\Gamma$ effect on the fireshell visible area, we found that the CBM clumps causing the spikes in the extended-afterglow emission have masses on the order of 10^{22-24} g. The value of the α parameter was found to be -1.8 along the total duration of the GRB.

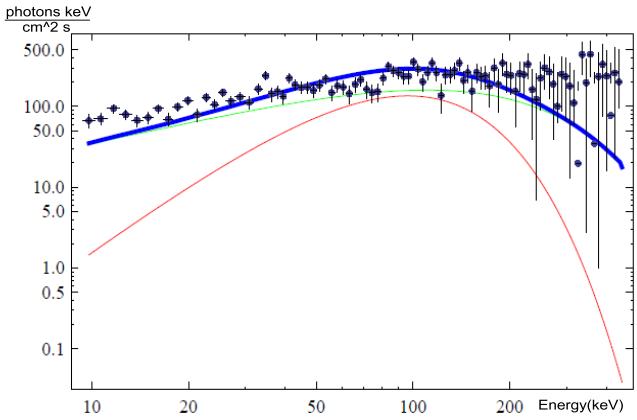

Figure 9.9.: Fireshell simulation, green line, and the sole blackbody emission, red line, of the time-integrated (t0+50, t0+54 s) spectrum of the P-GRB emission. The sum of the two components, the blue line, is the total simulated emission in the first 4 s of the second episode.

In Fig. 9.11 we show the simulated light curve (8-1000 keV) of the GRB and the corresponding spectrum, using the spectral model described in Bianco and Ruffini (2004) and Patricelli et al. (2011).

We focus our attention on the structure of the first spikes. The comparison between the spectra of the first main spike (t_0+59, t_0+66 s) of the extended afterglow of GRB 090618, obtained with three different assumptions is shown in Fig. 9.12: in the upper panel we show the fireshell simulation of the integrated spectrum (t0+59, t0+66 s) of the first main spike, in the middle panel we show the best fit with a blackbody and a power-law component model and in the lower panel the best fit using a simple power-law spectral model.

We can see that the fit with the last two models is not satisfactory: the corresponding $\tilde{\chi}^2$ is 7 for the blackbody + power-law and $\sim$ 15 for the simple power-law. We cannot give the $\tilde{\chi}^2$ of the fireshell simulation, since it is not represented by an explicit analytic fitting function, but it originates in a sequence of complex high non-linear procedure, summarized in Sec. 9.3. It is clear from a direct scrutiny that it correctly reproduces the low-energy emission, thanks in particular to the role of the α parameter, which was described previously. At higher energies, the theoretically predicted spectrum is affected by the cut-off induced by the thermal spectrum. The temporal variability of the first two spikes is well simulated.

We are not able to accurately reproduce the last spikes of the light curve, since the equations of motion of the accelerated baryons become very complicated after the first interactions of the fireshell with the CBM (Ruffini et al., 2007c). This happens for different reasons. First, a possible fragmentation of the fireshell can occur (Ruffini et al., 2007c). Moreover, at larger distances from the progenitor the fireshell visible area becomes larger than the trans-

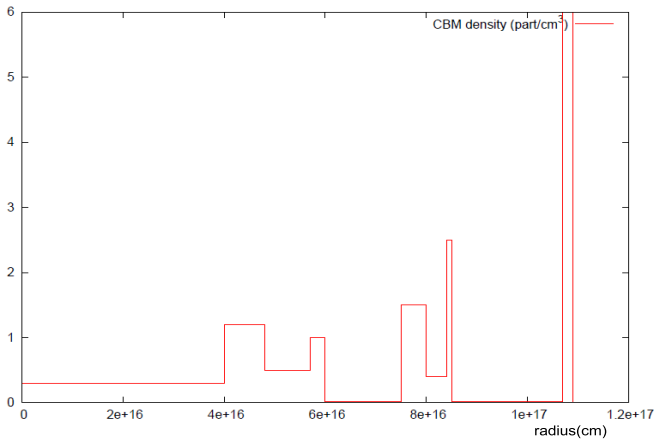

Figure 9.10.: Radial CBM density distribution for GRB 090618. The characteristic masses of each cloud are on the order of $\sim 10^{22-24}$ g and 10^{16} cm in radii.

verse dimension of a typical blob of matter, consequently a modification of the code for a three-dimensional description of the interstellar medium will be needed. This is unlike the early phases in the prompt emission, which is the main topic we address at the moment, where a spherically symmetric approximation applies. The fireshell visible area is smaller than the typical size of the CBM clouds in the early phases of the prompt radiation (Izzo et al., 2010).

The second episode, lasting from 50 to 151 s, agrees with a canonical GRB in the fireshell scenario. Particularly relevant is the problematic of the P-GRB. It interfaces with the fundamental physics problems, related to the physics of the gravitational collapse and the black hole formation. There is an interface between the reaching of transparency of the P-GRB and the early part of the extended afterglow. This connection has already been introduced in the literature (Pe'Er et al., 2012). We studied this interface in the fireshell by analyzing the thermal emission at the transparency with the early interaction of the baryons with the CBM matter, see Fig. 9.9.

We now aim to reach a better understanding of the meaning of the first episode, between 0 and 50 s of the GRB emission. To this end we examine the two episodes with respect to 1) the Amati relation, 2) the hardness variation, and 3) the observed time lag.

Table 9.3.: Final results of the simulation of GRB 090618 in the fireshell scenario

Parameter	Value
$E_{tot}^{e^+e^-}$	$2.49 \pm 0.02 \times 10^{53}$ ergs
B	$1.98 \pm 0.15 \times 10^{-3}$
Γ_0	495 ± 40
kT_{th}	29.22 ± 2.21 keV
$E_{P-GRB,th}$	$4.33 \pm 0.28 \times 10^{51}$ ergs
$< n >$	$0.6\, part/cm^3$
$< \delta n/n >$	$2\, part/cm^3$

Table 9.4.: Physical properties of the three clouds surrounding the burst site: the distance from the burst site (2^{nd} column), the radius r of the cloud (3^{rd} column), the particle density ρ (4^{th} column), and the mass M (the last column).

Cloud	Distance (cm)	r (cm)	ρ (#/cm^3)	M (g)
First	4.0×10^{16}	1×10^{16}	1	2.5×10^{24}
Second	7.4×10^{16}	5×10^{15}	1	3.1×10^{23}
Third	1.1×10^{17}	2×10^{15}	4	2.0×10^{22}

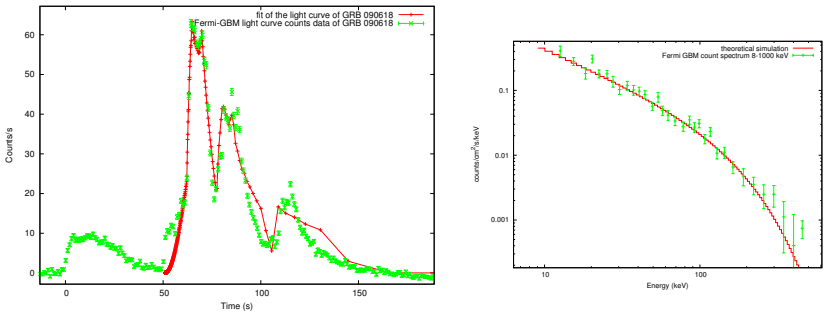

Figure 9.11.: Simulated light curve and time integrated (t0+58, t0+150 s) spectrum (8-440 keV) of the extended-afterglow of GRB 090618.

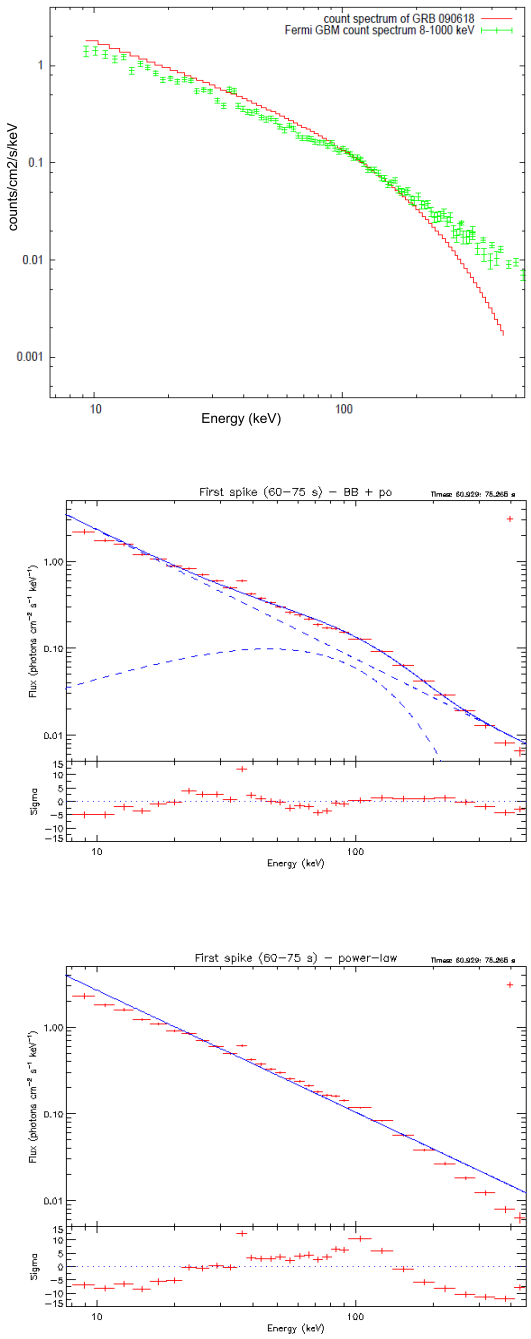

Figure 9.12.: Simulated time-integrated (t0+58, t0+66 s) count spectrum (8-440 keV) of the extended afterglow of GRB 090618 (upper panel), count spectrum (8 keV - 10 MeV) of the main pulse emission (t0+58, t0+66), and best fit with a blackbody + power-law model (middle panel) and a simple power-law model (lower panel).

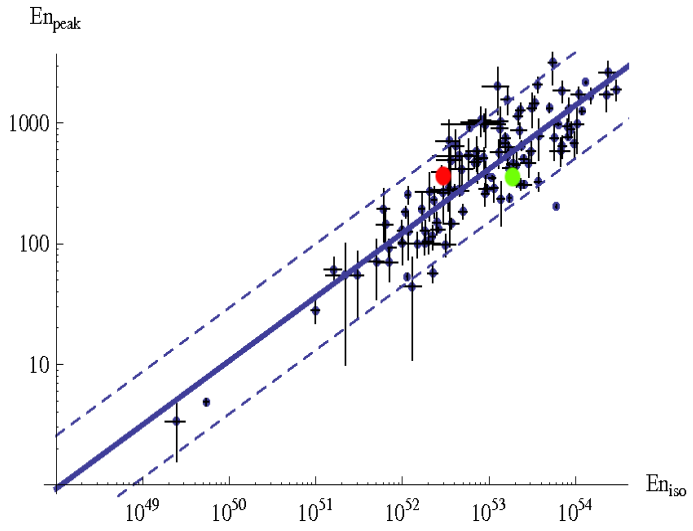

Figure 9.13.: Position of the first and second component of GRB 090618 in the $E_{p,i}$ - E_{iso} plane with respect to the best fit of the Amati relation, as derived following the procedure described in Capozziello and Izzo (2010). The red circle corresponds to the first emission while the green circle corresponds to the second one.

9.6. The Amati relation, the HR, and the time lag of the two episodes

9.6.1. The first episode as an independent GRB?

We first checked if the two episodes separately fulfill the Amati relation, (Amati et al., 2002). By using the Band spectrum we verified that the first episode presents an intrinsic peak energy value of $E_{p,1st}$ = 223.01 $\pm$ 24.15 keV, while the second episode presents an $E_{p,2nd}$ = 224.57 $\pm$ 17.4 keV. The isotropic energies emitted in each single episode are $E_{iso,1st}$ = 4.09 $\pm$ 0.07 $\times$ 10^{52} ergs and $E_{iso,2nd}$ = 2.49 $\pm$ 0.02 $\times$ 10^{53} ergs, therefore both episodes satisfy the Amati relation, see Fig. 9.13. The fulfillment of the Amati relation of episode 2 was expected, because the second episode is a canonical GRB. What we find surprising is the fulfillment of the Amati relation of the first episode.

We first examine episode 1 as a single GRB. We notice a sharp rise in the luminosity in the first 6 s of emission. We therefore attempted a first interpretation by assuming the first 6 s to the P-GRB component of this independent GRB, and the remaining 44 s to be the extended-afterglow of this GRB. A value of the fit gives $E_{tot}^{e^+e^-} = 3.87 \times 10^{52}$ ergs and $B = 1.5 \times 10^{-4}$. This would imply a very high value for the Lorentz factor at the transparency of $\sim$ 5000. In turn, this value would imply (Ruffini, 1999) a spectrum of the P-GRB peaking around $\sim$ 300 keV, which is in contrast with the observed temperature of

58 keV. Alternatively, we attempted a second simulation by assuming all observed data to be part of the extended afterglow of a GRB, with a P-GRB below the detector threshold. Assuming in this case $E_{iso} = E_{tot}^{e^+e^-}$, $B = 10^{-2}$, and assuming for the P-GRB a duration shorter than 10 s, as confirmed from the observations of all existing P-GRBs (Ruffini et al., 2007c), we should obtain an energy of the P-GRB greater than 10^{-8} ergs/cm^2/s, which should have been easily detectable from Fermi and Swift. This second possibility is therefore not viable either. We can then generally conclude that we cannot interpret this episode either as a P-GRB of the second episode, as proved in paragraph 3.2 or, as proved here, as a separate GRB. We then conclude that the fulfillment of the Amati relation does not imply that the source is necessarily a GRB.

9.6.2. The HR variation and the time lag of the two episodes

We finally address another difference between the two episodes, related to the hardness-ratio behavior (HR) and their observed time-lag. The first evidence of an evolution of the GRBs power-law slope indexes with time was observed in the BATSE GRB photon spectra (Crider et al., 1997). In the context of the fireshell scenario, as recalled earlier, the spectral evolution naturally develops from the evolution of the comoving temperature, the decrease of the bulk Lorentz Γ factor, and from the curvature effect (Bianco and Ruffini, 2004), with theoretically predicted values, in excellent agreement with observations in past GRBs.

To build the HR **ratio**, we considered the data from three different instruments: Swift-BAT, Fermi-GBM and the CORONAS-PHOTON-RT-2. The plots obtained with these instruments confirm the existence of a peculiar trend of the hardness behavior: in the first 50 s it shows a monotonic hard-to-soft behavior, as expected because of the blackbody evolution of the first episode. For the second episode, the following 50 to 151 s of the emission, there is a soft-to-hard trend in the first 4 s of emission, and a hard-to-soft behavior modulated by the spiky emission in the following 100 s. For the HR **ratio** we considered the ratio of the count rate detected from a higher energy channel to that of a lower energy channel: HR = ctg(HE)/ctg(LE). In particular, we considered the count rate subtracted for the background, although this choice provides poor HR data in the time region dominated by the background, where the count rate can be zero or negative. For the Swift data, we considered the HR for two different energy subranges: the HR1 shows the ratio of the (50-150 keV) over the (15-50 keV) emission while the HR2 **ratio** shows the ratio of the (25-50 keV) over the (15-25 keV) emission, see Fig. 9.14.

A similar trend was found for the Fermi-GBM NaI and RT-2 instruments, see Fig.9.15. In particular, the HR data from the Fermi observations were assembled the counts observed by the b0 BGO detector in the range (260 keV -

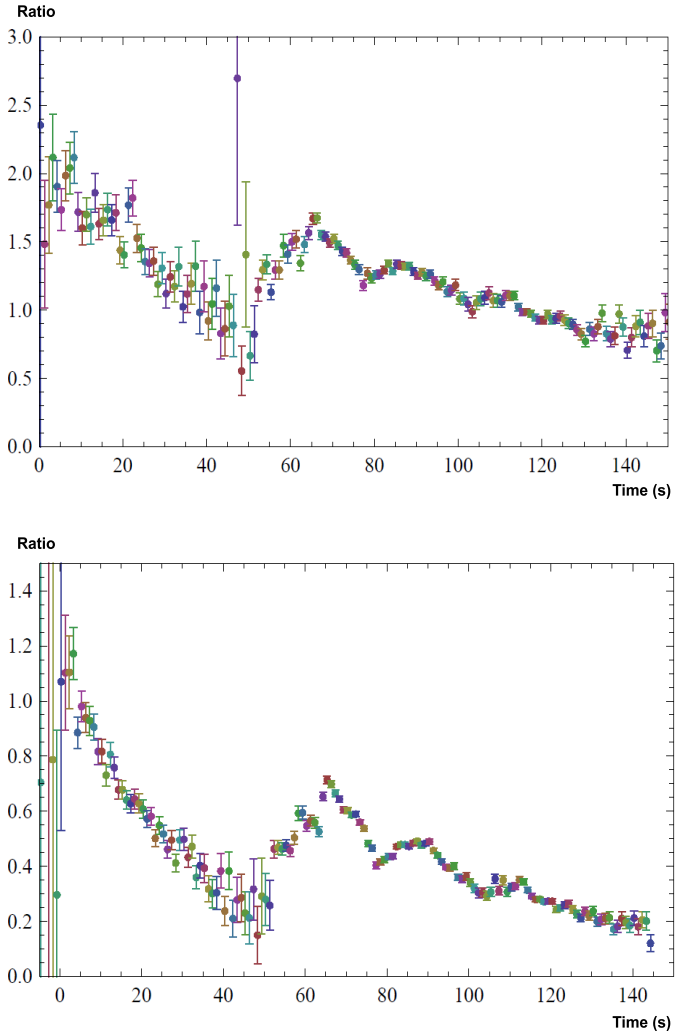

Figure 9.14.: Hardness-Ratio **ratios** for the Swift BAT data in two different energy channels: HR1 = cts(25-50 keV)/cts(15-25 keV), HR2 = cts(50-150 keV)/cts(15-50 keV).

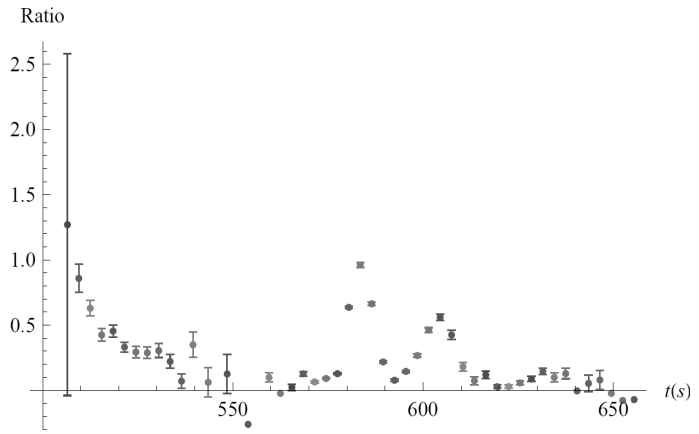

Figure 9.15.: Hardness-ratio for the Fermi data. We considered the cts observed in the (260 keV - 40 MeV) energy range over the (8 - 260 keV) energy range. The time on the x-axis is reported in terms of the mission elapsed time (MET). Several negative data points arise because of noise, in other words the non-presence of GRB emission, in the background-subtracted BGO count light curve.

40 MeV) and those observed by the n4 NaI detector in the range (8 - 260 keV). In Fig. 9.15 we show the HR for the Fermi observations, where we rebinned the counts in time intervals of 3 seconds. From this analysis we see that the HR peaks at the beginning of each pulse, also for the second-episode pulses, but each peak of the second-episode pulses is softer than the previous one, suggesting that these pulses are consequential in the second episode and generally agree with the advance of a fireshell in the CBM. Since RT-2 data clearly show both episodes up to 1 MeV, this complements the results obtained by Swift (up to 200 keV) and FERMI (up to 440 keV) in the high and the most interesting energy range. The hardness-ratio plot of (250-1000 keV)/(8-250 keV) indicates that the first phases of both episodes are the hardest.

Finally, the evident asymmetry of the first episode, supported by the observations of a long time lag in the high- and low-energy channels, see Fig. 9.2, suggests a different process at work. The first episode softens significantly, as reported in Rao et al. (2011), who observed a long time lag between the 15-25 keV energy range and 100-150 keV: the high-energy photons peak $\sim$ 7 seconds before the photons detected in the 15-25 keV energy range. This long time lag is not observed in the second episode, where the lags are on the order of $\sim$ 1 s.

Motivated by these results, we proceed to a most accurate time-resolved spectral analysis of the first episode to identify its physical and astrophysical origin.

9.7. A different emission process in the first episode

9.7.1. The time-resolved spectra and temperature variation

One of the most significant outcomes of the multi-year work of Felix Ryde and his collaborators, (see e.g. Ryde et al., 2010, and references therein), has been the identification and the detailed analysis of the thermal plus power-law features observed in time-limited intervals in selected BATSE GRBs. Similar features have also been observed in the data acquired by the Fermi satellite (Ryde et al., 2010; Guiriec et al., 2011). We propose to divide these observations into two broad families. The first family presents a thermal plus power-law(s) feature, with a temperature changing in time following a precise power-law behavior. The second family is also characterized by a thermal plus power-law component, but with the blackbody emission generally varying without a specific power-law behavior and on shorter time scales. It is our goal to study these features within the fireshell scenario to possibly identify the underlying physical processes. We have already showed in Sec. 4 that the emission of the thermal plus power-law component characterizes the P-GRB emission. We have also emphasized that the P-GRB emission is the most relativistic regime occurring in GRBs, uniquely linked to the process of the black hole formation, see Sec. 5. This process appears to belong to the second family considered above. Our aim here is to see if the first episode of GRB 090618 can lead to the identification of the first family of events: those whose temperature changes with time following a power-law behavior on time scales from 1 to 50 s. We have already pointed out in the previous section that the hardness-ratio evolution and the long time lag observed for the first episode (Rao et al., 2011) points to a distinct origin for the first 50 s of emission, corresponding to the first episode.

We made a detailed time-resolved analysis of the first episode, considering different time bin durations to obtain good statistics in the spectra and to take into account the sub-structures in the light curve. We then used two different spectral models to fit the observed data, a classical Band spectrum (Band et al., 1993), and a blackbody with a power-law component.

To obtain more accurate constraints on the spectral parameters, we made a joint fit considering the observations from both the n4 NaI and the b0 BGO detectors, covering a wider energy range in this way, from 8 keV to 40 MeV. To avoid some bias from low-photon statistics, we considered an energy upper limit of the value of 10 MeV. We report in the last three columns of Table 9.5 the spectral analysis performed in the energy range of the BATSE LAD instrument (20-1900 keV), as analyzed in Ryde and Pe'er (2009) as a comparison tool with the results described in that paper. Our analysis is summarized in Figs. 9.16, 9.17, and in Table 9.5, where we report the residual ratio diagram

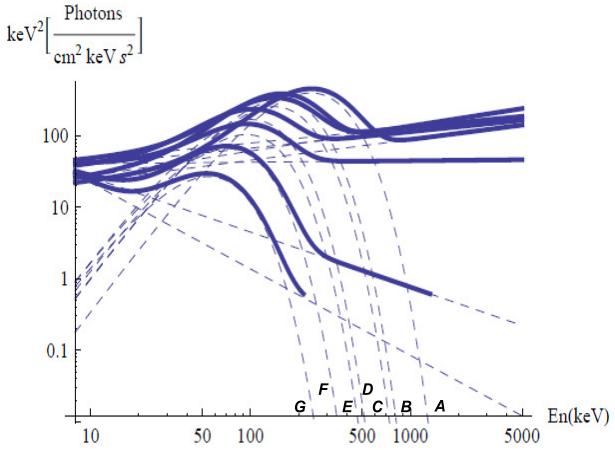

Figure 9.16.: Evolution of the BB+powerlaw spectral model in the $\nu F(\nu)$ spectrum of the first emission of GRB 090618. It shows the cooling of the blackbody and of the associated non-thermal component with time. We only plot the fitting functions for clarity.

and the reduced-χ^2 values for the spectral models.

We conclude that both the Band and the proposed blackbody + power-law spectral models fit the observed data very well. Particularly interesting is the clear evolution in the time-resolved spectra, which corresponds to the blackbody and power-law component, see Fig. 9.16. The kT parameter of the blackbody, in particular, presents a strong decay, with a temporal behavior well-described by a double broken power-law function, see upper panel in Fig. 9.17. From a fitting procedure we obtain that the best fit (R^2-statistic = 0.992) for the two decay indexes for the temperature variation are a_{kT} = -0.33 $\pm$ 0.07 and b_{kT} = -0.57 $\pm$ 0.11. In Ryde and Pe'er (2009) an average value for these parameters on a set of 49 GRBs is given: $\langle a_{kT} \rangle$ = -0.07 $\pm$ 0.19 and $\langle b_{kT} \rangle$

Table 9.5.: Time-resolved spectral analysis of the first episode in GRB 090618. We considered seven time intervals and used two spectral models, whose best-fit parameters are shown here. The last three columns, marked with a LAD subscript, report the same analysis but in the energy range $20 - 1900$ keV, which is the same energy range of the BATSE-LAD detector as used in the work of Ryde and Pe'er (2009).

Time	α	β	E_0 (keV)	$\tilde{\chi}^2_{BAND}$	kT (keV)	γ	$\tilde{\chi}^2_{BB+po}$	kT_{LAD} (keV)	γ_{LAD}	$\tilde{\chi}^2_{BB+po,LAD}$
A:0 - 5	-0.45 $\pm$ 0.11	-2.89 $\pm$ 0.78	208.9 $\pm$ 36.13	0.93	59.86 $\pm$ 2.72	1.62 $\pm$ 0.07	1.07	52.52 $\pm$ 23.63	1.42 $\pm$ 0.06	0.93
B:5 - 10	-0.16 $\pm$ 0.17	-2.34 $\pm$ 0.18	89.84 $\pm$ 17.69	1.14	37.57 $\pm$ 1.76	1.56 $\pm$ 0.05	1.36	37.39 $\pm$ 2.46	1.55 $\pm$ 0.06	1.27
C:10 - 17	-0.74 $\pm$ 0.08	-3.36 $\pm$ 1.34	149.7 $\pm$ 21.1	0.98	34.90 $\pm$ 1.63	1.72 $\pm$ 0.05	1.20	36.89 $\pm$ 2.40	1.75 $\pm$ 0.06	1.10
D:17 - 23	-0.51 $\pm$ 0.17	-2.56 $\pm$ 0.26	75.57 $\pm$ 16.35	1.11	25.47 $\pm$ 1.38	1.75 $\pm$ 0.06	1.19	25.70 $\pm$ 1.76	1.75 $\pm$ 0.08	1.19
E:23 - 31	-0.93 $\pm$ 0.13	unconstr.	104.7 $\pm$ 21.29	1.08	23.75 $\pm$ 1.68	1.93 $\pm$ 0.10	1.13	24.45 $\pm$ 2.24	1.95 $\pm$ 0.12	1.31
F:31 - 39	-1.27 $\pm$ 0.28	-3.20 $\pm$ 1.00	113.28 $\pm$ 64.7	1.17	18.44 $\pm$ 1.46	2.77 $\pm$ 0.83	1.10	18.69 $\pm$ 1.89	4.69 $\pm$ 4.2	1.08
G:39 - 49	-3.62 $\pm$ 1.00	-2.19 $\pm$ 0.17	57.48 $\pm$ 50.0	1.15	14.03 $\pm$ 2.35	3.20 $\pm$ 1.38	1.10	14.71 $\pm$ 3.52	3.06 $\pm$ 3.50	1.09

= -0.68 $\pm$ 0.24. We note, however, that in the sample considered in Ryde and Pe'er (2009) only few bursts shows a break time around 10 s, as in our case, see Fig. 9.17. Two of these bursts present many similarities with our source GRB 090618: GRB 930214 and GRB 990102. These bursts are characterized by a simple FRED pulse, whose total duration is $\sim$ 40 s, quite close to the one corresponding to the first episode of GRB 090618. The break time t_b in these two bursts are at 12.9 and 8.1 s respectively, while the decay indexes are a_{kT} = -0.25 $\pm$ 0.02 and b_{kT} = -0.78 $\pm$ 0.04 for GRB 930214 and a_{kT} = -0.36 $\pm$ 0.03 and b_{kT} = -0.64 $\pm$ 0.04 for GRB 990102, see Table 1 in Ryde and Pe'er (2009), which agrees very well with the values observed for the first episode of GRB 090618. We conclude that the values we observe in GRB 090618 are very close to the values of these two bursts. We return to compare and contrast our results with the other sources considered in Ryde and Pe'er (2009), and GRB 970828 (Pe'er et al., 2007) in a forthcoming publication.

The results presented in Figs. 9.16,9.17, and Table 9.5, point to a rapid cooling of the thermal emission with time of the first episode. The evolution of the corresponding power-law spectral component also appears to be strictly related to the change of the temperature kT. The power-law γ index falls, or softens, with temperature, see Fig. 9.16. An interesting feature appears to occur at the transition of the two power-laws describing the observed decrease of the temperature. The long time lag observed in the first episode that we reported in section 6.1 has a clear explanation in the power-law behavior of the temperature and corresponding evolution of the photon index γ, Figs. 9.16 and 9.17.

9.7.2. The radius of the emitting region

We turn now to estimate an additional crucial parameter for the identifying of the nature of the blackbody component: the radius of the emitter r_{em}. We have proved that the first episode is not an independent GRB and not part of a GRB. We can therefore provide the estimate of the emitter radius from non-relativistic considerations, just corrected for the cosmological redshift z. We have, in fact, that the temperature of the emitter $T_{em} = T_{obs}(1+z)$, and that the luminosity of the emitter, due to the blackbody emission, is

$$L = 4\pi r_{em}^2 \sigma T_{em}^4 = 4\pi r_{em}^2 \sigma T_{obs}^4 (1+z)^4, \tag{9.7.1}$$

where r_{em} is the emitter radius and σ is the Stefan-Boltzmann constant. From the luminosity distance definition, we also have that the observed flux ϕ_{obs} is given by

$$\phi_{obs} = \frac{L}{4\pi D^2} = \frac{r_{em}^2 \sigma T_{obs}^4 (1+z)^4}{D^2}. \tag{9.7.2}$$

We then obtain

$$r_{em} = \left(\frac{\phi_{obs}}{\sigma T_{ob}^4}\right)^{1/2} \frac{D}{(1+z)^2}. \tag{9.7.3}$$

The above radius differs from the radius r_{ph} given in Eq. (1) of Ryde and Pe'er (2009), which was also clearly obtained by interpreting the early evolution of GRB 970828 as belonging to the photospheric emission of a GRB and assuming a relativistic expansion with a Lorentz gamma factor Γ

$$r_{ph} = \hat{\Re} D \left(\frac{\Gamma}{(1.06)(1+z)^2}\right), \tag{9.7.4}$$

where $\hat{\Re} = \left(\phi_{obs}/(\sigma T_{ob}^4)\right)^{1/2}$ and the prefactor 1.06 arises from the dependence of r_{ph} on the angle of sight (Pe'er, 2008). Typical values of r_{ph} are at least two orders of magnitude higher than our radius r_{em}. We will return to the analysis of GRB 970828 in a forthcoming paper.

Assuming a standard cosmological model ($H_0 = 70$ km/s/Mpc, $\Omega_m = 0.27$ and $\Omega_\Lambda = 0.73$) for estimating the luminosity distance D, and using the values for the observed flux ϕ_{obs} and the temperature kT_{obs}, we give in Fig. 9.18 the evolution of the surface radius that emits the blackbody r_{em} as a function of time.

Assuming an exponential evolution with time t^δ of the radius in the comoving frame, we obtain the value $\delta = 0.59 \pm 0.11$ from a fitting procedure, which is well compatible with $\delta = 0.5$. We also notice a steeper behavior for the variation of the radius with time corresponding to the first 10 s, which corresponds to the emission before the break of the double power-law behavior of the temperature. We estimate an average velocity of $\bar{v} = 4067 \pm 918$ km/s, $R^2 = 0.91$, in these first 10 s of emission. In episode 1 the observations lead to a core of an initial radius of ~ 12000 km expanding in the early phase with a higher initial velocity of ~ 4000 km/s. The effective Lorentz Γ factor is very low, $\Gamma - 1 \sim 10^{-5}$.

9.8. Conclusions

GRB 090618 is one of the closest ($z = 0.54$) and most energetic ($E_{iso} = 2.9 \times 10^{53}$ ergs) GRBs up to date. It has been observed simultaneously by the largest number of X and γ ray telescopes: Fermi, Swift, AGILE, Konus-WIND, Suzaku-WAM, and the CORONAS-PHOTON-RT2. These circumstances have produced an unprecedented set of high-quality data as well as the coverage of the instantaneous spectral properties and of the time variability in luminosity of selected bandwidth of the source, see e.g. Figs. 9.1 and 9.2. In addition, there is also the possibility of identifying an underlying supernova event from the optical observations in the light curve of well-defined

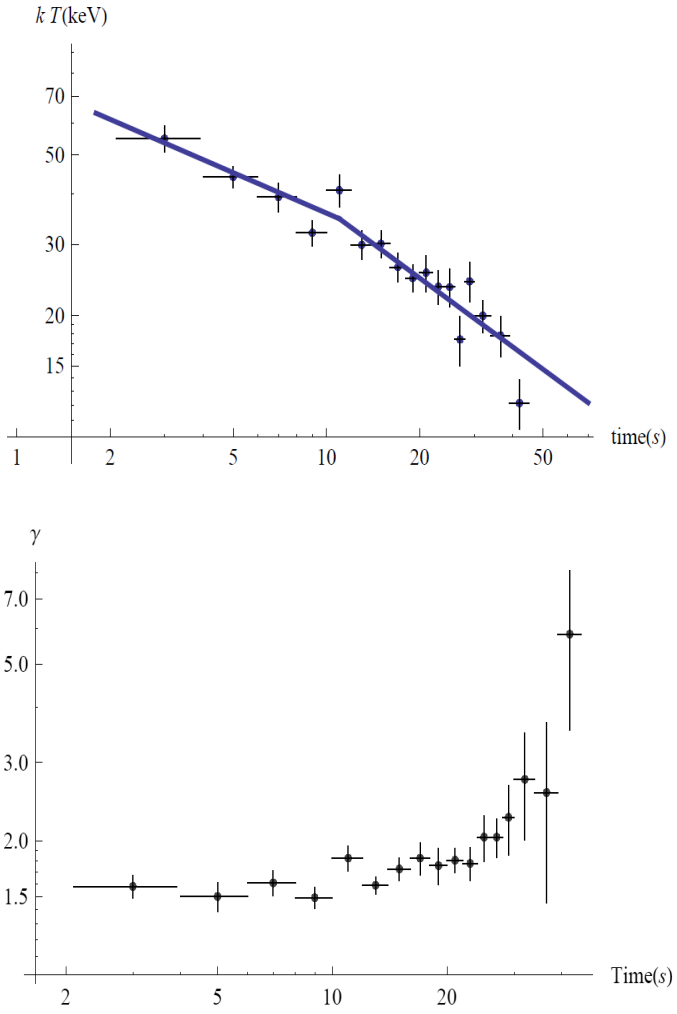

Figure 9.17.: Evolution of the kT observed temperature of the blackbody component and the corresponding evolution of the power-law photon index. The blue line in the upper panel corresponds to the fit of the time evolution of the temperature with a broken power-law function. It shows a break time t_b around 11 s after the trigger time, as obtained from the fitting procedure.

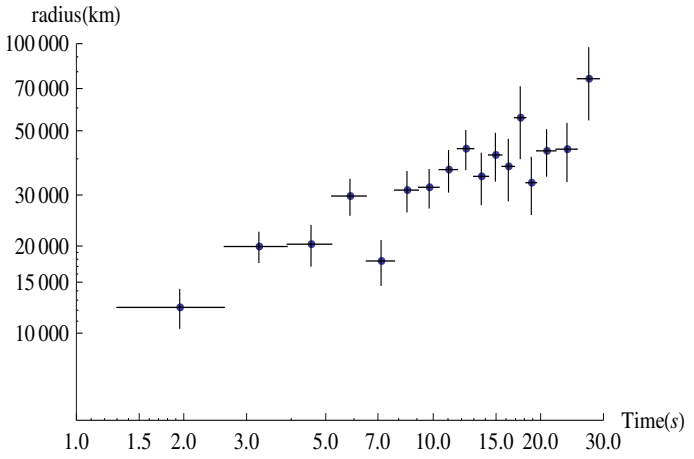

Figure 9.18.: Evolution of the first episode emitter radius, as given by Eq. (9.7.3).

bumps, as well as from the corresponding change in color after about 10 days from the main event (Cano et al., 2011). Unfortunately, a spectroscopic confirmation of this supernova is lacking. We have restricted our attention in this paper to the sole X- and γ-ray emission of the GRB, without addressing the possible supernova component.

By applying our analysis within the fireshell scenario, see section 4, we gained supporting evidence that GRB 090618 is indeed composed of two different episodes (Ruffini et al., 2010b): episode 1, lasting from 0 to 50 s, and episode 2 from 50 s to 151 s after the trigger time. We also illustrated the recent conclusions presented in Ruffini et al. (2011a) that episode 1 cannot be a GRB or part of a GRB, see section 5. With a time-resolved spectral analysis we fitted the instantaneous spectra with a blackbody plus an extra power-law component. The temperature of the blackbody appears to have a regular dependence with time, described by two power-law functions: a first power-law with decay index a_{kT} = -0.33 $\pm$ 0.07 and the second one with b_{kT} = -0.57 $\pm$ 0.11, see Section 7 . All these features precisely follow some of the results obtained by Felix Ryde and his collaborators (Ryde and Pe'er, 2009), who analyzed selected temporal episodes in some GRBs observed by BATSE.

We also examined with particular attention, see section 6, the radius r_{em} of the blackbody emitter observed in the first episode, given by Eq. (9.7.3). We interpreted the nature of this episode 1 as originating from what we have defined as a proto-black hole (Ruffini et al., 2010b): the collapsing bare core leading to the black hole formation. Within this interpretation, the radius r_{em} depends only on the observed energy flux of the blackbody component ϕ_{obs}, the temperature kT and on the luminosity distance of the source D. We obtained a radius of the emitting region that smoothly varies between $\sim$ 12000 and 70000 km, see Fig. 9.18. Other interpretations associating the origin of this early emission to the GRB main event (Pe'er et al., 2007) lead to a dif-

ferent definition for the radius of the blackbody emitter, which results to be larger than our radius by at least two orders of magnitude. We are planning a systematic search for other systems that present these particular features.

Episode 2 is identified as a canonical long GRB that originates from the black hole formation process and lasts in arrival time from 50 s to 151 s after the trigger time. The good quality of the data allowed us to search for the P-GRB signature in the early emission of the episode 2. From a detailed analysis we find that the first 4 s of episode 2 agree well with the theoretically predicted P-GRB emission, see section 5.2. The observed spectrum integrated over these 4 s is well-fitted by a blackbody with an extra power-law component, where this latter component is mainly due to the early emission of the extended-afterglow, see Fig. 9.8. From the temperature observed in the P-GRB, $kT_{PGRB} = 29.22 \pm 2.21$, and the $E_{tot}^{e^+e^-}$ energy of the second episode, which we assumed to be equal to the isotropic equivalent energy of this episode, $E_{tot}^{e^+e^-} = 2.49 \times 10^{53}$ ergs, we obtained the value of the baryon load of the GRB, see also Fig. 9.4, $B = (1.98 \pm 0.15) \times 10^{-3}$, and a consequent Lorentz Γ factor at the transparency of $\Gamma_\circ = 495 \pm 40$. We were able to simulate the temporal and spectral emission of the second episode as seen by the Fermi-GBM instrument (8 keV – 10 MeV). As we showed in Fig. 9.12, our simulation succeeds in fitting the light curves as well as the spectral energy distribution emitted in the first main spike of the second episode. The residual emission of the last spikes is reasonably well-fitted, taking into account the difficulties in integrating the equations of motion, which after the first interactions of the fireshell with the CBM become hardly predictable. The energetic of the simulation is fulfilled and we find that the emission is caused by blobs of matter in the CBM with typical dimensions of $r_{bl} = 10^{16}$ cm and average density contrast $\delta n/n \simeq 2$ particles/cm^3 in an overall average density of 1 particle/cm^3. We need to find additional cases of these phenomena to augment our statistics and improve our understanding of it.

Particularly relevant are the first two-dimensional hydrodynamical simulations of the progenitor evolution of a $23 M_\odot$ star close to core-collapse, leading to a naked core, as shown in the recent work of Arnett and Meakin (Arnett and Meakin, 2011). In that work, pronounced asymmetries and strong dynamical interactions between burning shells are seen: the dynamical behavior proceeds to high amplitudes, enlarging deviations from the spherical symmetry in the burning shells. It is highly desirable to find a possible connection between the proto-black-hole concept, introduced in this work, with the Arnett and Meakin results: to compare the radius, the temperature, and the dynamics of the core we found in the present work with the naked core obtained by Arnett and Meakin from the thermonuclear evolution of the progenitor star. Particularly relevant are the strong waves during this phase of collapse, which originate in the mixing of the different elements' shells. These waves should become able to compress, as they propagate inward, but they

should also dissipate in non-convective regions, causing heating and slow mixing in these regions of the star. Since the wave heating is faster than radiative diffusion (which is very slow), an expansion phase of the boundary layers will occur, while the iron (Fe) core will contract (Arnett and Meakin, 2011). There is also the interesting possibility that the CBM clouds observed in GRBs might be related to the vigorous dynamics in the violent activity of matter ejected in the evolution of the original massive star, well before the formation of the naked core (Arnett D., private communication).

It is appropriate to emphasize that these results have no relation with the study of precursors in GRBs performed in the current literature (see e.g. Burlon et al., 2008, and references therein). Episodes 1 and 2 are not temporally separated by a quiescent time. The spectral feature of episodes 1 and 2 are strikingly different and, moreover, episode 1 is very energetic, which is quite unusual for a typical precursor event. We finally conclude that for the first time we witness the process of formation of the black hole from the phases just preceding the gravitational collapse all the way up to the GRB emission.

There is now evidence that the proto black hole formation has been observed also in other GRB sources. After the submission of this article a second example has been found in GRB 101023, and a paper about this source was submitted on 4 November 2011 and was published on 1 February 2012 (Penacchioni et al., 2012). There, extremely novel considerations concerning the structure of the late phase of the emission in X-ray at times longer than 200 s have been presented which favor a standard signature in these sources (see also the considerations made in Page et al., 2011b). The possible use of this new family of GRBs as distance indicators is being considered.

10. Evidence for a proto-black hole and a double astrophysical component in GRB 101023

10.1. Introduction

Discovered at the end of the 60s (Strong, 1975), gamma-ray bursts (GRBs) are extremely intense flashes of hard X-radiation, coming from random directions in the sky at unpredictable times and typically lasting from a fraction of a second up to a few minutes. They are detected by satellites in low Earth orbit at a rate of $\sim$0.8 events/day. As outlined by breakthrough observations in the last $\sim$15 years, these phenomena are by far the most energetic sources in the Universe, observed in a range of cosmological redshift $0.0084 \leq z \lesssim 9$ (Salvaterra et al., 2009; Tanvir et al., 2009; Cucchiara et al., 2011), with isotropic equivalent radiated energy E_{iso} in the range $10^{49} - 10^{55}$ erg and a theoretically predicted upper limit to their energies of 10^{55} erg (Ruffini, 2009a). Since the early observation by BATSE (Meegan et al., 1992), they have been divided into two classes: the short GRBs, with a characteristic duration of $T_{90} < 2$ s, and the long GRBs, with a characteristic $T_{90} > 2$ s (Dezalay et al., 1992; Klebesadel, 1992; Kouveliotou et al., 1993).

Analysis of the GRBs within the fireshell model (see e.g. Ruffini et al., 2001b, 2009, and references therein) has led to identifying a canonical GRB structure described by two parameters: the total energy $E_{tot}^{e^\pm}$ of the initially optically thick electron-positron plasma and its baryon load $B = M_B c^2 / E_{tot}^{e^\pm}$. To this information characterizing the source is added the information on the density and filamentary distribution of the circumburst medium (CBM) (Ruffini et al., 2004b, 2005c; Patricelli et al., 2012, 2011).

Within this model the structure of a canonical GRB has been identified. It is composed by a proper-GRB (P-GRB), followed by an extended afterglow. The P-GRB originates at the moment of transparency of the relativistically expanding electron-positron plasma. The extended afterglow originates in the collision of the ultra-relativistic baryons with the filamentary structure of the CBM. The acceleration process of the baryons occurs in the optically thick phase of the self-accelerating electron-positron plasma. This explains the spiky emission observed in the prompt radiation (Ruffini et al., 2002). The average density, the porosity, and the dimensions of the clouds in the

CBM are in turn determined (see e.g. Ruffini et al., 2006b; Bernardini et al., 2007; Dainotti et al., 2007; Caito et al., 2009).

This model has allowed the nature of long GRBs to be explained and two new classes of short bursts to be introduced. A first class contains the disguised short GRBs (Bernardini et al., 2007; Caito et al., 2009, 2010; de Barros et al., 2011): just long GRBs exploding in low density CBM ($n = 10^{-3} part/cm^3$), and often referred to as short GRBs in the literature (see e.g. Gehrels et al., 2005). A second class contains the genuine short GRBs, theoretically foreseen in Ruffini et al. (2001b) as canonical GRBs occurring in the limit of a very low baryon load, $B < 10^{-5}$. This new class of genuine short GRBs is expected to occur on a much shorter time scale, $T_{90} \leq 10^{-2} - 10^{-3}$ s.

With the observation of GRB 090618, a novel situation has occurred with respect to the above classification. It had been shown in the pioneering works of Felix Ryde and his collaborators (Ryde, 2004) that, in the early emission of selected BATSE sources and also in some Fermi sources, a characteristic thermal component is present with temperature changing in time following a broken power law (Ryde, 2004, 2005; Ryde and Pe'er, 2009). They attempted to interpret this emission within the GRB fireball model (see e.g. Pe'er et al., 2007).

Ruffini et al. (2010a) showed that two very different episodes occur in GRB 090618: episodes 1 and 2. Episode 1 presents an emission "á la Ryde". There it was proposed that such an emission, alternatively to the Ryde interpretation, had to be interpreted as originating in a new kind of source in the late phase of a core collapse. The concept of proto-black hole was introduced there. Episode 2 was shown to be consistent with a canonical GRB.

Details of the data analysis showing the characteristic broken power law temporal variation of the temperature of the thermal component of episode 1 are presented in Izzo et al. (2012e). The radius of the emitting region and its time variation have been determined as well, along with the details of the GRB emission of episode 2, including the P-GRB structure, the porosity of the interstellar medium, the baryon load B, and the total energy. Identifying these two components has been made possible by the extraordinary coincidence of three major factors for this GRB: 1) precise determination of the cosmological redshift of this source $z = 0.54$, implying the fortunate occurrence of a very close source with an energy $E_{iso} = 2.7 \times 10^{53}$ erg; 2) joint observations by several X and gamma-ray telescopes; 3) the exceptional dataset on the instantaneous spectral distribution, light curve, and luminosity variation of this source (see section 10.2).

There is a striking morphological analogy between GRB 101023 and GRB 090618 (see Figs. 10.2 and 10.1). Both light curves present a first emission that lasts $\sim$ 50 s, followed by a spikier structure in the remaining part. We identify the first 45 s of GRB 101023 with episode 1 and the remaining 44 s with episode 2 (a canonical GRB). There is, however, a substantial difference between these two sources. In the present source, GRB 101023, the cosmolog-

ical redshift is unknown. This has not been a drawback for us but a challenge that probes our understanding of the GRB phenomenon. It is interesting, as a rough estimate, that if one were to assume that the two sources, GRB 101023 and GRB 090618 had not only the same morphology but also the same energy E_{iso}, one would infer $z = 1$ for the cosmological redshift of GRB 101023. A main result of this article is that, assuming the validity of the Amati relation (see Amati et al., 2009, and references therein) and Atteia criteria (Atteia, 2003), it is possible to theoretically derive an expected cosmological redshift $z = 0.9 \pm 0.084(stat.) \pm 0.2(sys.)$ for episode 2.

What is most striking is that we can have an independent verification of this redshift by comparing the late part of the afterglows of the two sources. Since we have verified that both GRB 090618 and GRB 101023 have similar energetics, and under the hypothesis of the same progenitor mechanism, we compare and contrast the luminosities of both GRBs in the late X-ray afterglow emission. We know that the X-ray afterglow is related to the residual kinetic energy of the outflow, although we do not attempt here to present a theoretical model for this emission. We rescaled, in the observed time interval and energy range, the X-ray afterglow luminosity of GRB 090618 for different redshifts in an interval between $0.04 < z < 3$ (see Fig. 10.15). The striking coincidence for $z = 0.9$ is presented in Fig. 10.14.

In section 10.2 we summarize the results of GRB 090618 and identify episode 1 and episode 2. In section 10.3 we present the observations of GRB 101023 by the different satellites. In section 10.4 we give a brief summary of the fireshell scenario. In section 10.5 we perform a spectral analysis of episodes 1 and 2 of this GRB. In section 10.6 we try to identify the P-GRB of the gamma-ray burst, taking different time intervals into account along the entire emission. In section 10.7 we present the methods we used to constrain the redshift. In section 10.8, after interpreting the second episode as a canonical GRB within the fireshell model, we build its light curve and spectrum. In Section 10.9 we go into further detail in the analysis of the first episode, making clear the evolution of the thermal component and the radius of the outermost shell and establishing the complete correspondence with GRB 090618. Finally, in Section 10.10 we present the conclusions.

10.2. Brief summary of GRB090618 analysis

We recall that GRB 0908618 is one of the most energetic among the nearest sources, with an isotropic energy of $E_{iso} = 2.7 \times 10^{53}$ erg, at redshift z= 0.54. It has been observed in a wide energy range by many satellites, such as as Fermi GBM (Meegan et al., 2009), Swift-BAT (Gehrels et al., 2009), AGILE (Longo et al., 2009b), Konus-WIND (Golenetskii et al., 2009a), Suzaku-WAM (Kono et al., 2009), and CORONAS-PHOTON (Kotov et al., 2008), and by many on-ground telescopes. We have shown (see the work of Izzo et al., 2012e) that

the light curve is quite particular, as it consists of two different emissions, of 50 s and 100 s of duration. A time-resolved spectral analysis showed that the first part is well fit by a black body and an extra power-law component. The temperature decays with time following a broken power law, in agreement with the results found by Ryde and collaborators (Ryde and Pe'er, 2009). The first power law has an index $a_{kT} = -0.33 \pm 0.07$, and the second one has an index $b_{kT} = -0.57 \pm 0.11$. The evolution of the radius r_{em} of the black body emitter has also been studied, finding an initial radius of 12000 km, expanding in the early phase with a velocity of $\sim$ 4000 km/s. By analyzing it within the fireshell model, we concluded that the first episode cannot be either a GRB or part of a GRB. Indeed, we relate this episode to the phases just preceding the gravitational collapse and define it as a "proto-black hole": the latest phase of the collapsing bare core leading to the black hole formation and the simultaneous emission of the GRB (Ruffini et al., 2010a). In this interpretation, the radius r_{em} only depends on the observed energy flux of the black body component ϕ_{obs}, the temperature kT and the luminosity distance to the source D. Episode 2 was identified as a canonical GRB, which comes from the black hole formation process. The first 4 s were identified as the P-GRB, and its spectrum is well fit by a black body with an extra power-law component, the latter mainly caused by the early emission of the extended afterglow. We found a P-GRB temperature of $kT = 29.22 \pm 2.21$ keV and a dyadosphere energy of the whole second episode of $E^{e^{\pm}}_{tot} = 2.49 \times 10^{53}$ erg. We performed a numerical simulation with the numerical code GRBsim and found a baryon load $B = (1.98 \pm 0.15) \times 10^{-3}$and a Lorentz Gamma factor at the transparency of $\Gamma = 495 \pm 40$. From this analysis we concluded that we are in the presence of a very interesting source, because for the first time we can witness the process of formation of a black hole from the phases just preceding the gravitational collapse to the GRB emission.

10.3. Observations of GRB 101023

On 23 October 2010 the Fermi GBM (Briggs, 2010) detector was triggered by a source quite similar to GRB 090618, with a trigger time of 309567006.726968 (in MET seconds). The burst was also detected by BAT (Saxton et al., 2010) (see Fig. 10.3), onboard the Swift satellite (Gehrels et al., 2004), with a trigger time of 436981 (in MET seconds) and the following location coordinates: $RA(J2000) = 21h11m49s$, $Dec(J2000) = -65°23'37''$ with an uncertainty of 3 arcmin. The Swift-XRT detector (Page and Saxton, 2010; Burrows et al., 2005a) has also observed this source from 88 s to 6.0 ks after the BAT trigger. GRB 101023 was also detected by the Wind instrument onboard Konus satellite, in the energy range $(10 - 770)$ keV (Golenetskii et al., 2010). The inferred location is in complete agreement with that determined by Swift and Fermi. Moreover, there have been detections in the optical band by the Gemini tele-

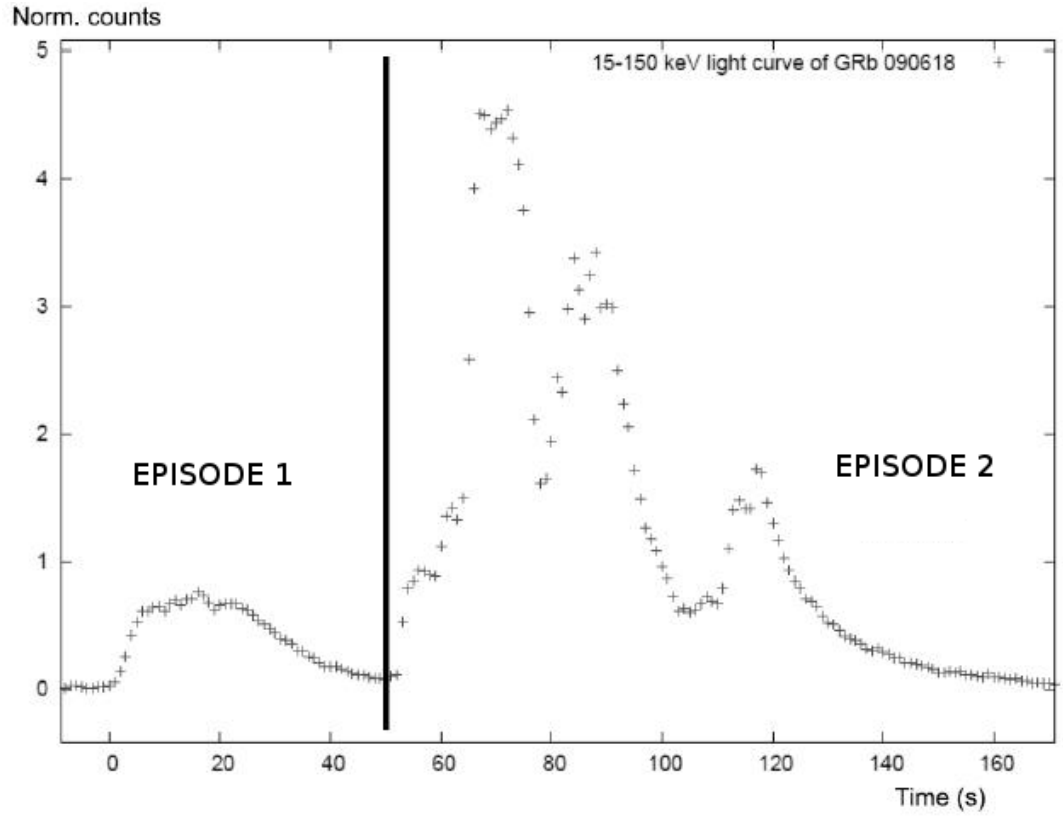

Figure 10.1.: Count light curve of GRB 090618 obtained from Fermi GBM detector, with a bin time of 1 s, and showing two-episode nature of the GRB.

scope (Levan et al., 2010).

The GBM light curve (Fig. 10.2) shows two major pulses.The first one starts at the trigger time and lasts 45 s. It consists of a small peak that lasts about 10 s, followed by a higher emission that decays slowly with time. The duration, as well as the topology of this curve, lead us to think that this may not be a canonical GRB, but its origin may lie on another kind of source, which remains unidentified. The second pulse starts at 45 s after the trigger time and lasts 44 s. It presents a peaky structure, composed of a short and weak peak at the beginning, followed by several bumps, big not only in magnitude but also in duration. This second emission, in contrast, does have all the characteristics that describe a canonical GRB (Ruffini et al., 2010c).

10.4. Theoretical model considered: Fireshell Scenario

In the fireshell scenario, the GRB emission comes from a process of vacuum polarization, resulting in pair creation in the so-called dyadosphere. In the

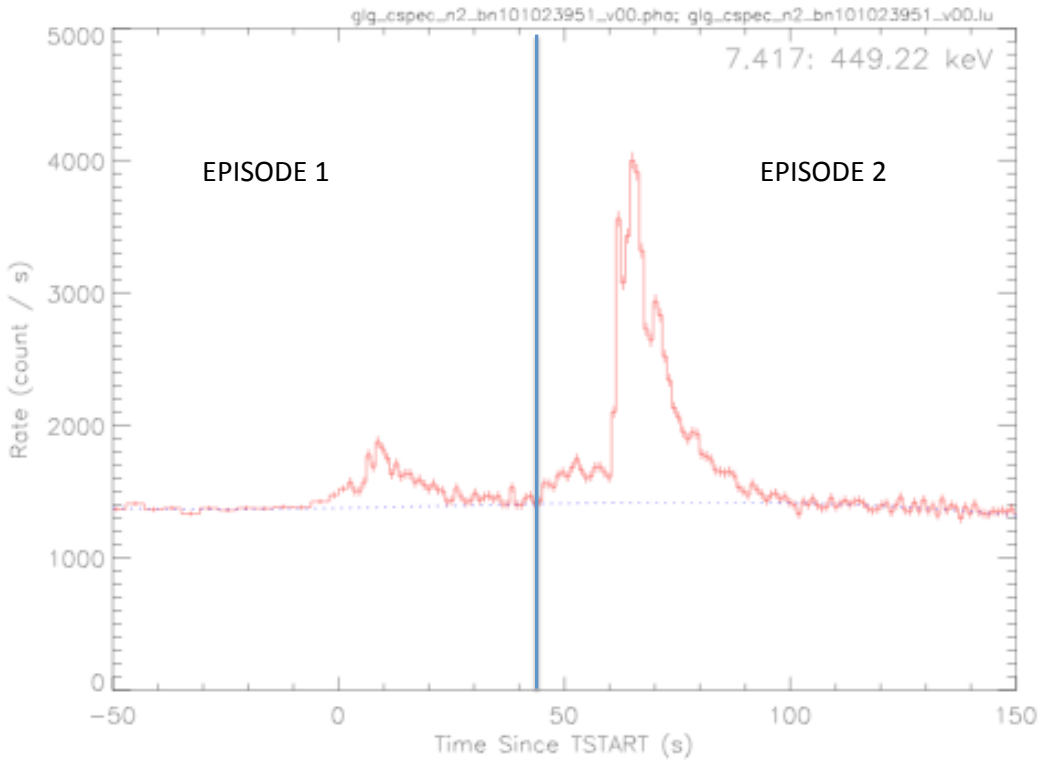

Figure 10.2.: Count light curve of GRB 101023 obtained from the Fermi GBM detector, with a bin time of 1 s. The time is given with respect to the GBM trigger time of 22:50:04.73 UT, 2010 October 23. The plot was obtained with the RMFIT program. The two-episode nature of the GRB is shown in analogy with GRB 090618.

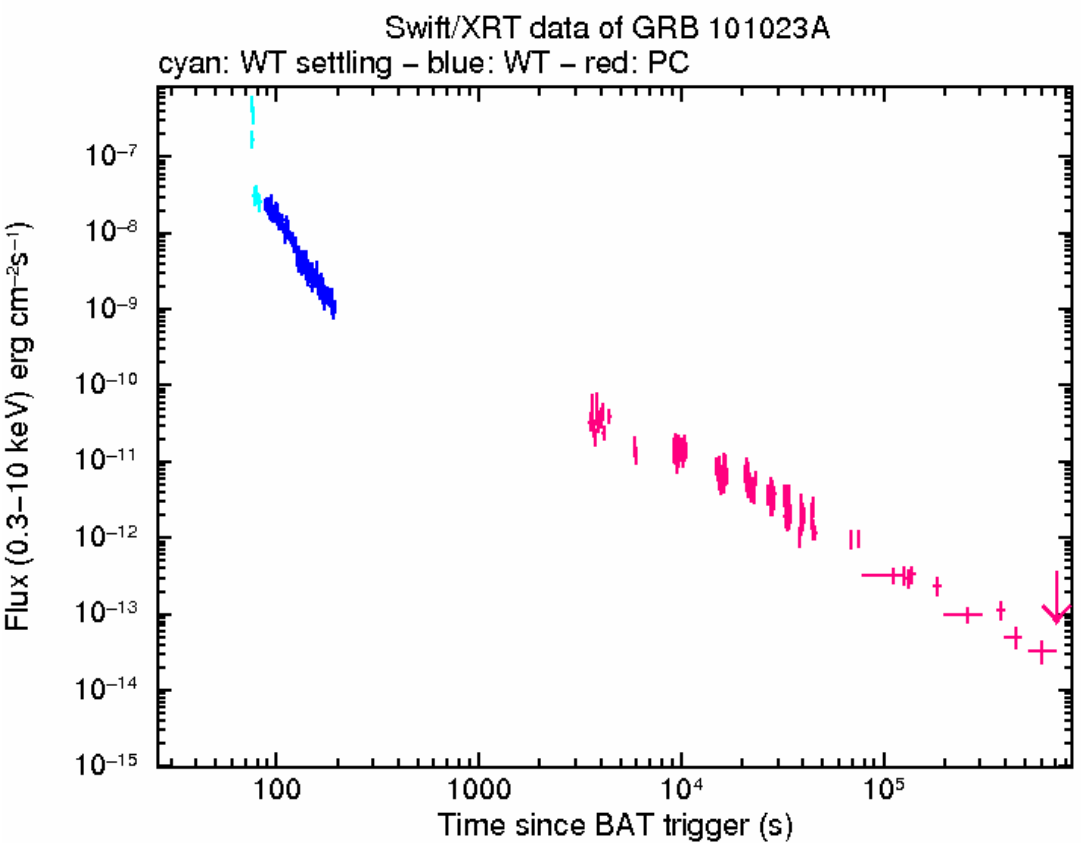

Figure 10.3.: Count light curve of GRB 101023 obtained from the Swift XRT detector.

process of gravitational collapse to a black hole (Ruffini et al., 2010e), an $e^{\pm}$ plasma is formed in thermal equilibrium, with total energy $E^{e^{\pm}}_{tot}$. The annihilation of these $e^{\pm}$ pairs occurs gradually and is confined in a shell, called "fireshell". This shell self-accelerates to relativistic velocities, engulfing the baryonic matter (of mass M_B) left over in the process of collapse and reaching a thermal equilibrium with it (Ruffini et al., 2000). The baryon loading is measured by the dimensionless parameter $B = M_B c^2 / E^{e^{\pm}}_{tot}$. The fireshell continues to self-accelerate up to relativistic velocities (Ruffini, 1999) until it reaches the transparency condition. At this time we have a first flash of radiation, the P-GRB (Ruffini et al., 2001b). The energy released in the P-GRB is a fraction of the initial energy of the dyadosphere $E^{e^{\pm}}_{tot}$. The residual plasma of leptons and baryons interacts with the circumburst medium (CBM) as it expands, giving rise to multi-wavelength emission: the "extended" afterglow. However, owing to these collisions, the plasma starts to slow down. We assume a fully-radiative condition in this model (Ruffini et al., 2003a). The structures observed in the prompt emission of a GRB come from the inhomogeneities in this CBM, while in the standard fireball scenario (Meszaros, 2006) they are caused by internal shocks. In this way we need few parameters for a complete description of a GRB: the dyadosphere energy $E^{e^{\pm}}_{tot}$, the baryon load B and the CBM density distribution, n_{CBM}. In addition, we assume that there is spherical symmetry, and the energy released in the explosion E_{iso} is equal to the energy of the dyadosphere $E^{e^{\pm}}_{tot}$. From this approach, to sum up, the GRB bolometric light curve will be composed of two main parts: the P-GRB and the extended afterglow. Their relative energetics and their observed time separation are functions of the parameters $E^{e^{\pm}}_{tot}$, B, and n_{CBM}. We want to stress that the emission of the P-GRB does not always coincide with what is called "prompt emission" in the fireball scenario. Indeed, within the fireshell model, this prompt emission corresponds to the gamma-ray emission, which addresses not only the P-GRB, but also the peak of the extended afterglow.

Instead of making use of the typical thermal spectrum, we introduced a modified black body spectrum (Patricelli et al., 2012, 2011), given by

$$\frac{dN_\gamma}{dVd\epsilon} = \left(\frac{8\pi}{h^3c^3}\right)\left(\frac{\epsilon}{k_B T}\right)^{\alpha} \frac{\epsilon^2}{exp\left(\frac{\epsilon}{k_B T}\right) - 1}. \tag{10.4.1}$$

This way we can also reach an agreement with the most energetic GRBs ($E_{iso} \geq 10^{53}$ erg). Furthermore, within the fireshell scenario we can naturally explain the hard-to-soft spectral variation observed in the extended afterglow emission. As the Lorentz gamma factor Γ decreases with time, the observed effective temperature of the fireshell also decreases, making the peak of the emission take place at lower energies. This effect is amplified by the curvature effect of the EQTS (Bianco and Ruffini, 2005a), which produces the observed time lag in the majority of the GRBs.

Table 10.1.: Time-resolved spectral analysis of GRB 101023.

Time $[s]$	α	β	E_0^{BAND}[keV]	χ^2	Norm	kT[keV]	γ	χ^2	Norm ^{Po}	Norm ^{BB}
0-44	-1.3±0.8	-1.9±0.2	87±147	0.98	0.006±0.01	14±6	-1.7±0.1	0.98	0.0003±0.0004	$(4.1 \pm 7.4) \times 10^{-5}$
45-89	-0.9±0.1	-2.02±0.1	151±24	1.09	0.043±0.008	26±1	-1.58±0.03	1.12	0.0124±0.0006	$(4.2 \pm 1.1) \times 10^{-5}$

We need to identify the P-GRB in the observed data so that we are able to determine the parameters $E_{tot}^{e^\pm}$ and B, via a trial and error procedure, and consequently the P-GRB energy E_{P-GRB}, the Lorentz gamma factor at the transparency γ, the theoretically predicted temperature kT_{th}, and the radius at the transparency (see Fig. 1 in (Ruffini et al., 2009)). The observed temperature kT_{obs} is related to the theoretically predicted temperature kT_{th} through

$$kT_{obs} = \frac{kT_{th}}{1+z}. \tag{10.4.2}$$

10.5. Analysis of data and results

To obtain the Fermi GBM light curve and spectrum in the band $8 - 440$ keV (see Fig. 10.2), we used the RMFIT program. We downloaded the data from the gsfc website[1]. We used the lightcurves corresponding to the second and fifth NaI detectors and the b0 BGO detector. We subtracted the background by fitting a cubic function from the intervals before and after the GRB (from 400 s to 200 s before the GRB and from 180 s to 220 s after it), where we suppose there is no data. Then we proceeded with the time-resolved spectral analysis.

To proceed with the fitting of the spectra, we defined first of all the time intervals we wanted to analyze: the first interval starts at the trigger time $t_0 = 0$ and lasts 45 s, while the other starts at $t_0 + 45$ s and lasts 44 s. For convenience, from now on we will refer to the first emission as episode 1 and the second emission as episode 2. For this source we considered two models: the black body plus power-law model and the Band spectral model (Band et al., 1993). We first analyzed each of the events separately, as if they were two GRBs and then subdivided each of the two emissions in the light curve into two other parts: the one that we think would correspond to the P-GRB emission and the one that would correspond to the afterglow. The results from the spectral analysis are shown in Table 10.1. The fit of the spectrum of the first episode with both models is shown in Fig. 10.4, while Fig. 10.5 shows the same fit for the second episode.

[1] ftp://legacy.gsfc.nasa.gov/fermi/data/gbm/bursts

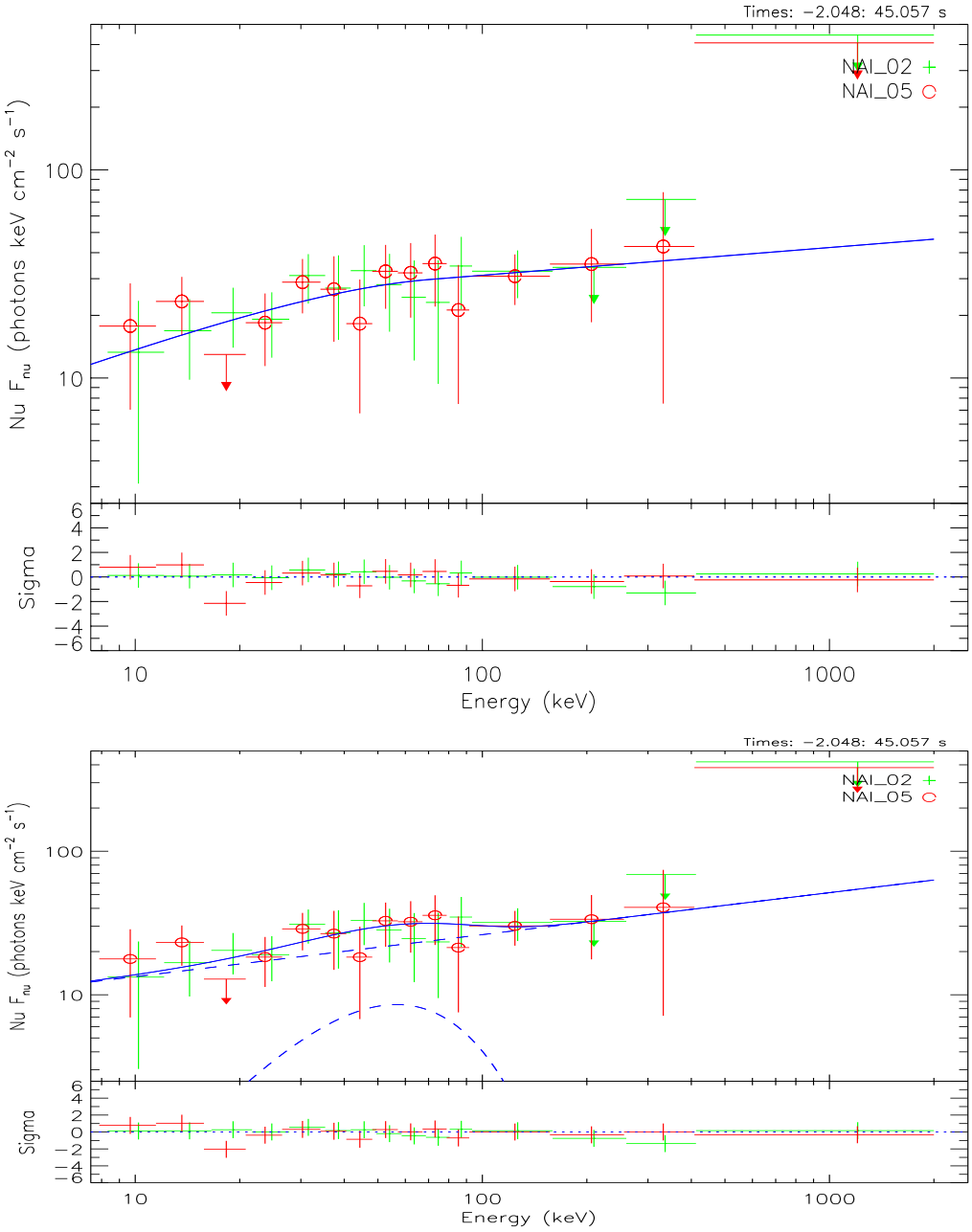

Figure 10.4.: Fit of the spectrum of episode 1, with a Band model (upper panel) and a black body plus power-law model (lower panel).

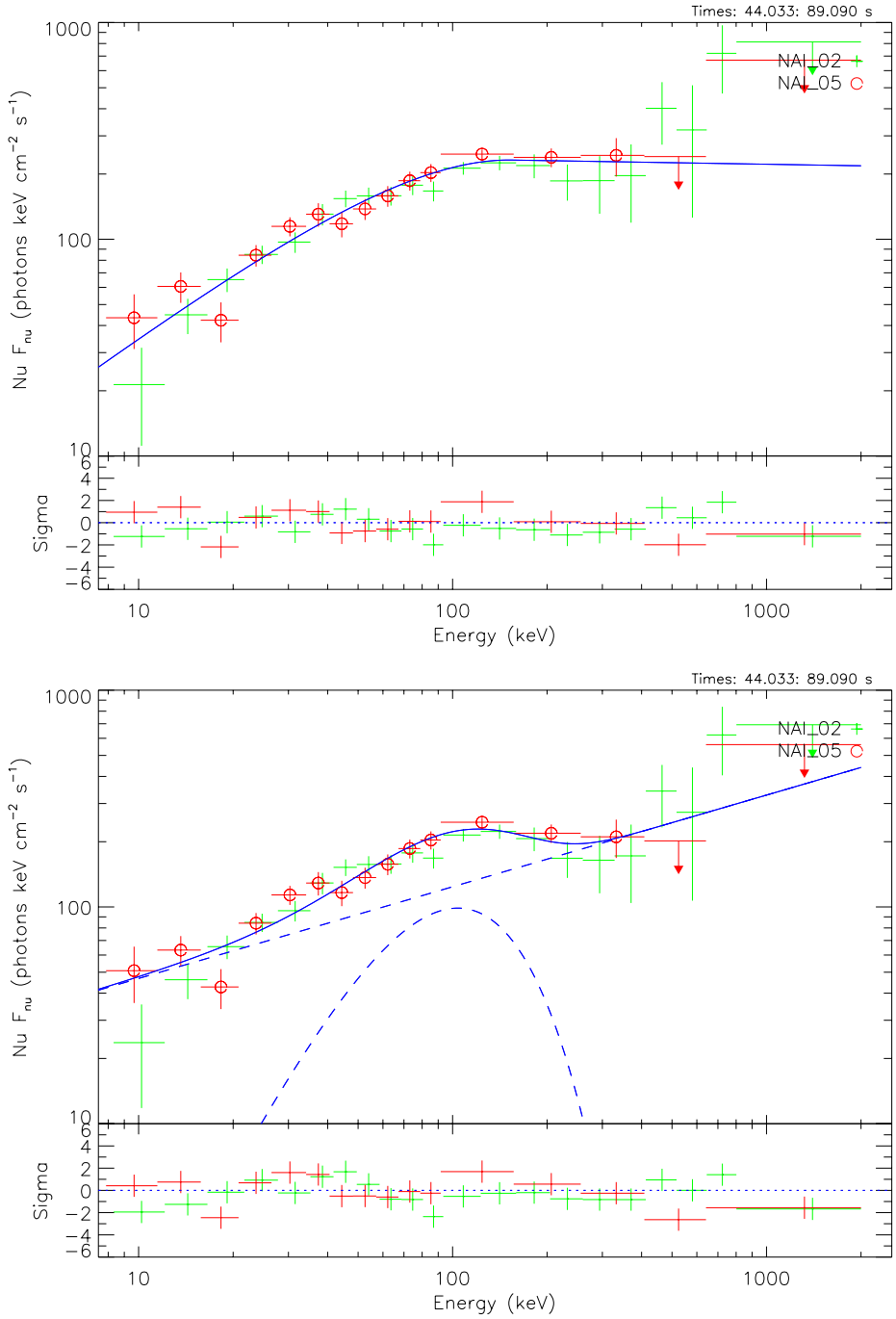

Figure 10.5.: Fit of the spectrum of episode 2, with a Band model (upper panel) and a black body plus a power-law model (lower panel). Both models fit the entire energy range well, with a chi squared of 0.79 and 0.84, respectively. The data points have been grouped according a signal-to-noise ratio of N=10, and rebinned at higher energies in order to have better statistics and reduce the error bars.

10.6. Identification of the P-GRB

10.6.1. Attempt for a single GRB scenario: the whole emission as a single GRB

The first step in our analysis was to attempt to interpret the whole emission as a single GRB, with episode 1 as the P-GRB. We performed a time-integrated analysis of the whole emission of episode 1, using a black body plus power-law model and a Band model. The results of this spectral analysis are shown in Table 10.1. We found a black-body temperature of $kT = 14 \pm 6$ keV with normalization factor $norm_{bbody} = (4.1 \pm 7.4) \times 10^{-5}$, a photon index of $\gamma = -1.7 \pm 0.1$ with normalization factor $norm_{po} = (3 \pm 4) \times 10^{-4}$ and a $\chi^2 = 0.98$ for both spectral models. The P-GRB energy is $E_{P-GRB} = 1.625 \times 10^{52}$ erg and the isotropic energy $E_{iso} = 4.03 \times 10^{53}$ erg, which gives a ratio $E_{P-GRB}/E_{iso} = 0.04$. This value in our simulations would imply a theoretically predicted temperature of $kT_{th} = 110.63$ keV, which is by far much bigger than the observed one. Consequently, the first episode cannot be the P-GRB of the whole emission.

10.6.2. The identification of the P-GRB of the first episode

Our second step in the analysis of this source was to attempt to interpret episodes 1 and 2 as two different GRBs. We first analyzed episode 1 by taking two different possibilities into account:

1) We considered a P-GRB that lasts 6 s and made the spectral analysis with XSPEC. We fitted a black body plus power-law model and found a black-body temperature of $kT = 25.4 \pm 6.9$ keV with normalization factor $norm_{bbody} = 0.9 \pm 0.5$, a photon index of $\gamma = 2.2 \pm 0.5$ with $norm_{po} = 30.9 \pm 35.3$ and a reduced chi squared of $\chi^2 = 1.01$. Considering that the P-GRB is the thermal component of the GRB, by using XSPEC we found a flux of 7.25×10^{-8}erg/cm^2/s in the range (8-5000) keV. Then we followed the same procedure for the whole of episode 1, fitting a cutoffpl model, and found a photon index of $\gamma = 1.16 \pm 0.3$, a cutoff energy of $E_{cutoff} = 73 \pm 27$ keV, a normalization factor of 2.9 ± 2.4, a reduced chi squared value of $\chi^2 = 1.08$, and a flux of 1.626×10^{-7}erg/cm^2/s. Using formula 10.7.2, we found a P-GRB energy of $E_{P-GRB} = 9.56 \times 10^{50}$ erg and a total energy of $E^{e^\pm}_{tot} = 1.625 \times 10^{52}$ erg, which gives a ratio $E_{P-GRB} = 5.9\% E^{e^\pm}_{tot}$. With these values we performed the simulation with the numerical code and found a baryon load $B = 8.5 \times 10^{-4}$ and a predicted temperature of $kT_{th} = 128.82$ keV, which is much higher than the one observed. Therefore, we concluded that the first 6 s of emission cannot be the P-GRB of episode 1, at least in the fireshell scenario. 2) We considered the P-GRB under the threshold of the detector. We took the first 6 s before the trigger time as the P-GRB and supposed that it is well fitted

by a Band model, with a flux of 10^{-8}erg/cm^2/s, which is comparable with the threshold of the detector. We derived a P-GRB energy of 10^{50} erg, which is the 0.9% of the total energy. For this ratio of the energies, we found with the numerical code a baryon load of $B = 10^{-2}$ and a predicted flux that is smaller than the detector threshold. This indicates that indeed this could be the P-GRB of the first emission, so that episode 1 could be a GRB, and we could be for the first time in the presence of a double GRB. However, in light of the results obtained from the analysis of GRB 090618 (Izzo et al., 2012e) and taking into account that the value of the redshift has not been precisely determined, we decided to discard this result. Therefore, we conclude that episode 1 is not a GRB but another source whose origin is still unidentified. We come back to this interpretation later.

10.6.3. Analysis of the second episode

After the analysis of episode 1, we moved on to the analysis of episode 2. We followed the same steps taking the first 12 s of episode 2 as the possible P-GRB. We also fitted a black body plus power-law model to the whole P-GRB and found a black-body temperature of $kT = 15.5 \pm 1.6$ keV with normalization factor $norm_{bbody} = 1.26 \pm 0.3$, a photon index of $\gamma = 2.5 \pm 0.4$ with normalization factor $norm_{po} = 141.79$ and a $\chi^2 = 0.96$. We computed a flux in the band (260-5000) keV of 2.54×10^{-7}erg/cm^2/s and a P-GRB energy of $E_{P-GRB} = 1.89 \times 10^{52}$ erg. By fitting a black body plus power-law model to the whole of episode 2 we found a flux in the band (8-5000) keV of 1.272×10^{-7}erg/cm^2/s and a total energy of $E^{e^\pm}_{tot} = 1.309 \times 10^{53}$ erg. The ratio is $E_{P-GRB} = 0.9\% E^{e^\pm}_{tot}$. This same value is reached with the numerical code for a baryon load $B = 7.6 \times 10^{-3}$ and a predicted temperature of $kT_{th} = 14.02$ keV, which after cosmological correction gives 7.38 keV (assuming z=0.9, see next section), which is not in good agreement with the observed one, $kT_{obs} = 26$ keV. Thus we conclude that the first 12 s of emission cannot be the P-GRB.

To be more accurate, we performed the following procedure: as we know that the P-GRB consists of a black-body emission, we performed a detailed spectral analysis every 1s with the Black body model to see the behavior of the black body component, i.e where the black body component dominates. That will indicate more precisely the time range and duration of the P-GRB. Table 10.2 shows the results of this analysis and Fig. 10.6 shows the behavior of the black body component with time. We see that in fact only the first 5 s of emission have a marked black body component, with a typical pulse shape. The emission that follows seems not to be related to the P-GRB, but to the afterglow. So we conclude that episode 2 is indeed a GRB and the first 5 s of emission are the P-GRB (see Section 10.8).

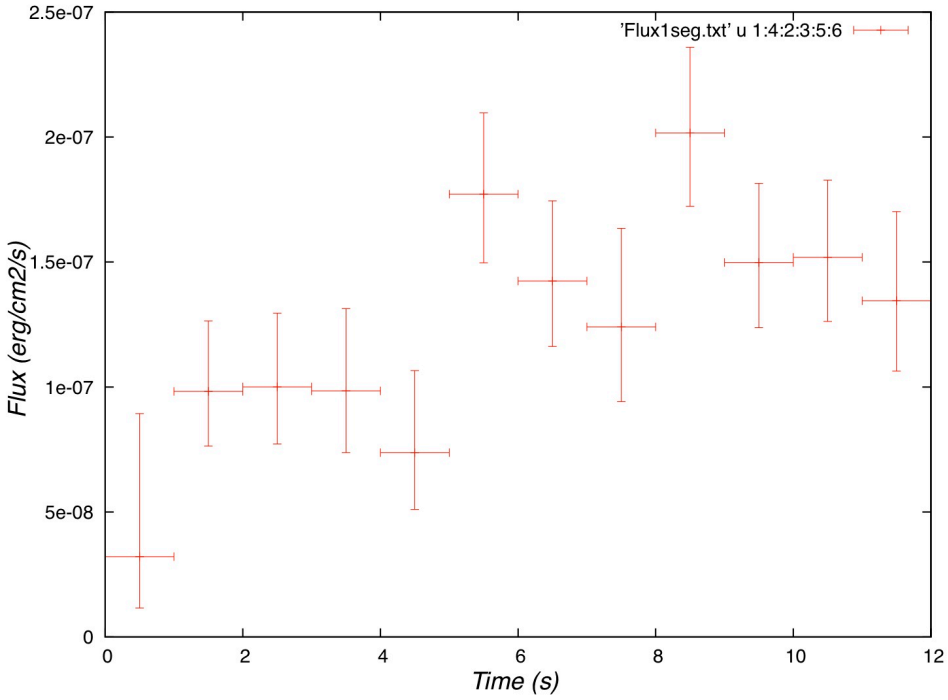

Figure 10.6.: Plot of the flux of the BB component vs time for the first 12 s of episode 2.

Table 10.2.: Detailed spectral analysis of the P-GRB of episode 2, of 12s of duration, using a BB+po model and performed every 1 second.

P-GRB of episode 2	(BB+po)			
Time Int	kT(keV)	norm factor	Flux 8-440 keV	χ^2
051-052	1.9±1.7	0.9±2	3.2525 $\times 10^{-8}$	1.40
052-053	5±1	1.3±0.3	9.8254×10^{-8}	1.06
053-054	7±1	1.2±0.3	9.9689×10^{-8}	0.99
054-055	10±2	1.2±0.3	9.8285×10^{-8}	1.17
055-056	7±1	1.6±0.3	1.3217×10^{-7}	0.96
056-057	10±1	2.1±0.4	1.7721×10^{-7}	1.42
057-058	10±1	1.7±0.4	1.4245×10^{-7}	0.96
058-059	11±1	2.1±0.4	1.7738×10^{-7}	1.16
059-060	10±1	2.6±0.4	2.1844×10^{-7}	1.38
060-061	10±1	1.8±0.3	1.4976×10^{-7}	1.51
061-062	9±1	1.8±0.3	1.5193×10^{-7}	1.18
062-063	14±2	1.6±0.4	1.3462×10^{-7}	1.74

10.7. Pseudo-redshift determination

The redshift of this source is unknown, owing to the lack of data in the optical band. However, to constrain it, we employed three different methods, mentioned below.

10.7.1. Method 1: nH column density

We first tried to estimate the redshift making use of the method developed in Grupe et al. (2007b) work, where the authors comment on the possible relation between the absorption column density in excess of the galactic absorption column density $\Delta N_H = N_{H,fit} - N_{H,gal}$ and the redshift z. To do this, we considered the galactic absorption component taken from Kalberla et al. (2005), with the following values of the galactic coordinates of the GRB: $l = 328.88$, $b = -38.88$. We used the Lab Survey website[2] and obtained the value of $n_H = 2.59 \times 10^{20} cm^{-2}$ for the galactic H column density.

Then we took the values of some parameters, the spectrum, and response files from the XRT website[3], selected the part of interest and carried out an analysis making use of the program XSPEC. We fit the model wabs, which is the photoelectric absorption using Wisconsin cross sections (Morrison and McCammon, 1983): $M(E) = exp[-n_H \sigma(E)]$, where $\sigma(E)$ is the photoelectric cross section (not including Thomson scattering) and n_H is the equivalent hydrogen column density, in units of 10^{22} atoms/cm^2. Once we knew these parameters, we fit the data with a power-law model, considering a phabs component related to the intrinsic absorption. We obtained a value of $n_H^{intr} = 0.18 \pm 0.019 \times 10^{22} cm^{-2}$. Wkth this result, we put them in formula (1) of Grupe et al. (2007b) paper:

$$log(1+z) < 1.3 - 0.5[log(1 + \Delta N_H)], \tag{10.7.1}$$

and we obtained an upper limit for the redshift of 3.8.

10.7.2. Method 2: Amati relation

We tried another method of constraining the redshift, making use of the Amati relation (Amati, 2006), shown in Fig. 10.7. This relates the isotropic energy E_{iso} emitted by a GRB to the peak energy in the rest frame $E_{p,i}$ of its νF_ν electromagnetic spectrum (see Amati et al., 2009, and references therein). E_{iso} is the isotropic-equivalent radiated energy, while $E_{p,i}$ is the photon energy at which the time averaged νF_ν spectrum peaks. The analytical expression of

[2] http://www.astro.uni-bonn.de/~webaiub/english/tools_labsurvey.php
[3] http://www.swift.ac.uk/xrt_curves/

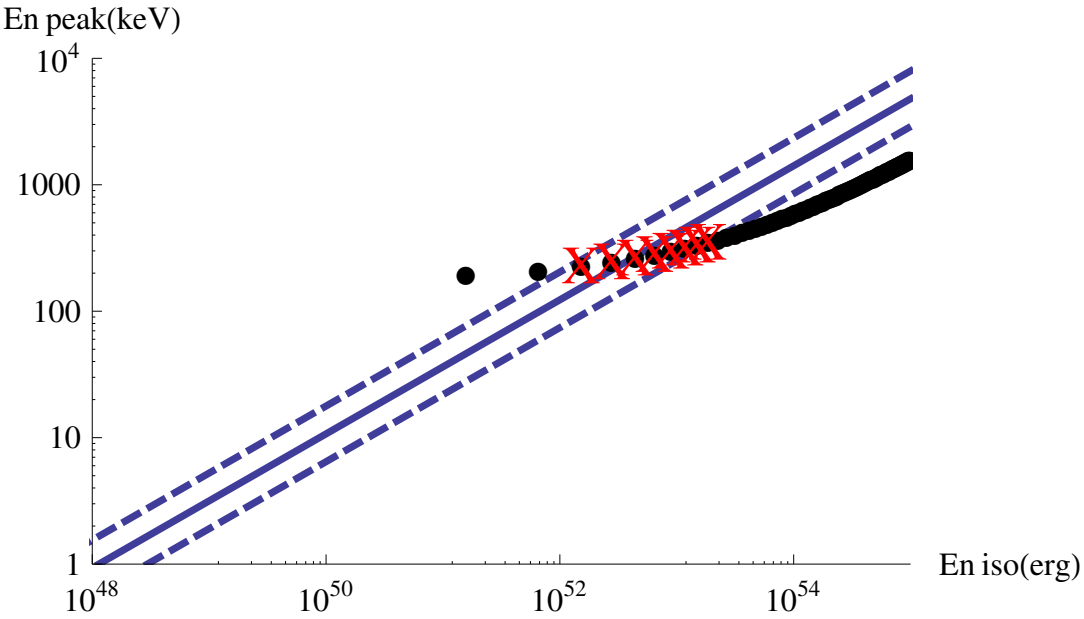

Figure 10.7.: Plot of the relation between $E_{p,i}$ and E_{iso} for the second episode of GRB 101023, considering different values of the redshift. It can be seen that the plot lies within 1σ for the range z= 0.3 - z= 1.0.

E_{iso} is

$$E_{iso} = \frac{4\pi d_l^2}{(1+z)} S_{bol}, \tag{10.7.2}$$

where d_l^2 is the luminosity distance, z is the redshift and S_{bol} is the bolometric fluence, related to the observed fluence in a given detection band (E_{min}, E_{max}) by

$$S_{bol} = S_{obs} \frac{\int_{1/(1+z)}^{10^4/(1+z)} E\phi(E)dE}{\int_{E^{min}}^{E^{max}} E\phi(E)dE}, \tag{10.7.3}$$

with ϕ the spectral model considered for the spectral data fit. The value of $E_{p,i}$ is related to the peak energy E_p in the observer's frame by

$$E_{p,i} = E_p(1+z)\,. \tag{10.7.4}$$

We started our analysis under the hypothesis that episode 2 is a long GRB. We computed the values of $E_{p,i}$ and E_{iso} for different given values of z and plotted them in Fig. 10.7. We found that the Amati relation is fulfilled by episode 2 for $0.3 < z < 1.0$. This interval has been calculated at 1σ from the best fit from the Amati relation, in order to obtain a tighter interval around the best fit than with the previous method.

10.7.3. Method 3: Empirical method for the pseudo-redshift

We also tried an empirical method, following Atteia (2003) and Pélangeon et al. (2006), which can be used as a redshift indicator. This method consists in determining a pseudo-redshift from the GRB spectral properties. Using the parameters from the Band model, namely the index of the low-energy power-law α and the break energy E_0, we can compute the value of the peak energy of the νF_ν spectrum, as $E_p = E_0(2+\alpha)$. Then, we define the isotropic-equivalent number of photons in a GRB, N_γ, as the number of photons below the break, integrated from $E_p/100$ to $E_p/2$. If we also know the T_{90}, we define the redshift indicator

$$X = \frac{N_\gamma}{E_p\sqrt{T_{90}}}. \tag{10.7.5}$$

From a sample of 17 GRBs with known redshift reported in Atteia (2003) we compute the theoretical evolution of X with the redshift z, that is $X = f(z)$. Then we invert the relation to derive a pseudo-redshift from the value of X. That way we obtain the pseudo-redshift as $\hat{z} = f^{-1}(X)$, for the GRB of interest.

We applied this treatment to episode 2 of GRB 101023, introducing the spectral parameters from the Band model on the Cosmos website[4] and obtained a value for the redshift of $z = 0.9 \pm 0.084$. It is important to mention here that this error is a statistical one, while the systematic error is much bigger (Atteia, 2003; Pélangeon et al., 2006, 2008), of a factor of ~ 1.5, i.e., $z = 0.9^{+0.45}_{-0.3}$.

This result agrees with the redshift range found from the Amati relation for episode 2 and is also consistent with the upper limit determined with method 1.

10.8. Simulation of the light curve and spectrum

To simulate the light curve we made use of a numerical code called GRB-sim. This numerical code simulates a GRB emission by solving the fireshell equations of motion, taking the effect of the EQuiTemporal Surfaces (EQTS, Bianco and Ruffini, 2005a) into account. We made the simulation for episode 2. We found, at the transparency point, a value of the laboratory radius of $1.34 \times 10^{14} cm$, a theoretically predicted temperature that after cosmological correction gives $kT_{th} = 13.26$ keV, a Lorentz Gamma factor of $\Gamma = 260.48$, a P-GRB laboratory energy of 2.51×10^{51} erg and a P-GRB observed temperature of 28.43keV. We adopted a value for the dyadosphere energy of $E^{e^\pm}_{tot} = 1.8 \times 10^{53}$ erg and a baryon loading of $B = 3.8 \times 10^{-3}$. The simulated light curve and spectrum of episode 2 are shown in Figs. 10.8 and 10.9, respectively.

[4] http://cosmos.ast.obs-mip.fr/projet/v2/fast_computation.html

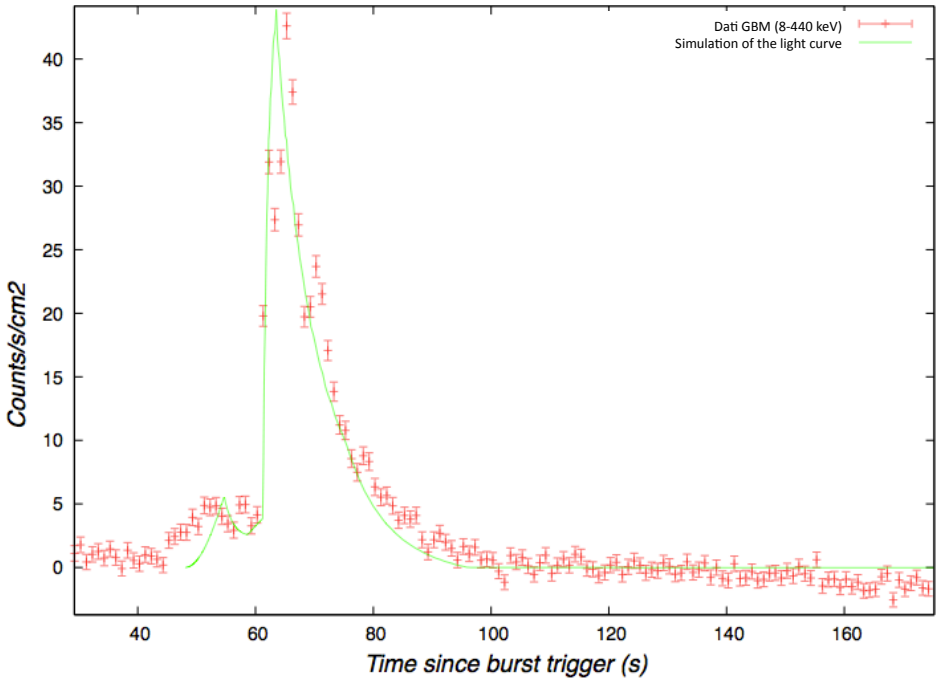

Figure 10.8.: Fit of the second major pulse of the light curve of GRB 101023.

Figure 10.10 shows the fitted spectrum with different models. We took the data points from the NaI n2 and BGO b0 detectors together. We note there is a good agreement between both fits, in the low and medium energy range. At high energies, the spectrum follows a power-law behavior, which cannot be reproduced by the modified black body model due to the exponential cutoff.

10.9. Analysis of the first episode

To analyze episode 1 more into detail, in order to identify the nature of this phenomenon, we plotted the temperature of the black body component as a function of time, for the first 20 s of emission (see Fig. 10.11). We note a strong evolution in the first 20 s of emission which, according to Ryde (2004) can be reproduced by a broken power-law behavior, with $\alpha = -0.47 \pm 0.34$ and $\beta = -1.48 \pm 1.13$ being the indices of the first and second power law, respectively. We also plotted the radius of the most external shell with time (see Fig. 10.12). Following Izzo et al. (2012e), the radius can be written as

$$r_{em} = \frac{\hat{R} D \Gamma}{(1+z)^2}, \tag{10.9.1}$$

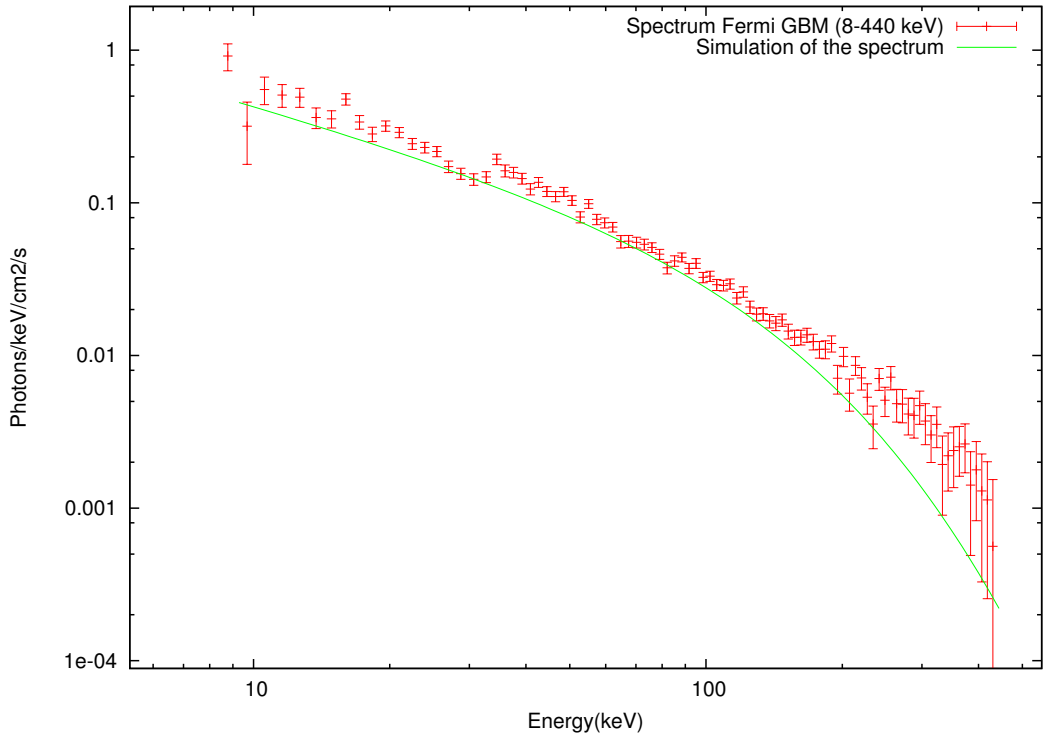

Figure 10.9.: Fit of the spectrum of episode 2.

where $\hat{R}^2 = \phi_{obs}/(4\pi\sigma T_{obs}^4)$ is a parameter, D the luminosity distance, Γ the Lorentz factor, and ϕ_{obs} the observed flux. We can see that the radius remains almost constant (in fact it increases, but only slightly). From this it is possible to see that the plasma is expanding at nonrelativistic velocities. According to the work of Arnett and Meakin (2011), there is an expansion phase of the boundary layers, while the iron core suffers a contraction. This is due to the presence of strong waves originated while the different shells of the progenitor mix during the collapse phase. This fact confirms the non-GRB nature for the first episode.

10.9.1. The X-ray afterglow as a possible redshift estimate ?

We have seen that GRB 090618 and GRB 101023 share similar properties. They seem to be composed of two different emission episodes, the first being connected to a quasi-thermal process before the collapse of the core, while the second is the canonical GRB (see Ruffini et al., 2010a,b).

Anyway, if both GRBs were created originated by the same physical mechanism and since the energetics are very similar, considering the value $z = 0.9$ for GRB 101023, we can expect similar luminosity behavior for the X-ray afterglow. Although we have not yet developed a theory for this late afterglow emission, we attempted a simple test that compared the observed X-ray af-

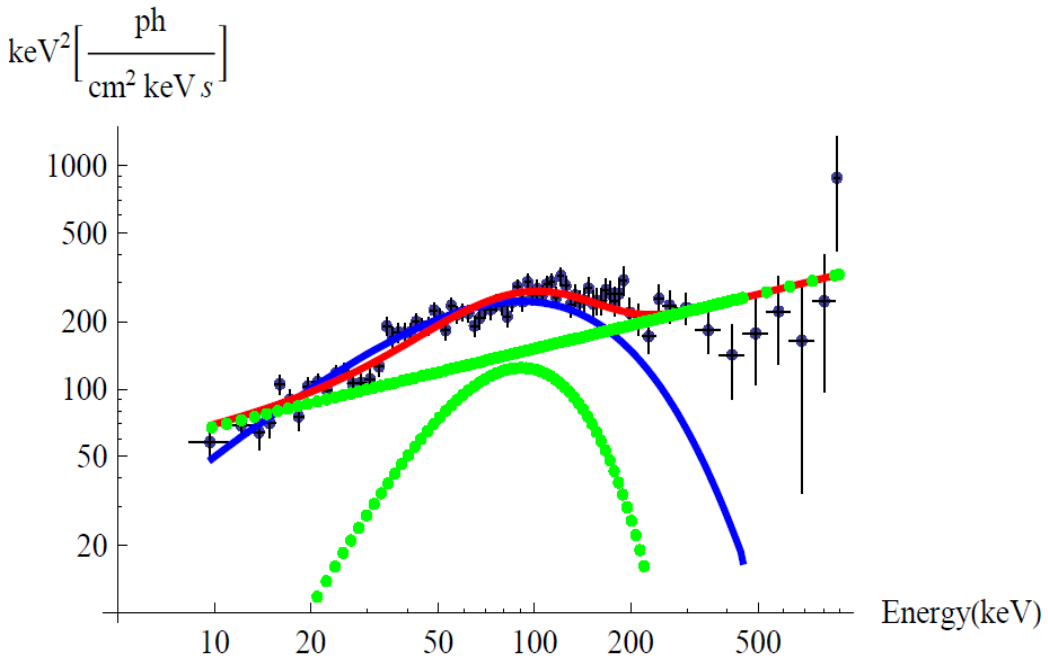

Figure 10.10.: Fit of the spectrum of episode 2. The green dotted lines represent the fit of a black body and a power-law components, separately. The red line is the sum of them, calculated with XSPEC (BB+po). The blue line is the fit with the modified black body spectrum given in Eq.(10.4.1), calculated with the GRBsim numerical code.

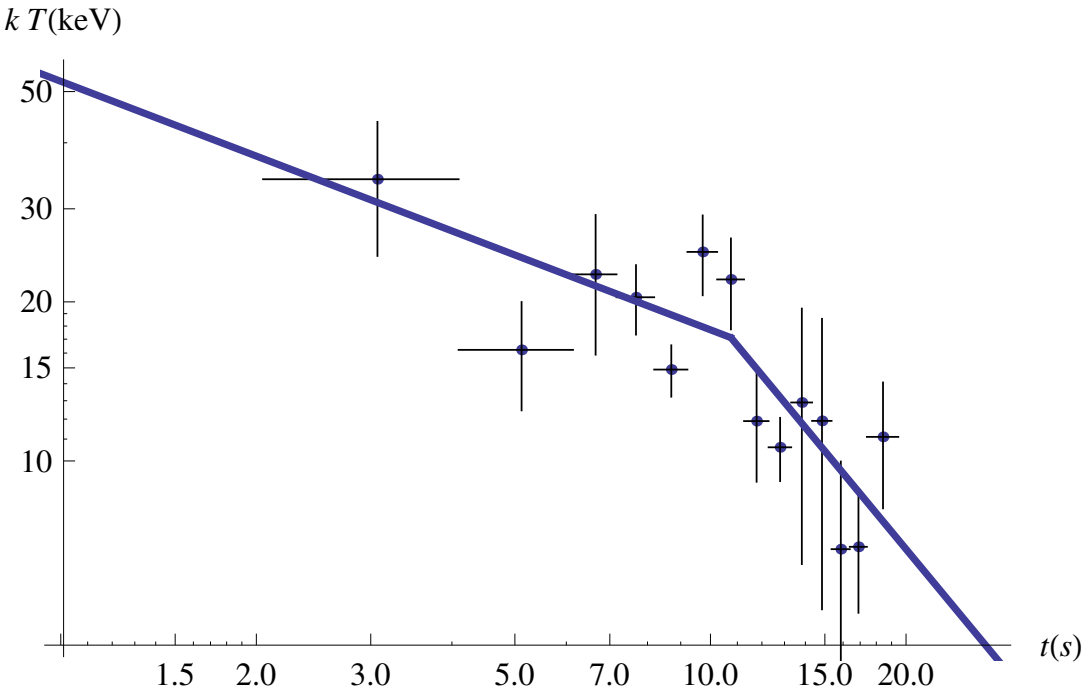

Figure 10.11.: Evolution of the observed temperature kT of the BB component. The blue line corresponds to a broken power-law fit. The indices of the first and second power laws are $\alpha = -0.47 \pm 0.34$ and $\beta = -1.48 \pm 1.13$, respectively. The break occurs at 11 s after the trigger time.

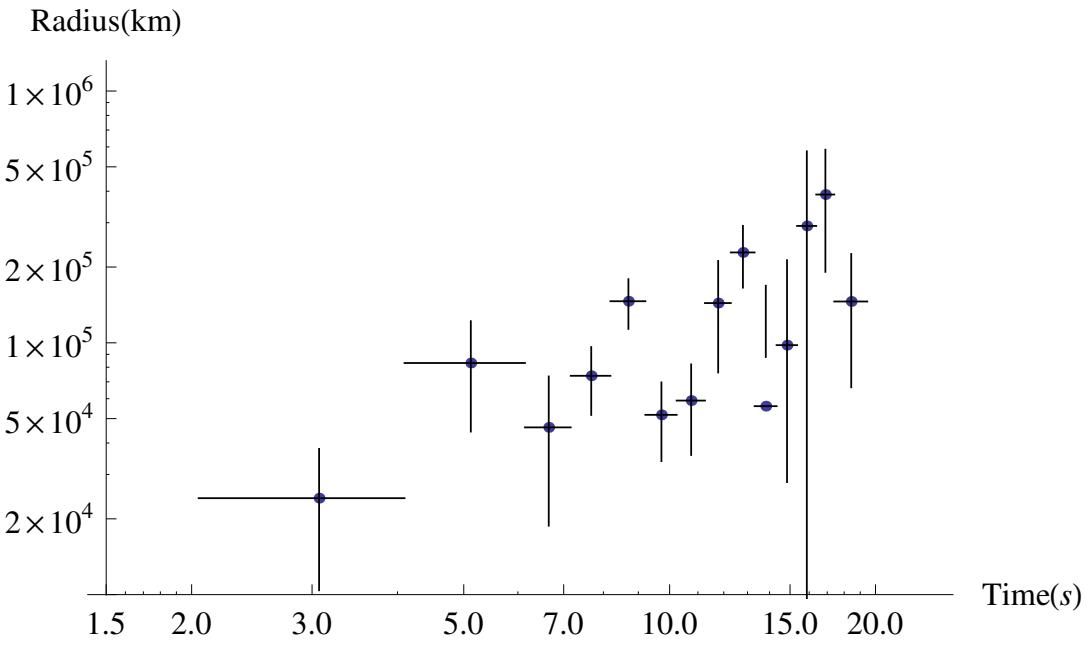

Figure 10.12.: Evolution of the radius of the first episode progenitor.

terglow of both GRBs as if they were located at the same redshift. Since there are different spectral components in the GRB X-ray afterglow, we built the pseudo-redshift light curves for both these different emissions. Thanks to the Swift-XRT observations, we know that the early X-ray afterglow of both GRBs shows a canonical behavior, where the emission can be divided in three distinct parts (Nousek, 2006): 1) a first very steep decay, associated with the late prompt emission; 2) a shallower decay, the plateau; 3) a final steeper decay. At first, we determined for GRB 090618 and GRB 101023 these three time intervals by using the phenomenological function introduced in the work of Willingale et al. (2007):

$$f(t) = \begin{cases} F_c exp\left(\alpha_c - \frac{t\alpha_c}{T_c}\right) exp\left(\frac{-t_c}{t}\right), & t < T_c; \\ F_c \left(\frac{t}{T_c}\right)^{-\alpha_c} exp\left(\frac{-t_c}{t}\right), & t > T_c, \end{cases} \tag{10.9.2}$$

which represents the transition from an exponential regime to a power law. This transition occurs at the point (T_c, F_c) where the two functional sections have the same value and gradient. The α_c parameter determines both the time constant of the exponential decay and the temporal decay index of the power law, while the t_c parameter marks the initial rise. The maximum flux occurs at $t = (t_c T_c/\alpha_c)^{1/2}$. We fit the afterglow data of the two GRBs with this model, and the results of our fits are shown in Fig. 10.13.

After the determination of these three time intervals, we built the X-ray light curve of GRB 090618 as if it was observed at redshift z = 0.9, which is our estimate for the redshift of GRB 101023. The Swift-XRT (which operates in the (0.3 - 10) keV energy range) light curve of GRB 090618 (Evans et al., 2007, 2009) corresponds to the emission in the rest frame at z = 0.54 in the energy range (0.462 - 15.4) keV, while for GRB 101023 the XRT window corresponds to the range (0.57 - 19) keV. We must obtain the emission of GRB 090618 in this last energy range, in order to compare the two light curves. At first we made the assumption that the spectrum of each time interval is best fitted by a simple power-law model. This assumption is supported by the hypothesis that the X-ray afterglow comes from a synchrotron emission mechanism (Sari and Piran, 1999), whose spectral emission is represented by a simple power law function. Then, we extrapolated the emission of the afterglow of GRB 090618 in the (0.57 - 19) keV energy range by considering the ratio between the number of photon counts in both energy ranges. This value corresponds to a conversion factor, which we consider for scaling the intensity of the light curve. We finally amplified, by a term $(1 + z_{101023})/(1 + z_{090618})$, the time interval of emission of GRB 090618, obtaining as a final result the afterglow light curve of GRB 090618 as if it was observed by XRT at redshift 0.9, see Fig. 10.14. It is, most remarkably, a perfect superposition of the light curve emission of both GRBs. This evidence delineates three important aspects:

- the X-ray afterglow of both GRBs clearly confirms a common physical

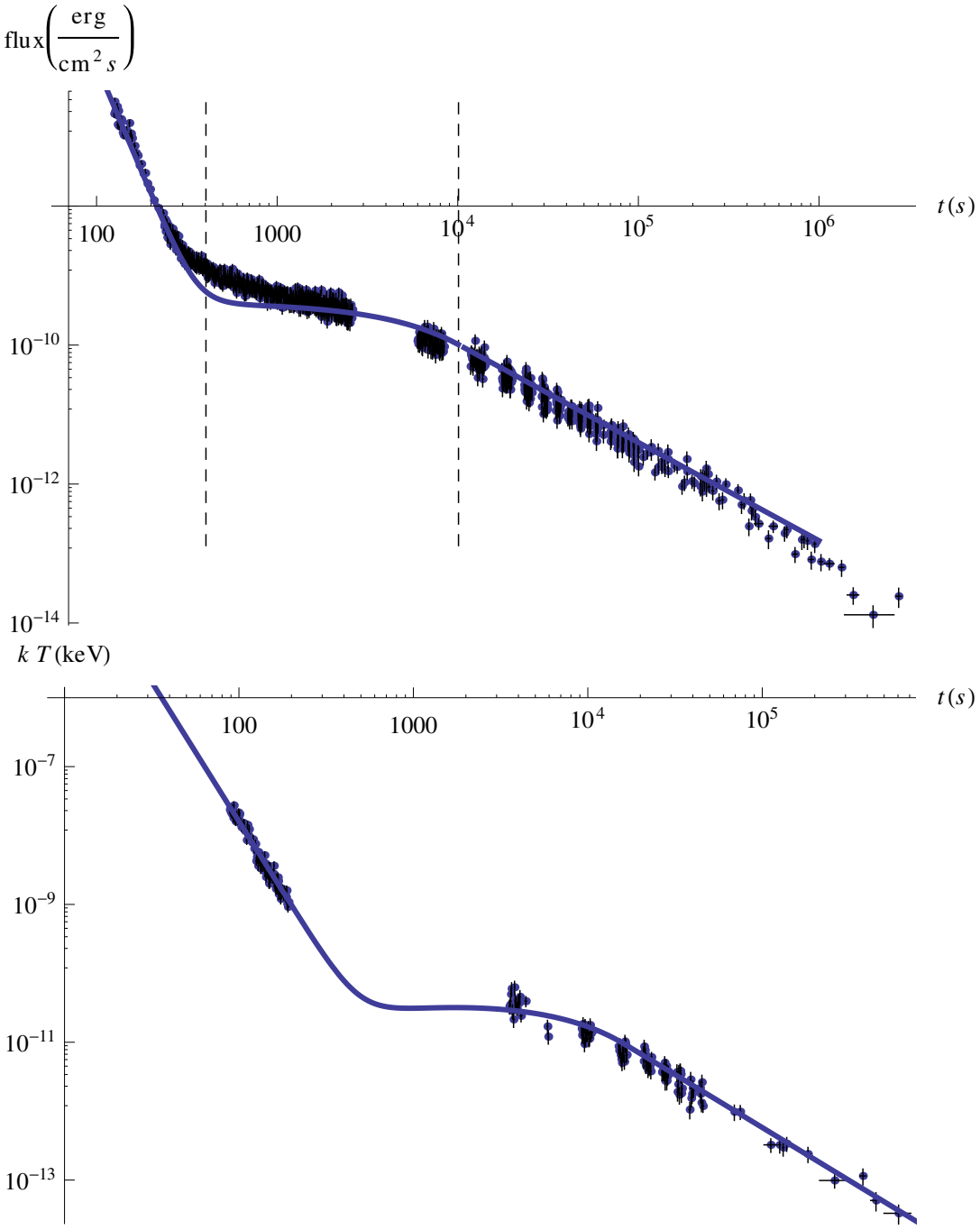

Figure 10.13.: The fit of the X-ray afterglow of GRB 090618 (upper panel) and GRB 101023 (lower panel) with the model of Willingale et al. (2007).

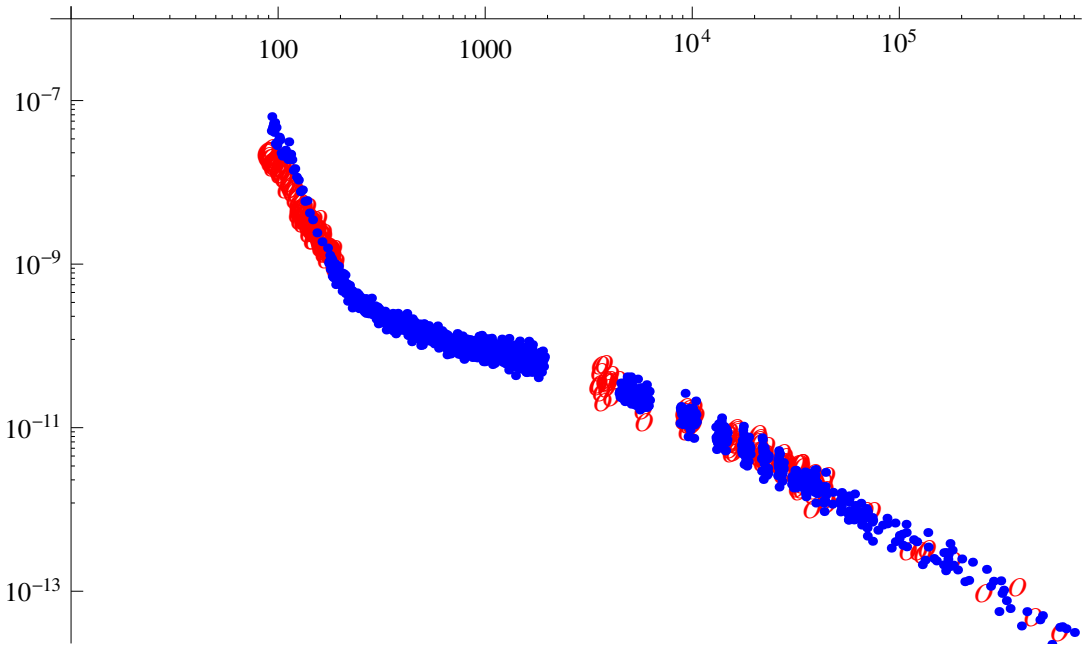

Figure 10.14.: The X-ray afterglow of GRB 090618 (blue data) as if it was observed at redshift $z = 0.9$ (see text). The X-ray afterglow of GRB 101023 is also shown as comparison (red data). Data on GRB 101023 are missing between $\sim$ 200 s and 3550 s. Where data are present, the superposition is striking.

mechanism for these GRBs;

- there is ample convergence and redundancy with different methods of determining a value of redshift $z = 0.9$ for GRB 101023. There has also been the unexpected result pointing to the late afterglow as a possibly independent redshift estimator;
- the redshift of GRB 101023 derived by the superposition of the two afterglow curves is consistent with the value of $z = 0.9$, which we have found before.

This last point led us to do another analysis consisting in the redshift-translation of the X-ray afterglow of GRB 090618 considering different values for the redshift. Following the same procedure and considering five different values for the redshift, $z = (0.4, 0.6, 1.2, 2, 3)$, we see that the X-ray emission of GRB 101023 is compatible with the X-ray afterglow of GRB 090618 as if it bursted between $z = 0.6$ and $z = 1.2$, see Fig. 10.15. Then we conclude that our estimate for the redshift of GRB 101023 of $z = 0.9$ is very reliable.

10.10. Conclusions

GRB 101023 is a very interesting source for the following reasons.

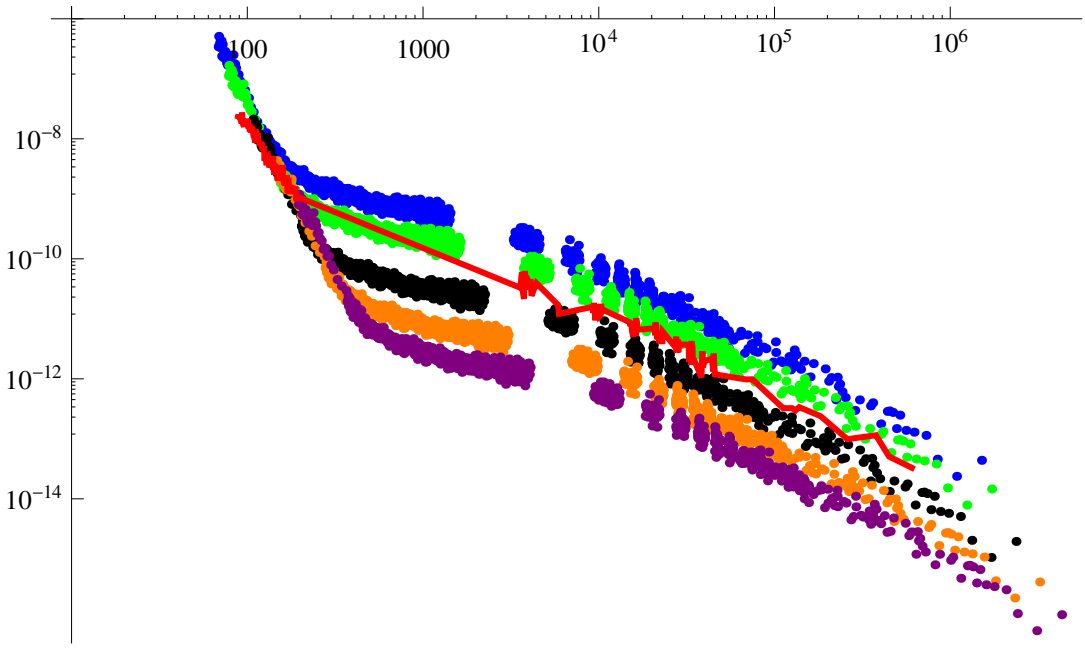

Figure 10.15.: The X-ray afterglow of GRB 090618 as if it was observed at different redshifts $z = (0.4, 0.6, 1.2, 2, 3)$, where each color corresponds to a different redshift. The X-ray afterglow of GRB 101023 is also shown for comparison (red data).

1) We find a striking similarity between GRB 101023 and GRB 090618, as can be seen from the light curves. Following the study of GRB 090618, we divided the emission into two episodes: episode 1, which lasts 45 s, presents a smooth emission without spikes that decays slowly with time. Episode 2, of 44 s of duration, presents a spiky structure, composed of a short and faint peak at the beginning, followed by several intense bumps, after which there is a fast decay with time. Episode 2 has all the characteristics of a canonical long GRB.

2) We performed a time-resolved analysis of episode 1. We fitted a black body plus a power-law model and plotted the evolution of the black body component with time. The observed temperature decreases during the first 20 s following a broken power law: the first with index $\alpha = -0.47 \pm 0.34$ and the second with index $\beta = -1.48 \pm 1.13$, see Sec. 9. This behavior is very similar to GRB 090618.

3) In the absence of a direct measurement of the redshift to the source, we have inferred it from several empirical methods. First, following the work of Grupe et al. (2007b), which considers the hydrogen equivalent column density in the direction of the source, we obtained an upper limit of $z < 3.8$. Then we performed a spectral analysis to episode 2, fitting a Band model. From the peak energy E_{peak} and using the Amati relation under the hypothesis that episode 2 is a canonical long GRB, we constrain the value of the redshift to

be between 0.3 and 1.0. Finally, using the parameters of the Band model and following the work of Atteia (2003), we determine a value of the redshift of $z = 0.9 \pm 0.084(stat.) \pm 0.2(sys.)$. The three methods are consistent, so we assumed for the redshift of this source $z = 0.9$.

4) From the knowledge of the redshift of the source, we have analyzed episode 2 within the fireshell model. We determined a total energy $E_{iso} = 1.79 \times 10^{53}$ erg and a P-GRB energy of 2.51×10^{51} erg, which we used to simulate the light curve and spectrum with the numerical code GRBsim. We find a baryon load $B = 3.8 \times 10^{-3}$ and, at the transparency point, a value of the laboratory radius of 1.34×10^{14} cm, a theoretically predicted temperature of $kT_{th} = 13.26$ keV (after cosmological correction) and a Lorentz gamma factor of $\Gamma = 260.48$, confirming that episode 2 is indeed a canonical GRB.

5) From the knowledge of the redshift, we can also evaluate the flux emitted by episode 1, and from the observed black body temperature, infer the radius of the black body emitter and its variation with time, see Fig. 12. We saw that it increases during the first 20 s of emission, with a velocity $\sim 1.5 \times 10^4$ km/s. In analogy with GRB 090618, we concluded that episode 1 originates in the last phases of gravitational collapse of a stellar core, just prior to the collapse to a black hole. We call this core a "proto-black hole" (Ruffini et al., 2010a). Immediately afterwards, the collapse occurs and the GRB is emitted (episode 2).

6) Finally, we performed the following test. Owing to the similarities between GRB 101023 and GRB 090618 regarding morphology and energetics, we expect them to be created by the same physical mechanism, so we compared the late observed X-ray afterglow of both GRBs as if they were located at the same redshift; i.e, we built the light curve of GRB 090618 (of $z = 0.54$) as if it had redshift $z = 0.9$, extrapolating it to the XRT energy window of GRB 101023. We found a surprising perfect superposition of the light curves for z=0.9, receiving a further confirmation of the correctness of the cosmological redshift determination. The same procedure for the redshift determination will be repeated for sources with a spectroscopical-determined redshift, as a further check of our proposal. This result points to a possible use of the late afterglow as a distance indicator.

We concluded that GRB 101023 and GRB 090618 have striking analogies and are members of a specific new family of GRBs developing out of a single core collapse. It is also appropriate to remark that this new kind of source does not present any GeV emission. The existence of precise scaling laws between these two sources opens a new window on the use of GRBs as distance indicators. We will go on to identify additional sources belonging to this family. This new paradigm is also being applied to sources at very high redshift to see how the absence of a signal under the threshold can affect the theoretical interpretation. We are also considering the possibility that proto-neutron stars in addition to proto-black holes may exist in the case of supernovae or hypernovae. Particularly interesting in this respect is the work of Soder-

berg et al. (2008) showing the X-ray emission prior to SN events, which may relate the observed X-ray emission prior to SN 2008D to episode 1 in GRB 090618 and GRB 101023. In this sense we are revisiting our considerations of GRB 980425 (see e.g. Fraschetti et al., 2004, 2005; Ruffini et al., 2004a, 2007c; Bernardini et al., 2008b), as well as of GRB 030329 (Bernardini et al., 2004, 2005b) and GRB 031203 (Bernardini et al., 2005a; Ruffini et al., 2007c, 2008c).

11. GRB 090227B: the missing link between the genuine short and long GRBs

11.1. Introduction

The understanding of GRBs is among the most fascinating and profound conceptual problems of relativistic astrophysics. Observations at high energies from space missions, such as BATSE (Meegan et al., 1992), Beppo-SAX (Metzger et al., 1997), Swift Burst Alert Telescope (BAT) (Gehrels et al., 2005), AGILE (Tavani et al., 2008), Fermi Gamma-ray Burst Monitor (GBM) (Meegan et al., 2009) and others, have revealed that GRBs emit in a few seconds of the time of the observer almost the energy equivalent to a solar mass. This allows the observability of these sources over the entire visible Universe.

The first systematic analysis on the large sample of GRBs observed by the BATSE instrument on board the Compton Gamma-Ray Observer (CGRO) satellite (Meegan et al., 1992), evidenced a bi-modal temporal distribution in the T_{90} observed duration of prompt emission of GRBs. The "long" and "short" GRBs were defined as being longer or shorter than $T_{90} = 2$ s.

Another fundamental progress was achieved by *Beppo-SAX* with the discovery of a prolonged soft X-ray emission, the "afterglow" (Costa et al., 1997), following the traditional hard X-ray emission observed by BATSE, that was called the "prompt emission".

In recent years, the observations by the *Swift* satellite (Gehrels et al., 2005) evidenced the existence of a possible third class of burst presenting hybrid properties between the short and the long ones: the Norris-Bonnell sources (Norris and Bonnell, 2006). The prompt emission of these sources is characterized by an initial short spike-like emission lasting a few seconds, followed by a prolonged softer extended emission lasting up to some hundred seconds. They were initially indicated in the literature as "short GRBs with an extended emission".

In parallel the theoretical progress in the Fireshell model of GRBs (see Ruffini et al., 2001a,b,c) has led to an alternative explanation of the Norris-Bonnell sources as "disguised short bursts" (Bernardini et al., 2007, 2008a; Caito et al., 2009, 2010; de Barros et al., 2011): canonical long bursts exploding in halos of their host galaxies, with $\langle n_{CBM} \rangle \approx 10^{-3}$ particles/cm^3 (see

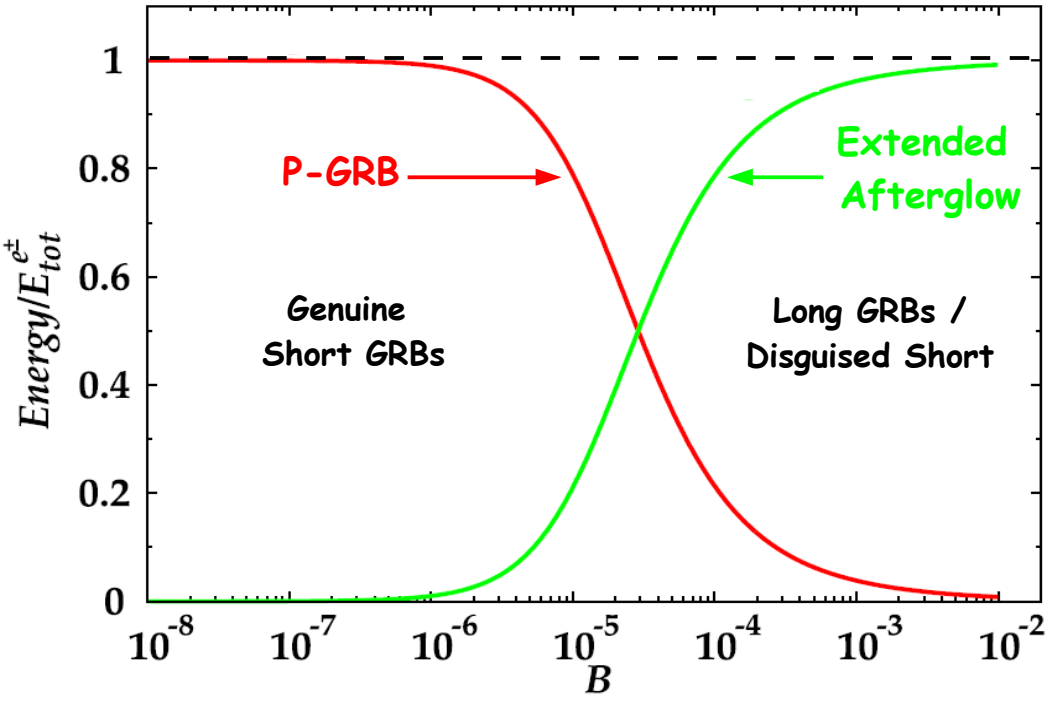

Figure 11.1.: The energy emitted in the extended afterglow (solid green curve) and in the P-GRB (solid red curve) in units of $E^{tot}_{e^+e^-} = 1.77 \times 10^{53}$ erg (dashed horizontal line), as functions of B. The crossing point, corresponding to the condition $E_{P-GRB} \equiv 50\% E^{tot}_{e^+e^-}$, marks the division between the genuine short and disguised short and long GRBs region.

Sec. 11.2.3).

The aim of this article, using the data obtained by the *Fermi*-GBM satellite (Meegan et al., 2009), is to probe the existence of a yet new class of GRBs which we here define "genuine short GRBs", theoretically predicted by the Fireshell model (Ruffini et al., 2001b, 2002). This class of canonical GRBs is characterized by severely small values of the Baryon load, $B \lesssim 10^{-5}$ (see Fig. 11.1). The energy emitted in the P-GRB is predominant and the characteristic duration is expected to be shorter than a fraction of a second (see Sec. 11.2.4).

We have started a search for these genuine short GRBs among the bursts detected by the Fermi GBM instrument, in its first three years of mission. The initial list of short GRBs was reduced requiring that no prominent X-rays and optical afterglows be observed. Among these bursts we have identified GRB 090227B. From its observed light curves, we have performed the spectral analysis of the source, and within the theory, we have inferred its cosmologi-

cal redshift, and all the basic parameters of the burst, as well as the isotropic energy, the Lorentz Γ factor at transparency, and the intrinsic duration.

In Sec. 11.2 we recall the relevant properties of the Fireshell model. In Sec. 11.3 we report the observation of GRB 090227B by the different satellites and the data analysis. In Sec. 11.4 we determine all the parameters characterizing GRB 090227B within the Fireshell scenario, including the redshift. In Sec. 11.5 we provide an estimation of the lower limit on the Lorentz Γ factor from the definition of opacity, finding the agreement with the theoretically determined Lorentz Γ factor. In the conclusions we show that GRB 090227B is the missing link between the genuine short and the long GRBs, with some common characteristics between the two classes. Further analysis of genuine short GRB with a yet small value of B should lead to P-GRB with a yet more pronounced thermal component. We identify the progenitor of GRB 090227B as a symmetric binary system of two neutron stars, each of $\sim 1.34 M_\odot$.

11.2. The Fireshell vs the Fireball model and the issue of the photospheric emission

Soon after the announcement of the discovery of GRBs (Strong et al., 1975), Damour and Ruffini (1975) proposed to explain the energy source of GRBs in terms of the e^+e^- pair plasma created in the process of vacuum polarization during the formation of a Kerr-Newman black hole. They mentioned that the energetics to be expected in this model is approximately 10^{54}–10^{55} erg for a $10 M_\odot$ black hole. At the time nothing was known about the energetics of GRBs, being their distance unknown. They did not pursue further the details of the model pending additional observational evidence.

The idea of the role of an e^+e^- pair plasma as energy source of GRBs was proposed again and independently by Cavallo and Rees (1978). They proposed a sudden release of energy in a process of gravitational collapse leading to a large number of e^+e^- pairs , whose instantaneous annihilation would lead to a vast release of energy pushing on the CBM: the concept of "fireball".

The concept of fireball was further examined by Goodman (1986), who quantified the dynamical effects of the expansion of the fireball computing the effect of the blue-shift due to the bulk Lorentz Γ factor on the observed temperature. Shemi and Piran (1990) were among the first to compute the dynamics of such a fireball in presence of baryonic matter, described by the adimensional parameter $\eta = E_0/M_B c^2$, in which E_0 is the initial total energy of the fireball. They clearly pointed out that for large values of η, photons carry most of the energy of the fireball. In the opposite regime most of E_0 is converted in the kinetic energy of the baryons and only a small fraction is carried away by the photons at transparency. Further works were presented by Meszaros et al. (1993), Piran et al. (1993) and Katz (1994b).

After the discovery by Beppo-SAX (Costa et al., 1997) of the cosmological nature of GRBs (van Paradijs et al., 1997), it became clear that the energetics presented by Damour and Ruffini (1975) was indeed correct and their work represented one of the handful GRB models still viable (Ruffini, 2001). The return to the model led to a further step in the comprehension of GRBs (Ruffini et al., 1999b, 2000) with the detailed analysis of the rate equation which accounts for the gradual annihilation of the pairs, in a relativistic expanding shell, during the entire optically thick acceleration phase of GRBs: the concept of "fireshell".

The main differences between the fireball and the fireshell scenarios are outlined in the paper of Bianco et al. (2006c), while in Aksenov et al. (2007) it was definitely proved that in an optically thick e^+e^- plasma the annihilation of the pairs does not occur instantaneously, as originally assumed by Cavallo and Rees. Instead the optically thick e^+e^- plasma reaches the thermal equilibrium in a very short time scale, $\sim 10^{-12}$ s, and then dynamically expands following the approach in Ruffini et al. (1999b, 2000).

In the meantime the BATSE observations led to a phenomenological classification of GRBs, based on their observed duration, into "long" and "short" GRBs (Klebesadel, 1992; Dezalay et al., 1992; Kouveliotou et al., 1993; Tavani, 1998). Initially this fact was interpreted in terms of different progenitors for these two classes (see Blinnikov et al., 1984; Woosley, 1993; Paczynski, 1998).

In 2001 an interpretation within the Fireshell model was proposed to explain the differences between the short and the long GRBs. This interpretation was based on the Baryon load B (inverse of η). In this picture, both long and short GRBs originate from the same basic machine, the dyadotorus, from an implosion leading to the formation of a Kerr-Newman black hole (Ruffini, 2009b). The long bursts correspond to GRBs with $B \gtrsim 3.0 \times 10^{-4}$ and the short ones to GRBs with $B \lesssim 10^{-5}$ (Fig. 11.1). For $10^{-5} \lesssim B \lesssim 3.0 \times 10^{-4}$ it depends also on the value of the total energy of the pairs $E^{tot}_{e^+e^-}$ (see Fig. 11.2). The short bursts should have in the limit of $B \to 0$ no afterglow. This was followed in 2002 by a further theoretical work evidencing also the relevance of an additional parameter influencing the interpretation above classification: the average density of the environment CBM (Ruffini et al., 2002, 2004b, 2005c). This led to the new concept of "disguised short" GRBs (Bernardini et al., 2007, 2008a; Caito et al., 2009, 2010; de Barros et al., 2011).

Let us briefly go in some more detail in the fireshell model. As we have recalled, the GRBs originate from the process of vacuum polarization occurring in the formation of a black hole, resulting in pair creation (Damour and Ruffini, 1975; Ruffini and Xue, 2008; Ruffini et al., 2010e). The formed e^+e^- plasma, with total energy $E^{tot}_{e^+e^-}$, reaches the thermal equilibrium almost instantaneously (Aksenov et al., 2007). The annihilation of these pairs occurs gradually and it is confined in an expanding shell, called *fireshell*, which self-accelerates up to ultra relativistic velocities (Ruffini et al., 1999b), and engulfs the baryonic matter (of mass M_B) left over in the process of col-

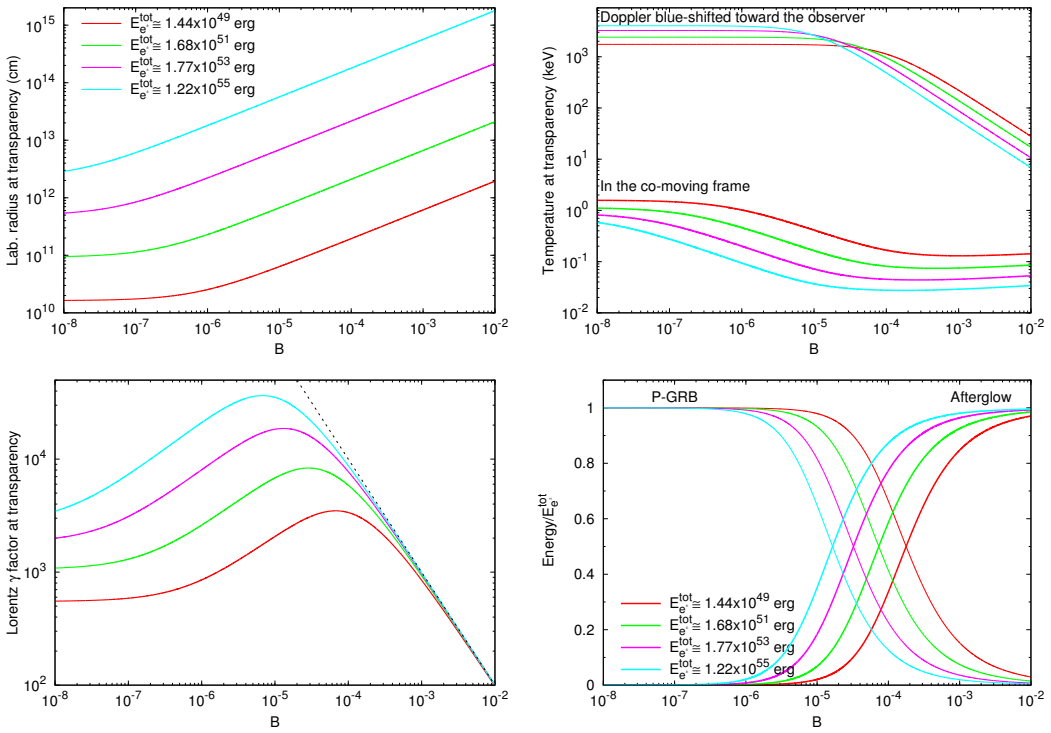

Figure 11.2.: The main quantities of the Fireshell model at the transparency for selected values of $E^{tot}_{e^+e^-}$: the radius in the laboratory frame, the co-moving frame and blue-shifted toward the observer temperatures of the plasma, the Lorentz Γ factor, and the fraction of energy radiated in the P-GRB and in the extended afterglow as functions of B. In these simulations a sudden transition between the optically thick adiabatic phase and the fully radiative condition at the transparency has been assumed.

lapse, which thermalizes with the pairs due to the large optical depth (Ruffini et al., 2000). The Baryon load is measured by the dimensionless parameter $B = M_B c^2 / E^{tot}_{e^+e^-}$. The fireshell continues to self-accelerate until it reaches the transparency condition and a first flash of radiation, the P-GRB, is emitted (Ruffini et al., 2001b). The radius at which the transparency occurs and the theoretical temperature, the Lorentz factor as well as the amount of the energy emitted in the P-GRB are functions of $E^{tot}_{e^+e^-}$ and B (see Fig. 11.2).

In recent years a systematic analysis of the possible presence of a thermal component in the early phases of the prompt emission of GRBs has been performed using the earlier data from BATSE all the way to the latest ones from Fermi (Ryde, 2004; Ryde and Pe'er, 2009; Guiriec et al., 2011). The presence of episodes with a significant thermal component lasting typically from 20 to 50 s has been evidenced. In some specific cases the thermal component has been shown to vary with time following a broken power-law (Ryde, 2004; Ryde and Pe'er, 2009). This problematic has led to the study of the

so-called photospheric emission (Rees and Mészáros, 2005; Pe'er et al., 2005, 2006; Lazzati and Begelman, 2010). It has been pointed out (Ruffini et al., 2011a; Izzo et al., 2012b,e; Penacchioni et al., 2012) that a marked difference exists between these prolonged emissions occurring at $\Gamma \sim 1$ and the specific ones of the e^+e^- recombination occurring at ultra relativistic regimes, $\Gamma > 10^2$, and lasting at most a few seconds. In the specific cases of GRB 970828 (Izzo et al., 2012b), GRB 090618 (Izzo et al., 2012e) and GRB 101023 (Penacchioni et al., 2012) the existence of these two components has been evidenced. The first component, at $\Gamma \sim 1$, has been associated to the Proto Black Hole (PBH), while the one at $\Gamma \geq 10^2$ has been identified with the P-GRB emission ($\Gamma = 495$, for GRB 090618, $\Gamma = 143$, for GRB 970828 , and $\Gamma = 261$ for GRB 101023).

11.2.1. The extended afterglow emission

After transparency, the residual expanding plasma of leptons and baryons interacts with the CBM and, due to these collisions, starts to slow down giving rise to a multi-wavelength emission: the extended afterglow. Assuming a fully-radiative condition, the structures observed in the extended afterglow of a GRB are described by two quantities associated with the environment: the CBM density profile n_{CBM}, which determines the temporal behavior of the light curve, and the fireshell surface filling factor $\mathcal{R} = A_{eff}/A_{vis}$, in which A_{eff} is the effective emitting area of the fireshell and A_{vis} its total visible area (Ruffini et al., 2002, 2005a). This second parameter takes into account the inhomogeneities in the CBM and its filamentary structure (Ruffini et al., 2004b). The emission process of the collision between the baryons and the CBM has been assumed in the comoving frame of the shell as a modified black body spectrum (Patricelli et al., 2012), given by

$$\frac{dN_\gamma}{dVd\epsilon} = \frac{8\pi}{h^3c^3}\left(\frac{\epsilon}{kT}\right)^\alpha \frac{\epsilon^2}{\exp(\epsilon/kT)-1}\,, \tag{11.2.1}$$

where α is a phenomenological parameter. It is appropriate to clarify that this emission is different from the photospheric one due to the e^+e^- plasma annihilation, since it originates from the interactions between the baryons and the CBM in an optically thin regime.

The observed GRB non-thermal spectral shape is then produced by the convolution of a very large number of modified thermal spectra with different temperatures and different Lorentz and Doppler factors. This convolution is performed over the surfaces of constant arrival time for the photons at the detector (EQuiTemporal Surfaces, EQTS, Bianco and Ruffini, 2005a,b) encompassing the total observation time. The observed hard-to-soft spectral variation comes out naturally from the decrease with time of the comoving temperature and of the bulk Lorentz Γ factor. This effect is amplified by the

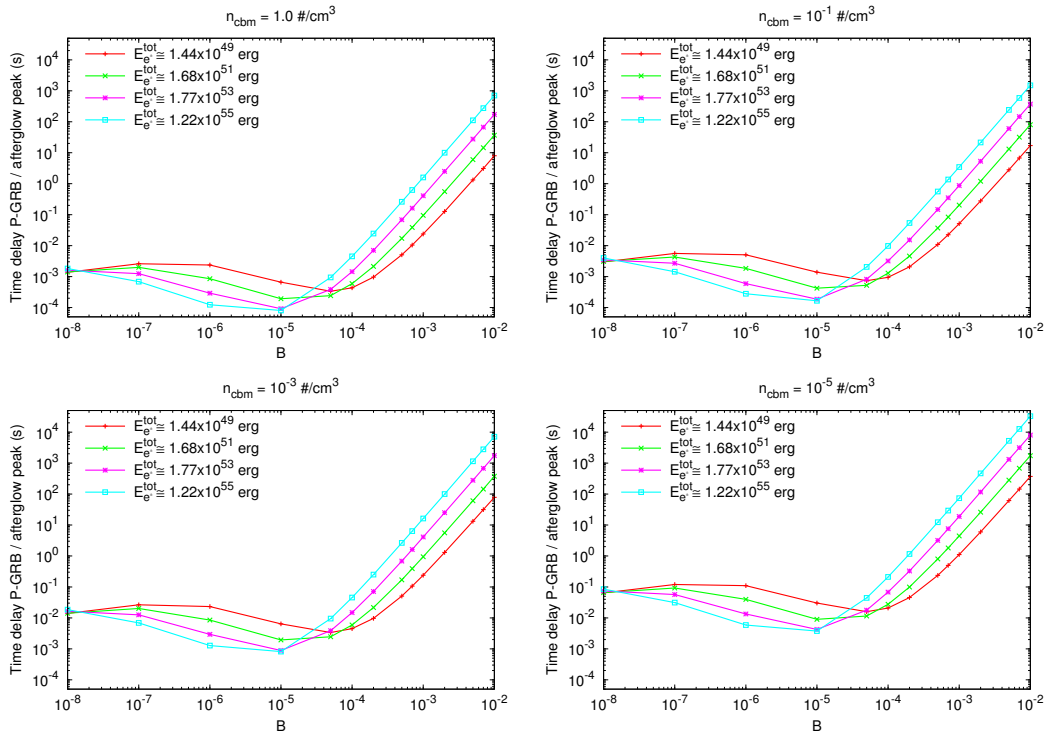

Figure 11.3.: Plots of the arrival time separation Δt_a between the P-GRB and the peak of the extended afterglow as function of B for four different values of $E^{tot}_{e^+e^-}$, measured in the source cosmological rest frame. This computation has been performed assuming four constant CBM density $n_{CBM} = 1.0$, 1.0×10^{-1}, 1.0×10^{-3}, 1.0×10^{-5} particles/cm^3.

curvature effect originated by the EQTS, which produce the observed time lag in the majority of the GRBs.

Assuming the spherical symmetry of the system, the isotropic energy emitted in the burst, E_{iso}, is equal to the energy of the e^+e^- plasma, $E^{tot}_{e^+e^-}$, and the GRB bolometric light curve is composed of the P-GRB and the extended afterglow. Their relative energetics and observed time separation are functions of the energy $E^{tot}_{e^+e^-}$, of the Baryon load B, and of the CBM density distribution n_{CBM} (see Fig. 11.3). In particular, for B decreasing, the extended afterglow light curve "squeezes" itself on the P-GRB and the P-GRB peak luminosity increases (see Fig. 11.4).

To reproduce the shape of the light curve we have to determine for each CBM clump the filling factor $\mathcal{R}$, which determines the effective temperature in the comoving frame and the corresponding peak energy of the spectrum, and of the CBM density n_{CBM}, which determines the temporal behavior of the light curve. It is clear that, since the EQTS encompass emission processes occurring at different comoving times weighted by their Lorentz and Doppler factors, the fit of a single spike is not only a function of the properties of the

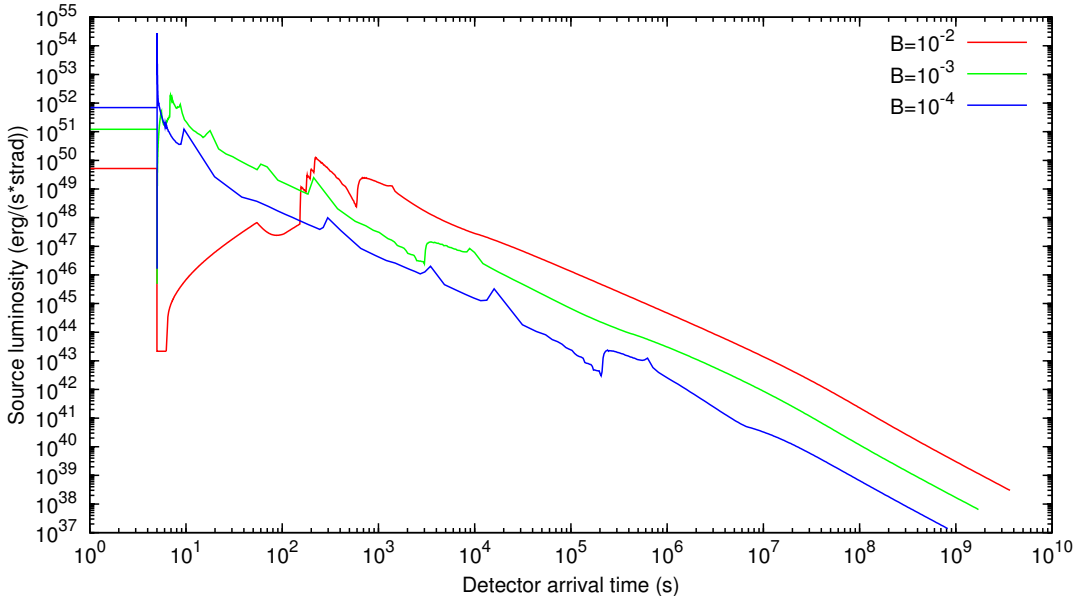

Figure 11.4.: The dependence of the shape of the light curve on B. The computations have been performed assuming $E^{tot}_{e^+e^-} = 4.83 \times 10^{53}$ ergs, $\langle n_{CBM} \rangle = 1.0$ particles/cm^3, three different values of the Baryon load $B = 10^{-2}, 10^{-3}, 10^{-4}$ and the P-GRBs duration fixed, i.e. 5 s. For B decreasing, the extended afterglow light curve squeezes itself on the P-GRB and the peak becomes sharper and higher.

specific CBM clump but of the entire previous history of the source. Due to the non-linearity of the system and to the EQTS, any change in the simulation produces observable effects up to a much later time. This brings to an extremely complex procedure by trial and error in the data simulation to reach the uniqueness.

It is appropriate to recall that in the Fireshell model the two phases, the one preceding the e^+e^- transparency and the following one, as well as their corresponding energetics, are directly linked by the Fireshell equations of motion (see Fig. 11.2). Consequently, their agreement with the data cannot be independently adjusted and optimized.

11.2.2. The canonical long GRBs

According to this theory, the canonical long GRBs are characterized by a Baryon load varying in the range $3.0 \times 10^{-4} \lesssim B \leq 10^{-2}$ and they occur in a typical galactic CBM with an average density $\langle n_{CBM} \rangle \approx 1$ particle/cm^3. As a result the extended afterglow is predominant with respect to the P-GRB (see Fig. 11.1).

11.2.3. The disguised short GRBs

After the observations by Swift of GRB 050509B (Gehrels et al., 2005), which was declared in the literature as the first short GRB with an extended emission ever observed, it has become clear that all such sources are actually disguised short GRBs (de Barros et al., 2011). It is conceivable and probable that also a large fraction of the declared short duration GRBs in the BATSE catalog, observed before the discovery of the afterglow, are members of this class. In the case of the disguised short GRBs the Baryon load varies in the same range of the long bursts, while the CBM density is of the order of 10^{-3} particles/cm^3. As a consequence, the extended afterglow results in a "deflated" emission that can be exceeded in peak luminosity by the P-GRB (Bernardini et al., 2007, 2008a; Caito et al., 2009, 2010; de Barros et al., 2011). Indeed the integrated emission in the extended afterglow is much larger than the one of the P-GRB (see Fig. 11.1), as expected for long GRBs. With these understandings long and disguised short GRBs are interpreted in terms of long GRBs exploding, respectively, in a typical galactic density or in a galactic halo density.

These sources have given the first evidence of GRBs originating from binary mergers, formed by two neutron stars and/or white dwarfs in all possible combinations, that have spiraled out from their host galaxies into the halos (Bernardini et al., 2007, 2008a; Caito et al., 2009, 2010; de Barros et al., 2011). This interpretation has been supported by direct optical observations of GRBs located in the outskirt of the host galaxies (Sahu et al., 1997; van

Paradijs et al., 1997; Bloom et al., 2006b; Troja et al., 2008; Fong et al., 2010; Berger, 2011b; Kopač et al., 2012).

11.2.4. The class of genuine short GRBs

The canonical genuine short GRBs occur in the limit of very low Baryon load, e.g. $B \lesssim 10^{-5}$ with the P-GRB predominant with respect to the extended afterglow. For such small values of B the afterglow peak emission shrinks over the P-GRB and its flux is lower than the P-GRB one (see Fig. 11.4).

The thermalization of photon-pairs plasma is reached in a very short timescale at the beginning of the expansion phase and the thermal equilibrium is implemented during the entire phase of the expansion (Aksenov et al., 2007), therefore the spectrum of these genuine short GRBs is expected to be characterized by a significant thermal-like emission. Since the baryon load is small but not zero, in addition to the predominant role of the P-GRB, a non-thermal component originating from the extended afterglow is expected.

11.3. Observations and Data Analysis of GRB 090227B

At 18:31:01.41 UT on 27^{th} February 2009, the Fermi GBM detector (Kono et al., 2009) triggered and located the short and bright burst, GRB 090227B (trigger 257452263/090227772). The on-ground calculated location, using the GBM trigger data, was (RA, Dec)(J2000)=($11^h48^m36^s, 32^o10'12''$), with an uncertainty of 1.77^o (statistical only). The angle from the Fermi LAT boresight was 72^o. The burst was also located by IPN (Golenetskii et al., 2009d) and detected by Konus-Wind (Golenetskii et al., 2009b), showing a single pulse with duration ~ 0.2 s (20 keV – 10 MeV). No X rays and optical observations were reported on the GCN Circular Archive, thus the redshift of the source is unknown.

To obtain the Fermi GBM light-curves and the spectrum in the energy range 8 keV – 40 MeV, we made use of the `RMFIT` program. For the spectral analysis, we have downloaded from the gsfc website [1] the `TTE` (Time-Tagged Events) files, suitable for short or highly structured events. We used the light curves corresponding to the NaI-n2 (8 – 900 keV) and the BGO-b0 (250 keV – 40 MeV) detectors. The 64 ms binned GBM light curves show one very bright spike with a short duration of 0.384 s, in the energy range 8 keV – 40 MeV, and a faint tail lasting up to 0.9 s after the trigtime T_0 in the energy range 10 keV – 1 MeV. After the subtraction of the background, we have proceeded with the time-integrated and time-resolved spectral analyses.

[1] ftp://legacy.gsfc.nasa.gov/fermi/data/gbm/bursts

11.3.1. Time-integrated spectral analysis

We have performed a time-integrated spectral analysis in the time interval from $T_0 - 0.064$ s to $T_0 + 0.896$ s, which corresponds to the T_{90} duration of the burst. We have fitted the spectrum in this time interval considering the following models: Comptonization (Compt) plus power-law (PL) and Band (Band et al., 1993) plus PL, as outlined e.g. in Guiriec et al. (2010), as well as a combination of Black Body (BB) and Band. We have evaluated the significance values from the differences in the C-STAT, considered as χ^2 variables for the change in the number of the model parameters. In Tab. 11.2 we have compared the model with different number of degrees of freedom (DOF). Within the T_{90} time interval, the BB+Band model improves the fit with respect to Compt+PL model at a significance level of 5%. The comparison between Band+PL and Compt+PL models is outside of such a confidence level (about 8%). The direct comparison between BB+Band and Band+PL models, which have the same number of dof (see Tab. 11.1), provides almost the same C-STAT values for BB+Band and Band+PL models (ΔC-STAT ≈ 0.89). This means that all the three models are viable. The results of the analysis are shown in Tab. 11.1 and Fig. 11.5. For BB+Band model, the ratio between the fluxes of the thermal component and the non-thermal one (NT) is $F_{BB}/F_{NT} \approx 0.22$. The BB component is important in the determination of the peak of the νF_ν spectrum and has an observed temperature $kT = (397 \pm 70)$ keV.

We have then focused our attention on the spike component, namely the time interval from $T_0 - 0.064$ s to $T_0 + 0.192$, which we indicate in the following as the T_{spike}. We have repeated the time-integrated analysis considering the same spectral models of the previous interval (see Tab. 11.1 and Fig. 11.6). As reported in Tab. 11.2, within the T_{spike} time interval, both BB+Band and Band+PL models marginally improve the fits of the data with respect to Compt+PL model within a confidence level of 5%. Again, the C-STAT values of BB+Band and Band+PL models are almost the same (ΔC-STAT ≈ 0.15) and they are statically equivalent in the T_{spike}. For the BB+Band model, the observed temperature of the thermal component is $kT = (515 \pm 28)$ keV and the flux ratio between the BB component and the NT one increases up to $F_{BB}/F_{NT} \approx 0.69$.

We have performed a further analysis in the time interval from $T_0 + 0.192$ s to $T_0 + 0.896$ s, which we indicate as T_{tail}, by considering BB+PL, Compt and PL models (see Fig. 11.7 and Tab. 11.1). The comparison in Tab. 11.2 shows that the best fit is the Compt model. The BB+PL model is the less preferred. From the data analysis in the T_{tail} time interval, we can conclude that a thermal component is ruled out.

In view of the above, we have focused our attention on the fit of the data of the BB+Band model within the Fireshell scenario, been equally probable from a mere statistical point of view with the other two choices, namely Band+PL and Compt+PL. According to the Fireshell scenario (see Sec. 11.2.1), the emis-

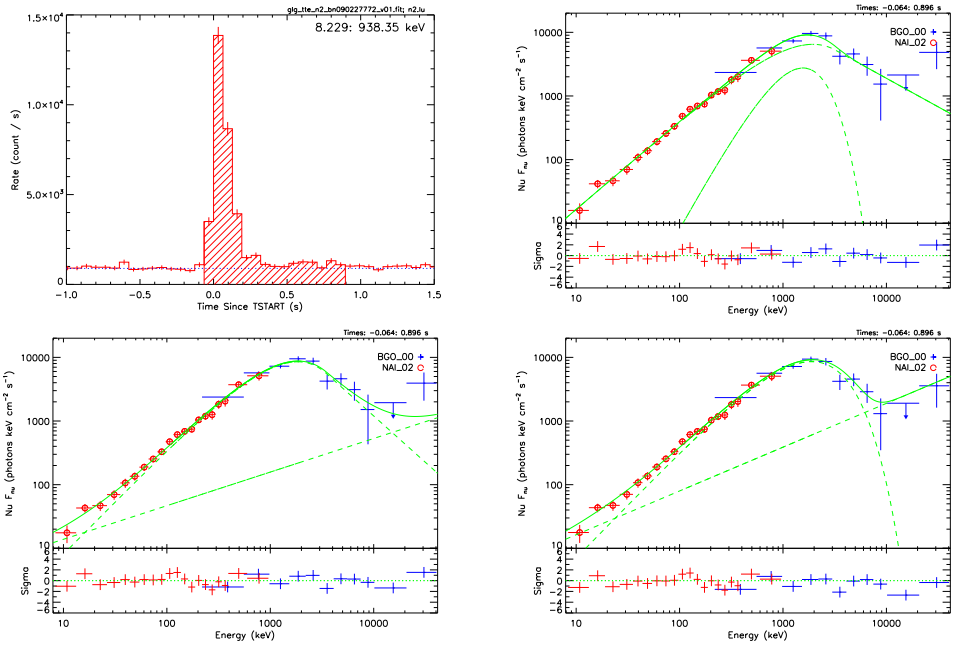

Figure 11.5.: The 64 ms time-binned NaI-n2 light curve (top left panel) and the NaI-n2+BGO-b0 νF_ν spectra (top right BB+Band, bottom left Band+PL, bottom right Compt+PL) of GRB 090227B in the T_{90} time interval.

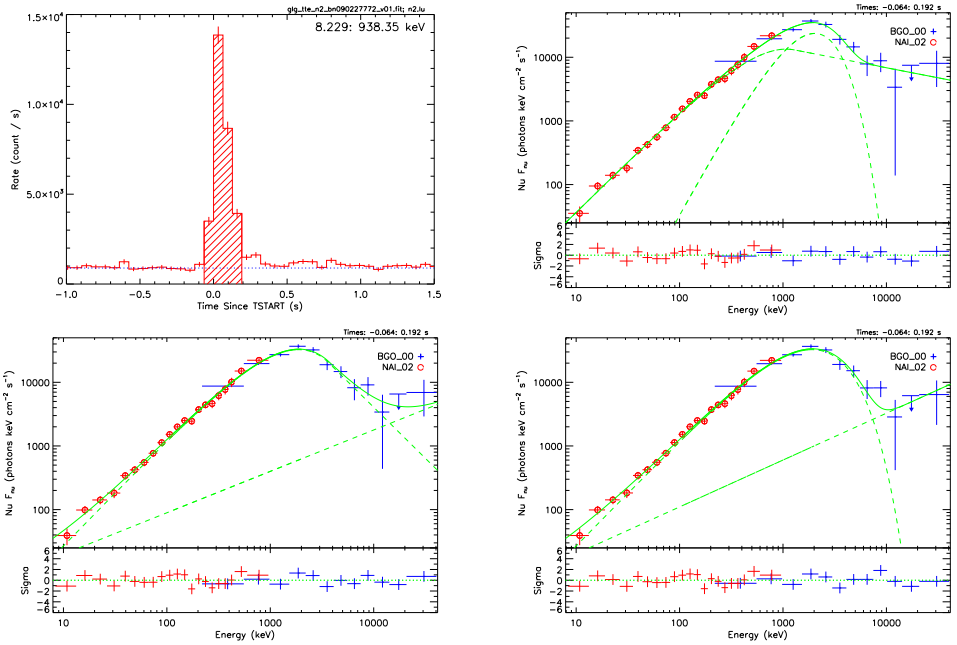

Figure 11.6.: The same considerations as in Fig. 11.5, in the T_{spike} time interval.

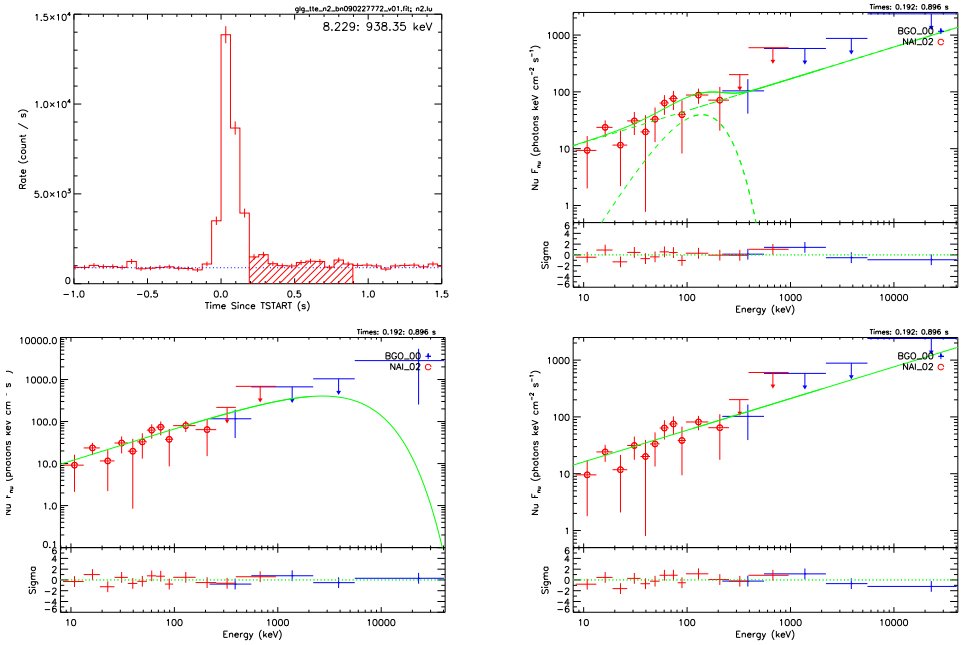

Figure 11.7.: The 64 ms time-binned NaI-n2 light curve (top left panel) and the NaI-n2+BGO-b0 νF_ν spectra (top right BB+PL, bottom left Compt, bottom right PL) of GRB 090227B in the T_{tail} time interval.

sion within the T_{spike} time interval is related to the P-GRB and is expected to be thermal. In addition the transition between the transparency emission of the P-GRB and the extended afterglow is not sharp. The time separation between the P-GRB and the peak of the extended afterglow depends on the energy of the e^+e^- plasma $E^{tot}_{e^+e^-}$, the Baryon load B and the CBM density n_{CBM} (see Fig. 11.4). As shown in Figs. 11.3 and 11.4, for decreasing values of B an early onset of the extended afterglow in the P-GRB spectrum occurs and thus, a NT component in the T_{spike} is expected. As a further check, the theory of the Fireshell model indeed predicts in the early part of the prompt emission of GRBs a thermal component due to the transparency of the e^+e^- plasma (see Sec. 11.2), while in the extended afterglow no thermal component is expected (see Sec. 11.2.1), as observed in the T_{tail} time interval.

Our theoretical interpretation is consistent with the observational data and the statistical analysis. From an astrophysical point of view the BB+Band model is preferred over the other two models, statistically equivalent in view of the above theoretical considerations.

11.3.2. Time-resolved spectral analysis

We have performed a time-resolved spectral analysis on shorter selected time intervals of 32 ms in order to correctly identify the P-GRB, namely finding out in which time interval the thermal component exceeds or at least has a com-

Int.	Model	kT [keV]	E_p [keV]	α	β	γ	F_{tot} [erg/cm^{2}s]	F_{BB}/F_{tot}	C-STAT/dof
T_{90}	BB+Band	397 ± 70	1942 ± 249	-0.60 ± 0.05	-2.90 ± 0.31		$(3.35 \pm 0.12) \times 10^{-5}$	0.22	286.84/240
	Band+PL		1835 ± 84	-0.35 ± 0.05	-3.46 ± 0.46	-1.47 ± 0.13	$(3.39 \pm 0.13) \times 10^{-5}$		287.73/240
	Compt+PL		1877 ± 72	-0.36 ± 0.05		-1.36 ± 0.05	$(3.44 \pm 0.13) \times 10^{-5}$		290.71/241
T_{spike}	BB+Band	515 ± 28	1072 ± 210	-0.40 ± 0.05	-2.32 ± 0.17		$(1.26 \pm 0.04) \times 10^{-4}$	0.69	266.17/240
	Band+PL		1879 ± 67	-0.33 ± 0.05	-3.61 ± 0.38	-1.35 ± 0.10	$(1.25 \pm 0.04) \times 10^{-4}$		266.32/240
	Compt+PL		1912 ± 58	-0.33 ± 0.05		-1.26 ± 0.07	$(1.26 \pm 0.04) \times 10^{-4}$		270.19/241
T_{tail}	BB+PL	36 ± 13				-1.44 ± 0.07	$(3.9 \pm 1.2) \times 10^{-6}$	*unc.*	293.85/242
	Compt		2703 ± 1760	-1.23 ± 0.09			$(2.03 \pm 0.79) \times 10^{-6}$		291.19/243
	PL					-1.44 ± 0.05	$(4.7 \pm 1.1) \times 10^{-6}$		296.07/244

Table 11.1.: The time-integrated spectral analyses performed using BB+Band, Band+PL and Compt+PL models in the T_{90} and T_{spike} time intervals, and BB+PL, Compt and PL in the T_{tail} time interval, in the energy range 8 keV – 40 MeV.

Int.	Models	ΔC-STAT	Significance
T_{90}	BB+Band over Compt+PL	3.87	0.049
	Band+PL over Compt+PL	2.98	0.084
T_{spike}	BB+Band over Compt+PL	4.02	0.045
	Band+PL over Compt+PL	3.87	0.049
T_{tail}	BB+PL over PL	2.22	0.33
	BB+PL over Compt	2.66	0.10
	Compt over PL	4.88	0.027

Table 11.2.: The C-STAT improvement with the addition of extra parameters in the T_{90}, T_{spike} and T_{tail} time intervals (see Tab. 11.1).

parable flux with respect to the NT one due to the onset of the extended afterglow. In this way we can single out the contribution of the NT component in the spectrum of the P-GRB.

A time-resolved spectral analysis has been performed by Guiriec et al. (2010) by selecting time intervals from 2 ms to 94 ms. In view of the low statistical content in some small time bins, the authors fitted the data by using simple Band functions. We have performed a time-resolved analysis on time intervals of 32 ms (see Fig. 11.8) in order to optimize the statistical content in each time bin and to test the presence of BB plus an extra NT component. The results are summarized in Tab. 11.3, where we have compared the BB+NT with the single Band function.

In the analysis we have preferred the χ^2 statistic because of the high photon fluxes in the first five time intervals, $\gtrsim 100$ photons/(cm^{2}s).

Within the first time-resolved interval the BB+PL model has a thermal flux (11.2 ± 3.4) **times bigger than the PL flux; the fit with BB+Band provides** $F_{BB} = (0.50 \pm 0.26) F_{NT}$**, where the NT component is in this case the Band model.** In the second and fourth intervals, the BB+Band model provides an improvement at a significance level of 5% in the fitting procedure with respect to the simple Band model (see Tab. 11.3, last column). In the third time interval as well as in the remaining time intervals up to $T_0 + 0.192$ s the Band spectral models provide better fits with respect to the BB+NT ones.

This is exactly what we expect from our theoretical understanding: from $T_0 - 0.032$ s to $T_0 + 0.096$ s we have found the edge of the P-GRB emission, in which the thermal components have fluxes higher or comparable to the NT

Interval [s]	Models	kT [keV]	E_p [keV]	α	β	$F_{tot} \times 10^{-5}$ [erg/cm^{2}s]	χ^2/DOF	F_{BB}/F_{NT}	BB+Band over Band
	BB+PL	274 ± 17		-1.75 ± 0.29		7.03 ± 0.76	$196.85/241 = 0.82$	11.2 ± 3.4	
$-0.032 \rightarrow 0.000$	**BB+Band**	280 ± 66	1703 ± 407	-0.50 ± 0.25	unc	8.22 ± 0.99	$180.23/239 = 0.75$	0.50 ± 0.26	0.051
	Band		1493 ± 155	-0.21 ± 0.11	unc	8.13 ± 0.88	$186.17/241 = 0.77$		
	BB+PL	377 ± 12		-1.20 ± 0.03		62.2 ± 3.6	$308.97/241 = 1.28$	1.04 ± 0.11	
$0.000 \rightarrow 0.032$	**BB+Band**	571 ± 44	858 ± 214	0.15 ± 0.17	-2.45 ± 0.26	46.2 ± 2.3	$222.54/239 = 0.93$	1.41 ± 0.38	0.041
	Band		2140 ± 102	-0.10 ± 0.06	-5.3 ± 1.9	47.2 ± 2.1	$228.95/241 = 0.95$		
	BB+PL	437 ± 20		-1.21 ± 0.03		43.4 ± 3.1	$247.41/241 = 1.03$	1.00 ± 0.24	
$0.032 \rightarrow 0.064$	**BB+Band**	572 ± 65	1713 ± 1045	-0.42 ± 0.14	-1.77 ± 0.26	35.0 ± 2.6	$222.18/239 = 0.93$	0.55 ± 0.35	0.081
	Band		2439 ± 257	-0.29 ± 0.07	-2.64 ± 0.22	36.4 ± 2.6	$227.21/241 = 0.94$		
	BB+PL	329 ± 21		-1.41 ± 0.04		17.8 ± 1.9	$241.91/241 = 1.00$	0.92 ± 0.27	
$0.064 \rightarrow 0.096$	**BB+Band**	373 ± 34	435 ± 297	-0.48 ± 0.09	-1.70 ± 0.14	17.5 ± 1.9	$221.50/239 = 0.93$	0.85 ± 0.28	0.020
	Band		1586 ± 281	-0.48 ± 0.29	-2.23 ± 0.19	17.5 ± 2.0	$229.31/241 = 0.95$		
	BB+PL	124.9 ± 8.4		-1.27 ± 0.04		18.9 ± 0.23	$258.17/241 = 1.07$	0.21 ± 0.08	
$0.096 \rightarrow 0.128$	**BB+Band**	144 ± 84	454 ± 162	0.11 ± 0.30	-1.80 ± 0.17	16.1 ± 2.1	$226.61/239 = 0.95$	unc	0.061
	Band		622 ± 112	-0.11 ± 0.17	-1.99 ± 0.11	13.8 ± 1.8	$232.21/241 = 0.96$		
	BB+PL	35.5 ± 4.8		-1.52 ± 0.08		2.87 ± 0.95	$202.44/241 = 0.84$	0.13 ± 0.06	
$0.128 \rightarrow 0.160$	**BB+Band**	39.6 ± 6.8	unc	-1.2 ± 1.4	-1.54 ± 0.26	2.8 ± 1.2	$198.00/239 = 0.83$	0.14 ± 0.08	0.067
	Band		193 ± 124	-0.75 ± 0.40	-1.84 ± 0.18	2.55 ± 0.91	$203.40/241 = 0.84$		
	BB+PL	30.2 ± 7.7		-1.19 ± 0.10		5.7 ± 1.4	$237.82/241 = 0.99$	0.020 ± 0.019	
$0.160 \rightarrow 0.192$	**BB+Band**	22 ± 10	unc	unc	-1.25 ± 0.08	unc	$203.37/239 = 0.85$	unc	0.0045
	Band		unc	-0.7 ± 1.2	-1.40 ± 0.08	6.0 ± 1.4	$214.19/241 = 0.89$		

Table 11.3.: Time-resolved analysis of GRB 090227B performed using BB+NT (NT=Band,PL) and a single Band model. In the first column we have indicated the time bin; in the following five columns we have indicated the spectral models and their parameters. In the next three columns we have listed, respectively, the total flux, the χ^2, and the ratio between the thermal (where considered) and the non-thermal fluxes. The last column reports the significance in the addition of the the BB with respect the sole Band model.

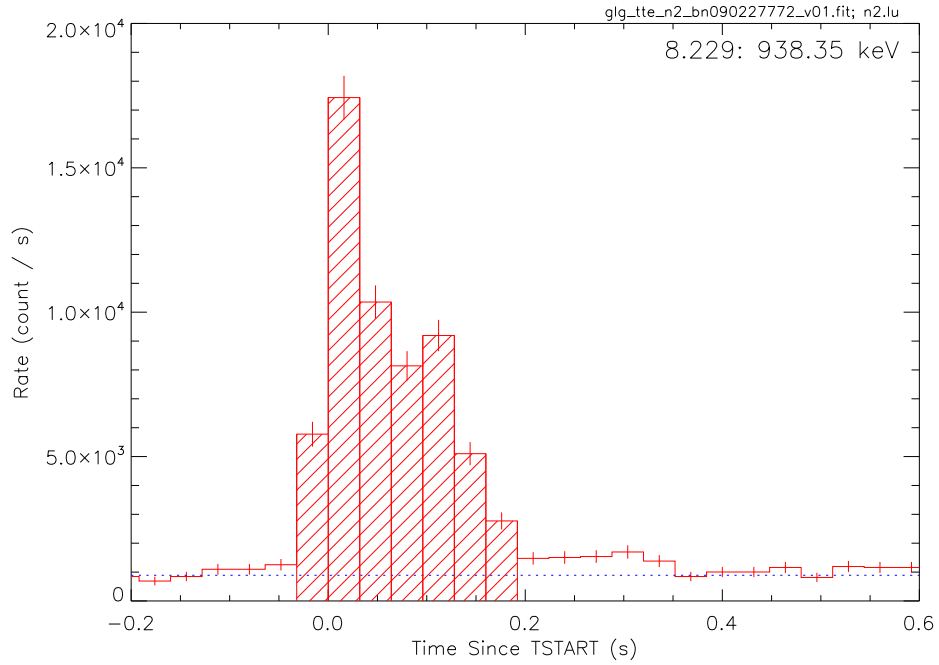

Figure 11.8.: The 32 ms time-binned NaI-n2 light curve of GRB 090227B in the time interval from $T_0 - 0.032$ s to $T_0 + 0.192$ s; each time bin corresponds to the time-resolved interval considered in the Sec. 11.3.2.

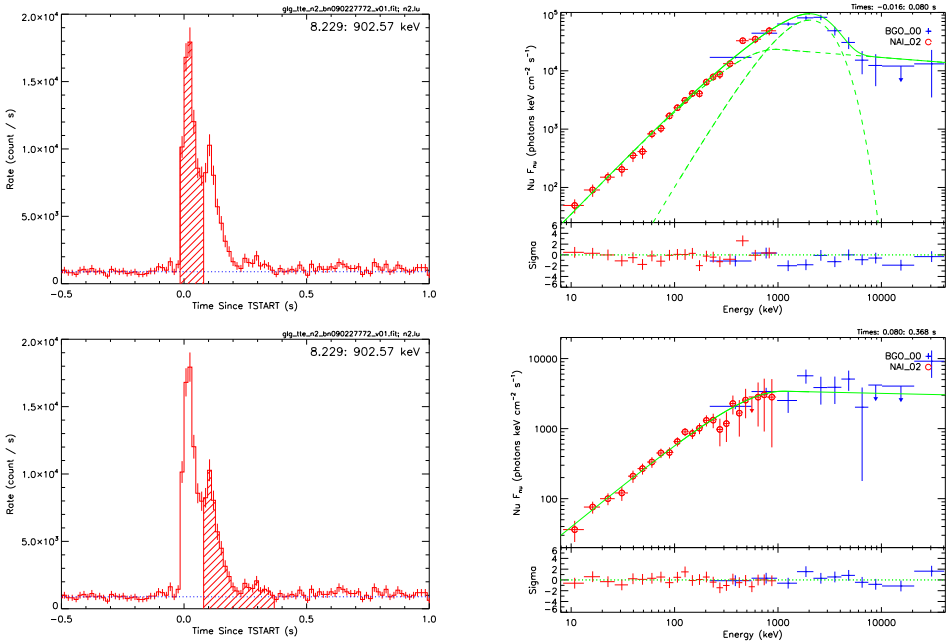

Figure 11.9.: The 16 ms time-binned NaI-n2 light curves of the P-GRB (left upper panel) and the extended afterglow (left lower panel) and their NaI-n2+BGO-b0 νF_ν spectra (on the right, the upper panel for the P-GRB and the lower one for the extended afterglow). The fit of the P-GRB is composed of a BB superimposed by a Band spectrum; the extended afterglow is well fitted by a simple Band function.

ones. The third interval corresponds to the peak emission of the extended afterglow (see Fig. 11.11). The contribution of the extended afterglow in the remaining time intervals increases, while the thermal flux noticeably decreases (see Tab. 11.3).

We have then explored the possibility of a further rebinning of the time interval T_{spike}, taking advantage of the large statistical content of each time bin. We have plotted the NaI-n2 light curve of GRB 090227B using time bins of 16 ms (see Fig. 11.9, left panels). The re-binned light curves show two spike-like substructures. The duration of the first spike is 96 ms and it is clearly distinct from the second spike. In this time range the observed BB temperature is $kT = (517 \pm 28)$ keV (see Tab. 11.4) and the ratio between the fluxes of the thermal component and the non-thermal one is $F_{BB}/F_{NT} \approx 1.1$. Consequently, we have interpreted the first spike as the P-GRB and the second spike as part of the extended afterglow. Their spectra are shown in Fig. 11.9, right panels, and the results of the spectral analysis are summarized in Tab. 11.4.

	Model	kT [keV]	α	β	E_{peak} [keV]	F_{tot} [erg/(cm^{2}s)]	F_{BB} [erg/(cm^{2}s)]	C-STAT/DOF
P-GRB	**Band+BB**	517 ± 28	-0.80 ± 0.05	-2.14 ± 0.17	952 ± 251	$(3.13 \pm 0.13) \times 10^{-4}$	$(1.61 \pm 0.47) \times 10^{-4}$	263.51/239
Ext. Aft.	**Band**		-0.79 ± 0.06	-2.01 ± 0.10	1048 ± 178	$(2.66 \pm 0.26) \times 10^{-5}$		276.50/241

Table 11.4.: The results of the spectral analysis of the P-GRB (from $T_0 - 0.016$ s to $T_0 + 0.080$ s, best fit BB+Band model) and the extended afterglow (from $T_0 + 0.080$ s to $T_0 + 0.368$ s, best fit Band model) of GRB 090227B in the energy range 8 keV – 40 MeV.

11.4. Analysis of GRB 090227B in the Fireshell model

The identification of the P-GRB is fundamental in order to determine the Baryon load and the other physical quantities characterizing the plasma at the transparency point (see Fig. 11.2). Crucial is the determination of the cosmological redshift, which can be derived combining the observed fluxes and the spectral properties of the P-GRB and of the extended afterglow with the equation of motion of our theory. From the cosmological redshift we derive $E^{tot}_{e^+e^-}$ and the relative energetics of the P-GRB and of the extended afterglow components (see Fig. 11.2). Having so derived the Baryon load B and the energy $E^{tot}_{e^+e^-}$, we can constrain the total energy and simulate the canonical light curve of the GRBs with their characteristic pulses, modeled by a variable number density distribution of the CBM around the burst site.

11.4.1. Estimation of the redshift of GRB 090227B

Having determined the redshift of the source, the analysis consists of equating $E^{tot}_{e^+e^-} \equiv E_{iso}$ (namely E_{iso} is a lower limit on $E^{tot}_{e^+e^-}$) and inserting a value of the Baryon load to complete the simulation. The right set of $E^{tot}_{e^+e^-}$ and B is determined when the theoretical energy and temperature of the P-GRB match the observed ones of the thermal emission [namely $E_{P-GRB} \equiv E_{BB}$ and $kT_{obs} = kT_{blue}/(1+z)$].

In the case of GRB 090227B we have estimated the ratio $E_{P-GRB}/E^{tot}_{e^+e^-}$ from the observed fluences

$$\frac{E_{P-GRB}}{E^{tot}_{e^+e^-}} = \frac{4\pi d_l^2 F_{BB} \Delta t_{BB}/(1+z)}{4\pi d_l^2 F_{tot} \Delta t_{tot}/(1+z)} = \frac{S_{BB}}{S_{tot}}\,, \tag{11.4.1}$$

where d_l is the luminosity distance of the source and $S = F\Delta t$ are the fluences. **The fluence of the BB component of the P-GRB (see Tab 11.4, first interval) is $S_{BB} = (1.54 \pm 0.45) \times 10^{-5}$ erg/cm^2. The total fluence of the burst is $S_{tot} = (3.79 \pm 0.20) \times 10^{-5}$ erg/cm^2 and has been evaluated in the time interval from $T_0 - 0.016$ s to $T_0 + 0.896$ s. This interval slightly differs from the T_{90} because of the new time boundaries defined after the rebin-**

Fireshell Parameter	Value
$E^{tot}_{e^+e^-}$ [erg]	$(2.83 \pm 0.15) \times 10^{53}$
B	$(4.13 \pm 0.05) \times 10^{-5}$
Γ_{tr}	$(1.44 \pm 0.01) \times 10^{4}$
r_{tr} [cm]	$(1.76 \pm 0.05) \times 10^{13}$
kT_{blue} [keV]	$(1.34 \pm 0.01) \times 10^{3}$
z	1.61 ± 0.14
$\langle n \rangle$ [particles/cm^3]	$(1.90 \pm 0.20) \times 10^{-5}$
$\langle \delta n/n \rangle$	0.82 ± 0.11

Table 11.5.: The results of the simulation of GRB 090227B in the Fireshell model.

ning of the light curve at resolution of 16 **ms.** Therefore the observed energy ratio is $E_{P-GRB}/E^{tot}_{e^+e^-} = (40.67 \pm 0.12)\%$. As is clear from the bottom right diagram in Fig. 11.2, for each value of this ratio we have a range of possible parameters B and $E^{tot}_{e^+e^-}$. In turn, for each value of them we can determine the theoretical blue-shifted toward the observer temperature kT_{blue} (see top right diagram in Fig. 11.2). Correspondingly, for each couple of value of B and $E^{tot}_{e^+e^-}$ we estimate the value of z by the ratio between kT_{blue} and the observed temperature of the P-GRB kT_{obs},

$$\frac{kT_{blue}}{kT_{obs}} = 1 + z \, . \tag{11.4.2}$$

In order to remove the degeneracy $[E^{tot}_{e^+e^-}(z), B(z)]$, we have made use of the isotropic energy formula

$$E_{iso} = 4\pi d_l^2 \frac{S_{tot}}{(1+z)} \frac{\int_{E_{min}/(1+z)}^{E_{max}/(1+z)} E\, N(E) dE}{\int_8^{40000} E\, N(E) dE} \, , \tag{11.4.3}$$

in which $N(E)$ is the photon spectrum of the burst and the integrals are due to the bolometric correction on S_{tot}. The correct value is the one for which the condition $E_{iso} \equiv E^{tot}_{e^+e^-}$ is satisfied.

We have found the equality at $z = 1.61 \pm 0.14$ for $B = (4.13 \pm 0.05) \times 10^{-5}$ and $E^{tot}_{e^+e^-} = (2.83 \pm 0.15) \times 10^{53}$ ergs. The complete quantities so determined are summarized in Tab. 11.5.

Cloud	Distance [cm]	n_{CBM} [#/cm^3]
1^{th}	1.76×10^{15}	$(1.9 \pm 0.2) \times 10^{-5}$
2^{th}	1.20×10^{17}	$(3.5 \pm 0.6) \times 10^{-6}$
3^{th}	1.65×10^{17}	$(9.5 \pm 0.5) \times 10^{-6}$
4^{th}	1.80×10^{17}	$(5.0 \pm 0.5) \times 10^{-6}$
5^{th}	2.38×10^{17}	$(2.6 \pm 0.2) \times 10^{-5}$
6^{th}	2.45×10^{17}	$(1.0 \pm 0.5) \times 10^{-7}$
7^{th}	4.04×10^{17}	$(6.0 \pm 1.0) \times 10^{-5}$

Table 11.6.: The density mask of GRB 090227B: in the first column we report the number of CBM clouds, in the second one their distance away from the BH, and in the third one the number density with the associated error box.

11.4.2. The analysis of the extended afterglow and the observed spectrum of the P-GRB

As recalled in Sec. 11.2, the arrival time separation between the P-GRB and the peak of the extended afterglow is a function of $E^{tot}_{e^+e^-}$ and B and depends on the detailed profile of the CBM density. For $B \sim 4 \times 10^{-5}$ (see Fig. 11.3) the time separation is $\sim 10^{-3}$–10^{-2} s in the source cosmological rest frame. In this light, there is an interface between the reaching of transparency of the P-GRB and the early part of the extended afterglow. This connection has already been introduced in literature (Pe'Er et al., 2012; Izzo et al., 2012e; Penacchioni et al., 2012).

From the determination of the initial values of the energy, $E^{tot}_{e^+e^-} = 2.83 \times 10^{53}$ ergs, of the Baryon load, $B = 4.13 \times 10^{-5}$, and of the Lorentz factor $\Gamma_{tr} = 1.44 \times 10^4$, we have simulated the light curve of the extended afterglow by deriving the radial distribution of the CBM clouds around the burst site (see Tab. 11.6 and Fig. 11.10). In particular, each spike in Fig. 11.10 corresponds to a CBM cloud. The error boxes on the number density on each cloud is defined as the maximum possible tolerance to ensure the agreement between the simulated light curve and the observed data. The average value of the CBM density is $\langle n \rangle = (1.90 \pm 0.20) \times 10^{-5}$ particles/cm^3 with an average density contrast $\langle \delta n/n \rangle = 0.82 \pm 0.11$ (see also Tab. 11.5). These values are typical of the galactic halos environment. The filling factor varies in the range $9.1 \times 10^{-12} \leq \mathcal{R} \leq 1.5 \times 10^{-11}$, up to 2.38×10^{17} cm away from the burst site, and then drops to the value $\mathcal{R} = 1.0 \times 10^{-15}$. The value of the α parameter has been found to be -1.99 along the total duration of the GRB. In Fig. 11.11 we show the NaI-n2 simulated light curve (8–1000 keV) of GRB 090227B and in Fig. 11.12 (left panel) the corresponding spectrum in the early ~ 0.4 s of the emission, using the spectral model described by Eq. 11.2.1 (Patricelli et al., 2012). The simulation of the extended afterglow starts $T_a - T_0 \sim 0.017$ s after the Trigtime T_0. After the submission of this

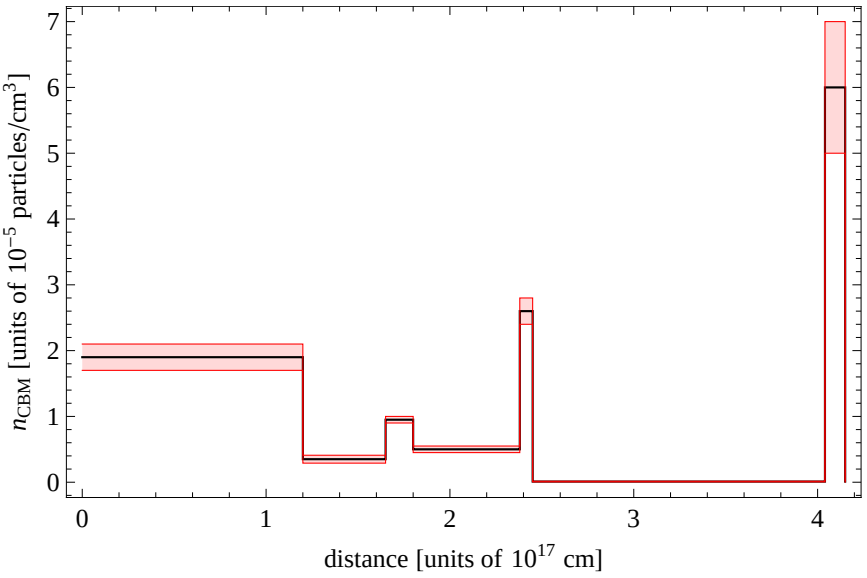

Figure 11.10.: The radial CBM density distribution of GRB 090227B (black line) and its range of validity (red shaded region).

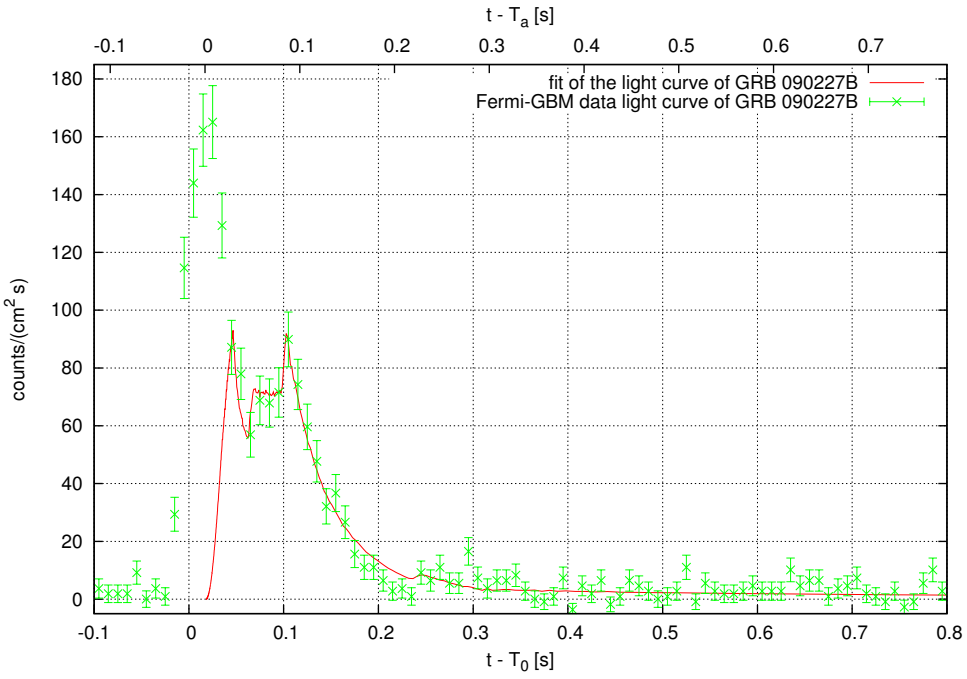

Figure 11.11.: The NaI-n2 simulated light curve of the extended-afterglow of GRB 090227B; each spike corresponds to the CBM density profile described in Tab. 11.6 and Fig. 11.10. The zero of the lower x-axis corresponds to the trig-time T_0; the zero of the upper x-axis is the time from which we have started the simulation of the extended afterglow, T_a, namely 0.017 s after T_0.

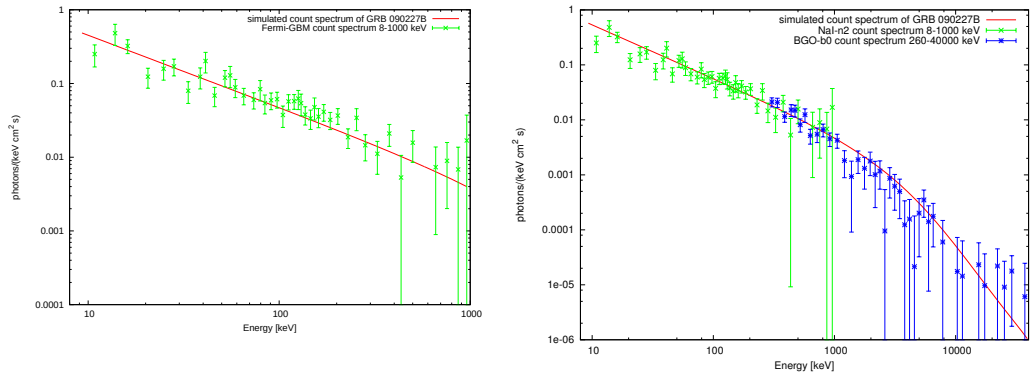

Figure 11.12.: Left panel: the simulated photon number spectrum of the extended-afterglow of GRB 090227B (from $T_0 + 0.015$ s to $T_0 + 0.385$ s) in the energy band 8–1000 keV, compared to the NaI-n2 data in the same time interval. Right panel: the same simulated spectrum, with the same parameters, extended up to 40 MeV and compared to the NaI-n2 and the BGO-b0 data in the same time interval.

manuscript, at the 13^{th} *Marcel Grossmann* meeting Dr. G. Vianello suggested to extend our simulations from 1 MeV all the way to 40 MeV, since significant data are available from the BGO detector. Without changing the parameters used in the theoretical simulation of the NaI-n2 data, we have extended the simulation up to 40 MeV and we compared the results with the BGO-b0 data (see Fig. 11.12, right panel). The theoretical simulation we performed, optimized on the NaI-n2 data alone, is perfectly consistent with the observed data all over the *entire* range of energies covered by the *Fermi*-GBM detector, both NaI and BGO.

We turn now to the emission of the early 96 ms. We have studied the interface between the P-GRB emission and the on-set of the extended afterglow emission. In Fig. 11.13 we have plotted the thermal spectrum of the P-GRB and the Fireshell simulation (from $T_0 + 0.015$ s to $T_0 + 0.080$ s) of the early interaction of the extended afterglow. The sum of these two components is compared with the observed spectrum from the NaI-n2 detector in the energy range 8–1000 keV (see Fig. 11.13, left panel). Then, again, from the theoretical simulation in the energy range of the NaI-n2 data, we have verified the consistency of the simulation extended up to 40 MeV with the observed data all over the range of energies covered by the *Fermi*-GBM detector, both NaI and BGO. The result is shown in Fig. 11.13 (right panel).

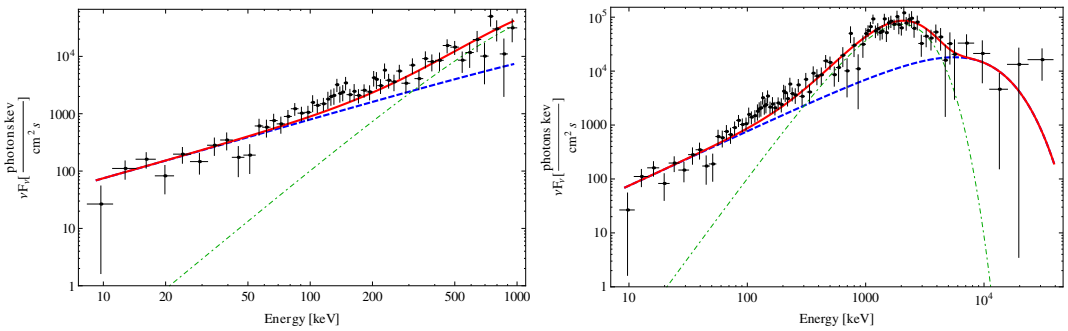

Figure 11.13.: Left panel: the time-integrated (from $T_0 + 0.015$ s to $T_0 + 0.080$ s) Fireshell simulation in the energy band 8–1000 keV, dashed blue line, and the BB emission, dashed-dotted green line; the sum of the two components, the solid red line, is compared to the observed P-GRB emission. Right panel: the same considerations including the BGO data up to 40 MeV.

11.5. Consistency with the opacity due to pair production

It is interesting to compare the Lorentz Γ factor theoretically determined from the P-GRB analysis with the lower limit coming from the opacity argument applied to the afterglow emission.

An estimate on this lower limit comes from the solution of the classical compactness problem for GRBs which arises from the combination of their large energy released, $\sim 10^{51}$ ergs, the short variability time scale δt of a few milliseconds and the observed hard non-thermal spectrum. Using the usual (Newtonian) causality limit on the size $R \leq c\delta t$ to estimate the density of photons, one finds that the optical depth for pair production at the source $\gamma\gamma \to e^+e^-$ would be $\sim 10^{15}$ (see Piran, 1999). Such an optically thick source could not emit the observed non-thermal spectrum.

As Ruderman (1975) pointed out, relativistic effects can solve this problem. The causality limit of a source moving relativistically with Lorentz factor $\Gamma \gg 1$ towards us is $R \leq c\delta t/\Gamma^2$. Additionally the observed photons have been blue-shifted. At the source they have lower energy, by a factor $\approx 1/\Gamma$, which may be insufficient for pair production. Together this leads to a decrease in the estimated optical depth by a factor $\Gamma^{2+2\beta}$ (Piran, 2012), where β is the high energy spectral index of the photon number distribution. Thus, the average optical depth, up to a factor due to the cosmological effects, is

$$\tau_{\gamma\gamma} = \frac{f_p}{\Gamma^{2+2\beta}} \frac{\sigma_T S d_l^2}{c^2 \delta t^2 m_e c^2} \,, \tag{11.5.1}$$

where f_p is the fraction of photon pairs at the source that can effectively produce pairs, σ_T is the Thompson cross-section and S is the observed fluence.

From the condition $\tau_{\gamma\gamma} < 1$, Eq. 11.5.1 becomes

$$\Gamma > \left(\frac{f_p \sigma_T S d_l^2}{c^2 \delta t^2 m_e c^2} \right)^{\frac{1}{2+2\beta}} . \tag{11.5.2}$$

By setting δt equal to minimum variability time scale observed for GRB 090227B, $\sim$ 2 ms (Guiriec et al., 2010), and using the observed total fluence, $S_{tot} = 3.79 \times 10^{-5}$ erg/cm^2, the high energy spectral index, $\beta = 2.90$, and the theoretically inferred redshift, $z = 1.61$, we obtain a lower limit $\Gamma > 594$.

The large quantitative difference between our theoretically estimated Lorentz factor from the P-GRB and the one derived from the opacity argument is not surprising in view of the very different approximations adopted. While the determination from the P-GRB consists in a precise analysis at the instant of transparency, the determination of the lower limit from the Eq. 11.5.2 is based on an estimate taking a time-averaged value on the entire extended afterglow.

Important, of course, is that the precise value determined from the P-GRB does fulfill the inequality given in Eq. 11.5.2.

11.6. Conclusions

The comprehension of this short GRB has been improved by analyzing the different spectra in the T_{90}, T_{spike} and T_{tail} time intervals. We have shown that within the T_{90} and the T_{spike} all the considered models (BB+Band, Band+PL, Compt+PL) are viable, while in the T_{tail} time interval, the presence of a thermal component is ruled out. The result of the analysis in the T_{tail} time interval gives an additional correspondence between the Fireshell model (see Sec. 11.2.1) and the observational data. According to this picture, the emission within the T_{spike} time interval is related to the P-GRB and it is expected to have a thermal spectrum with in addition an extra NT component due to an early onset of the extended afterglow. In this time interval a BB with an additional Band component has been observed and we have shown that it is statistically equivalent to the Compt+PL and the Band+PL models. Our theoretical interpretation is consistent with the observational data and statistical analysis. From an astrophysical point of view the BB+Band model is preferred over the Compt+PL and the Band+PL models, been described by a consistent theoretical model.

GRB 090227B is the missing link between the genuine short GRBs, with the Baryon load $B \lesssim 5 \times 10^{-5}$ and theoretically predicted by the Fireshell model (Ruffini et al., 2001a,b,c), and the long bursts.

From the observations, GRB 090227B has an overall emission lasting ~ 0.9 s with a fluence of 3.79×10^{-5} erg/cm^2 in the energy range 8 keV – 40 MeV. In absence of an optical identification, no determination of its cosmological

redshift and of its energetics was possible.

Thanks to the excellent data available from Fermi-GBM (Meegan et al., 2009), it has been possible to probe the comparison between the observation and the theoretical model. In this sense, we have then performed a more detailed spectral analysis on the time scale as short as 16 ms of the time interval T_{spike}. As a result we have found in the early 96 ms a thermal emission which we have identified with the theoretically expected P-GRB component. The subsequent emission of the time interval T_{spike} has been interpreted as part the extended afterglow. Consequently, we have determined the cosmological redshift, $z = 1.61 \pm 0.14$, as well as the Baryon load, $B = (4.13 \pm 0.05) \times 10^{-5}$, its energetics, $E^{tot}_{e^+e^-} = (2.83 \pm 0.15) \times 10^{53}$ ergs, and the extremely high Lorentz Γ factor at the transparency, $\Gamma_{tr} = (1.44 \pm 0.01) \times 10^4$.

We are led to the conclusion (see also Rueda and Ruffini, 2012a) that the progenitor of this GRB is a binary neutron star, which for simplicity we assume to have the same mass, by the following considerations:

1. the very low average number density of the CBM, $\langle n_{CBM} \rangle \sim 10^{-5}$ particles/cm^3; this fact points to two compact objects in a binary system that have spiraled out in the halo of their host galaxy (see Bernardini et al., 2007, 2008a; Bianco et al., 2008a; Caito et al., 2009, 2010; de Barros et al., 2011);

2. the large total energy, $E^{tot}_{e^+e^-} = 2.83 \times 10^{53}$ ergs, which we can indeed infer in view of the absence of beaming, and the very short time scale of emission point again to two neutron stars. We are led to a binary neutron star with total mass $m_1 + m_2$ larger than the neutron star critical mass, M_{cr}. In light of the recent neutron star theory in which all the fundamental interactions are taken into account (Belvedere et al., 2012), we obtain for simplicity in the case of equal neutron star masses, $m_1 = m_2 = 1.34 M_\odot$, radii $R_1 = R_2 = 12.24$ km, where we have used the NL3 nuclear model parameters for which $M_{cr} = 2.67 M_\odot$;

3. the very small value of the Baryon load, $B = 4.13 \times 10^{-5}$, is consistent with the above two neutron stars which have crusts ~ 0.47 km thick. The new theory of the neutron stars, developed in Belvedere et al. (2012), leads to the prediction of GRBs with still smaller Baryon load and, consequently, shorter periods. We indeed infer an absolute upper limit on the energy emitted via gravitational waves, $\sim 9.6 \times 10^{52}$ ergs (see Rueda and Ruffini, 2012a).

We can then generally conclude on the existence of three different possible structures of the canonical GRBs (see Fig. 11.14 and Tab. 11.7):

a. long GRB with Baryon load $3.0 \times 10^{-4} \lesssim B \leq 10^{-2}$, exploding in a CBM with average density of $\langle n_{CBM} \rangle \approx 1$ particle/cm^3, typical of the inner galactic regions;

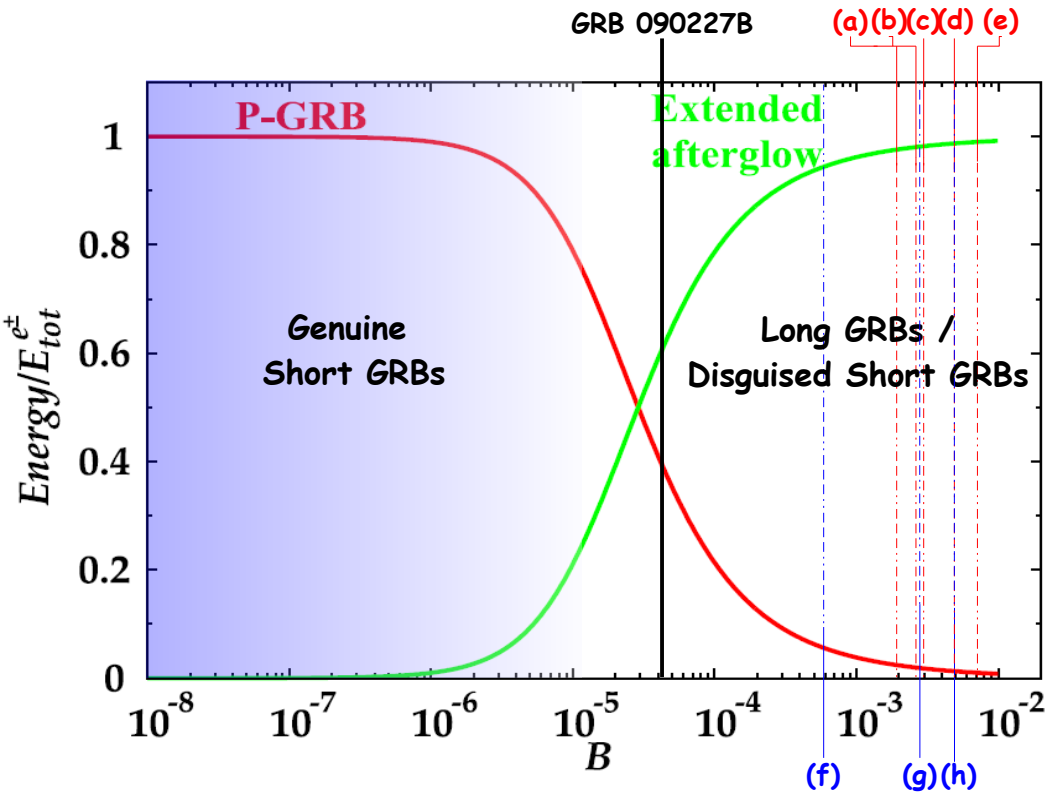

Figure 11.14.: The energy emitted in the extended afterglow (green curve) and in the P-GRB (red curve) in units of the total energy $E^{tot}_{e^+e^-} = 1.77 \times 10^{53}$ erg are plotted as functions of the B parameter. In the figure are also marked some values of the Baryon load: in black GRB 090227B and in red and blue some values corresponding to, respectively, some long and disguised short GRBs we analyzed.

label	GRB	$E^{tot}_{e^+e^-}$ [erg]	B	$\langle n_{CBM} \rangle$ [#/cm^3]
(a)	090618	2.49×10^{53}	1.98×10^{-3}	1.0
(b)	080319B	1.32×10^{54}	2.50×10^{-3}	6.0
(c)	991216	4.83×10^{53}	3.00×10^{-3}	1.0
(d)	030329	2.12×10^{52}	4.80×10^{-3}	2.0
(e)	031203	1.85×10^{50}	7.40×10^{-3}	0.3
(f)	050509B	5.52×10^{48}	6.00×10^{-4}	1.0×10^{-3}
(g)	060614	2.94×10^{51}	2.80×10^{-3}	1.0×10^{-3}
(h)	970228	1.45×10^{54}	5.00×10^{-3}	9.5×10^{-4}
	090227B	2.83×10^{53}	4.13×10^{-5}	1.9×10^{-5}

Table 11.7.: List of the long and disguised short GRBs labeled in Fig. 11.14 with in addition GRB 090227B. For each burst the total energy of the plasma, the Baryon load, and the average CBM density are indicated.

b. disguised short GRBs with the same Baryon load as the previous class, but occurring in a CBM with $\langle n_{CBM}\rangle \approx 10^{-3}$ particle/cm^3, typical of galactic halos (Bernardini et al., 2007, 2008a; Bianco et al., 2008a; Caito et al., 2009, 2010; de Barros et al., 2011);

c. genuine short GRBs which occur for $B \lesssim 10^{-5}$ with the P-GRB predominant with respect to the extended afterglow and exploding in a CBM with $\langle n_{CBM}\rangle \approx 10^{-5}$ particle/cm^3, typical again of galactic halos, being GRB 090227B the first example.

Both classes of GRBs occurring in galactic halos originate from binary mergers.

Finally, if we turn to the theoretical model within a general relativistic description of the gravitational collapse to a $10M_\odot$ black hole, see e.g. Ruffini et al. (2003b, 2005d) and Fig. 2 in Fraschetti et al. (2006), we find the necessity of time resolutions of the order the fraction of a ms, possibly down to μs, in order to follow such a process. One would need new space missions larger collecting area to prove with great accuracy the identification of a thermal component. It is likely that an improved data acquisition with high signal to noise on shorter time scale would evidence more clearly the thermal component as well as distinguish more effectively different fitting procedure.

12. GRB 110709B in the Induced Gravitational Collapse paradigm

12.1. Introduction

Of all the astrophysical processes currently being analyzed, few are more fundamental than the one presenting the coincidence of some Gamma-Ray Bursts (GRBs) with the explosion of a Supernova (SN). For this, the Induced Gravitational Collapse (IGC) paradigm was first introduced by Ruffini et al. (2001a) and further analyzed in Ruffini et al. (2007c), Ruffini et al. (2008b), Rueda and Ruffini (2012b) and Izzo et al. (2012a). Recently, it has been evidenced that indeed this process can explain the coincidence between the SN and GRB emission, both from an observational and a theoretical point of view (Izzo et al., 2012e; Penacchioni et al., 2012).

In the IGC paradigm (Ruffini et al., 2001a, 2007c), a binary system formed by an evolved star and a Neutron Star (NS) companion is considered as the progenitor.

The IGC paradigm implies a well determined time sequence. In a close binary system of a massive star in the latest phases of its thermonuclear evolution and a NS companion, the massive star undergoes a SN explosion. The accretion of the early-SN material onto the NS companion leads the NS to its critical mass and consequently to its gravitational collapse to form a black hole (BH). The emission of a canonical GRB in the collapse to the BH takes place. A young NS is born out of the SN explosion. Finally, a SN emission is either observed or expected in association with the GRB, ~ 10 days after the burst in the rest frame. We aim to find sources in which the data are of such a good quality to allow to see this complete sequence.

The prototype for the IGC paradigm has recently been given in the analysis of GRB 090618 (Izzo et al., 2012e), following the works of Rueda and Ruffini (2012b) and Izzo et al. (2012a). In this work we follow the same line and identify four different episodes in GRB 110709B. Episode 1 starts 40 s before the first trigger and lasts up to 60 s after it and is well fit by a blackbody (BB) plus a power-law (PL) spectral model . It corresponds to the trigger of the SN explosion of the compact core and its accretion onto the NS companion. We notice that the BB temperature decays with time following a broken power-

law (Ryde, 2004). Episode 2 starts 35 s before the second trigger and lasts up to 100 s after it. It corresponds to the emission of the canonical GRB emitted in the formation of a BH. Episode 3 starts at 800 s all the way to 10^6 s. It consists in a standard X-ray emission identified in all systems following the IGC paradigm (Pisani et al., in preparation). Episode 4 corresponds to the observation of the optical SN emission, observable after $T_{obs} = (1+z)T_{SN}$. In the present case, there is no evidence of an associated SN in the optical band. An explanation for this is given by Zauderer et al. (2013), who classified GRB 110709B as dark and stated that its optical emission may have been absorbed by the host galaxy and/or the interstellar medium. The ensemble of these four episodes characterize the IGC scenario.

As an outcome, at the endpoint of the IGC scenario, a binary system represented by a NS (formed by the SN explosion) and a BH (formed after the GRB explosion) should be expected.

As in the case of GRB 101023, we do not know the cosmological redshift of GRB 110709B due to the lack of optical data. Therefore, we infer it from phenomenological methods: 1) The Amati relation (Amati, 2006), 2) the Yonetoku relation (Yonetoku et al., 2004, 2010), 3) the work of Grupe et al. (2007b) and 4) the work by Penacchioni et al. (2012), Ruffini (2012) and by Pisani et al. (in preparation), which describe a scaling of the late X-ray emission of GRB 090618. In the case of GRB 111228, which we are currently analyzing, we find a striking coincidence between the values of the cosmological redshift determined by these methods for GRB 110709B.

In section 12.2 we report the observations of the two components of GRB 110709B by the different instruments, in space and on the ground. In section 12.3 we reduce the *Swift* data and perform a detailed spectral analysis of both Episode 1 and Episode 2. In section 12.4 we infer the redshift of the source using the four phenomenological methods mentioned above. In section 12.5 we determine the radius of the emitting region from the knowledge of the redshift and the BB flux of the first episode. In section 12.6 we give a brief description of the Fireshell model and we perform a deeper analysis of Episode 2 within this model, reproducing the light curve and the spectrum by a numerical simulation. In section 12.7 we calculate the parameters of the binary progenitor leading to the IGC of the NS to a BH by the SN explosion. Details on the accretion rate onto the NS, total accreted mass, SN ejecta density, NS mass, and binary orbital period are obtained for selected values of the SN progenitor mass. In section 12.8 we comment on the radio emission detected by EVLA (Zauderer and Berger, 2011). In section 12.9 we present the conclusions.

12.2. Observations of GRB 110709B

GRB 110709B has been detected by *Suzaku* (Ohmori et al., 2011) and *Swift* (Cummings et al., 2011) satellites, and by ground-based telescopes like *GROND* (Updike et al., 2011) and *Gemini* (Berger, 2011a).

The Burst Alert Telescope (BAT) on board *Swift* triggered a first time at 21:32:39 UT (trigger N°= 456967). The location of this event is RA= 164.6552, DEC= -23.4550. The light curve is composed of multiple peaks, with the whole emission extending up to 60 s after the trigger (see Fig. 12.1). What is most interesting is that there was another trigger at 21:43:25 UT (trigger N°=456969), $\sim$ 11 minutes after the first trigger. The on-board calculated location is RA=164.647, DEC=-23.464. This time *Swift* did not need to slew, because it was already pointing to that position. This second emission shows a bump that begins 100 s before the second trigger and lasts around 50 s, followed by several overlapping peaks with a total duration of about 40 s, and another isolated peak of 10 s of duration, 200 s after the second trigger. Fig. 12.1 shows the complete BAT light curve and Fig. 12.2 shows the light curve taken by the X-Ray Telescope (XRT) in the 0.3-10 keV band.

There have not been detections in the optical band by *Swift* UVOT, which started to observe 70 s after the first BAT trigger (Holland and Cummings, 2011). The observations with GROND at La Silla Observatory (Updike et al., 2011) simultaneously in the g' r' i 'z' JHK, reveal two point sources within the 5" .3 XRT error circle reported by Cummings et al. (2011). They suggest that one of them could be an afterglow candidate for GRB 110709B, although it is very faint.

It has been suggested by Zauderer et al. (2013) that this source is an "optically dark" GRB. The possible reasons for this are: 1) dust obscuration, 2) intrinsically dim event, and/or 3) high redshift (optical emission suppressed by Lyα absorption at $\lambda_{obs} \leq 1216\mathring{A}\,(1+z)$). However, they rule out the possibility of a high redshift event due to the association with an optically detected host galaxy. Furthermore, they have inferred the optical brightness of the afterglow according to the standard afterglow synchrotron model (Granot and Sari, 2002; Sari et al., 1999), and from the non-detection in the optical-NIR wavelengths they find a very large rest frame extinction for GRB 110709B . This can explain the lack of detections in the optical band.

There have been detections in the radio band on several occasions by EVLA (Zauderer and Berger, 2011), revealing a single unresolved radio source within the XRT error circle, which rebrightened by a factor of 1.6 between 2.1 and 7 days after the burst. The location of the source is RA=10:58:37.114, DEC=-23:27:16.760.

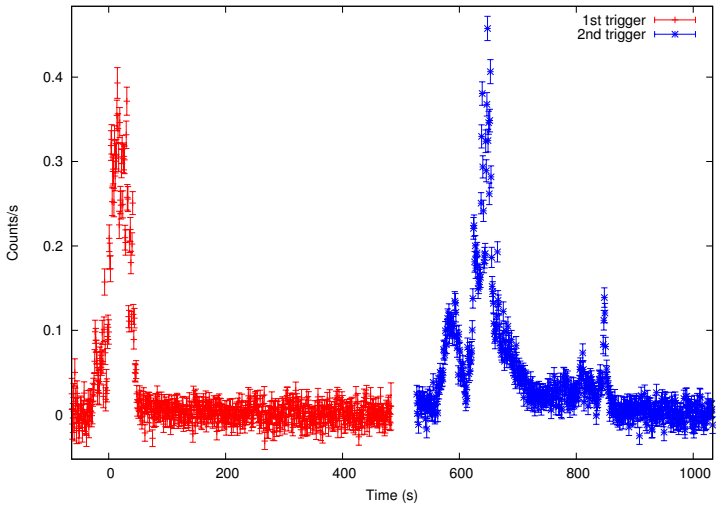

Figure 12.1.: BAT light curve of GRB 110709B, including both triggers. Here we can appreciate the time separation (about 10 minutes) between the first and the second trigger. The light curve is in the (15-150 keV) energy band. The time is relative to the first trigtime, of 331939966 s (in MET seconds). The second trigger was at 331940612 s in MET seconds.

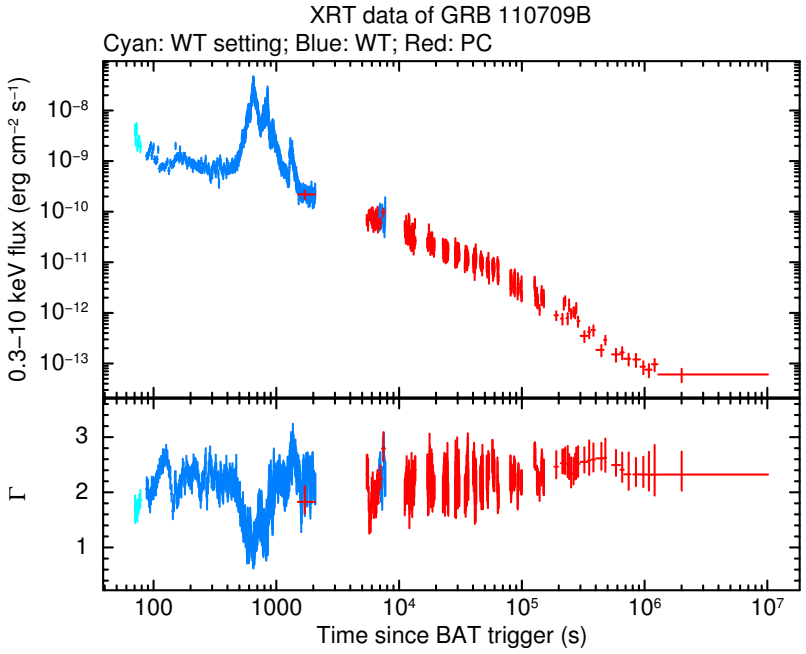

Figure 12.2.: Count light curve of GRB 110709B obtained from the *Swift*-XRT detector, in the (0.3-10 keV) energy band. The time is relative to the first trigtime, of 331939966 s (in MET seconds).

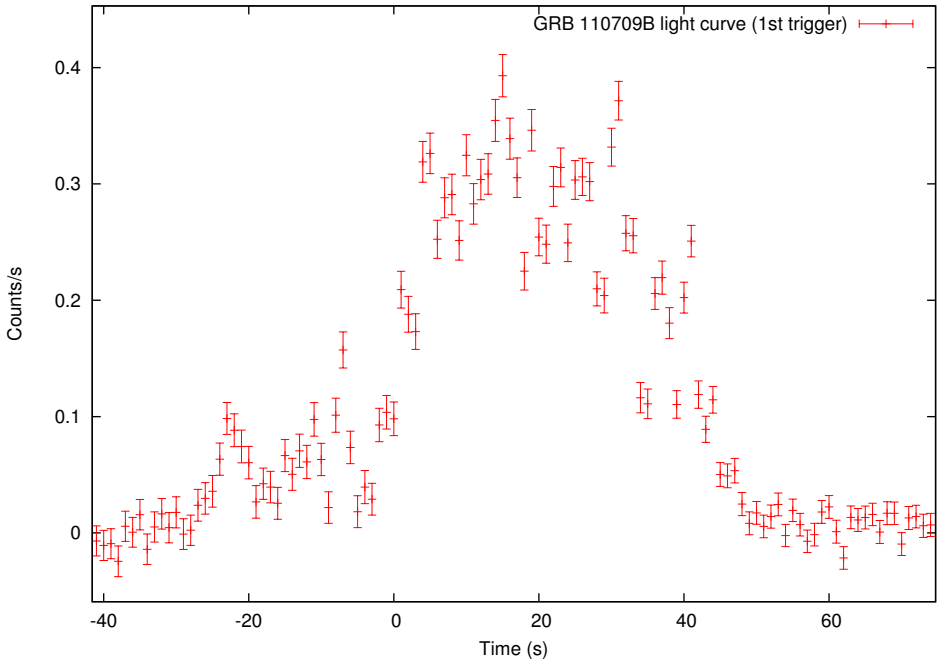

Figure 12.3.: Count light curve of Episode 1 of GRB 110709B obtained from the *Swift*-BAT detector, in the (15-150 keV) energy band. The time is relative to the first trigtime, of 331939966 s (in MET seconds).

Table 12.1.: Fit results of Episode 1 with five spectral models: BB, Band, BB+PL, PL and CutoffPL. The flux is in the energy band (15- 150) keV, in units of erg/cm^2/s.

BB	Band	BB+PL	PL	CutoffPL
$kT = 18.9 \pm 0.2$	$\alpha = -1.2 \pm 0.1$	$kT = 22 \pm 5$	$\gamma = 1.37 \pm 0.02$	$\gamma = 1.1 \pm 0.1$
$K_{BB} = 0.95 \pm 0.01$	β =unconstr.	$K_{BB} = 0.2 \pm 0.1$	$K_{PO} = 2.0 \pm 0.2$	$E_0 = 196 \pm 68$
	$E_0 = 296 \pm 255$	$\gamma = 1.4 \pm 0.1$		$K = 0.8 \pm 0.2$
		$K_{PO} = 2.2 \pm 0.8$		
Red$\chi^2 = 7.3$	Red$\chi^2 = 1.031$	Red$\chi^2 = 1.049$	Red$\chi^2 = 1.14$	Red$\chi^2 = 0.99$
56 DOF	54 DOF	54 DOF	56 DOF	55 DOF
Flux$= 7.52 \times 10^{-8}$	Flux$= 8.99 \times 10^{-8}$	Flux$= 8.96 \times 10^{-8}$	Flux$= 9.08 \times 10^{-8}$	Flux$= 8.93 \times 10^{-8}$

12.3. Data analysis

In the following we refer to the emission that goes from 40 s before the first BAT trigger to 60 s after it as Episode 1 (see Fig. 12.3). We call the emission going from 35 s before the second BAT trigger to 100 s after it as Episode 2. We make use of *Swift* BAT data to perform the spectral analysis with XSPEC.

12.3.1. Episode 1

We perform a time-integrated analysis to the whole Episode 1, using five different spectral models, namely BB, Band (Band et al., 1993), BB+PL, PL and CutoffPL. The results of the fits are shown in Table 12.1 and in Fig. 12.4. The

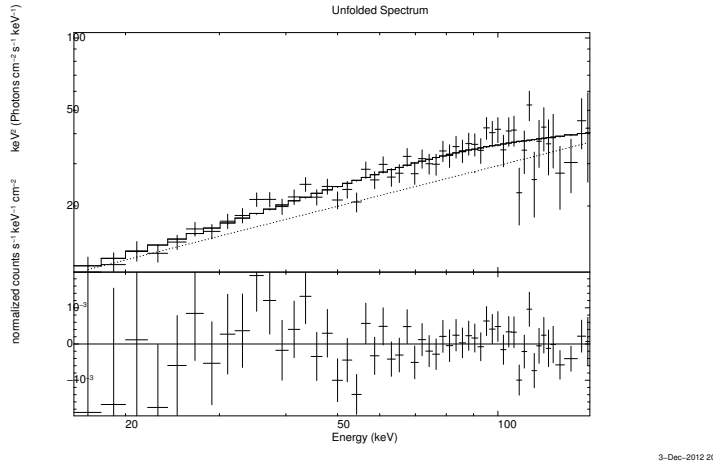

Figure 12.4.: Fit of Episode 1 with a BB+PL model. The parameters of the fit are: $kT = (22 \pm 5)$ keV, BB Amp$= 0.2 \pm 0.1$, $\gamma = 1.4 \pm 0.1$, PL Amp$= 2.2 \pm 0.8$, Red-$\chi^2 = 1.049$ (54 DOF).

Band function is not well constrained, so we have excluded it in the following analysis. A statistical test shows that the best models are BB+PL ($\chi^2 = 56.65$) and CutoffPL ($\chi^2 = 54.45$). Since the difference in the χ^2 between these two models is 2.2, the two models are statistically equivalent. So we discriminate between these two models based on the physical grounds expected from the IGC scenario. In this scenario, we expect a thermal emission from the expansion of the outer layers of the compact core SN progenitor. Thus, we have chosen the BB+PL model. We obtain a BB temperature $kT = (22 \pm 5)$ keV, a PL index $\gamma = 1.4 \pm 0.1$ and a $\chi^2 = 56.65$ (54 DOF). The flux of the BB component is $\sim$ 12% of the total flux. The total energy of Episode 1 is $E_{iso}^{Ep_1} = 1.42 \times 10^{53}$ erg. The results of the fit are shown in Table 12.1. Then we perform a time-resolved spectral analysis with a binning of 5 s fitting the same model and find that the temperature of the BB component follows a broken power-law, as mentioned in Ryde (2004), from 5 s before the trigger to 55 s after it (see Fig. 12.5). The broken power-law is indeed a constant function plus a simple power-law function. This is the same behavior as for the previously analyzed GRB 090618 (Izzo et al., 2012e) and GRB 101023 (Penacchioni et al., 2012). However, we notice that the temperatures for this GRB are lower. Nevertheless, the simultaneous presence of a BB and PL component is necessary in order to obtain an acceptable fit of the data (see Fig. 12.4).

12.3.2. Episode 2

We also performed a time-integrated spectral analysis of Episode 2, whose light curve is shown in Fig. 12.7. This episode starts 35 s before the sec-

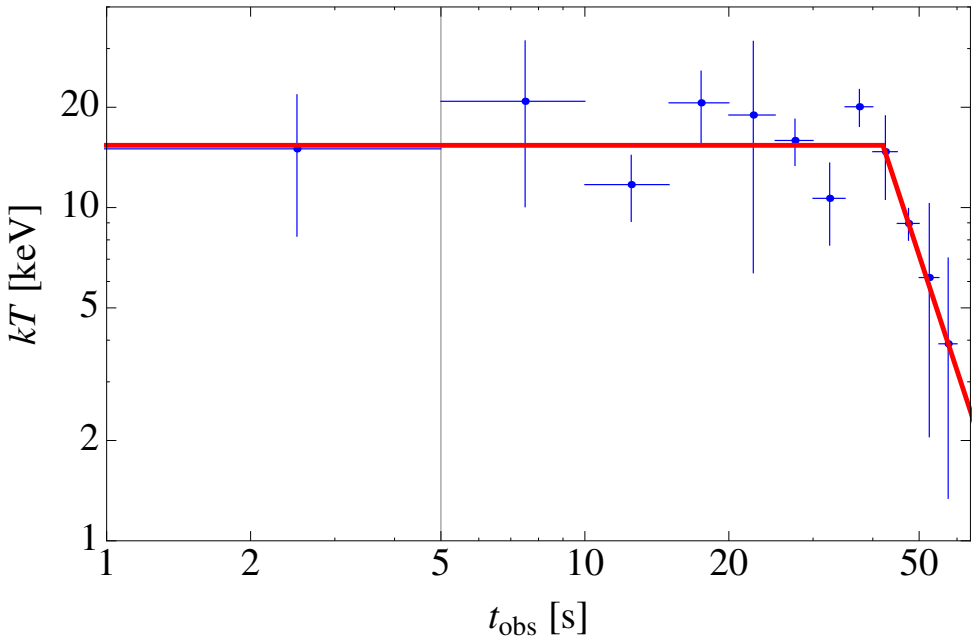

Figure 12.5.: Evolution of the kT component of the BB+PL model during Episode 1. The first data point corresponds to 5 s before the first BAT trigger. The vertical line corresponds to the trigger time. The time is in the observer frame. The temperature evolves in time following a broken power-law fit. There is a break at $t = 41.21$ s. The indices of the PL are $\alpha = 0$ (consistent with a constant function) and $\beta = -4 \pm 2$, respectively. The presence of the BB, although smaller than in previous cases, is essential to have an acceptable fit.

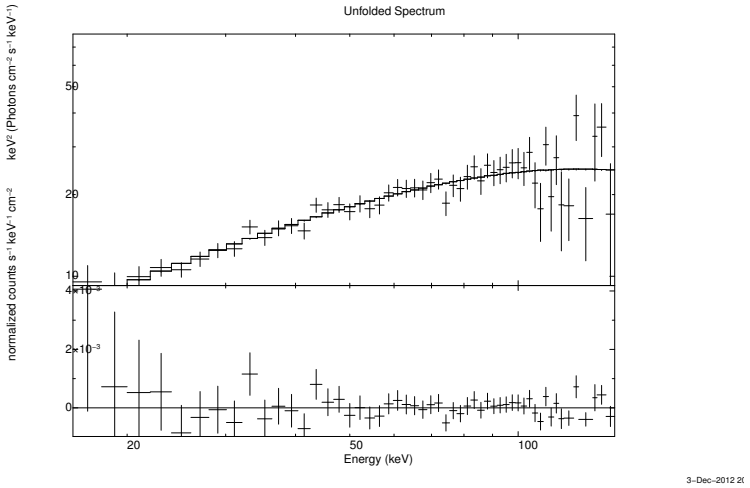

Figure 12.6.: Fit of Episode 2 with a Cutoffpl model. The photon index is $\gamma = 1.0 \pm 0.1$, the normalization constant is 0.5 ± 0.1, the cutoff energy is $E_0 = 132 \pm 31$ and the reduced chi squared of the fit is Red-$\chi^2 = 0.77$ (55 DOF).

ond trigger and last 135 s, until 100 s after the second trigger. We tried to fit the spectrum with the following spectral models: BB, PL, BB+PL, cutoffPL and Band (see Table 12.2). We can easily discard the BB and Band models because in one case the Red χ^2 is too high and in the other case there is an unconstrained parameter. As the PL and the BB+PL are nested models, we performed a statistical test to see which one is the best. We obtained a probability Prob=0.001 that the simpler model is better, so the BB+PL dominates over the PL. Then we have to compare between the BB+PL and the CutoffPL models. As they are not nested, we cannot apply the same test. So we chose the model that gives the lowest χ^2. We concluded that the model that best fits Episode 2 is the cutoffPL model.

It is clear from the analogies with GRB 090618 and GRB 101023 that Episode 2 has all the characteristics of a canonical GRB. A difference between GRB 110790B and the already analyzed ones is that the separation between Episode 1 and Episode 2, $\sim$ 10 min, is much bigger than previously, $\sim$ 50 s. This remarkable time separation between the two episodes is an additional new fact to propose a different astrophysical origin of these two components.

We turn now to the crucial analysis of the determination of the cosmological redshift of Episode 2.

Table 12.2.: Spectral fit of the whole Episode 2 with different models: BB, PL, BB+PL, cutoffPL and Band. The flux corresponds to the (15 -150) keV energy range. The model that best fits the data is the cutoffPL. We can easily see that the BB and Band models are not good. As the PL and BB+PL are nested models, we performed a statistical test to see which was the best one. We obtained a probability Prob=0.001, indicating that the BB+PL dominates over the PL model. Then, between BB+PL and CutoffPL (that are not nested, then we cannot apply the same test), we took the CutoffPL as the best model because it gives the lowest χ^2. Note that the models with which we fit the data are those defined in the XSPEC's Manual: http://heasarc.nasa.gov/xanadu/xspec/xspec11/manual/manual.html

BB	PL	BB+PL	CUTOFFPL	BAND
kT [keV]$= 17.5 \pm 0.2$	$\gamma = 1.46 \pm 0.02$	kT [keV]$= 20 \pm 3$	$\gamma = 1.0 \pm 0.1$	$\alpha = -1.0 \pm 0.1$
$K_{BB} = 0.661 \pm 0.009$	$K_{PO} = 2.1 \pm 0.2$	$K_{BB} = 0.16 \pm 0.06$	$E_0 = 132 \pm 31$	$\beta =$ unc
		$\gamma = 1.5 \pm 0.1$	$K = 0.5 \pm 0.1$	$E_0 = 142 \pm 42$
		$K_{PO} = 2.3 \pm 0.8$		$K = 0.0048 \pm 0.0008$
Red $\chi^2 = 7.16$	Red $\chi^2 = 1.109$	Red $\chi^2 = 0.78$	Red $\chi^2 = 0.77$	Red $\chi^2 = 0.79$
DOF= 56	DOF= 56	DOF=54	DOF= 55	DOF= 54
Flux= 5.2×10^{-8}	Flux= 6.52×10^{-8}	Flux =6.35×10^{-8}	Flux= 2.43×10^{-8}	Flux= 6.36×10^{-8}

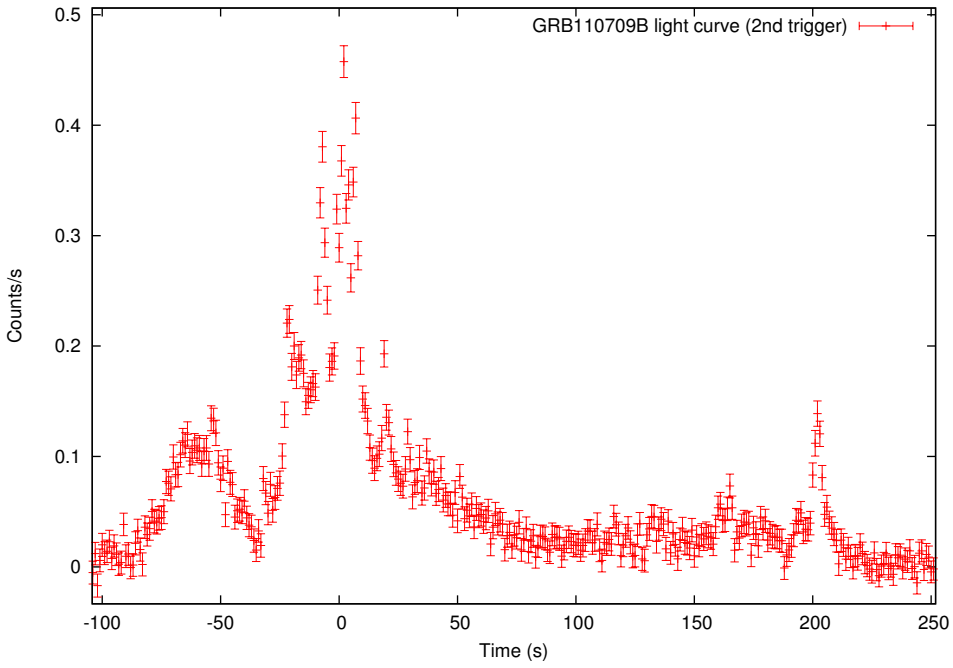

Figure 12.7.: Count light curve of Episode 2 of GRB 110709B obtained from the *Swift*-BAT detector, in the (15-150 keV) energy band. The time is relative to the second trigtime, of 331940612 s (in MET seconds).

12.4. Cosmological redshift determination

We used four phenomenological methods to constrain the redshift of the source, based on different relations, detailed below.

12.4.1. N_H column density

We first tried to get an upper limit for z following the work of Grupe et al. (2007b). They consider a relation between the absorption column density in excess of the galactic column density, given by $\Delta N_H = N_{H,fit} - N_{H,gal}$ and the redshift z, through the equation

$$log(1+z) < 1.3 - 0.5[log(1+\Delta N_H)]. \tag{12.4.1}$$

We calculated $N_{H,gal}$ from the radio map of the galaxy in the Lab Survey website[1] by entering the coordinates of the GRB (RA=164.64, DEC=-23.46). We obtained $N_{H,gal} = 10.5 \times 10^{20}$ cm^{-2}.

To obtain the value of $N_{H,fit}$ we took the XRT data from 2000 s to 10^6 s after the first BAT trigger and fitted the model *phabs*po* using the program XSPEC. The XRT data were reduced by the xrtpipeline software, version 0.10.4, which is part of the HEASOFT package, version 6.12. We use the standard response matrix swxpc0to12s6_20010101v013.rmf for the PC mode data. The model *phabs* represents the photoelectric absorption

$$M(E) = e^{-n_H \sigma(E)}, \tag{12.4.2}$$

where n_H is the equivalent hydrogen column density (in units of 10^{22} cm^{-2}) and $\sigma(E)$ is the photoelectric cross section, not including Thompson scattering. We obtained a value of $N_{H,fit} = 71.76 \times 10^{20}$ cm^{-2}. Using these values in (12.4.1) we obtained an upper limit for the redshift of $z < 1.35$.

12.4.2. Amati Relation

We also tried to determine the redshift of Episode 2 through the Amati relation (Amati, 2006), that relates the isotropic energy E_{iso} of the GRB to the peak Energy in the rest frame $E_{p,i}$ of the νF_ν spectrum (Amati et al., 2009). The analytical expression of E_{iso} is

$$E_{iso} = \frac{4\pi d_L^2}{(1+z)} S_{bol}, \tag{12.4.3}$$

where d_L^2 is the luminosity distance, z is the redshift and S_{bol} is the bolometric fluence, related to the observed fluence in a given detection band (E_{min}, E_{max})

[1] http://www.astro.uni-bonn.de/~webaiub/english/tools_labsurvey.php

by

$$S_{bol} = S_{obs} \frac{\int_{1/(1+z)}^{10^4/(1+z)} E\phi(E)dE}{\int_{E^{min}}^{E^{max}} E\phi(E)dE}. \tag{12.4.4}$$

Here, ϕ is the spectral model considered for the spectral data fit; in this case a Band model (Band et al., 1993), composed of two smoothly connected power-laws. $E_{p,i}$ is related to the peak energy E_p in the observer frame by

$$E_{p,i} = E_p(1+z). \tag{12.4.5}$$

The peak energy is the energy at the peak of the νF_ν spectrum. It can be written as

$$E_p = E_0(2+\alpha),$$

where E_0 is the energy at which the two power-laws intersect and α is the slope of the low-energy power-law, according to the Band model.

We calculate the luminosity distance d_L, as given by the standard cosmological model

$$d_L = \frac{c}{H_0}(1+z)\int_0^z \frac{dx}{\sqrt{\Omega_m(1+x)^3+\Omega_\Lambda}}, \tag{12.4.6}$$

where the Hubble constant is $H_0 = 70$ km s^{-1} Mpc^{-1}, $\Omega_m = 0.27$, $\Omega_\Lambda = 0.73$ and c is the speed of light.

Following the same procedure as described in (Penacchioni et al., 2012), we calculated E_{iso} and $E_{p,i}$ for different values of z, from 0.1 to 3, at steps of 0.1. Fig. 12.8 shows that the relation is satisfied for values of $z > 0.4$. This puts a lower limit to the estimation of the redshift.

12.4.3. Yonetoku Relation

We finally obtained a range of possible redshifts by using the Yonetoku relation (Yonetoku et al., 2004). This relation, also known as the E_p - Luminosity relation (E_p - L) , connects the observed isotropic luminosity L in units of 10^{52} erg s^{-1} with the peak energy $E_p(1+z)$ in the rest frame of the GRB. It is valid for values of E_p between 50 and 2000 keV, and a luminosity range of $10^{50} - 10^{54}$ erg s^{-1}.

The best fit function for the E_p - L relation is

$$\frac{L}{10^{52}\text{erg s}^{-1}} = (2.34^{+2.29}_{-1.76}) \times 10^{-5} \left[\frac{E_p(1+z)}{1\text{ keV}}\right]^{2.0\pm0.2} \tag{12.4.7}$$

The peak luminosity and the peak energy are calculated by integrating within a 1 s interval around the most intense peak of the light curve, be-

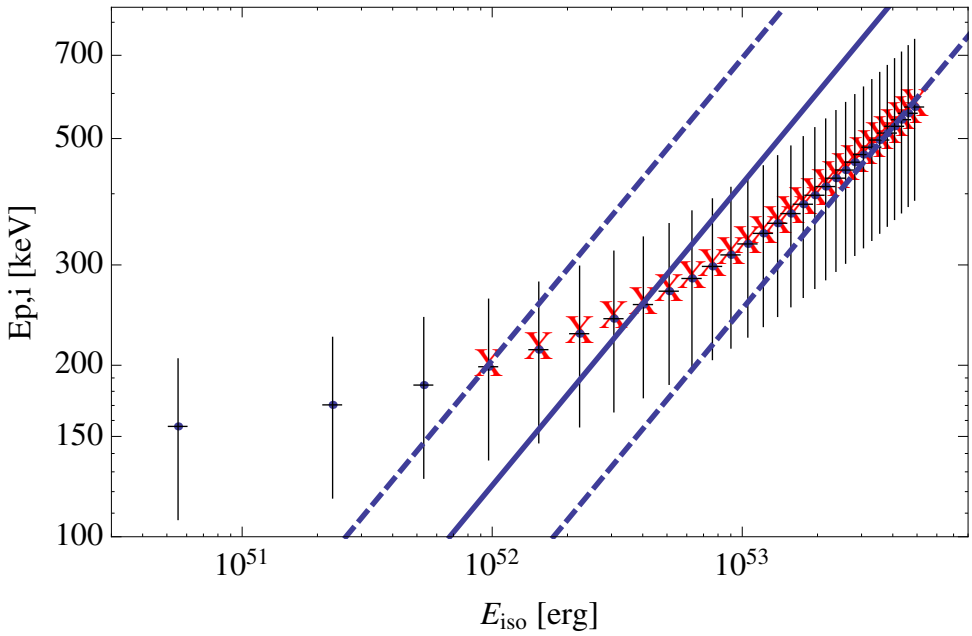

Figure 12.8.: Amati relation (solid line) with its $1-\sigma$ uncertainties (doted lines) and peak energy $E_{p.i}$ vs. E_{iso} for GRB 110709B, for different values of the redshift, from 0.1 to 3, at steps of 0.1. We can see that the data matches the theoretical function within $1-\sigma$ for $z > 0.4$.

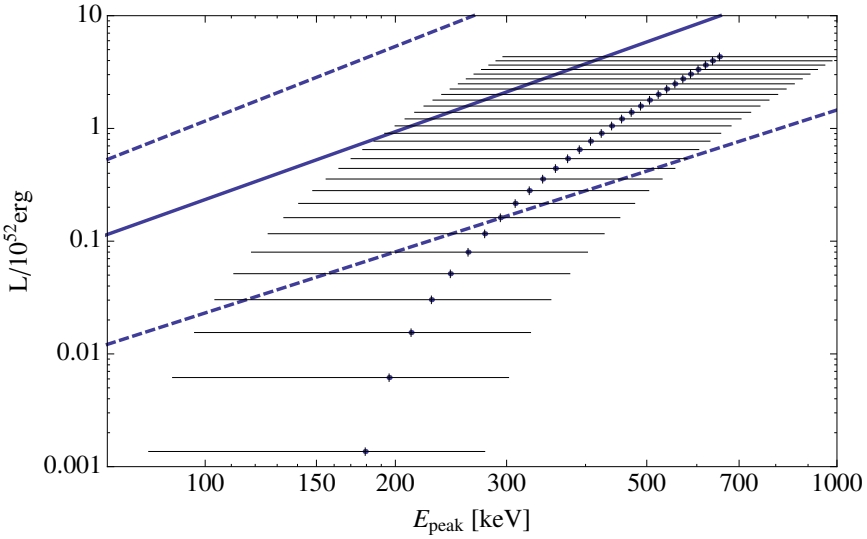

Figure 12.9.: Yonetoku relation (solid line) with its $1-\sigma$ uncertainties (doted lines) and peak Luminosity vs. $E_{p,i}$ for GRB 110709B, for different values of the redshift, from 0.1 to 3, at steps of 0.1. We can see that the data matches the theoretical function within $1-\sigma$ for $z > 0.6$.

cause this is a better distance indicator than the burst average luminosity. However, we took a 10s interval around the most intense peak in order to better constrain the value of the parameters (i.e., to increase the number of photons in the spectrum and obtain an error which is smaller than the value of the parameters). The peak luminosity in the rest frame (with the proper K-correction) can be calculated as

$$L = 4\pi d_L^2 F_{bol}, \tag{12.4.8}$$

where

$$F_{bol} = P_{obs} \frac{\int_{1/(1+z)}^{10000/(1+z)} EN(E)dE}{\int_{E_{min}}^{E_{max}} N(E)dE} \tag{12.4.9}$$

is the energy flux and P_{obs} is the photon flux.

Fig. 12.9 shows the Yonetoku relation (solid line) with its uncertainties (dotted lines), and the values of L and $E_{p,i}$ for each value of z, from 0.1 to 3, at steps of 0.1. We see that the Yonetoku relation is satisfied within 1σ for values of the redshift > 0.7, consistent with the results obtained with the Amati relation.

In conclusion, if we put together the three methods, we have a range of possible redshifts of $0.7 < z < 1.35$.

12.4.4. Estimate of the redshift using the X-ray afterglow

We already presented in (Penacchioni et al., 2012) a method to estimate the redshift of GRB 101023 by comparing its X-ray light curve to the one of GRB 090618, of known redshift ($z = 0.54$). Here we rescale the X-ray light curve of GRB 090618 as if it was seen at different redshifts and plot it together with GRB 110709B light curve, looking for the values of z for which these light curves overlap at late times. We find a remarkable consistency between this method and the phenomenological methods already mentioned.

In oder to compare in a common rest frame the two emissions from the GRBs, we apply the following operations only to GRB 090618:

1) determination of the starting time T_{start} of the late decay emission,

2) spectral analysis of this emission with an absorbed power-law model,

3) extrapolation of this spectral model in a common cosmological rest-frame energy range and, consequently, rescaling of GRB 090618 light curve for the different energy ranges,

4) cosmological correction for the arrival time by taking into due account the different scaling due to cosmological redshift, and

5) correction of the observed flux by changing the redshift of GRB 090618.

A detailed description of the method will be given in a forthcoming publication (Pisani et al., in preparation).

In this way we compare directly both light curves for different redshifts of GRB 090618. Fig. 12.10 shows GRB 090618 light curve seen as if the source was located at different redshifts: 0.2 (blue), 0.4 (green), 0.7 (grey), 1.0 (orange) and 2.0 (purple). The red light curve corresponds to GRB 110709B. We can see that it lies between the green and the orange ones. A more accurate scaling of the late X-ray afterglow suggests a redshift of $z = 0.75$ for this source.

Fig. 12.11 shows the superposition of GRB 110709B and GRB 090618 light curves in the observer frame, as if they were located at a redshift $z = 0.75$.

There is however a second aspect which is due to the peculiarity of the turn-on T_0 of the XRT detector. At the time BAT triggered for the second time, XRT was already pointing at the source and was able to detect the emission at very early times, making this GRB probably the first for which XRT has the earliest detection up to date. We need to shift GRB 110709B light curve in order to make the early steep decays (originating in the prompt in our interpretation) coincide. This is done by adding a time $T_* = +800$ s to GRB 090618 light curve. The superposition is very good. In this way we also make the early decays coincide. This factor is arbitrary, but we need to include it because GRB 110709B XRT light curve presents many spikes at the beginning, which according to our interpretation correspond not to the steep decay of the X-ray light curve but to the prompt emission.

In the case of GRB 110709B, thanks to the fact that XRT was already active and collecting data at the time of the second BAT trigger, we were able to

follow the behavior of the whole GRB emission of Episode 2. This is a key point to our understanding of GRB 110709B, since only in very few cases XRT had a response during the early emission.

In the big flare at $\sim$ 1000 s after the first BAT trigger we notice a strong correlation between the emission in X-rays and in γ-rays. We identify this emission as the prompt emission of Episode 2. After this prompt phase the traditional plateau phase is observed. After the plateau phase, there is the late decay phase in the X-ray light curve following a power-law behavior which has already been observed in other sources (i.e., GRB 101023, GRB 090618, GRB 111228). We study this decay in the IGC paradigm, and consider the possibility that it is produced by the early emission of the newly-born NS. It is interesting to notice that in GRB 110709B the typical flare in X-rays just preceding the plateau phase and following the prompt emission is not observed. This X-ray emission usually occurs without any associated γ-ray emission, since the data is usually below the BAT threshold. In the present case, it is conceivable that the flaring indeed occurred during some of the gaps of $\sim$ 4000 s in which there is no data due to Earth occultation.

We can then distinguish two types of flares in the X-ray light curve. The first type occurs at early times, previous to the steep decay, and belongs to the prompt emission. This flares can be seen in X-rays only when XRT starts its detection at early enough times, e.g., when the satellite was already pointing at a region near the burst position and did not need much time to slew. The light curve in X-rays generally follows the trend of the light curve in γ-rays. The second type of flares occurs at later times, just preceding the plateau phase. This flares are seen only in X-rays since their photon flux is much lower than the BAT threshold. In the ICG paradigm, we interpret this flares as possible indicators of the breakout of the SN.

We are currently analyzing more sources in the catalogue by Margutti et al. (2013) to look for these three very distinct phases, i.e., the flares in the prompt emission, the flares in the afterglow and the late decay after the plateau, each of them having a different physical origin within the IGC paradigm.

12.5. Episode 1: radius of the emitting region

With the knowledge of the redshift and the parameters of the fit with a BB + PL model, we computed the isotropic energy of the whole Episode 1, $E_{iso}^{(1)} = 1.42 \times 10^{53}$ erg.

With the energy flux of the BB component ϕ_{BB} as a function of time from the time-resolved spectral analysis and the luminosity distance d_L, we can compute the value of the radius of the emitter in cm (we then express it in km in Fig. 12.12) through

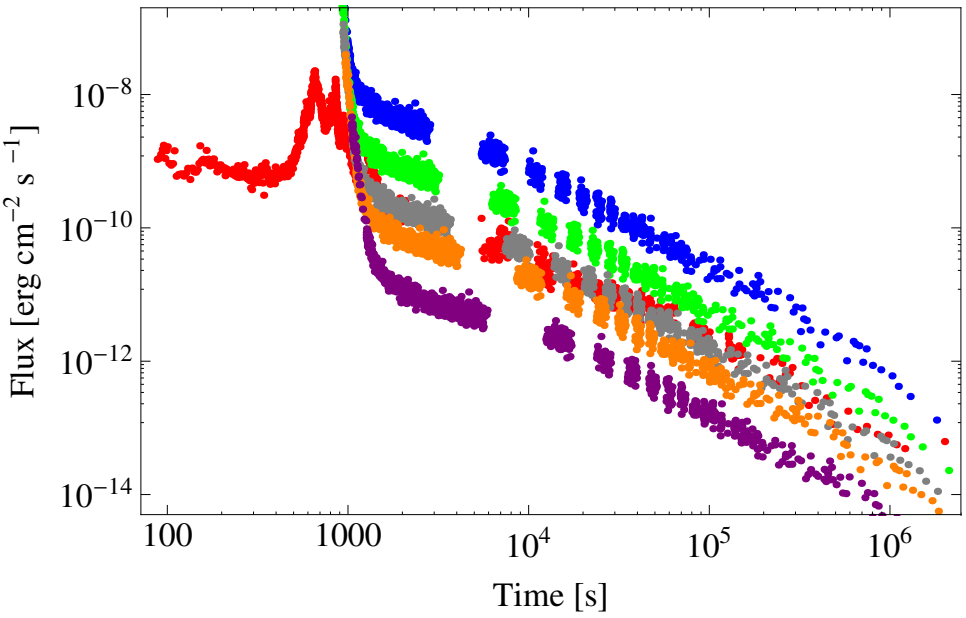

Figure 12.10.: Plot of GRB 090618 seen as if it was at different redshifts: 0.2 (blue), 0.4 (green), 0.7 (grey), 1.0 (orange) and 2.0 (purple). The red light curve corresponds to GRB 110709B. We can see that it lies between the green and the orange light curves, indicating that the redshift must be between 0.4 and 1.0.

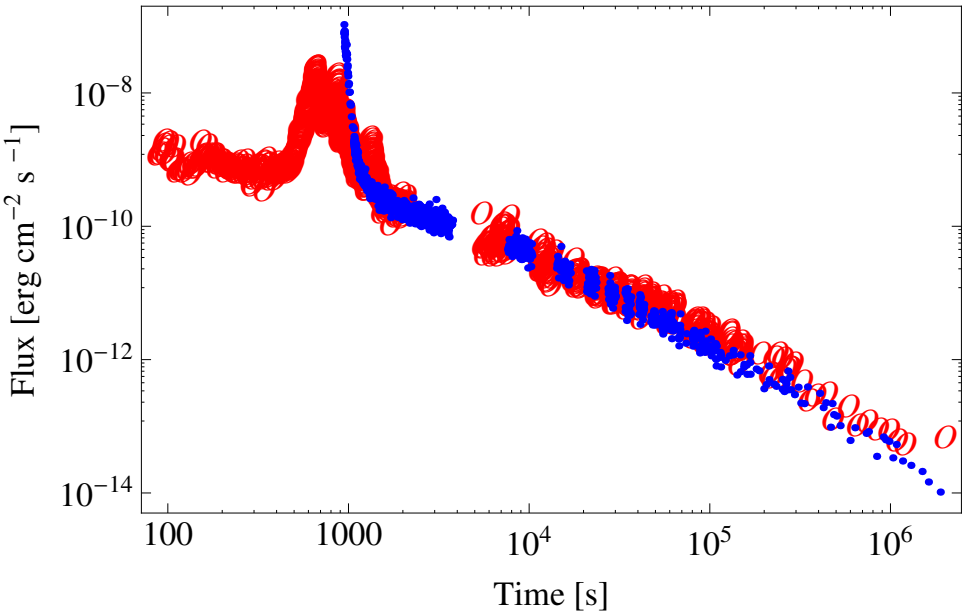

Figure 12.11.: GRB 090618 light curve (blue) as if it was seen at $z = 0.75$ together with GRB 110709B light curve (red). There is an excellent superposition in the late decay assuming a temporal shift of GRB 090618 of $T_* = 800$ s to the right to have the coincidence of the steep decays of the light curves.

$$r_{em} = \sqrt{\frac{\phi_{BB}}{\sigma T^4}} \frac{d_L}{(1+z)^2}. \tag{12.5.1}$$

Here ϕ_{BB} is the BB flux in units of $erg\ cm^{-2}s^{-1}$, $\sigma = 5.6704\ erg\ cm^2s^{-1}K^{-4}$ is the Stefan-Boltzmann constant and d_L is the luminosity distance in cm.

The best fit of the expanding radius is

$$r(t) = at^b, \tag{12.5.2}$$

where $a = (1.5 \pm 1.2) \times 10^4$ km s^{-b} and $b = 0.32 \pm 0.27$ (see Fig 12.12).

We associate the BB component to the expansion of the ejected material, while the power-law is associated (as we interpret from the IGC paradigm) with the accretion of part of this material onto the NS companion.

12.6. Analysis of Episode 2 in the Fireshell model

We recall that the Fireshell model (Damour and Ruffini, 1975; Ruffini et al., 2000; Ruffini, 2001; Ruffini et al., 2010e) is an alternative to the Fireball model, first proposed by Cavallo and Rees (1978), Goodman (1986) and Paczynski (1986). We assume, within the Fireshell model, that all GRBs originate from

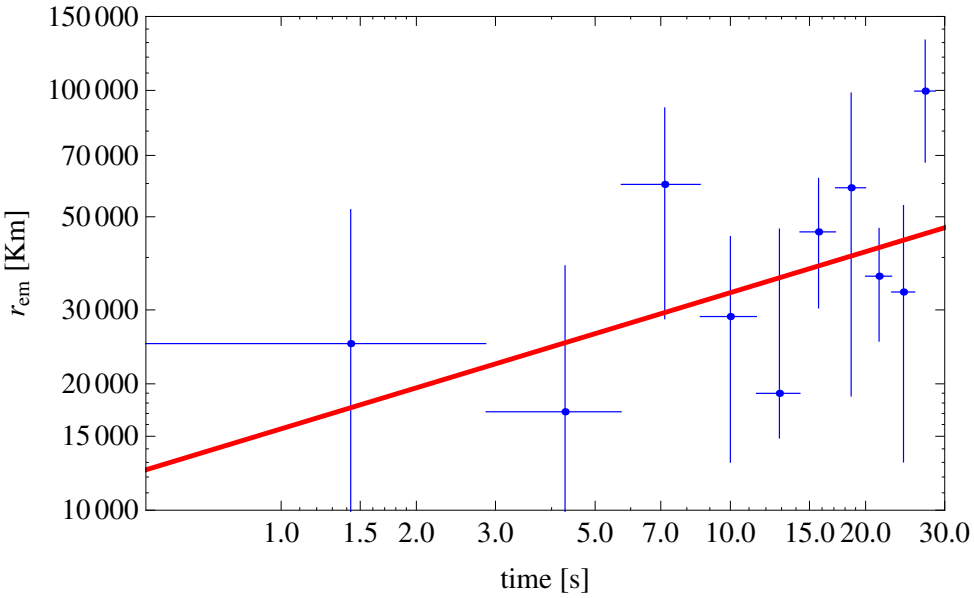

Figure 12.12.: Radius of the emitting region as a function of time (in the cosmological rest frame), corresponding to Episode 1. The radius increases with time following a power-law at^b, with $a = (1.5 \pm 1.2) \times 10^4$ km/s and $b = 0.32 \pm 0.27$.

the gravitational collapse of a star approaching asymptotically the formation of a Kerr-Newmann BH (Ruffini, 2009b). An electric field E is created just outside the collapsing core and in between the expanding outer shells that act as a capacitor (Preparata et al., 1998). This electrical field grows until it reaches a critical value, $E_c = m^2c^3/\hbar e$. At this time, vacuum polarization occurs, leading to pair creation at the expenses of the gravitational energy. An optically thick $e^\pm$ plasma forms with total energy $E^{e^\pm}_{tot}$ in the range 10^{49} - 10^{54} erg. The $e^\pm$ plasma reaches thermal equilibrium on a timescale of 10^{-12} s (Aksenov et al., 2007). Being optically thick, the plasma self-accelerates due to its internal radiation pressure (Ruffini et al., 1999b,a). After an early expansion in vacuum, the $e^\pm$-photon plasma engulfs the baryonic matter M_B of the outer shells and reaches thermal equilibrium with it. The baryonic matter is described by the dimensionless parameter $B = M_Bc^2/E^{e^\pm}_{tot}$. B must be less than 10^{-2}, otherwise there will not be any relativistic expansion (Ruffini et al., 2000). The optically thick fireshell composed by $e^\pm$-photon-baryon plasma self-accelerates to ultrarelativistic velocities, finally reaching the transparency condition. A flash of radiation is then emitted. This is the P-GRB (Ruffini et al., 2001b). The amount of energy radiated in the P-GRB is only a fraction of the initial energy $E^{e^\pm}_{tot}$. The remaining energy is stored in the kinetic energy of the optically thin baryonic and leptonic matter fireshell that expands ballistically and starts to slow down due to the inelastic collisions with the Cir-

cumburst Medium (CBM). This interaction gives rise to a multi-wavelength emission, the extended afterglow (Ruffini et al., 2001b). We can estimate the characteristic inhomogeneities of the CBM by fitting the luminosity of the X-ray source and imposing the fully radiative condition in the collision between the ultra relativistic baryonic shell and the clouds of the Interstellar Medium (ISM). The complete analytic solution has been developed in Bianco and Ruffini (2004, 2005a,b), together with the analytic expression of the Surfaces of Equal arrival Time of the photons at the detector (EQTS). The afterglow presents three different regimes: a rising part, a peak and a decaying tail. We therefore define a "canonical GRB" light curve with two sharply different components: 1) the P-GRB and 2) the extended afterglow. What is usually called "Prompt emission" in the current GRB literature mixes the P-GRB with the raising part and the peak of the extended afterglow (Ruffini et al., 2003a). The spectrum of the extended afterglow is initially assumed to be thermal in the comoving frame of the expanding shell. Recently, after the analysis of some highly energetic sources observed by *Swift* and *Fermi* satellites, this assumption of a pure comoving thermal spectrum has been relaxed and a phenomenological modification by a power-law of the low energy spectral slope has been introduced (Patricelli et al., 2012). The observed non thermal spectrum shape is due to a double convolution of thousands of instantaneous comoving spectra, with different temperatures and different Doppler factors, over both the EQTS and the observation time (Ruffini et al., 2004b).

Having fixed the value of the redshift to $z = 0.75$, we started the analysis of Episode 2 within the Fireshell model. We first looked for the P-GRB during the first bump of Episode 2 (from 100 to 40 s before the second trigger) by fitting the data with a BB + PL model. We selected several time intervals as the P-GRB during the first bump of Episode 2, but in some cases the fits were not good. In some other cases, to reproduce the ratio between the P-GRB energy and the total energy we needed to consider a baryon load $B > 10^{-2}$ (which has no sense within the Fireshell model) and, in other cases, there was a discrepancy between the observed temperature and the one given by the simulation. Thus we concluded that this bump should belong to Episode 1. The reason why we do not find a strong thermal signature in this bump is that Episode 1 starts ~ 10 minutes before the beginning of the bump and the temperature of the BB component decreases very rapidly following a power-law in the first seconds of emission.Consequently, after such a long time we do not expect to find any signature of a BB from Episode 1.

We finally selected the P-GRB as the 9 s from 35 to 26 s before the second trigger, and the following emission from -26 to 100 s as the afterglow. Table 12.3 shows the parameters of the fit. We calculated a P-GRB energy of $E_{P-GRB} = 3.44 \times 10^{50}$ erg and an isotropic energy of $E_{iso} = 2.43 \times 10^{52}$ erg.

We inserted these values of the energies into our numerical code and calculated the value of the baryon load, $B = 5.7 \times 10^{-3}$. We simulated the light

Table 12.3.: Fit of the P-GRB and the afterglow of GRB 110709B, Episode 2. The P-GRB is well fit with a BB model, while the whole Episode 2 is best fit by a CutoffPL model. From this fit and the value of the redshift we are able to calculate E_{iso} and E_{P-GRB}.

Parameter	P-GRB	P-GRB+Afterglow
kT [keV]	14 ± 1	
BB Amp	0.30 ± 0.02	
γ		1.03 ± 0.1
PL Amp		0.5 ± 0.1
Red χ^2	1.448 (56 DOF)	0.77 (55 DOF)
Energy Flux $(15-150$ keV) [erg cm^{-2} s^{-1}]	2.413×10^{-8}	6.34×10^{-8}
Energy [erg]	3.44×10^{50}	2.43×10^{52}

curve and the spectrum, obtaining, at the transparency point, a Laboratory Radius $r_{tr} = 6.04 \times 10^{13}$ cm, a gamma Lorentz factor $\Gamma = 1.73 \times 10^2$ and a P-GRB observed temperature (after cosmological correction) $kT = 12.36$ keV.

Figs. 12.13a and 12.13b show the simulation of the light curve and the spectrum of Episode 2, respectively. The photon index of the XRT and BAT spectra are in agreement with that predicted by the simulation. Details of this calculation will be given in a forthcoming letter (Penacchioni et al., in preparation). Fig. 12.14 shows the density mask of the ISM, i.e., the density of particles of the interstellar clouds as a function of the distance to the center of the BH. This density has to be interpreted as an effective density because fragmentation may occur in the expanding shell (Ruffini et al., 2007c; Dainotti et al., 2007).

12.7. Nature of the Progenitor

Following the works of Rueda and Ruffini (2012b) and Izzo et al. (2012a), we suggest for the origin of GRB 110709B a binary system formed by a massive evolved star on the verge of a SN explosion and a NS. The early-SN material expanding at non-relativistic velocities is then accreted by the NS companion at times larger than $t_{0,\mathrm{accr}}$, when the material reaches the NS gravitational capture region. The emission observed in Episode 1 is associated to this early-SN evolution, identified with the thermal component, and accretion process onto the NS, possibly related to the non-thermal component. The NS reaches in a time $t_{0,\mathrm{accr}} + \Delta t_{\mathrm{accr}}$ the critical mass and gravitationally collapses to a black hole, emitting the GRB seen in Episode 2. We assume the critical mass of a non-rotating NS $M_{\mathrm{crit}} = 2.67 M_\odot$ as given by Belvedere et al. (2012).

The amount of material that reaches the NS gravitational capture region

$$R_{\mathrm{cap}}(t) = \frac{2GM_{\mathrm{NS}}(t)}{v^2_{\mathrm{ej,rel}}(t)} \tag{12.7.1}$$

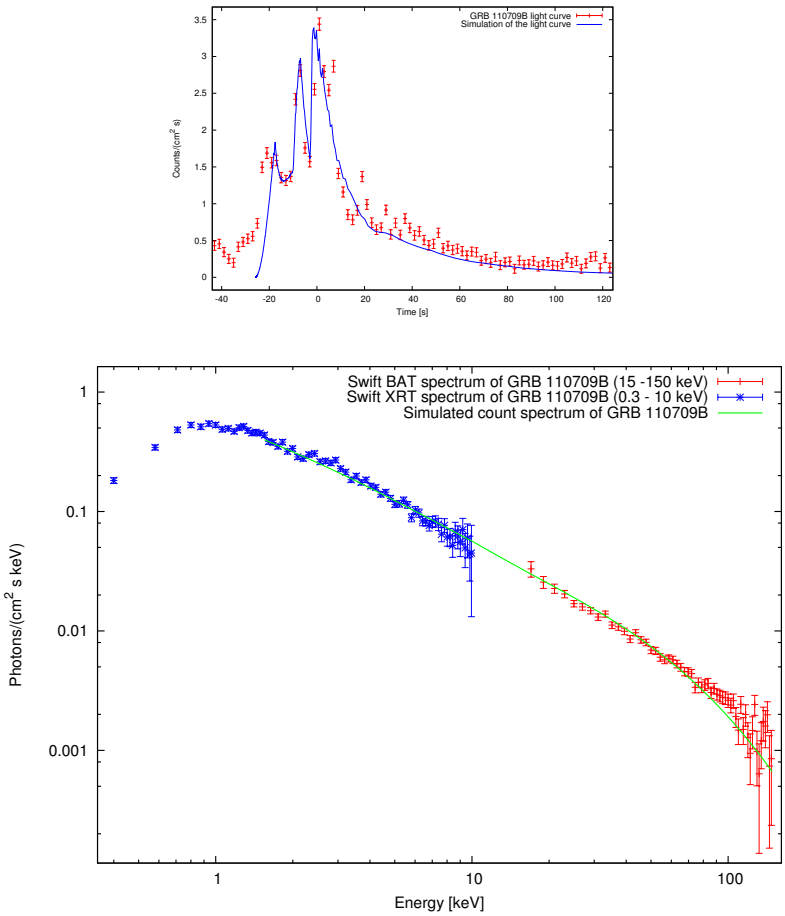

Figure 12.13.: Simulation of the BAT (a) light curve and (b) spectrum of Episode 2. We included XRT data in the fit of the spectrum to show that the slope predicted in the fireshell model is in agreement with the slope of the X-ray spectrum.

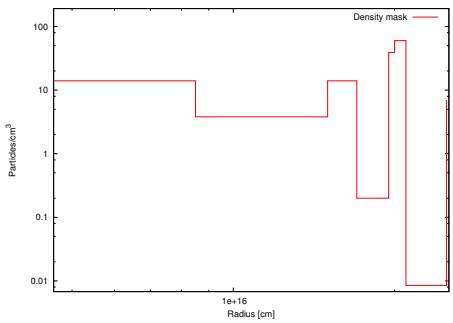

Figure 12.14.: Particle density of the ISM clouds as a function of the distance. The mean density is 76 part/cm^3.

per unit time is given by (see Rueda and Ruffini (2012b) and Izzo et al. (2012a))

$$\dot{M}(t) = \pi \rho_{\rm ej}(t) v_{\rm ej,rel}(t) R^2_{\rm cap}(t), \tag{12.7.2}$$

where $R_{\rm cap}$ is measured from the NS center.

In these expressions, $\rho_{\rm ej}(t) = 3M_{\rm ej}(t)/(4\pi r^3_{\rm ej}(t))$ is the density of the ejecta,

$$M_{\rm ej}(t) = M_{\rm ej}(0) - M(t) \tag{12.7.3}$$

is the total available mass to be accreted by the NS, $M_{\rm NS}(t)$ is the NS mass, and $v_{\rm ej,rel}(t)$ is the velocity of the ejecta relative to the NS

$$v_{\rm ej,rel}(t) = \sqrt{v^2_{\rm orb,NS}(t) + v^2_{\rm ej}(t)}. \tag{12.7.4}$$

In Eq. (12.7.3), $M_{\rm ej}(0)$ is the given initial mass of the ejecta (just at the beginning of the accretion process); we choose different values for it in Table 12.4. $M(t)$ is the mass of the ejecta that is lost because it passes through the capture region of the NS.

The actual mass accretion rate onto the NS, $\dot{M}_{\rm accr}(t)$, is a fraction $\eta_{\rm accr} \leq 1$ of Eq. (12.7.2), i.e.

$$\dot{M}_{\rm accr}(t) = \eta_{\rm accr} \dot{M}(t), \tag{12.7.5}$$

where η is the accretion efficiency onto the NS. So, there is an amount of material per unit time $\dot{M}_{out}(t) = (1 - \eta_{\rm accr})\dot{M}(t)$ not accreted by the NS.

In Eq. (12.7.4), $v_{\rm orb,NS}(t) = \sqrt{G(M_{\rm prog} + M_{\rm NS}(t))/a}$ is the orbital velocity relative to the SN core progenitor, a is the separation distance between the NS and the SN core progenitor, and

$$v_{\rm ej}(t) = \frac{dr_{\rm ej}(t)}{dt} = b\frac{r_{\rm ej}(t)}{t} \tag{12.7.6}$$

is the expansion velocity of the early-SN material, where we have used $r_{\rm ej}(t) = r_{\rm em}(t)$, given by Eq. (12.5.2).

We have already mentioned that the power-law component in the spectrum of Episode 1 might be due to the accretion onto the NS companion. As this power-law component is present since the beginning of Episode 1, we have fixed the value of $t_{0,\rm accr}$ to be equal to the starting time of Episode 1. This puts a constraint in the separation distance a of the binary, which under these conditions is given by

$$a = r_0 + R_{\rm cap}(0), \tag{12.7.7}$$

where $r_0 = r_{ej}(0)$ and $R_{\rm cap}(0)$ are the radius of the early-SN ejecta and the capture radius of the NS companion at the beginning of Episode 1. In this

$M_{\rm prog}/M_\odot$	$M_{\rm ej}(0)/M_\odot$	$\rho_{\rm ej}(0)$ (g cm^{-3})	$\eta_{\rm accr}$	$\Delta M_{\rm accr}/M_{\rm ej}(0)$	P (min)	$v_{\rm orb,NS}(0)$ (km s^{-1})	$\Delta t_{\rm accr}/P$	$a/R_\odot$
4	2.7	2.39×10^5	0.92	0.47	0.52	5.24×10^3	11.14	0.037
5	3.7	3.27×10^5	0.88	0.34	0.45	5.84×10^3	12.96	0.036
6	4.7	4.16×10^5	0.88	0.27	0.39	6.39×10^3	14.71	0.035
7	5.7	5.04×10^5	0.89	0.22	0.35	6.91×10^3	16.39	0.034
8	6.7	5.93×10^5	0.91	0.19	0.32	7.40×10^3	18.00	0.033
9	7.7	6.81×10^5	0.94	0.16	0.30	7.87×10^3	19.55	0.032
10	8.7	7.69×10^5	0.96	0.15	0.27	8.32×10^3	21.04	0.031

Table 12.4.: The massive star - neutron star binary progenitor of GRB 110709B. $M_{\rm prog}$ is the mass of the massive star (in solar masses), $M_{\rm ej}(0)$ is the mass of the ejected material in the early-SN phase (in solar masses), $\rho_{\rm ej}(0)$ is the density of the ejecta at the beginning of the expansion, $\eta_{\rm accr}$ is the efficiency of the accretion process onto the NS, $\Delta M_{\rm accr} = M_{\rm crit} - M_{\rm NS}(0)$ is the total mass accreted by the NS before the collapse, $P = 2\pi a/v_{\rm orb,NS}$ is the period of the binary, $v_{\rm orb,NS}(0)$ is the initial orbital velocity of the NS and $\Delta t_{\rm accr}/P$ is the arc-length travelled by the NS during the accretion process in units of the length of the whole orbit and $a/R_\odot$ is the binary separation (in units of solar radii). We suppose that the accretion process starts 5 s before the first trigger, i.e. $t_{0,\rm accr}$ coincides with the time corresponding to the first datapoint in Fig. 12.5.

case, $r_0 \approx 1.75\times10^9$ cm, see Fig. 12.12. The separation a is a function of the initial mass of the NS and of the SN core progenitor mass, as well as of the orbital velocity, through $R_{\rm cap}$. It is clear that the constraint given by Eq. (12.7.7) is a lower limit, since the accretion process onto the NS could have been triggered before by layers at lower densities (e.g. He). In such a case, the binary separation a could be higher.

In addition to this constraint, we must take into account that the NS must reach its critical mass $M_{\rm crit}$ at the beginning of Episode 2, since by that time the NS must collapse to a BH and emit the canonical GRB. This implies that

$$\Delta t_{\rm accr} \approx \frac{611}{(1+z)} \approx 349 \text{ s}. \tag{12.7.8}$$

We show in Table 12.4 the parameters of the binary system leading to IGC of the NS in a time interval equal to the duration of Episode 1. We adopt an initial mass for the NS, $M_{\rm NS}(0) = 1.4M_\odot$ and, correspondingly, a NS radius of $R_{\rm NS}(0) = 12.3$ km from the mass-radius relation of Belvedere et al. (2012). From the constraint given by Eq. (12.7.7) we fix the binary separation a. We then proceed with the numerical integration of the accretion rate equations by requiring that $M_{\rm NS}(t) = M_{\rm crit}$ at $t = \Delta t_{\rm accr}$, given by Eq. (12.7.8), from which we obtain the efficiency $\eta_{\rm accr}$.

It is interesting to analyze how the NS can accrete such a large mass, in some cases of the order of 47% of the early-SN material (see column 5 of Table 12.4), since one could think that solid angles of $\sim$ 50% between the early-SN material and the accreting NS are hard to obtain. Indeed, during the

accretion process the NS is moving with high orbital velocities of the order of 10^8 cm s^{-1} relative to the core progenitor (see column 7 of Table 12.4), and consequently travels effective arc-lengths several times larger than the circumference of the orbit (see column 8 of Table 12.4).

Assuming that the gain in gravitational energy of the accreted material into the NS can be released from the system leads to an upper limit of the luminosity

$$|\dot{E}_b(t)| = \frac{G\dot{M}_{\rm accr}(t)M_{\rm NS}(t)}{R_{\rm NS}(t)}, \tag{12.7.9}$$

where we take into account the dependence of the NS radius with time, due to the increment of the NS mass by the accretion process. The self-consistent radius is computed at each time from the mass-radius relation of Belvedere et al. (2012).

The actual luminosity depends on the efficiency $\eta_{\rm rad}$ in converting gravitational energy into electromagnetic energy by some still unknown process. Since in our model we assume that the BB component of Episode 1 is due to the early-SN expansion, we estimate the efficiency $\eta_{\rm rad}$ from the assumption that $|\dot{E}_b|$ is responsible for the power-law luminosity $L_{\rm PL}$, namely

$$\eta_{\rm rad}(t) = \frac{L_{\rm PL}}{|\dot{E}_b(t)|}. \tag{12.7.10}$$

In Fig. 12.15 we show the evolution of the efficiency $\eta_{\rm rad}$ in the first seconds of emission for the binary systems shown in Table 12.4. We assume a constant and isotropic power-law luminosity of Episode 1, $L_{\rm PL} \approx 1.8 \times 10^{50}$ erg s^{-1} $\approx$ $10^{-4}\ M_\odot$ s^{-1}, as found from the spectral analysis. For all the cases, we obtain the same evolution of the efficiency with time, i.e. the curves overlap. This is due to the fact that we constrained all the systems to have the same initial NS mass and $\Delta t_{\rm accr}$.

12.8. Radio observations

Zauderer and Berger (2011) report observations with the EVLA radio telescopes on several occasions between 11 and 16 July, at a frequency of 5.8 GHz. They found a radio source which brightened by about a factor of 1.6, between 2.1 and 7 days after the burst. The coincidence with the XRT position and the rising flux indicate that this is the radio afterglow of GRB 110709B. The position of the source is RA = 10:58:37.114, DEC = -23:27:16.760. We show in Fig. 12.16 the 5.8 GHz light curve presented in Zauderer et al. (2013), where there is evidence of a radio bump. Following the work of Chevalier and Soderberg (2010), we have reproduced the plot of the peak spectral radio Luminosity per unit frequency as a function of time (days) at which the peak

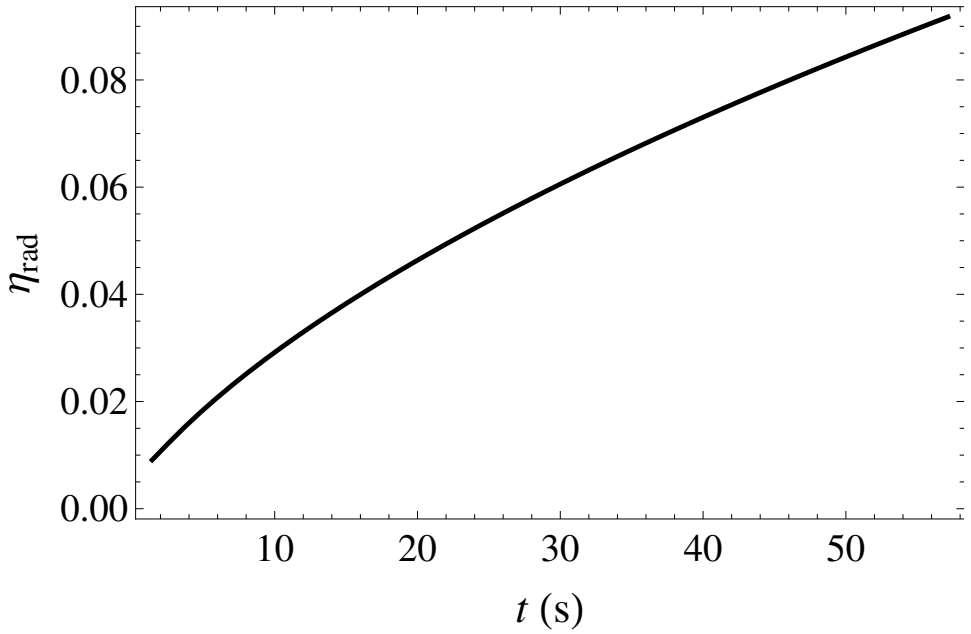

Figure 12.15.: Theoretical estimation of the efficiency $\eta_{\rm rad}$ given by Eq. (12.7.10) of the process to convert gravitational energy in radiation as a function of time. For this plot, we have assumed a constant and isotropic power-law luminosity of Episode 1, $L_{\rm PL} \approx 1.8 \times 10^{50}$ erg s^{-1} $\approx 10^{-4}\ M_\odot$ s^{-1}. We computed the values of the efficiency for the binary systems shown in Table 12.4. For all the cases, we obtain the same evolution of the efficiency with time, i.e. the curves overlap. The values of $\eta_{\rm rad}$ are always $< 10\%$.

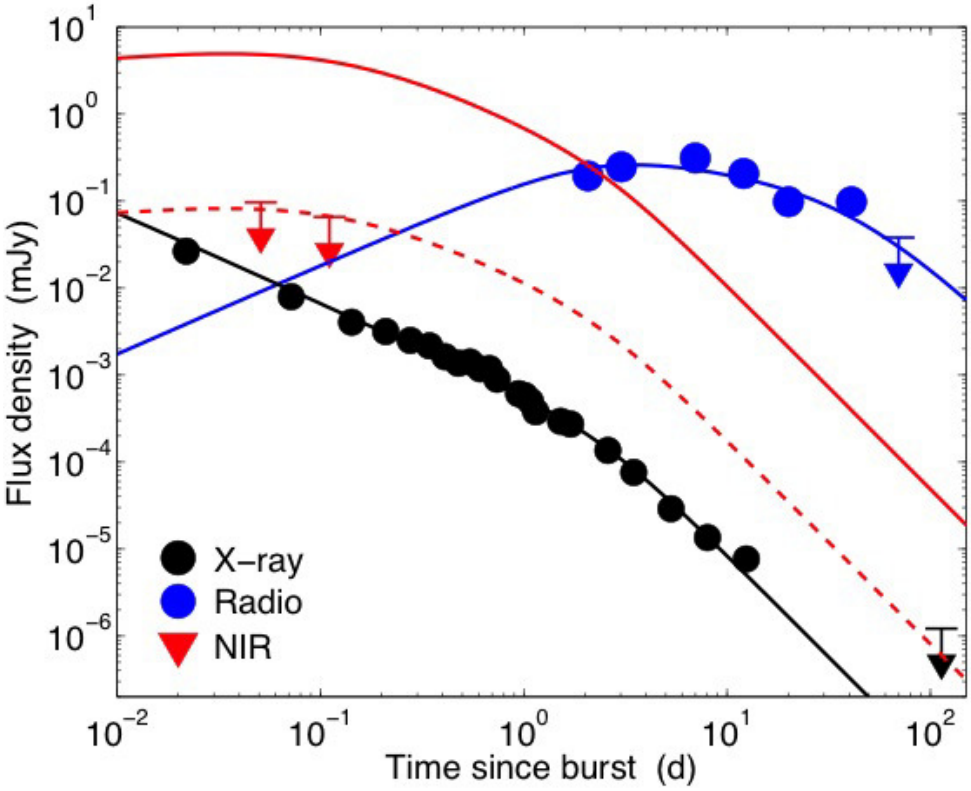

Figure 12.16.: X-Ray (black), radio (blue) and NIR (red, upper limits) light curves of GRB 110709B. Taken from Zauderer et al. (2013) with kind permission.

is produced for different SN associated with GRBs, including GRB 110709B (see Fig. 12.17). We find that the radio emission of this source is higher than the ones associated with typical SN.

12.9. Conclusions

GRB 110709B is a very peculiar source, since it is the first for which Swift BAT has triggered twice. Its *Swift* BAT light curve presents two well defined episodes, Episode 1 and Episode 2. Episode 1 lasts 100 s and Episode 2 lasts 135 s. Particularly interesting is the fact that the X-ray observations started well before the second trigger. The light curve and spectrum of this source share similar characteristics with GRB 090618 (Izzo et al., 2012a), GRB 101023 (Penacchioni et al., 2012) and GRB 970828 (Izzo et al., 2012b). It has been recently shown that these GRBs which show such distinct emissions, Episodes 1 and 2, form a new family of GRBs described by the IGC paradigm (Rueda and Ruffini, 2012b; Izzo et al., 2012a). Within this scenario, the GRB originates in a binary system formed by a massive star on the verge of a SN and a NS

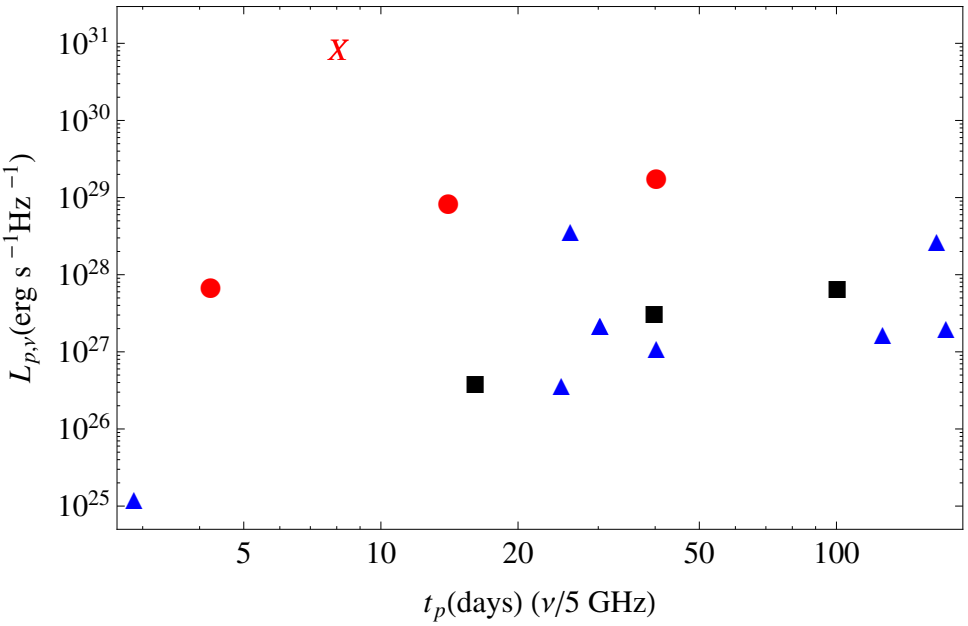

Figure 12.17.: Plot of the peak spectral radio Luminosity per unit frequency versus the time at which the peak occurs, for different SN associated to GRBs. The circles represent the SN emission associated to SN 2006aj (GRB 060218), SN 1998bw (GRB 980425) and SN 2003lw (GRB 031203). The triangles represent the SN Ib/c for which there are radio observations, namely SN 2002ap, SN 1990B, SN 2008D, SN 1994I, SN 2009bb and SN 2003L. The squares represent the SN IIb: SN 2008ax, SN 2001ig, SN 1993J, SN 2001gd and SN 2003bg. The red cross is the luminosity related to GRB 110709B afterglow. It is higher than the emissions of the other SN, considered "standard".

close to its critical mass for the gravitational collapse to a BH. The compact core SN progenitor ejects material in the very early phases of the SN explosion, that is then accreted by the NS; this process is identified with Episode 1. The accretion process onto the NS brings it to the critical mass, leading to its gravitational collapse to a BH and emitting the GRB, identified with Episode 2. Later on, we see a standard emission in X-rays, which we have called Episode 3. Several days after the burst, when it is present, we see an optical emission, associated to the SN (Episode 4). Following the recent works on GRB 090618 (Izzo et al., 2012a) and GRB 970828 (Izzo et al., 2012b), we here apply the IGC paradigm to GRB 110709B.

The redshift of GRB 110709B is unknown, so in Section 12.4 we used four phenomenological methods to constrain it; i.e., Grupe (Grupe et al., 2007b), Amati (Amati, 2006), Yonetoku (Yonetoku et al., 2004) and the scaling of the X-Ray afterglow (Izzo et al., 2012e; Penacchioni et al., 2012). The first method gives an upper limit of $z < 1.35$. The second and third methods give a lower limit of $z > 0.6$ and $z > 0.7$, respectively. The last method gives a precise value of $z = 0.75$, which lies within the range determined by three the above mentioned methods. We then fixed this last value as the redshift of GRB 110709B.

The spectral analysis of Episode 1 is given in Section 12.3.1 and 12.5. We find a value of the isotropic energy for Episode 1 of $E_{iso}^{(1)} = 1.42 \times 10^{53}$ erg (see Table 12.1). We fit the spectrum with a BB+PL model. The temperature of the BB component evolves with time following a broken power-law (see Fig. 12.5). The corresponding radius of the BB emitter evolves in time following a power-law given in Eq. (12.5.2) and shown in Fig. 12.12. We associate this radius and the BB component to the evolution of the SN ejecta, while the power-law is associated to the accretion of the ejected material onto the NS companion.

Episode 2 is analyzed in Sections 12.3.2 and 12.6. We find an isotropic energy of $E_{iso}^{(2)} = 2.43 \times 10^{52}$ erg (see Table 12.3). We interpret this episode as a canonical GRB and simulated its light curve and spectrum within the Fireshell model. We find at transparency a Lorentz factor $\Gamma \sim 1.73 \times 10^2$, laboratory radius of 6.04×10^{13} cm, P-GRB observed temperature $kT_{P-GRB} = 12.36$ keV, baryon load $B = 5.7 \times 10^{-3}$, P-GRB energy of $E_{P-GRB} = 3.44 \times 10^{50}$ erg, and a CBM mean density 76 part cm^{-3}. This value is consistent with a "dark GRB", as cited in Zauderer et al. (2013). The lack of detection of a SN emission for this particular GRB could be due to obscuration by the circumstellar dust in the host galaxy.

The nature of the progenitor is discussed in Section 12.7. We indicate that it is a binary system formed by a massive evolved star on the verge of a SN explosion and a NS. We associate the thermal component of Episode 1 mainly with the early-SN evolution and the power-law component to the accretion process onto the NS. There is the possibility that also the accretion process

has a thermal contribution. The energy due just to the thermal component is of the order of 10^{50} erg, which is reasonable for the expansion of the early-SN ejecta. We perform all the necessary calculations to obtain the parameters of the binary system. For all our calculations we assume a fixed NS mass of $1.4 M_{\odot}$. We compute the rate at which the early-SN material enters the capture region, for given values of the SN core progenitor mass. From this material, only a fraction will be accreted by the NS, so we introduced an efficiency factor $\eta_{\rm accr}$. As the power-law component is present since the beginning of Episode 1, we suppose that this episode starts at the same time $t_{0,\rm accr}$ as the accretion process, namely, when the outermost shell of expanding ejecta reaches the capture radius $R_{\rm cap}$ of the NS (measured from the center of the NS). This puts a constraint on the separation distance a of the binary. In addition, the NS must reach its critical mass and collapse to a BH at the beginning of Episode 2. This puts a constraint on the duration of the accretion process $\Delta t_{\rm accr}$. By integrating the accretion rate equations with these boundary conditions we obtain the efficiency $\eta_{\rm accr}$. We summarize the results in Table 12.4, for different values of the core-progenitor mass and the density of the early-SN ejecta. Assuming that the power-law radiation comes from the conversion of the binding energy of the accreted material onto the NS, we estimate the efficiency $\eta_{\rm rad}$ of this conversion process, which we show in Fig. 12.15 for an isotropic power-law luminosity $L_{\rm PL} \approx 1.8 \times 10^{50}$ erg $\rm s^{-1} \approx 10^{-4}\ M_{\odot}\ s^{-1}$ observed in Episode 1. For the parameters of the binary system shown in Table 12.4, we obtain values of $\eta_{\rm rad} < 10\%$. The efficiency of the radiation mechanism can be even lower if some beaming or boosting is present. However, we did not address any such possible mechanism in this work.

In section 12.8 we present the radio observations of GRB 110709B with the EVLA radio telescopes and the X-ray, radio and NIR light curves taken from Zauderer et al. (2013). We notice the presence of a bump in the radio afterglow, at ≈ 10 days after the burst. As GRB 110709B has been classified as an optically dark burst, we plotted the peak spectral radio luminosity per unit frequency as a function of time and compared it with the luminosities of typical SNe, to see if it was possible to find any coincidences that may indicate the presence of the SN in the radio band. However, the luminosity we find is much higher than the ones of the standard SNe.

We interpret, within the IGC paradigm, that GRB 110709B is a new member of the IGC family, in addition to GRB 090618, GRB 101023 and GRB 970828.

A remarkable support of the above IGC paradigm comes from the observations of the X-ray afterglow emission of these systems. The X-Ray light curve is composed of an early steep decay, a plateau and a late decay. The analysis of the late decay of the afterglow luminosity has been identified with the cooling of the newly born NS, left by the SN explosion (Negreiros et al., 2012).

13. GRB 090510: a disguised short GRB with the highest Lorentz factor and circumburst medium.

13.1. Introduction

In their earliest classification of the 4BATSE catalog (Meegan, 1997), all GRBs have been classified in short and long bursts being their T_{90} duration longer or shorter than 2 s (Klebesadel, 1992; Dezalay et al., 1992; Kouveliotou et al., 1993; Tavani, 1998). In the meantime, short bursts have been shown to originate from a variety of astrophysical origins and not form a homogeneous class. In the Fireshell model (Ruffini et al., 2001a,a,c, 2010e), the canonical GRB has two components: an emission occurring at the transparency of the optically thick expanding e^+e^--baryon plasma (Ruffini et al., 2000), the Proper-GRB (P-GRB), followed by the extended afterglow, due to the interactions between the accelerated baryons and the CircumBurst Medium (CBM). Such an extended afterglow comprises the prompt emission as well as the late phase of the afterglow (Bianco and Ruffini, 2005a,b). The relative energy of these two components, for a given total energy of the plasma $E^{tot}_{e^+e^-}$, is uniquely a function of the baryon load $B = M_B c^2 / E^{tot}_{e^+e^-}$, where M_B is the total baryons mass (see Fig. 13.1, left panel).

The genuine short GRBs (Ruffini et al., 2001a) are the bursts occurring for $B \lesssim 10^{-5}$. The first example of such systems has indeed been recently identified, originating in a binary neutron star merger (Muccino et al., 2013).

It has been also proved the existence of disguised short GRBs, with baryon load $3 \times 10^{-4} \leq B \leq 10^{-2}$ (Bernardini et al., 2007, 2008b). In this class the extended afterglow is indeed energetically predominant but results in a "deflated" emission, less intense than the P-GRB, due to the low density of the CBM, $\langle n_{CBM} \rangle \approx 10^{-3}$ particle/cm^3, much lower than the canonical value $\langle n_{CBM} \rangle \approx 1$ particle/cm^3. The majority of the declared short bursts in the current literature appears to be disguised short GRBs (Bernardini et al., 2007, 2008b; Caito et al., 2009, 2010; de Barros et al., 2011).

In this paper we show a yet different kind of a disguised short, GRB 090510, again, with $3 \times 10^{-4} \leq B \leq 10^{-2}$ and Lorentz factor $\Gamma_{tr} \approx 700$, occurring

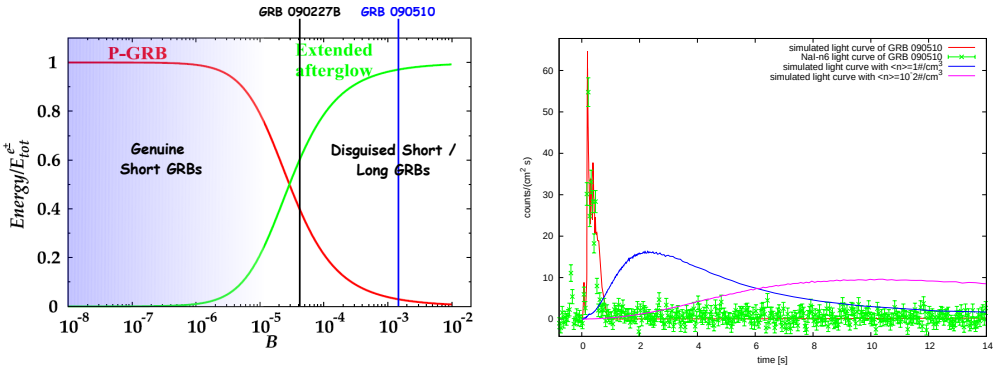

Figure 13.1.: Left panel: the energy emitted in the extended afterglow (green curve) and in the P-GRB (red curve) in units of $E^{tot}_{e^+e^-}$ are plotted as functions of B. The values of B of GRB 090510 (in blue) and of the genuinely short GRB 090227B (in black) are compared. Right panel: the 50 ms time-binned NaI-n6 light curve (green data) and the extended afterglow simulations corresponding to CBM average densities of a "disguised short GRB by excess" with $\langle n_{CBM}\rangle \approx 10^3$ particles/cm^3 (red curve), of a canonical long GRB with $\langle n_{CBM}\rangle = 1$ particle/cm^3 (blue curve), and of a "disguised short GRB by defect" with $\langle n_{CBM}\rangle = 10^{-2}$ particles/cm^3 (purple curve). For larger densities the extended afterglow compresses in time and "inflates" in intensity.

in a medium with $\langle n_{CBM}\rangle \approx 10^3$ particles/cm^3. We define, indeed, these GRBs as "disguised short burst by excess", being their $\langle n_{CBM}\rangle$ much larger than the canonical one. Correspondingly, we indicate the disguised short with a CBM density typical of the galactic halo environments, $\langle n_{CBM}\rangle \approx 10^{-3}$ particles/cm^3, as "disguised short GRBs by defect" (see Fig. 13.1, lower panel).

The possibility of GRBs exploding in high density CBM has been already considered in literature (Dai and Lu, 1999; Lazzati et al., 1999; Piro et al., 2001; Wang et al., 2003; Prochaska et al., 2008; Izzo et al., 2012b). In Dai and Lu (1999); Piro et al. (2001); Wang et al. (2003), the high density has been inferred from the steepening in the afterglows, respectively, of GRB 990123 in the R-band about $\sim$ 2.5 days after the burst, of GRB 000926 in the R-band after $\sim$ 2 days, and of GRB 990705 in the H-band after $\sim$ 1 day, due to the transition to the nonrelativistic regime of the fireball. Lazzati et al. (1999) discuss the possibility that the detection of Fe lines in the afterglows of GRB 970508 and GRB 970828 could be due to recombination processes in extremely high densities during the X-ray afterglow. In Prochaska et al. (2008), the authors inferred dense environments, $n \gtrsim 10^3$ particles/cm^3, from a survey for NV absorption in GRBs afterglow spectra. In particular, in Izzo et al. (2012b) the Fireshell model has been applied in the analysis of GRB 970828, discussed also in Lazzati et al. (1999), inferring a dense environment with $\langle n_{CBM}\rangle = 3.4 \times 10^3$ particle/cm^3, consistent with the large column density

environment in Yoshida et al. (2001). In the case of GRB 090510 the joint effect of the very dense CBM and the high Lorentz factor at the transparency, $\Gamma_{tr} \sim 700$, leads to an extended afterglow with $T_{90} < 2$ s (see Fig. 13.1, lower panel). These high values of the CBM density n_{CBM} and of the Lorentz factor Γ_{tr} may represent an important step towards the explanation of the GeV emission.

The work is organized as follow: in Sec. 13.2 we present the data analysis of GRB 090510; in Sec. 13.3 we give our theoretical interpretation on the source; in Sec. 13.4 we summarize our conclusions.

13.2. GRB 090510 Data Analysis

At 00:22:59.97 UT on 10^{th} May 2009, the Fermi-GBM detector (Guiriec et al., 2009) triggered and located the short and bright burst, GRB 090510, which was also detected by Swift (Hoversten et al., 2009), Fermi-LAT (Ohno and Pelassa, 2009), AGILE (Longo et al., 2009a), Konus-Wind (Golenetskii et al., 2009c), and Suzaku-WAM (Ohmori et al., 2009). Optical observations by VLT/FORS2 located the host galaxy of GRB 090510 at the redshift of $z = 0.903 \pm 0.003$ (Rau et al., 2009). The offset with respect to the NOT refined afterglow position (Olofsson et al., 2009) corresponds to 5.5 kpc.

We have analyzed the Fermi-GBM data from NaI-n6 (8 – 900 keV) and BGO-b1 (260 keV – 40 MeV) detectors and the LAT data in the energy range 100 MeV – 30 GeV.

The light curve of GRB 090510 is composed of two different episodes, 0.5 s apart. The first episode, from $T_0 - 0.064$ s to $T_0 + 0.016$ s (in the following ΔT_1; T_0 is the trigger time), has not been considered by Ackermann et al. (2010), Giuliani et al. (2010) and Guiriec et al. (2010) because of the small content of detected photons. Even though the statistical content of this first episode is very poor, in this letter we show its great relevance for the theoretical analysis, since it can be identified with the P-GRB. The second episode can be interpreted as the extended afterglow. In the statistical analysis of the first episode, we have considered power-law (PL), black body (BB) plus PL, Band (Band et al., 1993), Comptonized (Compt), Band+BB and Compt+BB models. Following the statistical analysis for nested models by Guiriec et al. (2010), models more complicated than the simplest Band and Compt are singled out (see the last column of Tab. 13.1). The direct statistical comparison between BB+PL and PL models gives a significance level of 3% (see Tab. 13.1). This means that the BB+PL model improves the fit of the data of the first episode with respect to the PL model, which is excluded at 97% confidence level. The simple Band model has an unconstrained α index and a large error on the energy peak E_p, as well as in the case of the Compt model, for which the total flux is underestimated with respect to the Band and BB+PL models. The quality of data does not allow us to favor the BB+PL model versus the Compt one

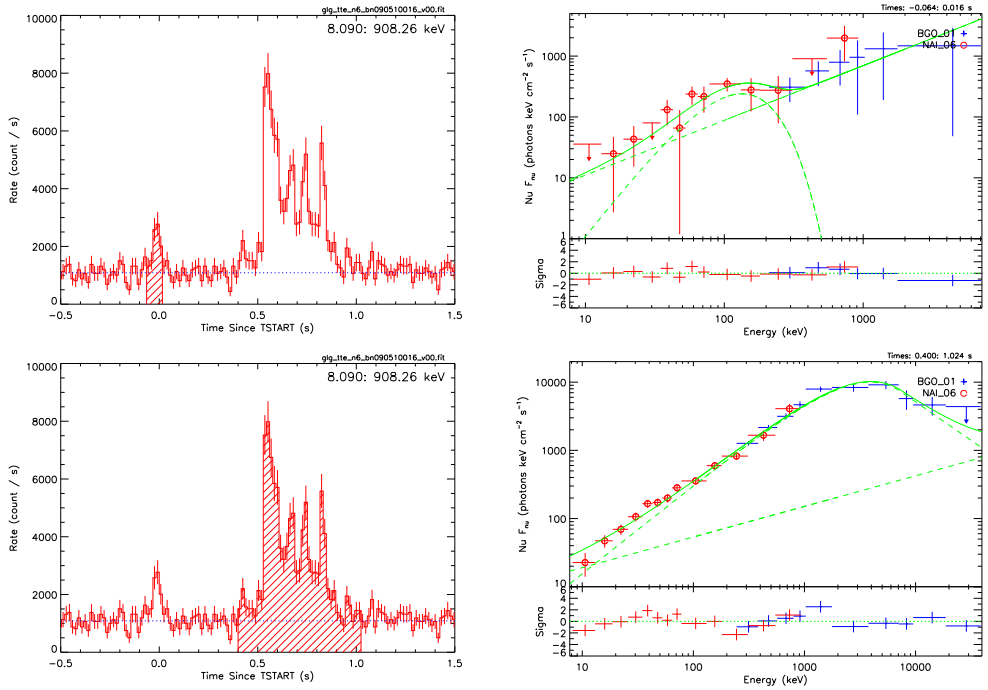

Figure 13.2.: Upper panels: on the left, the 16 ms time-binned NaI-n6 light curve and, on the right, the NaI-n6+BGO-b1 νF_ν spectrum (best fit BB+PL) in the ΔT_1 time interval. Lower panels: on the left, the 16 ms time-binned NaI-n6 light curve and, on the right, the NaI-n6+BGO-b1 νF_ν spectrum (best fit Band+PL) in the ΔT_2 time interval.

from a pure statistical analysis. In order to clarify such a fundamental issue, it is appropriate that future space missions with larger collecting area and X/γ-rays timing be flown in the near future (see e.g. LOFT mission, Feroci et al., 2012). From our theoretical interpretation the BB+PL, being equally probable than the Compt model, is adopted for its physical meaning and because it is not ruled out by the data. The BB observed temperature is $kT_{obs} = (34.2 \pm 7.5)$ keV (see Fig. 13.2, top right panel, and table below) and the total energy of the first episode is $E_1 = (2.28 \pm 0.39) \times 10^{51}$ erg.

We have then analyzed the second episode in the time interval from $T_0 + 0.400$ s to $T_0 + 1.024$ s (in the following ΔT_2). The best fit in the energy range 8 keV – 40 MeV is Band+PL (Ackermann et al., 2010) or, alternatively Compt+PL (Giuliani et al., 2010; Guiriec et al., 2010). The results are shown in Fig. 13.2 and in Tab. 13.1. Including the LAT data, the spectrum is again best fitted by Band+PL (see last row in Tab. 13.1), with the PL observed up to 30 GeV (Ackermann et al., 2010). The total energy is $E_2 = (1.08 \pm 0.06) \times 10^{53}$ erg.

Interval	Model	kT [keV]	α	β	E_p [keV]	γ
	PL	...	...	...	...	-1.22 ± 0.06
	BB+PL	34.2 ± 7.5	...	...	...	-1.10 ± 0.14
	Band	...	unc	-1.44 ± 0.11	94 ± 74	...
ΔT_1	**Compt**	...	-0.81 ± 0.22	...	990 ± 554	...
	Band+BB	24.3 ± 5.6	unc	-1.76 ± 0.62	unc	...
	Compt+BB	27.2 ± 6.7	-0.72 ± 0.39	...	2967 ± 1570	...
ΔT_2 (a)	**Band+PL**	...	-0.70 ± 0.10	-3.13 ± 0.97	3941 ± 346	-1.55 ± 0.54
ΔT_2 (b)	**Band+PL**	...	-0.71 ± 0.07	-2.97 ± 0.26	4145 ± 398	-1.62 ± 0.05

Table 13.1.: ΔT_1 time interval: parameters of PL, BB+PL, Band, Compt, Band+BB and Compt+BB models in the energy range 8–7000 keV. ΔT_2 time interval: parameters of the best fits (Band+PL) in the energy ranges (a) 8–40000 keV (GBM) and (b) 8 keV – 30 GeV (GBM+LAT). In the last column of ΔT_1 we list the significance levels from the comparison between nested models (BB+PL over PL, Band+BB over Band and Compt+BB over Compt).

13.3. GRB 090510 Theoretical Interpretation

In the Fireshell model (Ruffini et al., 2001a,a,c) GRBs originate from an optically thick e^+e^- plasma created by vacuum polarization processes in the gravitational collapse to a black hole (Damour and Ruffini, 1975; Ruffini et al., 2010e). The dynamics of such an expanding plasma in the optically thick phase is described by its total energy $E^{tot}_{e^+e^-}$ and by the amount of the engulfed baryons B. The spherical symmetry of the system is assumed. The canonical GRBs light curve is then characterized by a first emission due to the transparency of the e^+e^--photon-baryon plasma, the P-GRB, followed by a multi-wavelength emission, the extended afterglow, due to the collisions, in a fully radiative regime, between the accelerated baryons and the CBM. The radius at which the transparency occurs, r_{tr}, the theoretical temperature blue-shifted toward the observer kT_{blue} and the Lorentz factor Γ_{tr} as well as the amount of the energy emitted in the P-GRB are functions of $E^{tot}_{e^+e^-}$ and B (Ruffini et al., 2001a, 2009). The structures observed in the extended afterglow of a GRB are described by two quantities associated with the environment: the CBM density profile n_{CBM}, which determines the temporal behavior of the light curve, and the filling factor $\mathcal{R} = A_{eff}/A_{vis}$, where A_{eff} is the effective emitting area of the fireshell and A_{vis} its total visible area (Ruffini et al., 2002, 2005a). This second parameter takes into account the inhomogeneities in the CBM and its filamentary structure (Ruffini et al., 2004b). The density of each filament is simply defined as $n_{fil} = n_{CBM}/\mathcal{R}$.

We have identified the first episode, where the thermal component is not statistically excluded, with the P-GRB. Then we have started the simulation

Distance [cm]	n_{CBM} **[#/cm^3]**	$\mathcal{R}$	n_{fil} **[#/cm^3]**
6.5×10^{14}	550 ± 45	$(3.2 \pm 0.3) \times 10^{-9}$	$(1.72 \pm 0.21) \times 10^{11}$
9.2×10^{14}	1.90 ± 0.60		$(5.94 \pm 0.84) \times 10^{8}$
1.6×10^{15}	60.0 ± 4.1		$(1.88 \pm 0.22) \times 10^{10}$
2.3×10^{15}	$(2.50 \pm 0.20) \times 10^{3}$		$(7.81 \pm 0.96) \times 10^{11}$
2.5×10^{15}	0.15 ± 0.01		$(4.69 \pm 0.53) \times 10^{7}$
3.3×10^{15}	$(1.90 \pm 0.20) \times 10^{4}$	$(1.5 \pm 0.2) \times 10^{-10}$	$(1.27 \pm 0.22) \times 10^{14}$
3.4×10^{15}	0.15 ± 0.02		$(1.00 \pm 0.19) \times 10^{9}$
3.5×10^{15}	$(2.50 \pm 0.14) \times 10^{4}$	$(3.8 \pm 0.4) \times 10^{-8}$	$(6.58 \pm 0.78) \times 10^{11}$
3.6×10^{15}	0.10 ± 0.02		$(2.63 \pm 0.59) \times 10^{6}$

Table 13.2.: We report for each cloud, respectively, the distance from the black hole, the average number density (assuming spherically distributed clouds), the filling factor and the number density of the filaments.

using our numerical code (for details, see e.g. Ruffini et al., 2007a). The input parameters are $E^{tot}_{e^+e^-}$, constrained to the isotropic energy of the burst, $E_{iso} = (1.10 \pm 0.06) \times 10^{53}$ erg, and the Baryon load $B = (1.45 \pm 0.28) \times 10^{-3}$, determined by matching the theoretically simulated energy E_{tr} and temperature $kT_{th} = kT_{blue}/(1+z)$ of the P-GRB with the ones observed in the faint pulse, E_1 and kT_{obs}. The results of our simulation are the following:

$$\Gamma_{tr} = (6.7 \pm 1.6) \times 10^2 \ , \ r_{tr} = (6.51 \pm 0.92) \times 10^{13} \, \text{cm} \, , \\ E_{tr} = (2.94 \pm 0.50)\% E^{tot}_{e^+e^-} \ , \ kT_{th} = (34.2 \pm 7.5) \, \text{keV}. \qquad (13.3.1)$$

The theoretically predicted P-GRB energy slightly differs from the observed $E_1 = (2.28 \pm 0.39) \times 10^{51}$ erg $= (2.08 \pm 0.35)\% E_{iso}$, since emission below the threshold is expected between the small precursor and the main emission (see light curves in Fig. 13.2), thus the value of E_1 is certainly underestimated.

In the following analysis we focus our attention on the main emission. Since in ΔT_2 no evidence of a thermal component has been found (see Fig. 13.2, bottom right panel, and table below), we have interpreted this emission as the extended afterglow. Using the above values of $E^{tot}_{e^+e^-}$ and B, we have simulated the light curve of the extended afterglow by defining the radial number density distribution of the CBM (assuming spherically distributed clouds) and the value of the filling factor $\mathcal{R}$, following a trial and error procedure to reproduce the pulses observed in the light curve and the corresponding spectrum. The errors on the densities and the filling factors are obtained varying them within the observational errors; typically the errors are about 10% of the value. The average value is indeed very high, $\langle n_{CBM} \rangle = (1.85 \pm 0.14) \times 10^3$ particles/cm^3, assuming spherically distributed clouds (see Fig. 13.3, upper plot). Basically this high average density is due to the second and the third

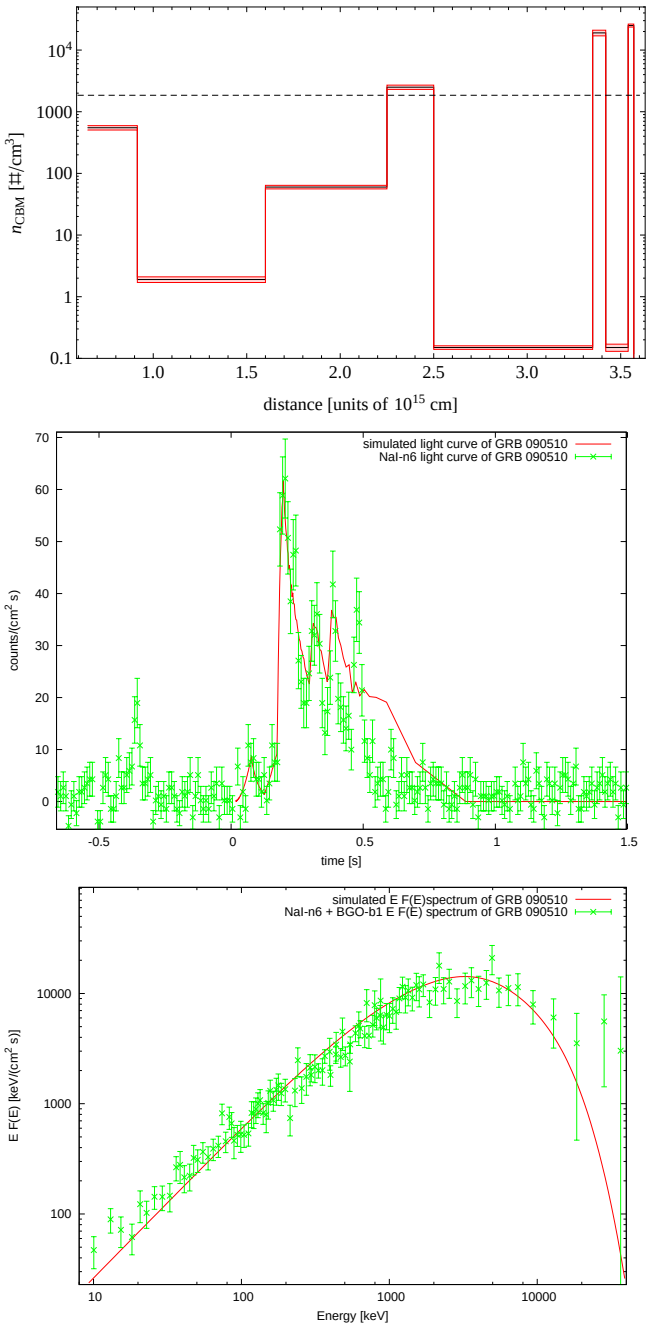

Figure 13.3.: In the upper panel the radial CBM density distribution of GRB 090510 (red solid line) with its uncertainty (light red shaded region) and the mean value (black dashed line) are shown. The simulated NaI-n6 light curve (8–1000 keV) of the extended afterglow (middle panel) and the corresponding spectrum of the early $\sim$ 0.4 s of the emission in the energy range 8 keV – 40 MeV (lower panel) are consequently obtained.

brightest spikes of the light curve (see Fig. 13.3, middle panel), where the density of the clouds is $\sim 2 \times 10^4$ particles/cm^3 (see Tab. 13.2, second column). The filling factor assumes values $1.5 \times 10^{-10} \leq \mathcal{R} \leq 3.8 \times 10^{-8}$ (see Tab. 13.2, third column). Correspondingly, the values of the densities of the filaments n_{fil} are estimated (see Tab. 13.2, fourth column). In Fig. 13.3 we show also the simulated extended afterglow light curve from the NaI-n6 detector (middle panel) and the corresponding spectrum of the early $\sim$ 0.4 s of the emission (lower panel) in the energy range 8 keV – 40 MeV, using the spectral model described in Ruffini et al. (2004b) and Patricelli et al. (2012). The last part of the simulation requires a more detailed 3-dimensional code to take into due account the distribution of the CBM.

13.4. Conclusions

We list our conclusions.

1) The simulated spectrum of the extended afterglow in the time interval ΔT_2, considered in the analysis by Ackermann et al. (2010), is in excellent agreement with the one in Fig. 13.2 in the sub-MeV and in the MeV region. The baryon load $B = (1.45 \pm 0.28) \times 10^{-3}$ used in this simulation has been determined from the analysis of the first episode, which has been identified with the P-GRB. The current quality of the data does not allow us to properly distinguish between BB+PL and Compt spectral models. From our theoretical interpretation, BB+PL model was adopted, since it is not ruled out by the data. Such a fundamental issue will be further clarified by future space missions with larger collecting area and X/γ-rays timing, as e.g. the LOFT mission (Feroci et al., 2012).

2) We have stressed a key difference between the Fireshell and the Fireball approaches. In the Fireshell model the extended afterglow encompasses the prompt emission and the afterglow of the traditional Fireball model. The density of the CBM is inferred from the prompt emission by assuming the fully radiative condition emission in a optically thin regime (Ruffini et al., 2002, 2004b, 2005a) and a precise spectrum in the comoving frame is assumed (Patricelli et al., 2012) and convoluted over the EquiTemporal Surfaces (EQTS, Bianco and Ruffini, 2005a,b). In the Fireball model, instead, the density is estimated from the afterglow emission by analyzing emission or absorption lines in the X-ray spectra (see e.g. Lazzati et al., 1999; Prochaska et al., 2008), or by observing steepening or breaks of the optical afterglow light curves (see e.g. Dai and Lu, 1999; Piro et al., 2001; Wang et al., 2003). From the fully radiative condition, we have found that GRB 090510 occurs in an over-dense medium with an average value of $\langle n_{CBM} \rangle \approx 10^3$ particles/cm^3 (for spherically symmetric distributed clouds). This high CBM density and the small value of the filling factor, $1.5 \times 10^{-10} \leq \mathcal{R} \leq 3.8 \times 10^{-8}$, leads to local over-dense CBM clouds, in the form of filaments, bubbles and clumps, with a range of

densities $n_{fil} = n_{CBM}/\mathcal{R} \approx (10^6 - 10^{14})$ particles/cm^3.

3) The joint effect of the high value of the Lorentz factor, $\Gamma_{tr} = (6.7 \pm 1.6) \times 10^2$, and the high density compresses in time the emission of the extended afterglow. Therefore its light curve is shortened in time and "inflated" in intensity with respect to the canonical one for disguised short bursts (see Fig. 13.1, lower panel), making it apparently closer to the genuine short class of GRBs (Muccino et al., 2013). It is interesting to note that in this GRB, with an abnormally high value of the CBM density, the extended afterglow does not fulfill the Amati relation (Amati, 2006).

4) From the values of n_{fil} we obtain a range of grammages of $m_H n_{fil} \Delta r_c \approx (10^{-2} - 10^4)$ g/cm^2, where m_H is the mass of the Hydrogen atom and Δr_c is the size of the cloud inferred from our simulation (see Fig. 13.3 and the first column in Tab. 13.2). This high value of the grammage may be relevant in the explanation of the observed GeV emission as originating in the collisions between ultra high energy protons, with bulk Lorentz factor of $\Gamma_{tr} = (6.7 \pm 1.6) \times 10^2$, and the CBM.

14. Novel distance indicator for Gamma-Ray Bursts associated with Supernovae

Recently, Ruffini et al. (2001a, 2007c) proposed that the temporal coincidence of some gamma-ray bursts (GRBs) and a type Ib/c supernovae (SNe) can be explained with the concept of induced gravitational collapse (IGC) of a neutron star (NS) to a black hole (BH) induced by accretion of matter ejected by the SN Ib/c. More recently, this concept has been extended, including a precise description of the progenitor system of such GRB-SN systems (Rueda and Ruffini, 2012b).

The main new result presented here is that the IGC GRB-SN class shows a standard late X-ray luminosity light curve in the common energy range 0.3 – 10 keV (Ruffini, 2012).

The prototype is GRB 090618 (Ruffini et al., 2011a; Izzo et al., 2012e,a) at redshift $z = 0.54$, where four different emission episodes have been identified.

Episode 1, corresponding to the SN onset, has been observed to have thermal as well as power-law emission. The thermal emission changes in time following a precise power-law behavior (Izzo et al., 2012e; Penacchioni et al., 2012, 2013).

Episode 2 follows and in the IGC model corresponds to the GRB emission coincident with the BH formation. The characteristic parameters of the GRB, including baryon load, the Lorentz factor, and the nature of the circumburst medium (CBM), have been computed (Izzo et al., 2012e; Penacchioni et al., 2012, 2013).

Episode 3 is characterized in the X-ray light curve by a shallow phase (a plateau) followed by a final steeper decay. Typically, it is observed in the range $10^2 - 10^6$ s after the GRB trigger.

Episode 4 occurs after a time of about ten days in the cosmological rest-frame, corresponding to the SN emission due to the Ni decay (see Arnett, 1996, for a complete review). This emission is clearly observed in GRB 090618 during the late optical GRB afterglow emission.

Here we analyze the X-ray emission of a sample of eight GRBs with $E_{iso} \geq 10^{52}$ erg that satisfy at least one of the following three requirements:

- there is a double emission episode in the prompt emission: Episode 1,

GRB	z	$E_{iso}(erg)$
GRB 060729	0.54	1.6×10^{52}
GRB 061007	1.261	1.0×10^{54}
GRB 080319B	0.937	1.3×10^{54}
GRB 090618	0.54	2.9×10^{53}
GRB 091127	0.49	1.1×10^{52}
GRB 111228	0.713	2.4×10^{52}
GRB 101023	0.9^*	1.8×10^{53}
GRB 110709B	0.75^*	1.7×10^{53}

Table 14.1.: GRB sample considered in this work. The redshifts of GRB 101023 and GRB 110709B, which are marked with an asterisk, were deduced theoretically by using the method outlined here (Penacchioni et al., 2012) and the corresponding isotropic energy computed by assuming these redshifts.

with a decaying thermal feature, and Episode 2, a canonical GRB, as in GRB 090618 (Izzo et al., 2012e), GRB 101023 (Penacchioni et al., 2012), and in GRB 110709B (Penacchioni et al., 2013);

- there is a shallow phase followed by a final steeper decay in the X-ray light curve: Episode 3;
- an SN is detected after about ten days from the GRB trigger in the rest-frame: Episode 4.

We found eight GRBs that satisfy our requirements (see Table 14.1).

GRB 060729. In this source an SN bump was observed in the optical GRB afterglow (Cano et al., 2011). It is at the same redshift $z = 0.54$ as GRB 090618 and shows a small precursor plus a main event in the prompt light curve and a peculiar prolonged duration for the X-ray afterglow. The isotropic energy emitted in this burst is $E_{iso} = 1.6 \times 10^{52}$ erg (Grupe et al., 2007a).

GRB 061007. This GRB has no associated SN but is characterized by a precursor with a clear evolving thermal emission (Larsson et al., 2011). With an energetic E_{iso} of 1.0×10^{54} erg (Golenetskii et al., 2006b) at $z = 1.261$, it is the farthest GRB in our sample. The large distance makes the detection of an SN from this GRB difficult.

GRB 080319B. A tentative SN was reported also for GRB 080319B, well-known as the naked-eye GRB, whose prompt emission also shows a possible double-emission episode (Kann et al., 2008b). Its measured redshift is $z = 0.937$. This is one of the most energetic GRB, with $E_{iso} = 1.3 \times 10^{54}$ erg (Golenetskii et al., 2008), and its X-ray light curve is well fit by a simple decaying power-law.

GRB 090618. This GRB is the prototype of the IGC GRB-SN subclass. Its prompt emission shows a clear Episode 1 plus Episode 2 structure in light

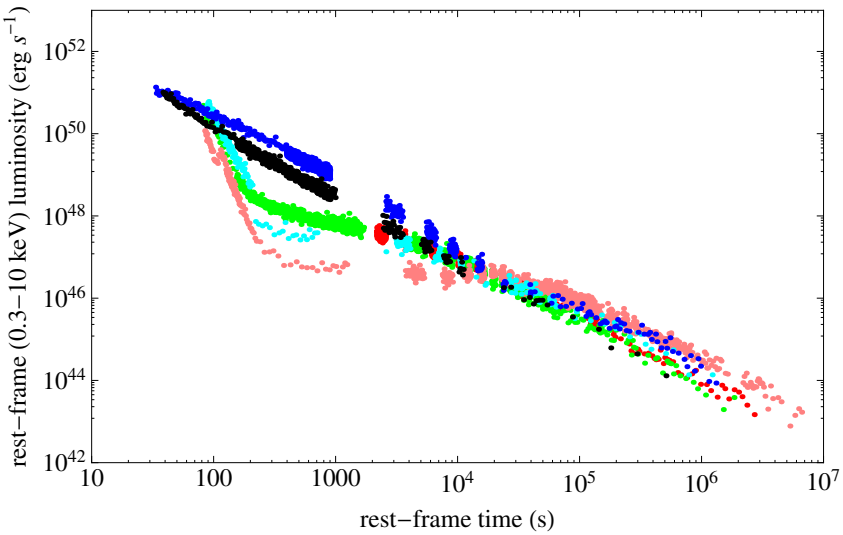

Figure 14.1.: X-ray luminosity light curves of the six GRBs with measured redshift in the 0.3 – 10 keV rest-frame energy range: in pink GRB 060729, $z = 0.54$; black GRB 061007, $z = 1.261$; blue GRB 080319B, $z = 0.937$; green GRB 090618, $z = 0.54$, red GRB 091127, $z = 0.49$, and in cyan GRB 111228, $z = 0.713$.

curve and spectrum. The measured redshift is $z = 0.54$ and the $E_{iso} = 2.9 \times 10^{53}$ erg (Izzo et al., 2012e). There is a clear optical bump, about ten days of rest-frame time after the GRB trigger, in the afterglow light curve of GRB 090618 that is associated with the SN emission (Cano et al., 2011). The characteristic parameters of this GRB, including the baryon load ($B = 1.98 \times 10^{-3}$), the Lorentz factor at the trasparency ($\Gamma_{tr} = 495$), and the nature of the CBM ($\langle n_{CBM} \rangle = 0.6\, part/cm^3$), have been estimated previously (Izzo et al., 2012e).

GRB 091127. GRB 091127 is associated with SN 2009nz at a redshift of $z = 0.49$ (Cobb et al., 2010). The E_{iso} for this burst is 1.1×10^{52} erg (Wilson-Hodge and Preece, 2009).

GRB 111228. An SN feature was also reported in the literature for GRB 111228 (D'Avanzo et al., 2012), which shows a multiply peaked prompt light curve in the Fermi-GBM data. The measured redshift of this GRB is $z = 0.713$, its $E_{iso} = 2.4 \times 10^{52}$ erg (Briggs and Younes, 2011), and a dedicated analysis of this GRB will be presented elsewhere. The detection of an SN in GRB 111228 is debated, since the subsequent optical bump has the same flux as the host galaxy of the source, but SN features were observed in the differential photometry between the last epochs of observations, where a transient component was detected that was unrelated to the afterglow, and was consequently attributed to the SN.

GRB 101023. This GRB shows clear Episode 1 and Episode 2 emissions in the prompt light curve and spectrum, but there is no detection of an SN and

no measured redshift because of the lack of optical observations at late times. We estimated the redshift of this source at $z = 0.9$ by analogy to the late X-ray afterglow decay observed in the six GRBs with a measured redshift. This leads to an estimate of $E_{iso} = 1.8 \times 10^{53}$ erg, a baryon load of $B = 3.8 \times 10^{-3}$, a Lorentz factor at transparency of $\Gamma_{tr} = 260$, and an average density for the CBM of ($\langle n_{CBM} \rangle \approx 16\, part/cm^3$ (Penacchioni et al., 2012).

GRB 110709B. Like GRB 101023, this GRB shows clear Episode 1 plus Episode 2 emission in the prompt light curve and spectrum, but there is no detection of an SN. This can be explained by the fact that it is a dark GRB, whose emission is strongly influenced by absorption. Particularly interesting is the detection of clear radio emission (Zauderer et al., 2013). There is no measurement for the redshift but, as for GRB 101023, we estimated it to be $z = 0.75$ by analogy to the late X-ray afterglow decay observed in the six GRBs with measured redshifts. This leads to an estimate of an isotropic energy of $E_{iso} = 1.7 \times 10^{53}$ erg, a baryon load of $B = 5.7 \times 10^{-3}$, a Lorentz factor at the trasparency of $\Gamma_{tr} = 174$, and an average density of the CBM of $\langle n_{CBM} \rangle \approx 76 part/cm^3$ (Penacchioni et al., 2013).

We focused the analysis of all available XRT data of these sources. Characteristically, XRT follow-up starts only about 100 seconds after the BAT trigger (typical repointing time of Swift after the BAT trigger). Because the behavior was similar in all sources, we compared the analyzed XRT luminosity light curve L_{rf} for the six GRBs with measured redshifts in the common rest-frame energy range 0.3 – 10 keV. As a first step we converted the observed XRT flux f_{obs} to one in the 0.3 – 10 keV rest-frame energy range. In the detector frame, the 0.3 – 10 keV rest-frame energy range becomes $[0.3/(1+z)] - [10/(1+z)]$ keV, where z is the redshift of the GRB. We assumed a simple power-law function as the best fit for the spectral energy distribution of the XRT data[1]:

$$\frac{dN}{dA\, dt\, dE} \propto E^{-\gamma}\,. \tag{14.0.1}$$

We can then write the flux light curve, f_{rf}, in the 0.3 – 10 keV rest-frame energy range as

$$f_{rf} = f_{obs} \frac{\int_{\frac{0.3\,keV}{1+z}}^{\frac{10\,keV}{1+z}} E^{-\gamma} dE}{\int_{0.3\,keV}^{10\,keV} E^{-\gamma} dE} = f_{obs}(1+z)^{\gamma-1}\,. \tag{14.0.2}$$

Then, we have to multiply f_{rf} by the luminosity distance to derive L_{rf}:

$$L_{rf} = 4\,\pi\, d_l^2(z) f_{rf}\,, \tag{14.0.3}$$

where we assume a standard cosmological ΛCDM model with $\Omega_m = 0.27$

[1] http://www.swift.ac.uk/

and $\Omega_\Lambda = 0.73$. Clearly, this luminosity must be plotted as a function of the rest-frame time t_{rf}, namely

$$t_{rf} = \frac{t_{obs}}{1+z}\,. \tag{14.0.4}$$

The X-ray luminosity light curves of the six GRBs with measured redshifts in the 0.3–10 keV rest-frame energy band are plotted in Fig. 14.1. What is most striking is that these six GRBs, with redshifts in the range $0.49-1.261$, show a remarkably common behavior of the late X-ray afterglow luminosity light curves (Episode 3), despite their very different prompt emissions (Episode 1 and 2) and energetics spanning more than two orders of magnitude. The common behavior starts between 10^4-10^5 s after the trigger and continues until the emission falls below the XRT threshold. This standard behavior of Episode 3 represents a strong evidence of very low or even absent beaming in this particular phase of the X-ray afterglow emission process. We have proposed that this late-time X-ray emission in Episode 3 is related to the process of the SN explosion within the IGC scenario, possibly emitted by the newly born NS, and not by the GRB itself (Negreiros et al., 2012). This scaling law, when confirmed in sources with Episode 1 plus Episode 2 emissions, offers a powerful tool for estimating the redshift of GRBs that belong to this subclass of events. As an example, Fig. 14.2 plots the rest-frame X-ray luminosity (0.3 - 10 keV) light curve of GRB 090618 (considered the prototype of the common behavior shown in Fig. 14.1) with the rest-frame X-ray luminosity light curves of GRB 110709B estimated for selected values of its redshifts $z = 0.4, 0.6, 0.8, 1.0, and 1.2$, and similarly the corresponding analysis for GRB 101023 for redshifts $z = 0.6, 0.8, 1.0, 1.2, and 1.5$. This shows that GRB 101023 should have been located at $z \sim 0.9$ and GRB 110709B at $z \sim 0.75$. These redshift estimates are within the range expected using the Amati relation as shown in Penacchioni et al. (2012, 2013). This is an important independent validity confirmation for this new redshift estimator we are proposing for the family of IGC GRB-SN systems. We stress, however, that the redshift was determined assuming the validity of the standard ΛCDM cosmological model for sources with redshift in the range $z = 0.49-1.216$. We are currently testing the validity of this assumption for sources at higher cosmological redshifts.

Before concluding, it is appropriate to recall once again that we assumed that these binary systems give rise to the IGC GRB-SN sources, which are a subclass of all GRBs. Their special binary nature is very different from that corresponding to the genuine short GRBs, for instance. For these the progenitors are thought by many to be binary neutron stars and there is no expected observable afterglow emission (see e.g. the case of GRB 090227B presented in Muccino et al., 2013). They are also different from disguised short GRBs, which again may originate from binary systems drifting to the galactic halo (Bernardini et al., 2007; Caito et al., 2009, 2010; de Barros et al., 2011). In par-

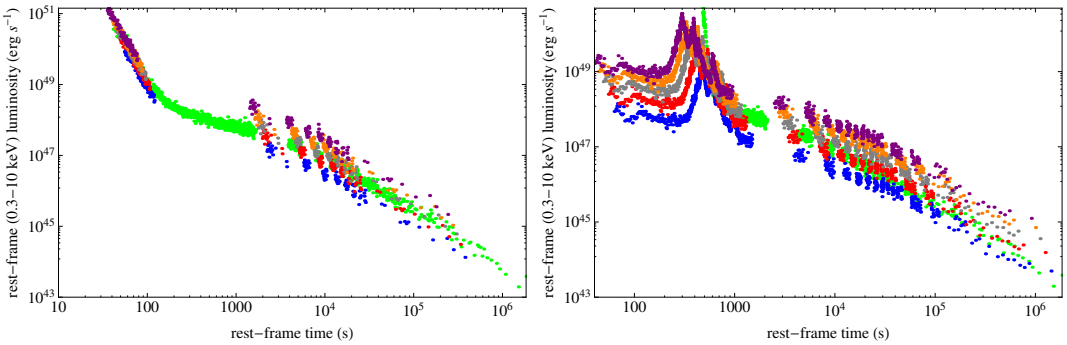

Figure 14.2.: In green we show the rest-frame X-ray luminosity light curve of GRB 090618 in the 0.3 – 10 keV energy range in comparison with the one of GRB 101023 (left) and GRB 110709B (right), computed for different hypothetical redshifts: respectively, from blue to purple: $z = 0.6, 0.8, 1.0, 1.2, 1.5$ (left) and $z = 0.4, 0.6, 0.8, 1.0, 1.2$ (right). The overlapping at late time of the two X-ray luminosity light curves is obtained for a redshift of $z = 0.9$ (left) and $z = 0.75$ (right). For further details see Penacchioni et al. (2012, 2013).

ticular, they may differ from GRB 060614, where there is strong evidence that it has no associated SN (Della Valle et al., 2006; Gal-Yam et al., 2006; Gehrels et al., 2006). We were also able to show explicitly that the X-ray luminosity light curve of the IGC GRB-SN prototype, GRB 090618, is drastically different both from that of GRB 060614 and that of GRB 090510, which may be an example of a disguised short GRB that may have instead exploded in a very high density region (Muccino et al., 2013), see Fig. 14.3. In all the above examples we have considered very energetic sources ($E_{iso} \geq 10^{52}$ erg). Less energetic GRB-SN sources, e.g. GRB 980425 (Pian et al., 2000), also show a late X-ray emission different from the typical emission of the IGC GRB-SN sources, and we will discuss this matter elsewhere.

We presented a sample of IGC GRB-SN systems with a standard late-time ($10^4 - 10^5$ s after the trigger) X-ray luminosity light curve in the 0.3 – 10 keV rest-frame energy band. This standard behavior points to a common physical origin of this emission, possibly related to a newly born NS out of the SN event (Negreiros et al., 2012). This scaling law can provide a new distance indicator for this subclass of GRBs, allowing one to predict the redshift of the source as well as the presence of an associated SN.

We are currently testing the predictive power of our results on three different observational scenarios for sources of the IGC GRB-SN subclass:

- GRBs at high redshift. We are able to predict the existence of an SN in these systems, which is expected to emerge after $t \sim 10\,(1+z)$ days, the canonical time sequence of an SN explosion. This offers a new challenge to detect SNe at high redshift, e.g., by observing radio emission (Penacchioni et al., 2013);

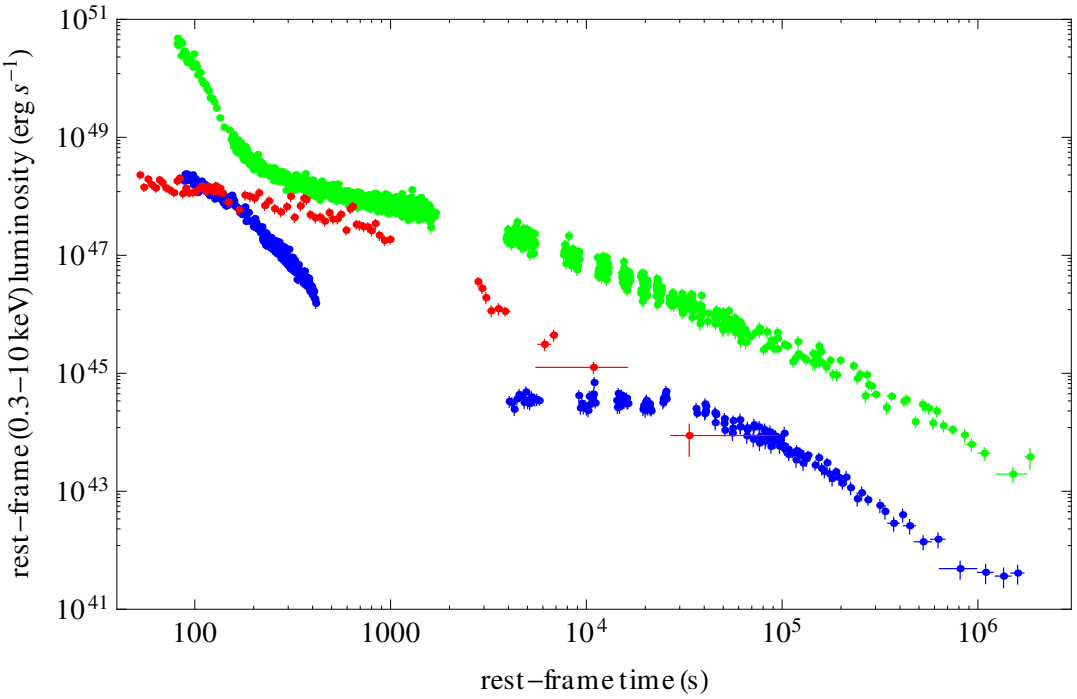

Figure 14.3.: X-ray luminosity light curves of GRB 090618 (green), GRB 060614 (blue), and GRB 090510 (red) in the 0.3 – 10 keV rest-frame energy range.

- for GRBs with $z \leq 1$ we can indicate in advance from the X-ray luminosity light curve observed by XRT the expected time for the observations of an SN and alert direct observations from ground- and space-based telescopes;
- as we showed here, we can infer the redshift of GRBs in the same way we did for GRB 110709B and GRB 101023A.

We are currently expanding the sample to increase the statistical validity of our approach and its cosmological implications.

15. Induced Gravitational Collapse Paradigm

It is by now clear that not all gamma-ray bursts (GRBs) are associated with Supernovae (SNe). One of the best example is the case of GRB 090227b where the GRB originate by the merging of a binary neutron star (Muccino et al., 2013).

Soon after the observation of GRB 980425 by Galama et al. (1998), it was clear that some GRBs were associated with SNe. It was then advanced the working hypothesis that all long GRBs originate from an SN explosion and a specific model was adopted to explain this phenomenon: the collapsar model by Woosley (1993) (see e.g. Woosley and Bloom, 2006, and references therein).

Since 2001, a different approach was presented by our group based on the following assumptions:

1. the only possible outcome of a SN is a neutron star (NS) and not a black hole (BH);

2. GRBs originate in the formation process of a BH, following the vacuum polarization process and the creation of an electron-positron plasma (see Damour and Ruffini, 1975);

3. the concurrent occurrence of a SN and a GRB takes place in a binary system via a process of "induced collapse".

In 2001 we considered the case of a binary system in which the GRB generated by a collapse to a BH would induce an SN explosion on a duly evolved companion star (Ruffini et al., 2001a).

In 2006 we have proposed an alternative picture still based on a binary system, formed by an evolved Carbon-Oxygen core, left over by the late thermonuclear evolution of a massive star, and a NS. In such a binary system a "cosmic carom" is taking place: the evolved core gives rise to a SN, whose ejecta accrete on the companion NS and *induces* its gravitational collapse to a BH; in the formation process of the BH the GRB is emitted (see left panel in Fig. 15.1 and Ruffini et al., 2007c). However, the "cosmic carom" is not yet finished: out of the SN a newly born NS is formed. After 10–13 days the SN gives rise to its traditional optical emission. The crucial sequence of this "cosmic carom" takes place in less than one minute with very specific signatures.

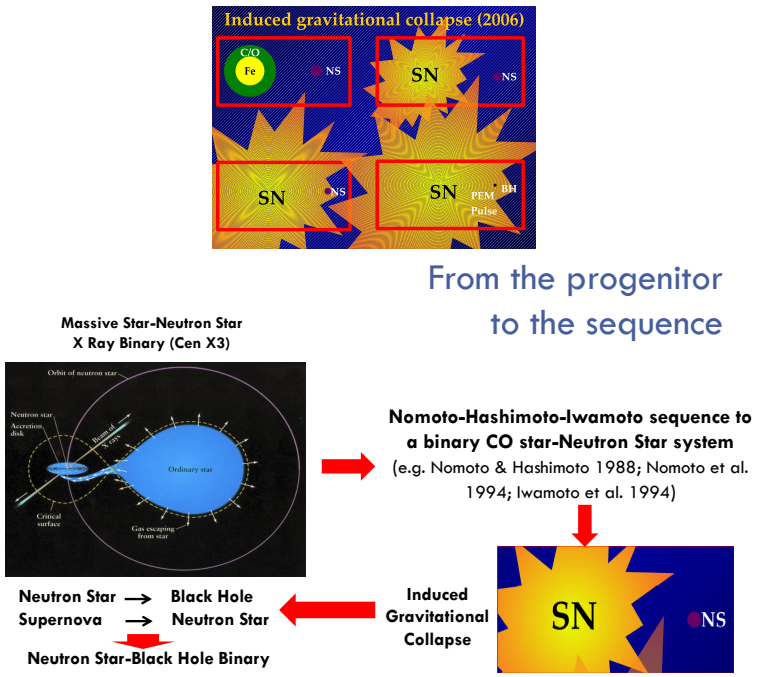

Figure 15.1.: Time-sequence of the IGC paradigm. Details in Ruffini et al. (2007c); Ruffini (2012); Rueda and Ruffini (2012b).

This process can be astrophysically fitted in the very late evolution of an X-ray binary system (see right panel in Fig. 15.1). The corresponding accretion process is schematically shown in Fig. 15.2.

This induced gravitational collapse (IGC) paradigm has been tested (see Fig. 15.3) on GRB-SN associations in the following sources: GRB101023 (Penacchioni et al., 2012), GRB 090618 Izzo et al. (2012e), GRB 110709B (Penacchioni et al., 2013) and from a theoretical point of view in Rueda and Ruffini (2012b); Izzo et al. (2012a).

Right now, this model has been tested in such details that it has become predictive (see Pisani et al., 2013). We can identify from their prompt emissions the GRBs that are members of this family of IGC systems, and consequently predict the occurrence of an associated SN and its luminosity. This has led us to the prediction, on May 2^{nd}, of an SN in association with GRB 130427A (see Ruffini et al., 2013):

```
TITLE:   GCN CIRCULAR
NUMBER:  14526
SUBJECT: GRB 130427A: Predictions about the occurrence of a supernova
DATE:    13/05/02 09:15:09 GMT
FROM:    Remo Rufinni at ICRA  <ruffini@icra.it>

R. Ruffini, C.L. Bianco, M. Enderli, M. Muccino, A.V. Penacchioni,
G.B. Pisani, J.A. Rueda, N. Sahakyan, Y. Wang, L. Izzo report:
```

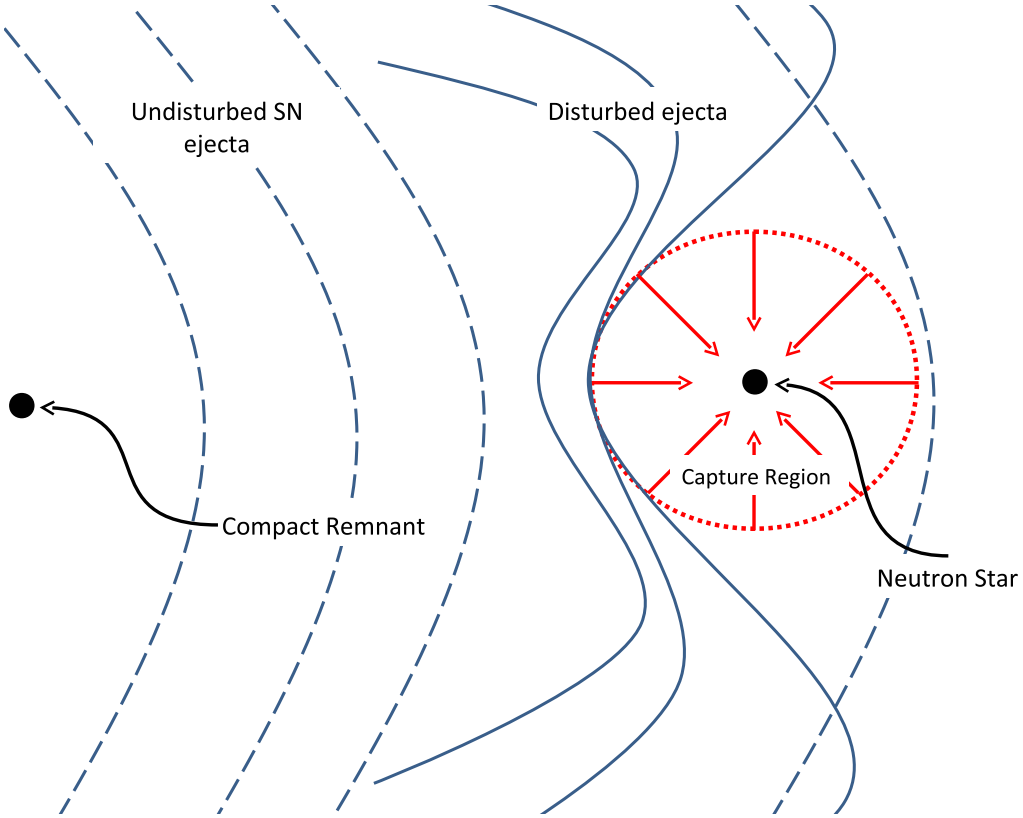

Figure 15.2.: Details of the accretion of the SN ejecta into the NS. Details in Ruffini (2012); Rueda and Ruffini (2012b).

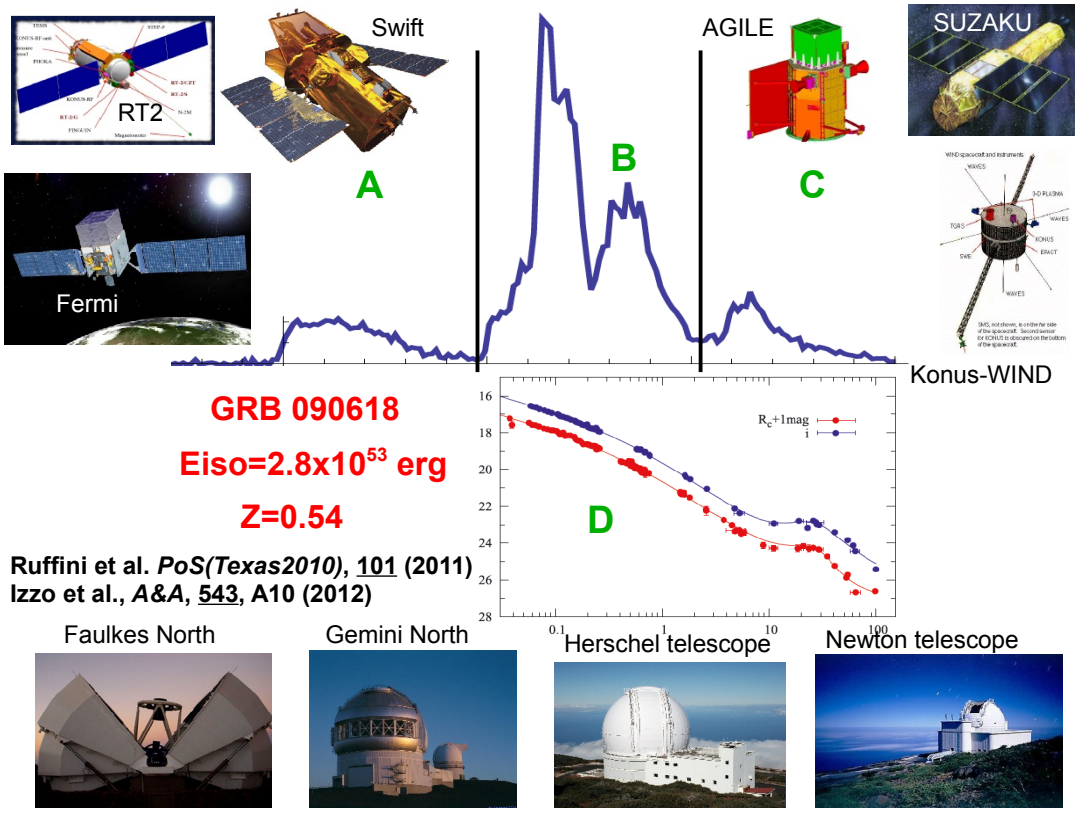

Figure 15.3.: Different phases in GRB 090618. Details in Izzo et al. (2012e,a).

```
The late x ray observations of GRB 130427A by Swift-XRT clearly
evidence a pattern typical of a family of GRBs associated to supernova
(SN) following the Induce Gravitational Collapse (IGC) paradigm (Rueda
& Ruffini 2012; Pisani et al. 2013). We assume that the luminosity of
the possible SN associated to GRB 130427A would be the one of 1998bw,
as found in the IGC sample described in Pisani et al. 2013. Assuming
the intergalactic absorption in the I-band (which corresponds to the
R-band rest-frame) and the intrinsic one, assuming a Milky Way type
for the host galaxy, we obtain a magnitude expected for the peak of
the SN of I = 22 - 23 occurring 13-15 days after the GRB trigger,
namely between the 10th and the 12th of May 2013.

Further optical and radio observations are encouraged.
```

This prediction has been observationally tested by the best telescopes in the world, including GTC, Keck and VLT, and it was fully confirmed (see Xu et al., 2013a; Trotter et al., 2013a; Garnavich, 2013; Watson et al., 2013a; Perley and Tang, 2013; Wiersema et al., 2013; Kann et al., 2013; Volnova et al., 2013; de Ugarte Postigo et al., 2013; Trotter et al., 2013b; Watson et al., 2013b; Sokolov et al., 2013; Levan et al., 2013). The new discovered SN was named SN 2013cq (Xu et al., 2013b).

This signed a change of paradigm in the understanding of GRBs and of SN-GRB association. The following sequence appears to occur (see Fig. 15.4 and details in Rueda and Ruffini, 2012b; Negreiros et al., 2012; Izzo et al., 2012e,a):

a) A binary system formed by an evolved Carbon-Oxygen core and a companion NS.

b) The occurrence of the SN and the accretion of the ejecta into the NS.

c) Gravitational collapse of the NS into a BH and concurrent emission of the GRB.

d) Birth of a new NS out of the SN.

e) New binary system formed by a BH and a newly born NS.

f) Final observation of the SN in the optical band, which has been the object of our prediction in the case of GRB 130427A (see the above GCN).

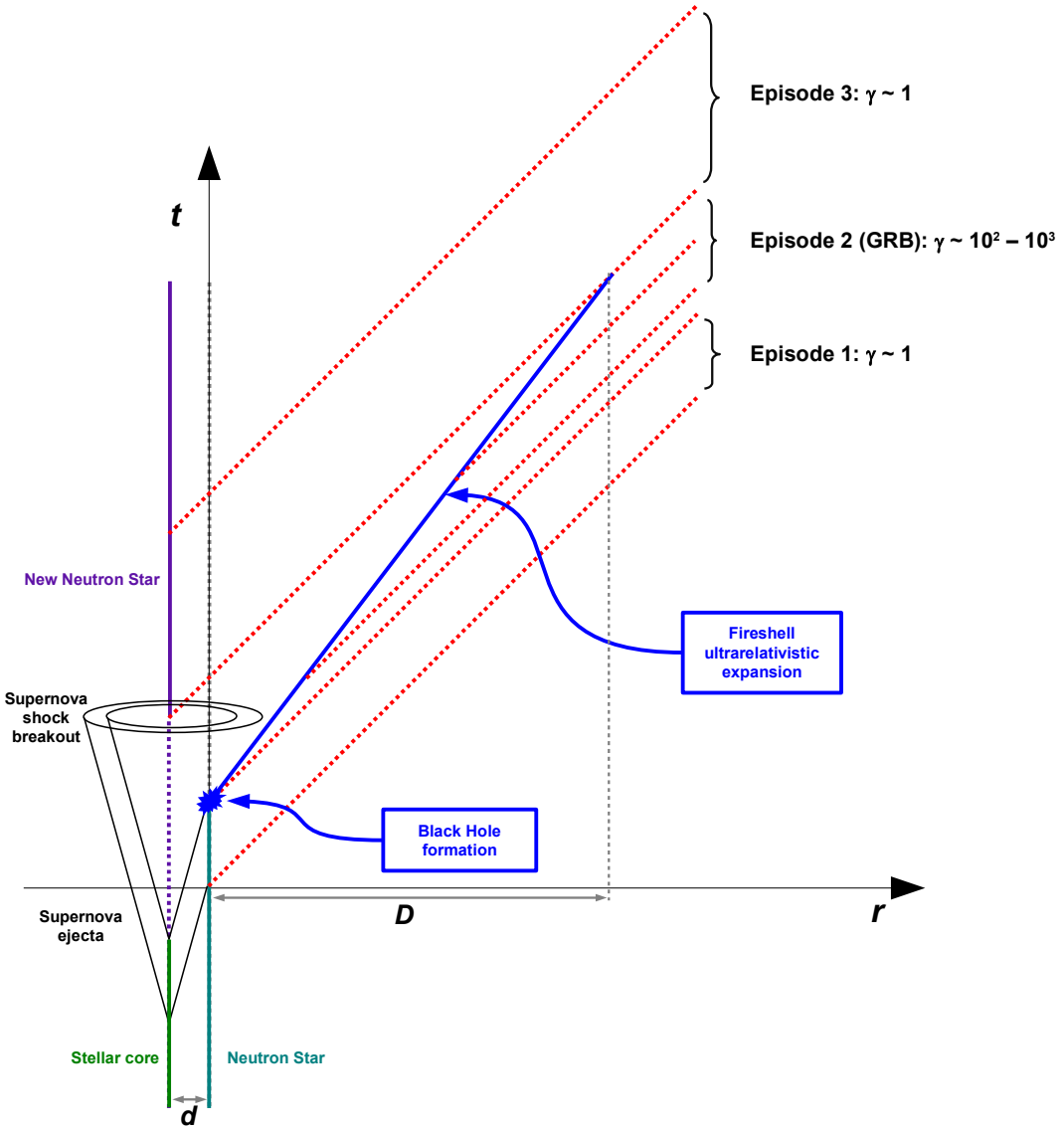

Figure 15.4.: Space time diagram.

16. GRB 090423 : a canonical GRB at redshift 8.1

GRB 090423 is the most distant GRB known to-date, with a spectroscopically determined redshift of $z \simeq 8.1$, (Tanvir et al. 2009), that was confirmed with an in-depth analysis of the TNG spectrum of GRB 090423 taken on Apr 23 at 22:16 UT using the Italian TNG 3.6m telescope located in the Canary Islands (Spain), (Guidorzi et al. 2009). The Swift satellite triggered GRB 090423 on April 09, 2009 at 07:55:19 UT, (Krimm et al. 2009). At almost the same instant also the Fermi Gamma Ray Burst Monitor (GBM) triggered on GRB 090423. The two light curves show a structured single peak lasting ~ 19 seconds, while the T-90, in the Swift (15-150 keV) band, is equal to 12 ± 1.4 s. This measure, and the estimate of the redshift, suggests that this GRB is intrinsically a short-GRB. Nevertheless GRB 090423 is fully consistent with the Amati relation, (Amati et al. 2009), so that it is considered as a long-GRB. Moreover if we consider the Swift-BAT sensitivity of $\sim 10^{-8}$ ergs cm^{-2} s^{-1}, and considering the redshift of ~ 8.1, it is likely that part of the emission of gamma-rays from GRB 090423 has not been detected because it was below the threshold of Swift-BAT. This evidence is supported by observations of Swift-XRT, which started to observe GRB 090423 ~ 72 seconds after the BAT trigger time. The XRT light curve of GRB 090423 is a classical 3-steps X-ray light curve, showing in particular a flare just before the start of the plateau phase. This flare is a signature of a prolonged activity of the peak of the afterglow up to ~ 400 seconds, so when the flare stops then it starts the plateau component.

This second phase in the X-ray afterglow was discovered with the launch of the Swift satellite, which was the first instrument to obtain early X-ray light curves immediately following GRBs. In literature there are several possible explanation for this second component, (Butler & Kovevski 2007, Nousek et al. 2006, Zhang et al. 2006). In the standard model it was attributed to the outflow, being jet-like, and the break in the X-ray light curve occurs when the edge of the jet becomes visible, as the jet slows down, (Meszaros & Rees 2009, Roads 1997, Roads 1999, Sari et al. 1999), while the other models, which exclude a jet-emission model, need a mechanism that allows a prolonged injection of energy, (Kumar & Piran 2000, O'Brien et al. 2006). Here we consider the application of the fireshell model, (Ruffini et al. 2001, Ruffini et al. 2001b, Ruffini 2007a), to GRB 090423, in which a possible alternative to the existing models to explain this second component is the following : we

Table 16.1.: Starting parameters for the fireshell fit of GRB 090423

Parameter	Starting value
E_{dya}	$1.00 \times 10^{53}\ ergs$
M_{BH}	$10\ M\odot$
B	$\sim 10^{-3}$

consider the shell, which expands in the medium surrounding the burst, as a shell structured, which consists of the classical compact front, but ending more smoothly with a tail of the matter distribution less energetic. As the forward shell collides with the circumburst medium (CBM), it loses energy and velocity while the tail moves forward undisturbed by the collision with the CBM. At a certain time, t_r, the forward shell, which continues to lose energy and slow down, reaching a Lorentz Gamma factor, Γ_2, value such that it is catched up by the delayed shells, which constitute the tail of the total fireshell. This second shell does not interact with the CBM, since the first one, after its passage, cleaned up most of the interstellar medium near the GRB site, leaving this second shell in a quasi empty space. It's important to note the existence of a correlation between the value of the bulk Lorentz Gamma factor at the transparency, Γ_0, and at the collision of these two shells, Γ_2. This fact is known only for a tens of GRBs, (Bernardini in preparation), and it could be interesting for constraining better the fireshell dynamics.

At this moment it starts the second component, the plateau, which lasts $10^2 - 10^4$ seconds until a break occurs in the light curve at a time t_b, where the radiation flow begins to decline steadily. The physical origin of this second component is to seek in the collision of the shell which occurs at t_r. The collision would generate a sort of refreshed shock, whose following dominant radiation emission process is due to magnetohydrodynamics of electrons accelerated in the shell's collisions.

In the literature there are several indications, see for example (Butler & Kocevski 2007), that the late afterglows is due to a synchrotron-like emission scenario, whose radiation emission theory is well known in the case, (Sari et al. 1998, Granot & Sari 2002). For this reason we strongly believe that the plateau phase and the following X-ray emission is due to another emission process and for the first time we do not expect the equations of motion to hold.

16.1. GRB 090423 in the fireshell model

We start the fit of the *Swift*-BAT light curve and the spectrum of GRB 090423 considering as starting parameters the values indicated in the Table 16.2.

In Fig. 16.1 we report the theoretical fit of *Swift*-BAT (15-150 keV) light

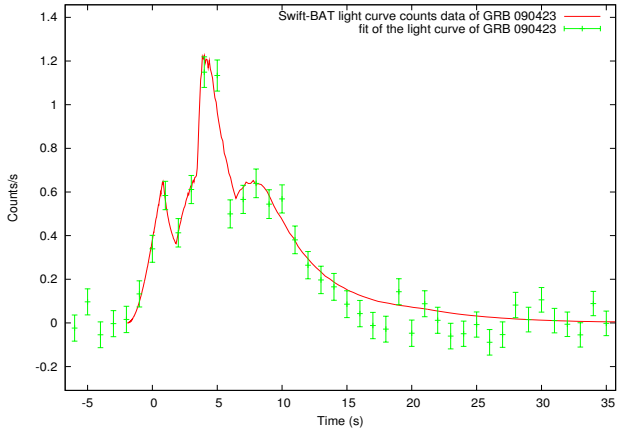

Figure 16.1.: *Swift*-BAT (15-150 keV) light curve (green bars) compared with the theoretical fit (red lines).

curve of GRB 090423 prompt emission. As said before, we find the P-GRB below the detector threshold, so we identify all of the gamma-pulses with the afterglow peak emission, in the context of the "fireshell" scenario. These pulses have been reproduced in our simulations assuming a spherical distribution of the density of the CBM. In particular each pulse corresponds to an overdense shell of matter around the site of the burst. On average, we find that during the prompt emission we have for the CBM density the value of $< n >= 5 \times 10^{-2}$ particles/cm^3. Nevertheless after the prompt emission, when it starts the X-afterglow, the density decreases abruptly up to the lower value of 10^{-7} at the onset of the plateau. In particular the big X-flare, starting at $T_0 + 170$ s is fitted considering a density shell of 10^{-5}. This value is quite low, but it could be reconsidered in light of the possible shell's fragmentations, e.g. (Dainotti et al. 2008), as we can see in the next subsection.

Last we obtain for the two parameters characterizing the source in the Fireshell model the value of $E_{dya} = 1.20 \times 10^{53}$ ergs, and $B = 8 \times 10^{-4}$. With these values we obtain an initial plasma created between the radii $r_1 = 2.93 \times 10^6$ cm and $r_2 = 1.39 \times 10^8$ cm, with a total number of pairs $N_{e^\pm} = 4.10 \times 10^{57}$ and an initial temperature of about 2.3 MeV. So we can estimate the energy emitted in the P-GRB, which turns out to be $E_{P-GRB} = 4.5\,\% \, E_{dya} = 5.4 \times 10^{51}$ ergs. Immediately we note that, at that redshift and with the energy given by E_{P-GRB}, the P-GRB should not be visible, as we verify in the observations. The transparency point happens to the radius of $r_0 = 5.03 \times 10^{13}$ cm, when the fireshell has a Lorentz Gamma factor of about 1100.

For the fit of the energy spectrum we assume that the spectral energy distribution of photons emitted in the co-moving frame of the fireshell is:

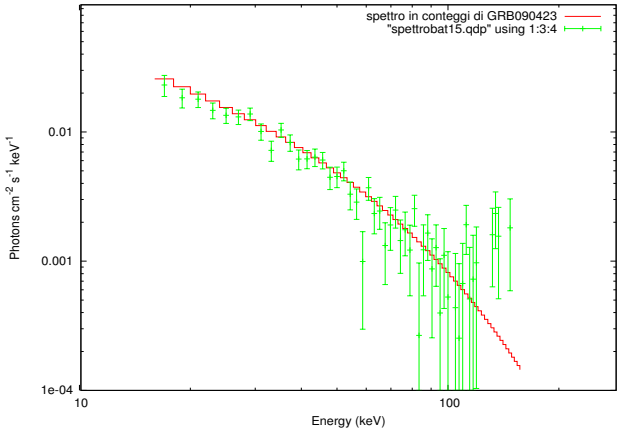

Figure 16.2.: *Swift*-BAT (15-150 keV) energy spectrum (green bars) compared with the theoretical fit (red lines).

$$\frac{dE}{dAd\Omega d\nu dt} = \frac{2h\nu^3}{c^2}\left(\frac{h\nu}{k_B T}\right)^{\alpha}\frac{1}{exp\left(\frac{h\nu}{k_B T}\right)-1} \tag{16.1.1}$$

which is characterized by the parameter α. The spectrum in the observer's frame is obtained by the convolution over the EquiTemporal Surfaces (EQTS, (Biacno et aa. 2001)) and the observational time, (Patricelli et al. in preparation). Here we show the application of this spectral model, for which we find for the α-index in Eq.(16.1.1) the value of $\alpha = -1.8$. The fit of the energy spectrum is plotted in Fig.16.2.

16.1.1. The fragmentation of the fireshell

The fit of the X-afterglow of GRB 090423 appears to have a significant lower effective CBM density. This fact could be due to the possible fragmentation of the incoming baryon fireshell. One of the possible causes of the fireshell fragmentation is attributable to the interaction of the same shell with the CBM. In particular at a certain radius the surface of the fireshell, responsible for the radiation emission, does not increase as r^2, but as r^β, with $\beta < 2$, (Ruffini et al. 2007). So the effective CBM density n is linked to the actual one n_{act} by the following relation:

$$n = \mathcal{R}\, n_{act} \tag{16.1.2}$$

where $\mathcal{R} = (r^\star/r)^\delta$, with $r^\star$ the starting radius at which the fragmentation occurs and $\delta = 2 - \beta$. Considering a constant density of the CBM, exactly $n_{act} = 10^{-2}$ particles/cm^3 at $r^\star = 6 \times 10^{16}$ cm, we obtain from the fit of the late-prompt light curve, the value of $\beta = -3$.

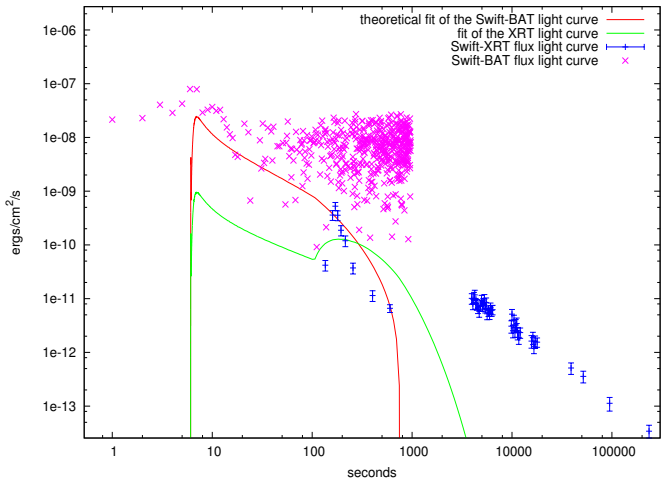

Figure 16.3.: The fit of the Swift BAT and XRT light curve of 090423, obtained considering the prompt emission as due to the P-GRB. Note the lack of efficiency for the simulation of the x-ray flare.

16.1.2. GRB 090423 considered as a disguised short GRB

In light of the new results from the disguised short GRBs, see Secs. C.3, C.1 and C.2 an intriguing possible explanation for the emission observed in GRB 090423 could be that this GRB is a disguised short GRB. We tried to simulate the emission observed considering the prompt light curve, and of consequence the most energetic part of the GRB, as due to the P-GRB emission, and an intermediate case, where we considered both the contributes, the P-GRB and the extended afterglow, in the GRB prompt light curve.

In the first case, see Fig. 16.3, we don't see the peak of the afterglow and, more important, we are not able to simulate the x-ray flare observed in the XRT light curve. Moreover we don't have in this case enough energy to model the following x-ray emission (the plateau and the late decay), which we consider as due to a different emission mechanism, see next section. In the latter case the simulation of the light curve is in good agreemente with the observed data, see Fig. 16.4, but in order to simulate it we must take into account a strong variation of the emitting fireshell area.

In all cases the CBM average density exhibits a sharp variation at a certain radius. This fact seems in agreement with an initial wind density of the CBM, $\rho \propto r^{-2}$, and a subsequent high-density cloud, $\rho \sim 10$ particles/cm^3.

The work about this source is still in progress, and it would be very interesting in particular to take some other similar results from other high-redshift sources as, for example, GRB 080913.

Finally we note that these two extra possibilities can be discarded by the fact that, at that redshift, the detector threshold act as a sort of selection effect for the GRB emission. In particular there could be a hidden emission that

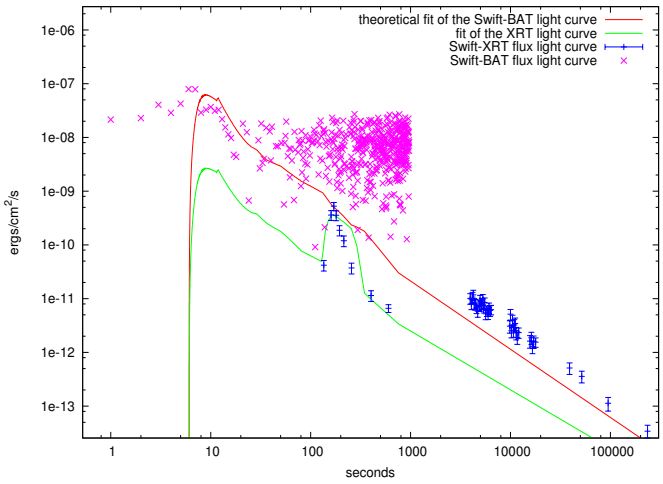

Figure 16.4.: The fit of the Swift BAT and XRT light curve of 090423, obtained considering the first 4 seconds of the prompt light curve as due to the P-GRB emission.

was not detected by Swift BAT, and it can be happened both before and after the observed prompt light curve. However we cannot speculate more on this argument, but there is the possibility that the prompt emission is due to the most energetic pulse of the intrinsic hard x-ray emission of the GRB.

16.2. A new component in the afterglow scenario

This GRB was first detected in the X-ray by Swift-XRT, which began observing the region of the explosion 72.5 s after the Swift-BAT trigger. The analysis of the first 8.4 ks in the 0.3-10 keV band,(Stratta et al. 2009), reveals a classical 3-steps X-ray trend. In the first steep phase, at T0+170 s, there is a big flare, ending at about T0+260 s when immediately the plateau component starts. At about T0+3.9ks the light curve is well-described by a power-law model with index $\alpha = -1.30 \pm 0.10$.

Then we consider the time integrated and time resolved spectral analysis, in particular analyzing the spectrum emitted during each of the X-ray phase. All of these spectrum are well fit by an absorbed power-law spectral model whose energy indexes β are shown in the second column of the Table 16.2. For these spectrum we impose as the Galactic column density the value of $6.9 \times 10^{22} cm^{-2}$, which was found for the fit of the total spectrum, while as intrinsic column density we obtain the value of $2.9 \times 10^{20} cm^{-2}$.

As a result of the previous analysis we report an evident spectral variation in the respective energy index between the first phase and the remaining ones of the X-ray light curve. Nevertheless we note that a similar spectral variation was also noted in the past, (Butler). In that work the authors describe this

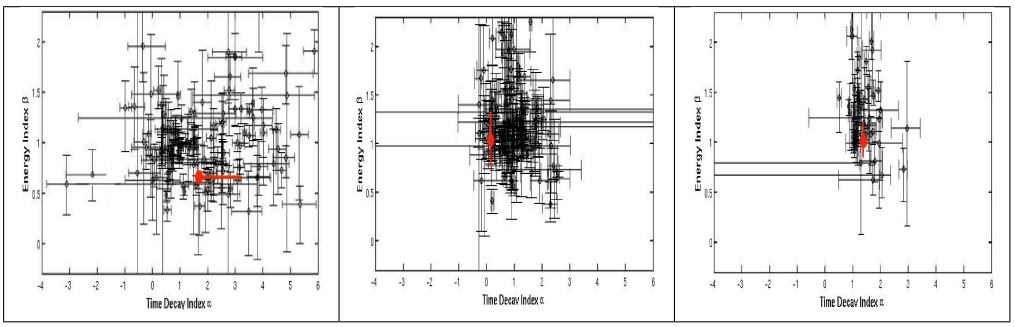

Figure 16.5.: Time decay index α versus Energy index β for the X-ray afterglows for each of the three afterglow phases described in the text. We consider a sample of 133 GRBs with time decay α and energy index β taken in (Evans2). In particular we consider only energy spectra taken by the Swift-XRT satellite in Photon Countig mode for at least the first two afterglow phases. Note the data sample clustering in the second and the third phase, as delineated in (Butler & Kocevski 2007).

variation as the signature of a second component in the afterglow of GRBs, (Nousek). In particular a detailed spectral analysis of a sample of GRBs, that we reproduce in Fig. 16.5, where the red dot represents GRB090423, led the authors to state that this second component has all of the observational characteristics of an adiabatic external shock synchrotron radiation, e.g. see (Sari). In this work we don't tackle directly this argument, but we assert that after a certain time, the fireshell emission drops down so that the following dominant radiation emission process is due to the magnetohydrodynamics of electrons accelerated in the previous shell's collision. A complete analysis and explanation of these considerations will be explained in a forthcoming paper.

In this way we stop our analysis of GRB 090423 at the start of the plateau component. As delineated previously, the plateau component starts after a big flare lasting about 150 s. It is also the presence of this flare which bring us to the conclusion that 090423 is a long GRB. Indeed it is seen in the X-ray part of the e.m. spectrum, but if we consider the correction for the redshift of the GRB, we obtain that this emission should be stay in the γ-ray part of the e.m. spectrum. Moreover the flare is the signature of a prolonged activity of the shell with the CBM. From our analysis we preliminarily obtain that this flare is due to some blob of interstellar matter located at ≈ 0.5 l. y. along the line of sight from the Black Hole formed. At these high distances from the progenitor we have that the fireshell visible area (defined by the condition $\cos\theta = v/c$, where θ is the angle between the emitted photon and the line of sight, and v is the fireshell velocity, (Bernardini et al. 2009), is wider than that at short distances, see Fig. , and this fact translates in the fit with a different treatment for the flare: we consider a bidimensional structure

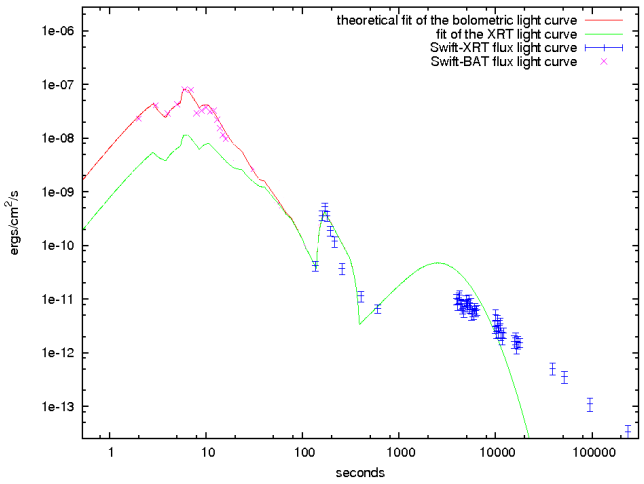

Figure 16.6.: The fit of the X-ray light curve of 090423. Note the end-point t the start of the plateau and the fit of the BAT light curve (in purple).

Table 16.2.: Time-resolved X-light curve analysis. The light curve index for the plateau and late decay phase are taken from the XRT refined analysis, (Stratta et a. 2009)

Phase	β	α	$C-STAT$
Total	0.825 ± 0.09	xxx	$308.11(345)$
Flare	0.44 ± 0.20	< -1.4	$152.65(168)$
Plateau	1.01 ± 0.33	0.13 ± 0.11	$109.19(118)$
Late	0.901 ± 0.15	-1.30 ± 0.10	$238.63(271)$
Plateau + Late	0.93 ± 0.14	xxx	$279.81(301)$

of the CBM clump along the line of sight, as already done for GRB 011121, (Caito et al. 2009). For this reason we integrate up to a well-defined angle θ_c from the line of sight, corresponding to the transverse dimension of the CBM clump which in this case is given by $d_c = 2r_c \sin\theta_c$, where r_c is the distance of the clump from the formed black hole. We obtain a good fit for the flare considering a cut at 170 s after the initial emission, which corresponds to a distance from the black hole formed of $r_{cut} = 3.25 \times 10^{17}$ cm. The final fit of the flare is shown in Fig.16.8 while a graphical explanation of our flare analysis is shown in Fig.16.9. Even if the fireshell emission after the cut is different from that simulated, our procedure confirms the fact that we can obtain a good representations of the flares in the context of the interactions of the fireshell with the CircumBurst medium. However, in order to simulate the effective emission after a cut to the fireshell visible area, it is required a net improvement of the code, also for a fully treatment in a three-dimensional context of the CBM clump responsible for the flare.

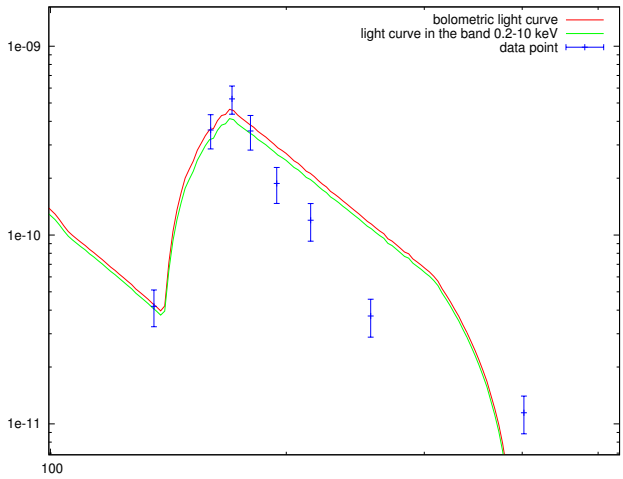

Figure 16.7.: The fit of the X-ray flare of 090423 considering that all of the emission from the fireshell contributes to it.

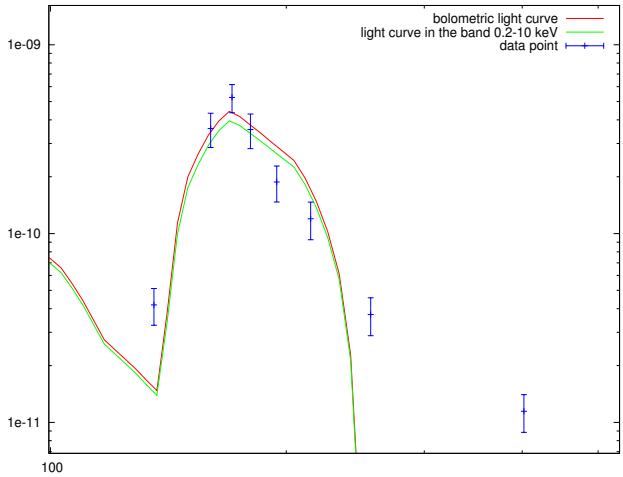

Figure 16.8.: The fit of the X-ray flare of 090423. In order to obtain a good fit, we consider a cut to the fireshell visible area corresponding to the total emission up to 170 s after the initial emission.

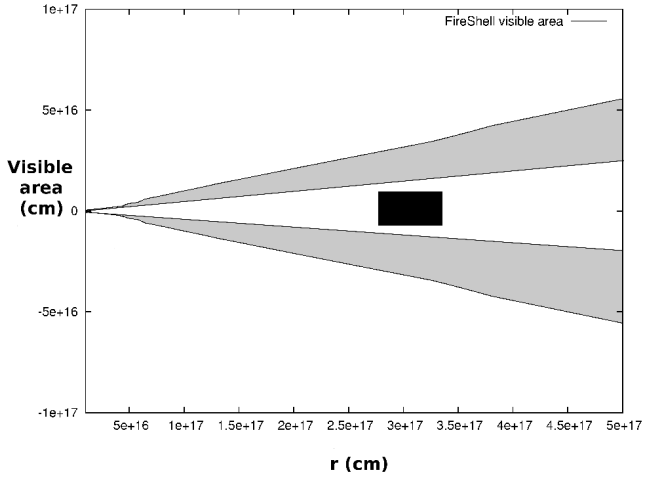

Figure 16.9.: A graphical expanation for the cut to the fireshell visible area expaining the flare in the X-ray light curve.

16.3. Discussions and conclusions

GRB 090423 is the most distant GRB up to date, with a redshift of about $z = 8.1$. In the cosmological ΛCDM standard model this means that 090423 bursted about 700.000 years after the Big Bang. For this reason we argue that 090423 originated from the collapse of a massive star, generating a Black Hole with a minimum mass of 10 solar masses. A binary merging origin is rejected since the time for the formation and the merging of two compact binary stars is supposed greater than 700.000 years.

The fit in the fireshell scenario suggests that 090423 is a canonical Gamma Ray Burst. We obtain a CBM average density of about $10^{-2}\,\#/cm^3$, and a high value of the Lorentz Gamma factor at the transparency $\Gamma \approx 10^3$. The presence of a big flare in the X-ray light curve is a signature of the late interaction of the fireshell with the CBM and, more important, is the confirmation that 090423 is a long GRB. This fact is supported also by the fact that this GRB satisfies the Amati relation.

The X-ray light curve consists of 3 distinct power-law segments. The first one consists of a rapid flux decay (if we do not consider the flare) and it represents the residual emission of the fireshell. In the second phase the flux is approximately constant so the light curve become shallower than the previous phase, while in the last one we have another flux decay but with a different time decay index α than the first phase. Nevertheless we note a variation in the power-law spectral index β between the first and the remaining 2 X-ray light curve phases. This fact is more evident in the diagram shown in Fig.16.5, where is reported the same analysis but considering a sample of 133 GRBs.

In particular it is clearly evident a clustering of the data sample in the second and the third phases. This fact suggests the presence of a second component in the GRB scenario. We are studying this possibility in the FireShell scenario and in particular we believe that this second component is due to the structure of the FireShell, (De Barros et al. 2009). In particular the ejecta should have a range of bulk Lorentz factor Γ, interacting with each other when the outer shells slow down due to the interaction with the CBM. This interaction should generate some bumps, turning off the FireShell emission and highlighting sub-process of emission due to the magnetohydrodynamics of the electrons accelerated in the previous shell's collisions. One of the possible evolutions of the model will be the explanation of this second component in terms of this electron-generated emission.

17. The high-energy emission in the fireshell scenario

The launch of the *Fermi* satellite opened a new window on the GRB science. Thanks to the Large Area Telescope (LAT) (Atwood et al., 2009) on-board the Fermi spacecraft, we can detect very high energy photons (> 100 MeV) from GRBs. The first result we obtained from Fermi is that not all GRBs own this high energy component, but just a fraction of them: currently LAT has detected energetic photons from ~ 20 GRBs upon the whole set of ~ 480 GRBs detected by the Fermi Gamma-ray Burst Monitor (GBM) (Meegan et al., 2009). However this last evidence has been already noticed by the EGRET detector on board the Compton Gamma-Ray Observer satellite, which detected high energy photons just from few GRBs.

The other very interesting discovery of the Fermi LAT was that this high energy component is delayed compared to the emission observed by the GBM detector. Moreover when the GBM signal fades in the canonical way, the high energy one is prolonged and can last for hundreds of seconds. The case of GRB 080916c (Abdo et al., 2009b) is remarkable: it is currently the most energetic GRB to date, with an estimated isotropic energy of $E_{iso} = 8.8 \times 10^{54}$ ergs. A significant contribution to this value was provided by the high-energy gamma-rays (¿ 100 MeV) emitted by this GRB. Moreover this high energy emission started ~ 3.6 s after the GBM trigger and persisted up to 1400 s after the GBM trigger. The spectral energy distribution of these high energy photons is best represented by a power-law function, whose photon index was found to be the same of the harder component of the GBM Band spectrum. This observed feature suggested the possibility that the origin of the high energy component can be the same of the GRB emission in the "canonical" electromagnetic energy range. The case of GRB 090902b on the contrary is quite different. Its energy distribution shows a deviation from the Band function obtained from fitting GBM data between 50 keV and 40 MeV (Bissaldi and Connaughton, 2009). This deviation is apparent both below 50 keV in the GBM and above 100 MeV in the LAT. It is well-fit by a single power-law, with a well-constrained index that is retrieved from a fit of the GBM data alone, the LAT data alone, and when jointly fitting the entire data set, see Fig. 17.1. Moreover the time-resolved spectral analysis shows an evolution with the time for the peak energy E_p, (Abdo et al., 2009a).

In the case of the fireshell scenario, since the adopted modified black-body spectrum can never produce large MeV and GeV photons, a new mechanism

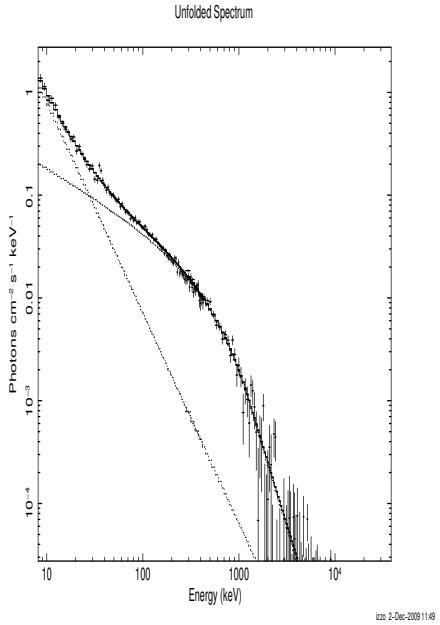

Figure 17.1.: The fit of the spectrum of 090902B considering as spectral model a Band model plus a power-law component.

is needed in the fireshell to explain the high energy component. Following an idea first formulated by Katz (1994a), we propose that the GeV emission is originated by the collision between relativistic baryons in the fireshell after the transparency and the nucleons located in some giant molecular clouds (GMC) near the burst site. This collision should give rise pion production, whose immediate decay provides high energy photons, neutrinos and leptons. In these GMCs, there are structures composed mainly of molecules and nucleons, so that the interaction of relativistic nucleons of the Fireshell and the nucleons at rest in the GMC could happen. For this reason we consider the proton-proton interaction as responsible for the high energy emission in GRBs. So we have that the interaction of the fireshell with these GMCs will happen at a certain radius $R_{ext} \sim 10^{16-17}$ cm. If the radius of these GMCs is of the same order, from the fact that the mean free path in p-p collisions is $l = (n\sigma_{pp})^{-1}$, with $\sigma_{pp} \simeq 30$ mbarn the cross section in the case of a pp interaction, we obtain an average density n of the cloud of about 10^{9-10} particles/cm^3 if l and the GMC radius are similar. However from the IR and radio observations of GMCs, we know that the particle density in these regions reaches high values (10^{3-4} particles/cm^3) but there are substructures in these clouds, in the forms of filaments, bubbles and clumps, in which the density reaches very high values (10^{4-6} particles/cm^3) (Williams et al., 2000). Moreover, if we consider a magnetic field of the cloud such that the respective gyroradius is of the order of the cloud size, the relativistic protons could spend a

greater time inside the cloud, giving a possible explanation for the prolonged emission in the MeV-GeV energy range. We have that for a gyroradius of the order of 1016 cm, and for a proton energy of 3 TeV, the average magnetic field should be of $\sim 10^{-7}$-10^{-6} G, a value in agreement with the magnetic field of interstellar medium (Beck, 2005). Nevertheless a very detailed dimensional analysis is needed, in order to constraining better the physics underlying the p-p process in the fireshell.

Our scope consists in determining the spectral shape of the pp fireshell process, or at least some estimates which connect the canonical GRB fireshell emission with this latter one. The interaction of the ABM-pulse with the CBM, including the GMC, will generate the extended afterglow emission, which is simulated using the GRBsim code (Bianco and Ruffini, 2005b), whose results (light curve and spectrum) are shown in Figs. 17.3, 17.4. In our simulation we consider as dyadosphere energy the value $E_{dya} = 8.8 \times 10^{54}$ ergs, but the fraction of this energy going in the extended afterglow emission is the 75 % of the totality. In this picture, the onset of the high energy emission allow us to distinguish the P-GRB emission from the extended afterglow. In fact, since the P-GRB is the emission at the transparency of the original fireball, there should be no signatures of particle interaction in its spectrum. So we have a powerful tool for identify the P-GRB emission in a GRB.

In GRB 080916c the P-GRB should correspond with the first pulse visible in the Fermi-GBM light curve, see Fig 17.3. From the observed flux, we have estimated the energy emitted in the P-GRB, $E_{P-GRB} = 2.8 \times 10^{53}$ ergs, in order to compute the baryon loading of the GRB (Ruffini et al., 2001a), which results to be $B = 3.3 \times 10^{-4}$. From the simulation we have obtained an average CBM density of $< n > = 2.2 \times$" 10^{-3} particles/cm^{-3}, which seems to be inconsistent with the predicted value of the GMC responsible for the pp interaction. However, we note that this value correspond to an ISM in a volume spherically-distributed around the burst site, while the GMC should occupy only a tiny fraction of the entire solid angle so that the real density is larger. The first important result that we obtain from the simulation is that the Lorentz γ factor at the transparency is very high, $\gamma = 3170$. We found very high value for the Lorentz factor also for the other GRBs with high energy emission, so that it is possible to conclude that a requirement for the presence of high energy in GRBs is a very large value for γ. Moreover, the very large energy emitted in these GRBs reflects in the number of baryons located in the incoming fireshell, so that in these GRBs there will be a large number of pp collisions and of consequence a large probability to observe very high energy photons incoming from them.

Likewise, in GRB 090902b the P-GRB should correspond with the first 6 s and its energy emitted is constrained to be $\sim$ 5-6% of the dyadosphere, which in this case is $E_{dya} = 3.63 \times 10^{54}$ ergs. With a baryon loading of 3×10^{-4}, the Lorentz γ factor at the transparency also in this case is very high,

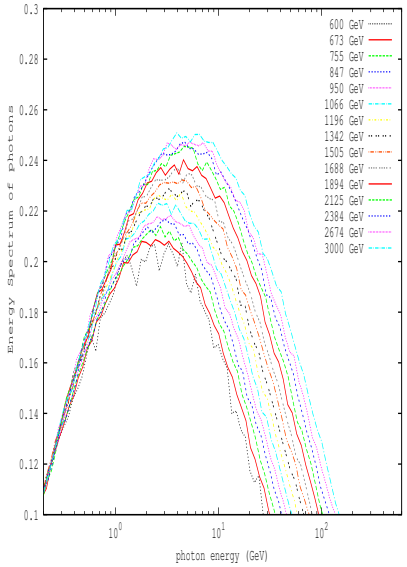

Figure 17.2.: Energy spectrum of photons obtained from our simulations of proton-proton interactions, with different values for the energy of the relativistic proton incoming.

$\gamma = 2386$. This fact seems to suggest a sort of energy threshold for the high energy component in the GRBs.

We tried to model this high energy emission considering the pp interaction in the center of mass (c.m.) frame. We note that the threshold for the creation of pion is relatively low: the Lorentz γ value of the incident proton can be $\sim$ 2.2. From the previous analysis, we have obtained a very high value for the Lorentz γ of the incoming baryons so their energy in the interaction is very large $E_p = (\gamma 1) m_p c^2$,that for $\gamma \propto 10^3$ is of the order of some TeV.

In order to obtain an energy distribution of the high energy photons obtained from the pion decay, we used the Monte Carlo code SIBYLL (Fletcher et al., 1994) to reproduce the spectra of the collisions for different energies of the incident protons. Using the SIBYLL code, we could note that $\sim$ 83% of the radiation produced is from the decay of the neutral pion π^0, where the decay $\pi^0 \rightarrow 2\gamma$ is by 98.8 %. In the Fig. 17.2 it is shown the count spectrum of emission for fifteen different energies of the incident protons, so that we can note how the most part of the emitted photons increases from 2 to 5 GeV while the incident proton energy increase from 600 to 3000 GeV. In the case of incident protons with the highest energy, the production of photons with 300 MeV and 100 GeV is the half of the peak production (5 GeV).

Note that for the data of GRB 080916c we consider the Fermi GBM observations (8 keV - 5000 MeV), reduced with the standard FTOOLS package for

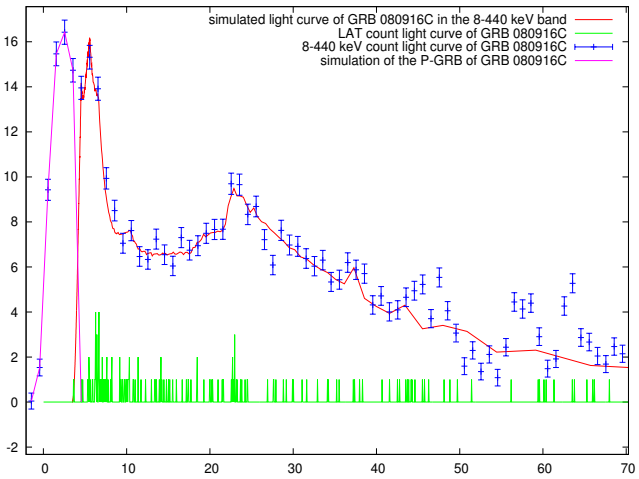

Figure 17.3.: Fermi-GBM (8-440 keV) light curve (blue points) compared with the results of our simulation of the light curve of GRB 080916C (red lines) and the P-GRB emission (pink line). The green bars correspond to the LAT ($>$ 100 MeV count light curve. Note the P-GRB emission starting before the LAT data.

the Fermi satellite [1].

17.1. Spectral analysis of the P-GRB candidates

According to the Fireshell scenario, the main emission in a GRB, the extended afterglow, is due to the interaction of the baryonic and leptonic shell with the interstellar medium surrounding the GRB. Before the extended afterglow, we should see a flash of X and gamma radiation, the P-GRB, due to the initial plasma composed of $e^{\pm}$-pairs and photons, that reaches the condition of transparency. This relativistic plasma thermalizes before the transparency, so the energy spectrum of the P-GRB should have the characteristics of a black-body spectrum. However, as it is well known, the spectrum of a GRB, and of a typical pulse observed in a burst, is not thermal. This seems could have interesting consequences for the Fireshell model. The possibilities are different: among the many ones considered are those that 1) in addition to a thermal emission there is another dominant process together the P-GRB emission, 2) the spectrum is purely thermal, but not of the type described above, i.e. a convolution of one or more black-body with the EQTS, 3) what is observed is not the P-GRB.

Since in GRB 080916c we the delayed onset of the high-energy emission could be due to the interaction of the fireshell with the CBM, and the emission previously observed in the lower energy bands associated with another

[1] `http://heasarc.gsfc.nasa.gov/ftools/ftools_menu.html`

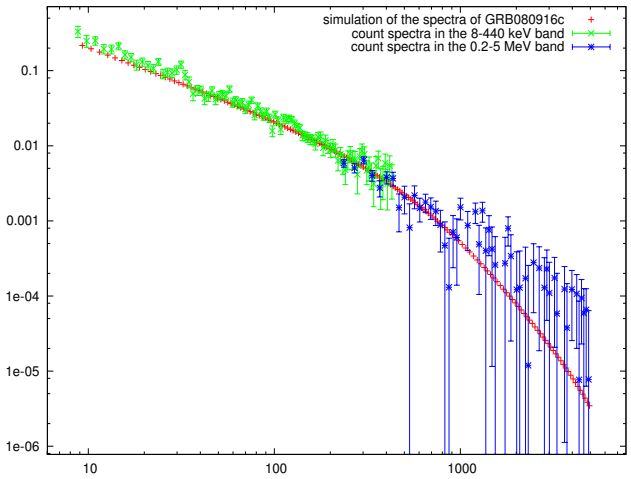

Figure 17.4.: Fermi-GBM (8-440 keV - green bars) and Fermi-BGO (260-5000 keV - blue bars) energy spectrum compared with the results of our simulation for the energy spectrum of GRB 080916C (red lines).

Table 17.1.: Time-resolved spectral analysis in the range (8 keV - 5 MeV) for the first pulse of GRB 080916C using a blackbody spectral model with an extra power-law $kE^{-\gamma}$ component, a classical Band function and a modified blackbody spectral model.

GRB 080916C			
BB+po	kT = 56.91 $\pm$ 2.49	-1.26 $\pm$ 0.03	
Band	α = -0.33 $\pm$ 0.08	β = -2.11 $\pm$ 0.18	E_0 = 209.98 $\pm$ 30.83
ModifiedBB	kT = 199.74 $\pm$ 17.99	-0.52 $\pm$ 0.05	

phenomenon, as the P-GRB, we made a spectral analysis of this emission, in order to find some signatures of the P-GRB thermal emission. We note that the duration of this first pulse in GRB 080916c is comparable with what is expected for a P-GRB, e.g. of the order of few seconds (Ruffini et al., 1999b). Moreover a time-resolved analysis of the different pulses seen in all GRBs shows a soft-to-hard trend for the first two pulses, becoming the canonical hard-to-soft one for the following emission. We consider three different spectral models in our analysis: 1) a classical Band model, represented by two broken power-laws smoothly connected at a given energy E_0; 2) a black-body model with an extra power-law component; 3) the modified black-body spectral model described in a previous section. A simple black-body model didn't explain the observed energy distribution. All of these spectral models are in agreement with the observed Fermi-GBM spectrum (8 - 5000 keV), and the final results are shown in Table 17.1 and in Figs. 17.5.

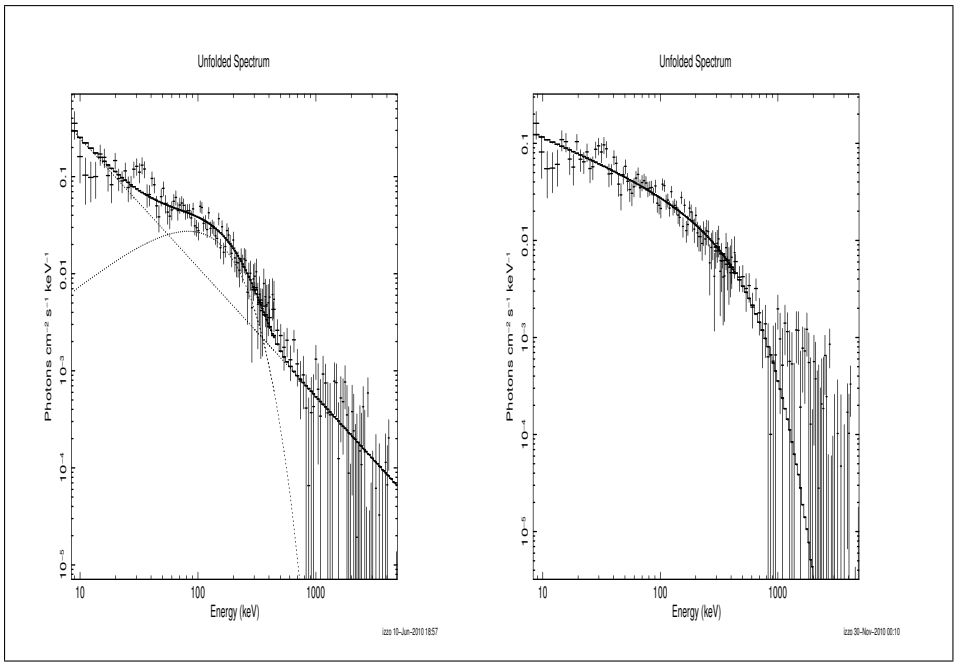

Figure 17.5.: Spectral fits of the Fermi GBM and BGO count spectra of the P-GRBs of GRB 080916C in the range (8 keV - 5 MeV). We consider in these cases a blackbody spectral model with an extra power-law component and a modified blackbody spectral model respectively.

A. On the GRB-SN association

Models of GRBs based on a single source (the "collapsar") generating both the SN and the GRB abounds in the literature (see e.g. Woosley and Bloom, 2006). Since the two phenomena are qualitatively very different, in our approach we have emphasized the concept of induced gravitational collapse, which occurs strictly in a binary system. The SN originates from a star evolved out of the main sequence and the GRB from the collapse to a black hole. The concept of induced collapse implies at least two alternative scenarios. In the first, the GRB triggers a SN explosion in the very last phase of the thermonuclear evolution of a companion star (Ruffini et al., 2001a). In the second, the early phases of the SN induce gravitational collapse of a companion neutron star to a black hole (Ruffini, 2006). Of course, in absence of SN, there is also the possibility that the collapse to a black hole, generating the GRB, occurs in a single star system or in the final collapse of a binary neutron star system. Still, in such a case there is also the possibility that the black hole progenitor is represented by a binary system composed by a white dwarf and/or a neutron star and/or a black hole in various combinations. What is most remarkable is that, following the "uniqueness of the black hole" (see Ruffini, 2009b), all these collapses lead to a common GRB independently of the nature of their progenitors.

Having obtained success in the fit of GRB 991216, as well as of GRB 031203 and GRB 050315 (see sections C.6 and C.7), we turn to the application of our theoretical analysis to the GRBs associated with SNe. We start with GRB 980425 / SN 1998bw. We have however to caution about the validity of this fit. From the available data of BeppoSAX, BATSE, XMM and Chandra, only the data of the prompt emission ($t_a^d < 10^2$ s) and of the latest afterglow phases ($t_a^d > 10^5$ s all the way to more than 10^8 s!) were available. Our fit refers only to the prompt emission, as usually interpreted as the peak of the afterglow. The fit, therefore, represents an underestimate of the GRB 980425 total energy and in this sense it is not surprising that it does not fit the Amati et al. (2002) relation. The latest afterglow emission, the URCA-1 emission, presents a different problematic which we will shortly address (see below).

A.1. GRB 980425 / SN 1998bw / URCA-1

The best fit of the observational data of GRB 980425 (Pian et al., 2000; Frontera et al., 2000) leads to $E_{e^\pm}^{tot} = 1.2 \times 10^{48}$ erg and $B = 7.7 \times 10^{-3}$. This implies

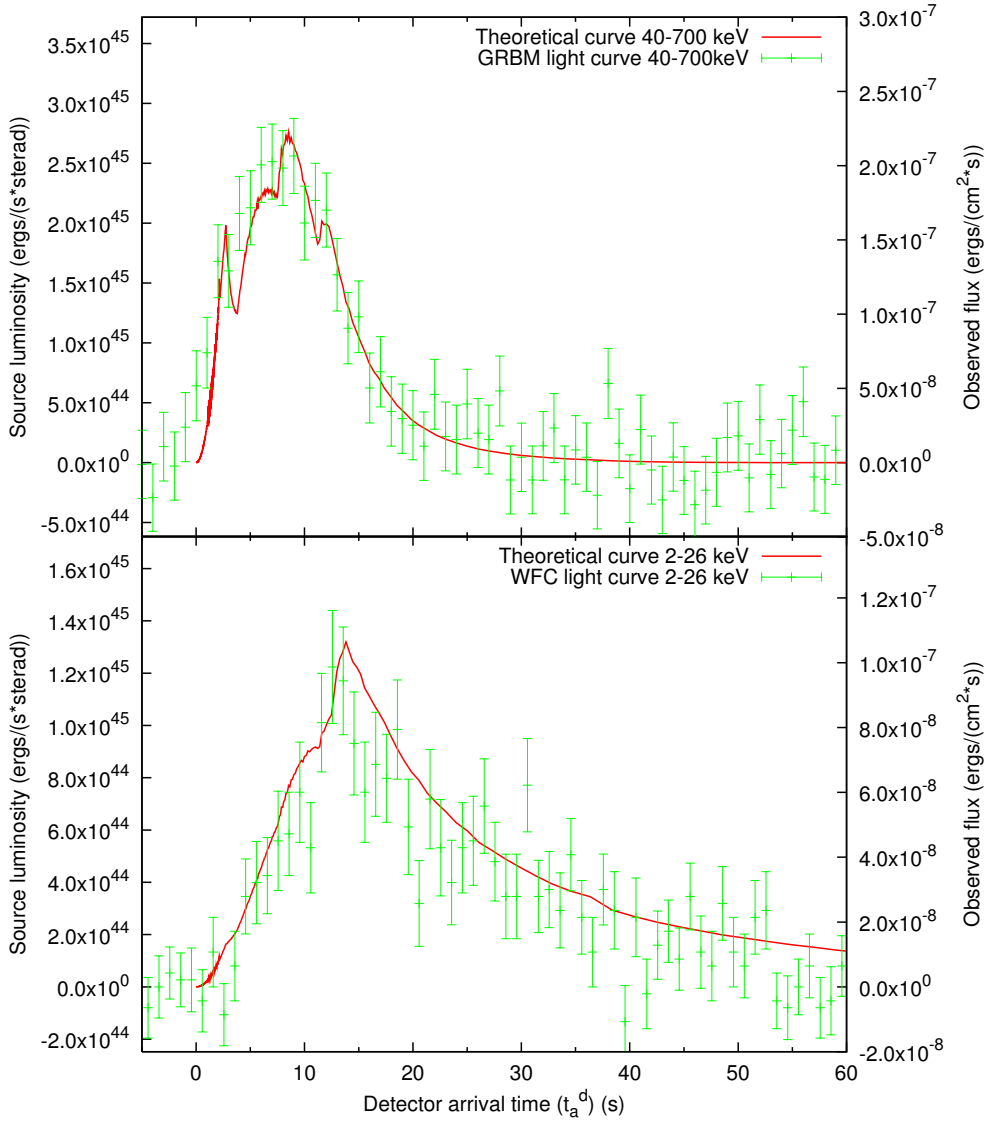

Figure A.1.: Theoretical light curves of GRB 980425 prompt emission in the 40–700 keV and 2–26 keV energy bands (red line), compared with the observed data respectively from Beppo-SAX GRBM and WFC (see Pian et al., 2000; Frontera et al., 2000).

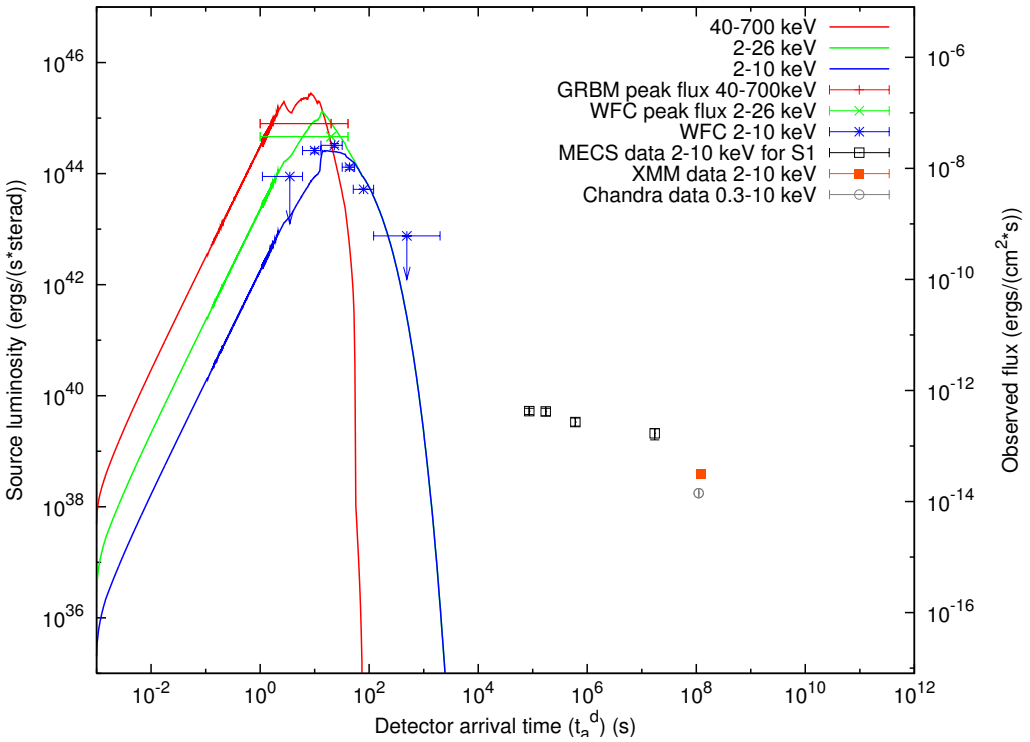

Figure A.2.: Theoretical light curves of GRB 980425 in the 40–700 keV (red line), 2–26 keV (green line), 2–10 keV (blue line) energy bands, represented together with URCA-1 observational data. All observations are by BeppoSAX (Pian et al., 2000), with the exception of the last two URCA-1 points, which is observed by XMM and Chandra (Pian et al., 2004; Kouveliotou et al., 2004).

an initial $e^{\pm}$ plasma with $N_{e^+e^-} = 3.6 \times 10^{53}$ and with an initial temperature $T = 1.2$ MeV. After the transparency point, the initial Lorentz gamma factor of the accelerated baryons is $\gamma_\circ = 124$. The variability of the luminosity, due to the inhomogeneities of the CBM, is characterized by a density contrast $\delta n/n \sim 10^{-1}$ on a length scale of $\Delta \sim 10^{14}$ cm. We determine the effective CBM parameters to be: $\langle n_{cbm} \rangle = 2.5 \times 10^{-2}$ particle/cm^3 and $\langle \mathcal{R} \rangle = 1.2 \times 10^{-8}$.

In Fig. A.1 we test our specific theoretical assumptions comparing our theoretically computed light curves in the 40–700 and 2–26 keV energy bands with the observations by the BeppoSAX GRBM and WFC during the first 60 s of data (see Pian et al., 2000; Frontera et al., 2000). The agreement between observations and theoretical predictions in Fig. A.1 is very satisfactory.

In Fig. A.2 we summarize some of the problematic implicit in the old pre-*Swift* era: data are missing in the crucial time interval between 60 s and 10^5 s, when the BeppoSAX NFI starts to point the GRB 980425 location. In this region we have assumed, for the effective CBM parameters, constant values inferred by the last observational data. Currently we are relaxing this condition, also in view of the interesting paper by Ghisellini et al. (2006).

The follow-up of GRB980425 with BeppoSAX NFI 10 hours, one week and 6 months after the event revealed the presence of an X-ray source consistent with SN1998bw (Pian et al., 2000), confirmed also by observations by XMM (Pian et al., 2004) and Chandra (Kouveliotou et al., 2004). The S1 X-ray light curve shows a decay much slower than usual X-ray GRB afterglows (Pian et al., 2000). We then address to this peculiar X-ray emission as "URCA-1" (see the following sections). In Fig. A.3A we represent the URCA-1 observations (Pian et al., 2000, 2004; Kouveliotou et al., 2004). The separation between the light curves of GRB 980425 in the 2–700 keV energy band, of SN 1998bw in the optical band (Nomoto et al., 2007; Pian et al., 2006), and of the above mentioned URCA-1 observations is evident.

A.2. GRB 030329 / SN 2003dh / URCA-2

For GRB 030329 we have obtained (see Bernardini et al., 2004, 2005b; Ruffini et al., 2007b) a total energy $E^{tot}_{e^\pm} = 2.12 \times 10^{52}$ erg and a baryon loading $B = 4.8 \times 10^{-3}$. This implies an initial $e^{\pm}$ plasma with $N_{e^+e^-} = 1.1 \times 10^{57}$ and with an initial temperature $T = 2.1$ MeV. After the transparency point, the initial Lorentz gamma factor of the accelerated baryons is $\gamma_\circ = 206$. The effective CBM parameters are $\langle n_{cbm} \rangle = 2.0$ particle/cm^3 and $\langle \mathcal{R} \rangle = 2.8 \times 10^{-9}$, with a density contrast $\delta n/n \sim 10$ on a length scale of $\Delta \sim 10^{14}$ cm. The resulting fit of the observations, both of the prompt phase and of the afterglow have been presented in Bernardini et al. (2004, 2005b). We compare in Fig. A.3B the light curves of GRB 030329 in the 2–400 keV energy band, of SN 2003dh in the optical band (Nomoto et al., 2007; Pian et al., 2006) and of the possible

Table A.1.: a) see Kaneko et al. (2007); b) Mazzali, P., private communication at MG11 meeting in Berlin, July 2006; c) evaluated fitting the URCAs with a power law followed by an exponentially decaying part; d) evaluated assuming a mass of the neutron star $M = 1.5 M_{\odot}$ and $T \sim$ 5–7 keV in the source rest frame; e) see Galama et al. (1998); Greiner et al. (2003a); Prochaska et al. (2004); Mirabal et al. (2006).

GRB	$E^{tot}_{e^{\pm}}$ (erg)	B	γ_0	E^{bolom}_{SN} (erg)[a]	E^{kin}_{SN} (erg)[b]	E_{URCA} (erg)[c]	$\frac{E^{tot}_{e^{\pm}}}{E_{URCA}}$	$\frac{E^{kin}_{SN}}{E_{URCA}}$	R_{NS} (km)[d]	z^e
980425	1.2×10^{48}	7.7×10^{-3}	124	2.3×10^{49}	1.0×10^{52}	3×10^{48}	0.4	1.7×10^{4}	8	0.0085
030329	2.1×10^{52}	4.8×10^{-3}	206	1.8×10^{49}	8.0×10^{51}	3×10^{49}	6×10^{2}	1.2×10^{3}	14	0.1685
031203	1.8×10^{50}	7.4×10^{-3}	133	3.1×10^{49}	1.5×10^{52}	2×10^{49}	8.2	3.0×10^{3}	20	0.105
060218	1.8×10^{50}	1.0×10^{-2}	99	9.2×10^{48}	2.0×10^{51}	?	?	?	?	0.033

URCA-2 emission observed by XMM-EPIC in 2–10 keV energy band (Tiengo et al., 2003, 2004).

A.3. GRB 031203 / SN 2003lw / URCA-3

We will show in section C.6 the detailed analysis of GRB 031203 which leads to a total energy $E^{tot}_{e^{\pm}} = 1.85 \times 10^{50}$ erg and to a baryon loading $B = 7.4 \times 10^{-3}$. This implies an initial $e^{\pm}$ plasma with $N_{e^+e^-} = 3.0 \times 10^{55}$ and with an initial temperature $T = 1.5$ MeV. After the transparency point, the initial Lorentz gamma factor of the accelerated baryons is $\gamma_{\circ} = 132$. The effective CBM parameters are $\langle n_{cbm} \rangle = 1.6 \times 10^{-1}$ particle/cm^3 and $\langle \mathcal{R} \rangle = 3.7 \times 10^{-9}$, with a density contrast $\delta n/n \sim 10$ on a length scale of $\Delta \sim 10^{15}$ cm. In Fig. A.3C we compare the light curves of GRB 031203 in the 2–200 keV energy band, of SN 2003lw in the optical band (Nomoto et al., 2007; Pian et al., 2006) and of the possible URCA-3 emission observed by XMM-EPIC in the 0.2–10 keV energy band (Watson et al., 2004) and by Chandra in the 2–10 keV energy band (Soderberg et al., 2004).

A.4. The GRB / SN / URCA connection

In Tab. A.1 we summarize the representative parameters of the above three GRB-SN systems together with GRB 060218-SN 2006aj which will be presented in section C.8, including the very large kinetic energy observed in all SNe (Mazzali, 2006). Some general conclusions on these weak GRBs at low redshift, associated to SN Ib/c, can be established on the ground of our analysis:

1) From the detailed fit of their light curves, as well as their accurate spectral analysis, it follows that all the above GRB sources originate consistently from the formation of a black hole. This result extends to this low-energy GRB class at small cosmological redshift the applicability of our model, which

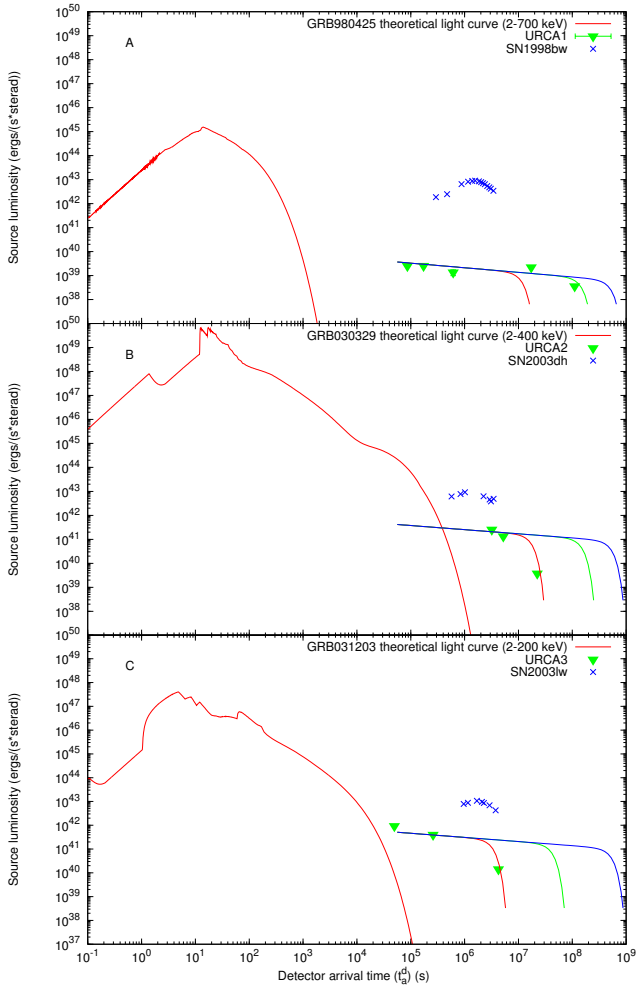

Figure A.3.: Theoretically computed light curves of GRB 980425 in the 2–700 keV band (A), of GRB 030329 in the 2–400 keV band (B) and of GRB 031203 in the 2–200 keV band (C) are represented, together with the URCA observational data and qualitative representative curves for their emission, fitted with a power law followed by an exponentially decaying part. The luminosity of the SNe in the $3000 - 24000$ Å are also represented (Nomoto et al., 2007; Pian et al., 2006).

now spans over a range of energy of six orders of magnitude from 10^{48} to 10^{54} ergs (Ruffini et al., 2003a, 2004a, 2007b; Bernardini et al., 2004, 2005b,a; Ruffini et al., 2006b). Distinctive of this class is the very high value of the baryon loading which in one case (GRB 060218, see section C.8 and Dainotti et al., 2007) is very close to the maximum limit compatible with the dynamical stability of the adiabatic optically thick acceleration phase of the GRBs (Ruffini et al., 2000). Correspondingly, the maximum Lorentz gamma factors are systematically smaller than the ones of the more energetic GRBs at large cosmological distances. This in turn implies the smoothness of the observed light curves in the so-called "prompt phase". The only exception to this is the case of GRB 030329.
2) The accurate fits of the GRBs allow us to infer also some general properties of the CBM. While the size of the clumps of the inhomogeneities is $\Delta \approx 10^{14}$ cm, the effective CBM average density is consistently smaller than in the case of more energetic GRBs: we have in fact $\langle n_{cbm} \rangle$ in the range between $\sim 10^{-6}$ particle/cm^3 (GRB 060218) and $\sim 10^{-1}$ particle/cm^3 (GRB 031203), while only in the case of GRB 030329 it is ~ 2 particle/cm^3. We are also currently studying a characteristic trend in the variability of $\mathcal{R}$ during some specific bursts as well as the physical origin of the consistently smaller effective CBM density $\langle n_{cbm} \rangle$ values observed in these sources (see Dainotti et al., 2007).
3) Still within their weakness these four GRB sources present a large variability in their total energy: a factor 10^4 between GRB 980425 and GRB 030329. Remarkably, the SNe emission both in their very high kinetic energy and in their bolometric energy appear to be almost constant respectively 10^{52} erg and 10^{49} erg. The URCAs present also a remarkably steady behavior around a "standard luminosity" and a typical temporal evolution. The weakness in the energetics of GRB 980425 and GRB 031203, and the sizes of their dyadospheres, suggest that they originate from the formation of the smallest possible black hole, just over the critical mass of the neutron star (see Fig. A.4 and Ruffini, 2006).

A.5. URCA-1, URCA-2 and URCA-3

We turn to the search for the nature of URCA-1, URCA-2 and URCA-3. These systems are not yet understood and may have an important role in the comprehension of the astrophysical scenario of GRB sources. It is important to perform additional observations in order to verify if the URCA sources are related to the black hole originating the GRB phenomenon or to the SN. Even a single observation of an URCA source with a GRB in absence of a SN would prove their relation with the black hole formation. Such a result is today theoretically unexpected and would open new problematics in relativistic astrophysics and in the physics of black holes. Alternatively, even a single observation of an URCA source during the early expansion phase of a Type Ib/c

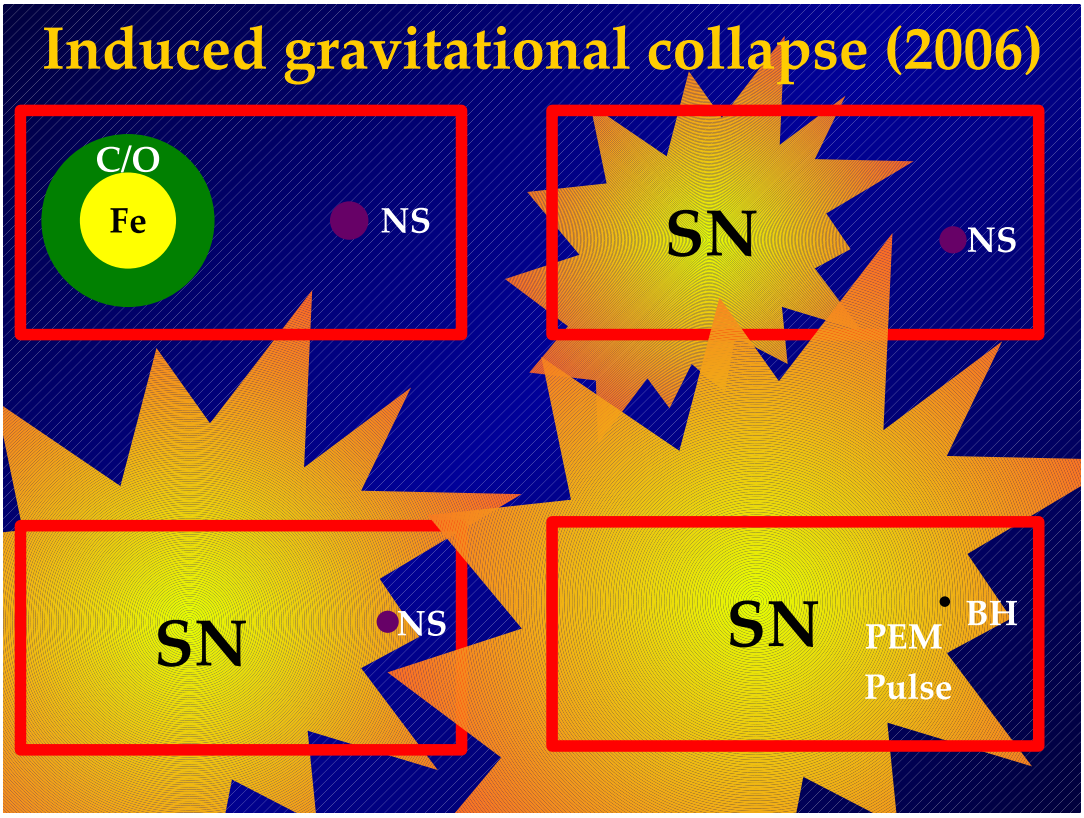

Figure A.4.: A possible process of gravitational collapse to a black hole "induced" by the Ib/c SN on a companion neutron star in a close binary system. Details in Ruffini (2006).

SN in absence of a GRB would prove the early expansion phases of the SN remnants. In the case that none of such two conditions are fulfilled, then the URCA sources must be related to the GRBs occurring in presence of a SN. In such a case, one of the possibilities would be that for the first time we are observing a newly born neutron star out of the supernova phenomenon unveiled by the GRB. This last possibility would offer new fundamental information about the outcome of the gravitational collapse, and especially about the equations of state at supranuclear densities and about a variety of fundamental issues of relativistic astrophysics of neutron stars.

The names of "URCA-1" and "URCA-2" for the peculiar late X-ray emission of GRB 980425 and GRB 030329 were given in the occasion of the Tenth Marcel Grossmann meeting held in Rio de Janeiro (Brazil) in the Village of Urca (see Ruffini et al., 2005b). Their identification was made at that time and presented at that meeting. However, there are additional reasons for the choice of these names. Another important physical phenomenon was indeed introduced in 1941 in the same Village of Urca by George Gamow and Mario Schoenberg (see Gamow and Schoenberg, 1941). The need for a rapid cooling process due to neutrino anti-neutrino emission in the process of gravitational collapse leading to the formation of a neutron star was there considered for the first time. It was Gamow who named this cooling as "Urca process" (see Gamow, 1970a). Since then, a systematic analysis of the theory of neutron star cooling was advanced by Tsuruta (1964, 1979); Tsuruta and Cameron (1966); Tsuruta et al. (2002); Canuto (1978). The coming of age of X-ray observatories such as Einstein (1978-1981), EXOSAT (1983-1986), ROSAT (1990-1998), and the contemporary missions of Chandra and XMM-Newton since 1999 dramatically presented an observational situation establishing very embarrassing and stringent upper limits to the surface temperature of neutron stars in well known historical supernova remnants (see e.g. Romani, 1987). It was so that, for some remnants, notably SN 1006 and the Tycho supernova, the upper limits to the surface temperatures were significantly lower than the temperatures given by standard cooling times (see e.g. Romani, 1987). Much of the theoretical works has been mainly directed, therefore, to find theoretical arguments in order to explain such low surface temperature $T_s \sim 0.5$–1.0×10^6 K — embarrassingly low, when compared to the initial hot ($\sim 10^{11}$ K) birth of a neutron star in a supernova explosion (see e.g. Romani, 1987). Some important contributions in this researches have been presented by van Riper (1988, 1991); Burrows and Lattimer (1986); Lattimer et al. (1994); Yakovlev and Pethick (2004). The youngest neutron star to be searched for thermal emission has been the pulsar PSR J0205+6449 in 3C 58 (see e.g. Yakovlev and Pethick, 2004), which is 820 years old! Trümper (2005) reported evidence for the detection of thermal emission from the crab nebula pulsar which is, again, 951 years old.

URCA-1, URCA-2 and URCA-3 may explore a totally different regime: the X-ray emission possibly from a recently born neutron star in the first days –

months of its existence. The thermal emission from the young neutron star surface would in principle give information on the equations of state in the core at supranuclear densities and on the detailed mechanism of the formation of the neutron star itself with the related neutrino emission. It is also possible that the neutron star is initially fast rotating and its early emission could be dominated by the magnetospheric emission or by accretion processes from the remnant which would overshadow the thermal emission. A periodic signal related to the neutron star rotational period should in principle be observable in a close enough GRB-SN system. In order to attract attention to this problematic, we have given in Tab. A.1 an estimate of the corresponding neutron star radius for URCA-1, URCA-2 and URCA-3. It has been pointed out (see e.g. Pian et al., 2000) the different spectral properties between the GRBs and the URCAs. It would be also interesting to compare and contrast the spectra of all URCAs in order to evidence any analogy among them. Observations of a powerful URCA source on time scales of 0.1–10 seconds would be highly desirable.

B. Collisions in the slowing down phase of the prompt emission

One of the main results of the *Swift* satellite was to unveil the unknown window time of the early afterglow ($10^2 - 10^4$ s) with multiwavelength observations, in order to answer some questions concerning in particular the possibility that the prompt emission and the afterglow originate from the same physical process (Meszaros and Rees, 1993; Rees and Meszaros, 1994; Ruffini et al., 2001b). These observations allowed the identification in a good sample of bursts of a so-called canonical behavior (Nousek et al., 2006; Evans et al., 2009): a steep decay followed by a shallow decline, the "plateau phase", followed then by a more conventional decay.

The origin of this "plateau phase" is a puzzle. Within the standard fireball model, a variety of explanations have been advanced. In particular, Zhang et al. (2006) summarizes three possible physical origins: **1)** the central engine itself is long lasting, behaving like $L(t) \propto t^{-q}$ (Dai and Lu, 1998; Zhang and Mészáros, 2001); **2)** the central engine activity may be brief but at the end of the prompt phase the ejecta have a range of Lorentz factors such that the amount of mass with Lorentz factor greater than γ is $M(> \gamma) \propto \gamma^{-s}$ (Rees and Meszaros, 1998; Panaitescu et al., 1998; Sari and Mészáros, 2000); **3)** the energy injection is also brief but the outflow has a significant fraction of Poynting flux (Usov, 1992; Thompson, 1994; Meszaros and Rees, 1997b; Lyutikov and Blandford, 2003). In this case the energy transfer to the ambient medium can be delayed with respect to the standard case (Zhang and Kobayashi, 2005).

In this Letter we consider one of these possibilities within the fireshell model. Following the Rees and Meszaros (1998) proposal, we consider the material stored inside the fireshell not as a unique shell, instead it moves with a range of Lorentz factors. During the prompt emission phase, the fastest material that is in front is slowed by the interaction of the CircumBurst Medium (CBM) so that at the end of the prompt emission the slower material will catch up with it. Therefore, the plateau phase is the result of this injection, that produces a modification both in the dynamics of the fireshell and in the spectrum of the emitted radiation.

We postulate that this spread in the fireshell Lorentz factor occurs when the fireshell becomes transparent, and some hints on this directions have been provided by studies of the Proper-GRB (P-GRB) structure with different baryon loadings (see De Barros et al, in preparation). This hypothesis is

compatible with the basic idea of the fireshell model that all GRBs originate from the gravitational collapse to a black hole that provides the initial energy of the system, but all the following evolution is unconnected from the progenitor's details and do not depend on a prolonged activity of the central engine. The novelty in this approach is that while the prompt phase has an "external" origin, being the result of the interaction of the fireshell with the CBM, the shallow decaying phase paradoxically has an "internal" origin.

The aim of this section is to characterize dynamically the system in order to understand the nature of that material. In doing so, we schematically represent the outflow as two shells: one is the main fireshell that moves with an initial Lorenz factor $\gamma_\circ$ that decreases due to the interaction with the CBM and the other represent the trailing slow material that expands ballistically with constant speed. We examine the several GRBs for which we have all details of the parameters characterizing the dynamics of the system. The aim is to see is we can find a quantitative correlation between the two Lorentz gamma factors considered in this process.

B.1. Dynamics of the Collision and determination of γ_2

Suppose that the fireshell moves with an initial Lorenz factor $\gamma_\circ$ that decreases due to the interaction with the CBM, and that the injecting material is contained in a second shell with constant Lorentz factor $\gamma_2 \leq \gamma_\circ$ (see Fig. B.1). The second shell will catch up with the fireshell at a certain radius r^* and laboratory time t^* such that:

$$r^* = \beta_2 c t^* \,, \tag{B.1.1}$$

where $\beta_2 = \sqrt{1 - 1/\gamma_2^2}$ is the velocity of the second shell, and r^* and t^* are fixed by the dynamics of the fireshell.

If we assume that the X-ray plateau is the result of the collision between the fireshell and the second shell, we can identify its onset with the moment at which the collision occurs. We determine this time in the observer frame t^*_{ob} by fitting the X-ray afterglow with a broken power law:

$$F(t_{ob}) = N \left(\left(\frac{t_{ob}}{t^*_{ob}} \right)^a + \left(\frac{t_{ob}}{t^*_{ob}} \right)^b \right) . \tag{B.1.2}$$

Since the second shell expands with constant velocity, the corresponding laboratory time at which a photon is emitted along the line of sight is (neglecting the initial time that corresponds to the time at which the transparency occurs

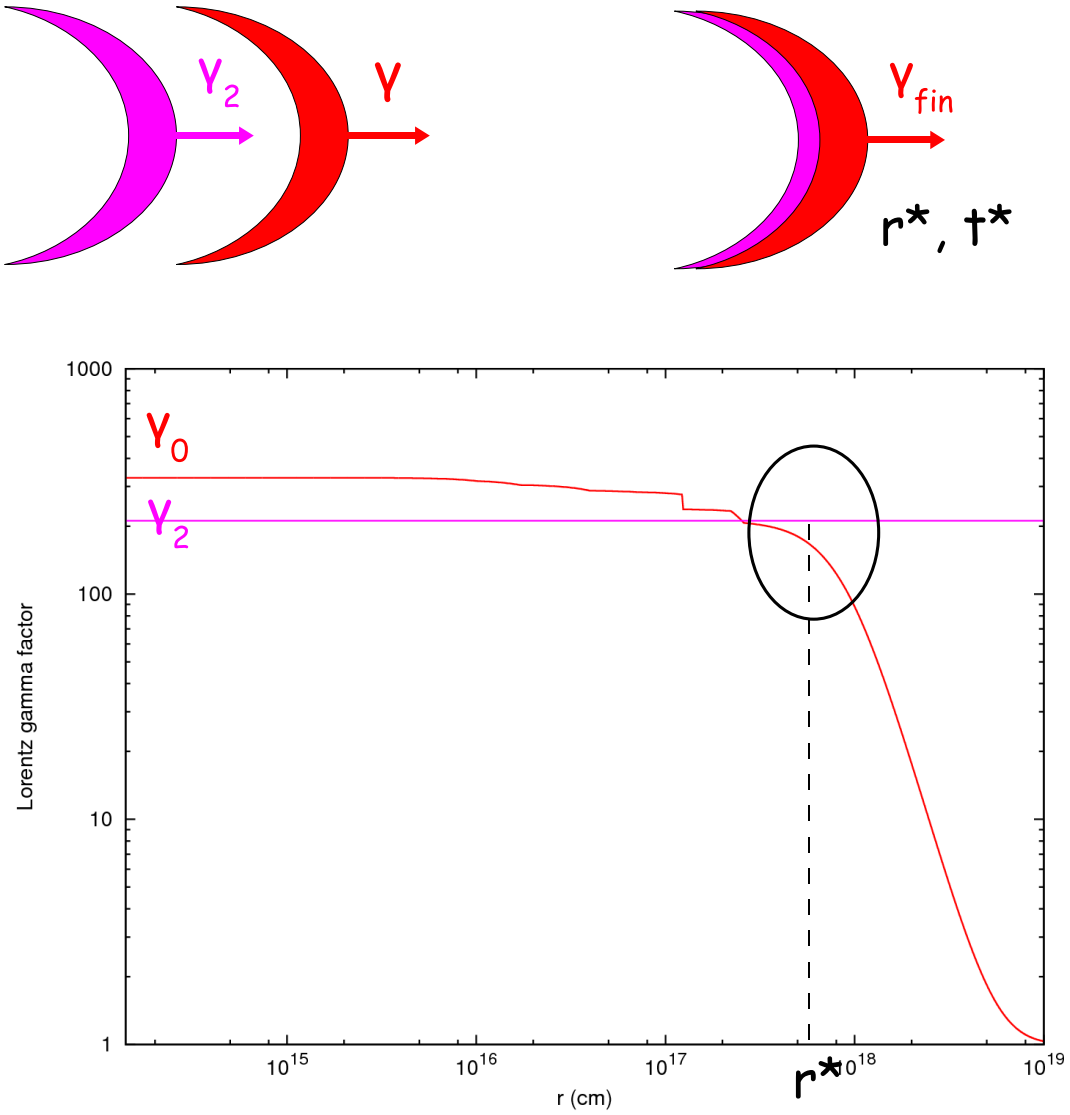

Figure B.1.: The fireshell (red shell) moves with an initial Lorenz factor $\gamma_\circ$ that decreases due to the interaction with the CBM, and the injecting material, represented by the second shell (pink shell), moves with constant Lorentz factor $\gamma_2 \leq \gamma_\circ$. The second shell will catch up with the fireshell at a certain radius r^*.

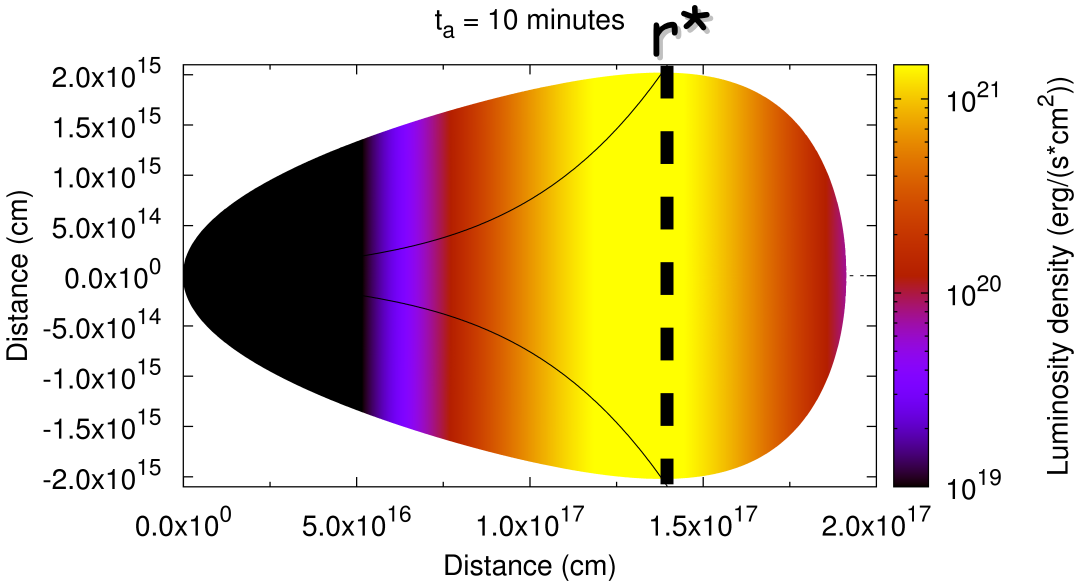

Figure B.2.: Emitted bolometric luminosity on an EQTS corresponding to an observed time of 10 minutes. It is manifest how the most luminous emitting region corresponds to the boundary of the visible region (solid line). The dashed line therefore traces the radius that we assume to be the collision radius r^*.

$t_\circ \ll t^*$):

$$t^* = 2\gamma_2^2 \frac{t^*_{ob}}{1+z}\,, \tag{B.1.3}$$

where we accounted also for the cosmological redshift of the source z.

The second step is to identify the radius r^*. For relativistic extended emitters, the photons observed at the same time are emitted by the source at different radii, and they describe a surface called EQuiTemporal Surface (EQTS, see Fig. B.2 and Bianco and Ruffini, 2005b). Therefore, it is not obvious to establish in the evolution of the fireshell which is the collision radius, i.e. which radius corresponds to the t^*_{ob} determined above. From the analysis of the luminosity emitted by a fixed EQTS (see Section ...Carlo..EQTS...) it results that at observed times corresponding to the onset of the plateau the most luminous region is the boundary of the visible region, $\theta_{max} \sim 1/\gamma$, where γ is the Lorentz factor of the fireshell at the moment of the collision and depends strongly on the details of the CircumBurst Medium (CBM) adopted. The most reasonable choice is to estimate tentatively r^* as the radius corresponding to the boundary of the EQTS visible area associated to t^*_{ob} (dashed line in Fig. B.2), which is approximately smaller than the head on radius by a factor 2 for a constant speed motion.

We can now evaluate the Lorentz factor that the second shell should have

in order to produce a collision observed at t^*_{ob} with the fireshell:

$$\gamma_2 \simeq \sqrt{\frac{r^*(1+z)}{ct^*_{ob}} + \frac{1}{2}}\,. \tag{B.1.4}$$

We select 6 GRBs among those examined within the fireshell model that show in the X-ray afterglow a behavior compatible with the X-ray plateau. In Table B.1 the results obtained for the GRBs of the sample are reported.

Table B.1.: Table of the GRBs of our sample including also GRB080319B (see Sec. B.2). For these GRBs there are reported the observed time with error and radius of the collision (t^*_{ob} and r^*), the Lorentz gamma factor of the fireshell at r^* (γ_1) and at the transparency ($\gamma_\circ$), the redshift z, the value adopted for the free parameters of the fireshell model ($E^{e\pm}_{tot}$ and B) and the Lorentz gamma factor of the second shell derived γ_2 with error.

GRB	t^*_{ob} (s)	Δt^*_{ob} (s)	r^* (cm)	γ_1	$\gamma_\circ$	z	$E^{e\pm}_{tot}$ (erg)	B	γ_2	$\Delta\gamma_2$
060218	1.05×10^4	1.57×10^3	1.12×10^{18}	53.6	99.3	0.03	2.32×10^{50}	1.00×10^{-2}	60.6	6.15
050315	4.64×10^2	2.98×10^1	7.30×10^{16}	102.0	220.0	1.95	1.46×10^{53}	4.55×10^{-3}	124.0	3.76
060607A	1.18×10^3	5.41×10^2	3.87×10^{17}	196.0	328.0	3.08	2.50×10^{53}	3.00×10^{-3}	211.0	43.1
060614	1.20×10^3	4.60×10^1	9.40×10^{17}	146.0	345.0	0.13	2.94×10^{51}	2.80×10^{-3}	171.0	11.5
080319B	3.00×10^1	2.00×10^1	5.65×10^{16}	335.0	394.0	0.94	1.00×10^{54}	2.50×10^{-3}	349.0	111.0
090423	3.94×10^2	5.13×10^1	4.26×10^{17}	548.0	1190.0	8.1	1.20×10^{53}	8.00×10^{-4}	572.0	35.7
050904	6.46×10^2	4.54×10^1	1.68×10^{17}	201.0	489.0	6.29	5.00×10^{53}	2.00×10^{-3}	251.0	47.0

B.2. γ_2-$\gamma_\circ$ correlation

The result of this analysis reveals (see Fig. B.3) the existence of a correlation between the Lorentz factor of the second shell γ_2 and the maximum Lorentz factor of the fireshell $\gamma_\circ$, $\gamma_2 \propto \gamma_\circ^{0.9}$, with $\chi^2/dof = 0.67$ and a Spearman rank coefficient $r_s = 0.91$ (null hypothesis probability $nhp = 0.0083$).

This correlation is not trivial since the dynamics of the fireshell after the transparency is determined uniquely by the CBM distribution that is different for each GRB. It reveals indeed that the second shell in not erratic, emitted in a second episode of the engine activity, but it is intertwined with the main fireshell until the transparency. Therefore, the correlation provides some hints on the origin of the second shell (see e.g. De Barros et al., in preparation).

The correlation between γ_2 and $\gamma_\circ$ can also be used to "predict" the X-ray plateau when it is not observed. We use as an example GRB080319B (Racusin et al., 2008, , Patricelli et al., in preparation). This GRB exhibits an X-ray afterglow well monitored from 51 s (Racusin et al., 2008) that decays as a simple power-law. Moreover, it has been pointed out (Margutti et al., 2008; Stamatikos et al., 2009) that the prompt emission can be divided in two different episodes on the basis of different properties of the temporal variability. We guessed therefore that the plateau phase could be occurred during the

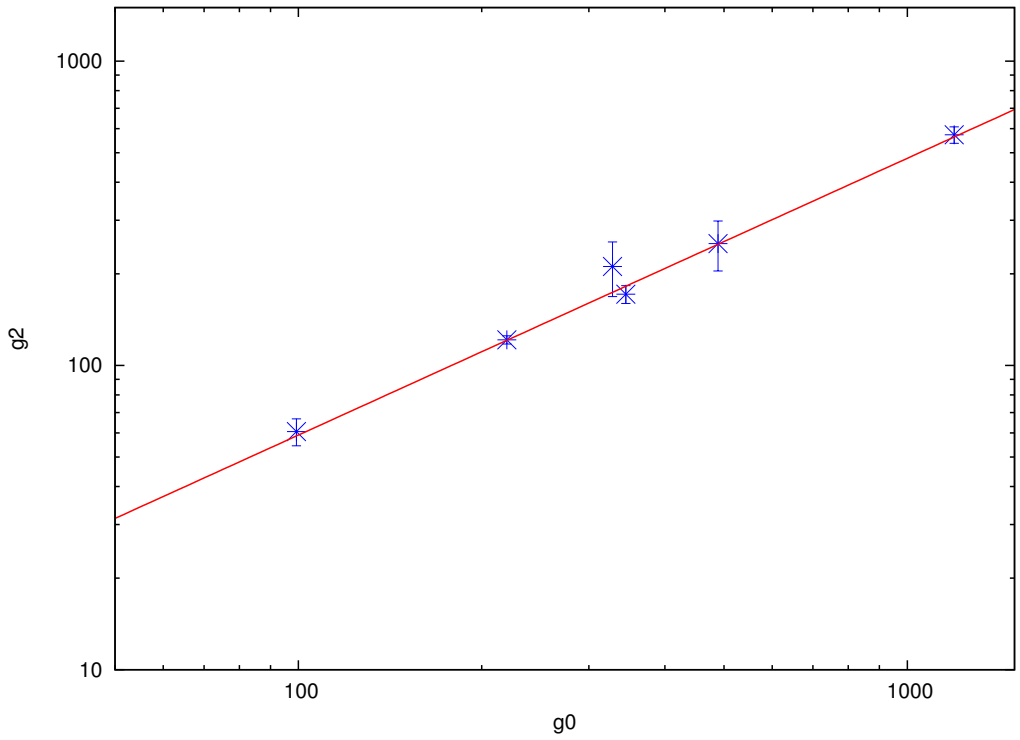

Figure B.3.: Lorentz gamma factor of the second shell γ_2 versus the maximum Lorentz factor of the fireshell $\gamma_\circ$ for the 6 GRBs of the sample. The correlation between the two quantities is manifest.

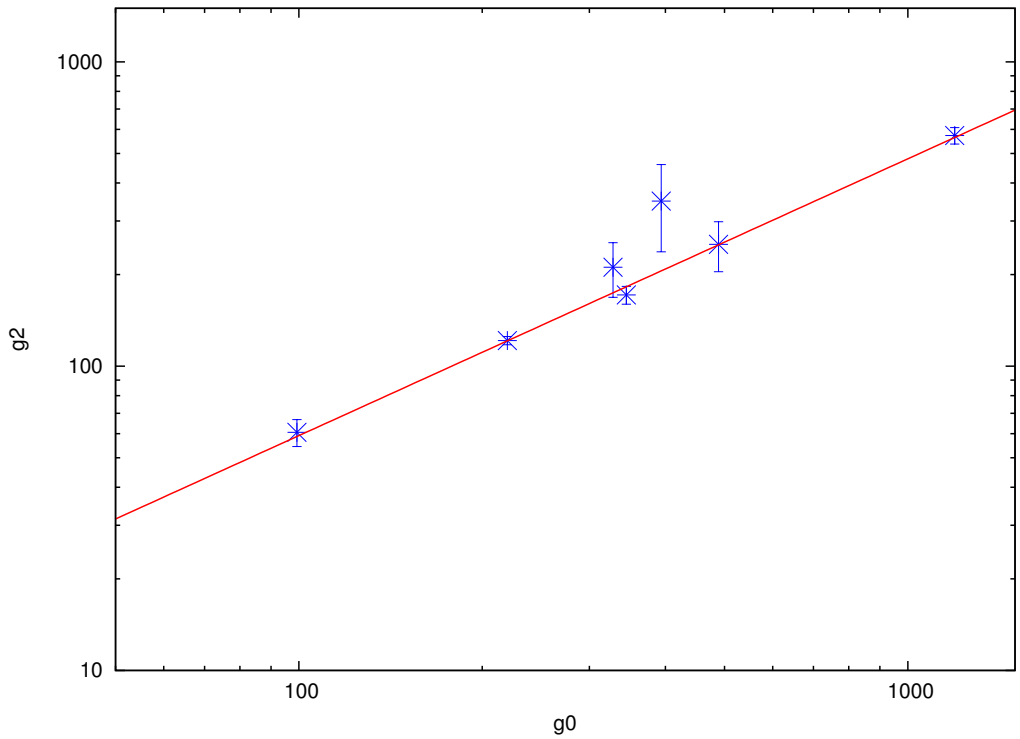

Figure B.4.: Same as Fig. B.3 with in addition the values for GRB080319B, assuming that the plateau phase occurs during the prompt emission. A correlation is still present.

prompt emission as a "γ-ray plateau", coincident with the second episode. With this assumption we performed the analysis described before and we found that the γ_2 obtained is only marginally correlated with $\gamma_\circ$, thus neither confirming nor excluding this possibility (see Fig. B.4).

C. Applications to various sources from previous year reports

C.1. Application to GRB 970228

GRB 970228 was detected by the Gamma-Ray Burst Monitor (GRBM, 40–700 keV) and Wide Field Cameras (WFC, 2–26 keV) on board BeppoSAX on February 28.123620 UT (Frontera et al., 1998). The burst prompt emission is characterized by an initial 5 s strong pulse followed, after 30 s, by a set of three additional pulses of decreasing intensity (Frontera et al., 1998). Eight hours after the initial detection, the NFIs on board BeppoSAX were pointed at the burst location for a first target of opportunity observation and a new X-ray source was detected in the GRB error box: this is the first "afterglow" ever detected (Costa et al., 1997). A fading optical transient has been identified in a position consistent with the X-ray transient (van Paradijs et al., 1997), coincident with a faint galaxy with redshift $z = 0.695$ (Bloom et al., 2001). Further observations by the Hubble Space Telescope clearly showed that the optical counterpart was located in the outskirts of a late-type galaxy with an irregular morphology (Sahu et al., 1997).

The BeppoSAX observations of GRB 970228 prompt emission revealed a discontinuity in the spectral index between the end of the first pulse and the beginning of the three additional ones (Costa et al., 1997; Frontera et al., 1998, 2000). The spectrum during the first 3 s of the second pulse is significantly harder than during the last part of the first pulse (Frontera et al., 1998, 2000), while the spectrum of the last three pulses appear to be consistent with the late X-ray afterglow (Frontera et al., 1998, 2000). This was soon recognized by Frontera et al. (1998, 2000) as pointing to an emission mechanism producing the X-ray afterglow already taking place after the first pulse.

As recalled aboce, the simultaneous occurrence of an afterglow with total time-integrated luminosity larger than the P-GRB one, but with a smaller peak luminosity, is indeed explainable in terms of a peculiarly small average value of the CBM density and not due to the intrinsic nature of the source. In this sense, GRBs belonging to this class are only "fake" short GRBs. We show that GRB 970228 is a very clear example of this situation. We identify the initial spikelike emission with the P-GRB, and the late soft bump with the peak of the afterglow. GRB 970228 shares the same morphology and observational features with the sources analyzed by Norris and Bonnell (2006) as well as

with e.g. GRB 050709 (Villasenor et al., 2005), GRB 050724 (Campana et al., 2006b) and GRB 060614 (see appendix C.2 and Gehrels et al., 2006). Therefore, we propose GRB 970228 as a prototype for this new GRB class.

C.1.1. The analysis of GRB 970228 prompt emission

In Fig. C.1 we present the theoretical fit of BeppoSAX GRBM (40–700 keV) and WFC (2–26 keV) light curves of GRB 970228 prompt emission (Frontera et al., 1998). Within our "canonical GRB" scenario we identify the first main pulse with the P-GRB and the three additional pulses with the afterglow peak emission, consistently with the above mentioned observations by Costa et al. (1997) and Frontera et al. (1998). Such last three pulses have been reproduced assuming three overdense spherical CBM regions (see Fig. C.2) with a very good agreement (see Fig. C.1).

We therefore obtain for the two parameters characterizing the source in our model $E^{tot}_{e^\pm} = 1.45 \times 10^{54}$ erg and $B = 5.0 \times 10^{-3}$. This implies an initial $e^\pm$ plasma created between the radii $r_1 = 3.52 \times 10^7$ cm and $r_2 = 4.87 \times 10^8$ cm with a total number of $e^\pm$ pairs $N_{e^\pm} = 1.6 \times 10^{59}$ and an initial temperature $T = 1.7$ MeV. The theoretically estimated total isotropic energy emitted in the P-GRB is $E_{P-GRB} = 1.1\% E^{tot}_{e^\pm} = 1.54 \times 10^{52}$ erg, in excellent agreement with the one observed in the first main pulse ($E^{obs}_{P-GRB} \sim 1.5 \times 10^{52}$ erg in $2 - 700$ keV energy band, see Fig. C.1), as expected due to their identification. After the transparency point at $r_0 = 4.37 \times 10^{14}$ cm from the progenitor, the initial Lorentz gamma factor of the fireshell is $\gamma_0 = 199$. On average, during the afterglow peak emission phase we have for the CBM $\langle \mathcal{R} \rangle = 1.5 \times 10^{-7}$ and $\langle n_{cbm} \rangle = 9.5 \times 10^{-4}$ particles/cm^3. This very low average value for the CBM density is compatible with the observed occurrence of GRB 970228 in its host galaxy's halo (Sahu et al., 1997; van Paradijs et al., 1997; Panaitescu, 2006) and it is crucial in explaining the light curve behavior.

The values of $E^{tot}_{e^\pm}$ and B we determined are univocally fixed by two tight constraints. The first one is the total energy emitted by the source all the way up to the latest afterglow phases (i.e. up to $\sim 10^6$ s). The second one is the ratio between the total time-integrated luminosity of the P-GRB and the corresponding one of the whole afterglow (i.e. up to $\sim 10^6$ s). In particular, in GRB 970228 such a ratio results to be $\sim 1.1\%$ (see Fig. 3.8). However, the P-GRB peak luminosity actually results to be much more intense than the afterglow one (see Fig. C.1). This is due to the very low average value of the CBM density $\langle n_{cbm} \rangle = 9.5 \times 10^{-4}$ particles/cm^3, which produces a less intense afterglow emission. Since the afterglow total time-integrated luminosity is fixed, such a less intense emission lasts longer than what we would expect for an average density $\langle n_{cbm} \rangle \sim 1$ particles/cm^3.

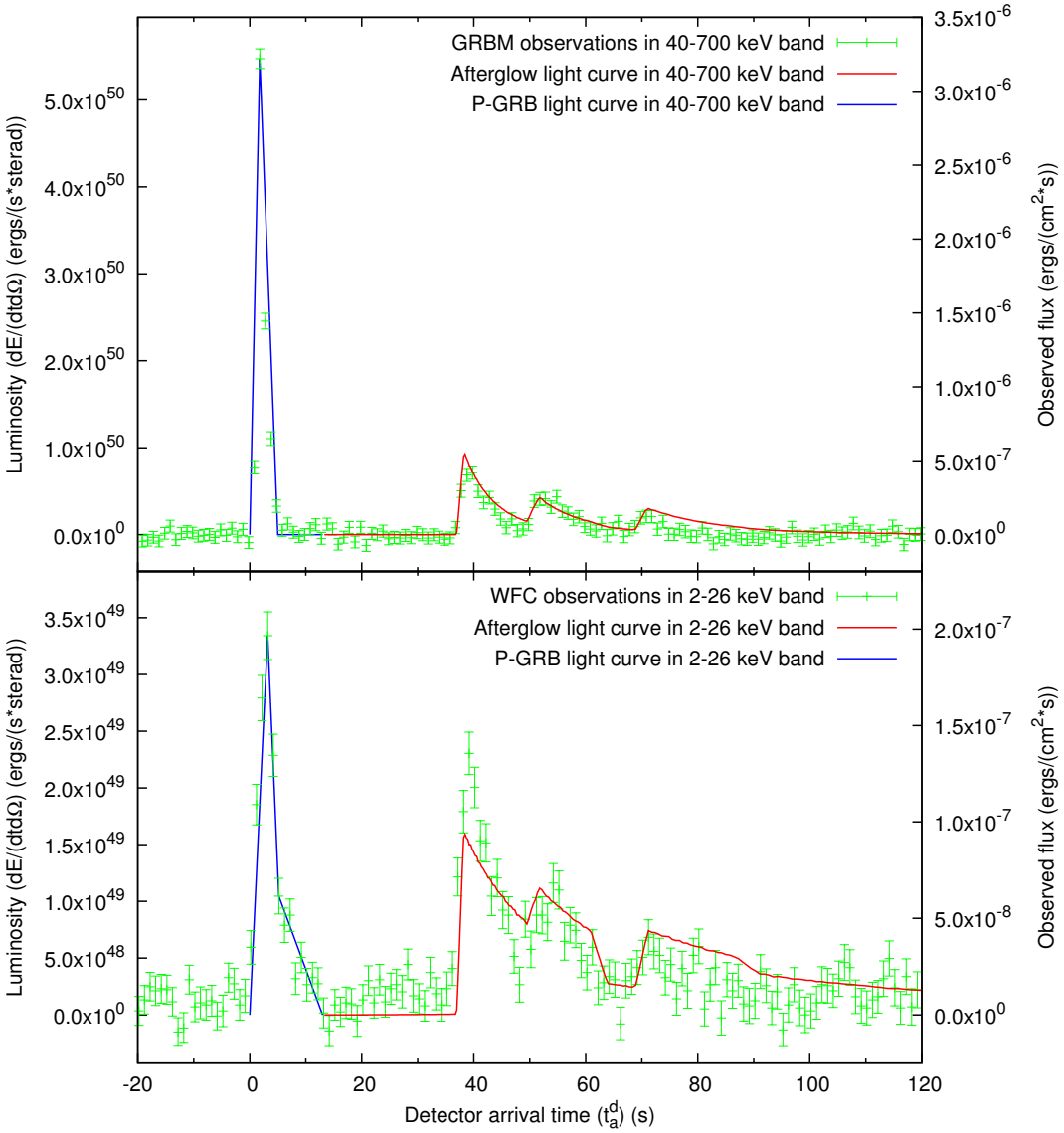

Figure C.1.: The "canonical GRB" light curve theoretically computed for the prompt emission of GRB 970228. BeppoSAX GRBM (40–700 keV, above) and WFC (2–26 keV, below) light curves (data points) are compared with the afterglow peak theoretical ones (solid lines). The onset of the afterglow coincides with the end of the P-GRB (represented qualitatively by the dotted lines). For this source we have $B \simeq 5.0 \times 10^{-3}$ and $\langle n_{cbm} \rangle \sim 10^{-3}$ particles/cm^3.

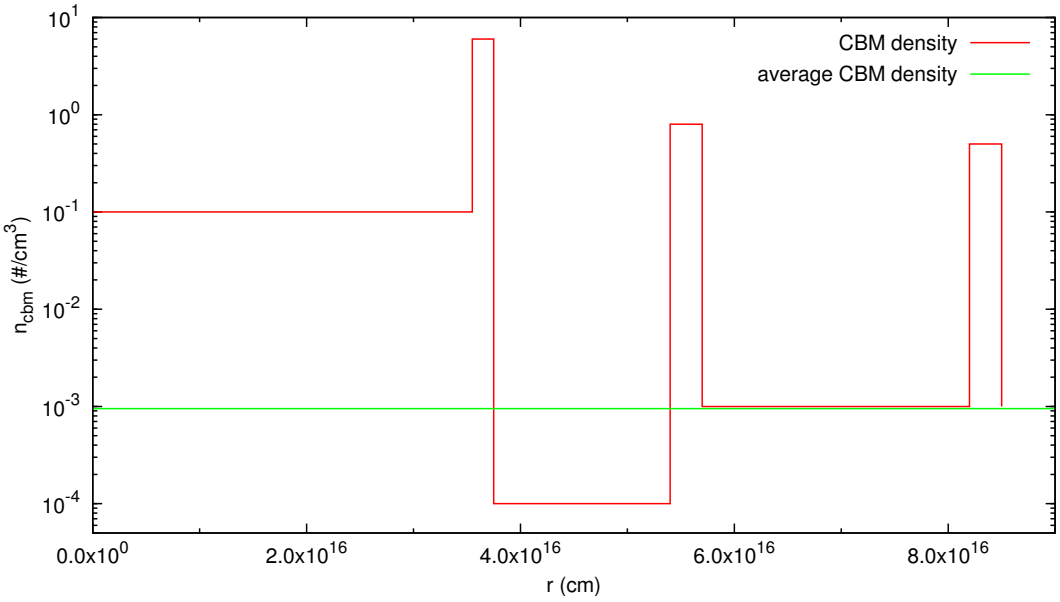

Figure C.2.: The CBM density profile we assumed to reproduce the last three pulses of the GRB 970228 prompt emission (red line), together with its average value $\langle n_{cbm} \rangle = 9.5 \times 10^{-4}$ particles/cm^3 (green line).

C.1.2. Rescaling the CBM density

We present now an explicit example in order to probe the crucial role of the average CBM density in explaining the relative intensities of the P-GRB and of the afterglow peak in GRB 970228. We keep fixed the basic parameters of the source, namely the total energy $E_{e^\pm}^{tot}$ and the baryon loading B, therefore keeping fixed the P-GRB and the afterglow total time-integrated luminosities. Then we rescale the CBM density profile given in Fig. C.2 by a constant numerical factor in order to raise its average value to the standard one $\langle n_{ism} \rangle = 1$ particle/cm^3. We then compute the corresponding light curve, shown in Fig. C.3.

We notice a clear enhancement of the afterglow peak luminosity with respect to the P-GRB one in comparison with the fit of the observational data presented in Fig. C.1. The two light curves actually crosses at $t_a^d \simeq 1.8 \times 10^4$ s since their total time-integrated luminosities must be the same. The GRB "rescaled" to $\langle n_{ism} \rangle = 1$ particle/cm^3 appears to be totally similar to, e.g., GRB 050315 (Ruffini et al., 2006b) and GRB 991216 (Ruffini et al., 2003a, 2004b, 2005a).

It is appropriate to emphasize that, although the two underlying CBM density profiles differ by a constant numerical factor, the two afterglow light curves in Fig. C.3 do not. This is because the absolute value of the CBM density at each point affects in a non-linear way all the following evolution of the fireshell due to the feedback on its dynamics (Bianco and Ruffini, 2005a).

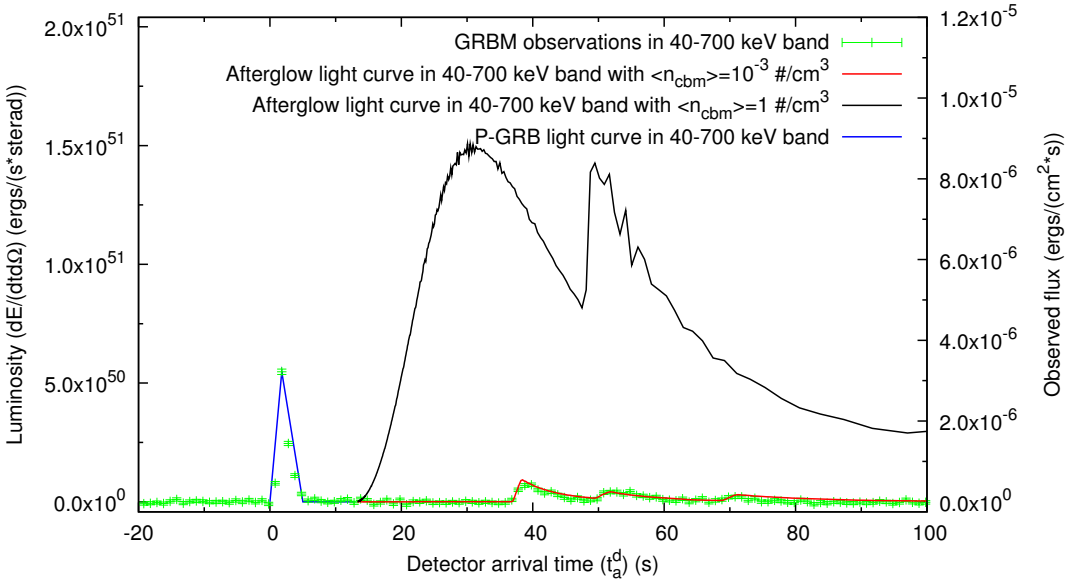

Figure C.3.: The theoretical fit of the BeppoSAX GRBM observations (red line, see Fig. C.1) is compared with the afterglow light curve in the 40–700 keV energy band obtained rescaling the CBM density to $\langle n_{cbm} \rangle = 1$ particle/cm^3 keeping constant its shape and the values of the fundamental parameters of the theory $E^{tot}_{e^\pm}$ and B (black line). The P-GRB duration and luminosity (blue line), depending only on $E^{tot}_{e^\pm}$ and B, are not affected by this process of rescaling the CBM density.

Moreover, the shape of the surfaces of equal arrival time of the photons at the detector (EQTS) is strongly elongated along the line of sight (Bianco and Ruffini, 2005b). Therefore photons coming from the same CBM density region are observed over a very long arrival time interval.

C.1.3. GRB 970228 and the Amati relation

We turn now to the "Amati relation" (Amati et al., 2002; Amati, 2006) between the isotropic equivalent energy emitted in the prompt emission E_{iso} and the peak energy of the corresponding time-integrated spectrum $E_{p,i}$ in the source rest frame. It has been shown by Amati et al. (2002); Amati (2006) that this correlation holds for almost all the "long" GRBs which have a redshift and an $E_{p,i}$ measured, but not for the ones classified as "short" (Amati, 2006). If we focus on the "fake" short GRBs, namely the GRBs belonging to this new class, at least in one case (GRB 050724 Campana et al., 2006b) it has been shown that the correlation is recovered if also the extended emission is considered (Amati, 2007).

It clearly follows from our treatment that for the "canonical GRBs" with large values of the baryon loading and high $\langle n_{cbm} \rangle$, which presumably are most of the GRBs for which the correlation holds, the leading contribution to the prompt emission is the afterglow peak emission. The case of the "fake" short GRBs is completely different: it is crucial to consider separately the two components since the P-GRB contribution to the prompt emission in this case is significant.

To test this scenario, we evaluated from our fit of GRB 970228 E_{iso} and $E_{p,i}$ only for the afterglow peak emission component, i.e. from $t_a^d = 37$ s to $t_a^d = 81.6$ s. We found an isotropic energy emitted in the 2–400 keV energy band $E_{iso} = 1.5 \times 10^{52}$ erg, and $E_{p,i} = 90.3$ keV. As it is clearly shown in Fig. C.4, the sole afterglow component of GRB 970228 prompt emission is in perfect agreement with the Amati relation. If this behavior is confirmed for other GRBs belonging to this new class, this will enforce our identification of the "fake" short GRBs. This result will also provide a theoretical explanation for the the apparent absence of such correlation for the initial spikelike component in the different nature of the P-GRB.

C.1.4. Conclusions

We conclude that GRB 970228 is a "canonical GRB" with a large value of the baryon loading quite near to the maximum $B \sim 10^{-2}$ (see Fig. 3.8). The difference with e.g. GRB 050315 (Ruffini et al., 2006b) or GRB 991216 (Ruffini et al., 2003a, 2004b, 2005a) is the low average value of the CBM density $\langle n_{cbm} \rangle \sim 10^{-3}$ particles/cm^3 which deflates the afterglow peak luminosity. Hence, the predominance of the P-GRB, coincident with the initial

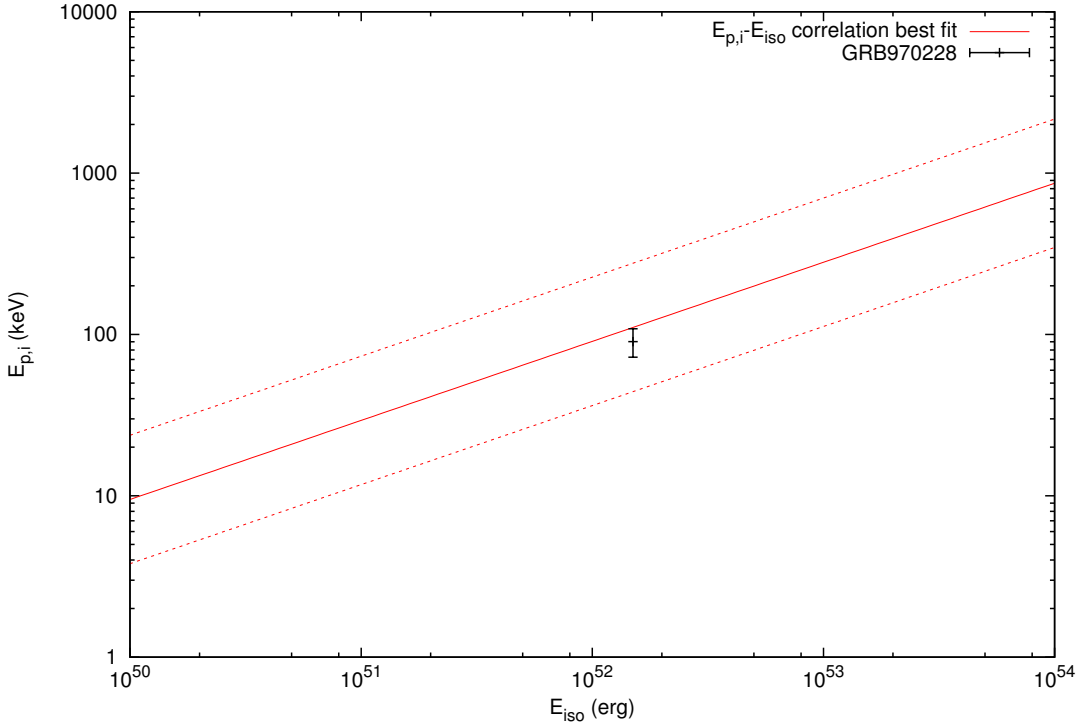

Figure C.4.: The estimated values for $E_{p,i}$ and E_{iso} obtained by our analysis (black dot) compared with the "Amati relation" (Amati et al., 2002): the solid line is the best fitting power law (Amati, 2006) and the dashed lines delimit the region corresponding to a vertical logarithmic deviation of 0.4 (Amati, 2006). The uncertainty in the theoretical estimated value for $E_{p,i}$ has been assumed conservatively as 20%.

spikelike emission, over the afterglow is just apparent: 98.9% of the total time-integrated luminosity is indeed in the afterglow component. Such a low average CBM density is consistent with the occurrence of GRB 970228 in the galactic halo of its host galaxy (Sahu et al., 1997; van Paradijs et al., 1997), where lower CBM densities have to be expected (Panaitescu, 2006).

We propose GRB 970228 as the prototype for the new class of GRBs comprising GRB 060614 and the GRBs analyzed by Norris and Bonnell (2006). We naturally explain the hardness and the absence of spectral lag in the initial spikelike emission with the physics of the P-GRB originating from the gravitational collapse leading to the black hole formation. The hard-to-soft behavior in the afterglow is also naturally explained by the physics of the relativistic fireshell interacting with the CBM, clearly evidenced in GRB 031203 (Bernardini et al., 2005a) and in GRB 050315 (Ruffini et al., 2006b). Also justified is the applicability of the Amati relation to the sole afterglow component (see Amati, 2006, 2007).

This class of GRBs with $z \sim 0.4$ appears to be nearer than the other GRBs detected by *Swift* ($z \sim 2.3$, see Guetta, 2006). This may be explained by the afterglow peak luminosity deflation. The absence of a jet break in those afterglows has been pointed out (Campana et al., 2006b; Watson et al., 2006), consistently with our spherically symmetric approach. Their association with non-star-forming host galaxies appears to be consistent with the merging of a compact object binary (Barthelmy et al., 2005b; Fox et al., 2005). It is here appropriate, however, to caution on this conclusion, since the association of GRB 060614 and GRB 970228 with the explosion of massive stars is not excluded (Della Valle et al., 2006; Galama et al., 2000).

Most of the sources of this class appear indeed not to be related to bright "Hypernovae", to be in the outskirts of their host galaxies (Fox et al., 2005, see above) and a consistent fraction of them are in galaxy clusters with CBM densities $\langle n_{cbm} \rangle \sim 10^{-3}$ particles/cm^3 (see e.g. Lewis et al., 2003; Berger et al., 2007). This suggests a spiraling out binary nature of their progenitor systems (Kramer, 2008) made of neutron stars and/or white dwarfs leading to a black hole formation.

Moreover, we verified the applicability of the Amati relation to the sole afterglow component in GRB 970228 prompt emission, in analogy with what happens for some of the GRBs belonging to this new class. In fact it has been shown by Amati (2006, 2007) that the "fake" short GRBs do not fulfill the $E_{p,i}$–E_{iso} correlation when the sole spiklike emission is considered, while they do if the long soft bump is included. Since the spikelike emission and the soft bump contributions are comparable, it is natural to expect that the soft bump alone will fulfill the correlation as well.

Within our "canonical GRB" scenario the sharp distinction between the P-GRB and the afterglow provide a natural explanation for the observational features of the two contributions. We naturally explain the hardness and the absence of spectral lag in the initial spikelike emission with the physics of the

P-GRB originating from the gravitational collapse leading to the black hole formation. The hard-to-soft behavior in the afterglow is also naturally explained by the physics of the relativistic fireshell interacting with the CBM, clearly evidenced in GRB 031203 (Bernardini et al., 2005a) and in GRB 050315 (Ruffini et al., 2006b). Therefore, we expect naturally that the $E_{p,i}$–E_{iso} correlation holds only for the afterglow component and not for the P-GRB. Actually we find that the correlation is recovered for the afterglow peak emission of GRB 970228.

In the original work by Amati et al. (2002); Amati (2006) only the prompt emission is considered and not the late afterglow one. In our theoretical approach the afterglow peak emission contributes to the prompt emission and continues up to the latest GRB emission. Hence, the meaningful procedure within our model to recover the Amati relation is to look at a correlation between the total isotropic energy and the peak of the time-integrated spectrum of the whole afterglow. A first attempt to obtain such a correlation has already been performed using GRB 050315 as a template, giving very satisfactory results (Guida et al., 2008b).

C.2. Application to GRB 060614

GRB060614 (Gehrels et al., 2006; Mangano et al., 2007) has drawn the general attention of the gamma-ray burst's (GRB) scientific community because it is the first clear example of a nearby ($z = 0.125$), long GRB not associated with a bright Ib/c supernova (SN) (Della Valle et al., 2006; Gal-Yam et al., 2006). It has been estimated that, if present, the SN-component should be about 200 times fainter than the archetypal SN 1998bw associated with GRB980425; moreover, it would also be fainter (at least 30 times) than any stripped-envelope SN ever observed (Richardson et al., 2006).

Within the standard scenario, long duration GRBs ($T_{90} > 2$ s) are thought to be produced by SN events during the collapse of massive stars in star forming regions ("collapsar", see Woosley, 1993). The observations of broad-lined and bright type Ib/c SNe associated with GRBs are often reported to favor this scenario (Woosley and Bloom, 2006, and references therein). The *ansatz* has been advanced that every long GRB should have a SN associated with it (Zhang et al., 2007). Consequently, in all nearby long GRBs ($z \leq 1$), SN emission should be observed.

For these reasons the case of GRB060614 is unusual. Some obvious hypotheses have been proposed and ruled out: the chance superposition with a galaxy at low redshift (Gal-Yam et al., 2006) and strong dust obscuration and extinction (Fynbo et al., 2006). Appeal has been made to the possible occurrence of an unusually low luminosity stripped-envelope core-collapse SN (Della Valle et al., 2006).

The second novelty of GRB060614 is that it challenges the traditional sepa-

ration between Long Soft GRBs and Short Hard GRBs. Traditionally (Klebesadel, 1992; Dezalay et al., 1992), the "short" GRBs have $T_{90} < 2$ s, present an harder spectrum and negligible spectral lag, and are assumed to originate from the merging of two compact objects, i.e. two neutron stars or a neutron star and a black hole (see e.g. Blinnikov et al., 1984; Paczynski, 1986; Goodman, 1986; Eichler et al., 1989; Piran, 2005; Meszaros, 2006, and references therein). GRB060614 lasts about one hundred seconds ($T_{90} = (102 \pm 5)$ s; Gehrels et al., 2006), it fulfills the $E_p^{rest} - E_{iso}$ correlation (Amati et al., 2007), and therefore traditionally it should be classified as a "long" GRB. However, its morphology is different from typical long GRBs, being similar to the one of GRB050724, traditionally classified as a short GRB (Zhang et al., 2007; Piro, 2005). Its optical afterglow luminosity is intermediate between the traditional long and short ones (Kann et al., 2008a). Its host galaxy has a moderate specific star formation rate ($R_{Host} \approx 2 M_s y^{-1} (L^*)^{-1}$, $M_{vHost} \approx -15.5$; Fynbo et al., 2006; Della Valle et al., 2006). The spectral lag in its light curves is very small or absent (Gehrels et al., 2006). All these features are typical of short GRBs.

A third peculiarity of GRB060614 is that its 15–150 keV light curve presents a short, hard and multi-peaked episode (about 5 s). The episode is followed by a softer, prolonged emission that manifests a strong hard to soft evolution in the first 400 s of data (Mangano et al., 2007). The total fluence in the 15–150 keV energy band is $F = (2.17 \pm 0.04) \times 10^{-5}$ erg/cm^2, the 20% emitted during the initial spikelike emission, where the peak luminosity reaches the value of 300 keV before decreasing to 8 keV during the BAT-XRT overlap time (about 80 s).

These apparent contradictions find a natural explanation in the framework of the "fireshell" model[1]. Within the fireshell model, the occurrence of a GRB-SN is not a necessity. The origin of all GRBs is traced back to the formation of a black hole, either occurring in a single process of gravitational collapse, or in a binary system composed of a neutron star and a companion star evolved out of the main sequence, or in a merging binary system composed of neutron stars and/or white dwarfs in all possible combinations. The occurrence of a GRB-SN is indeed only one of the possibilities, linked, for example, to the process of "induced gravitational collapse" (Ruffini et al., 2001a, 2007b; Dainotti et al., 2007).

Within the "fireshell" model, the difference between the "short" and "long" GRBs does not rely uniquely on the time scale of the event, as in the traditional classification. It is theoretically explained by the fireshell baryon loading affecting the structure of the "canonical" GRB light curve. The "canoni-

[1] We indicate here and in the following by the "fireshell" model the one we have consistently developed encompassing the three basic paradigms presented in Ruffini et al. (2001c,b,a) as well as all the technical developments in the emission process, in the equations of motion and in the relativistic treatment of the extended afterglow as summarized in Ruffini et al. (2007a).

cal" GRB light curve is indeed composed of a proper-GRB (P-GRB, often labeled as "precursor"), emitted at the fireshell transparency, and an extended afterglow. The peak of such an extended afterglow is traditionally included in the prompt emission. The relative energetics of two such components and the temporal separation of the corresponding peaks are ruled by the fireshell baryon loading. In the limit of vanishing baryon loading, all the GRB energy is emitted in the P-GRB: these are the "genuine" short GRBs (Ruffini et al., 2001b, 2008a; Bernardini et al., 2007; Bianco et al., 2008a,b).

Within the "fireshell" model, in addition to the determination of the baryon loading, it is possible to infer a detailed description of the circumburst medium (CBM), its average density and its porosity and filamentary structure, all the way from the black hole horizon to a distance $r \lesssim 10^{17}$ cm. This corresponds to the prompt emission. This description is lacking in the traditional model based on the synchrotron emission. The attempt to use the internal shock model for the prompt emission (see e.g. Rees and Meszaros, 1994; Piran, 2005; Meszaros, 2006, and references therein) only applies to regions where $r > 10^{17}$ cm (Kumar and McMahon, 2008).

Our aim is to show how the "fireshell" model can explain all the abovementioned GRB060614 peculiarities and solve the apparent contradictions. In doing so, we also infer constraints on the astrophysical nature of the GRB060614 progenitors. In turn, these conclusions lead to a new scenario for all GRBs. We can confirm a classification of GRBs as "genuine" short, "fake" or "disguised" short, and all the remaining "canonical" GRBs. The connection between this new classification and the nature of GRB progenitors is quite different from the traditional one in the current literature.

C.2.1. The fit of the observed luminosity

In this scenario, GRB060614 is naturally interpreted as a "disguised" short GRB. We have performed the analysis of the observed light curves in the 15–150 keV energy band, corresponding to the γ-ray emission observed by the BAT instrument on the Swift satellite, and in the 0.2–10 keV energy band, corresponding to the X-ray component from the XRT instrument on Swift satellite. We do not address in this paper the issue of the optical emission, which represent less than 10% of the total energy of the GRB. From this fit (see Figs. C.5, C.7) we have derived the total initial energy $E_{tot}^{e^\pm}$, the value of B as well as the effective CBM distribution (see Fig. C.6). We find $E_{tot}^{e^\pm} = 2.94 \times 10^{51}$ erg, that accounts for the bolometric emission of both the P-GRB and the extended afterglow. Such a value is compatible with the observed $E_{iso} \simeq 2.5 \times 10^{51}$ erg (Gehrels et al., 2006). The value of B is $B = 2.8 \times 10^{-3}$, which corresponds to the lowest one of all the GRBs we have examined (see Fig. 6.4). It corresponds to a canonical GRB with a very clear extended afterglow predominance over the P-GRB. From the model, having determined $E_{tot}^{e^\pm}$ and

B, we can compute the theoretical expected P-GRB energetics E_{P-GRB} (Ruffini et al., 2001b). We obtain $E_{P-GRB} \simeq 1.15 \times 10^{50}$ erg, that is in good agreement with the observed $E_{iso,1p} \simeq 1.18 \times 10^{50}$ erg (Gehrels et al., 2006). The Lorentz Gamma Factor at the transparency is $\gamma_\circ = 346$, one of the highest of all the GRBs we have examined.

In Fig. C.5 we plot the comparison between the BAT observational data of the GRB0606014 prompt emission in the 15–150 keV energy range and the P-GRB and extended afterglow light curves computed within our model. The temporal variability of the extended afterglow peak emission is due to the inhomogeneities in the effective CBM density (see Figs. C.5, C.6). Toward the end of the BAT light curve, the good agreement between the observations and the fit is affected by the Lorentz gamma factor decrease and the corresponding increase of the maximum viewing angle. The source visible area becomes larger than the typical size of the filaments. This invalidates the radial approximation we use for the CBM description. To overcome this problem it is necessary to introduce a more detailed three-dimensional CBM description, in order to avoid an over-estimated area of emission and, correspondingly, to describe the sharpness of some observed light curves. We are still working on this issue (Ruffini et al., 2002; Caito et al., 2008; Bianco et al., 2006b; Guida et al., 2008a).

We turn now to the crucial determination of the CBM density, which is derived from the fit. At the transparency point it was $n_{cbm} = 4.8 \times 10^{-3}$ particles/cm^3 (see Fig. C.6). This density is compatible with the typical values of the galactic halos. During the peak of the extended afterglow emission the effective average CBM density decreases reaching $\langle n_{cbm} \rangle = 2.25 \times 10^{-5}$ particles/cm^3, possibly due to an occurring fragmentation of the shell (Dainotti et al., 2007) or due to a fractal structure in the CBM. The $\mathcal{R}$ value on average was $\langle \mathcal{R} \rangle = 1.72 \times 10^{-8}$. Note the striking analogy of the numerical value and the overall radial dependence of the CBM density in the present case of GRB060614 when compared and contrasted with the ones of GRB970228 (Bernardini et al., 2007).

Concerning the 0.2–10 keV light curve of the decaying phase of the afterglow observed with the XRT instrument, we have also reproduced very satisfactorily both the hard decrease in the slope and the plateau of the light curve, keeping constant the effective CBM density and changing only $\mathcal{R}$. The result of this analysis is reported in Fig. C.7. We assume in this phase $n_{cbm} = 4.70 \times 10^{-6}$ particles/cm^{-3}. The average value of the $\mathcal{R}$ parameter is $\langle \mathcal{R} \rangle = 1.27 \times 10^{-2}$. The drastic enhancement in the $\mathcal{R}$ parameter with respect to the values at the peak of the extended afterglow is consistent with similar features encountered in other sources we have studied: GRB060218 presents an enhancement of five orders of magnitude (Dainotti et al., 2007), in GRB060710 the enhancement is of about four orders of magnitude (see Izzo et al., in preparation) while in GRB050315 there is a three orders of magnitude enhancement (Ruffini et al., 2006b). In these last two cases, we find

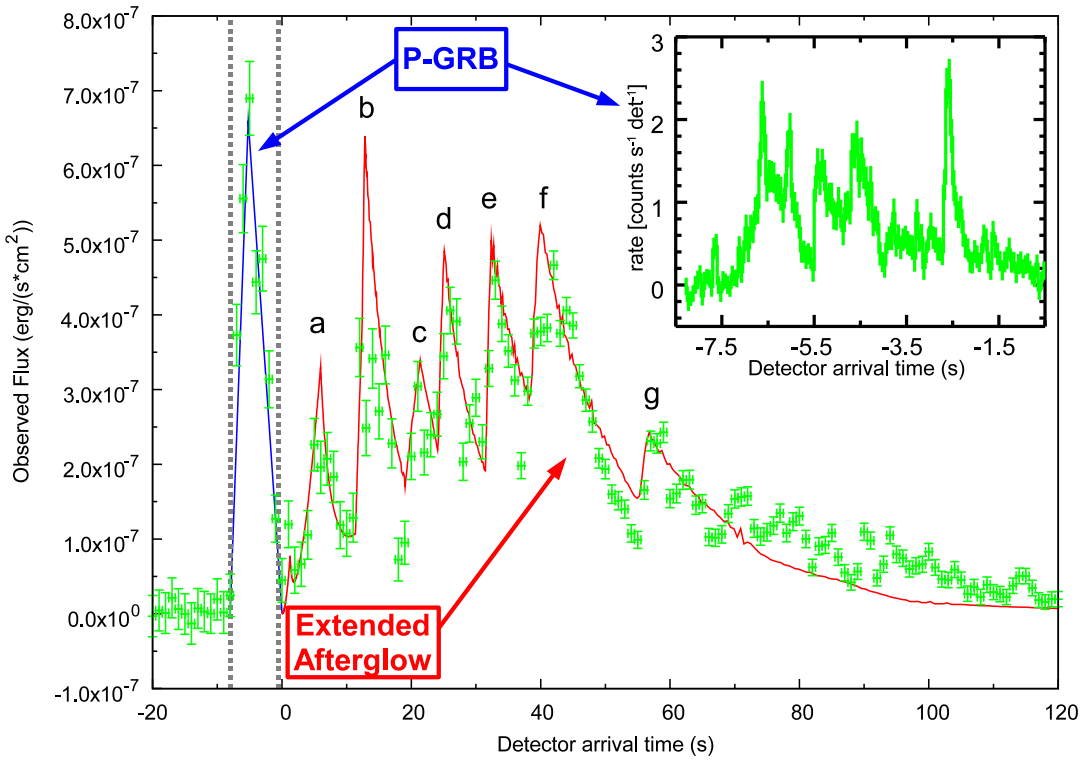

Figure C.5.: The BAT 15–150 keV light curve (green points) at 1 s time resolution compared with the corresponding theoretical extended afterglow light curve we compute (red line). The onset of the extended afterglow is at the end of the P-GRB (qualitatively sketched in blue lines and delimited by dashed gray vertical lines). Therefore the zero of the temporal axis is shifted by 5.5 s with respect to the BAT trigger time. The peaks of the extended afterglow light curves are labeled to match them with the corresponding CBM density peak in Fig. C.6. In the upper right corner there is an enlargement of the P-GRB at 50ms time resolution (reproduced from Mangano et al., 2007), showing its structure.

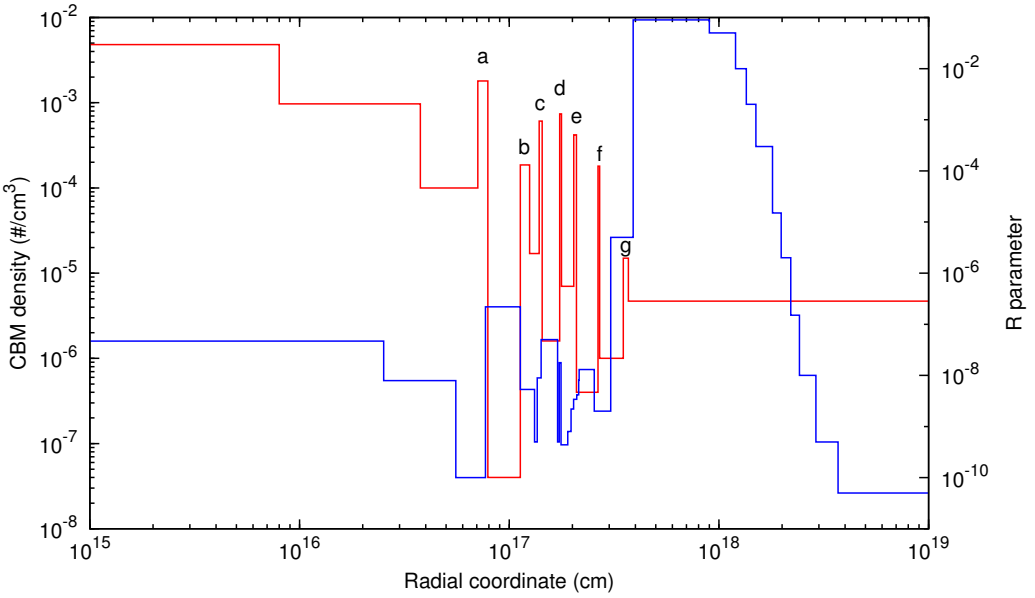

Figure C.6.: The effective CBM density (red line) and the $\mathcal{R}$ parameter (blue line) versus the radial coordinate of the shell. The CBM density peaks are labeled to match them with the corresponding extended afterglow light curve peaks in Fig. C.5. They correspond to filaments of characteristic size $\Delta r \sim 10^{15}$ cm and density contrast $\Delta n_{cbm}/\langle n_{cbm}\rangle \sim 20$ particles/cm^3.

the enhancement of $\mathcal{R}$ between r=2 $\times$ 10^{17} cm and r=3 $\times$ 10^{17} cm, just as for GRB060614, for which we have the enhancement at r=3.5 $\times$ 10^{17} cm. The time of the bump approximately corresponds to the appearance of the optical emission observed in GRB060614 and, more in general, to the onset of the second component of the Willingale et al. (2007) scheme for GRBs.

C.2.2. Open issues in current theoretical models

The "fireshell" model addresses mainly the γ and X-ray emission, which are energetically the most relevant part of the GRB phenomenon. The model allows a detailed identification of the fundamental three parameters of the GRB source: the total energy, the baryon loading, as well as the CBM density, filamentary structure and porosity. Knowledge of these phenomena characterizes the region surrounding the black hole up to a distance which in this source reaches $\sim 10^{17}$–10^{18} cm. When applied, however, to larger distances, which correspond to the latest phases of the X-ray afterglow, since the beginning of the "plateau" phase, the model reveals a different regime which has not yet been fully interpreted in its astrophysical implications. To fit the light curve in the soft X-ray regime for $r > 4 \times 10^{17}$ cm, we require an enhancement of about six orders of magnitude in the $\mathcal{R}$ factor (see Fig. C.6). This would correspond to a more diffuse CBM structure, with a smaller porosity,

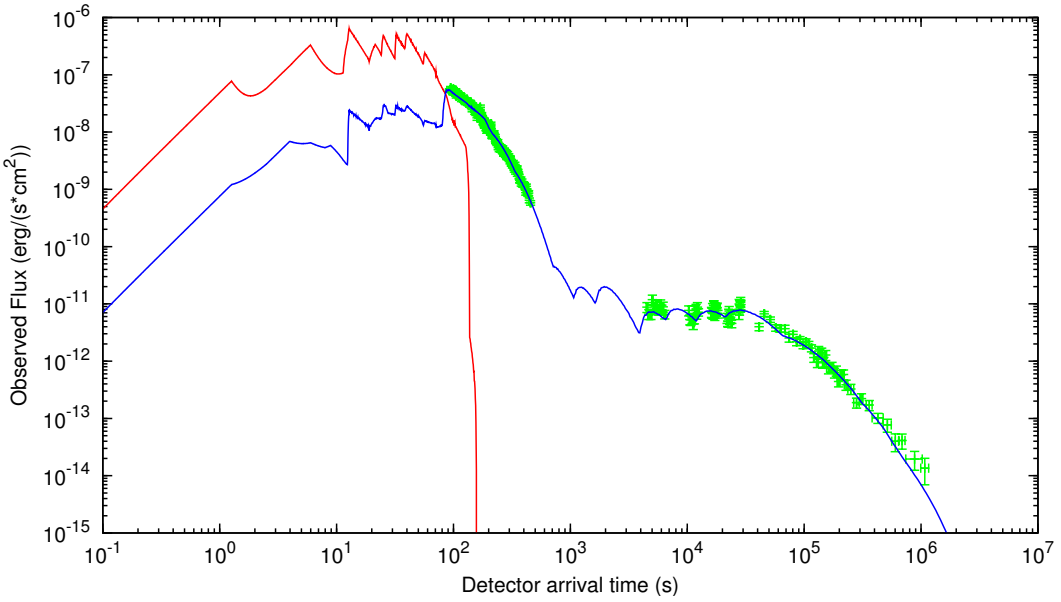

Figure C.7.: The XRT 0.2–10 keV light curve (green points) compared with the corresponding theoretical extended afterglow light curve we compute (blue line). In this case also we have a good correspondence between data and theoretical results. For completeness, the red line shows the theoretical extended afterglow light curve in the 15–150 keV energy range presented in Fig. C.5.

interacting with the fireshell. This implies a different main physical process during the latest X-ray afterglow phases. For the optical, IR and radio emission, the fireshell model leads to a much lower flux than the observed one, especially for $r \sim 10^{17}$–10^{18} cm. Although the optical, IR, and radio luminosities have a minor energetic role, they may lead to the identification of crucial parameters and new phenomena occurring in the source, and they deserve careful attention.

In these late phases for $r \geq 10^{17}$ cm the treatment based on synchrotron emission, pioneered by Meszaros and Rees (1997a) even before the discovery of the afterglow (Costa et al., 1997), is currently applied. Such a model has been further developed (see Sari et al., 1998; Piran, 2005; Meszaros, 2006, and references therein). Also in this case, however, some difficulties remain since it is necessary to invoke the presence of an unidentified energy injection mechanism (Zhang et al., 2006). Such a model appears to be quite successful in explaining the late phases of the X-ray emission of GRB060614, as well as the corresponding optical emission, in terms of different power-law indexes for the different parts of the afterglow light curves (Mangano et al., 2007; Xu et al., 2008). However, also in this case an unidentified energy injection mechanism between $\sim$ 0.01 days and $\sim$ 0.26 days appears to be necessary (Xu et al., 2008).

The attempt to describe the prompt emission via the synchrotron process

by the internal shock scenario (see e.g. Rees and Meszaros, 1994; Piran, 2005; Meszaros, 2006, and references therein) also encounters difficulties: Kumar and McMahon (2008) have shown that the traditional synchrotron model can be applied to the prompt emission only if it occurs at $r > 10^{17}$ cm. A proposed solution to this problem, via the inverse Compton process, suffers from an "energy crisis" (see e.g. Piran et al., 2008).

Interestingly, the declared region of validity of the traditional synchrotron model ($r > 10^{17}$ cm) is complementary to the one successfully described by our model ($r < 10^{17}$–10^{18} cm). Astrophysically, Xu et al. (2008) have reached, within the framework of the traditional synchrotron model, two conclusions which are consistent with the results of our analysis. First, they also infer from their numerical fit a very low density environment, namely $n_{cbm} \sim 0.04$ particles/cm^3. Second, they also mention the possibility that the progenitor of GRB0606014 is a merging binary system formed by two compact objects.

C.2.3. Conclusions

As recalled in the introduction, GRB060614 presents three major novelties, which challenge the most widespread theoretical models and which are strongly debated in the current literature. The first one is that it challenges the traditional separation between long soft GRBs and short hard GRBs (Gehrels et al., 2006). The second one is that it presents a short, hard and multi-peaked episode, followed by a softer, prolonged emission with a strong hard to soft evolution (Gehrels et al., 2006; Mangano et al., 2007). The third one is that it is the first clear example of a nearby, long GRB not associated with a bright SN Ib/c (Della Valle et al., 2006; Gal-Yam et al., 2006). All these three issues are naturally explained within our "fireshell" model, which allows a detailed analysis of the temporal behavior of the signal originating up to a distance $r \sim 10^{17}$–10^{18} cm from the black hole, and relates, with all the relativistic transformation, the arrival time to the CBM structure and the relativistic parameters of the fireshell.

One of the major outcomes of the Swift observation of, e.g., GRB050315 (Vaughan et al., 2006; Ruffini et al., 2006b) has been the confirmation that long GRB duration is not intrinsic to the source but it is merely a function of the instrumental noise threshold (Ruffini et al., 2006a). GRB060614 represents an additional fundamental progress in clarifying the role of the CBM density in determining the GRB morphology. It confirms the results presented in GRB970228 (Bernardini et al., 2007), that is the prototype of the new class of "fake" short GRBs, or, better, of canonical GRBs "disguised" as short ones. They correspond to canonical GRBs with an extended afterglow emission energetically predominant relative to the P-GRB one and a baryon loading $B > 10^{-4}$. The sharp spiky emission corresponds to the P-GRB. As recalled before, a comparison of the luminosities of the P-GRB and of the extended

afterglow is indeed misleading: it follows from the low average CBM density inferred from the fit of the fireshell model, which leads to $n_{cbm} \sim 10^{-3}$ particles/cm^3. Therefore such a feature is neither intrinsic to the progenitor nor to the black hole, but it is only indicative of the CBM density at the location where the final merging occurs. GRB060614 is a canonical GRB and it is what would be traditionally called a "long" GRB if it had not exploded in an especially low CBM density environment. GRB060614 must necessarily fulfill, and indeed it does, the Amati relation. This happens even taking into account the entire prompt emission mixing together the P-GRB and the extended afterglow (Amati et al., 2007), due to the energetic predominance of the extended afterglow discussed above (see also Guida et al., 2008b). These results justify the occurrence of the abovementioned first two novelties.

The low value of the CBM density is compatible with a galactic halo environment. This result points to an old binary system as the progenitor of GRB060614 and it justifies the abovementioned third novelty: the absence of an associated SN Ib/c (see also Davies et al., 2007). Such a binary system departed from its original location in a star-forming region and spiraled out in a low density region of the galactic halo (see e.g. Kramer, 2008). The energetics of this GRB is about two orders of magnitude lower than the one of GRB970228 (Bernardini et al., 2007). A natural possible explanation is that instead of a neutron star - neutron star merging binary system we are in the presence of a white dwarf - neutron star binary. We therefore agree, for different reasons, with the identification proposed by Davies et al. (2007) for the GRB060614 progenitor. In principle, the nature of the white dwarf, with a typical radius of the order of 10^3 km, as opposed to the one of the neutron star, typically of the order of 10 km, may manifest itself in characteristic signatures in the structure of the P-GRB (see Fig. C.5).

It is interesting that these results lead also to three major new possibilities:

- The majority of GRBs declared as shorts (see e.g. Piro, 2005) are likely "disguised" short GRBs, in which the extended afterglow is below the instrumental threshold.

- The observations of GRB060614 offer the opportunity, for the first time, to analyze in detail the structure of a P-GRB lasting 5 s. This feature is directly linked to the physics of the gravitational collapse that generated the GRB. Recently, there has been a crucial theoretical physics result showing that the characteristic time constant for the thermalization of an $e^{\pm}$ plasma is of the order of 10^{-13} s (Aksenov et al., 2007). Such a time scale still applies for an $e^{\pm}$ plasma with a baryon loading of the order of the one observed in GRBs (Aksenov et al., 2008). The shortness of such a time scale, as well as the knowledge of the dynamical equations of the optically thick phase preceding the P-GRB emission (Bianco et al., 2006c), implies that the structure of the P-GRB is a faithful representation of the gravitational collapse process leading to the formation

of the black hole (Ruffini et al., 2005d). In this respect, it is indeed crucial that the Swift data on the P-GRB observed in GRB060614 (see Fig. C.5) appear to be highly structured all the way to a time scale of 0.1 s. This opens a new field of research: the study of the P-GRB structure in relation to the process of gravitational collapse leading to the GRB.

- If indeed the binary nature of the progenitor system and the peculiarly low CBM density $n_{cbm} \sim 10^{-3}$ particles/cm^3 will be confirmed for all "fake" or "disguised" GRBs, then it is very likely that the traditionally "long" high luminosity GRBs at higher redshift also originates in the merging of binary systems formed by neutron stars and/or white dwarfs occurring close to their birth location in star-forming regions with $n_{cbm} \sim 1$ particle/cm^3 (see Fig. C.3).

C.3. Application to GRB 071227: an additional case of a disguised short burst

GRB 071227 presents some intriguing anomalies. As for the "Norris and Bonnel" GRBs, its BAT light curve shows in the 15–150 keV range a multi-peaked structure lasting $T_{90} = (1.8 \pm 0.4)$ s, followed by an extended but much softer emission up to $t_0 + 100$ s (D'Avanzo et al., 2009). A fading X-ray (0.3–10 keV) and a faint optical afterglow have also been identified. The optical afterglow emission allowed to measure its redshift, $z = 0.383$, and therefore its isotropic equivalent energy, $E_{iso} = 5.8 \times 10^{50}$ erg in 20–1300 keV (D'Avanzo et al., 2009). The observed X-ray and optical afterglow is superimposed on the plane of the host galaxy, at (15.0 ± 2.2) kpc from its center.

On the basis of these characteristics, GRB 071227 has been classified as a short burst. This statement is supported by other main features: **1)** If we consider the first and apparently predominant short-duration episode, it does not fulfill the Amati relation between the isotropic equivalent radiated energy of the prompt emission E_{iso} and the cosmological rest-frame νF_ν spectrum peak energy $E_{p,i}$ (Amati et al., 2002; Amati, 2006; Amati et al., 2007, 2009). **2)** The spectral lag of the first spike-like emission in 25–50 keV to 100–350 keV bands is consistent with zero (Sakamoto et al., 2007). **3)** Multiwavelength observations performed over many days have displayed that there is no association with a Ib/c hypernova, the type of SN generally observed with GRBs, even if it is a nearby burst and its isotropic energy is compatible with that of other GRBs associated with them (D'Avanzo et al., 2009), although the upper limits are not deep enough to rule out a low-energetic core-collapse event. Nevertheless, the explosion of this burst in a star-forming region of a spiral galaxy, and its prolonged tail of emission, makes it most likely to be a long burst.

In this paper, we show that all these ambiguities and peculiarities can be explained in the framework of the fireshell model if we assume GRB 071227 to be a *disguised* short burst, in which the first spike-like emission coincides with the P-GRB and the prolonged softer tail with the peak of the extended afterglow emitted in a low CircumBurst Medium (CBM) density region. We show, moreover, that this tail satisfies the Amati relation, and this is consistent with our interpretation.

C.3.1. The interpretation of GRB 071227 light curves

We examine the possibility that GRB 071227 can also be classified as a "disguised" burst. We analyzed the observed light curves of this burst in the 15–50 keV bandpass, corresponding to the lowest band of the γ-ray emission, detected by the BAT instrument on the *Swift* satellite, and in the 0.3–10 keV energy band, corresponding to the X-ray component from the XRT instrument. To model the CBM structure, we assume that n_{cbm} is a function of only the radial coordinate, $n_{cbm} = n_{cbm}(r)$ (radial approximation). The CBM is arranged in spherical shells of width $\sim 10^{15} - 10^{16}$ cm arranged in such a way that the corresponding modulation of the emitted flux closely resembles the observed shape. We assumed that the first short spike-like emission represents the P-GRB and the γ-ray tail is the peak of the extended afterglow. We therefore began the simulation in such a way that the extended afterglow light curve begins in coincidence with the peak of the P-GRB (about 1s), as shown in Fig. C.8. To reproduce the observational data and the energetics observed for the P-GRB emission ($E_{iso} \sim 1.0 \times 10^{51}$ erg), we require the initial conditions $E_{tot}^{e^\pm} = 5.04 \times 10^{51}$ erg and $B = 2.0 \times 10^{-4}$. In Figs. C.8 and C.9 we plot the comparison of the GRB 071227 BAT and XRT data with the theoretical extended afterglow light curves. We obtained a good result in the prompt emission for the 15–50 keV bandpass (see Fig. C.8), while, for 0.3–10 keV, we only succeeded in reproducing the first decaying part of the XRT light curve (see Fig. C.9). We assumed this to correspond to the possible onset of the "plateau" phase of the extended afterglow (Nousek et al., 2006).

From our simulation, the amount of energy stored in the P-GRB is found to be about 20% of the total energetics of the explosion. Hence, this burst cannot be a short burst within the fireshell scenario. The baryon loading obtained ($B = 2.0 \times 10^{-4}$) remains in the range of long duration GRBs. This is a very critical value, because it is very close to the crossing point of the plot of the energetics of GRBs as a function of B (see above). This is the lowest baryon loading that we have ever found in our analysis within the fireshell scenario. From our analysis, we found a peculiar result for the average CBM density. We obtained a density of $n_{cbm} = 1.0 \times 10^{-2}$ particles/cm^3 at the beginning of the process, later decreasing to $n_{cbm} = 1.0 \times 10^{-4}$ particles/cm^3. This low average density, inferred from the analysis, is responsible for the strong de-

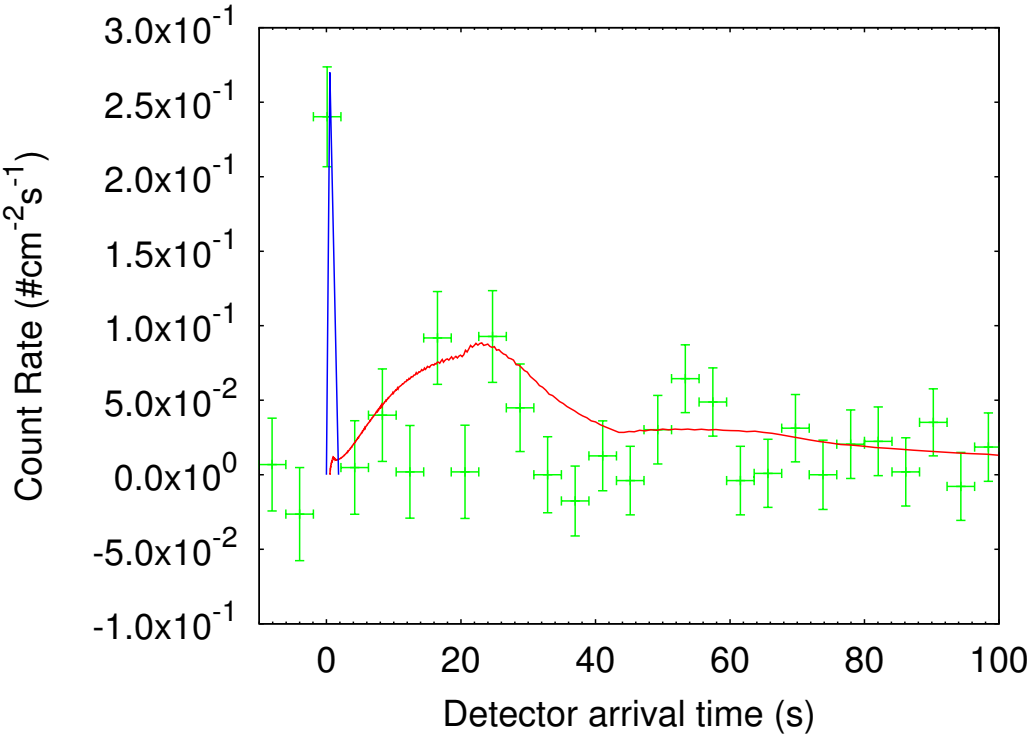

Figure C.8.: The BAT 15–50 keV light curve (green points) compared with the corresponding theoretical extended afterglow light curve (red line). The P-GRB is qualitatively sketched by the blue line.

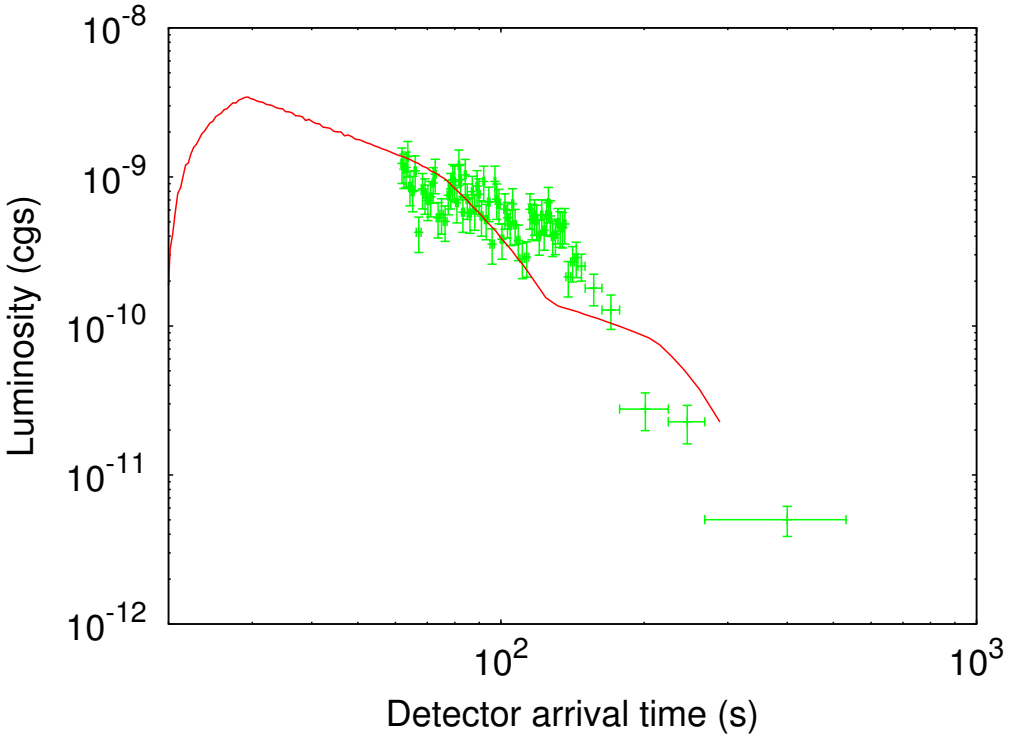

Figure C.9.: The XRT 0.3–10 keV light curve (green points) compared with the corresponding theoretical extended afterglow light curve we obtain (red line). The X-ray data corresponding to the first 60 seconds are not available since XRT starts to observe only 60 seconds after the BAT trigger. We stop our analysis at $\gamma \sim 5$ when our relativistic dynamical model can no longer be applied

flation of the γ-ray tail. However, at the radius of about 2.0×10^{17} cm, the density becomes higher and reaches the value of $n_{cbm} = 10$ particles/cm^3 (the complete profiles of n_{cbm} and $\mathcal{R}$ as functions of the radial coordinate are reported in Fig. C.10). This is compatible with the observations. The observed X-ray and optical afterglow of GRB 071227 is indeed superimposed on the plane of the host galaxy, at (15.0 ± 2.2) kpc from its center (D'Avanzo et al., 2009). An interesting possibility observed by D. Arnett (private communication) is that this very low density "cavity" could be formed in the coalescing phase of a binary formed by a neutron star and a white dwarf. Accurate studies on compact object mergers have shown the distribution of merger locations for different host galaxies (Belczynski et al., 2006; Berger, 2010). In starburst galaxies, most of the mergers are expected to be found within hosts, while in elliptical galaxies a substantial fraction of mergers take place outside hosts. Spiral galaxies, hosting both young and old stellar populations, represent the intermediate case between the preceding two. This result is therefore compatible with our hypothesis about the binary nature of the progenitor of GRB 071227. Although they did not consider the case of binary systems formed by a neutron star and a white dwarf, the progenitor of GRB 071227 would fit into the tight binary scenario described by Belczynski et al. (2006).

These results clearly imply that GRB 071227 is another example of a disguised burst.

C.3.2. GRB 071227 within the Amati relation

One of the most effective tools for discriminating between "short" and "long" bursts, and possibly clarifying the interpretation of these different classes of events, is the Amati relation (Amati et al., 2002; Amati, 2006; Amati et al., 2007, 2009).

This empirical spectrum-energy correlation states that the isotropic-equivalent radiated energy of the prompt emission E_{iso} is correlated with the cosmological rest-frame νF_ν spectrum peak energy $E_{p,i}$: $E_{p,i} \propto (E_{iso})^a$, with $a \approx 0.5$ (Amati et al., 2002). The existence of the Amati relation, discovered when analyzing the *BeppoSAX* long duration bursts, has been confirmed by studying a sample of GRBs observed by *Swift*, intense or soft, with available measurements of redshift and spectral parameters, and also by *HETE-2* and *Konus/WIND*. When the "afterglow revolution" allowed the redshift estimation of also some short GRBs, it was found that these bursts are inconsistent with the Amati relation, holding instead for long GRBs (Amati, 2006, 2010; Antonelli et al., 2009). The most recent updating of the correlation (95 GRBs with the data available up to April 2009) also includes two high-energetic events detected by *Fermi* (GRB 090323 and GRB 080916C), which are fully consistent with the $E_{p,i}$–E_{iso} relation (Amati et al., 2009). We also note that the short event

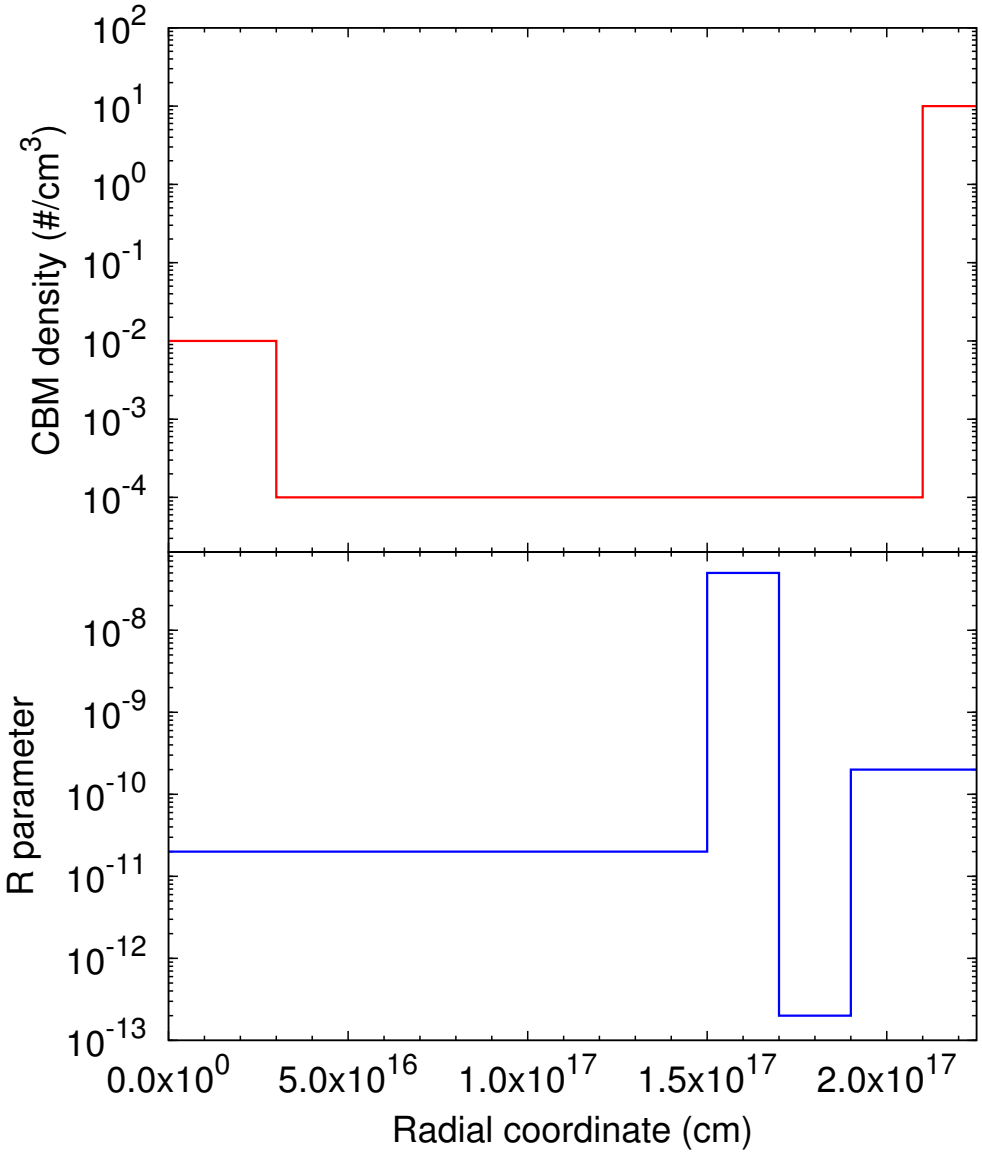

Figure C.10.: The CBM particle number density n_{cbm} (upper panel, red line) and the $\mathcal{R}$ parameter (lower panel, blue line) as functions of the radial coordinate

GRB 090510, observed by the same satellite, is an outlier of the relation, as expected for short bursts. This dichotomy finds a natural explanation within the fireshell model. As recalled above, within this theoretical framework the prompt emission of long GRBs is dominated by the peak of the extended afterglow, while the one of the short GRBs is dominated by the P-GRB. Only the extended afterglow emission follows the Amati relation (see Guida et al., 2008b, for details). Therefore, all GRBs in which the P-GRB provides a negligible contribution to the prompt emission (namely the long ones, where the P-GRB is at most a small precursor) fulfill the Amati relation, while all GRBs in which the extended afterglow provides a negligible contribution to the prompt emission (namely the short ones) do not.

Apart from this general feature, there are peculiar cases. One of these is GRB 050724, a short burst followed by a long, softer tail in the γ-ray energy band. While the first short emission is inconsistent with the Amati relation, the soft tail is again consistent with it. Another one, the intriguing case of GRB 060614, a *disguised* short burst within the fireshell scenario (Caito et al., 2009), shows similar behavior: the first hard episode does not fulfill the Amati relation, while the whole event is fully consistent with it (Amati et al., 2007). This is again fully consistent with the predictions of the fireshell model for the disguised GRB class. Since the first short and hard episode is the P-GRB and the prolonged softer tail is the peak of the extended afterglow, the Amati relation must be fulfilled only when the softer tail is considered alone, or considered together with the first episode if this episode provides a negligible contribution (see Bernardini et al., 2008a, for details). Thus, to discriminate its nature, we studied the position of GRB 071227 in the $E_{p,i}$-E_{iso} plane. At the observed redshift, we assumed a "flat Λ-CDM model" with $H_0 = 70 Km/s/Mpc$ and $\Omega_\Lambda = 0.73$. For the first, hard spike, lasting about 1.8s, using *Konus/WIND* data (Golenetskii et al., 2007), and integrating between 1 and 10 000 keV, we found that $E_{p,i} = (1384 \pm 277)$ keV and $E_{iso} = (1.0 \pm 0.2) \times 10^{51}$ erg. As shown in Fig. C.11, this is inconsistent with the $E_{p,i}$-E_{iso} relation, and instead occupies the short-populated region of the plane. For the long tail, lasting about 100s, we used a Band model with $\alpha = -1.5$ and $\beta = -3$, which are typical of soft events. These values are compatible with the low quality statistics of this event. We found that $E_{p,i} = 20^{+19}_{-11}$ keV and $E_{iso} = (2.2 \pm 0.1) \times 10^{51}$ erg. With these values, the tail of emission is fully consistent with the Amati relation, as for any long GRB (see Fig. C.11). This clearly supports our hypothesis about the nature of GRB 071227.

C.3.3. Conclusions

GRB 071227 has been classified in the current literature as a short GRB not fulfilling the Amati relation. By analyzing it using the fireshell model, we have

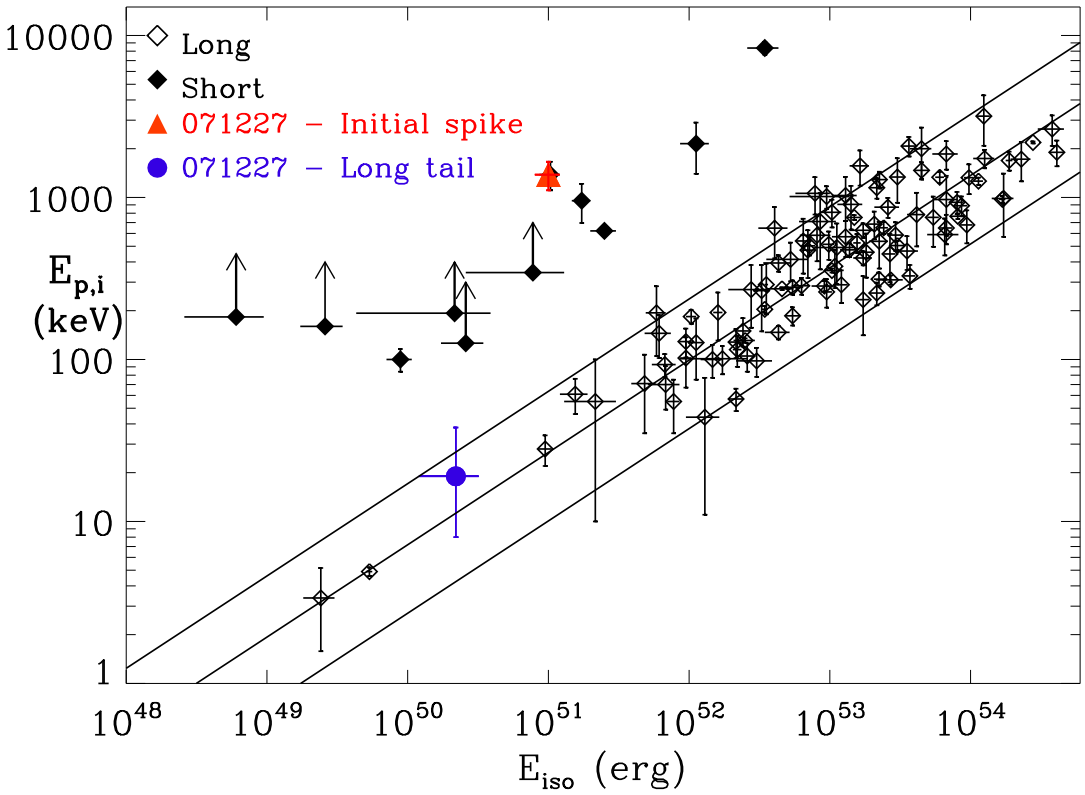

Figure C.11.: Location of the initial short spike and soft long tail of GRB 071227 in the $E_{p,i} - E_{iso}$ plane. The data points of long GRBs are from Amati et al. (2008, 2009), the data points and limits of short GRBs are from Amati (2006); Amati et al. (2009); Piranomonte et al. (2008). The continuous lines show the best-fit power law and the 2σ confidence region of the correlation, as determined by Amati et al. (2008).

identified the first spike-like emission with the P-GRB and consequently the prolonged softer tail with the peak of the extended afterglow. We have shown that this tail indeed fulfills the Amati relation. We have shown that the Amati relation is a characteristic of the extended afterglow phase of GRBs and does not occur during the P-GRB emission. As presented above, the relative energy of the P-GRB with respect to the extended afterglow is a strong function of the baryon loading. For $B \to 10^{-2}$, the energetic relevance of the P-GRB decreases and its contribution to the total GRB energetics can be neglected with respect to the extended afterglow: in this limit, the Amati relation always applies. In the present case, we have $B = 2.0 \times 10^{-4}$ and the exclusion of the P-GRB from the total energetics of the GRB is indeed essential to fulfill the Amati relation. This is similar to the case of GRB 050724. With the considerations given above, it is appropriate to consider GRB 071227 to be another "Norris and Bonnell" kind of burst. It is quite similar to the bright GRB 060614, which we have previously analyzed (Caito et al., 2009), although underluminous. The value of $B = 2.0 \times 10^{-4}$ that we obtained appears to be the smallest of all GRBs we examined. It is particularly interesting that the CBM distribution is given by $\langle n_{cbm} \rangle < 10^{-2}$ particles/cm^3 to a radius of the order of $\sim 2.1 \times 10^{17}$ cm and then monotonically rises to a value of $\langle n_{cbm} \rangle = 10$ particles/cm^3. While this last value is expected in the region where the GRB occurred, at (15.0 ± 2.2) kpc from the center of its host galaxy, the existence of a very low density "cavity" appears to be of great interest. On the other side, as for GRB 060614, the energetics of GRB 071227 is compatible with the progenitor being the merging of a binary system of a neutron-star and a white-dwarf. This binary system, during the long-lasting merging process, may have swept the CBM around by means of the pulsar radiation emission (D. Arnett, private communication). This remains under investigation and may be an additional factor affecting the analogous low density observed in GRB 060614. In that burst, the progenitor was also consistent with a binary system formed by a white dwarf and a neutron star.

C.4. Application to GRB 050509b: an additional case of a disguised short burst

C.4.1. Introduction

The traditional classification of gamma ray bursts (GRBs) is based on the observed time duration of the prompt emission measured with the criterion of "T_{90}", which is the time duration in which the cumulative counts increase from 5% to 95% above the background, encompassing 90% of the total GRB counts. This parameter shows that there are two groups of GRBs, the short ones with $T_{90} < 2$ s, and the long ones with $T_{90} > 2$ s. This analysis mo-

tivated the standard classification in the literature of short and long GRBs (Klebesadel, 1992; Dezalay et al., 1992; Kouveliotou et al., 1993).

The observations of GRB 050509b by BAT and XRT on board the *Swift* satellite (see Gehrels et al., 2004; Burrows et al., 2005a) represent a new challenge to the classification of GRBs as long and short, since it is the first short GRB associated with an afterglow (Gehrels et al., 2005). Its prompt emission observed by BAT lasts 40 milliseconds, but it also has an afterglow in the X-ray band observed by XRT, which begins 100 seconds after the BAT trigger (time needed to point XRT to the position of the burst) and lasts until ≈ 1000 seconds. It is located 40 kpc away from the center of its host galaxy (Bloom et al., 2006b, , see Fig. C.12), which is a luminous, non-star-forming elliptical galaxy with redshift $z = 0.225$ (Gehrels et al., 2005). Although an extensive observational campaign has been performed using many different instruments, no convincing optical-IR candidate afterglow nor any trace of any supernova has been found associated with GRB 050509b (see Cenko et al., 2005; Bersier et al., 2005; Hjorth et al., 2005; Castro-Tirado et al., 2005; Bloom et al., 2005a,b, 2006b). An upper limit in the R-band 18.5 days after the event onset imply that the peak flux of any underlying supernova should have been ~ 3 mag fainter than the one observed for the type Ib/c supernova SN 1998bw associated with GRB 980425, and 2.3 mag fainter than a typical type Ia supernova (Castro-Tirado et al., 2005, see also Hjorth et al., 2005). An upper limit to the brightening caused by a supernova or supernova-like emission has also been established at 8.17 days after the GRB: $R_c \sim 25.0$ mag (Bloom et al., 2006b). While some core-collapse supernovae might be as faint as (or fainter than) this limit (Pastorello et al., 2007), the presence of this supernova in the outskirts of an elliptical galaxy would be truly extraordinary (Mannucci et al., 2005; van den Bergh et al., 2005).

Unfortunately, we cannot obtain exhaustive observational constraints for this GRB because XRT data are missing in-between the first 40 milliseconds and 100 seconds. However, this makes the theoretical work particularly interesting, because we can infer from first principles some characteristics of the missing data, which are inferred by our model, and consequently reach a definite understanding of the source. This is indeed the case, specifically, for the verification of the Amati relation (Amati et al., 2002; Amati, 2006; Amati et al., 2009) for these sources as we see in section C.4.4.

GRB 050509b is an example that the usual classification is at least incomplete. Within the fireshell model, we propose three classes of GRBs: long, genuine short and disguised short (Ruffini et al., 2009, and references therein). We have a well-defined way of differentiating between the classes, which is based on two parameters, the baryon loading parameter B and the Circum-Burst Medium (CBM) number density n_{CBM} (see next section), that help to make the classification clearer. In this paper, we analyze GRB 050509b within the fireshell model. We proceed with the identification of the two basic parameters, B and n_{CBM}, within two different scenarios. We first investigate the

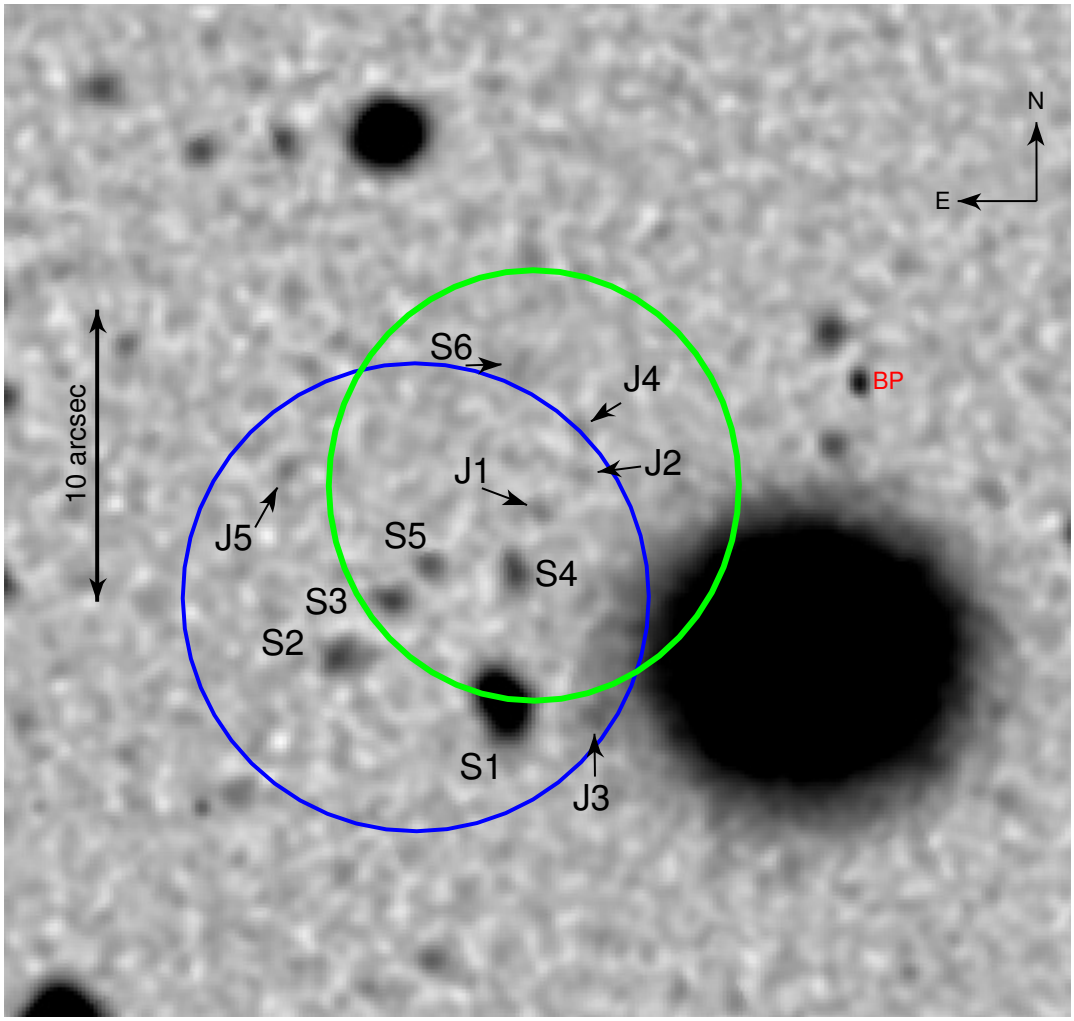

Figure C.12.: Keck LRIS G-band image, zoomed to show the XRT error circle. The larger, blue circle is the revised XRT position from Rol et al. (2005); the smaller, green circle to the west and north of that is the 2σ confidence region of the XRT position computed in Bloom et al. (2006b). The 11 sources consistent with the Rol et al. (2005) X-ray afterglow localization are labeled in the image. North is up and east is to the left. G1 is the large galaxy to the west and south of the XRT. Bad pixel locations are denoted with "BP". Figure reproduced from Bloom et al. (2006b) with the kind permission of J. Bloom and of the AAS.

"ansatz" that this GRB is the first example of a "genuine" short bursts. After disproving this possibility, we show that this GRB is indeed another example of a disguised short burst.

In the next section, we briefly introduce the fireshell model and explain the classification, in section C.4.3 we show the analysis of the data, in section C.4.4 we present the theoretical spectrum and the study of the fulfillment of the Amati relation, in section C.4.5 we comment on the results, and in section C.4.6 we finally present our conclusions.

C.4.2. Fireshell model

Within the fireshell model (Ruffini et al., 2002, 2004b, 2005c, 2009; Bianco and Ruffini, 2005b,a), all GRBs originate from an optically thick $e^{\pm}$ plasma of total energy $E_{tot}^{e^{\pm}}$ in the range 10^{49}–10^{54} ergs and a temperature T in the range 1–4 MeV. After an early expansion, the $e^{\pm}$-photon plasma reaches thermal equilibrium with the engulfed baryonic matter M_B described by the dimensionless parameter $B = M_B c^2 / E_{tot}^{e^{\pm}}$, which must be $B < 10^{-2}$ to allow the fireshell to expand further. As the optically thick fireshell composed of $e^{\pm}$-photon-baryon plasma self-accelerates to ultrarelativistic velocities, it finally reaches the transparency condition. A flash of radiation is then emitted. This represents the proper-GRB (P-GRB). The amount of energy radiated in the P-GRB is only a fraction of the initial energy $E_{tot}^{e^{\pm}}$. The remaining energy is stored in the kinetic energy of the optically thin baryonic and leptonic matter fireshell that, by inelastic collisions with the CBM, gives rise to multiwavelength emission. This is the extended afterglow.

Within this model, the value of B strongly affects the ratio of the energetics of the P-GRB to the kinetic energy of the baryonic and leptonic matter within the extended afterglow phase. It also affects the time separation between the corresponding peaks (Ruffini et al., 2009). For baryon loading $B \lesssim 10^{-5}$, the P-GRB component is always energetically dominant over the extended afterglow (see Fig. C.13). In the limit $B \to 0$, it gives rise to a "genuine" short GRB. Otherwise, when $3.0 \times 10^{-4} \lesssim B \leq 10^{-2}$, the kinetic energy of the baryonic and leptonic matter, and consequently the extended afterglow emission, predominates with respect to the P-GRB (Ruffini et al., 2002; Bernardini et al., 2007). Since the "critical" value of B corresponding to the crossing point in Fig. C.13 is a slowly varying function of the total energy $E_{tot}^{e^{\pm}}$, for $10^{-5} \lesssim B \lesssim 3.0 \times 10^{-4}$ the ratio of the total energies of the P-GRB and the extended afterglow is also a function of $E_{tot}^{e^{\pm}}$.

The extended afterglow luminosity in the different energy bands is governed by two quantities associated with the environment: the CBM density profile, n_{CBM}, and the ratio of the effective emitting area A_{eff} to the total area A_{tot} of the expanding baryonic shell, $\mathcal{R} = A_{eff} / A_{tot}$. This second parameter takes into account the CBM filamentary structure (Ruffini et al., 2004b). Typi-

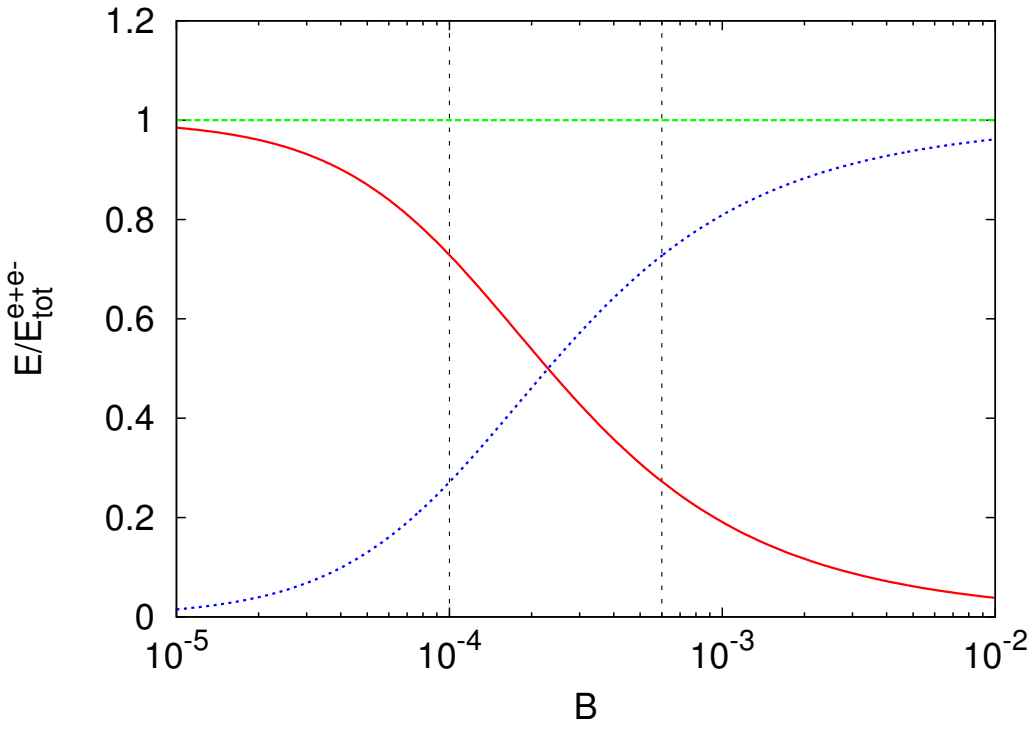

Figure C.13.: The dashed (blue) curve is the energy emitted in the extended afterglow, the solid (red) curve is the energy emitted in the P-GRB, their sum is $E_{tot}^{e^{\pm}}$. From left to right, the first vertical line corresponds to the value of $B = 1.0 \times 10^{-4}$ of scenario 1, the second to the value of $B = 6.0 \times 10^{-4}$ of scenario 2 (see Sec. C.4.3).

cal values of $\mathcal{R}$ ranges between 10^{-10} and 10^{-6} (see e.g. Bernardini et al., 2007, 2005a; Caito et al., 2009, 2010; Dainotti et al., 2007; Ruffini et al., 2006b).

The emission from the baryonic matter shell is spherically symmetric. This allows us to assume, to a first approximation, a modeling of thin spherical shells for the CBM distribution and consequently only consider their radial dependence (Ruffini et al., 2002). The emission process is assumed to be thermal in the comoving frame of the shell (Ruffini et al., 2004b). The observed GRB non-thermal spectral shape is produced by the convolution of a very large number of thermal spectra with different temperatures and different Lorentz and Doppler factors. This convolution is performed over the surfaces of constant arrival times for the photons at the detector (EQuiTemporal Surfaces, EQTSs; Bianco and Ruffini, 2005b,a) encompassing the total observation time. The fireshell model does not address the plateau phase described by Nousek et al. (2006), which may not be related to the interaction of the single baryonic shell with the CBM (Bernardini et al., 2010).

In the context of the fireshell model, we considered a new class of GRBs, pioneered by Norris and Bonnell (2006). This class is characterized by an occasional softer extended emission after an initial spike-like emission. The softer extended emission has a peak luminosity lower than the one of the initial spike-like emission. As shown in the prototypical case of GRB 970228 (Bernardini et al., 2007) and then in both GRB 060614 (Caito et al., 2009) and GRB 071227 (Caito et al., 2010), we can identify the initial spike-like emission with the P-GRB and the softer extended emission with the peak of the extended afterglow. A crucial point is that the time-integrated extended afterglow luminosity (i.e. its total radiated energy) is much higher than the P-GRB one. This unquestionably identifies GRB 970228 and GRB 060614 as canonical GRBs with $B > 10^{-4}$. The consistent application of the fireshell model allows us to infer the CBM filamentary structure and average density, which, in that specific case, is $n_{CBM} \sim 10^{-3}$ particles/cm^3, typical of a galactic halo environment (Bernardini et al., 2007). This low CBM density value explains the peculiarity of the low extended afterglow peak luminosity and its more protracted time evolution. These features are not intrinsic to the progenitor, but depend uniquely on the peculiarly low value of the CBM density. This led us to expand the traditional classification of GRBs to three classes: "genuine" short GRBs, "fake" or "disguised" short GRBs, and the remaining "long duration" ones.

A CBM density $n_{CBM} \sim 10^{-3}$ particles/cm^3 is typical of a galactic halo environment, and GRB 970228 was indeed found to be in the halo of its host galaxy (Sahu et al., 1997; van Paradijs et al., 1997). We therefore proposed that the progenitors of this new class of disguised short GRBs are merging binary systems, formed by neutron stars and/or white dwarfs in all possible combinations, which spiraled out from their birth place into the halo (see Bernardini et al., 2007; Caito et al., 2009; Kramer, 2008). This hypothesis can also be supported by other observations. Assuming that the soft-tail peak lu-

minosity is directly related to the CBM density, short GRBs displaying a prolonged soft tail should have a systematically smaller offset from the center of their host galaxy. Some observational evidence was found in this sense (Troja et al., 2008). However, the present sample of observations does not enable us to derive any firm conclusion that short GRBs with extended emission have smaller physical offsets than those without extended emission (Fong et al., 2010; Berger, 2011b).

C.4.3. Data analysis of GRB 050509b

Scenario 1

We first attempt to analyze GRB 050509b under the scenario that assumes it is a "genuine" short GRB, namely a GRB in which more than 50% of the total energy is emitted in the P-GRB. This would be the first example of an identified "genuine" short GRB.

Within our model, the only consistent solution that does not contradict this assumption leads to the interpretation that all the data belongs to the extended afterglow phase; the BAT data of the prompt emission (see figure 2 in Gehrels et al., 2005) are then the peak of the extended afterglow, and the XRT data represents the decaying phase of the extended afterglow (which in the literature is simply called "the afterglow", see section C.4.2).

In figure C.14, we show the result of this analysis. We obtained the following set of parameters: $E_{tot}^{e^\pm} = 2.8 \times 10^{49}$ erg, $B = 1.0 \times 10^{-4}$, and $n_{CBM} = 1.0 \times 10^{-3}$ particles/cm^3. These parameters would imply, however, that the energy emitted in the P-GRB should be almost 72% of the total value. This P-GRB should have been clearly observable, and has not been detected. Consequently, this scenario is ruled out and we conclude that GRB 050509b cannot be interpreted as a "genuine" short GRB.

Scenario 2

We now analyze GRB 050509b under the alternative scenario that assumes the energy of the extended afterglow is higher than the P-GRB one. Within our model, the only consistent solution that does not contradict this assumption leads to the prompt emission observed by BAT (see Fig. 2 in Gehrels et al., 2005) being interpreted as the P-GRB, and the X-ray decaying afterglow data observed by XRT being interpreted as the extended afterglow.

In Fig. C.15, we show the result of this analysis. We obtained the parameters $E_{tot}^{e^\pm} = 5.52 \times 10^{48}$ erg, $B = 6 \times 10^{-4}$, and an almost constant CBM density $n_{CBM} = 1.0 \times 10^{-3}$ particles/cm^3. The low value of the number density is justified by the GRB being located 40 kpc away from the center of the host galaxy (Bloom et al., 2006b, , see Fig. C.12). The initial value of $\mathcal{R}$ is

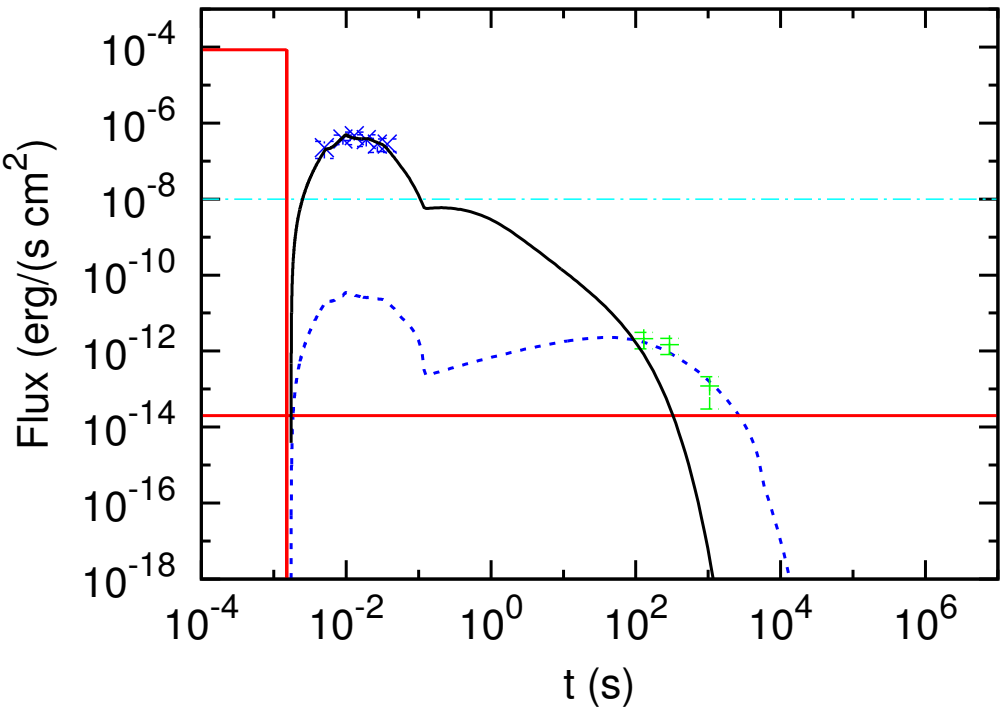

Figure C.14.: Our numerical simulation within scenario 1, assuming that GRB 050509b is a "genuine" short GRB, i.e. that the P-GRB is energetically predominant over the extended afterglow. The BAT data (crosses) are interpreted as the peak of the extended afterglow. In this case, the predicted P-GRB (solid rectangle) total energy is more than twice the extended afterglow one. The solid line is the theoretical light curve in the 15-150 keV energy band, and the dashed one is the theoretical light curve in the 0.3-10 keV energy band. The dot-dashed horizontal line represents the BAT threshold and the solid horizontal one represents the XRT threshold.

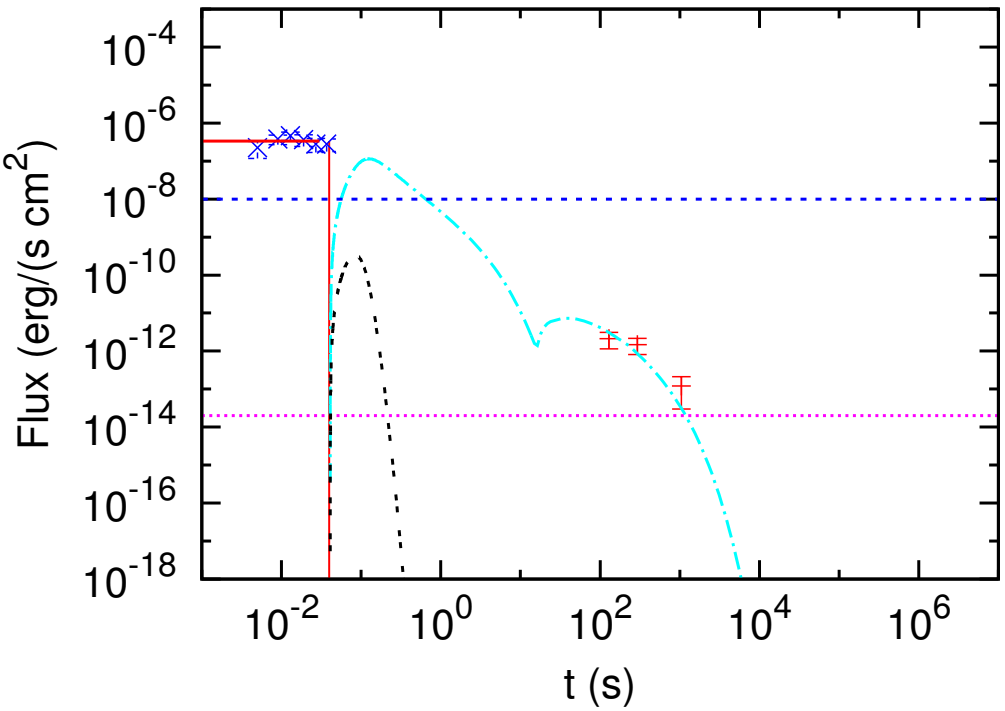

Figure C.15.: Our numerical simulation within scenario 2, assuming that the extended afterglow is energetically predominant over the P-GRB. In this case, the predicted P-GRB (solid rectangle) is less then twice the extended afterglow. We interpret the BAT data (crosses) as the P-GRB and the XRT data as the extended afterglow. The P-GRB has just 28% of the total energy. The double-dashed line is the theoretical light curve in the band 15–150 keV, and the dot-dashed line is the theoretical light curve in the band 0.3–10 keV. The two horizontal lines are from above to below: the BAT threshold and the XRT threshold.

quite large, $\mathcal{R} = 1.2 \times 10^{-1}$, which indicates that there is a very homogeneous CBM in the region close to the progenitor system. However, at $t \approx 10$ seconds, corresponding to a fireshell radius of $\sim 2 \times 10^{16}$ cm, the effective area of interaction between the expanding plasma and the CBM drops six orders of magnitude and we have $\mathcal{R} = 3 \times 10^{-7}$, a value pointing to the typical CBM filamentary structure also encountered in other sources (see Sec. C.4.2). The P-GRB has an estimated energy of $E_{P-GRB} = 28\% E^{e^{\pm}}_{tot}$, which means that 72% of the energy is released in the extended afterglow. The peak of the extended afterglow, theoretically predicted by our model in figure C.15, was not observed by BAT, since the energy was below its threshold, and also not observed by XRT, since unfortunately its data collection started only 100 seconds after the BAT trigger.

Following our classification, therefore, due to the values of the baryon loading and of the CBM density, as well as due to the offset with respect to the host galaxy, GRB 050509b is consistent with being another example of a disguised short GRB. This follows the previous identification of GRB 970228 (Bernardini et al., 2007) GRB 060614 (Caito et al., 2009) and GRB 071227 (Caito et al., 2010).

C.4.4. The theoretical spectrum and Amati relation

We turn now to the most interesting aspects of our theoretical work, namely the possibility of inferring some characteristics of the missing data and finally the nature of the burst from first principles. The most effective tool for determining the nature and, then, interpreting the different classes of GRBs, is the Amati relation (Amati et al., 2002; Amati, 2006; Amati et al., 2009). This empirical spectrum-energy correlation states that the isotropic-equivalent radiated energy of the prompt emission E_{iso} is correlated with the cosmological rest-frame νF_ν spectrum peak energy $E_{p,i}$: $E_{p,i} \propto (E_{iso})^a$, where $a \approx 0.5$ and a dispersion $\sigma(\log_{E_p}) \sim 0.2$. The Amati relation holds only for long duration bursts, while short ones, as it has been possible to prove after the "afterglow revolution" and the measurement of their redshift, are inconsistent with it (Amati, 2006; Amati et al., 2009).

This dichotomy can naturally be explained by the fireshell model. As recalled in Sect. C.4.2, within this theoretical framework the prompt emission of long GRBs is dominated by the peak of the extended afterglow, while that of the short GRBs is dominated by the P-GRB. Only the extended afterglow emission follows the Amati relation (see Guida et al., 2008b; Caito et al., 2010). Therefore, all GRBs in which the P-GRB provides a negligible contribution to the prompt emission (namely the long ones, where the P-GRB is at most a small precursor) fulfill the Amati relation, while all GRBs in which the extended afterglow provides a negligible contribution to the prompt emission (namely the short ones) do not (see Bernardini et al., 2007, 2008a; Guida et al.,

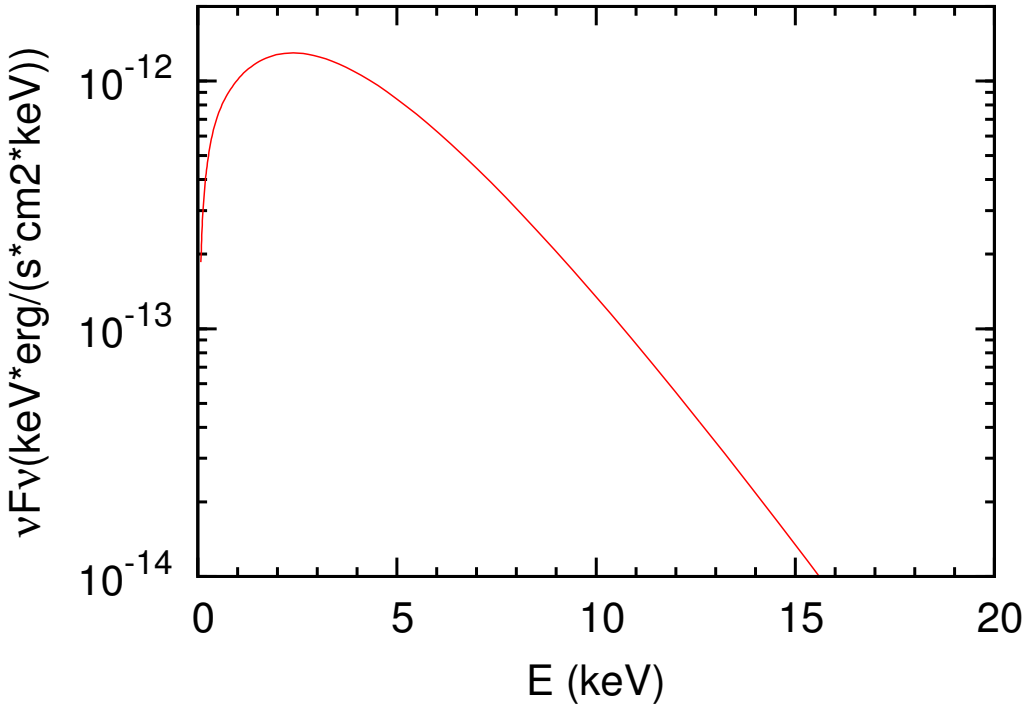

Figure C.16.: Our theoretical spectrum in the observer frame integrated over the entire extended afterglow up to 10^4 s, see also Guida et al. (2008b).

2008b; Caito et al., 2009, 2010). As a consequence, for disguised short bursts the two components of the prompt emission must be analyzed separately. The first spikelike emission alone, which is identified with the P-GRB, should not follow the Amati relation; the prolonged soft tail, which is identified with the peak of the extended afterglow, should instead follow the Amati relation. This has been confirmed in the cases of GRB 060614 and GRB 071227 (Caito et al., 2010).

Owing to the lack of extended afterglow observational data before 100 seconds, there is no way to confirm whether this source follows the Amati relation on an observational ground. To verify whether GRB 050509b follows the Amati relation, and so clarify its nature, we simulated a theoretical spectrum (see figure C.16), following scenario 2, to verify a posteriori the consistency of this source with the Amati relation.

We first calculate E_{iso}, which, as mentioned above, in our case is not the total energy of the GRB but the total energy of the extended afterglow, $E_{iso} \equiv E_{after} = 72\% E^{e^\pm}_{tot} = 4 \times 10^{48}$ erg. To calculate $E_{p,i}$, we simulated the $\nu F\nu$ theoretical spectrum integrated over the entire extended afterglow up to 10^4 s, as described in Guida et al. (2008b). The theoretical $\nu F\nu$ spectrum in the observer frame is shown in figure C.16: it peaks at $E_p \sim 2.3$ keV, which implies that $E_{p,i} = (1+z)E_p \sim 2.8$ keV.

We also checked the position of GRB 050509b in the $E_{p,i}/E_{iso}$ plane considering only the short hard spikelike emission observed by BAT, which is identified with the P-GRB. In this case, only a lower limit to $E_{p,i}$ can be established from the observational data. The νF_ν observed spectrum in the BAT 15–150 keV energy range indeed increase with energy and does not exhibit any peak (Bloom et al., 2006b). Therefore, a first estimate would lead us to conclude that $E_p > 150$ keV and then that $E_{p,i} > 184$ keV. The corresponding value of the isotropic equivalent energy emitted in the BAT 15–150 keV energy range is $E_{iso,15-150} = (2.7 \pm 1) \times 10^{48}$ ergs (Bloom et al., 2006b). Bloom et al. (2006b) conclude that the total isotropic equivalent energy emitted can be $E_{iso} \gtrsim 3E_{iso,15-150}$ if $E_p \gtrsim$ 1–2 MeV. A more conservative estimate of $E_{p,i}$ and E_{iso} can be found by fitting the observed BAT spectrum with a Band model where α and β indices are fixed to typical values ($\alpha = -1$ and $\beta = -2.3$). This leads to the following lower limit to E_p at 90% c.l. of $E_p > 55$ keV, which corresponds to $E_{p,i} > 67$ keV. To compute the corresponding total isotropic equivalent energy E_{iso}, we must integrate this Band spectrum from 1 keV to 10000 keV. Since the exact value of E_p is not known, but we have only a lower limit, the result of this integration, and therefore E_{iso}, will depend on E_p. We find that E_{iso} can range from 5×10^{48} erg, if E_p is equal to its lower limit (i.e. $E_p = 55$ keV), all the way up to 3×10^{49} erg, if E_p is as high as the upper limit of the integration (i.e. $E_p = 10000$ keV).

In Fig. C.17, the result of this analysis are shown. When considering both the upper limit following Bloom et al. (2006b), namely $E_{p,i} > 184$ keV and $2.6 \times 10^{48} < E_{iso} \lesssim 7.8 \times 10^{48}$ erg, and the more conservative upper limit computed above, namely $E_{p,i} > 67$ keV and $5 \times 10^{48} < E_{iso} < 3 \times 10^{49}$ erg, we find that the short hard spikelike emission observed by BAT, which is identified with the P-GRB, does not fulfill the Amati relation. When, instead, we consider the peak of the extended afterglow alone ($E_{p,i} \sim 2.8$ keV, $E_{iso} \sim 4 \times 10^{48}$ erg, see above), as should be done according to the fireshell scenario (Guida et al., 2008b; Caito et al., 2010), GRB 050509b is fully consistent with the Amati relation.

This result allows us to conclude that, within the theoretical fireshell model, GRB 050509b is consistent with the Amati relation. It implies that this is not a genuine short burst, but instead a long burst disguised as a short one, confirming our hypothesis.

C.4.5. Discussion

In a set of papers based on the fireshell model, it has been introduced a new class of GRBs, called "disguised" short GRBs (see Bernardini et al., 2007, 2008a; Caito et al., 2009, 2010; Ruffini et al., 2009, and references therein). These are canonical long GRBs with an extended afterglow that is energetically predominant with respect to the P-GRB (see Fig. C.13). Their main

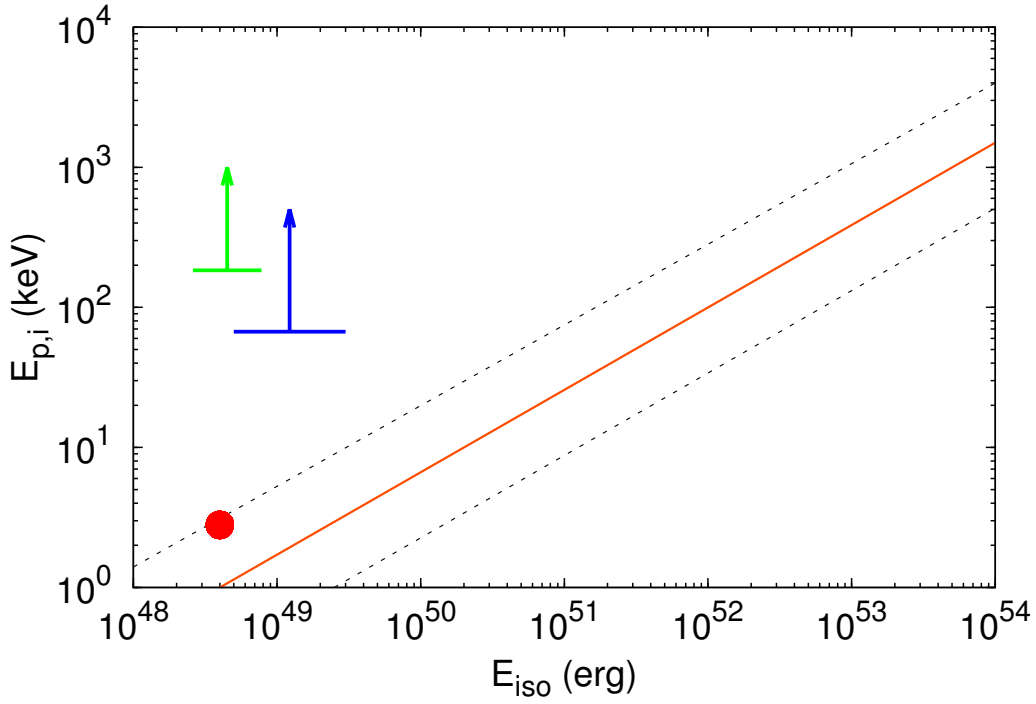

Figure C.17.: GRB 050509b position in the $E_{p,i}/E_{iso}$ plane. The continuous orange lines show the best-fit power law of the $E_{p,i} - E_{iso}$ correlation and the dotted gray ones are the 2σ confidence region, as determined by Amati et al. (2009). The green lower limit ($2.6 \times 10^{48} < E_{iso} \lesssim 7.8 \times 10^{48}$ erg and $E_{p,i} > 184$ keV, computed following Bloom et al., 2006b) and the blue lower limit ($5 \times 10^{48} < E_{iso} < 3 \times 10^{49}$ erg and $E_{p,i} > 67$ keV, computed following the more conservative approach described in this paper) correspond to the short hard spikelike emission observed by BAT. The red dot ($E_{iso} \sim 4 \times 10^{48}$ erg, $E_{p,i} \sim 2.8$ keV) corresponds to the unobserved peak of the extended afterglow theoretically computed within the fireshell model.

characteristic is that the emission of the afterglow occurs in an environment characterized by a peculiarly low value of the average CBM density ($n_{CBM} = 1.0 \times 10^{-3}$ particles/cm^3), which is a value typical of a galactic halo environment. Under this condition, the extended afterglow peak luminosity is much lower than the one expected for a canonical value of the average CBM density inside the galaxy ($n_{CBM} = 1.0$ particle/cm^3). Consequently, the extended afterglow peak luminosity is "deflated" and the energy of the extended afterglow is released on a much longer timescale. The energetic predominance of the afterglow with respect to the P-GRB is quantified by the value of the baryon loading B (see Fig. C.13) and can be verified by integrating over time the luminosity of the extended afterglow. Examples of this class are GRB 970228 (Bernardini et al., 2007), GRB 060614 (Caito et al., 2009), and GRB 071227 (Caito et al., 2010).

We have shown that GRB 050509b cannot be considered a "genuine" short GRB and proposed that it be classified as a disguised short GRB. We have tested two alternative scenarios for this GRB, one assuming it is a "genuine" short GRB and an alternative one assuming it is a disguised short GRB. We have demonstrated that the only interpretation of the data compatible with the first scenario would lead to an extremely intense P-GRB that is not observed (see Fig. C.14); therefore this scenario should be discarded and GRB 050509b cannot be interpreted as a "genuine" short GRB. We have instead obtained a reasonable interpretation within the second scenario for $B = 6.0 \times 10^{-4}$, corresponding to a long GRB, and an average CBM density of $n_{CBM} = 1.0 \times 10^{-3}$ particles/cm^3, which clearly implies that GRB 050509b is a disguised short GRB (see Fig. C.15).

GRB 050509b does not have XRT data before 100 s. The BAT light curve went beneath its threshold at $\sim$ 40 ms. All the data about the peak of the extended afterglow is therefore missing, which is the relevant part for the calculation of the energy peak $E_{p,i}$ of the $\nu F\nu$ spectrum for the Amati relation. Despite this lack of data, it has been possible, from our theoretical simulation, to infer both the spectrum of the extended afterglow peak emission and a value of $E_{p,i}$, and to check a posteriori whether GRB 050509b fulfills the Amati relation. This has been done, as already shown in previous papers (Guida et al., 2008b; Caito et al., 2010), by duly neglecting the contribution of the P-GRB, assuming that the Amati relation is connected only to the extended afterglow emission process. It has been proven indeed (see Fig. C.17) that GRB 050509b, when the P-GRB contribution in neglected, is in perfect agreement with the Amati relation. This interpretation is also supported by the P-GRB alone being inconsistent with the Amati relation (see also Fig. C.17, Sec. C.4.4 and e.g. Bloom et al., 2006b, and references therein).

The understanding reached for this source and others of the same class points also to a difficulty in identifing a "genuine" short GRB. A selection effect is at work: a genuine short GRB must have a very weak extended afterglow (see Fig. C.13); consequently, it is very difficult to determine its redshift.

C.4.6. Conclusion

It has been shown that GRB 050509b originates from the gravitational collapse to a black hole of a merging binary system consisting of two degenerate stars according to three different and complementary considerations:

1. Very stringent upper limits on an associated supernova event have been established (see Cenko et al., 2005; Bersier et al., 2005; Hjorth et al., 2005; Castro-Tirado et al., 2005; Bloom et al., 2005a,b, 2006b);

2. The host galaxy has been identified with a luminous, non-star-forming elliptical galaxy (Prochaska et al., 2005; Gehrels et al., 2005; Bloom et al., 2005a, 2006b);

3. The GRB exploded in the halo of the host galaxy (Bloom et al., 2006b), because the binary system spiraled out before merging.

From an astrophysical point of view, there are three possible cases of merging binary systems that must be considered:

1. Neutron star / neutron star: unlike the case of GRB 970228 (Bernardini et al., 2007), the low energetics of GRB 050509b disfavor this hypothesis;

2. Neutron star / white dwarf: this appears to be the most likely case for GRB 050509b, as in GRB 060614 (Caito et al., 2009) and in GRB 071227 (Caito et al., 2010);

3. White dwarf / white dwarf: this case is viable only for two very massive white dwarfs, allowing the critical mass of neutron stars against gravitational collapse to a black hole to be overcome in the merging process; that low massive white dwarf / white dwarf merging binary systems may lead to low energetics events has been widely expressed in the literature (see e.g. Iben and Tutukov, 1984; Paczynski, 1985; Pakmor et al., 2010).

From the point of view of GRB classification, we conclude that:

1. GRB 050509b is a disguised short GRB occurring in a low CBM density environment ($n_{CBM} < 10^{-3}$ particles/cm^3), typical of a galactic halo;

2. The baryon loading of GRB 050509b, and consequently the ratio of the P-GRB to the extended afterglow energetics, is typical of canonical long-duration GRBs;

3. The possible origin of a genuine short GRB from a merging binary system, as often purported in the literature (see e.g. Meszaros, 2006 but also Gehrels et al., 2009), still remains an open issue both from an observational and a theoretical point of view; in theory, this will crucially

depend on the amount of baryonic matter left over in the process of gravitational collapse originating the fireshell baryon loading, which must be $B \lesssim 10^{-5}$.

From all the above considerations, it also follows that a binary system merging in a higher density region (i.e. $n_{CBM} \sim 1$ particles/cm^3) would give rise to a canonical long-duration GRB without an associated supernova (see also Bernardini et al., 2007; Caito et al., 2009).

C.5. Application to GRB 011121

C.5.1. A widely debated issue: the interpretation of flares

A flare is a large scale activity in excess on the underlying light curve that manifests as a bump in luminosity rather intense and sharp in the decaying phase of the X-Ray afterglow.

When the first flare was detected by BeppoSAX, on the X-Ray light curve of GRB 011121, it was assumed as an extremely peculiar phenomenon. However, by the advent of the Swift Mission, many flares have been discovered in the light curves of about the 50% of the total amount of X-Ray afterglows observed: it was clear that flares are a very typical feature of GRBs phenomenon. The many observations collected until today show that flares are random events that manifest in different shapes and in all sizes, in each kind of burst (both long and short) and at each measure of redshift. X-Ray flares have been observed in all phases of the X-Ray light curve, the peak time ranges between 95 s and 75 ks. There are light curves with more than one flare, although the more frequent case exhibits one single pulse on the Gamma-Ray peak followed by one or two flares. They are often characterized by large flux variations, can be strongly energetics and in some cases flares have surpassed the original GRB (ex. GRB 060526). This extreme variability and, in particular, the smallness of the time interval in which these big variation of flux happens, makes hard to give reason of such a phenomenon.

As discussed in the previous sections, in our theory the multiwavelength emission is entirely due to the fully inelastic collisions of the baryonic remnants of the fireshell with the CBM. Flares also, as characteristic parts of the afterglow, can be naturally explained in this context. The most relevant results of recent data analysis made on big samples (Chincarini et al., 2007b; Falcone et al., 2007a) are consistent with our hypothesis of inelastic collisions as the origin of flares. In fact, first of all, flares manifest until very late times and follow the typical hard to soft evolution; then, bumps become broader as the time increases, consistently with a general trend of GRB light curves. Moreover, the distribution of intensity ratios between successive Gamma-Ray pulses and that between successive X-Ray flares is the same, while there is no correlation between the number of pulses of the Gamma-Ray emission and

the number of X-Ray flares. These last features seem to establish a common origin of Gamma-Ray bumps and X-Ray flares, and this is consistent with our hypothesis concerning to which the entire emission (from the Gamma 'Prompt emission' to the late Afterglow phase) is generated by the same inelastic collisions process.

On the other hand, it is difficult to conciliate all these aspects within the standard model or any other model founded on an internal shock process (eventually followed by an external shock phase). In particular, is hardly explained the presence of flares at very late times and their strong, rapid variation of flux. As already said, this is one of the most debated peculiarity of the appearing flares. It has been found that $\langle dt/t \rangle = 0.13 \pm 0.10$, corresponding to variations of flux of one or also two orders of magnitude. It's a shared opinion that an external shock scenario can't reproduce a similar range of variability, but we are able to show that this is consistent with our fully inelastic collision hypothesis. This assumption implies just the consideration of the three-dimensional structure of the CBM, until now neglected for the radial approximation modeling for the CBM profile. We realized a first attempt to check this idea by its application on the burst with the first flare observed, GRB 011121.

C.5.2. The first step on the first flare: analysis of GRB 011121

GRB 011121 is a near, long burst with $T_{90} = 28$ s and redshift $z = 0.36$ (Infante et al., 2001). Its fluence (Price et al., 2002) is 2.4×10^{-5} erg/cm^2 that corresponds, in the hypothesis of isotropic emission at the observed redshift, to an energy in the band $2 - 700$ keV of 2.8×10^{52} erg. This is the second brightest source detected by BeppoSAX in γ-rays and X-rays. At the time $t = 240$ s, in the X-ray $2 - 26$ keV energy band, there is a big flare(Piro et al., 2005; Greiner et al., 2003a). It lasts about seventy seconds ($dt/t \sim 0.29$) and corresponds to a bump of an order of magnitude in luminosity. It is however very soft, since its energy is about 3% of the total amount of the prompt emission (Piro et al., 2005).

In figure C.18 we present the observed GRB 011121 light curves in the three different energy bands we analyzed, together with their theoretical fit in the framework of our model: $40 - 700$ keV, $2 - 26$ keV, $2 - 10$ keV. Looking at the observational data we can see that the $40 - 700$ keV energy band light curve presents a temporal profile particularly regular, smooth and homogeneous, while the $2 - 26$ keV light curve has a remarkably irregular profile. This is quite anomalous, in fact generally the light curves in these energy bands presents just the opposite trend.

In figure C.18 there is also an enlargement of the flare of this source that shows in detail the comparison between the theoretical light curve and the

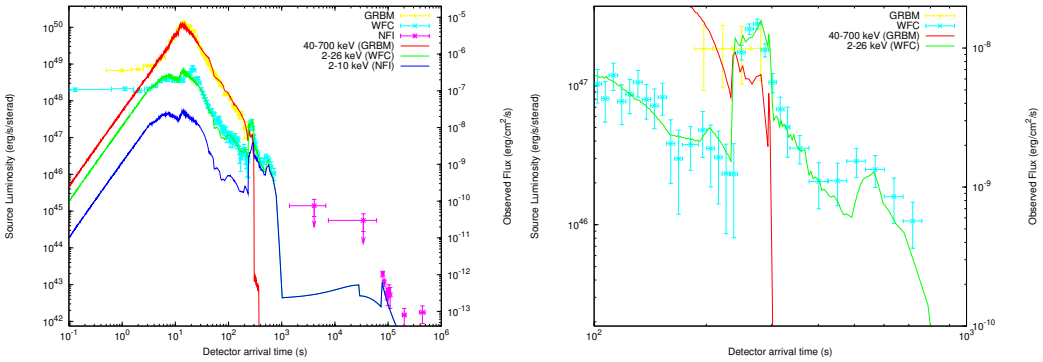

Figure C.18.: Left: Theoretical fit of the GRB 011121 light curves in the $40 - 700$ keV (BeppoSAX GRBM), $2 - 26$ keV (BeppoSAX WFC), 2/10 keV (BeppoSAX NFI). **Right:** Enlargement of the Flare.

observational data.

In the computation of the theoretical light curve for the flare we reproduce it as due to a spherical cloud of CBM along the line of sight introducing, in this way, a three-dimensional structure for the Circum Burst Medium. In fact, in the first approximation, we assume a modeling of thin spherical shells for the distribution of the CBM. This allows us to consider a purely radial profile in the expansion (Ruffini et al., 2002, 2003a) . This radial approximation is valid until the visible area of emission of photons is sufficiently small with respect to the characteristic size of the CBM shell. The visiblre area of emission is defined by the maximum value of the viewing angle; it varies with time and is inversely proportional to the Lorentz Gamma Factor(see the previous). So it happens that, at the beginning of the expansion, when the Gamma Factor is big (about 10^2), the effective distribution of the CBM doesn't matter for the narrowness of the viewing angle but, at the end of the expansion, the remarkable lessening of the Gamma Factor produces a strong increase of the viewing angle and a correct estimation of the CBM by the introduction of the angular coordinate distribution becomes necessary.

We can see that our results are in very good agreement with the observational data, also in the late tail of the flare. In particular, the short time variability has been successfully reproduced.

Here we performed just a first attempt of application of our interpretation of flares and we found an encouraging result. Now we plan to verify our hypothesis by its application to other sources and to produce a detailed cinematic and dynamic theory concerning this fundamental features of Gamma-Ray Burst.

C.6. Application to GRB 031203

GRB 031203 was observed by IBIS, on board of the INTEGRAL satellite (see Mereghetti and Gotz, 2003), as well as by XMM (Watson et al., 2004) and Chandra (Soderberg et al., 2004) in the $2-10$ keV band, and by VLT (Soderberg et al., 2004) in the radio band. It appears as a typical long burst (Sazonov et al., 2004a), with a simple profile and a duration of ≈ 40 s. The burst fluence in the $20-200$ keV band is $(2.0 \pm 0.4) \times 10^{-6}$ erg/cm^2 (Sazonov et al., 2004a), and the measured redshift is $z = 0.106$ (Prochaska et al., 2004). We analyze in the following the gamma-ray signal received by INTEGRAL. The observations in other wavelengths, in analogy with the case of GRB 980425 (Pian et al., 2000; Ruffini et al., 2004a, 2007b), could be related to the supernova event, as also suggested by Soderberg et al. (2004), and they will be examined elsewhere.

The INTEGRAL observations find a direct explanation in our theoretical model. We reproduce correctly the observed time variability of the prompt emission (see Fig. C.19 and Bernardini et al., 2005a). The radiation produced by the interaction of the optically thin fireshell with the CBM agrees with observations both for intensity and time structure.

The progress in reproducing the X and $\gamma-$ray emission as originating from a thermal spectrum in the comoving frame of the burst (Ruffini et al., 2004b) leads to the characterization of the instantaneous spectral properties which are shown to drift from hard to soft during the evolution of the system. The convolution of these instantaneous spectra over the observational time scale is in very good agreement with the observed power-law spectral shape.

C.6.1. The initial conditions

The best fit of the observational data leads to a total energy of the electron-positron plasma $E^{tot}_{e^\pm} = 1.85 \times 10^{50}$ erg. Assuming a black hole mass $M = 10 M_\odot$, we then have a black hole charge to mass ratio $\xi = 6.8 \times 10^{-3}$; the plasma is created between the radii $r_1 = 2.95 \times 10^6$ cm and $r_2 = 2.81 \times 10^7$ cm with an initial temperature $T = 1.52$ MeV and a total number of pairs $N_{e^\pm} = 2.98 \times 10^{55}$. The amount of baryonic matter in the remnant is $B = 7.4 \times 10^{-3}$.

After the transparency point and the P-GRB emission, the initial Lorentz gamma factor of the accelerated baryons is $\gamma_\circ = 132.8$ at an arrival time at the detector $t^d_a = 8.14 \times 10^{-3}$ s and a distance from the Black Hole $r_\circ = 6.02 \times 10^{12}$ cm. The CBM parameters are: $< n_{cbm} >= 0.3$ particle$/cm^3$ and $< \mathcal{R} >= 7.81 \times 10^{-9}$.

C.6.2. The GRB luminosity in fixed energy bands

The aim of our model is to derive from first principles both the luminosity in selected energy bands and the time resolved/integrated spectra. We recall that the luminosity in selected energy bands is evaluated integrating over the EQTSs (see Ruffini et al., 2004b) the energy density released in the interaction of the accelerated baryons with the CBM measured in the co-moving frame, duly boosted in the observer frame. The radiation viewed in the comoving frame of the accelerated baryonic matter is assumed to have a thermal spectrum and to be produced by the interaction of the CBM with the front of the expanding baryonic shell.

In order to evaluate the contributions in the band $[\nu_1, \nu_2]$ we have to multiply the bolometric luminosity with an "effective weight" $W(\nu_1, \nu_2, T_{arr})$, where T_{arr} is the observed temperature. $W(\nu_1, \nu_2, T_{arr})$ is given by the ratio of the integral over the given energy band of a Planckian distribution at temperature T_{arr} to the total integral aT_{arr}^4 (Ruffini et al., 2004b). The resulting expression for the emitted luminosity is Eq.(7.3.1).

C.6.3. The "prompt emission"

In order to compare our theoretical prediction with the observations, it is important to notice that there is a shift between the initial time of the GRB event and the moment in which the satellite instrument has been triggered. In fact, in our model the GRB emission starts at the transparency point when the P-GRB is emitted. If the P-GRB is under the threshold of the instrument, the trigger starts a few seconds later with respect to the real beginning of the event. Therefore it is crucial, in the theoretical analysis, to estimate and take into due account this time delay. In the present case it results in $\Delta t_a^d = 3.5$ s (see the bold red line in Fig. C.19). In what follows, the detector arrival time is referred to the onset of the instrument.

The structure of the prompt emission of GRB 031203, which is a single peak with a slow decay, is reproduced assuming an CBM which has not a constant density but presents several density spikes with $< n_{cbm} >= 0.16$ particle/cm^3. Such density spikes corresponding to the main peak are modeled as three spherical shells with width Δ and density contrast $\Delta n/n$: we adopted for the first peak $\Delta = 3.0 \times 10^{15}$ cm and $\Delta n/n = 8$, for the second peak $\Delta = 1.0 \times 10^{15}$ cm and $\Delta n/n = 1.5$ and for the third one $\Delta = 7.0 \times 10^{14}$ cm and $\Delta n/n = 1$. To describe the details of the CBM filamentary structure we would require an intensity vs. time information with an arbitrarily high resolving power. With the finite resolution of the INTEGRAL instrument, we can only describe the average density distribution compatible with the given accuracy. Only structures at scales of 10^{15} cm can be identified. Smaller structures would need a stronger signal and/or a smaller time resolution of the detector. The three clouds here considered are necessary and sufficient to re-

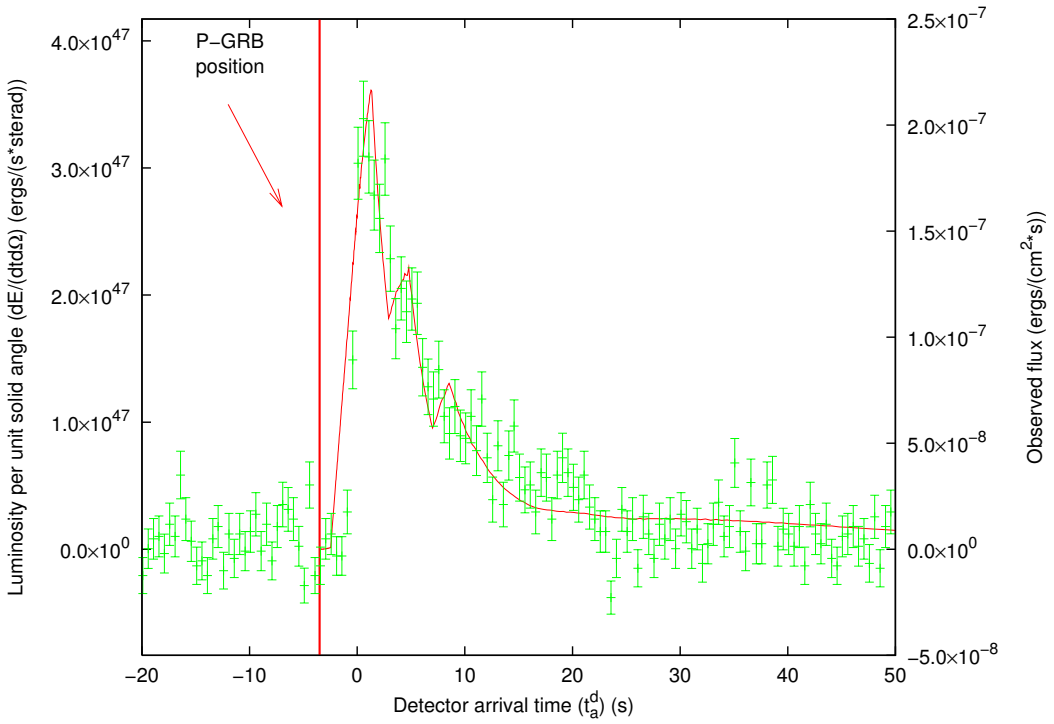

Figure C.19.: Theoretically simulated light curve of the GRB 031203 prompt emission in the $20 - 200$ keV energy band (solid red line) is compared with the observed data (green points) from Sazonov et al. (2004a). The vertical bold red line indicates the time position of P-GRB.

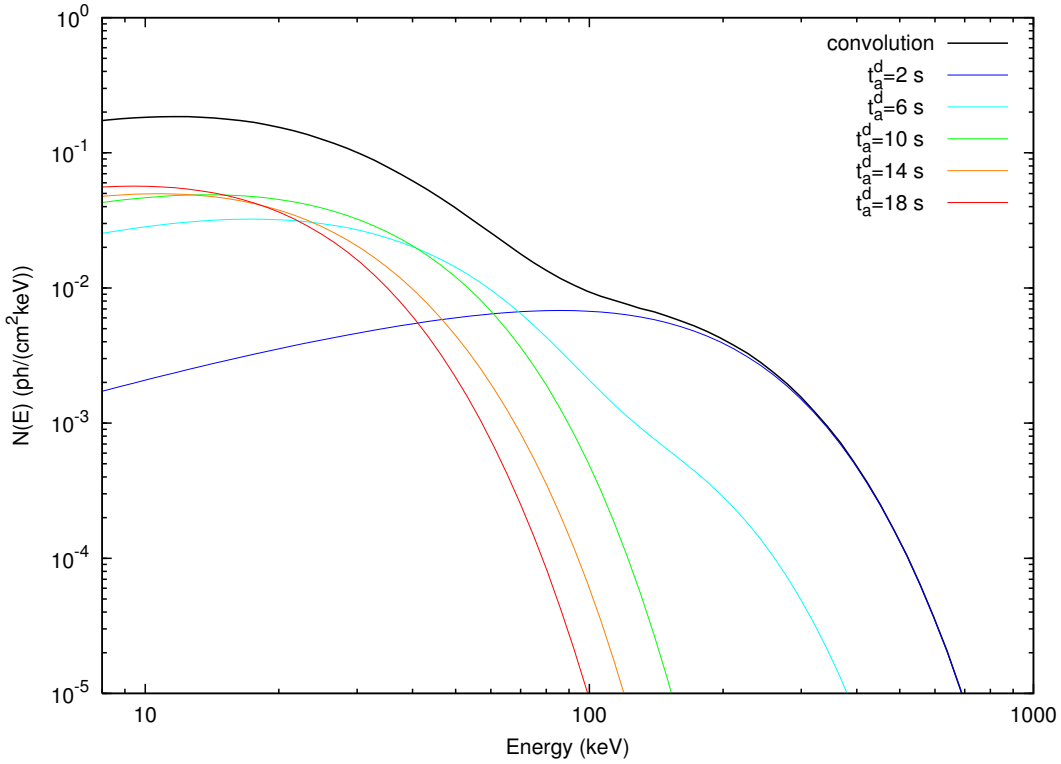

Figure C.20.: Five different theoretically predicted instantaneous photon number spectrum $N(E)$ for $t_a^d = 2, 6, 10, 14, 18$ s are here represented (colored curves) together with their own temporal convolution (black bold curve). The shapes of the instantaneous spectra are not blackbodies due to the spatial convolution over the EQTS (see text).

produce the observed light curve: a smaller number would not fit the data, while a larger number is unnecessary and would be indeterminable.

The result (see Fig. C.19) shows a good agreement with the light curve reported by Sazonov et al. (2004a), and it provides a further evidence for the possibility of reproducing light curves with a complex time variability through CBM inhomogeneities (Ruffini et al., 2002, 2003a, 2005a).

C.6.4. The instantaneous spectrum

As outlined in previous sections, in addition to the the luminosity in fixed energy bands we can derive also the instantaneous photon number spectrum $N(E)$. In Fig. C.20 are shown samples of time-resolved spectra for five different values of the arrival time which cover the whole duration of the event.

It is manifest from this picture that, although the spectrum in the comoving frame of the expanding pulse is thermal, the shape of the final spectrum in the laboratory frame is clearly non thermal. In fact, as explained in Ruffini et al.

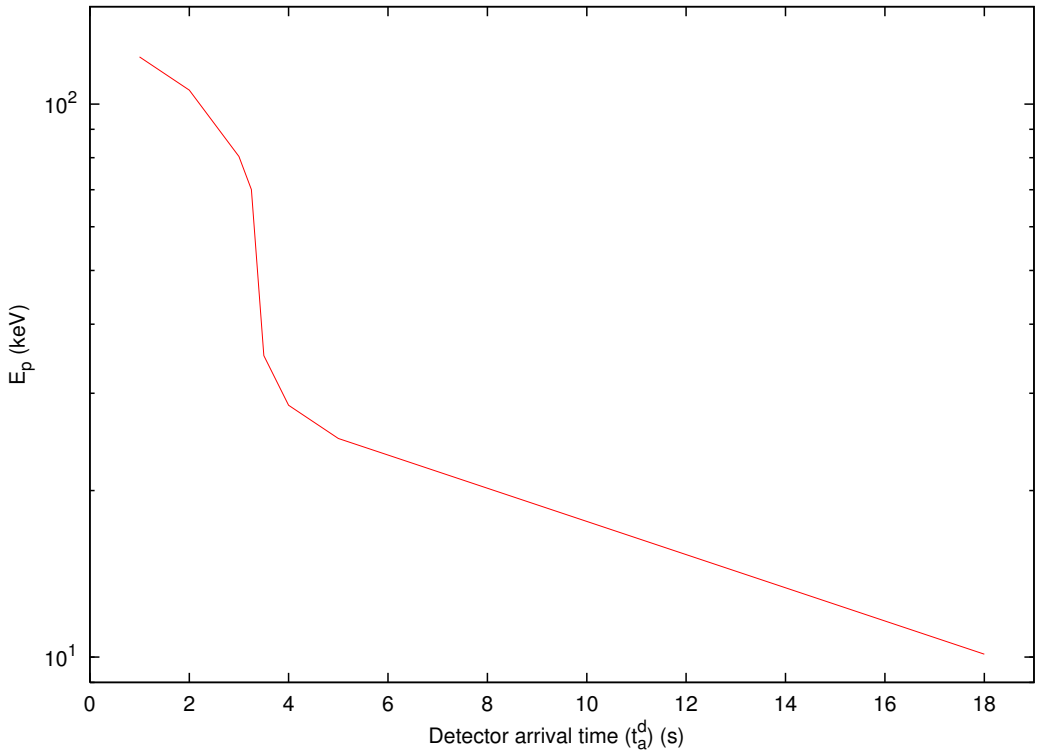

Figure C.21.: The energy of the peak of the instantaneous photon number spectrum $N(E)$ is here represented as a function of the arrival time during the "prompt emission" phase. The clear hard to soft behavior is shown.

(2004b), each single instantaneous spectrum is the result of an integration of hundreds of thermal spectra over the corresponding EQTS. This calculation produces a non thermal instantaneous spectrum in the observer frame (see Fig. C.20).

Another distinguishing feature of the GRBs spectra which is also present in these instantaneous spectra, as shown in Fig. C.20, is the hard to soft transition during the evolution of the event (Crider et al., 1997; Piran, 1999; Frontera et al., 2000; Ghirlanda et al., 2002). In fact the peak of the energy distributions E_p drift monotonically to softer frequencies with time (see Fig. C.21). This feature explains the change in the power-law low energy spectral index α (Band et al., 1993) which at the beginning of the prompt emission of the burst ($t_a^d = 2$ s) is $\alpha = 0.75$, and progressively decreases for later times (see Fig. C.20). In this way the link between E_p and α identified by Crider et al. (1997) is explicitly shown. This theoretically predicted evolution of the spectral index during the event unfortunately cannot be detected in this particular burst by INTEGRAL because of the not sufficient quality of the data (poor photon statistics, see Sazonov et al., 2004a).

C.6.5. The time-integrated spectrum: comparison with the observed data

The time-integrated observed GRB spectra show a clear power-law behavior. Within a different framework Shakura, Sunyaev and Zel'dovich (see e.g. Pozdniakov et al., 1983, and references therein) argued that it is possible to obtain such power-law spectra from a convolution of many non power-law instantaneous spectra evolving in time. This result was recalled and applied to GRBs by Blinnikov et al. (1999) assuming for the instantaneous spectra a thermal shape with a temperature changing with time. They showed that the integration of such energy distributions over the observation time gives a typical power-law shape possibly consistent with GRB spectra.

Our specific quantitative model is more complicated than the one considered by Blinnikov et al. (1999): as pointed out in previous sections, the instantaneous spectrum here is not a black body. Each instantaneous spectrum is obtained by an integration over the corresponding EQTS: it is itself a convolution, weighted by appropriate Lorentz and Doppler factors, of $\sim 10^6$ thermal spectra with variable temperature. Therefore, the time-integrated spectra are not plain convolutions of thermal spectra: they are convolutions of convolutions of thermal spectra (see Fig. C.20).

The simple power-law shape of the integrated spectrum is more evident if we sum tens of instantaneous spectra, as in Fig. C.22. In this case we divided the prompt emission in three different time interval, and for each one we integrated on time the energy distribution. The resulting three time-integrated spectra have a clear non-thermal behavior, and still present the characteristic hard to soft transition.

Finally, we integrated the photon number spectrum $N(E)$ over the whole duration of the prompt event (see again Fig. C.22): in this way we obtain a typical non-thermal power-law spectrum which results to be in good agreement with the INTEGRAL data (see Sazonov et al., 2004a,b) and gives a clear evidence of the possibility that the observed GRBs spectra are originated from a thermal emission.

The precise knowledge we have here acquired on GRB 031203 helps in clarifying the overall astrophysical system GRB 031203 - SN 2003lw - the $2-10$ keV XMM and Chandra data (see sections A.3 and A.5, where the late $2-10$ keV XMM and Chandra data are also discussed).

C.7. Application to GRB 050315

GRB 050315 (Vaughan et al., 2006) has been triggered and located by the BAT instrument (Barthelmy, 2004; Barthelmy et al., 2005a) on board of the *Swift* satellite (Gehrels et al., 2004) at 2005-March-15 20:59:42 UT (Parsons et al., 2005). The narrow field instrument XRT (Burrows et al., 2004, 2005a) began

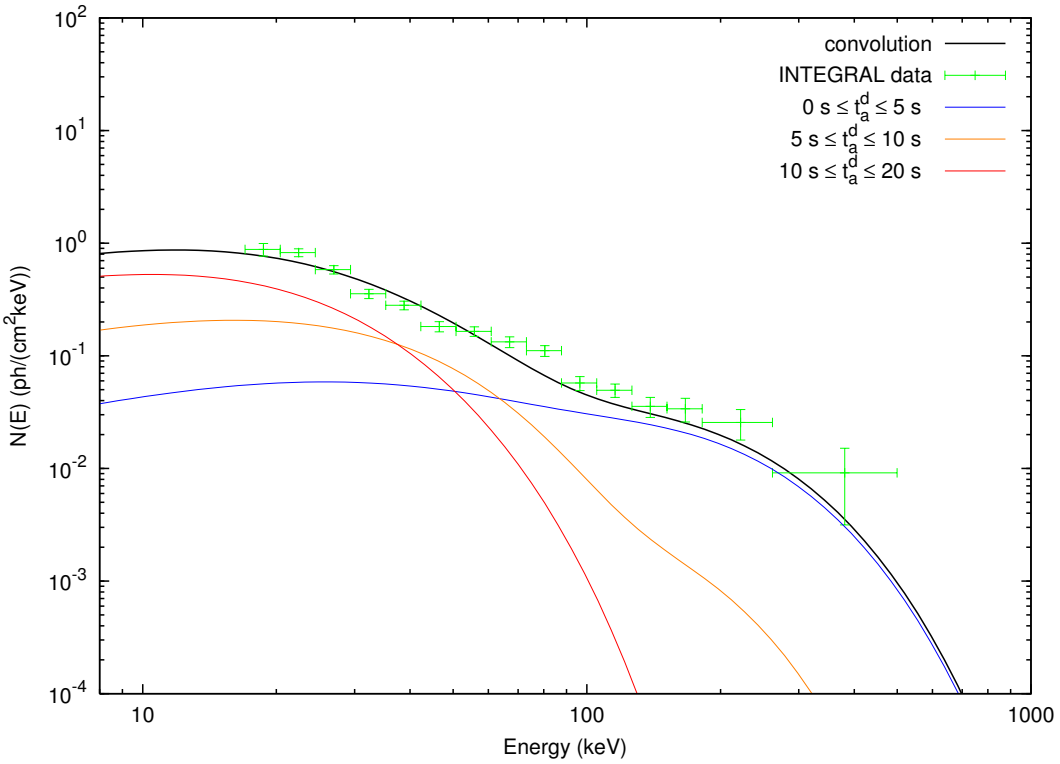

Figure C.22.: Three theoretically predicted time-integrated photon number spectra $N(E)$ are here represented for $0 \leq t_a^d \leq 5$ s, $5 \leq t_a^d \leq 10$ s and $10 \leq t_a^d \leq 20$ s (colored curves). The hard to soft behavior presented in Fig. C.21 is confirmed. Moreover, the theoretically predicted time-integrated photon number spectrum $N(E)$ corresponding to the first 20 s of the "prompt emission" (black bold curve) is compared with the data observed by INTEGRAL (green points, see Sazonov et al., 2004a,b). This curve is obtained as a convolution of 108 instantaneous spectra, which are enough to get a good agreement with the observed data.

observations $\sim$ 80 s after the BAT trigger, one of the earliest XRT observations yet made, and continued to detect the source for $\sim$ 10 days (Vaughan et al., 2006). The spectroscopic redshift has been found to be $z = 1.949$ (Kelson and Berger, 2005).

We present here the results of the fit of the *Swift* data of this source in 5 energy bands in the framework of our theoretical model, pointing out a new step toward the uniqueness of the explanation of the overall GRB structure. We first recall the essential features of our theoretical model; then we fit the GRB 050315 observations by both the BAT and XRT instruments; we also present the instantaneous spectra for selected values of the detector arrival time ranging from 60 s (i.e. during the so called "prompt emission") all the way to 3.0×10^4 s (i.e. the latest afterglow phases).

C.7.1. The fit of the observations

The best fit of the observational data leads to a total energy of the black hole dyadosphere, generating the $e^{\pm}$ plasma, $E^{tot}_{e^{\pm}} = 1.46 \times 10^{53}$ erg (the observational *Swift* E_{iso} is $> 2.62 \times 10^{52}$ erg, see Vaughan et al., 2006), so that the plasma is created between the radii $r_1 = 5.88 \times 10^6$ cm and $r_2 = 1.74 \times 10^8$ cm with an initial temperature $T = 2.05 MeV$ and a total number of pairs $N_{e^+e^-} = 7.93 \times 10^{57}$. The second parameter of the theory, the amount M_B of baryonic matter in the plasma, is found to be such that $B \equiv M_B c^2 / E_{dya} = 4.55 \times 10^{-3}$. The transparency point and the P-GRB emission occurs then with an initial Lorentz gamma factor of the accelerated baryons $\gamma_\circ = 217.81$ at a distance $r = 1.32 \times 10^{14}$ cm from the black hole.

The BAT data

In Fig. C.23 we represent our theoretical fit of the BAT observations in the three energy channels 15–25 keV, 25–50 keV and 50–100 keV and in the whole 15–350 keV energy band.

In our model the GRB emission starts at the transparency point when the P-GRB is emitted; this instant of time is often different from the moment in which the satellite instrument triggers, due to the fact that sometimes the P-GRB is under the instrumental noise threshold or comparable with it. In order to compare our theoretical predictions with the observations, it is important to estimate and take into account this time shift. In the present case of GRB 050315 it has been observed (see Vaughan et al., 2006) a possible precursor before the trigger. Such a precursor is indeed in agreement with our theoretically predicted P-GRB, both in its isotropic energy emitted (which we theoretically predict to be $E_{P-GRB} = 1.98 \times 10^{51}$ erg) and its temporal separation from the peak of the afterglow (which we theoretically predicted to be $\Delta t^d_a = 51$ s). In Fig. C.23a the blue line shows our theoretical prediction for the P-GRB in agreement with the observations.

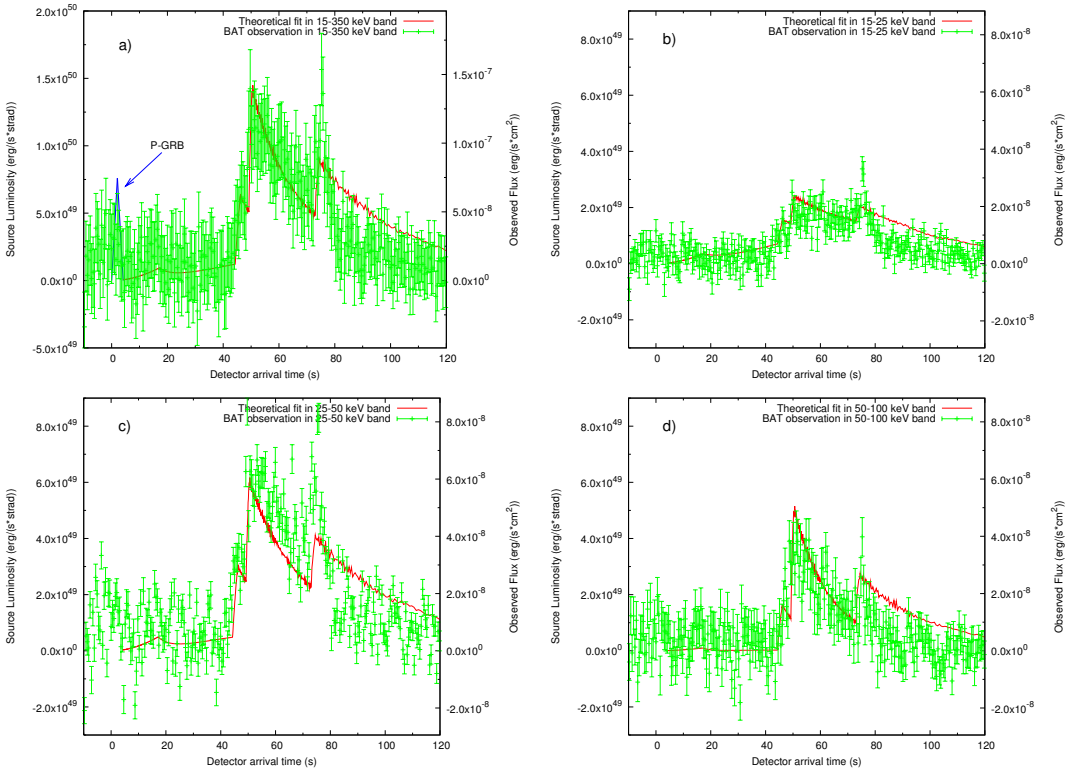

Figure C.23.: Our theoretical fit (red line) of the BAT observations (green points) of GRB 050315 in the 15–350 keV (a), 15–25 keV (b), 25–50 keV (c), 50–100 keV (d) energy bands (Vaughan et al., 2006). The blue line in panel (a) represents our theoretical prediction for the intensity and temporal position of the P-GRB.

After the P-GRB emission, all the observed radiation is produced by the interaction of the expanding baryonic shell with the interstellar medium. In order to reproduce the complex time variability of the light curve of the prompt emission as well as of the afterglow, we describe the CBM filamentary structure, for simplicity, as a sequence of overdense spherical regions separated by much less dense regions. Such overdense regions are nonhomogeneously filled, leading to an effective emitting area A_{eff} determined by the dimensionless parameter $\mathcal{R}$ (see previous sections and Ruffini et al., 2004b, 2005c, for details). Clearly, in order to describe any detailed structure of the time variability an authentic three dimensional representation of the CBM structure would be needed. However, this finer description would not change the substantial agreement of the model with the observational data. Anyway, in the "prompt emission" phase, the small angular size of the source visible area due to the relativistic beaming makes such a spherical approximation an excellent one (see also for details Ruffini et al., 2002).

The structure of the "prompt emission" has been reproduced assuming three overdense spherical CBM regions with width Δ and density contrast $\Delta n/\langle n\rangle$: we chose for the first region, at $r = 4.15 \times 10^{16}$ cm, $\Delta = 1.5 \times 10^{15}$ cm and $\Delta n/\langle n\rangle = 5.17$, for the second region, at $r = 4.53 \times 10^{16}$ cm, $\Delta = 7.0 \times 10^{14}$ cm and $\Delta n/\langle n\rangle = 36.0$ and for the third region, at $r = 5.62 \times 10^{16}$ cm, $\Delta = 5.0 \times 10^{14}$ cm and $\Delta n/\langle n\rangle = 85.4$. The CBM mean density during this phase is $\langle n_{cbm}\rangle = 0.81$ particles/cm^3 and $\langle \mathcal{R}\rangle = 1.4 \times 10^{-7}$. With this choice of the density mask we obtain agreement with the observed light curve, as shown in Fig. C.23. A small discrepancy occurs in coincidence with the last peak: this is due to the fact that at this stage the source visible area due to the relativistic beaming is comparable with the size of the clouds, therefore the spherical shell approximation should be duly modified by a detailed analysis of a full three-dimensional treatment of the CBM filamentary structure. Such a topic is currently under investigation (see also for details Ruffini et al., 2002). Fig. C.23 shows also the theoretical fit of the light curves in the three BAT energy channels in which the GRB has been detected (15–25 keV in Fig. C.23b, 25–50 keV in Fig. C.23c, 50–100 keV in Fig. C.23d).

The XRT data

The same analysis can be applied to explain the features of the XRT light curve in the afterglow phase. It has been recently pointed out (Nousek et al., 2006) that almost all the GRBs observed by *Swift* show a "canonical behavior": an initial very steep decay followed by a shallow decay and finally a steeper decay. In order to explain these features many different approaches have been proposed (Meszaros, 2006; Nousek et al., 2006; Panaitescu et al., 2006; Zhang et al., 2006). In our treatment these behaviors are automatically described by the same mechanism responsible for the prompt emission described above: the baryonic shell expands in an CBM region, between

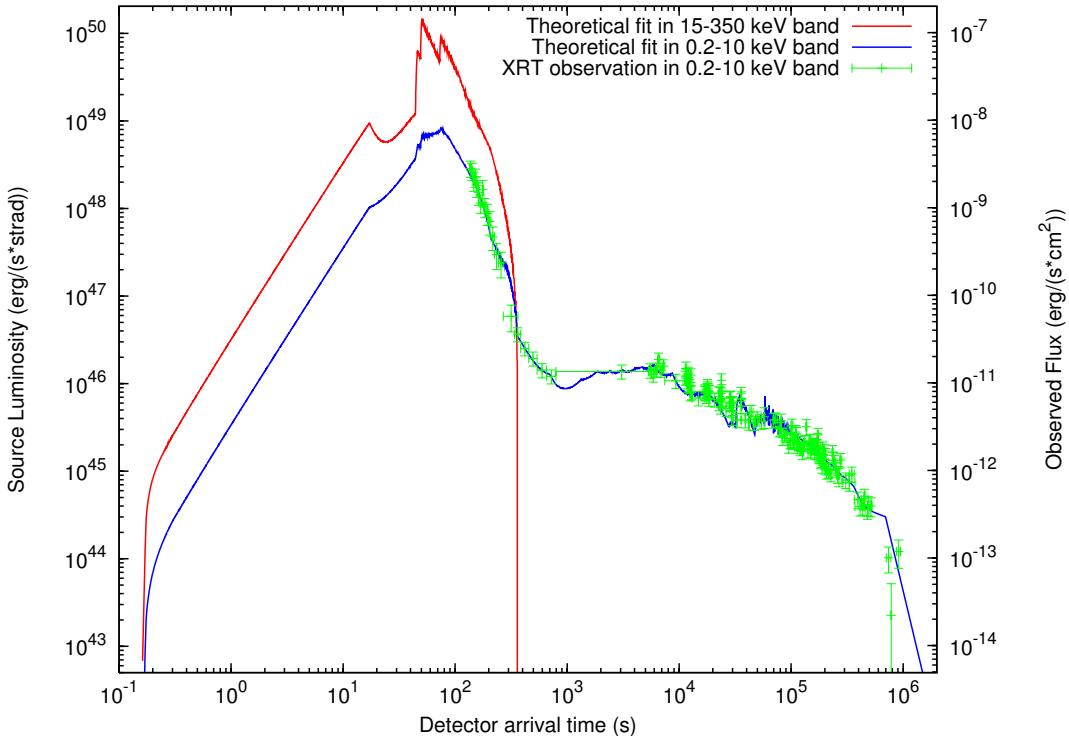

Figure C.24.: Our theoretical fit (blue line) of the XRT observations (green points) of GRB 050315 in the 0.2–10 keV energy band (Vaughan et al., 2006). The theoretical fit of the BAT observations (see Fig. C.23a) in the 15–350 keV energy band is also represented (red line).

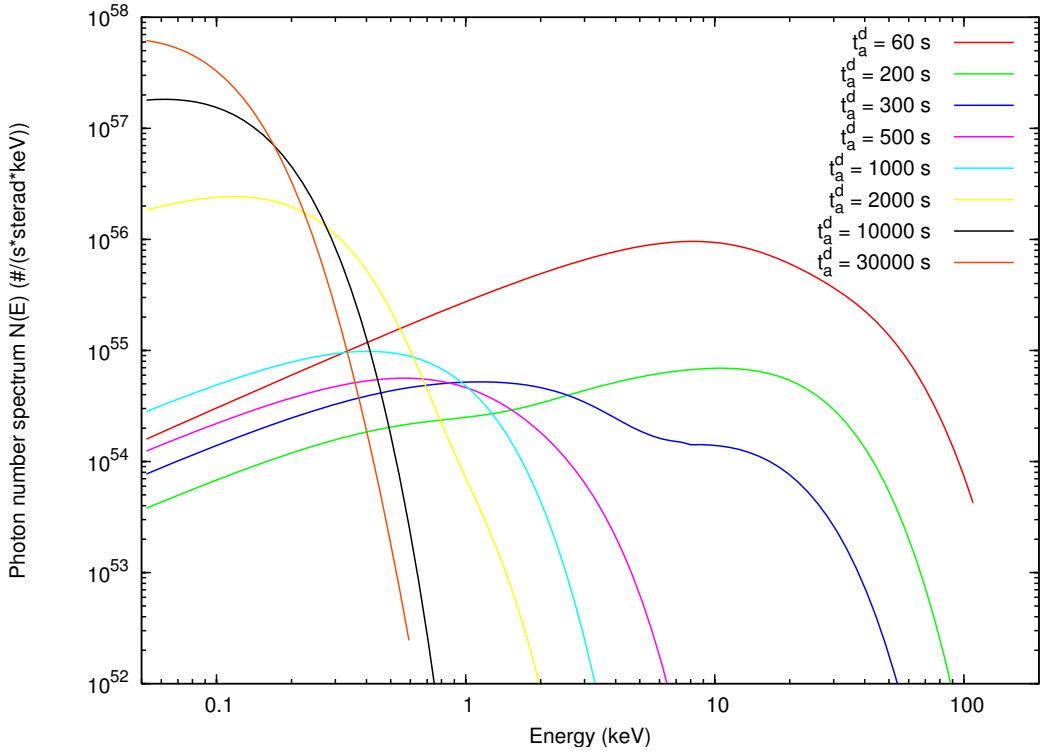

Figure C.25.: Eight theoretically predicted instantaneous photon number spectra $N(E)$ are here represented for different values of the arrival time (colored curves). The hard to soft behavior is confirmed.

$r = 9.00 \times 10^{16}$ cm and $r = 5.50 \times 10^{18}$ cm, which is significantly at lower density ($\langle n_{cbm} \rangle = 4.76 \times 10^{-4}$ particles/cm^3, $\langle \mathcal{R} \rangle = 7.0 \times 10^{-6}$) then the one corresponding to the prompt emission, and this produces a slower decrease of the velocity of the baryons with a consequent longer duration of the afterglow emission. The initial steep decay of the observed flux is due to the smaller number of collisions with the CBM. In Fig. C.24 is represented our theoretical fit of the XRT data, together with the theoretically computed 15–350 keV light curve of Fig. C.23a (without the BAT observational data to not overwhelm the picture too much).

What is impressive is that no different scenarios need to be advocated in order to explain the features of the light curves: both the prompt and the afterglow emission are just due to the thermal radiation in the comoving frame produced by inelastic collisions with the CBM duly boosted by the relativistic transformations over the EQTSs.

C.7.2. The instantaneous spectrum

In addition to the the luminosity in fixed energy bands we can derive also the instantaneous photon number spectrum $N(E)$ starting from the same as-

sumptions. In Fig. C.25 are shown samples of time-resolved spectra for eight different values of the arrival time which cover the whole duration of the event. It is manifest from this picture that, although the spectrum in the comoving frame of the expanding pulse is thermal, the shape of the final spectrum in the laboratory frame is clearly non thermal. In fact, as explained in Ruffini et al. (2004b), each single instantaneous spectrum is the result of an integration of thousands of thermal spectra over the corresponding EQTS. This calculation produces a non thermal instantaneous spectrum in the observer frame (see Fig. C.25).

A distinguishing feature of the GRBs spectra which is also present in these instantaneous spectra is the hard to soft transition during the evolution of the event (Crider et al., 1997; Piran, 1999; Frontera et al., 2000; Ghirlanda et al., 2002). In fact the peak of the energy distribution E_p drifts monotonically to softer frequencies with time. This feature is linked to the change in the power-law low energy spectral index α (Band et al., 1993), so the correlation between α and E_p (Crider et al., 1997) is explicitly shown.

It is important to stress that there is no difference in the nature of the spectrum during the prompt and the afterglow phases: the observed energy distribution changes from hard to soft, with continuity, from the "prompt emission" all the way to the latest phases of the afterglow.

C.7.3. Problems with the definition of "long" GRBs

The confirmation by *Swift* of our prediction of the overall afterglow structure, and especially the coincidence of the "prompt emission" with the peak of the afterglow, opens a new problematic in the definition of the long GRBs. It is clear, in fact, that the identification of the "prompt emission" in the current GRB literature is not at all intrinsic to the phenomenon but is merely due to the threshold of the instruments used in the observations (e.g. BATSE in the 50–300 keV energy range, or BeppoSAX GRBM in 40–700 keV, or *Swift* BAT in 15–350 keV). As it is clear from Fig. C.26, there is no natural way to identify in the source a special extension of the peak of the afterglow that is not the one purely defined by the experimental threshold. It is clear, therefore, that long GRBs, as defined till today, are just the peak of the afterglow and there is no way, as explained above, to define their "prompt emission" duration as a characteristic signature of the source. As the *Swift* observations show, the duration of the long GRBs has to coincide with the duration of the entire afterglow. A Kouveliotou - Tavani plot of the long GRBs, done following our interpretation which is clearly supported by the recent *Swift* data (see Fig. C.26), will present enormous dispersion on the temporal axis.

We recall that in our theory both "short" and "long" GRBs originate from the same process of black hole formation. The major difference between the two is the value of the baryon loading parameter B (see Fig. 3.8). In the limit

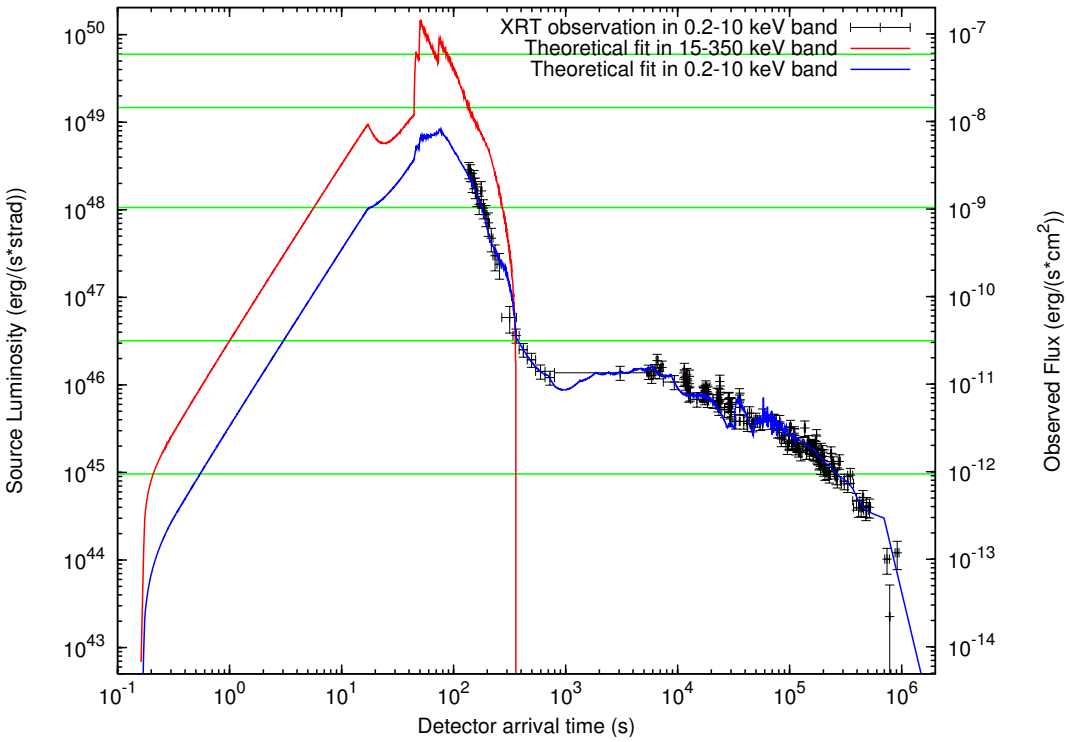

Figure C.26.: Same as Fig. C.24. The horizontal green lines corresponds to different possible instrumental thresholds. It is clear that long GRB durations are just functions of the observational threshold.

of small baryon loading, all the plasma energy is emitted at the transparency in the P-GRB, with negligible afterglow observed flux. For higher values of the baryon loading, the relative energy content of the P-GRB with respect to the afterglow diminishes (see Ruffini et al., 2005a, and references therein).

C.8. Application to GRB 060218

GRB 060218 triggered the BAT instrument of *Swift* on 18 February 2006 at 03:36:02 UT and has a $T_{90} = (2100 \pm 100)$ s (Cusumano et al., 2006). The XRT instrument (Kennea et al., 2006; Cusumano et al., 2006) began observations ~ 153 s after the BAT trigger and continued for ~ 12.3 days (Sakamoto et al., 2006). The source is characterized by a flat γ-ray light curve and a soft spectrum (Barbier et al., 2006). It has an X-ray light curve with a long, slow rise and gradual decline and it is considered an X-Ray Flash (XRF) since its peak energy occurs at $E_p = 4.9^{+0.4}_{-0.3}$ keV (Campana et al., 2006a). It has been observed by the *Chandra* satellite on February 26.78 and March 7.55 UT ($t \simeq 8.8$ and 17.4 days) for 20 and 30 ks respectively (Soderberg et al., 2006b). The spectroscopic redshift has been found to be $z = 0.033$ (Sollerman et al., 2006; Mirabal et al., 2006). The corresponding isotropic equivalent energy is $E_{iso} = (1.9 \pm 0.1) \times 10^{49}$ erg (Sakamoto et al., 2006) which sets this GRB as a low luminous one, consistent with most of the GRBs associated with SNe (Liang et al., 2007; Cobb et al., 2006; Guetta and Della Valle, 2007).

GRB 060218 is associated with SN2006aj whose expansion velocity is $v \sim 0.1c$ (Pian et al., 2006; Fatkhullin et al., 2006; Soderberg et al., 2006a; Cobb et al., 2006). The host galaxy of SN2006aj is a low luminosity, metal poor star forming dwarf galaxy (Ferrero et al., 2007) with an irregular morphology (Wiersema et al., 2007), similar to the ones of other GRBs associated with SNe (Modjaz et al., 2006; Sollerman et al., 2006).

C.8.1. The fit of the observed data

In this section we present the fit of our fireshell model to the observed data (see Figs. C.27, C.30). The fit leads to a total energy of the $e^{\pm}$ plasma $E^{tot}_{e^{\pm}} = 2.32 \times 10^{50}$ erg, with an initial temperature $T = 1.86$ MeV and a total number of pairs $N_{e^{\pm}} = 1.79 \times 10^{55}$. The second parameter of the theory, $B = 1.0 \times 10^{-2}$, is the highest value ever observed and is close to the limit for the stability of the adiabatic optically thick acceleration phase of the fireshell (for further details see Ruffini et al., 2000). The Lorentz gamma factor obtained solving the fireshell equations of motion (Bianco and Ruffini, 2005b,a) is $\gamma_\circ = 99.2$ at the beginning of the afterglow phase at a distance from the progenitor $r_\circ = 7.82 \times 10^{12}$ cm. It is much larger than $\gamma \sim 5$ estimated by Kaneko et al. (2007) and Toma et al. (2007).

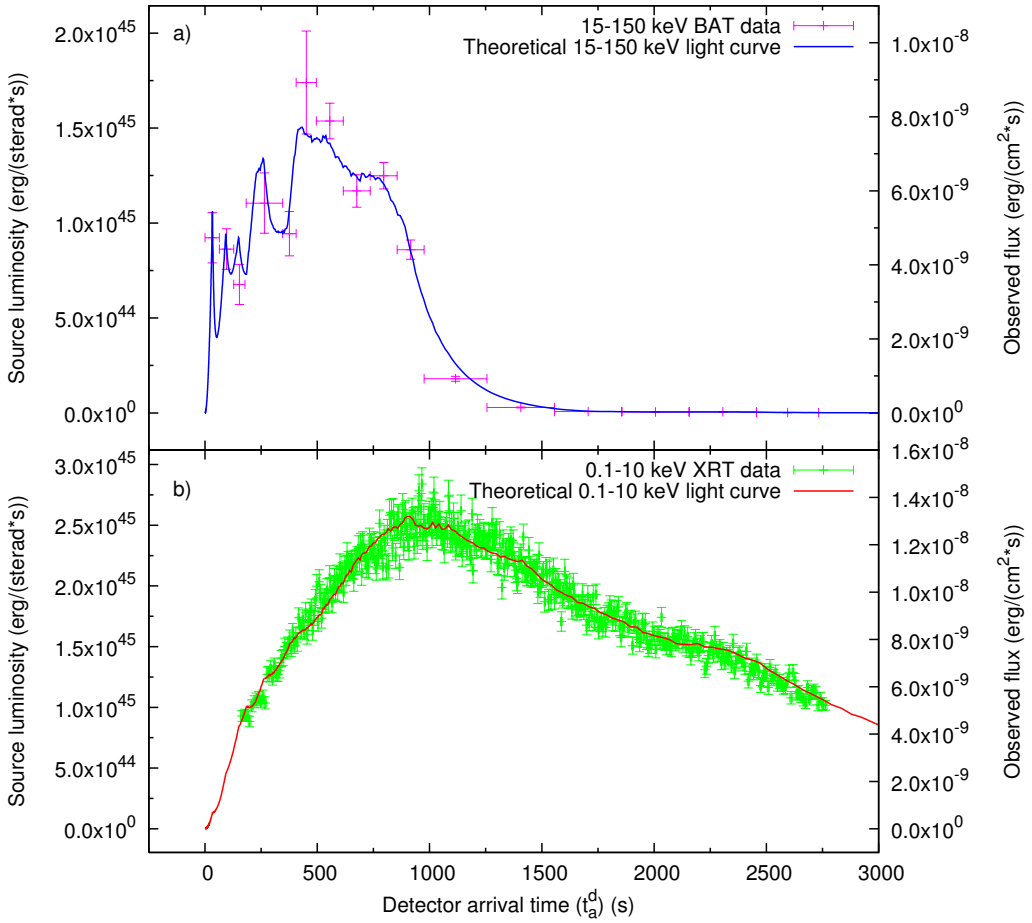

Figure C.27.: GRB 060218 prompt emission: a) our theoretical fit (blue line) of the BAT observations in the 15–150 keV energy band (pink points); b) our theoretical fit (red line) of the XRT observations in the 0.3–10 keV energy band (green points) (Data from: Campana et al., 2006a).

In Fig. C.27 we show the afterglow light curves fitting the prompt emission both in the BAT (15–150 keV) and in the XRT (0.3–10 keV) energy ranges, as expected in our "canonical GRB" scenario (Dainotti et al., 2007). Initially the two luminosities are comparable to each other, but for a detector arrival time $t_a^d > 1000$ s the XRT curves becomes dominant. The displacement between the peaks of these two light curves leads to a theoretically estimated spectral lag greater than 500 s in perfect agreement with the observations (see Liang et al., 2006b). We obtain that the bolometric luminosity in this early part coincides with the sum of the BAT and XRT light curves (see Fig. C.30) and the luminosity in the other energy ranges is negligible.

We recall that at $t_a^d \sim 10^4$ s there is a sudden enhancement in the radio luminosity and there is an optical luminosity dominated by the SN2006aj emission (see Campana et al., 2006a; Soderberg et al., 2006b; Fan et al., 2006). Although our analysis addresses only the BAT and XRT observations, for $r > 10^{18}$ cm corresponding to $t_a^d > 10^4$ s the fit of the XRT data implies two new features: **1)** a sudden increase of the $\mathcal{R}$ factor from $\mathcal{R} = 1.0 \times 10^{-11}$ to $\mathcal{R} = 1.6 \times 10^{-6}$, corresponding to a significantly more homogeneous effective CBM distribution (see Fig.C.31b); **2)** an XRT luminosity much smaller than the bolometric one (see Fig. C.30). These theoretical predictions may account for the energetics of the enhancement of the radio and possibly optical and UV luminosities. Therefore, we identify two different regimes in the afterglow, one for $t_a^d < 10^4$ s and the other for $t_a^d > 10^4$ s. Nevertheless, there is a unifying feature: the determined effective CBM density decreases with the distance r monotonically and continuously through both these two regimes from $n_{cbm} = 1$ particle/cm^3 at $r = r_\circ$ to $n_{cbm} = 10^{-6}$ particle/cm^3 at $r = 6.0 \times 10^{18}$ cm: $n_{cbm} \propto r^{-\alpha}$, with $1.0 \lesssim \alpha \lesssim 1.7$ (see Fig. C.31a).

Our assumption of spherical symmetry is supported by the observations which set for GRB 060218 an opening beaming angle larger than $\sim 37^\circ$ (Liang et al., 2007; Campana et al., 2006a; Soderberg et al., 2006b; Guetta and Della Valle, 2007).

C.8.2. The procedure of the fit

The arrival time of each photon at the detector depends on the entire previous history of the fireshell (Ruffini et al., 2001c). Moreover, all the observables depends on the EQTS (Bianco and Ruffini, 2004, 2005b) which, in turn, depend crucially on the equations of motion of the fireshell. The CBM engulfment has to be computed self-consistently through the entire dynamical evolution of the fireshell and not separately at each point. Any change in the CBM distribution strongly influences the entire dynamical evolution of the fireshell and, due to the EQTS structure, produces observable effects up to a much later time. For example if we change the density mask at a certain distance from the black hole we modify the shape of the lightcurve and con-

sequently the evolution changes at larger radii corresponding to later times. Anyway the change of the density is not the only problem to face in the fitting of the source, in fact first of all we have to choose the energy in order to have Lorentz gamma factor sufficiently high to fit the entire GRB. In order to show the sensitivity of the fitting procedure I also present two examples of fits with the same value of B and different value of $E^{tot}_{e^\pm}$.

The first example has an $E^{tot}_{e^\pm} = 1.36 \times 10^{50}$ erg . This fit resulted unsuccessfully as we see from the Fig.C.28, because the bolometric lightcurve is under the XRT peak of the afterglow. This means that the value of the energy chosen is too small to fit any data points after the peak of the afterglow. So we have to increase the value of the Energy to a have a better fit. In fact the parameters values have been found with various attempt in order to obtain the best fit.

The second example is characterized by $E^{tot}_{e^\pm} = 1.61 \times 10^{50}$ erg and the all the data are fitted except for the last point from 2.0×10^2s to the end (see Fig. C.29). I attempt to fit these last points trying to diminuishes the R values in order to enhance the energy emission, but again the low value of the Lorentz gamma factor, that in this case is 3 prevent the fireshell to expand. So again in this case the value of the Energy chosen is too small, but it is better than the previous attempt. In this case we increased the energy value of the 24%, but it is not enough so we decide to increase 16%.

So the final fit is characterized by the $B = 1.0 \times 10^{-2}$ and by the $E^{tot}_{e^\pm} = 2.32 \times 10^{50}$ erg. With this value of the energy we are able to fit all the experimental points.

C.8.3. The fireshell fragmentation

GRB 060218 presents different peculiarities: the extremely long T_{90}, the very low effective CBM density decreasing with the distance and the largest possible value of $B = 10^{-2}$. These peculiarities appear to be correlated. Following Ruffini et al. (2007b), we propose that in the present case the fireshell is fragmented. This implies that the surface of the fireshell does not increase any longer as r^2 but as r^β with $\beta < 2$. Consequently, the effective CBM density n_{cbm} is linked to the actual one n^{act}_{cbm} by:

$$n_{cbm} = \mathcal{R}_{shell} n^{act}_{cbm}, \quad \text{with} \quad \mathcal{R}_{shell} \equiv (r^\star/r)^\alpha , \tag{C.8.1}$$

where $r^\star$ is the starting radius at which the fragmentation occurs and $\alpha = 2 - \beta$ (see Fig. C.31a). For $r^\star = r_\circ$ we have $n^{act}_{cbm} = 1$ particles/cm^3, as expected for a "canonical GRB" (Ruffini et al., 2007a) and in agreement with the apparent absence of a massive stellar wind in the CBM (Soderberg et al., 2006b; Fan et al., 2006; Li, 2007).

The $\mathcal{R}$ parameter defined in Eq.(C.8.2) has to take into account both the effect of the fireshell fragmentation ($\mathcal{R}_{shell}$) and of the effective CBM porosity

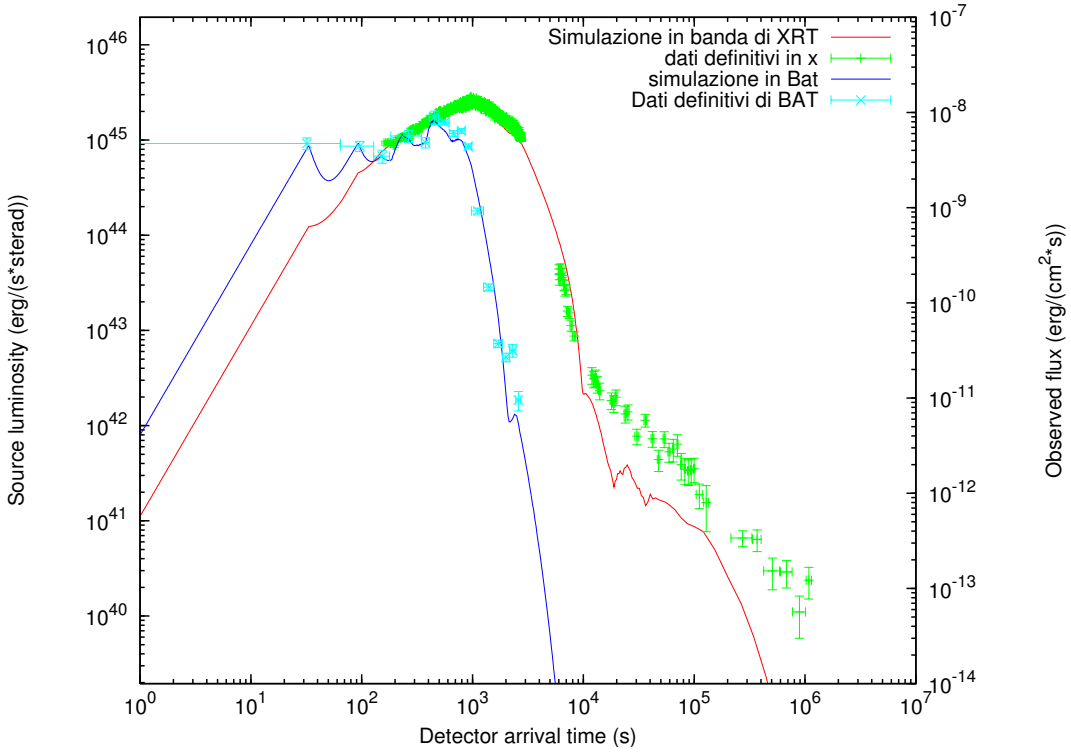

Figure C.28.: GRB 060218 light curves with $E^{tot}_{e^{\pm}} = 1.36 \times 10^{50}$ erg: our theoretical fit (blue line) of the 15–150 keV BAT observations (pink points), our theoretical fit (red line) of the 0.3–10 keV XRT observations (green points) and the 0.3–10 keV *Chandra* observations (black points) are represented together with our theoretically computed bolometric luminosity (black line) (Data from: Campana et al. (2006a); Soderberg et al. (2006b)).

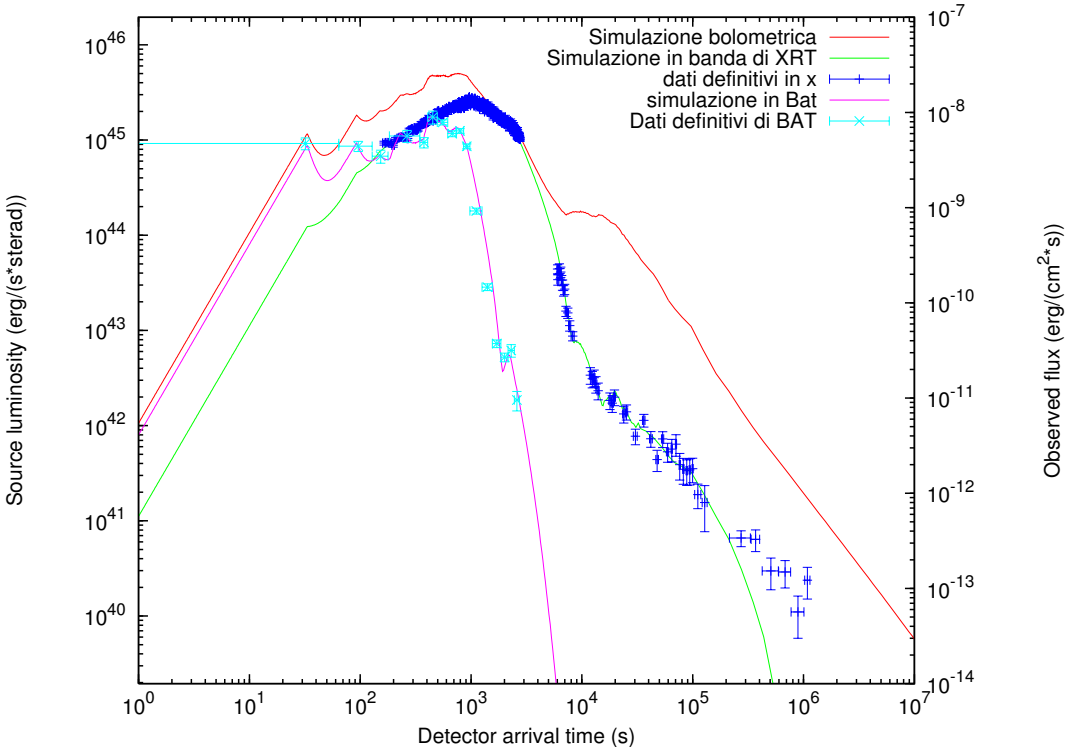

Figure C.29.: GRB 060218 light curves with $E^{tot}_{e^{\pm}} = 1.61 \times 10^{50}$ erg: our theoretical fit (blue line) of the 15–150 keV BAT observations (pink points), our theoretical fit (red line) of the 0.3–10 keV XRT observations (green points) and the 0.3–10 keV *Chandra* observations (black points) are represented together with our theoretically computed bolometric luminosity (black line). Data from: Campana et al. (2006a); Soderberg et al. (2006b).

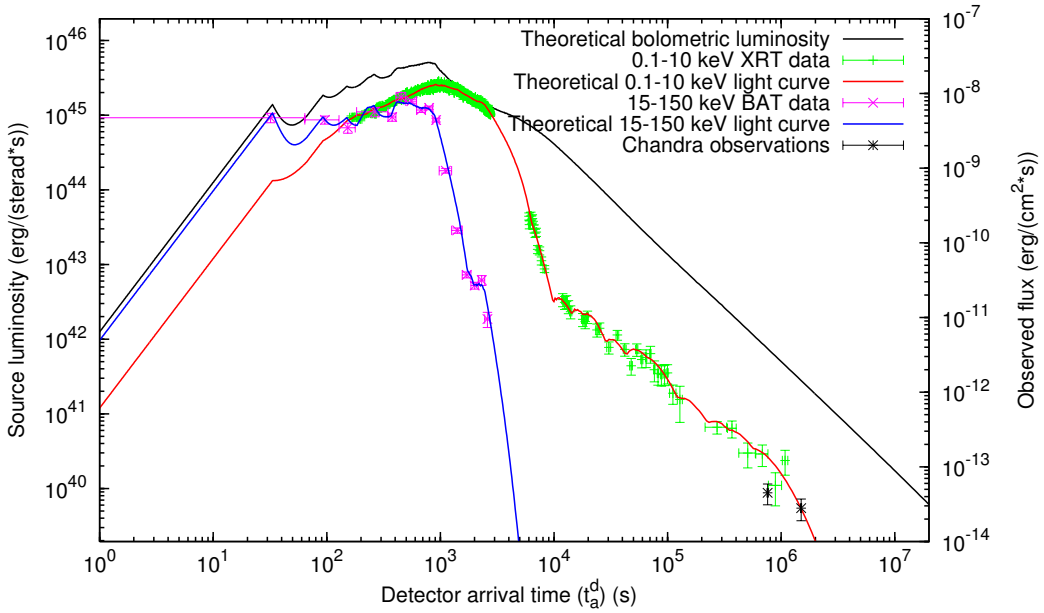

Figure C.30.: GRB 060218 complete light curves: our theoretical fit (blue line) of the 15–150 keV BAT observations (pink points), our theoretical fit (red line) of the 0.3–10 keV XRT observations (green points) and the 0.3–10 keV *Chandra* observations (black points) are represented together with our theoretically computed bolometric luminosity (black line) (Data from: Campana et al., 2006a; Soderberg et al., 2006b).

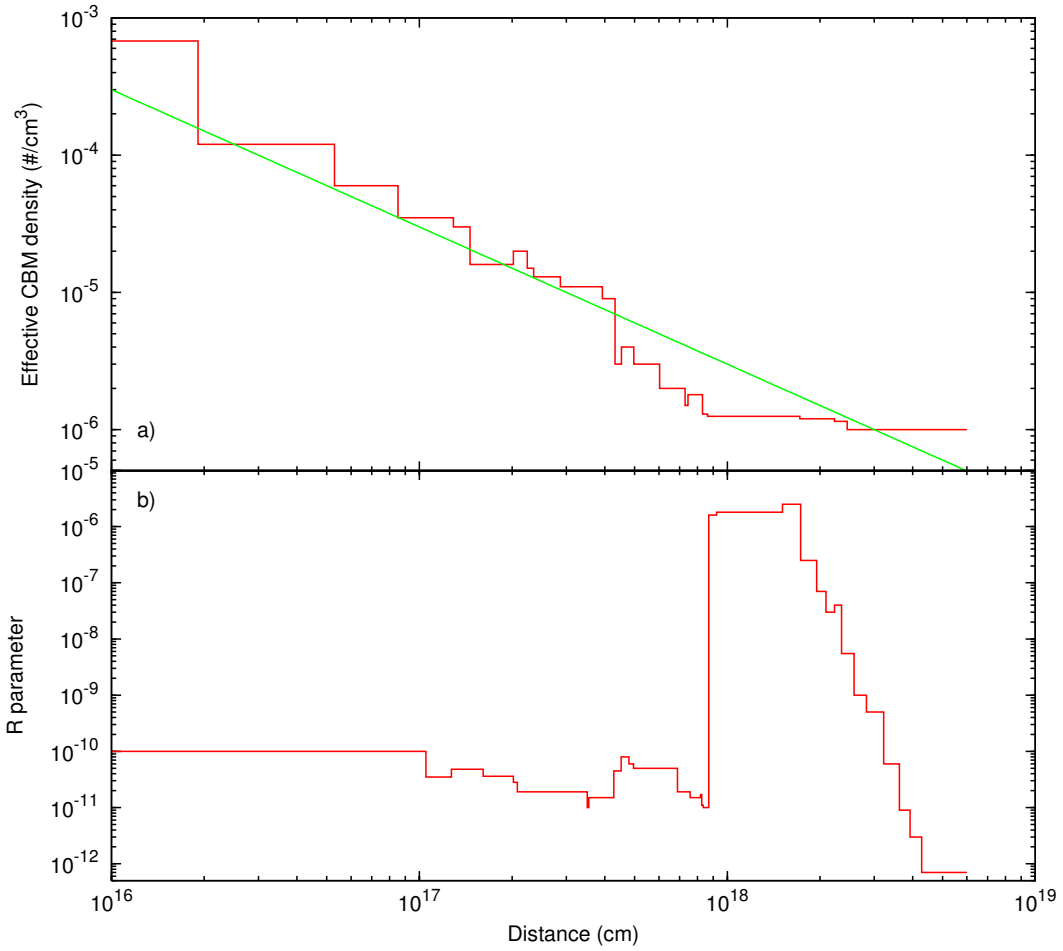

Figure C.31.: The CBM distribution parameters: a) the effective CBM number density (red line) monotonically decreases with the distance r following Eq.(C.8.1) (green line); b) the $\mathcal{R}$ parameter vs. distance.

($\mathcal{R}_{cbm}$):

$$\mathcal{R} \equiv \mathcal{R}_{shell} \times \mathcal{R}_{cbm} \,. \tag{C.8.2}$$

The phenomenon of the clumpiness of the ejecta, whose measure is the filling factor, is an aspect well known in astrophysics. For example, in the case of Novae the filling factor has been measured to be in the range 10^{-2}–10^{-5} (Ederoclite et al., 2006). Such a filling factor coincides, in our case, with $\mathcal{R}_{shell}$.

C.8.4. Binaries as progenitors of GRB-SN systems

The majority of the existing models in the literature appeal to a single astrophysical phenomenon to explain both the GRB and the SN ("collapsar", see e.g. Woosley and Bloom, 2006). On the contrary, a distinguishing feature of our theoretical approach is to differentiate between the SN and the GRB process. The GRB is assumed to occur during the formation process of a black hole. The SN is assumed to lead to the formation of a neutron star (NS) or to a complete disruptive explosion without remnants and, in no way, to the formation of a black hole. In the case of SN2006aj the formation of such a NS has been actually inferred by Maeda et al. (2007) because of the large amount of ^{58}Ni ($0.05 M_\odot$). Moreover the significantly small initial mass of the SN progenitor star $M \approx 20 M_\odot$ is expected to form a NS rather than a black hole when its core collapses (Maeda et al., 2007; Ferrero et al., 2007; Mazzali et al., 2006; Nomoto et al., 2007). In order to fulfill both the above requirement, we assume that the progenitor of the GRB and the SN consists of a binary system formed by a NS close to its critical mass collapsing to a black hole, and a companion star evolved out of the main sequence originating the SN. The temporal coincidence between the GRB and the SN phenomenon is explained in term of the concept of "induced" gravitational collapse (Ruffini et al., 2001a, 2007b). There is also the distinct possibility of observing the young born NS out of the SN (see e.g. Ruffini et al., 2007b, and references therein).

It has been often proposed that GRBs associated with SNe Ib/c, at smaller redshift $0.0085 < z < 0.168$ (see e.g. Della Valle, 2006, and references therein), form a different class, less luminous and possibly much more numerous than the high luminosity GRBs at higher redshift (Pian et al., 2006; Soderberg et al., 2004; Maeda et al., 2007; Della Valle, 2006). Therefore they have been proposed to originate from a separate class of progenitors (Liang et al., 2007; Cobb et al., 2006). In our model this is explained by the nature of the progenitor system leading to the formation of the black hole with the smallest possible mass: the one formed by the collapse of a just overcritical NS (Ruffini et al., 2008b, 2007b).

The recent observation of GRB 060614 at $z = 0.125$ without an associated SN (Della Valle et al., 2006; Mangano et al., 2007) gives strong support to our scenario, alternative to the collapsar model. Also in this case the progenitor

of the GRB appears to be a binary system composed of two NSs or a NS and a white dwarf.

C.8.5. Conclusions

GRB 060218 presents a variety of peculiarities, including its extremely large T_{90} and its classification as an XRF. Nevertheless, a crucial point of our analysis is that we have successfully applied to this source our "canonical GRB" scenario.

Within our model there is no need for inserting GRB 060218 in a new class of GRBs, such as the XRFs, alternative to the "canonical" ones. This same point recently received strong observational support in the case of GRB 060218 (Liang et al., 2006b) and a consensus by other models in the literature (Kaneko et al., 2007).

The anomalously long T_{90} led us to infer a monotonic decrease in the CBM effective density giving the first clear evidence for a fragmentation in the fireshell. This phenomenon appears to be essential in understanding the features of also other GRBs (see e.g. GRB 050315 in Ruffini et al., 2007b; Bernardini et al., 2007).

Our "canonical GRB" scenario originates from the gravitational collapse to a black hole and is now confirmed over a 10^6 range in energy (see e.g. Ruffini et al., 2007a, and references therein). It is clear that, although the process of gravitational collapse is unique, there is a large variety of progenitors which may lead to the formation of black holes, each one with precise signatures in the energetics. The low energetics of the class of GRBs associated with SNe, and the necessity of the occurrence of the SN, naturally leads in our model to identify their progenitors with the formation of the smallest possible black hole originating from a NS overcoming his critical mass in a binary system. For GRB 060218 there is no need within our model for a new or unidentified source such as a magnetar or a collapsar.

GRB 060218 is the first GRB associated with SN with complete coverage of data from the onset all the way up to $\sim 10^6$ s. This fact offers an unprecedented opportunity to verify theoretical models on such a GRB class. For example, GRB 060218 fulfills the Amati et al. (2002) relation unlike other sources in its same class. **This is particularly significant, since GRB 060218 is the only source in such a class to have an excellent data coverage without gaps. We are currently examining if the missing data in the other sources of such a class may have a prominent role in their non-fulfillment of the Amati et al. (2002) relation (Dainotti et al., in preparation; see also Ghisellini et al., 2006).**

C.9. Application to GRB 060607A: prompt emission, X-ray flares and late afterglow phase.

GRB060607A is a very distant ($z = 3.082$, Ledoux et al., 2006) and energetic event ($E_{iso} \sim 10^{53}$ erg, Molinari et al., 2007). Its BAT light curve shows a double-peaked structure with a duration of $T_{90} = (100 \pm 5)$ s (Tueller et al., 2006). The time-integrated spectrum over the T_{90} is best fit with a simple power-law model with an index $\Gamma = 1.45 \pm 0.08$ (Guidorzi, private communication). The XRT light curve shows a prominent flaring activity (at least two flares) superimposed to the normal afterglow decay (Page et al., 2006a).

GRB060607A main peculiarity is that the peak of the near-infrared (NIR) afterglow has been observed with the REM robotic telescope (Molinari et al., 2007). Interpreting the NIR light curve as corresponding to the afterglow onset as predicted by the fireball forward shock model (Sari and Piran, 1999; Meszaros, 2006), it is possible to infer the initial Lorentz gamma factor of the emitting system that results to be $\Gamma_\circ \sim 400$ (Molinari et al., 2007; Covino et al., 2008; Jin and Fan, 2007). Moreover, these measurements seem to be consistent with an interstellar medium environment within the standard fireball scenario, ruling out the wind-like medium predicted by the Collapsar model (Molinari et al., 2007; Jin and Fan, 2007).

We analyze GRB060607A within the fireshell model (Ruffini et al., 2001c,b, 2007a). We deal only with the BAT and XRT observations, that are the basic contribution to the extended afterglow emission up to a distance from the progenitor $r \sim 4 \times 10^{17}$ cm. Such observations are usually neglected in the treatments adopted in current literature to characterize the fireball dynamics (Molinari et al., 2007; Sari and Piran, 1999). The complete numerical modeling of the fireshell dynamics (see e.g. Ruffini et al., 2007a), from the creation of the initial plasma up to the interaction of the optically thin fireshell with the surrounding medium, allows to calculate all its characteristic quantities. In particular, the exact value of the Lorentz gamma factor of the fireshell at the transparency can be therefore calculated ($\gamma_\circ = 328$) once we fix the two free parameter from the gamma and X-ray light curves analysis.

According to the "canonical GRB" scenario (Ruffini et al., 2001b, 2007a) we interpret the whole prompt emission as the joint contribution of both the Proper-GRB (P-GRB), emitted at the fireshell transparency, and the peak of the extended afterglow, which follows the P-GRB emission. While the variability of the P-GRB is linked to the collapse mechanism of the progenitor (Caito et al., 2009), the observed temporal variability of the peak of the extended afterglow is shown to be produced by the interaction of the fireshell with CircumBurst Medium (CBM) clumps with density contrast $\delta n/n \sim 2$. The corresponding theoretical light curves obtained are in good agreement with the observations in all the *Swift* BAT energy bands.

We analyze the GRB060607A prompt emission time-integrated spectrum. The fireshell model postulates that the GRB spectrum is thermal in the comoving frame, and that the non-thermal power-law observed spectrum can be recovered by integrating over the EQuiTemporal Surfaces (EQTS, see Bianco and Ruffini, 2004, 2005b) and the observation time. The assumption of a pure thermal spectrum in the comoving frame has been chosen for simplicity as an *ansatz* on general thermal emission processes expected in high energy collisions. It can be subject to improvements when data on instantaneous spectra are available (Patricelli et al., in preparation). Indeed the resulting time-integrated spectrum is compatible with the one observed by BAT in different time intervals covering the whole prompt emission, despite a small discrepancy at low energy.

We turn to the analysis of the X-ray flares observed by *Swift* XRT in the early part of the decaying phase of the X-ray afterglow (Page et al., 2006a). According to the fireshell model these flares have the same nature than the peaks observed in the prompt emission, namely they are produced by the interaction of the fireshell with different CBM clumps. This idea is consistent with the correlation between the late peaks in the gamma-ray light curve and the X-ray flares when they are observed simultaneously (Molinari et al., 2007; Ziaeepour et al., 2008). What is peculiar in the late afterglow phases is that the typical dimensions of the clumps become smaller than the visible area of the fireshell. Under this condition, a three dimensional description would be necessary to substitute the assumption of spherical symmetry and to take into due account the structure of the clumps. We propose here a simplified bi-dimensional model for the CBM clump along the line of sight, the emission being limited to a small fraction of the entire EQTS. We show that even with this simplified model it is possible to fully explain flares with $\Delta t/t$ compatible with the observations.

The NIR emission shows no significant evidence for correlation with the prompt emission (Ziaeepour et al., 2008): while the common gamma and X-ray flares light curves appear to be very close and correlate (Ziaeepour et al., 2008), in the NIR band the flaring activity, if any, is much weaker (Molinari et al., 2007). On the contrary, when both the NIR and X-ray light curve are decaying regularly, these curves appear to be correlated (Molinari et al., 2007). We propose a possible scenario in which this second decaying phase arises from the injection of slower material into the fireshell. This leads to a collision which is assumed to be responsible for the X-ray plateau, producing a modification in the comoving thermal spectrum, as well as in the equations of the dynamics of the afterglow. This phase characterized by high level of instabilities may account for both the observed X-ray and NIR emission.

C.9.1. GRB060607A prompt emission light curve

It is commonly believed that the observed temporal variability of the prompt emission and the X-ray flares are related to the activity of a "central engine" and originate from internal rather than external shocks (Sari and Piran, 1995; Daigne and Mochkovitch, 1998; Fenimore et al., 1999; Panaitescu and Mészáros, 1999; Liang et al., 2006a; Chincarini et al., 2007a). This interpretation claims that it can account for both the duration ($\delta t/t \ll 1$) and the observed spectral properties of such a variability (Norris et al., 1996; Chincarini et al., 2007a; Falcone et al., 2007b). Indeed the internal shock model reveals some problems in the radiation mechanisms assumed for the gamma-ray emission: recently it has been pointed out that the synchrotron mechanisms apply successfully only for the late afterglow (Kumar and McMahon, 2008) and the inverse Compton scattering suffers of "energy crisis" (Piran et al., 2009).

Unlike treatments in the current literature, we recall that within the fireshell model the prompt emission consists of two sharply different components: the P-GRB and the peak of the extended afterglow (Ruffini et al., 2001b, 2007a). The variability of the P-GRB is linked to the collapse mechanism of the progenitor (Caito et al., 2009), while the observed temporal variability of the peak of the extended afterglow is described by the interaction of the fireshell with different CBM clumps (Ruffini et al., 2002).

We identify the whole prompt emission with the peak of the extended afterglow emission, and the remaining part of the light curve with the decaying tail of the afterglow, according to our "canonical GRB" scenario (Ruffini et al., 2001b, 2007a). The temporal variability of the light curve has been reproduced assuming spherical CBM regions with different densities (Ruffini et al., 2002). The structure of the CBM adopted is presented in Fig. C.33. This distribution of the CBM is just an approximation of the real one, where the CBM density shows some smooth fluctuations around its trend during the fireshell evolution. Nevertheless it is representative of the global properties of the medium and it is sufficient to account for the observed variability in the luminosity. The decreasing trend of the CBM density up to very low values (see Fig. C.33) is not real but it is probably the result of the fragmentation occurring in the fireshell, as already proposed by Dainotti et al. (2007): $n_{cbm} = n^{\circ}_{cbm}\,(r^*/r)^{\alpha}$, with in this case $\alpha \sim -2.5$. The adopted density contrast with respect to the real CBM density n°_{cbm} is $\delta n/n \sim 2$ or less (see Fig. C.32).

For the two parameters characterizing the initial dynamics of the fireshell we adopt $E^{e^{\pm}}_{tot} = 2.5 \times 10^{53}$ erg and $B = 3.0 \times 10^{-3}$. This choice is motivated by the requirement that the total energy of the system should account for the GRB isotropic emission up to the latest phase of the afterglow ($E_{iso} = 1.1 \times 10^{53}$ erg, Tueller et al., 2006). The baryonic content of the fireshell (B) determines how much kinetic energy should be dissipated during the afterglow that, we recall, in the fireshell model encompasses the prompt emis-

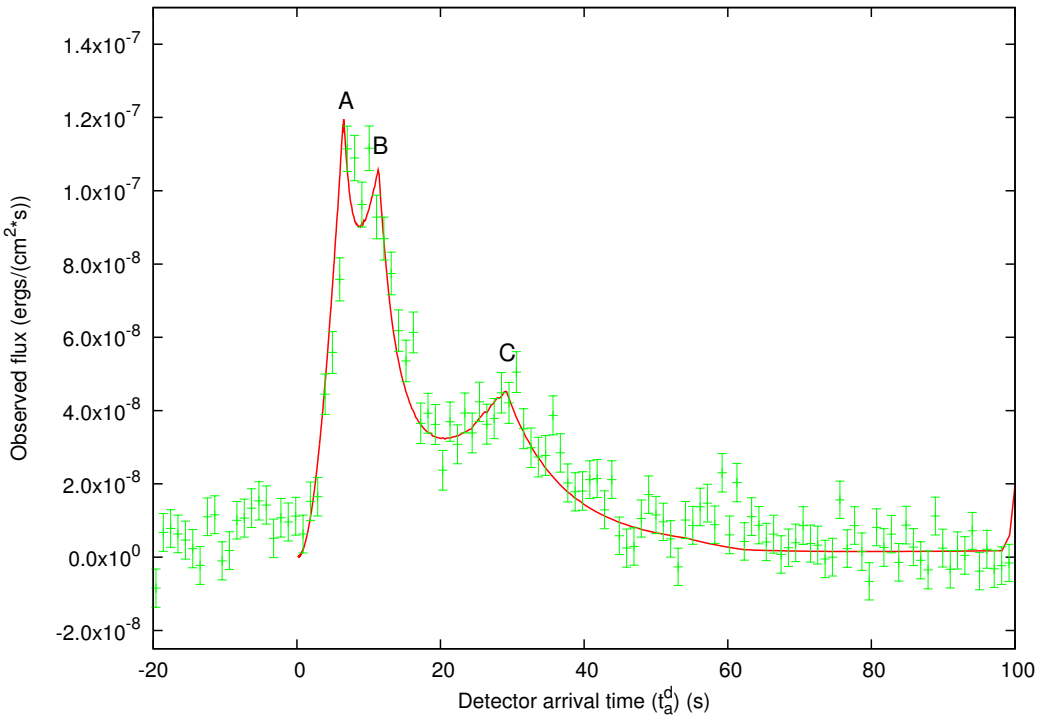

Figure C.32.: *Swift* BAT 15–150 keV light curve (green points) compared with the theoretical one (red line). The labels A, B, C identifies the three major peaks.

sion as well. Then, it is involved in the determination of the total energy emitted in the P-GRB and in the afterglow, in the determination of the overall duration of the phenomenon and in the occurrence of the peak of the afterglow emission (see Sec. 6). The baryon loading adopted for this GRB is fixed by the requirement that the P-GRB is under the BAT threshold: the total isotropic energy emitted in the P-GRB is expected to be $E^{iso}_{P-GRB} = 1.9\%\, E^{e^\pm}_{tot} = 4.7 \times 10^{51}$ erg, hence it is below the BAT threshold if we assume an observed duration $\Delta t_{p-grb} \gtrsim 10$ s. Therefore this is the minimum B acceptable. Larger values of B would result in an afterglow peak emission with a much slower rise time than the observed one. In Fig. C.32 we present a simulation of the light curve of GRB060607A in the *Swift* BAT (15–150 keV) energy band obtained with this choice of the parameters.

The initial conditions adopted for the optically thick fireshell ($E^{e^\pm}_{tot}$ and B) estimated from the simultaneous analysis of the BAT and XRT light curves imply an initial number of $e^\pm$ pairs $N_{e^\pm} = 2.6 \times 10^{58}$ and an initial temperature $T = 1.7$ MeV. After the transparency point at $r_\circ = 1.4 \times 10^{14}$ cm from the progenitor, the initial Lorentz gamma factor of the fireshell is $\gamma_\circ = 328$. This value confirms that the fireshell is highly relativistic, as expected to avoid the "compactness problem" (Piran, 2005). The Lorentz factor at the transparency $\gamma_\circ$ is an exact value calculated by solving numerically the equation of motion of the fireshell. In particular this is the maximum value of $\gamma_\circ$ since it has been obtained with the minimum baryon loading acceptable for this GRB (see sec. 6 and e.g. Ruffini et al., 2008a). The value of 400 that has been claimed in the literature within the fireball forward shock model (Molinari et al., 2007; Covino et al., 2008; Jin and Fan, 2007) cannot be reached by the fireshell, otherwise the P-GRB would be visible.

C.9.2. GRB spectrum

We turn now to the analysis of the GRB060607A prompt emission time-integrated spectrum. As discussed in previous works (Ruffini et al., 2004b, 2005c; Bernardini et al., 2005a), the fireshell model postulates that:

- the resulting radiation as viewed in the comoving frame has a thermal spectrum
- the CBM swept up by the front of the optically thin fireshell is responsible for this thermal emission.

In our case the radiation is produced in the inelastic collision between the accelerated baryons and the CBM. The structure of the collision is determined by mass, momentum and energy conservation, i.e. by the constancy of the specific enthalpy, which are standard conditions in the expanding matter rest frame (Zeldovich and Raizer, 1966). The only additional free parameter to

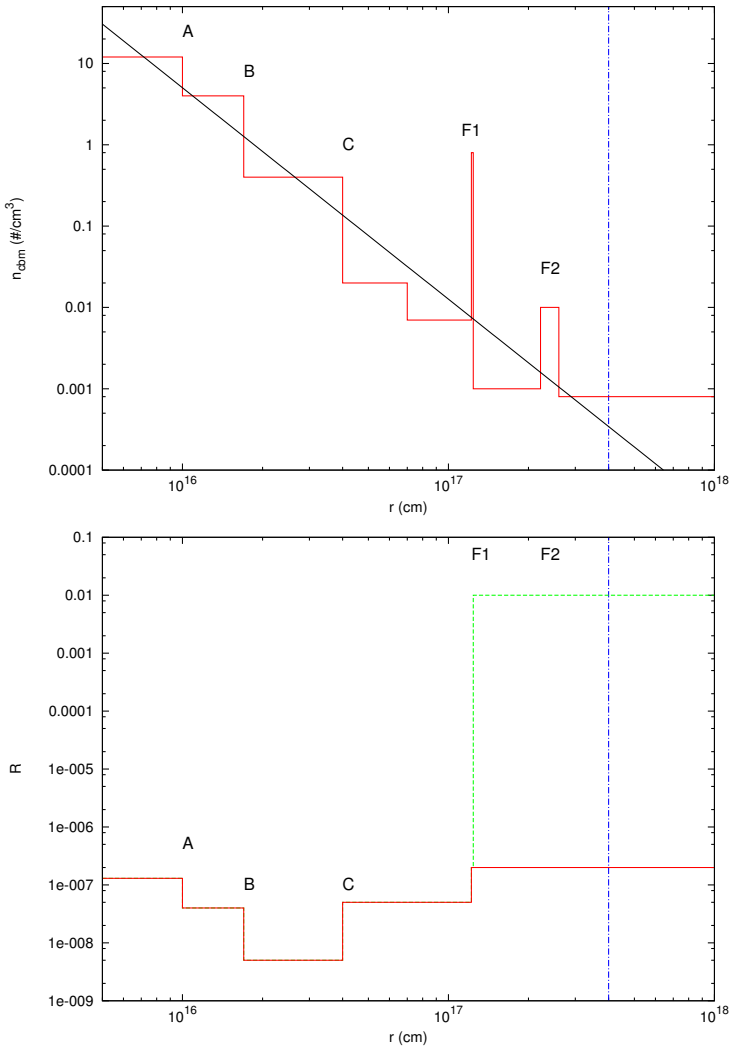

Figure C.33.: Structure of the CBM adopted: effective particle number density n_{cbm} (upper panel) and fraction of effective emitting area $\mathcal{R}$ (lower panel) versus distance from the progenitor. The labels A, B, C indicate the values corresponding to the peaks in the BAT light curve (see Fig. C.32). The black solid line represents the decreasing trend of the CBM density that probably reflects a fragmentation in the fireshell. The two X-ray flares, indicated by the labels F1, F2, corresponds in the upper panel to the huge increase in the CBM density that departs from the roughly power-law decrease observed. In the lower panel, the X-ray flares produce an increase of the emitting area which is not real but due to the lack of a complete three-dimensional treatment of the interaction between the fireshell and the CBM (green dashed line). In fact if we adopt a bi-dimensional structure for the CBM clumps responsible for the flares we obtain a constant value (red solid line, see Sec. C.9.3). The blue vertical dashed-dotted line sets the limit of our analysis (for details see Sec. C.9.4).

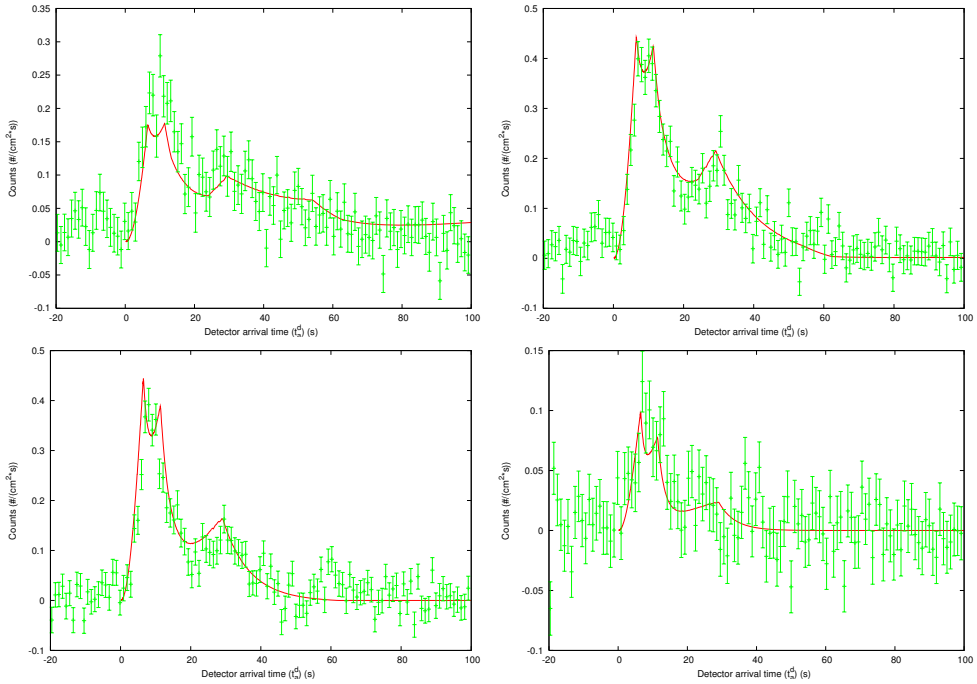

Figure C.34.: *Swift* BAT (15–25 keV, 25–50 keV, 50–100 keV, 100–150 keV) light curves (green points) compared with the theoretical ones (red lines).

model this emission process is the size of the "effective emitting area" of the fireshell: A_{eff}.

The power emitted in the interaction of the fireshell with the CBM measured in the comoving frame is:

$$\frac{dE_{\rm int}}{dt} = 4\pi r^2 \mathcal{R} \sigma T^4 \,, \tag{C.9.1}$$

where $dE_{\rm int}$ is the internal energy developed in the collision, T is the black body temperature, σ is the Stefan-Boltzmann constant and

$$\mathcal{R} = \frac{A_{eff}}{A_{tot}} \tag{C.9.2}$$

is the "surface filling factor" which accounts for the fraction of the shell surface becoming active, being the ratio between the "effective emitting area" and the total area A_{tot}. The ratio $\mathcal{R}$ is a priori a function that varies as the system evolves so it is evaluated at every given value of the radius r (for the variability of $\mathcal{R}$ in the case of GRB060607A see Fig. C.33).

We are now ready to calculate the source luminosity in a given energy band (Ruffini et al., 2004b). The source luminosity at a detector arrival time t_a^d, per

unit solid angle $d\Omega$ and in the energy band $[\nu_1, \nu_2]$ is given by:

$$\frac{dE^{[\nu_1,\nu_2]}}{dt_a^d d\Omega} = \int_{EQTS} \frac{\Delta\varepsilon}{4\pi}\, v\, \cos\vartheta\, \Lambda^4\, \frac{dt}{dt_a^d} W\left(\nu_1, \nu_2, T_{arr}\right) d\Sigma\,, \tag{C.9.3}$$

where $\Delta\varepsilon = \Delta E_{int}/V$ is the energy density released in the comoving frame assuming, for simplicity, that all the shell is emitting, $\Lambda = 1/(\gamma(1-(v/c)\cos\vartheta))$ is the Doppler factor, $d\Sigma$ is the surface element of the EQTS at detector arrival time t_a^d on which the integration is performed and T_{arr} is the observed temperature of the radiation emitted from $d\Sigma$:

$$T_{arr} = \frac{\Lambda\, T}{(1+z)}\,. \tag{C.9.4}$$

The "effective weight" $W\left(\nu_1, \nu_2, T_{arr}\right)$ is given by the ratio of the integral over the given energy band of a Planckian distribution at a temperature T_{arr} to the total integral aT_{arr}^4 (Ruffini et al., 2004b):

$$W\left(\nu_1, \nu_2, T_{arr}\right) = \frac{\frac{2}{h^2c^3}\int_{\nu_1}^{\nu_2} \frac{(h\nu)^3}{\exp^{h\nu/(kT_{arr})}-1} d\nu}{aT_{arr}^4}\,. \tag{C.9.5}$$

Fig. C.34 shows the simulations performed with the parameters derived in Sec. C.9.1 and with a variable surface filling factor $\mathcal{R}$ as in Fig. C.33: they match quite well the observed prompt emission light curves of GRB060607A in all the BAT sub-energy bands, with just a small discrepancy in the first few seconds in the lowest channel ($15-25$ keV).

Once we have the luminosity in a given energy band in the same way we can obtain the instantaneous and the time-integrated photon number spectrum. It is clear from Eq. C.9.3 that each single instantaneous spectrum is the result of a convolution of thermal spectra since photons observed at the same arrival time are emitted at different comoving time, hence with different temperatures. This calculation produces a non-thermal instantaneous spectrum in the observer frame. This effect is enhanced if we calculate the time-integrated spectrum: we perform two different integrations, one on the observation time and one on the EQTSs, and what we get is a non-thermal spectrum that is comparable with the one observed by BAT in different time intervals covering the whole prompt emission (see Fig. C.35).

It is clear that this description attempts to identify the leading process of the GRB spectrum, and more details will be needed as soon as instantaneous spectra will become available. It is also clear that, in case of GRBs with Lorentz gamma factor well above the ones considered in the present source ($\gamma_\circ > 10^3$), additional high energy processes have to be considered, eventually including hadronic interactions.

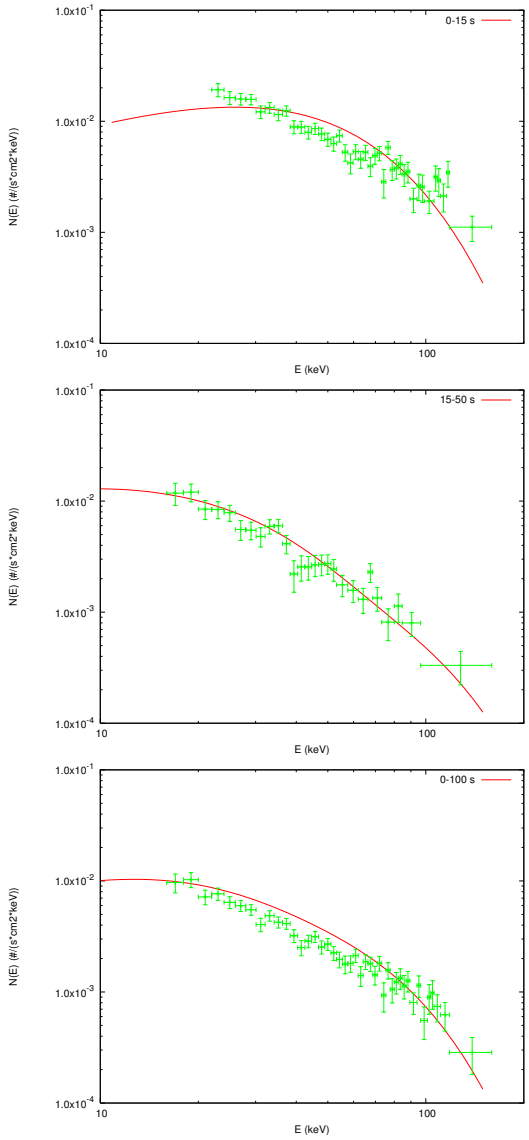

Figure C.35.: Theoretically predicted time-integrated photon number spectrum $N(E)$ corresponding to the $0-15$ s (upper panel), $15-50$ s (middle panel), and to the whole duration ($T_{90} = 100$ s, lower panel) of the prompt emission (solid lines) compared with the observed spectra integrated in the same intervals.

C.9.3. The X-ray flares

The last step to the understanding of the prompt emission of GRB060607A is the analysis of the X-ray flares observed by *Swift* XRT ($0.3 - 10$ keV) in the early part of the decaying phase of the afterglow. As already mentioned, in the current literature this emission is associated to the prompt emission due to their temporal and spectral behavior (Burrows et al., 2005b; Falcone et al., 2006; Zhang et al., 2006; Chincarini et al., 2007a; Falcone et al., 2007b). Even GRB060607A reveals a close correlation between the light curve observed by BAT and the X-ray flares observed by XRT (Ziaeepour et al., 2008).

Accordingly with these observations, the fireshell model predicts that these flares have the same origin of the prompt emission, namely they are produced by the interaction of the fireshell with overdense CBM, and their appearance in the X-ray energy band depends on the hard-to-soft evolution of the GRB spectrum. Initially, the result obtained is not compatible with the observations (we choose as an example the second flare labeled as F2, see Fig. C.36, upper panel). This discrepancy is due to the simple "radial approximation" adopted, namely the CBM inhomogeneities are assumed to be in spherical shells (Ruffini et al., 2002). Clearly this approximation fails when the visible area of the fireshell is comparable with the size of the CBM clump. This is indeed the case of the X-ray flares, since at those times the fireshell visible area (defined by the condition $\cos\theta \geq v/c$, where θ is the angle between the emitted photon and the line of sight, and v is the fireshell velocity) is much larger than during the prompt phase (for F2 see Fig. C.36, lower panel).

Following the results obtained for GRB011121 (Caito et al., 2008), we simulated the flare F2 light curve assuming a bi-dimensional structure of the CBM clump along the line of sight. We integrate over the emitting surface only up to a certain angle θ_c from the line of sight, corresponding to the transverse dimension of the CBM clump which in this case results $d_c = 2r_c \sin\theta_c \sim 10^{15}$ cm $\sim 0.5\, d_f$, where d_c and d_f are respectively the CBM clump and the fireshell transverse dimensions, and r_c is the distance of the clump from the source. We obtain in this way a flare whose duration $\Delta t/t$ is compatible with the observation (see Fig. C.36, middle panel). In general, we expect that the ratio $\Delta t/t$ would be approximately constant for flares occurring at different times (as observationally found Chincarini et al., 2010) if the corresponding CBM clumps have similar size. This is due to the decrease of the Lorentz gamma factor of the fireshell.

It is worth to observe that with this procedure the value of $\mathcal{R}$ remains constant during the flare (see Fig. C.33, lower panel, red solid line). Hence the increase in $\mathcal{R}$ that we obtained in our previous analysis (see Fig. C.33, lower panel, green dashed line) was only a compensation for the failure of the radial approximation.

At this preliminary stage this procedure does not affect the dynamics of the fireshell in the proper way since the "cut" at θ_c is performed only on

the emitted flux, but the fireshell is supposed to interact still with a spherical CBM shell. Nevertheless, it is a confirmation that it is possible to obtain arbitrarily short flares when a fully three dimensional code for the CBM is implemented.

C.9.4. The decaying afterglow regime

The NIR emission shows no significant evidence for correlation with the prompt emission (Ziaeepour et al., 2008): while the common gamma and X-ray light curves appear to be very close and correlate (Ziaeepour et al., 2008), in the NIR band the flaring activity, if any, is much weaker (Molinari et al., 2007). Even if in GRB060607A it is not possible to perform a comparison between the NIR light curve and the X-ray one after the plateau phase (Molinari et al., 2007), generally they show similar trends (see e.g. Rykoff et al., 2009).

We propose a possible scenario in which the plateau phase and the following decaying phase of the X-ray afterglow originate from a delayed emission produced by a "second component" of the fireshell. This component can be identified with the trailing edge of the matter distribution inside the fireshell (see Sec. 6) that, being slower than the main shell, engulfs it at later times. We tried to analyze the dynamics of this second shell and we found that its Lorentz factor is correlated with the one of the fireshell at the moment of transparency, thus confirming that the second shell in not erratic, emitted in a distinct episode of the engine activity, but it is intertwined with the main fireshell until the transparency (Bernardini et al., 2010).

We expect that during the collision a turbulent regime onsets and the description of the fireshell dynamics presented in Sec. 6 does not hold anymore. Therefore we limit our analysis to the onset of the plateau, which in the case of GRB060607A occurs at a radius $r_{on} \sim 4.0 \times 10^{17}$ cm (see Fig. C.33). The existence of these collisions implies that the subsequent expansion of the fireshell will not follow a ballistic description. Therefore, any inference on the nature of the emitting process based on a ballistic picture of the expanding shell and power-law extrapolations will be necessarily incorrect.

C.9.5. Conclusions

The "canonical GRB" scenario (Ruffini et al., 2001b, 2007a) implies that the GRB prompt emission is formed by two different components: the P-GRB and the peak of the extended afterglow. Therefore the analysis of the prompt emission light curve and spectrum is necessary and sufficient in order to fix the initial parameters which characterize the dynamics of the fireshell both in the optically thick and in the optically thin regimes through the equations of motion that we explicitly derived. This is one major difference between our approach and the ones in the current literature, where emphasis is usually

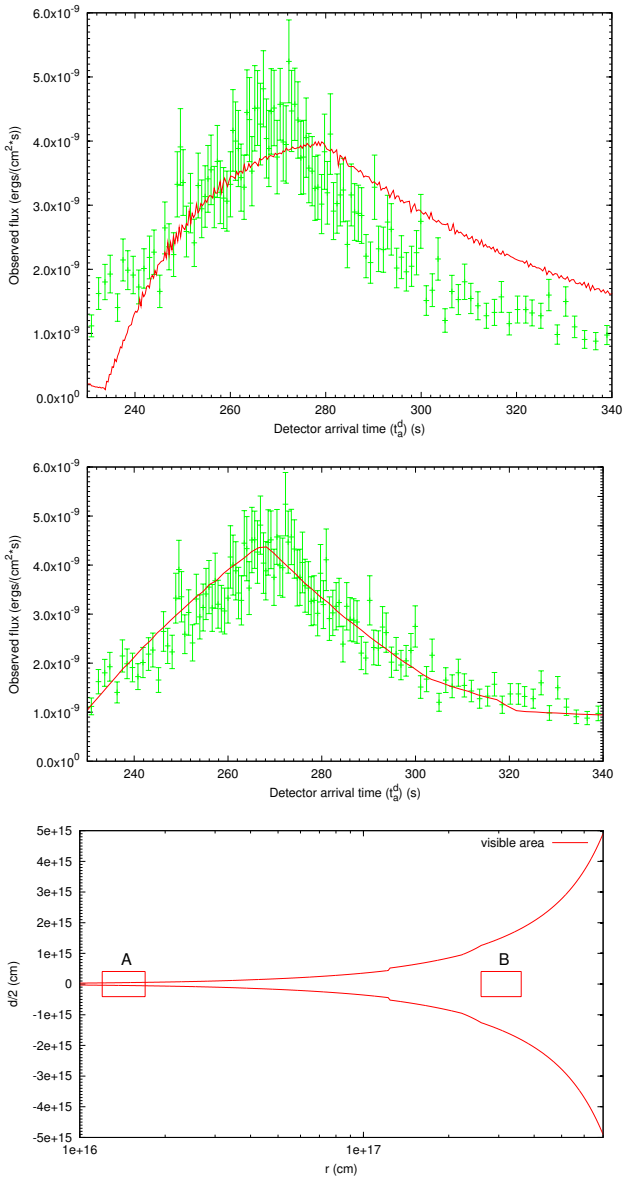

Figure C.36.: Upper panel: *Swift* XRT (0.3–10 keV) light curve of flare F2 compared with the theoretical one obtained under the "radial approximation" assumption (red line). Middle panel: *Swift* XRT (0.3–10 keV) light curve of flare F2 compared with the theoretical one obtained imposing a finite transverse dimension for the CBM clump (red line). Lower panel: the boundaries of the fireshell visible area ($\cos\theta = v/c$) compared with the dimensions of two CBM clumps corresponding to the first spike of the prompt emission (A) and of the flare (B). It is manifest how similar clumps produce different observational results depending on the evolution of the fireshell visible area (see text).

given to the latest parts of the GRB emission (Optical, NIR) and the dynamics of the early phases is just extrapolated backwards by power-laws (Molinari et al., 2007; Sari and Piran, 1999).

In this paper we explicitly show in the case of GRB060607A how the analysis of the prompt emission spectra and luminosities in different energy bands allows to determine the total energy of the electron positron pairs $E^{e^\pm}_{tot} = 2.5 \times 10^{53}$ erg. The engine powering the GRB is the gravitational collapse to a black hole and from our analysis this energetics points to a binary neutron star merger as the progenitor (Ruffini et al., 2009; Cherubini et al., 2009; Caito et al., 2009). The complete numerical modeling of the fireshell dynamics allows to calculate also the value of its Lorentz gamma factor at the transparency: $\gamma_\circ = 328$.

According to the fireshell model the X-ray flares have the same nature than the peaks observed in the prompt emission, namely they are produced by the interaction of the fireshell with different CBM clumps. What is peculiar in the late afterglow phases is that the typical dimensions of the clumps become smaller than the visible area of the fireshell. Under these conditions, we propose a bi-dimensional model for the CBM clump along the line of sight, the emission being limited to a small fraction of the entire EQTS, to substitute the assumption of spherical symmetry and to take into due account the structure of the clumps. We show that in this condition it is possible to obtain flares with $\Delta t/t_{tot}$ compatible with the observations. In order to fully describe all the X-ray flares properties a three dimensional description will be necessary.

We stop our analysis at the starting of the X-ray plateau. We propose a possible scenario in which this phase arises from the injection of slower material into the fireshell. This phase is characterized by high level of instabilities and may account for both the observed X-ray and NIR emission. Clearly its dynamics does not follow a simple ballistic law. Therefore, any backward extrapolation based on power-law equations of motion approximating a ballistic dynamics may lead to unphysical results.

Bibliography

ABDO, A.A., ACKERMANN, M., AJELLO, M., ASANO, K., ATWOOD, W.B., AXELSSON, M., BALDINI, L., BALLET, J., BARBIELLINI, G., BARING, M.G. ET AL.
≪Fermi Observations of GRB 090902B: A Distinct Spectral Component in the Prompt and Delayed Emission≫.
ApJ, **706**, pp. L138–L144 (2009a).

ABDO, A.A., ACKERMANN, M., ARIMOTO, M., ASANO, K., ATWOOD, W.B., AXELSSON, M., BALDINI, L., BALLET, J., BAND, D.L., BARBIELLINI, G. ET AL.
≪Fermi Observations of High-Energy Gamma-Ray Emission from GRB 080916C≫.
Science, **323**, p. 1688 (2009b).

ACKERMANN, M., AJELLO, M., ASANO, K., AXELSSON, M., BALDINI, L., BALLET, J., BARBIELLINI, G., BARING, M.G., BASTIERI, D., BECHTOL, K. ET AL.
≪Detection of a Spectral Break in the Extra Hard Component of GRB 090926A≫.
ApJ, **729**, 114 (2011).

ACKERMANN, M., ASANO, K., ATWOOD, W.B., AXELSSON, M., BALDINI, L., BALLET, J., BARBIELLINI, G., BARING, M.G., BASTIERI, D., BECHTOL, K. ET AL.
≪Fermi Observations of GRB 090510: A Short-Hard Gamma-ray Burst with an Additional, Hard Power-law Component from 10 keV TO GeV Energies≫.
ApJ, **716**, pp. 1178–1190 (2010).

AKSENOV, A., RUFFINI, R. AND VERESHCHAGIN, G.
≪Thermalization of nonequilibrium electron-positron-photon plasmas≫.
Phys. Rev. Lett., **99(12)**, p. 125003 (2007).

AKSENOV, A., RUFFINI, R. AND VERESHCHAGIN, G.
submitted to Phys. Rev. D (2008).

AKSENOV, A.G., BERNARDINI, M.G., BIANCO, C.L., CAITO, L., CHERUBINI, C., DE BARROS, G., GERALICO, A., IZZO, L., MASSUCCI, F.A., PATRICELLI, B. ET AL.

≪The fireshell model for gamma-ray bursts≫.
In G. Chincarini, P. D'Avanzo, R. Margutti and R. Salvaterra (eds.), *The Shocking Universe*, volume 102 of *SIF Conference Proceedings*, p. 451 (2010).

AKSENOV, A.G., RUFFINI, R. AND VERESHCHAGIN, G.V.
≪Thermalization of the mildly relativistic plasma≫.
Phys. Rev. D, **79(4)**, p. 043008 (2009).

AMATI, L.
≪The $e_{p,i}$-e_{iso} correlation in gamma-ray bursts: updated observational status, re-analysis and main implications≫.
MNRAS, **372**, pp. 233–245 (2006).

AMATI, L.
talk presented at the congress "10^{th} Italian-Korean Meeting", Pescara, Italy, June 25-29 (2007).

AMATI, L.
≪The Ep,i - Eiso correlation and Fermi Gamma-Ray Bursts≫.
ArXiv:1002.2232 (2010).

AMATI, L., DELLA VALLE, M., FRONTERA, F., MALESANI, D., GUIDORZI, C., MONTANARI, E. AND PIAN, E.
≪On the consistency of peculiar grbs 060218 and 060614 with the $e_{p,i}$ - e_{iso} correlation≫.
A&A, **463**, pp. 913–919 (2007).

AMATI, L., FEROCI, M., FRONTERA, F., LABANTI, C., VACCHI, A., ARGAN, A., CAMPANA, R., COSTA, E., RUFFINI, R., BOMBACI, I. ET AL.
≪A proposed Italian contribution to the MIRAX Scientific Payload≫.
Nuovo Cimento C, **34**, p. 49 (2011).

AMATI, L., FRONTERA, F. AND GUIDORZI, C.
≪Extremely energetic Fermi gamma-ray bursts obey spectral energy correlations≫.
A&A, **508**, pp. 173–180 (2009).

AMATI, L., FRONTERA, F., TAVANI, M., IN'T ZAND, J.J.M., ANTONELLI, A., COSTA, E., FEROCI, M., GUIDORZI, C., HEISE, J., MASETTI, N. ET AL.
≪Intrinsic spectra and energetics of bepposax gamma-ray bursts with known redshifts≫.
A&A, **390**, pp. 81–89 (2002).

AMATI, L., GUIDORZI, C., FRONTERA, F., DELLA VALLE, M., FINELLI, F., LANDI, R. AND MONTANARI, E.
≪Measuring the cosmological parameters with the $E_{p,i}$-E_{iso} correlation of gamma-ray bursts≫.

MNRAS, **391**, pp. 577–584 (2008).

ANTONELLI, L.A., D'AVANZO, P., PERNA, R., AMATI, L., COVINO, S., CUTINI, S., D'ELIA, V., GALLOZZI, S., GRAZIAN, A., PALAZZI, E. ET AL.
«GRB 090426: the farthest short gamma-ray burst?»
A&A, **507**, pp. L45–L48 (2009).

APTEKAR, R.L., FREDERIKS, D.D., GOLENETSKII, S.V., ILYNSKII, V.N., MAZETS, E.P., PANOV, V.N., SOKOLOVA, Z.J., TEREKHOV, M.M., SHESHIN, L.O., CLINE, T.L. ET AL.
«Konus-W Gamma-Ray Burst Experiment for the GGS Wind Spacecraft».
Space Science Reviews, **71**, pp. 265–272 (1995).

ARNAUD, K.A.
«XSPEC: The First Ten Years».
In G.H. Jacoby and J. Barnes (eds.), *Astronomical Data Analysis Software and Systems V*, volume 101 of *Astronomical Society of the Pacific Conference Series*, p. 17 (1996).

ARNETT, D.
Supernovae and Nucleosynthesis (Princeton University Press, 1996).

ARNETT, W.D. AND MEAKIN, C.
«Toward Realistic Progenitors of Core-collapse Supernovae».
ApJ, **733**, p. 78 (2011).

ATTEIA, J.L.
«A simple empirical redshift indicator for gamma-ray bursts».
A&A, **407**, pp. L1–L4 (2003).

ATWOOD, W.B., ABDO, A.A., ACKERMANN, M., ALTHOUSE, W., ANDERSON, B., AXELSSON, M., BALDINI, L., BALLET, J., BAND, D.L., BARBIELLINI, G. ET AL.
«The Large Area Telescope on the Fermi Gamma-Ray Space Telescope Mission».
ApJ, **697**, pp. 1071–1102 (2009).

BAND, D., MATTESON, J., FORD, L., SCHAEFER, B., PALMER, D., TEEGARDEN, B., CLINE, T., BRIGGS, M., PACIESAS, W., PENDLETON, G. ET AL.
«Batse observations of gamma-ray burst spectra. i - spectral diversity».
ApJ, **413**, pp. 281–292 (1993).

BARBIER, L., BARTHELMY, S., CUMMINGS, J., CUSUMANO, G., FENIMORE, E., GEHRELS, N., HULLINGER, D., KRIMM, H., MARKWARDT, C., PALMER, D. ET AL.
«Preliminary refined analysis of the swift-bat trigger 191157.»
GCN Circ., **4780** (2006).

BARTHELMY, S.D.
«Burst alert telescope (bat) on the swift midex mission».
In K.A. Flanagan and O.H.W. Siegmund (eds.), *X-Ray and Gamma-Ray Instrumentation for Astronomy XIII.*, volume 5165 of *Society of Photo-Optical Instrumentation Engineers (SPIE) Conference Proceedings*, pp. 175–189 (2004).

BARTHELMY, S.D., BARBIER, L.M., CUMMINGS, J.R., FENIMORE, E.E., GEHRELS, N., HULLINGER, D., KRIMM, H.A., MARKWARDT, C.B., PALMER, D.M., PARSONS, A. ET AL.
«The burst alert telescope (bat) on the swift midex mission».
Space Science Reviews, **120**, pp. 143–164 (2005a).

BARTHELMY, S.D., CHINCARINI, G., BURROWS, D.N., GEHRELS, N., COVINO, S., MORETTI, A., ROMANO, P., O'BRIEN, P.T., SARAZIN, C.L., KOUVELIOTOU, C. ET AL.
«An origin for short γ-ray bursts unassociated with current star formation».
Nature, **438**, pp. 994–996 (2005b).

BARTOLINI, C., GRECO, G., GUARNIERI, A., PICCIONI, A., BESKIN, G., BONDAR, S., KARPOV, S. AND MOLINARI, E.
«Analysis of the prompt optical emission of the naked-eye grb 080319b».
arXiv:0906.4144 (2009).

BAUMGARTNER, W.H., BARTHELMY, S.D., CUMMINGS, J.R., FENIMORE, E.E., GEHRELS, N., KRIMM, H.A., MARKWARDT, C.B., PALMER, D.M., SAKAMOTO, T., SATO, G. ET AL.
«GRB 090618: Swift-BAT refined analysis.»
GCN Circ., **9530**, p. 1 (2009).

BEARDMORE, A.P. AND SCHADY, P.
«GRB090618: Swift-XRT team refined analysis.»
GCN Circ., **9528**, p. 1 (2009).

BECK, R.
«Observations of Magnetic Fields in Galaxies».
In E. M. de Gouveia dal Pino, G. Lugones, & A. Lazarian (ed.), *Magnetic Fields in the Universe: From Laboratory and Stars to Primordial Structures.*, volume 784 of *American Institute of Physics Conference Series*, pp. 343–353 (2005).

BELCZYNSKI, K., PERNA, R., BULIK, T., KALOGERA, V., IVANOVA, N. AND LAMB, D.Q.
«A Study of Compact Object Mergers as Short Gamma-Ray Burst Progenitors».
ApJ, **648**, pp. 1110–1116 (2006).

BELVEDERE, R., PUGLIESE, D., RUEDA, J.A., RUFFINI, R. AND XUE, S.S.
«Neutron star equilibrium configurations within a fully relativistic theory with strong, weak, electromagnetic, and gravitational interactions».
Nuclear Physics A, **883**, pp. 1–24 (2012).

BERGER, E.
«The Host Galaxies of Short-Duration Gamma-Ray Bursts: Luminosities, Metallicities, and Star Formation Rates».
ApJ, **690**, pp. 231–237 (2009).

BERGER, E.
«The Environments of Short-Duration Gamma-Ray Bursts and Implications for their Progenitors».
ArXiv:1005.1068 (2010).

BERGER, E.
«GRB 110709B: gemini-south optical observations.»
GCN Circ., **12128**, p. 1 (2011a).

BERGER, E.
«The environments of short-duration gamma-ray bursts and implications for their progenitors».
New. Astron. Rev., **55**, pp. 1–22 (2011b).

BERGER, E., SHIN, M.S., MULCHAEY, J.S. AND JELTEMA, T.E.
«Galaxy clusters associated with short grbs. i. the fields of grbs 050709, 050724, 050911, and 051221a».
ApJ, **660**, pp. 496–503 (2007).

BERNARDINI, M.G., BIANCO, C.L., CAITO, L., DAINOTTI, M.G., GUIDA, R. AND RUFFINI, R.
«Grb 970228 and a class of grbs with an initial spikelike emission».
A&A, **474**, pp. L13–L16 (2007).

BERNARDINI, M.G., BIANCO, C.L., CAITO, L., DAINOTTI, M.G., GUIDA, R. AND RUFFINI, R.
«Grb970228 and the class of grbs with an initial spikelike emission: do they follow the amati relation?»
In C.L. Bianco and S.S. Xue (eds.), *Relativistic Astrophysics*, volume 966 of *American Institute of Physics Conference Series*, pp. 7–11 (2008a).

BERNARDINI, M.G., BIANCO, C.L., CAITO, L., DAINOTTI, M.G., GUIDA, R. AND RUFFINI, R.
«GRB970228 as a Prototype for the Class of GRBs with AN Initial Spikelike Emission».

In H. Kleinert, R.T. Jantzen and R. Ruffini (eds.), *The Eleventh Marcel Grossmann Meeting On Recent Developments in Theoretical and Experimental General Relativity, Gravitation and Relativistic Field Theories*, pp. 1992–1994 (2008b).

BERNARDINI, M.G., BIANCO, C.L., CAITO, L., DAINOTTI, M.G., GUIDA, R. AND RUFFINI, R.
≪GRB980425 and the Puzzling URCA1 Emission≫.
In H. Kleinert, R.T. Jantzen and R. Ruffini (eds.), *The Eleventh Marcel Grossmann Meeting On Recent Developments in Theoretical and Experimental General Relativity, Gravitation and Relativistic Field Theories*, pp. 1959–1961 (Singapore: World Scientific, 2008c).

BERNARDINI, M.G., BIANCO, C.L., CAITO, L., DAINOTTI, M.G., GUIDA, R. AND RUFFINI, R.
≪Preliminary analysis of GRB060607A within the fireshell model≫.
In Y.F. Huang, Z.G. Dai and B. Zhang (eds.), *2008 Nanjing Gamma-Ray Burst Conference*, volume 1065 of *American Institute of Physics Conference Series*, pp. 227–230 (2008d).

BERNARDINI, M.G., BIANCO, C.L., CAITO, L., IZZO, L., PATRICELLI, B. AND RUFFINI, R.
≪The end of the prompt emission within the fireshell model≫.
In G. Chincarini, P. D'Avanzo, R. Margutti and R. Salvaterra (eds.), *The Shocking Universe*, volume 102 of *SIF Conference Proceedings*, p. 489 (2010).

BERNARDINI, M.G., BIANCO, C.L., CHARDONNET, P., FRASCHETTI, F., RUFFINI, R. AND XUE, S.S.
≪A new astrophysical "triptych": Grb030329/sn2003dh/urca-2≫.
In E. Fenimore and M. Galassi (eds.), *Gamma-Ray Bursts: 30 Years of Discovery*, volume 727 of *American Institute of Physics Conference Series*, pp. 312–315 (2004).

BERNARDINI, M.G., BIANCO, C.L., CHARDONNET, P., FRASCHETTI, F., RUFFINI, R. AND XUE, S.S.
≪Theoretical interpretation of the luminosity and spectral properties of grb 031203≫.
ApJ, **634**, pp. L29–L32 (2005a).

BERNARDINI, M.G., BIANCO, C.L., RUFFINI, R., XUE, S.S., CHARDONNET, P. AND FRASCHETTI, F.
≪General features of grb 030329 in the embh model≫.
In M. Novello, S. Perez Bergliaffa and R. Ruffini (eds.), *The Tenth Marcel Grossmann Meeting. On recent developments in theoretical and experimental general relativity, gravitation and relativistic field theories*, p. 2459 (Singapore: World Scientific, 2005b).

BERNARDINI, M.G., DAINOTTI, M.G., BIANCO, C.L., CAITO, L., GUIDA, R. AND RUFFINI, R.
≪Prompt emission and X-ray flares: the case of GRB 060607 A≫.
In G. Giobbi, A. Tornambe, G. Raimondo, M. Limongi, L. A. Antonelli, N. Menci, & E. Brocato (ed.), *Probing Stellar Populations out to the Distant Universe*, volume 1111 of *American Institute of Physics Conference Series*, pp. 383–386 (2009).

BERSIER, D., FRUCHTER, A., RHOADS, J., LEVAN, A. AND TANVIR, N.
≪Limits on a SN in the field of GRB 050509b.≫
GCN Circ., **3521** (2005).

BIANCO, C.L., BERNARDINI, M.G., CAITO, L., DAINOTTI, M.G., GUIDA, R. AND RUFFINI, R.
≪The "fireshell" model and the "canonical" grb scenario.≫
In C.L. Bianco and S.S. Xue (eds.), *Relativistic Astrophysics*, volume 966 of *American Institute of Physics Conference Series*, pp. 12–15 (2008a).

BIANCO, C.L., BERNARDINI, M.G., CAITO, L., DAINOTTI, M.G., GUIDA, R. AND RUFFINI, R.
≪Short and canonical grbs≫.
In M. Galassi, D. Palmer and E. Fenimore (eds.), *GAMMA-RAY BURSTS 2007: Proceedings of the Santa Fe Conference*, volume 1000 of *American Institute of Physics Conference Series*, pp. 305–308 (2008b).

BIANCO, C.L., BERNARDINI, M.G., CAITO, L., DAINOTTI, M.G., GUIDA, R. AND RUFFINI, R.
≪The "fireshell" model and the "canonical GRB" scenario≫.
In Y.F. Huang, Z.G. Dai and B. Zhang (eds.), *2008 Nanjing Gamma-Ray Burst Conference*, volume 1065 of *American Institute of Physics Conference Series*, pp. 223–226 (2008c).

BIANCO, C.L., CAITO, L. AND RUFFINI, R.
≪Theoretical interpretation of GRB 011121≫.
Nuovo Cimento B, **121**, pp. 1441–1442 (2006a).

BIANCO, C.L., CAITO, L. AND RUFFINI, R.
≪Theoretical interpretation of grb 011121≫.
Il Nuovo Cimento B, **121**, p. 1441 (2006b).

BIANCO, C.L. AND RUFFINI, R.
≪Exact versus approximate equitemporal surfaces in gamma-ray burst afterglows≫.
ApJ, **605**, pp. L1–L4 (2004).

BIANCO, C.L. AND RUFFINI, R.

≪Exact versus approximate solutions in gamma-ray burst afterglows≫.
ApJ, **633**, pp. L13–L16 (2005a).

BIANCO, C.L. AND RUFFINI, R.
≪On the exact analytic expressions for the equitemporal surfaces in gamma-ray burst afterglows≫.
ApJ, **620**, pp. L23–L26 (2005b).

BIANCO, C.L. AND RUFFINI, R.
≪Exact versus approximate beaming formulae in gamma-ray burst afterglows≫.
ApJ, **644**, pp. L105–L108 (2006).

BIANCO, C.L., RUFFINI, R., VERESHCHAGIN, G. AND XUE, S.S.
≪Equations of motion and initial and boundary conditions for gamma-ray burst≫.
Journal of the Korean Physical Society, **49**, p. 722 (2006c).

BIANCO, C.L., RUFFINI, R. AND XUE, S.S.
≪The elementary spike produced by a pure e^+e^- pair-electromagnetic pulse from a black hole: The pem pulse≫.
A&A, **368**, pp. 377–390 (2001).

BISSALDI, E. AND CONNAUGHTON, V.
≪GRB 090902B: Fermi GBM detection of a bright burst.≫
GRB Coordinates Network, **9866**, pp. 1–+ (2009).

BLANDFORD, R.D. AND MCKEE, C.F.
≪Fluid dynamics of relativistic blast waves≫.
Physics of Fluids, **19**, pp. 1130–1138 (1976).

BLASCHKE, D., KLAHN, T. AND VOSKRESENSKY, D.
≪Diquark condensates and compact star cooling≫.
ApJ, **533**, p. 406412 (2000).

BLASCHKE, D., VOSKRESENSKY, D. AND GRIGORIAN, H.
≪Cooling of Neutron Stars with Color Superconducting Quark Cores≫.
Nuclear Physics A, **774**, pp. 815–818 (2006).
ISSN 03759474.

BLINNIKOV, S.I., KOZYREVA, A.V. AND PANCHENKO, I.E.
≪Gamma-ray bursts: When does a blackbody spectrum look non-thermal?≫
Astronomy Reports, **43**, pp. 739–747 (1999).

BLINNIKOV, S.I., NOVIKOV, I.D., PEREVODCHIKOVA, T.V. AND POLNAREV, A.G.

«Exploding neutron stars in close binaries».
Soviet Astronomy Letters, **10**, p. 177 (1984).

BLOOM, J., BLAKE, C., PROCHASKA, J.X., HENNAWI, J., GLADDERS, M. AND KOESTER, B.
«GRB 050509b: PAIRITEL and WIYN observations.»
GCN Circ., **3386** (2005a).

BLOOM, J.S., DJORGOVSKI, S.G. AND KULKARNI, S.R.
«The redshift and the ordinary host galaxy of grb 970228».
ApJ, **554**, pp. 678–683 (2001).

BLOOM, J.S., FOLEY, R.J., POOLEY, D., FILIPPENKO, A.V., CHORNOCK, R., BLAKE, C., PROCHASKA, J.X., HENNAWI, J., GLADDERS, M., KOESTER, B. ET AL.
«GRB 050509b: Keck/Chandra cross-correlation.»
GCN Circ., **3417** (2005b).

BLOOM, J.S., PERLEY, D.A. AND CHEN, H.W.
«GRB061121: spectroscopic redshift.»
GCN Circ., **5826** (2006a).

BLOOM, J.S., PROCHASKA, J.X., POOLEY, D., BLAKE, C.H., FOLEY, R.J., JHA, S., RAMIREZ-RUIZ, E., GRANOT, J., FILIPPENKO, A.V., SIGURDSSON, S. ET AL.
«Closing in on a Short-Hard Burst Progenitor: Constraints from Early-Time Optical Imaging and Spectroscopy of a Possible Host Galaxy of GRB 050509b».
ApJ, **638**, pp. 354–368 (2006b).

BOËR, M., ATTEIA, J.L., DAMERDJI, Y., GENDRE, B., KLOTZ, A. AND STRATTA, G.
«Detection of a Very Bright Optical Flare from the Gamma-Ray Burst GRB 050904 at Redshift 6.29».
ApJ, **638**, pp. L71–L74 (2006).

BRIGGS, M.S.
«GRB 101023A: Fermi GBM observation.»
GCN Circ., **11376**, p. 1 (2010).

BRIGGS, M.S. AND YOUNES, G.
«GRB 111228A: Fermi GBM observation.»
GCN Circ., **12744**, p. 1 (2011).

BURLON, D., GHIRLANDA, G., GHISELLINI, G., LAZZATI, D., NAVA, L., NARDINI, M. AND CELOTTI, A.
«Precursors in Swift Gamma Ray Bursts with Redshift».

ApJ, **685**, pp. L19–L22 (2008).

BURROWS, A. AND LATTIMER, J.M.
≪The birth of neutron stars≫.
ApJ, **307**, pp. 178–196 (1986).

BURROWS, D.N., HILL, J.E., NOUSEK, J.A., KENNEA, J.A., WELLS, A., OSBORNE, J.P., ABBEY, A.F., BEARDMORE, A., MUKERJEE, K., SHORT, A.D.T. ET AL.
≪The swift x-ray telescope≫.
Space Science Reviews, **120**, pp. 165–195 (2005a).

BURROWS, D.N., HILL, J.E., NOUSEK, J.A., WELLS, A.A., CHINCARINI, G., ABBEY, A.F., BEARDMORE, A.P., BOSWORTH, J., BRÄUNINGER, H.W., BURKERT, W. ET AL.
≪The swift x-ray telescope≫.
In K.A. Flanagan and O.H.W. Siegmund (eds.), *X-Ray and Gamma-Ray Instrumentation for Astronomy XIII*, volume 5165 of *Society of Photo-Optical Instrumentation Engineers (SPIE) Conference Proceedings*, pp. 201–216 (2004).

BURROWS, D.N., ROMANO, P., FALCONE, A., KOBAYASHI, S., ZHANG, B., MORETTI, A., O'BRIEN, P.T., GOAD, M.R., CAMPANA, S., PAGE, K.L. ET AL.
≪Bright x-ray flares in gamma-ray burst afterglows≫.
Science, **309**, pp. 1833–1835 (2005b).

CAITO, L., AMATI, L., BERNARDINI, M.G., BIANCO, C.L., DE BARROS, G., IZZO, L., PATRICELLI, B. AND RUFFINI, R.
≪GRB 071227: an additional case of a disguised short burst≫.
A&A, **521**, p. A80 (2010).

CAITO, L., BERNARDINI, M.G., BIANCO, C.L., DAINOTTI, M.G., GUIDA, R. AND RUFFINI, R.
In R.T. Jantzen, H. Kleinert and R. Ruffini (eds.), *The Eleventh Marcel Grossmann Meeting.* (Singapore: World Scientific, 2008).

CAITO, L., BERNARDINI, M.G., BIANCO, C.L., DAINOTTI, M.G., GUIDA, R. AND RUFFINI, R.
≪GRB060614: a "fake" short GRB from a merging binary system≫.
A&A, **498**, pp. 501–507 (2009).

CAMPANA, S., MANGANO, V., BLUSTIN, A.J., BROWN, P., BURROWS, D.N., CHINCARINI, G., CUMMINGS, J.R., CUSUMANO, G., DELLA VALLE, M., MALESANI, D. ET AL.
≪The association of grb 060218 with a supernova and the evolution of the shock wave≫.
Nature, **442**, pp. 1008–1010 (2006a).

CAMPANA, S., TAGLIAFERRI, G., LAZZATI, D., CHINCARINI, G., COVINO, S., PAGE, K., ROMANO, P., MORETTI, A., CUSUMANO, G., MANGANO, V. ET AL.
≪The x-ray afterglow of the short gamma ray burst 050724≫.
A&A, **454**, pp. 113–117 (2006b).

CANO, Z., BERSIER, D., GUIDORZI, C., MARGUTTI, R., SVENSSON, K.M., KOBAYASHI, S., MELANDRI, A., WIERSEMA, K., POZANENKO, A., VAN DER HORST, A.J. ET AL.
≪A tale of two GRB-SNe at a common redshift of z=0.54≫.
MNRAS, **413**, pp. 669–685 (2011).

CANUTO, V.
≪Neutron stars≫.
In R. Giacconi and R. Ruffini (eds.), *Physics and Astrophysics of Neutron Stars and Black Holes*, pp. 448–527 (1978).

CAPOZZIELLO, S. AND IZZO, L.
≪A cosmographic calibration of the $E_{p,i}$ - E_{iso} (Amati) relation for GRBs≫.
A&A, **519**, A73 (2010).

CASTRO-TIRADO, A.J., DE UGARTE POSTIGO, A., GOROSABEL, J., FATHKULLIN, T., SOKOLOV, V., BREMER, M., MÁRQUEZ, I., MARÍN, A.J., GUZIY, S., JELÍNEK, M. ET AL.
≪GRB 050509b: the elusive optical/nIR/mm afterglow of a short-duration GRB≫.
A&A, **439**, pp. L15–L18 (2005).

CAVALLO, G. AND REES, M.J.
≪A qualitative study of cosmic fireballs and gamma-ray bursts≫.
MNRAS, **183**, pp. 359–365 (1978).

CENKO, S.B., PERLEY, D.A., JUNKKARINEN, V., BURBIDGE, M., DIEGO, U.S. AND MILLER, K.
≪GRB 090618: Lick/KAST spectroscopy.≫
GCN Circ., **9518** (2009).

CENKO, S.B., SOIFER, B.T., BIAN, C., DESAI, V., KULKARNI, S.R., BERGER, E., DEY, A. AND JANNUZI, B.T.
≪GRB 050509b: further analysis of Keck LRIS images.≫
GCN Circ., **3401** (2005).

CHERUBINI, C., GERALICO, A., J. A. RUEDA, H. AND RUFFINI, R.
≪e^--e^+ pair creation by vacuum polarization around electromagnetic black holes≫.
Phys. Rev. D, **79(12)**, p. 124002 (2009).

CHEVALIER, R.A. AND SODERBERG, A.M.
«Type IIb Supernovae with Compact and Extended Progenitors».
ApJ, **711**, pp. L40–L43 (2010).

CHEVALIER, R.A.
«Neutron star accretion in a supernova».
ApJ, **346**, p. 847 (1989).
ISSN 0004-637X.

CHIANG, J. AND DERMER, C.D.
«Synchrotron and synchrotron self-compton emission and the blast-wave model of gamma-ray bursts».
ApJ, **512**, pp. 699–710 (1999).

CHINCARINI, G., MAO, J., MARGUTTI, R., BERNARDINI, M.G., GUIDORZI, C., PASOTTI, F., GIANNIOS, D., DELLA VALLE, M., MORETTI, A., ROMANO, P. ET AL.
«Unveiling the origin of X-ray flares in gamma-ray bursts».
MNRAS, **406**, pp. 2113–2148 (2010).

CHINCARINI, G., MORETTI, A., ROMANO, P., FALCONE, A.D., MORRIS, D., RACUSIN, J., CAMPANA, S., COVINO, S., GUIDORZI, C., TAGLIAFERRI, G. ET AL.
«The First Survey of X-Ray Flares from Gamma-Ray Bursts Observed by Swift: Temporal Properties and Morphology».
ApJ, **671**, pp. 1903–1920 (2007a).

CHINCARINI, G., MORETTI, A., ROMANO, P., FALCONE, A.D., MORRIS, D., RACUSIN, J., CAMPANA, S., GUIDORZI, C., TAGLIAFERRI, G., BURROWS, D.N. ET AL.
«The first survey of x-ray flares from gamma ray bursts observed by swift: Temporal properties and morphology».
ArXiv:astro-ph/0702371 (2007b).

COBB, B.E., BAILYN, C.D., VAN DOKKUM, P.G. AND NATARAJAN, P.
«Sn 2006aj and the nature of low-luminosity gamma-ray bursts».
ApJ, **645**, pp. L113–L116 (2006).

COBB, B.E., BLOOM, J.S., PERLEY, D.A., MORGAN, A.N., CENKO, S.B. AND FILIPPENKO, A.V.
«Discovery of SN 2009nz Associated with GRB 091127».
ApJ, **718**, pp. L150–L155 (2010).

COSTA, E., FRONTERA, F., HEISE, J., FEROCI, M., IN'T ZAND, J., FIORE, F., CINTI, M.N., DAL FIUME, D., NICASTRO, L., ORLANDINI, M. ET AL.
«Discovery of an x-ray afterglow associated with the γ-ray burst of 28 february 1997».

Nature, **387**, pp. 783–785 (1997).

COVINO, S., VERGANI, S.D., MALESANI, D., MOLINARI, E., D'AVANZO, P., CHINCARINI, G., ZERBI, F.M., ANTONELLI, L.A., CONCONI, P., TESTA, V. ET AL.
«The Afterglow Onset for GRB 060418 and GRB 060607A».
Chinese Journal of Astronomy and Astrophysics Supplement, **8**, pp. 356–360 (2008).

CRIDER, A., LIANG, E.P. AND PREECE, R.D.
«Confronting synchrotron shock and inverse Comptonization models with GRB spectral evolution».
In C.A. Meegan, R.D. Preece and T.M. Koshut (eds.), *Gamma-Ray Bursts, 4th Hunstville Symposium*, volume 428 of *American Institute of Physics Conference Series*, pp. 359–363 (1998).

CRIDER, A., LIANG, E.P., SMITH, I.A., PREECE, R.D., BRIGGS, M.S., PENDLETON, G.N., PACIESAS, W.S., BAND, D.L. AND MATTESON, J.L.
«Evolution of the low-energy photon spectral in gamma-ray bursts».
ApJ, **479**, p. L39 (1997).

CUCCHIARA, A., LEVAN, A.J., FOX, D.B., TANVIR, N.R., UKWATTA, T.N., BERGER, E., KRÜHLER, T., KÜPCÜ YOLDAŞ, A., WU, X.F., TOMA, K. ET AL.
«A Photometric Redshift of z ˜ 9.4 for GRB 090429B».
ApJ, **736**, 7 (2011).

CUMMINGS, J., ANGELINI, L., BARTHELMY, S., CUCCHIARA, A., GEHRELS, N., GRONWALL, C., HOLLAND, S.T., MANGANO, V., MARSHALL, F., PAGANI, C. ET AL.
«GRB050904: Swift-BAT detection of a probable burst.»
GCN Circ., **3910**, pp. 1–+ (2005).

CUMMINGS, J.R., BARTHELMY, S.D., BURROWS, D.N., GRONWALL, C., HOLLAND, S.T., KENNEA, J.A., MARKWARDT, C.B., PALMER, D.M., SIEGEL, M.H., STARLING, R.L.C. ET AL.
«GRB 110709B: Swift detection of a burst.»
GCN Circ., **12122**, p. 1 (2011).

CURRAN, P.A., VAN DER HORST, A.J. AND WIJERS, R.A.M.J.
«Are the missing X-ray breaks in gamma-ray burst afterglow light curves merely hidden?»
MNRAS, **386**, pp. 859–863 (2008).

CUSUMANO, G., BARTHELMY, S., GEHRELS, N., HUNSBERGER, S., IMMLER, S., MARSHALL, F., PALMER, D. AND SAKAMOTO, T.

«Grb 060218: Swift-bat detection of a possible burst.»
GCN Circ., **4775** (2006).

CUSUMANO, G., MANGANO, V., CHINCARINI, G., PANAITESCU, A., BURROWS, D.N., LA PAROLA, V., SAKAMOTO, T., CAMPANA, S., MINEO, T., TAGLIAFERRI, G. ET AL.
«Swift observations of GRB 050904: the most distant cosmic explosion ever observed».
A&A, **462**, pp. 73–80 (2007).

DAI, Z.G. AND LU, T.
«Gamma-ray burst afterglows and evolution of postburst fireballs with energy injection from strongly magnetic millisecond pulsars».
A&A, **333**, pp. L87–L90 (1998).

DAI, Z.G. AND LU, T.
«The Afterglow of GRB 990123 and a Dense Medium».
ApJ, **519**, pp. L155–L158 (1999).

DAIGNE, F., BOSNJAK, Z. AND DUBUS, G.
«The origin of the prompt GRB spectrum».
ArXiv:0912.3743 (2009).

DAIGNE, F. AND MOCHKOVITCH, R.
«Gamma-ray bursts from internal shocks in a relativistic wind: temporal and spectral properties».
MNRAS, **296**, pp. 275–286 (1998).

DAIGNE, F. AND MOCHKOVITCH, R.
«The expected thermal precursors of gamma-ray bursts in the internal shock model».
MNRAS, **336**, pp. 1271–1280 (2002).

DAINOTTI, M.G., BERNARDINI, M.G., BIANCO, C.L., CAITO, L., GUIDA, R. AND RUFFINI, R.
«Grb 060218 and grbs associated with supernovae ib/c».
A&A, **471**, pp. L29–L32 (2007).

DAINOTTI, M., BERNARDINI, M.G., BIANCO, C.L., CAITO, L., GUIDA, R. AND RUFFINI, R.
«The astrophysical trypthic: Grb, sn and urca can be extended to grb060218?»
J. Kor. Phys. Soc., **56**, p. 1588 (2010).

DAMOUR, T. AND RUFFINI, R.
«Quantum electrodynamical effects in kerr-newman geometries.»
Physical Review Letters, **35**, pp. 463–466 (1975).

D'AVANZO, P., MALESANI, D., COVINO, S., PIRANOMONTE, S., GRAZIAN, A., FUGAZZA, D., MARGUTTI, R., D'ELIA, V., ANTONELLI, L.A., CAMPANA, S. ET AL.
«The optical afterglows and host galaxies of three short/hard gamma-ray bursts».
A&A, **498**, pp. 711–721 (2009).

D'AVANZO, P., MELANDRI, A., PALAZZI, E., CAMPANA, S., DELLA VALLE, M., PIAN, E., SALVATERRA, R. AND TAGLIAFERRI, G.
«GRB 111228A: possible detection of the SN with the TNG.»
GCN Circ., **13069**, p. 1 (2012).

DAVIES, M.B., LEVAN, A.J., LARSSON, J., KING, A.R. AND FRUCHTER, A.S.
«Progenitors of long gamma-ray bursts».
In M. Axelsson and F. Ryde (eds.), *Gamma-Ray Bursts: Prospects for GLAST*, volume 906 of *American Institute of Physics Conference Series*, pp. 69–78 (2007).

DE BARROS, G., AMATI, L., BERNARDINI, M.G., BIANCO, C.L., CAITO, L., IZZO, L., PATRICELLI, B. AND RUFFINI, R.
«On the nature of GRB 050509b: a disguised short GRB».
A&A, **529**, p. A130 (2011).

DE UGARTE POSTIGO, A., XU, D., LELOUDAS, G., KRUEHLER, T., MALESANI, D., GOROSABEL, J., THOENE, C.C., SANCHEZ-RAMIREZ, R., SCHULZE, S., FYNBO, J.P.U. ET AL.
«GRB 130427A: spectroscopic detection of the SN from the 10.4m GTC.»
GCN Circ., **14646**, p. 1 (2013).

DELLA VALLE, M.
«Supernova and grb connection: Observations and questions».
In S.S. Holt, N. Gehrels and J.A. Nousek (eds.), *Gamma-Ray Bursts in the Swift Era*, volume 836 of *American Institute of Physics Conference Series*, pp. 367–379 (2006).

DELLA VALLE, M., CHINCARINI, G., PANAGIA, N., TAGLIAFERRI, G., MALESANI, D., TESTA, V., FUGAZZA, D., CAMPANA, S., COVINO, S., MANGANO, V. ET AL.
«An enigmatic long-lasting γ-ray burst not accompanied by a bright supernova».
Nature, **444**, pp. 1050–1052 (2006).

DERMER, C.D.
«External shocks, UHECRs, and the early afterglow of GRBs».
Nuovo Cimento B, **121**, pp. 1331–1336 (2006).

DERMER, C.D.
≪Nonthermal Synchrotron Radiation from Gamma-Ray Burst External Shocks and the X-Ray Flares Observed with Swift≫.
ApJ, **684**, pp. 430–448 (2008).

DERMER, C.D. AND MITMAN, K.E.
≪Short-timescale variability in the external shock model of gamma-ray bursts≫.
ApJ, **513**, pp. L5–L8 (1999).

DEZALAY, J.P., BARAT, C., TALON, R., SYUNYAEV, R., TEREKHOV, O. AND KUZNETSOV, A.
≪Short cosmic events - a subset of classical grbs?≫
In W.S. Paciesas and G.J. Fishman (eds.), *American Institute of Physics Conference Series*, volume 265 of *American Institute of Physics Conference Series*, pp. 304–309 (1992).

DUCCI, L., SIDOLI, L., MEREGHETTI, S., PAIZIS, A. AND ROMANO, P.
≪The structure of blue supergiant winds and the accretion in supergiant high-mass X-ray binaries≫.
MNRAS, **398**, pp. 2152–2165 (2009).

DUNCAN, R.C., SHAPIRO, S.L. AND WASSERMAN, I.
≪Neutrino-driven winds from young, hot neutron stars≫.
ApJ, **309**, p. 141 (1986).
ISSN 0004-637X.

EDEROCLITE, A., MASON, E., DELLA VALLE, M., GILMOZZI, R., WILLIAMS, R.E., GERMANY, L., SAVIANE, I., MATTEUCCI, F., SCHAEFER, B.E., WALTER, F. ET AL.
≪Early spectral evolution of nova sagittarii 2004 (v5114 sagittarii)≫.
A&A, **459**, pp. 875–883 (2006).

EICHLER, D. AND LEVINSON, A.
≪A Compact Fireball Model of Gamma-Ray Bursts≫.
ApJ, **529**, pp. 146–150 (2000).

EICHLER, D., LIVIO, M., PIRAN, T. AND SCHRAMM, D.N.
≪Nucleosynthesis, neutrino bursts and gamma-rays from coalescing neutron stars≫.
Nature, **340**, pp. 126–128 (1989).

EVANS, P.A., BEARDMORE, A.P., PAGE, K.L., OSBORNE, J.P., O'BRIEN, P.T., WILLINGALE, R., STARLING, R.L.C., BURROWS, D.N., GODET, O., VETERE, L. ET AL.
≪Methods and results of an automatic analysis of a complete sample of Swift-XRT observations of GRBs≫.

MNRAS, **397**, pp. 1177–1201 (2009).

EVANS, P.A., BEARDMORE, A.P., PAGE, K.L., TYLER, L.G., OSBORNE, J.P., GOAD, M.R., O'BRIEN, P.T., VETERE, L., RACUSIN, J., MORRIS, D. ET AL.
≪An online repository of Swift/XRT light curves of γ-ray bursts≫.
A&A, **469**, pp. 379–385 (2007).

FALCONE, A.D., BURROWS, D.N., LAZZATI, D., CAMPANA, S., KOBAYASHI, S., ZHANG, B., MÉSZÁROS, P., PAGE, K.L., KENNEA, J.A., ROMANO, P. ET AL.
≪The Giant X-Ray Flare of GRB 050502B: Evidence for Late-Time Internal Engine Activity≫.
ApJ, **641**, pp. 1010–1017 (2006).

FALCONE, A.D., MORRIS, D., RACUSIN, J., CHINCARINI, G., MORETTI, A., ROMANO, P., BURROWS, D.N., PAGANI, C., STROH, M., GRUPE, D. ET AL.
≪The first survey of x-ray flares from gamma ray bursts observed by swift: Spectral properties and energetics≫.
ArXiv:0706.1564 (2007a).

FALCONE, A.D., MORRIS, D., RACUSIN, J., CHINCARINI, G., MORETTI, A., ROMANO, P., BURROWS, D.N., PAGANI, C., STROH, M., GRUPE, D. ET AL.
≪The First Survey of X-Ray Flares from Gamma-Ray Bursts Observed by Swift: Spectral Properties and Energetics≫.
ApJ, **671**, pp. 1921–1938 (2007b).

FAN, Y.Z., PIRAN, T. AND XU, D.
≪The interpretation and implication of the afterglow of grb 060218≫.
Journal of Cosmology and Astro-Particle Physics, **9**, p. 13 (2006).

FATKHULLIN, T.A., SOKOLOV, V.V., MOISEEV, A.V., GUZIY, S. AND CASTRO-TIRADO, A.J.
≪Grb 060218: emergence of the underlying sn spectrum.≫
GCN Circ., **4809** (2006).

FENIMORE, E.E., COOPER, C., RAMIREZ-RUIZ, E., SUMNER, M.C., YOSHIDA, A. AND NAMIKI, M.
≪Gamma-ray bursts and relativistic shells: The surface filling factor≫.
ApJ, **512**, pp. 683–692 (1999).

FERMI, E.
≪On the Origin of the Cosmic Radiation≫.
Physical Review, **75**, pp. 1169–1174 (1949).

FERMI, E.
≪Galactic Magnetic Fields and the Origin of Cosmic Radiation.≫
ApJ, **119**, p. 1 (1954).

FEROCI, M., DEN HERDER, J.W., BOZZO, E., BARRET, D., BRANDT, S., HERNANZ, M., VAN DER KLIS, M., POHL, M., SANTANGELO, A., STELLA, L. ET AL.
«LOFT: the Large Observatory For X-ray Timing».
In *Space Telescopes and Instrumentation 2012: Ultraviolet to Gamma Ray*, volume 8443 of *Society of Photo-Optical Instrumentation Engineers (SPIE) Conference Series* (2012).

FEROCI, M. AND THE LOFT CONSORTIUM.
«The Large Observatory for X-ray Timing (LOFT)».
arXiv:1107.0436 (2011).

FERRERO, P., PALAZZI, E., PIAN, E. AND SAVAGLIO, S.
«Optical observations of grb 060218/sn 2006aj and its host galaxy».
In *American Institute of Physics Conference Series*, volume 924 of *American Institute of Physics Conference Series*, pp. 120–125 (2007).

FINKELSTEIN, S.L., RHOADS, J.E., MALHOTRA, S. AND GROGIN, N.
«Lyman Alpha Galaxies: Primitive, Dusty, or Evolved?»
ApJ, **691**, pp. 465–481 (2009).

FISHMAN, G.J., MEEGAN, C.A., WILSON, R.B., BROCK, M.N., HORACK, J.M., KOUVELIOTOU, C., HOWARD, S., PACIESAS, W.S., BRIGGS, M.S., PENDLETON, G.N. ET AL.
«The first BATSE gamma-ray burst catalog».
ApJSS, **92**, pp. 229–283 (1994).

FLETCHER, R.S., GAISSER, T.K., LIPARI, P. AND STANEV, T.
«sibyll: An event generator for simulation of high energy cosmic ray cascades».
Phys. Rev. D, **50**, pp. 5710–5731 (1994).

FONG, W., BERGER, E. AND FOX, D.B.
«Hubble Space Telescope Observations of Short Gamma-Ray Burst Host Galaxies: Morphologies, Offsets, and Local Environments».
ApJ, **708**, pp. 9–25 (2010).

FOX, D.B., FRAIL, D.A., PRICE, P.A., KULKARNI, S.R., BERGER, E., PIRAN, T., SODERBERG, A.M., CENKO, S.B., CAMERON, P.B., GAL-YAM, A. ET AL.
«The afterglow of grb 050709 and the nature of the short-hard γ-ray bursts».
Nature, **437**, pp. 845–850 (2005).

FRASCHETTI, F., BERNARDINI, M.G., BIANCO, C.L., CHARDONNET, P., RUFFINI, R. AND XUE, S.S.

≪The grb 980425-sn1998bw association in the embh model≫.
In E. Fenimore and M. Galassi (eds.), *Gamma-Ray Bursts: 30 Years of Discovery*, volume 727 of *American Institute of Physics Conference Series*, pp. 424–427 (2004).

FRASCHETTI, F., BERNARDINI, M.G., BIANCO, C.L., RUFFINI, R., XUE, S.S. AND CHARDONNET, P.
≪Inferences on the ism structure around grb 980425 and grb 980425-sn1998bw association in the embh model≫.
In M. Novello, S. Perez Bergliaffa and R. Ruffini (eds.), *The Tenth Marcel Grossmann Meeting. On recent developments in theoretical and experimental general relativity, gravitation and relativistic field theories*, p. 2451 (Singapore: World Scientific, 2005).

FRASCHETTI, F., RUFFINI, R., VITAGLIANO, L. AND XUE, S.S.
≪Theoretical predictions of spectral evolution of short GRBs≫.
Nuovo Cimento B, **121**, pp. 1477–1478 (2006).

FREDERIKS, D. AND PAL'SHIN, V.
≪GRB 110918A: rest-frame energetics in gamma-gays.≫
GCN Circ., **12370**, p. 1 (2011).

FRONTERA, F., AMATI, L., COSTA, E., MULLER, J.M., PIAN, E., PIRO, L., SOFFITTA, P., TAVANI, M., CASTRO-TIRADO, A., DAL FIUME, D. ET AL.
≪Prompt and delayed emission properties of gamma-ray bursts observed with bepposax≫.
ApJSS, **127**, pp. 59–78 (2000).

FRONTERA, F., COSTA, E., PIRO, L., MULLER, J.M., AMATI, L., FEROCI, M., FIORE, F., PIZZICHINI, G., TAVANI, M., CASTRO-TIRADO, A. ET AL.
≪Spectral properties of the prompt x-ray emission and afterglow from the gamma-ray burst of 1997 february 28≫.
ApJ, **493**, p. L67 (1998).

FYNBO, J.P.U., WATSON, D., THÖNE, C.C., SOLLERMAN, J., BLOOM, J.S., DAVIS, T.M., HJORTH, J., JAKOBSSON, P., JØRGENSEN, U.G., GRAHAM, J.F. ET AL.
≪No supernovae associated with two long-duration γ-ray bursts≫.
Nature, **444**, pp. 1047–1049 (2006).

GAL-YAM, A., FOX, D.B., PRICE, P.A., OFEK, E.O., DAVIS, M.R., LEONARD, D.C., SODERBERG, A.M., SCHMIDT, B.P., LEWIS, K.M., PETERSON, B.A. ET AL.
≪A novel explosive process is required for the γ-ray burst grb 060614≫.
Nature, **444**, pp. 1053–1055 (2006).

GALAMA, T.J., TANVIR, N., VREESWIJK, P.M., WIJERS, R.A.M.J., GROOT, P.J., ROL, E., VAN PARADIJS, J., KOUVELIOTOU, C., FRUCHTER, A.S., MASETTI, N. ET AL.
≪Evidence for a supernova in reanalyzed optical and near-infrared images of grb 970228≫.
ApJ, **536**, pp. 185–194 (2000).

GALAMA, T.J., VREESWIJK, P.M., VAN PARADIJS, J., KOUVELIOTOU, C., AUGUSTEIJN, T., BÖHNHARDT, H., BREWER, J.P., DOUBLIER, V., GONZALEZ, J.F., LEIBUNDGUT, B. ET AL.
≪An unusual supernova in the error box of the γ-ray burst of 25 april 1998≫.
Nature, **395**, pp. 670–672 (1998).

GAMOW, G.
My wordlines - an informal autobiography (New York: Viking press, 1970a).

GAMOW, G.
My world line: An informal autobiography. (New York, NY (USA): Viking Press, 1970b).

GAMOW, G. AND SCHOENBERG, M.
≪Neutrino theory of stellar collapse≫.
Physical Review, **59**, pp. 539–547 (1941).

GARNAVICH, P.
≪GRB 130427A, LBT optical spectrum≫.
GCN Circ., **14605**, p. 1 (2013).

GEHRELS, N., CHINCARINI, G., GIOMMI, P., MASON, K.O., NOUSEK, J.A., WELLS, A.A., WHITE, N.E., BARTHELMY, S.D., BURROWS, D.N., COMINSKY, L.R. ET AL.
≪The swift gamma-ray burst mission≫.
ApJ, **611**, pp. 1005–1020 (2004).

GEHRELS, N., NORRIS, J.P., BARTHELMY, S.D., GRANOT, J., KANEKO, Y., KOUVELIOTOU, C., MARKWARDT, C.B., MÉSZÁROS, P., NAKAR, E., NOUSEK, J.A. ET AL.
≪A new γ-ray burst classification scheme from grb060614≫.
Nature, **444**, pp. 1044–1046 (2006).

GEHRELS, N., RAMIREZ-RUIZ, E. AND FOX, D.B.
≪Gamma-Ray Bursts in the Swift Era≫.
ARAA, **47**, pp. 567–617 (2009).

GEHRELS, N., SARAZIN, C.L., O'BRIEN, P.T., ZHANG, B., BARBIER, L., BARTHELMY, S.D., BLUSTIN, A., BURROWS, D.N., CANNIZZO, J., CUMMINGS, J.R. ET AL.
«A short γ-ray burst apparently associated with an elliptical galaxy at redshift z = 0.225».
Nature, **437**, pp. 851–854 (2005).

GENDRE, B., GALLI, A., CORSI, A., KLOTZ, A., PIRO, L., STRATTA, G., BOËR, M. AND DAMERDJI, Y.
«The gamma-ray burst 050904: evidence for a termination shock?»
A&A, **462**, pp. 565–573 (2007).

GHIRLANDA, G., CELOTTI, A. AND GHISELLINI, G.
«Time resolved spectral analysis of bright gamma ray bursts».
A&A, **393**, pp. 409–423 (2002).

GHIRLANDA, G., CELOTTI, A. AND GHISELLINI, G.
«Extremely hard GRB spectra prune down the forest of emission models».
A&A, **406**, pp. 879–892 (2003).

GHISELLINI, G. AND CELOTTI, A.
«Quasi-thermal comptonization and GRBs».
A&AS, **138**, pp. 527–528 (1999).

GHISELLINI, G., GHIRLANDA, G., MEREGHETTI, S., BOSNJAK, Z., TAVECCHIO, F. AND FIRMANI, C.
«Are grb980425 and grb031203 real outliers or twins of grb060218?»
MNRAS, **372**, pp. 1699–1709 (2006).

GIANNIOS, D.
«Prompt emission spectra from the photosphere of a GRB».
A&A, **457**, pp. 763–770 (2006).

GIULIANI, A., FUSCHINO, F., VIANELLO, G., MARISALDI, M., MEREGHETTI, S., TAVANI, M., CUTINI, S., BARBIELLINI, G., LONGO, F., MORETTI, E. ET AL.
«AGILE Detection of Delayed Gamma-ray Emission From the Short Gamma-Ray Burst GRB 090510».
ApJ, **708**, pp. L84–L88 (2010).

GNEDIN, O.Y., YAKOVLEV, D.G. AND POTEKHIN, A.Y.
«Thermal relaxation in young neutron stars».
MNRAS, **324(3)**, pp. 725–736 (2001).
ISSN 0035-8711.

GOLENETSKII, S., APTEKAR, R., FREDERIKS, D., MAZETS, E., PAL'SHIN, V., OLEYNIK, P., ULANOV, M., SVINKIN, D. AND CLINE, T.

≪Konus-wind observation of GRB 101023A.≫
GCN Circ., **11384**, p. 1 (2010).

GOLENETSKII, S., APTEKAR, R., MAZETS, E., PAL'SHIN, V., FREDERIKS, D. AND CLINE, T.
≪Konus-wind and konus-a observations of GRB 061121.≫
GCN Circ., **5837** (2006a).

GOLENETSKII, S., APTEKAR, R., MAZETS, E., PAL'SHIN, V., FREDERIKS, D. AND CLINE, T.
≪Konus-wind observation of GRB 061007.≫
GCN Circ., **5722**, p. 1 (2006b).

GOLENETSKII, S., APTEKAR, R., MAZETS, E., PAL'SHIN, V., FREDERIKS, D. AND CLINE, T.
≪Konus-wind observation of GRB 071227.≫
GCN Circ., **7155**, pp. 1–+ (2007).

GOLENETSKII, S., APTEKAR, R., MAZETS, E., PAL'SHIN, V., FREDERIKS, D. AND CLINE, T.
≪Konus-wind observation of GRB 080319B.≫
GCN Circ., **7482** (2008).

GOLENETSKII, S., APTEKAR, R., MAZETS, E., PAL'SHIN, V., FREDERIKS, D., OLEYNIK, P., ULANOV, M., SVINKIN, D. AND CLINE, T.
≪Konus-wind and Konus-RF observations of GRB 090618.≫
GCN Circ., **9553**, p. 1 (2009a).

GOLENETSKII, S., APTEKAR, R., MAZETS, E., PAL'SHIN, V., FREDERIKS, D., OLEYNIK, P., ULANOV, M., SVINKIN, D. AND CLINE, T.
≪Konus-wind observation of bright short GRB 090227B.≫
GCN Circ., **8926**, p. 1 (2009b).

GOLENETSKII, S., APTEKAR, R., MAZETS, E., PAL'SHIN, V., FREDERIKS, D., OLEYNIK, P., ULANOV, M., SVINKIN, D. AND CLINE, T.
≪Konus-wind observation of GRB 091005.≫
GCN Circ., **9344**, p. 1 (2009c).

GOLENETSKII, S., APTEKAR, R., MAZETS, E., PAL'SHIN, V., FREDERIKS, D., OLEYNIK, P., ULANOV, M., SVINKIN, D., CLINE, T., YAMAOKA, K. ET AL.
≪IPN localization of short bright GRB 090227B.≫
GCN Circ., **8925**, p. 1 (2009d).

GOODMAN, J.
≪Are gamma-ray bursts optically thick?≫
ApJ, **308**, pp. L47–L50 (1986).

GORIELY, S., BAUSWEIN, A. AND JANKA, H.T.
«r-process Nucleosynthesis in Dynamically Ejected Matter of Neutron Star Mergers».
ApJ, **738**, p. L32 (2011a).

GORIELY, S., CHAMEL, N., JANKA, H.T. AND PEARSON, J.M.
«The decompression of the outer neutron star crust and r-process nucleosynthesis».
A&A, **531**, p. A78 (2011b).

GRANOT, J., PIRAN, T. AND SARI, R.
«Images and spectra from the interior of a relativistic fireball».
ApJ, **513**, pp. 679–689 (1999).

GRANOT, J. AND SARI, R.
«The Shape of Spectral Breaks in Gamma-Ray Burst Afterglows».
ApJ, **568**, pp. 820–829 (2002).

GREINER, J., KLOSE, S., SALVATO, M., ZEH, A., SCHWARZ, R., HARTMANN, D.H., MASETTI, N., STECKLUM, B., LAMER, G., LODIEU, N. ET AL.
«Grb 011121: A collimated outflow into wind-blown surroundings».
ApJ, **599**, pp. 1223–1237 (2003a).

GREINER, J., PEIMBERT, M., ESTABAN, C., KAUFER, A., JAUNSEN, A., SMOKE, J., KLOSE, S. AND REIMER, O.
«Redshift of GRB 030329.»
GCN Circ., **2020** (2003b).

GRIGORIAN, H., BLASCHKE, D. AND VOSKRESENSKY, D.
«Cooling of neutron stars with color superconducting quark cores».
Phys. Rev. C, **71(4)**, pp. 1–8 (2005).
ISSN 0556-2813.

GRUPE, D., GRONWALL, C., WANG, X.Y., ROMING, P.W.A., CUMMINGS, J., ZHANG, B., MÉSZÁROS, P., TRIGO, M.D., O'BRIEN, P.T., PAGE, K.L. ET AL.
«Swift and XMM-Newton Observations of the Extraordinary Gamma-Ray Burst 060729: More than 125 Days of X-Ray Afterglow».
ApJ, **662**, pp. 443–458 (2007a).

GRUPE, D., NOUSEK, J.A., VANDEN BERK, D.E., ROMING, P.W.A., BURROWS, D.N., GODET, O., OSBORNE, J. AND GEHRELS, N.
«Redshift Filtering by Swift Apparent X-Ray Column Density».
AJ, **133**, pp. 2216–2221 (2007b).

GRUZINOV, A. AND WAXMAN, E.
«Gamma-ray burst afterglow: Polarization and analytic light curves».

ApJ, **511**, pp. 852–861 (1999).

GUDMUNDSSON, E.H., PETHICK, C.J. AND EPSTEIN, R.I.
≪Structure of neutron star envelopes≫.
ApJ, **272**, p. 286 (1983).
ISSN 0004-637X.

GUETTA, D.
≪Short grbs: Rates and luminosity function implications≫.
ArXiv:astro-ph/0610408 (2006).

GUETTA, D. AND DELLA VALLE, M.
≪On the rates of gamma-ray bursts and type ib/c supernovae≫.
ApJ, **657**, pp. L73–L76 (2007).

GUETTA, D., PIAN, E. AND WAXMAN, E.
≪FERMI constraints on the high energy, ˜1 GeV, emission of long gamma ray bursts≫.
A&A, **525**, A53 (2011).

GUIDA, R., BERNARDINI, M.G., BIANCO, C.L., CAITO, L., DAINOTTI, M.G. AND RUFFINI, R.
In R.T. Jantzen, H. Kleinert and R. Ruffini (eds.), *The Eleventh Marcel Grossmann Meeting.* (Singapore: World Scientific, 2008a).

GUIDA, R., BERNARDINI, M.G., BIANCO, C.L., CAITO, L., DAINOTTI, M.G. AND RUFFINI, R.
≪The amati relation in the "fireshell" model≫.
A&A, **487**, pp. L37–L40 (2008b).

GUIDORZI, C., LACAPRA, M., FRONTERA, F., MONTANARI, E., AMATI, L., CALURA, F., NICASTRO, L. AND ORLANDINI, M.
≪Spectral catalogue of bright gamma-ray bursts detected with the BeppoSAX/GRBM≫.
A&A, **526**, p. A49 (2011).

GUIRIEC, S., BRIGGS, M.S., CONNAUGTHON, V., KARA, E., DAIGNE, F., KOUVELIOTOU, C., VAN DER HORST, A.J., PACIESAS, W., MEEGAN, C.A., BHAT, P.N. ET AL.
≪Time-resolved Spectroscopy of the Three Brightest and Hardest Short Gamma-ray Bursts Observed with the Fermi Gamma-ray Burst Monitor≫.
ApJ, **725**, pp. 225–241 (2010).

GUIRIEC, S., CONNAUGHTON, V. AND BRIGGS, M.
≪GRB 090510: Fermi GBM detection.≫
GCN Circ., **9336**, p. 1 (2009).

GUIRIEC, S., CONNAUGHTON, V., BRIGGS, M.S., BURGESS, M., RYDE, F., DAIGNE, F., MÉSZÁROS, P., GOLDSTEIN, A., MCENERY, J., OMODEI, N. ET AL.
≪Detection of a Thermal Spectral Component in the Prompt Emission of GRB 100724B≫.
ApJ, **727**, L33 (2011).

HJORTH, J., SOLLERMAN, J., GOROSABEL, J., GRANOT, J., KLOSE, S., KOUVELIOTOU, C., MELINDER, J., RAMIREZ-RUIZ, E., STARLING, R., THOMSEN, B. ET AL.
≪GRB 050509B: Constraints on Short Gamma-Ray Burst Models≫.
ApJ, **630**, pp. L117–L120 (2005).

HOLLAND, S.T. AND CUMMINGS, J.R.
≪GRB 110709B: Swift/UVOT observations.≫
GCN Circ., **12157**, p. 1 (2011).

HOVERSTEN, E.A., BARTHELMY, S.D., BURROWS, D.N., CHESTER, M.M., GRUPE, D., KENNEA, J.A., KRIMM, H.A., KUIN, N.P.M., PALMER, D.M. AND UKWATTA, T.N.
≪GRB 090510: Swift detection of a short hard burst.≫
GCN Circ., **9331**, p. 1 (2009).

IBEN, JR., I. AND TUTUKOV, A.V.
≪Supernovae of type I as end products of the evolution of binaries with components of moderate initial mass (M not greater than about 9 solar masses)≫.
ApJSS, **54**, pp. 335–372 (1984).

IMMLER, S., WILSON, A.S. AND TERASHIMA, Y.
≪X-Ray Emission from the Type Ic Supernova 1994I Observed with Chandra≫.
ApJ, **573**, pp. L27–L30 (2002).

INFANTE, L., GARNAVICH, P.M., STANEK, K.Z. AND WYRZYKOWSKI, L.
≪Grb011121: possible redshift, continued decay.≫
GCN Circ., **1152** (2001).

IWAMOTO, K., MAZZALI, P.A., NOMOTO, K., UMEDA, H., NAKAMURA, T., PATAT, F., DANZIGER, I.J., YOUNG, T.R., SUZUKI, T., SHIGEYAMA, T. ET AL.
≪A hypernova model for the supernova associated with the γ-ray burst of 25 april 1998≫.
Nature, **395**, pp. 672–674 (1998).

IZZO, L., BERNARDINI, M.G., BIANCO, C.L., CAITO, L., PATRICELLI, B. AND RUFFINI, R.

≪GRB 090423 at Redshift 8.1: a Theoretical Interpretation≫.
Journal of Korean Physical Society, **57**, p. 551 (2010).

IZZO, L., RUEDA, J.A. AND RUFFINI, R.
≪GRB 090618: a candidate for a neutron star gravitational collapse onto a black hole induced by a type Ib/c supernova≫.
A&A, **548**, L5 (2012a).

IZZO, L., RUFFINI, R., BIANCO, C.L., DERELI, H., MUCCINO, M., PENACCHIONI, A.V., PISANI, G. AND RUEDA, J.A.
≪On the thermal and double episode emissions in GRB 970828≫.
ArXiv:1205.6651 (2012b).

IZZO, L., RUFFINI, R., PENACCHIONI, A.V., BIANCO, C.L., CAITO, L., CHAKRABARTI, S.K., RUEDA, J.A., NANDI, A. AND PATRICELLI, B.
≪A double component in GRB 090618: a proto-black hole and a genuinely long gamma-ray burst≫.
In Izzo et al. (2012e), p. A10.

IZZO, L., RUFFINI, R., PENACCHIONI, A.V., BIANCO, C.L., CAITO, L., CHAKRABARTI, S.K., RUEDA, J.A., NANDI, A. AND PATRICELLI, B.
≪A double component in GRB 090618: a proto-black hole and a genuinely long gamma-ray burst≫.
In Izzo et al. (2012e), p. A10.

IZZO, L., RUFFINI, R., PENACCHIONI, A.V., BIANCO, C.L., CAITO, L., CHAKRABARTI, S.K., RUEDA, J.A., NANDI, A. AND PATRICELLI, B.
≪A double component in GRB 090618: a proto-black hole and a genuinely long gamma-ray burst≫.
A&A, **543**, A10 (2012e).

JIN, Z.P. AND FAN, Y.Z.
≪GRB 060418 and 060607A: the medium surrounding the progenitor and the weak reverse shock emission≫.
MNRAS, **378**, pp. 1043–1048 (2007).

KALBERLA, P.M.W., BURTON, W.B., HARTMANN, D., ARNAL, E.M., BAJAJA, E., MORRAS, R. AND PÖPPEL, W.G.L.
≪The Leiden/Argentine/Bonn (LAB) Survey of Galactic HI. Final data release of the combined LDS and IAR surveys with improved stray-radiation corrections≫.
A&A, **440**, pp. 775–782 (2005).

KANEKO, Y., GONZÁLEZ, M.M., PREECE, R.D., DINGUS, B.L. AND BRIGGS, M.S.
≪Broadband Spectral Properties of Bright High-Energy Gamma-Ray Bursts Observed with BATSE and EGRET≫.

ApJ, **677**, pp. 1168–1183 (2008).

KANEKO, Y., PREECE, R.D., BRIGGS, M.S., PACIESAS, W.S., MEEGAN, C.A. AND BAND, D.L.
«The Complete Spectral Catalog of Bright BATSE Gamma-Ray Bursts».
ApJSS, **166**, pp. 298–340 (2006).

KANEKO, Y., RAMIREZ-RUIZ, E., GRANOT, J., KOUVELIOTOU, C., WOOSLEY, S.E., PATEL, S.K., ROL, E., ZAND, J.J.M.I., VAN DER HORST, A.J., WIJERS, R.A.M.J. ET AL.
«Prompt and afterglow emission properties of gamma-ray bursts with spectroscopically identified supernovae».
ApJ, **654**, pp. 385–402 (2007).

KANN, D.A., KLOSE, S., ZHANG, B., MALESANI, D., NAKAR, E., POZANENKO, A., WILSON, A.C., BUTLER, N.R., JAKOBSSON, P., SCHULZE, S. ET AL.
«The Afterglows of Swift-era Gamma-ray Bursts. I. Comparing pre-Swift and Swift-era Long/Soft (Type II) GRB Optical Afterglows».
ApJ, **720**, pp. 1513–1558 (2010).

KANN, D.A., KLOSE, S., ZHANG, B., WILSON, A.C., BUTLER, N.R., MALESANI, D., NAKAR, E., ANTONELLI, L.A., CHINCARINI, G., COBB, B.E. ET AL.
«The afterglows of swift-era gamma-ray bursts. ii. short/hard (type i) vs. long/soft (type ii) optical afterglows».
ArXiv:0804.1959 (2008a).

KANN, D.A., MASETTI, N. AND KLOSE, S.
«The Prompt Optical/Near-Infrared Flare of GRB 050904: The Most Luminous Transient Ever Detected».
AJ, **133**, pp. 1187–1192 (2007).

KANN, D.A., SCHULZE, S. AND UPDIKE, A.C.
«GRB 080319B: jet break, energetics, supernova.»
GCN Circ., **7627**, p. 1 (2008b).

KANN, D.A., STECKLUM, B. AND HOEGNER, C.
«GRB 130427A: Tautenburg 2nd epoch: No break, no clear SN».
GCN Circ., **14631**, p. 1 (2013).

KATZ, J.I.
«Delayed hard photons from gamma-ray bursts».
ApJ, **432**, pp. L27–L29 (1994a).

KATZ, J.I.
«Two populations and models of gamma-ray bursts».

ApJ, **422**, pp. 248–259 (1994b).

KAWAI, N., YAMADA, T., KOSUGI, G., HATTORI, T. AND AOKI, K.
«Grb 050904: Subaru optical spectroscopy.»
GCN Circ., **3937** (2005).

KELSON, D. AND BERGER, E.
«Grb 050315: absorption redshift.»
GCN Circ., **3101** (2005).

KENNEA, J.A., BURROWS, D.N., CUSUMANO, G. AND TAGLIAFERRI, G.
«Subject: Grb 060218: Swift xrt position.»
GCN Circ., **4776** (2006).

KIM, S., STAVELEY-SMITH, L., SAULT, R.J., KESTEVEN, M.J., MCCONNELL, D., DOPITA, M.A. AND BESSELL, M.
«HI supergiant shells in the Large Magellanic Cloud».
Pub. Astron. Soc. Austr., **15**, pp. 132–35 (1998).

KLEBESADEL, R.W.
«The durations of gamma-ray bursts».
In C. Ho, R.I. Epstein and E.E. Fenimore (eds.), *Gamma-Ray Bursts - Observations, Analyses and Theories*, pp. 161–168 (Cambridge University Press, 1992).

KLEBESADEL, R.W., STRONG, I.B. AND OLSON, R.A.
«Observations of Gamma-Ray Bursts of Cosmic Origin».
ApJ, **182**, p. L85 (1973).

KONO, K., DAIKYUJI, A., SONODA, E., OHMORI, N., HAYASHI, H., NODA, K., NISHIOKA, Y., YAMAUCHI, M., OHNO, M., SUZUKI, M. ET AL.
«GRB 090618: Suzaku WAM observation of the prompt emission.»
GCN Circ., **9568**, p. 1 (2009).

KOPAČ, D., D'AVANZO, P., MELANDRI, A., CAMPANA, S., GOMBOC, A., JAPELJ, J., BERNARDINI, M.G., COVINO, S., VERGANI, S.D., SALVATERRA, R. ET AL.
«On the environment of short gamma-ray bursts».
MNRAS, **424**, pp. 2392–2399 (2012).

KOTOV, Y., KOCHEMASOV, A., KUZIN, S., KUZNETSOV, V., SYLWESTER, J. AND YUROV, V.
«Set of instruments for solar EUV and soft X-ray monitoring onboard satellite Coronas-Photon».
In *37th COSPAR Scientific Assembly*, volume 37 of *COSPAR Meeting*, p. 1596 (2008).

KOUVELIOTOU, C., MEEGAN, C.A., FISHMAN, G.J., BHAT, N.P., BRIGGS, M.S., KOSHUT, T.M., PACIESAS, W.S. AND PENDLETON, G.N.
«Identification of two classes of gamma-ray bursts».
ApJ, **413**, pp. L101–L104 (1993).

KOUVELIOTOU, C., WOOSLEY, S.E., PATEL, S.K., LEVAN, A., BLANDFORD, R., RAMIREZ-RUIZ, E., WIJERS, R.A.M.J., WEISSKOPF, M.C., TENNANT, A., PIAN, E. ET AL.
«Chandra observations of the x-ray environs of sn 1998bw/grb 980425».
ApJ, **608**, pp. 872–882 (2004).

KRAMER, M.
In R.T. Jantzen, H. Kleinert and R. Ruffini (eds.), *The Eleventh Marcel Grossmann Meeting* (Singapore: World Scientific, 2008).

KUMAR, P.
«Gamma-Ray Burst Energetics».
ApJ, **523**, pp. L113–L116 (1999).

KUMAR, P. AND MCMAHON, E.
«A general scheme for modelling γ-ray burst prompt emission».
MNRAS, **384**, pp. 33–63 (2008).

KUMAR, P. AND NARAYAN, R.
«GRB 080319B: evidence for relativistic turbulence, not internal shocks».
MNRAS, **395**, pp. 472–489 (2009).

KUMAR, P. AND PANAITESCU, A.
«What did we learn from gamma-ray burst 080319B?»
MNRAS, **391**, pp. L19–L23 (2008).

LARSSON, J., RYDE, F., LUNDMAN, C., MCGLYNN, S., LARSSON, S., OHNO, M. AND YAMAOKA, K.
«Spectral components in the bright, long GRB 061007: properties of the photosphere and the nature of the outflow».
MNRAS, **414**, pp. 2642–2649 (2011).

LATTIMER, J.M., VAN RIPER, K.A., PRAKASH, M. AND PRAKASH, M.
«Rapid cooling and the structure of neutron stars».
ApJ, **425**, pp. 802–813 (1994).

LAZZATI, D. AND BEGELMAN, M.C.
«Non-thermal Emission from the Photospheres of Gamma-ray Burst Outflows. I. High-Frequency Tails».
ApJ, **725**, pp. 1137–1145 (2010).

LAZZATI, D., CAMPANA, S. AND GHISELLINI, G.
«Iron line in the afterglow: a key to unveil gamma-ray burst progenitors».
MNRAS, **304**, pp. L31–L35 (1999).

LAZZATI, D., GHISELLINI, G., CELOTTI, A. AND REES, M.J.
«Compton-dragged Gamma-Ray Bursts Associated with Supernovae».
ApJ, **529**, pp. L17–L20 (2000).

LEDOUX, C., VREESWIJK, P., SMETTE, A., JAUNSEN, A. AND KAUFER, A.
«VLT/UVES observations of GRB 060607.»
GCN Circ., **5237** (2006).

LEVAN, A.J., FRUCHTER, A.S., GRAHAM, J., TANVIR, N.R., HJORTH, J., FYNBO, J., PERLEY, D., CENKO, S.B., PIAN, E., CANO, Z. ET AL.
«Grb 130427a / sn 2013cq: Hubble space telescope observations».
GCN Circ., **14686**, p. 1 (2013).

LEVAN, A.J., WARWICK, U., PERLEY, D. AND D'AVANZO, P.
«GRB 101023A: Gemini discovery of optical afterglow.»
GCN Circ., **11366**, p. 1 (2010).

LEWIS, A.D., BUOTE, D.A. AND STOCKE, J.T.
«Chandra observations of a2029: The dark matter profile down to below $0.01r_{vir}$ in an unusually relaxed cluster».
ApJ, **586**, pp. 135–142 (2003).

LI, L.X.
«Shock breakout in type ibc supernovae and application to grb 060218/sn 2006aj».
MNRAS, **375**, pp. 240–256 (2007).

LIANG, E., ZHANG, B., VIRGILI, F. AND DAI, Z.G.
«Low-luminosity gamma-ray bursts as a unique population: Luminosity function, local rate, and beaming factor».
ApJ, **662**, pp. 1111–1118 (2007).

LIANG, E.W., ZHANG, B., O'BRIEN, P.T., WILLINGALE, R., ANGELINI, L., BURROWS, D.N., CAMPANA, S., CHINCARINI, G., FALCONE, A., GEHRELS, N. ET AL.
«Testing the curvature effect and internal origin of gamma-ray burst prompt emissions and x-ray flares with swift data».
ApJ, **646**, pp. 351–357 (2006a).

LIANG, E.W., ZHANG, B.B., STAMATIKOS, M., ZHANG, B., NORRIS, J., GEHRELS, N., ZHANG, J. AND DAI, Z.G.
«Temporal profiles and spectral lags of xrf 060218».
ApJ, **653**, pp. L81–L84 (2006b).

LOCKMAN, F.J.
«Discovery of a Population of H I Clouds in the Galactic Halo».
ApJ, **580**, pp. L47–L50 (2002).

LONGO, F., MORETTI, E., BARBIELLINI, G., VALLAZZA, E., GIULIANI, A., CUTINI, S., PITTORI, C., MARISALDI, M., BULGARELLI, A., GIANOTTI, F. ET AL.
«AGILE detection of GRB 090510.»
GCN Circ., **9343**, p. 1 (2009a).

LONGO, F., MORETTI, E., BARBIELLINI, G., VALLAZZA, E., TRIFOGLIO, M., BULGARELLI, A., GIANOTTI, F., FUSCHINO, F., MARISALDI, M., LABANTI, C. ET AL.
«GRB 090618: AGILE observations.»
GCN Circ., **9524** (2009b).

LYUTIKOV, M. AND BLANDFORD, R.
«Gamma Ray Bursts as Electromagnetic Outflows».
arXiv:astro-ph/0312347 (2003).

MAEDA, K., KAWABATA, K., TANAKA, M., NOMOTO, K., TOMINAGA, N., HATTORI, T., MINEZAKI, T., KURODA, T., SUZUKI, T., DENG, J. ET AL.
«Sn 2006aj associated with xrf 060218 at late phases: Nucleosynthesis signature of a neutron star-driven explosion».
ApJ, **658**, pp. L5–L8 (2007).

MANGANO, V., HOLLAND, S.T., MALESANI, D., TROJA, E., CHINCARINI, G., ZHANG, B., LA PAROLA, V., BROWN, P.J., BURROWS, D.N., CAMPANA, S. ET AL.
«Swift observations of grb 060614: an anomalous burst with a well behaved afterglow».
A&A, **470**, pp. 105–118 (2007).

MANNUCCI, F., DELLA VALLE, M., PANAGIA, N., CAPPELLARO, E., CRESCI, G., MAIOLINO, R., PETROSIAN, A. AND TURATTO, M.
«The supernova rate per unit mass».
A&A, **433**, pp. 807–814 (2005).

MARGUTTI, R., BERNARDINI, M.G., BARNIOL DURAN, R., GUIDORZI, C., SHEN, R.F. AND CHINCARINI, G.
«On the average gamma-ray burst X-ray flaring activity».
MNRAS, **410**, pp. 1064–1075 (2011a).

MARGUTTI, R., CHINCARINI, G., GRANOT, J., GUIDORZI, C., BERGER, E., BERNARDINI, M.G., GEHRELS, N., SODERBERG, A.M., STAMATIKOS, M. AND ZANINONI, E.

«X-ray flare candidates in short gamma-ray bursts».
MNRAS, **417**, pp. 2144–2160 (2011b).

MARGUTTI, R., GUIDORZI, C., CHINCARINI, G., PASOTTI, F., COVINO, S. AND MAO, J.
«Temporal variability of GRB early X-ray afterglows and GRB080319B prompt emission».
In Y.F. Huang, Z.G. Dai and B. Zhang (eds.), *2008 Nanjing Gamma-Ray Burst Conference*, volume 1065 of *American Institute of Physics Conference Series*, pp. 259–262 (2008).

MARGUTTI, R., ZANINONI, E., BERNARDINI, M.G., CHINCARINI, G., PASOTTI, F., GUIDORZI, C., ANGELINI, L., BURROWS, D.N., CAPALBI, M., EVANS, P.A. ET AL.
«The prompt-afterglow connection in gamma-ray bursts: a comprehensive statistical analysis of Swift X-ray light curves».
MNRAS, **428**, pp. 729–742 (2013).

MAZZALI, P.
talk presented at the congress "Swift and GRBs: unveiling the relativistic universe", Venice, Italy, June 5-9 (2006).

MAZZALI, P.A., DENG, J., NOMOTO, K., SAUER, D.N., PIAN, E., TOMINAGA, N., TANAKA, M., MAEDA, K. AND FILIPPENKO, A.V.
«A neutron-star-driven x-ray flash associated with supernova sn 2006aj».
Nature, **442**, pp. 1018–1020 (2006).

MCBREEN, S.
«GRB 090618: Fermi GBM observation.»
GCN Circ., **9535** (2009).

MEDVEDEV, M.V.
«Theory of "Jitter" Radiation from Small-Scale Random Magnetic Fields and Prompt Emission from Gamma-Ray Burst Shocks».
ApJ, **540**, pp. 704–714 (2000).

MEDVEDEV, M.V. AND LOEB, A.
«Generation of Magnetic Fields in the Relativistic Shock of Gamma-Ray Burst Sources».
ApJ, **526**, pp. 697–706 (1999).

MEDVEDEV, M.V. AND SPITKOVSKY, A.
«Radiative Cooling in Relativistic Collisionless Shocks: Can Simulations and Experiments Probe Relevant Gamma-ray Burst Physics?»
ApJ, **700**, pp. 956–964 (2009).

MEEGAN, C., LICHTI, G., BHAT, P.N., BISSALDI, E., BRIGGS, M.S., CONNAUGHTON, V., DIEHL, R., FISHMAN, G., GREINER, J., HOOVER, A.S. ET AL.
«The Fermi Gamma-ray Burst Monitor».
ApJ, **702**, pp. 791–804 (2009).

MEEGAN, C.A.
«The BATSE Catalog of Gamma-Ray Bursts».
NASA STI/Recon Technical Report N, **1**, p. 70758 (1997).

MEEGAN, C.A., FISHMAN, G.J., WILSON, R.B., HORACK, J.M., BROCK, M.N., PACIESAS, W.S., PENDLETON, G.N. AND KOUVELIOTOU, C.
«Spatial distribution of gamma-ray bursts observed by BATSE».
Nature, **355**, pp. 143–145 (1992).

MEREGHETTI, S. AND GOTZ, D.
«Grb 031203: further analysis of integral data.»
GCN Circ., **2460** (2003).

MÉSZÁROS, P.
«Theories of gamma-ray bursts».
ARAA, **40**, pp. 137–169 (2002).

MESZAROS, P.
«Gamma-ray bursts.»
Reports of Progress in Physics, **69**, pp. 2259–2322 (2006).

MESZAROS, P., LAGUNA, P. AND REES, M.J.
«Gasdynamics of relativistically expanding gamma-ray burst sources - kinematics, energetics, magnetic fields, and efficiency».
ApJ, **415**, pp. 181–190 (1993).

MÉSZÁROS, P., RAMIREZ-RUIZ, E., REES, M.J. AND ZHANG, B.
«X-Ray-rich Gamma-Ray Bursts, Photospheres, and Variability».
ApJ, **578**, pp. 812–817 (2002).

MESZAROS, P. AND REES, M.J.
«Relativistic fireballs and their impact on external matter - Models for cosmological gamma-ray bursts».
ApJ, **405**, pp. 278–284 (1993).

MESZAROS, P. AND REES, M.J.
«Optical and Long-Wavelength Afterglow from Gamma-Ray Bursts».
ApJ, **476**, pp. 232–237 (1997a).

MESZAROS, P. AND REES, M.J.
«Poynting Jets from Black Holes and Cosmological Gamma-Ray Bursts».
ApJ, **482**, p. L29 (1997b).

MÉSZÁROS, P. AND REES, M.J.
≪Steep Slopes and Preferred Breaks in Gamma-Ray Burst Spectra: The Role of Photospheres and Comptonization≫.
ApJ, **530**, pp. 292–298 (2000).

METZGER, M.R., DJORGOVSKI, S.G., KULKARNI, S.R., STEIDEL, C.C., ADELBERGER, K.L., FRAIL, D.A., COSTA, E. AND FRONTERA, F.
≪Spectral constraints on the redshift of the optical counterpart to the γ-ray burst of 8 May 1997≫.
Nature, **387**, pp. 878–880 (1997).

MIRABAL, N., HALPERN, J.P., AN, D., THORSTENSEN, J.R. AND TERNDRUP, D.M.
≪Grb 060218/sn 2006aj: A gamma-ray burst and prompt supernova at z = 0.0335≫.
ApJ, **643**, pp. L99–L102 (2006).

MODJAZ, M., STANEK, K.Z., GARNAVICH, P.M., BERLIND, P., BLONDIN, S., BROWN, W., CALKINS, M., CHALLIS, P., DIAMOND-STANIC, A.M., HAO, H. ET AL.
≪Early-time photometry and spectroscopy of the fast evolving sn 2006aj associated with grb 060218≫.
ApJ, **645**, pp. L21–L24 (2006).

MOLINARI, E., VERGANI, S.D., MALESANI, D., COVINO, S., D'AVANZO, P., CHINCARINI, G., ZERBI, F.M., ANTONELLI, L.A., CONCONI, P., TESTA, V. ET AL.
≪REM observations of GRB 060418 and GRB 060607A: the onset of the afterglow and the initial fireball Lorentz factor determination≫.
A&A, **469**, pp. L13–L16 (2007).

MORRISON, R. AND MCCAMMON, D.
≪Interstellar photoelectric absorption cross sections, 0.03-10 keV≫.
ApJ, **270**, pp. 119–122 (1983).

MUCCINO, M., RUFFINI, R., BIANCO, C.L., IZZO, L. AND PENACCHIONI, A.V.
≪GRB 090227B: The Missing Link between the Genuine Short and Long Gamma-Ray Bursts≫.
ApJ, **763**, 125 (2013).

NAKAR, E. AND GRANOT, J.
≪Smooth light curves from a bumpy ride: relativistic blast wave encounters a density jump≫.
MNRAS, **380**, pp. 1744–1760 (2007).

NANDI, A., RAO, A.R., CHAKRABARTI, S.K., MALKAR, J.P., SREEKUMAR, S., DEBNATH, D., HINGAR, M.K., KOTOCH, T., KOTOVK, Y. AND ARKHANGELSKIY, A.
«Indian Payloads (RT-2 Experiment) Onboard CORONAS-PHOTON Mission».
ArXiv:0912.4126 (2009).

NEGREIROS, R., RUFFINI, R., BIANCO, C.L. AND RUEDA, J.A.
«Cooling of young neutron stars in GRB associated to supernovae».
A&A, **540**, A12 (2012).

NEGREIROS, R., DEXHEIMER, V. AND SCHRAMM, S.
«Modeling hybrid stars with an SU(3) nonlinear σ model».
Phys. Rev. C, **82(3)**, pp. 1–9 (2010).
ISSN 0556-2813.

NOMOTO, K., TOMINAGA, N., TANAKA, M., MAEDA, K., SUZUKI, T., DENG, J.S. AND MAZZALI, P.A.
«Diversity of the supernova - gamma-ray burst connection».
ArXiv:astro-ph/0702472 (2007).

NORRIS, J.P. AND BONNELL, J.T.
«Short gamma-ray bursts with extended emission».
ApJ, **643**, pp. 266–275 (2006).

NORRIS, J.P., NEMIROFF, R.J., BONNELL, J.T., SCARGLE, J.D., KOUVELIOTOU, C., PACIESAS, W.S., MEEGAN, C.A. AND FISHMAN, G.J.
«Attributes of Pulses in Long Bright Gamma-Ray Bursts».
ApJ, **459**, pp. 393–412 (1996).

NOUSEK, J.A.
«Swift Gamma-Ray Burst Explorer: The First Results».
Chinese Journal of Astronomy and Astrophysics Supplement, **6(1)**, pp. 010000–360 (2006).

NOUSEK, J.A., KOUVELIOTOU, C., GRUPE, D., PAGE, K.L., GRANOT, J., RAMIREZ-RUIZ, E., PATEL, S.K., BURROWS, D.N., MANGANO, V., BARTHELMY, S. ET AL.
«Evidence for a canonical gamma-ray burst afterglow light curve in the swift xrt data».
ApJ, **642**, pp. 389–400 (2006).

OHMORI, N., AKIYAMA, M., YAMAUCHI, M., OHNO, M., HANABATA, Y., UEHARA, T., TAKAHASHI, T., MIZUNO, M., FUKAZAWA, Y., YAMAOKA, K. ET AL.
«GRB 110709B : Suzaku WAM observation of the prompt emission.»
GCN Circ., **12172**, p. 1 (2011).

OHMORI, N., NODA, K., SONODA, E., YAMAUCHI, M., KONO, K., HAYASHI, H., DAIKYUJI, A., NISHIOKA, Y., OHNO, M., SUZUKI, M. ET AL.
«GRB 090510: Suzaku WAM observation of the prompt emission.»
GCN Circ., **9355**, p. 1 (2009).

OHNO, M. AND PELASSA, V.
«Fermi LAT detection of GRB 090510.»
GCN Circ., **9334**, p. 1 (2009).

OLOFSSON, G., ERGON, M., MALESANI, D., FYNBO, J.P.U., JAKOBSSON, P., TANVIR, N.R., WIERSEMA, K. AND LEVAN, A.J.
«GRB 090510: NOT afterglow confirmation.»
GCN Circ., **9338**, p. 1 (2009).

PACIESAS, W.S., MEEGAN, C.A., PENDLETON, G.N., BRIGGS, M.S., KOUVELIOTOU, C., KOSHUT, T.M., LESTRADE, J.P., MCCOLLOUGH, M.L., BRAINERD, J.J., HAKKILA, J. ET AL.
«The fourth batse gamma-ray burst catalog (revised)».
ApJSS, **122**, pp. 465–495 (1999).

PACZYNSKI, B.
«Evolution of cataclysmic binaries».
In D. Lamb and J. Patterson (eds.), *Cataclysmic Variables and Low-Mass X-ray Binaries*, volume 113 of *Astrophysics and Space Science Library*, pp. 1–12 (1985).

PACZYNSKI, B.
«Gamma-ray bursters at cosmological distances».
ApJ, **308**, pp. L43–L46 (1986).

PACZYNSKI, B.
«Are gamma-ray bursts in star-forming regions?»
ApJ, **494**, p. L45 (1998).

PAGE, D., GEPPERT, U. AND WEBER, F.
«The cooling of compact stars».
Nuclear Physics A, **777**, pp. 497–530 (2006).
ISSN 03759474.

PAGE, D., LATTIMER, J., PRAKASH, M. AND STEINER, A.W.
«Minimal Cooling of Neutron Stars: A New Paradigm».
ApJSS, **155(2)**, pp. 623–650 (2004).
ISSN 0067-0049.

PAGE, D., LATTIMER, J., PRAKASH, M. AND STEINER, A.W.

«Neutrino Emission From Cooper Pairs and Minimal Cooling of Neutron Stars».
ApJ, **707(2)**, pp. 1131–1140 (2009).
ISSN 0004-637X.

PAGE, D., PRAKASH, M., LATTIMER, J.M. AND STEINER, A.W.
«Rapid Cooling of the Neutron Star in Cassiopeia A Triggered by Neutron Superfluidity in Dense Matter».
Phys. Rev. Lett., **106(8)**, p. 081101 (2011a).

PAGE, K., GOAD, M. AND BEARDMORE, A.
«GRB 060607: Swift-XRT team refined analysis.»
GCN Circ., **5240** (2006a).

PAGE, K.L. AND SAXTON, C.J.
«GRB 101023A: Swift-XRT team refined analysis.»
GCN Circ., **11368**, p. 1 (2010).

PAGE, K.L., STARLING, R.L.C., FITZPATRICK, G., PANDEY, S.B., OSBORNE, J.P., SCHADY, P., MCBREEN, S., CAMPANA, S., UKWATTA, T.N., PAGANI, C. ET AL.
«GRB 090618: detection of thermal X-ray emission from a bright gamma-ray burst».
MNRAS, **416**, pp. 2078–2089 (2011b).

PAGE, K.L., STARLING, R.L.C., OSBORNE, J.P., TROJA, E. AND MORRIS, D.
«GRB 061121: Swift-XRT team refined analysis.»
GCN Circ., **5832** (2006b).

PAGE, K.L., WILLINGALE, R., OSBORNE, J.P., ZHANG, B., GODET, O., MARSHALL, F.E., MELANDRI, A., NORRIS, J.P., O'BRIEN, P.T., PAL'SHIN, V. ET AL.
«GRB 061121: Broadband Spectral Evolution through the Prompt and Afterglow Phases of a Bright Burst».
ApJ, **663**, pp. 1125–1138 (2007).

PAKMOR, R., KROMER, M., RÖPKE, F.K., SIM, S.A., RUITER, A.J. AND HILLEBRANDT, W.
«Sub-luminous type Ia supernovae from the mergers of equal-mass white dwarfs with mass $\sim 0.9 M_{solar}$».
Nature, **463**, pp. 61–64 (2010).

PANAITESCU, A.
«The energetics and environment of the short-grb afterglows 050709 and 050724».
MNRAS, **367**, pp. L42–L46 (2006).

PANAITESCU, A. AND MESZAROS, P.
«Rings in fireball afterglows».
ApJ, **493**, p. L31 (1998).

PANAITESCU, A. AND MÉSZÁROS, P.
«Dynamical evolution, light curves, and spectra of spherical and collimated gamma-ray burst remnants».
ApJ, **526**, pp. 707–715 (1999).

PANAITESCU, A. AND MÉSZÁROS, P.
«Gamma-Ray Bursts from Upscattered Self-absorbed Synchrotron Emission».
ApJ, **544**, pp. L17–L21 (2000).

PANAITESCU, A., MÉSZÁROS, P., GEHRELS, N., BURROWS, D. AND NOUSEK, J.
«Analysis of the x-ray emission of nine swift afterglows».
MNRAS, **366**, pp. 1357–1366 (2006).

PANAITESCU, A., MESZAROS, P. AND REES, M.J.
«Multiwavelength Afterglows in Gamma-Ray Bursts: Refreshed Shock and Jet Effects».
ApJ, **503**, pp. 314–+ (1998).

PARSONS, A., BARTHELMY, S., BARBIER, L., CUMMINGS, J., FENIMORE, E., FINK, R., GEHRELS, N., HOLLAND, S., HULLINGER, D., HURLEY, K. ET AL.
«Swift-bat detection of grb 050315.»
GCN Circ., **3094** (2005).

PASTORELLO, A., DELLA VALLE, M., SMARTT, S.J., ZAMPIERI, L., BENETTI, S., CAPPELLARO, E., MAZZALI, P.A., PATAT, F., SPIRO, S., TURATTO, M. ET AL.
«A very faint core-collapse supernova in M85».
Nature, **449** (2007).

PATNAUDE, D., LOEB, A. AND JONES, C.
«Evidence for a possible black hole remnant in the Type IIL Supernova 1979C».
New Astronomy, **16(3)**, pp. 187–190 (2011).
ISSN 13841076.

PATRICELLI, B., BERNARDINI, M.G., BIANCO, C.L., CAITO, L., DE BARROS, G., IZZO, L., RUFFINI, R. AND VERESHCHAGIN, G.V.
«Analysis of GRB 080319B and GRB 050904 within the Fireshell Model: Evidence for a Broader Spectral Energy Distribution».
ApJ, **756**, 16 (2012).

PATRICELLI, B., BERNARDINI, M.G., BIANCO, C.L., CAITO, L., IZZO, L., RUFFINI, R. AND VERESHCHAGIN, G.
«A New Spectral Energy Distribution of Photons in the Fireshell Model of GRBS».
IJMPD, **20**, pp. 1983–1987 (2011).

PE'ER, A.
«Temporal Evolution of Thermal Emission from Relativistically Expanding Plasma».
ApJ, **682**, pp. 463–473 (2008).

PE'ER, A., MÉSZÁROS, P. AND REES, M.J.
«Peak Energy Clustering and Efficiency in Compact Objects».
ApJ, **635**, pp. 476–480 (2005).

PE'ER, A., MÉSZÁROS, P. AND REES, M.J.
«The Observable Effects of a Photospheric Component on GRB and XRF Prompt Emission Spectrum».
ApJ, **642**, pp. 995–1003 (2006).

PE'ER, A. AND RYDE, F.
«A Theory of Multicolor Blackbody Emission from Relativistically Expanding Plasmas».
ApJ, **732**, p. 49 (2011).

PE'ER, A., RYDE, F., WIJERS, R.A.M.J., MÉSZÁROS, P. AND REES, M.J.
«A New Method of Determining the Initial Size and Lorentz Factor of Gamma-Ray Burst Fireballs Using a Thermal Emission Component».
ApJ, **664**, pp. L1–L4 (2007).

PE'ER, A. AND ZHANG, B.
«Synchrotron Emission in Small-Scale Magnetic Fields as a Possible Explanation for Prompt Emission Spectra of Gamma-Ray Bursts».
ApJ, **653**, pp. 454–461 (2006).

PE'ER, A., ZHANG, B.B., RYDE, F., MCGLYNN, S., ZHANG, B., PREECE, R.D. AND KOUVELIOTOU, C.
«The connection between thermal and non-thermal emission in gamma-ray bursts: general considerations and GRB 090902B as a case study».
MNRAS, **420**, pp. 468–482 (2012).

PÉLANGEON, A., ATTEIA, J.L., LAMB, D.Q. AND HETE-2 SCIENCE TEAM.
«An improved redshift indicator for Gamma-Ray Bursts, based on the prompt emission».
In S.S. Holt, N. Gehrels and J.A. Nousek (eds.), *Gamma-Ray Bursts in the Swift Era*, volume 836 of *American Institute of Physics Conference Series*, pp. 149–152 (2006).

PÉLANGEON, A., ATTEIA, J.L., NAKAGAWA, Y.E., HURLEY, K., YOSHIDA, A., VANDERSPEK, R., SUZUKI, M., KAWAI, N., PIZZICHINI, G., BOËR, M. ET AL.
≪Intrinsic properties of a complete sample of HETE-2 gamma-ray bursts. A measure of the GRB rate in the Local Universe≫.
A&A, **491**, pp. 157–171 (2008).

PENACCHIONI, A.V., RUFFINI, R., BIANCO, C.L., IZZO, L., MUCCINO, M., PISANI, G.B. AND RUEDA, J.A.
≪GRB 110709B in the induced gravitational collapse paradigm≫.
A&A, **551**, A133 (2013).

PENACCHIONI, A.V., RUFFINI, R., IZZO, L., MUCCINO, M., BIANCO, C.L., CAITO, L., PATRICELLI, B. AND AMATI, L.
≪Evidence for a proto-black hole and a double astrophysical component in GRB 101023≫.
A&A, **538**, A58 (2012).

PENG, Z.Y., YIN, Y., BI, X.W., BAO, Y.Y. AND MA, L.
≪Spectral lag of gamma-ray bursts caused by the intrinsic spectral evolution and the curvature effect≫.
Astronomische Nachrichten, **332**, p. 92 (2011).

PERLEY, D.A. AND TANG, S.
≪GRB 130427A: Keck/LRIS Observations≫.
GCN Circ., **14615**, p. 1 (2013).

PIAN, E., AMATI, L., ANTONELLI, L.A., BUTLER, R.C., COSTA, E., CUSUMANO, G., DANZIGER, J., FEROCI, M., FIORE, F., FRONTERA, F. ET AL.
≪Bepposax observations of grb 980425: Detection of the prompt event and monitoring of the error box≫.
ApJ, **536**, pp. 778–787 (2000).

PIAN, E., GIOMMI, P., AMATI, L., COSTA, E., DANZIGER, J., FEROCI, M., FIOCCHI, M.T., FRONTERA, F., KOUVELIOTOU, C., MASETTI, N. ET AL.
≪Xmm-newton observations of the field of γ-ray burst 980425≫.
Advances in Space Research, **34**, pp. 2711–2714 (2004).

PIAN, E., MAZZALI, P.A., MASETTI, N., FERRERO, P., KLOSE, S., PALAZZI, E., RAMIREZ-RUIZ, E., WOOSLEY, S.E., KOUVELIOTOU, C., DENG, J. ET AL.
≪An optical supernova associated with the x-ray flash xrf 060218≫.
Nature, **442**, pp. 1011–1013 (2006).

PIAN, E. ET AL.

Proposal for Chandra Observations: The X-Ray Remnant of XRF100316D/SN2010BH (2011).

PIRAN, T.
«Gamma-ray bursts and the fireball model».
Phys. Rep., **314**, pp. 575–667 (1999).

PIRAN, T.
«The physics of gamma-ray bursts».
Reviews of Modern Physics, **76**, pp. 1143–1210 (2004).

PIRAN, T.
«The physics of gamma-ray bursts».
Reviews of Modern Physics, **76**, pp. 1143–1210 (2005).

PIRAN, T.
«Gamma-Ray Bursts as Relativistic Objects».
In *Twelfth Marcel Grossmann Meeting on General Relativity*, p. 269 (2012).

PIRAN, T., SARI, R. AND ZOU, Y.C.
«Observational Limits on Inverse Compton Processes in GRBs».
ArXiv:0807.3954 (2008).

PIRAN, T., SARI, R. AND ZOU, Y.
«Observational limits on inverse Compton processes in gamma-ray bursts».
MNRAS, **393**, pp. 1107–1113 (2009).

PIRAN, T., SHEMI, A. AND NARAYAN, R.
«Hydrodynamics of relativistic fireballs».
MNRAS, **263**, p. 861 (1993).

PIRANOMONTE, S., D'AVANZO, P., COVINO, S., ANTONELLI, L.A., BEARDMORE, A.P., CAMPANA, S., CHINCARINI, G., D'ELIA, V., DELLA VALLE, M., FIORE, F. ET AL.
«The short GRB 070707 afterglow and its very faint host galaxy».
A&A, **491**, pp. 183–188 (2008).

PIRO, L.
«Astrophysics: Short-burst sources».
Nature, **437**, pp. 822–823 (2005).

PIRO, L., DE PASQUALE, M., SOFFITTA, P., LAZZATI, D., AMATI, L., COSTA, E., FEROCI, M., FRONTERA, F., GUIDORZI, C., IN'T ZAND, J.M.J. ET AL.
«Probing the environment in gamma-ray bursts: The case of an x-ray precursor, afterglow late onset, and wind versus constant density profile in grb 011121 and grb 011211».
ApJ, **623**, pp. 314–324 (2005).

PIRO, L., GARMIRE, G., GARCIA, M.R., ANTONELLI, L.A., COSTA, E., FEROCI, M., FRAIL, D.A., HARRISON, F., HURLEY, K., MÉSZÁROS, P. ET AL.
«The X-Ray Afterglow of GRB 000926 Observed by BeppoSAX and Chandra: A Mildly Collimated Fireball in a Dense Medium?»
ApJ, **558**, pp. 442–447 (2001).

PISANI, G.B., IZZO, L., RUFFINI, R., BIANCO, C.L., MUCCINO, M., PENACCHIONI, A.V., RUEDA, J.A. AND WANG, Y.
«Novel distance indicator for gamma-ray bursts associated with supernovae».
A&A, **552**, L5 (2013).

POPOV, V.
«From super-charged nuclei to massive nuclear density cores».
In R. Ruffini and G. Vereshchagin (eds.), *The Sun, the stars, the universe and general relativity*, volume 1205 of *American Institute of Physics Conference Series*, pp. 127–131 (2010).

POTEKHIN, A.Y., CHABRIER, G. AND YAKOVLEV, D.G.
«Internal temperatures and cooling of neutron stars with accreted envelopes».
A&A, **323**, pp. 415–428 (1997).

POZDNIAKOV, L.A., SOBOL, I.M. AND SYUNYAEV, R.A.
«Comptonization and the shaping of x-ray source spectra - monte carlo calculations».
Astrophysics and Space Physics Reviews, **2**, pp. 189–331 (1983).

PRAKASH, M., LATTIMER, J., PONS, J., STEINER, A. AND REDDY, S.
«Evolution of a neutron star from its birth to old age».
Physics of Neutron Star Interiors, pp. 364–423 (2001).

PREECE, R.D., BRIGGS, M.S., GIBLIN, T.W., MALLOZZI, R.S., PENDLETON, G.N., PACIESAS, W.S. AND BAND, D.L.
«On the Consistency of Gamma-Ray Burst Spectral Indices with the Synchrotron Shock Model».
ApJ, **581**, pp. 1248–1255 (2002).

PREECE, R.D., BRIGGS, M.S., MALLOZZI, R.S., PENDLETON, G.N., PACIESAS, W.S. AND BAND, D.L.
«The BATSE Gamma-Ray Burst Spectral Catalog. I. High Time Resolution Spectroscopy of Bright Bursts Using High Energy Resolution Data».
ApJSS, **126**, pp. 19–36 (2000).

PREECE, R.D., PENDLETON, G.N., BRIGGS, M.S., MALLOZZI, R.S., PACIESAS, W.S., BAND, D.L., MATTESON, J.L. AND MEEGAN, C.A.

«BATSE Observations of Gamma-Ray Burst Spectra. IV. Time-resolved High-Energy Spectroscopy».
ApJ, **496**, p. 849 (1998).

PREPARATA, G., RUFFINI, R. AND XUE, S.S.
«The dyadosphere of black holes and gamma-ray bursts».
A&A, **338**, pp. L87–L90 (1998).

PRICE, P.A., BERGER, E., REICHART, D.E., KULKARNI, S.R., YOST, S.A., SUBRAHMANYAN, R., WARK, R.M., WIERINGA, M.H., FRAIL, D.A., BAILEY, J. ET AL.
«Grb 011121: A massive star progenitor».
ApJ, **572**, pp. L51–L55 (2002).

PROCHASKA, J.X., BLOOM, J.S., CHEN, H.W., HURLEY, K.C., MELBOURNE, J., DRESSLER, A., GRAHAM, J.R., OSIP, D.J. AND VACCA, W.D.
«The host galaxy of grb 031203: Implications of its low metallicity, low redshift, and starburst nature».
ApJ, **611**, pp. 200–207 (2004).

PROCHASKA, J.X., COOPER, M., NEWMAN, J., BLOOM, J.S., HURLEY, K., BLAKE, C., GERKE, B. AND CHEN, H.W.
«Keck/DEIMOS spectrum of possible host galaxy for GRB050509b.»
GCN Circ., **3390** (2005).

PROCHASKA, J.X., DESSAUGES-ZAVADSKY, M., RAMIREZ-RUIZ, E. AND CHEN, H.W.
«A Survey for N V Absorption at z˜z_{GRB} in GRB Afterglow Spectra: Clues to Gas Near the Progenitor Star».
ApJ, **685**, pp. 344–353 (2008).

QIN, Y.P.
«Doppler effect of gamma-ray bursts in the fireball framework».
A&A, **396**, pp. 705–713 (2002).

RACUSIN, J.L., KARPOV, S.V., SOKOLOWSKI, M., GRANOT, J., WU, X.F., PAL'SHIN, V., COVINO, S., VAN DER HORST, A.J., OATES, S.R., SCHADY, P. ET AL.
«Broadband observations of the naked-eye γ-ray burst GRB080319B».
Nature, **455**, pp. 183–188 (2008).

RAMIREZ-RUIZ, E. AND FENIMORE, E.E.
«Pulse Width Evolution in Gamma-Ray Bursts: Evidence for Internal Shocks».
ApJ, **539**, pp. 712–717 (2000).

RAO, A.R., MALKAR, J.P., HINGAR, M.K., AGRAWAL, V.K., CHAKRABARTI, S.K., NANDI, A., DEBNATH, D., KOTOCH, T.B., SARKAR, R., CHIDAMBARAM, T.R. ET AL.
≪Detection of GRB 090618 with the RT-2 Experiment on Board the Coronas-Photon Satellite≫.
ApJ, **728**, p. 42 (2011).

RAU, A., MCBREEN, S. AND KRUEHLER, T.
≪GRB090510: VLT/FORS2 spectroscopic redshift.≫
GCN Circ., **9353**, p. 1 (2009).

REES, M., RUFFINI, R. AND WHEELER, J.A.
Black holes, gravitational waves and cosmology: an introduction to current research, volume 10 of *Topics in Astrophysics and Space Physics* (New York: Gordon and Breach, Science Publishers, Inc., 1974).

REES, M.J. AND MESZAROS, P.
≪Relativistic fireballs - Energy conversion and time-scales≫.
MNRAS, **258**, pp. 41P–43P (1992).

REES, M.J. AND MESZAROS, P.
≪Unsteady outflow models for cosmological gamma-ray bursts≫.
ApJ, **430**, pp. L93–L96 (1994).

REES, M.J. AND MESZAROS, P.
≪Refreshed shocks and afterglow longevity in gamma-ray bursts≫.
ApJ, **496**, p. L1 (1998).

REES, M.J. AND MÉSZÁROS, P.
≪Dissipative Photosphere Models of Gamma-Ray Bursts and X-Ray Flashes≫.
ApJ, **628**, pp. 847–852 (2005).

RICHARDSON, D., BRANCH, D. AND BARON, E.
≪Absolute magnitude distributions and light curves of stripped-envelope supernovae≫.
AJ, **131**, pp. 2233–2244 (2006).

ROL, E., PAGE, K., BURROWS, D.N., GEHRELS, N., GOAD, M., HURKETT, C., KENNEA, J. AND BRIAN, P.
≪GRB 050509B: Swift/XRT refined analysis.≫
GCN Circ., **3395** (2005).

ROMANI, R.W.
≪Model atmospheres for cooling neutron stars≫.
ApJ, **313**, pp. 718–726 (1987).

ROMING, P.W.A., KENNEDY, T.E., MASON, K.O., NOUSEK, J.A., AHR, L., BINGHAM, R.E., BROOS, P.S., CARTER, M.J., HANCOCK, B.K., HUCKLE, H.E. ET AL.
«The Swift Ultra-Violet/Optical Telescope».
Sp. Sci. Rev., **120**, pp. 95–142 (2005).

ROTONDO, M., RUEDA, J.A., RUFFINI, R. AND XUE, S.S.
«On the equilibrium of self-gravitating neutrons, protons and electrons in \beta-equilibrium».
ArXiv: 1107.2777 (2011a).

ROTONDO, M., RUEDA, J.A., RUFFINI, R. AND XUE, S.S.
«Relativistic Thomas-Fermi treatment of compressed atoms and compressed nuclear matter cores of stellar dimensions».
Phys. Rev. C, **83(4)**, p. 045805 (2011b).

ROTONDO, M., RUEDA, J.A., RUFFINI, R. AND XUE, S.S.
«The self-consistent general relativistic solution for a system of degenerate neutrons, protons and electrons in β-equilibrium».
Physics Letters B, **701**, pp. 667–671 (2011c).

ROTONDO, M., RUFFINI, R., XUE, S.S. AND POPOV, V.
«On Gravitationally and Electrodynamically Bound Nuclear Matter Cores of Stellar Dimensions».
IJMPD, **20**, pp. 1995–2002 (2011d).

RUDERMAN, M.
«Theories of gamma-ray bursts».
In P.G. Bergman, E.J. Fenyves and L. Motz (eds.), *Seventh Texas Symposium on Relativistic Astrophysics*, volume 262 of *Annals of the New York Academy of Sciences*, pp. 164–180 (1975).

RUEDA, J.A., ROTONDO, M., RUFFINI, R. AND XUE, S.S.
«A self-consistent approach to neutron stars».
Journal of the Korean Physical Society, **57**, p. 560 (2010a).

RUEDA, J.A., ROTONDO, M., RUFFINI, R. AND XUE, S.S.
«On Compressed Nuclear Matter:. from Nuclei to Neutron Stars».
IJMPD, **20**, pp. 1789–1796 (2011a).

RUEDA, J.A. AND RUFFINI, R.
«Gravitational Waves versus Electromagnetic Emission in Gamma-Ray Bursts».
ArXiv:1205.6915 (2012a).

RUEDA, J.A. AND RUFFINI, R.

≪On the Induced Gravitational Collapse of a Neutron Star to a Black Hole by a Type Ib/c Supernova≫.
ApJ, **758**, L7 (2012b).

RUEDA, J.A., RUFFINI, R. AND XUE, S..
≪The Klein first integrals in an equilibrium system with electromagnetic, weak, strong and gravitational interactions≫.
Nucl. Phys. A, in press; ArXiv: 1104.4062 (2011b).

RUEDA, J.A., RUFFINI, R. AND XUE, S.S.
≪On the electrostatic structure of neutron stars≫.
In R. Ruffini and G. Vereshchagin (eds.), *The Sun, the stars, the universe and general relativity*, volume 1205 of *American Institute of Physics Conference Series*, pp. 143–147 (2010b).

RUFFINI, R.
≪The dyadosphere of black holes and gamma-ray bursts≫.
Astronomy and Astrophysics, Supplement Series, **138**, pp. 513–514 (1999).

RUFFINI, R.
≪Analogies, new paradigms and observational data as growing factors of relativistic astrophysics≫.
In W. Janke, A. Pelster, H.J. Schmidt and M. Bachmann (eds.), *Fluctuating Paths and Fields* (Singapore: World Scientific, 2001).

RUFFINI, R.
talk presented at the congress "Eleventh Marcel Grossmann Meeting", Berlin, Germany, July 23-29 (2006).

RUFFINI, R.
≪The Role of Thomas-Fermi Approach in Neutron Star Matter≫.
In W. Janke and A. Pelster (eds.), *Path Integrals - New Trends and Perspectives*, pp. 207–218 (2008).

RUFFINI, R.
talk presented at the congress "Twelfth Marcel Grossmann Meeting", Paris, France, July 12-18 (2009a).

RUFFINI, R.
≪The ergosphere and dyadosphere of black holes≫.
In D.L. Wiltshire, M. Visser and S. Scott (eds.), *The Kerr Spacetime* (Cambridge University Press, 2009b).

RUFFINI, R.
In Z. Cao, X. Chen, R. Ruffini, S.S. Xue, C. Zhang and S. Zhang (eds.), *Proceedings of the Third Galileo-Xu Guangqi Meeting, to appear.* (2011a).

RUFFINI, R.
≪Fundamental physics from black holes, neutron stars and gamma-ray bursts≫.
arXiv:1107.0862 (2011b).

RUFFINI, R.
talk presented at the congress "Thirteenth Marcel Grossmann Meeting", Stockholm, Sweden, July 1-7 (2012).

RUFFINI, R., AKSENOV, A.G., BERNARDINI, M.G., BIANCO, C.L., CAITO, L., CHARDONNET, P., DAINOTTI, M.G., DE BARROS, G., GUIDA, R., IZZO, L. ET AL.
≪The Blackholic energy and the canonical Gamma-Ray Burst IV: the "long," "genuine short" and "fake-disguised short" GRBs≫.
In M. Novello and S. Perez Bergliaffa (eds.), *XIII Brazilian School on Cosmology and Gravitation*, volume 1132 of *American Institute of Physics Conference Series*, pp. 199–266 (2009).

RUFFINI, R., AKSENOV, A.G., BERNARDINI, M.G., BIANCO, C.L., CAITO, L., DAINOTTI, M.G., DE BARROS, G., GUIDA, R., VERESHCHAGIN, G.V. AND XUE, S.S.
≪The canonical Gamma-Ray Bursts and their "precursors"≫.
In Y.F. Huang, Z.G. Dai and B. Zhang (eds.), *2008 Nanjing Gamma-Ray Burst Conference*, volume 1065 of *American Institute of Physics Conference Series*, pp. 219–222 (2008a).

RUFFINI, R., BERNARDINI, M.G., BIANCO, C.L., CAITO, L., CHARDONNET, P., CHERUBINI, C., DAINOTTI, M.G., FRASCHETTI, F., GERALICO, A., GUIDA, R. ET AL.
≪On Gamma-Ray Bursts≫.
In H. Kleinert, R.T. Jantzen and R. Ruffini (eds.), *The Eleventh Marcel Grossmann Meeting On Recent Developments in Theoretical and Experimental General Relativity, Gravitation and Relativistic Field Theories*, pp. 368–505 (Singapore: World Scientific, 2008b).

RUFFINI, R., BERNARDINI, M.G., BIANCO, C.L., CAITO, L., CHARDONNET, P., DAINOTTI, M.G., FRASCHETTI, F., GUIDA, R., ROTONDO, M., VERESHCHAGIN, G. ET AL.
≪The blackholic energy and the canonical gamma-ray burst≫.
In M. Novello and S.E. Perez Bergliaffa (eds.), *XII Brazilian School of Cosmology and Gravitation*, volume 910 of *American Institute of Physics Conference Series*, pp. 55–217 (2007a).

RUFFINI, R., BERNARDINI, M.G., BIANCO, C.L., CAITO, L., CHARDONNET, P., DAINOTTI, M.G., FRASCHETTI, F., GUIDA, R., VERESHCHAGIN, G. AND XUE, S.S.

≪The role of grb 031203 in clarifying the astrophysical grb scenario≫.
In Ruffini et al. (2007c), p. 561.

RUFFINI, R., BERNARDINI, M.G., BIANCO, C.L., CAITO, L., CHARDONNET, P., DAINOTTI, M.G., FRASCHETTI, F., GUIDA, R., VERESHCHAGIN, G. AND XUE, S.S.
≪The role of grb 031203 in clarifying the astrophysical grb scenario≫.
In S. Grebenev, R. Sunyaev, C. Winkler, A. Parmar and L. Ouwehand (eds.), *The 6th Integral Workshop - The Obscured Universe*, volume SP-622 of *ESA Special Publication*, p. 561 (2007c).

RUFFINI, R., BERNARDINI, M.G., BIANCO, C.L., CAITO, L., DE BARROS, G., IZZO, L., PATRICELLI, B. AND VERESHCHAGIN, G.
≪The flares, the plateau phase and the P-GRB structure of GRBs within the fireshell model≫.
In *38th COSPAR Scientific Assembly*, volume 38, p. 2593 (2010a).

RUFFINI, R., BERNARDINI, M.G., BIANCO, C.L., CHARDONNET, P., FRASCHETTI, F., GUIDA, R. AND XUE, S.S.
≪Grb 050315: A step toward the uniqueness of the overall grb structure≫.
N.Cim.B, **121**, pp. 1367–1372 (2006a).

RUFFINI, R., BERNARDINI, M.G., BIANCO, C.L., CHARDONNET, P., FRASCHETTI, F., GUIDA, R. AND XUE, S.S.
≪Grb 050315: A step toward understanding the uniqueness of the overall gamma-ray burst structure≫.
ApJ, **645**, pp. L109–L112 (2006b).

RUFFINI, R., BERNARDINI, M.G., BIANCO, C.L., CHARDONNET, P., FRASCHETTI, F., GURZADYAN, V., VITAGLIANO, L. AND XUE, S.S.
≪The blackholic energy: long and short gamma-ray bursts (new perspectives in physics and astrophysics from the theoretical understanding of gamma-ray bursts, ii)≫.
In M. Novello and S.E. Perez Bergliaffa (eds.), *XI Brazilian School of Cosmology and Gravitation*, volume 782 of *American Institute of Physics Conference Series*, pp. 42–127 (2005a).

RUFFINI, R., BERNARDINI, M.G., BIANCO, C.L., CHARDONNET, P., FRASCHETTI, F. AND XUE, S.S.
≪Grb 980425, sn1998bw and the embh model≫.
Advances in Space Research, **34**, pp. 2715–2722 (2004a).

RUFFINI, R., BERNARDINI, M.G., BIANCO, C.L., CHARDONNET, P., FRASCHETTI, F. AND XUE, S.
≪Theoretical Interpretation of GRB 031203 and URCA-3≫.

In B. Aschenbach, V. Burwitz, G. Hasinger and B. Leibundgut (eds.), *Relativistic Astrophysics Legacy and Cosmology - Einstein's Legacy*, p. 399 (2008c).

RUFFINI, R., BERNARDINI, M.G., BIANCO, C.L., VITAGLIANO, L., XUE, S.S., CHARDONNET, P., FRASCHETTI, F. AND GURZADYAN, V.
≪Black hole physics and astrophysics: The grb-supernova connection and urca-1 - urca-2≫.
In M. Novello, S. Perez Bergliaffa and R. Ruffini (eds.), *The Tenth Marcel Grossmann Meeting. On recent developments in theoretical and experimental general relativity, gravitation and relativistic field theories*, p. 369 (Singapore: World Scientific, 2005b).

RUFFINI, R., BIANCO, C.L., CHARDONNET, P., FRASCHETTI, F., GURZADYAN, V. AND XUE, S.S.
≪On the instantaneous spectrum of gamma-ray bursts≫.
IJMPD, **13**, pp. 843–851 (2004b).

RUFFINI, R., BIANCO, C.L., CHARDONNET, P., FRASCHETTI, F., GURZADYAN, V. AND XUE, S.S.
≪Emergence of a filamentary structure in the fireball from grb spectra≫.
IJMPD, **14**, pp. 97–105 (2005c).

RUFFINI, R., BIANCO, C.L., CHARDONNET, P., FRASCHETTI, F., VITAGLIANO, L. AND XUE, S.S.
≪New perspectives in physics and astrophysics from the theoretical understanding of gamma-ray bursts≫.
In M. Novello and S.E. Perez Bergliaffa (eds.), *Cosmology and Gravitation*, volume 668 of *American Institute of Physics Conference Series*, pp. 16–107 (2003a).

RUFFINI, R., BIANCO, C.L., CHARDONNET, P., FRASCHETTI, F. AND XUE, S.S.
≪On a possible gamma-ray burst-supernova time sequence≫.
ApJ, **555**, pp. L117–L120 (2001a).

RUFFINI, R., BIANCO, C.L., CHARDONNET, P., FRASCHETTI, F. AND XUE, S.S.
≪On the interpretation of the burst structure of gamma-ray bursts≫.
ApJ, **555**, pp. L113–L116 (2001b).

RUFFINI, R., BIANCO, C.L., CHARDONNET, P., FRASCHETTI, F. AND XUE, S.S.
≪Relative spacetime transformations in gamma-ray bursts≫.
ApJ, **555**, pp. L107–L111 (2001c).

RUFFINI, R., BIANCO, C.L., CHARDONNET, P., FRASCHETTI, F. AND XUE, S.S.

«On the structures in the afterglow peak emission of gamma-ray bursts».
ApJ, **581**, pp. L19–L22 (2002).

RUFFINI, R., BIANCO, C.L., ENDERLI, M., MUCCINO, M., PENACCHIONI, A.V., PISANI, G.B., RUEDA, J.A., SAHAKYAN, N., WANG, Y. AND IZZO, L.
«GRB 130427A: predictions about the occurrence of a supernova.»
GCN Circ., **14526**, p. 1 (2013).

RUFFINI, R., BIANCO, C.L., FRASCHETTI, P.C.F. AND XUE, S.S.
«On the physical processes which lie at the bases of time variability of grbs».
Nuovo Cimento B Serie, **116**, p. 99 (2001d).

RUFFINI, R., CHAKRABARTI, S.K. AND IZZO, L.
«Possible multiple components in a GRB: the case of GRB 090618».
Submitted to Adv. Sp. Res. (2010b).

RUFFINI, R., FRASCHETTI, F., VITAGLIANO, L. AND XUE, S.S.
«Observational signatures of an electromagnetic overcritical gravitational collapse».
IJMPD, **14**, pp. 131–141 (2005d).

RUFFINI, R., IZZO, L., PENACCHIONE, A. AND CHAKRABARTI, S.K.
«Request for supernova related data for GRB 101023A.»
GCN Circ., **11459**, p. 1 (2010c).

RUFFINI, R., IZZO, L., PENACCHIONI, A.V., BIANCO, C.L., CAITO, L., CHAKRABARTI, S.K. AND NANDI, A.
«GRB 090618: a possible case of multiple GRB?»
PoS(Texas2010), p. 101 (2011a).

RUFFINI, R., ROTONDO, M. AND XUE, S.S.
«Electrodynamics for nuclear matter in bulk».
IJMPD, **16**, pp. 1–9 (2007d).

RUFFINI, R., SALMONSON, J.D., WILSON, J.R. AND XUE, S.S.
«On evolution of the pair-electromagnetic pulse of a charged black hole».
Astronomy and Astrophysics, Supplement Series, **138**, pp. 511–512 (1999a).

RUFFINI, R., SALMONSON, J.D., WILSON, J.R. AND XUE, S.S.
«On the pair electromagnetic pulse of a black hole with electromagnetic structure».
A&A, **350**, pp. 334–343 (1999b).

RUFFINI, R., SALMONSON, J.D., WILSON, J.R. AND XUE, S.S.

«On the pair-electromagnetic pulse from an electromagnetic black hole surrounded by a baryonic remnant».
A&A, **359**, pp. 855–864 (2000).

RUFFINI, R., SIUTSOU, I.A. AND VERESHCHAGIN, G.V.
«Theory of photospheric emission from relativistic outflows».
arXiv:1110.0407 (2011b).

RUFFINI, R., VERESHCHAGIN, G. AND XUE, S.
«Electron-positron pairs in physics and astrophysics: From heavy nuclei to black holes».
In Ruffini et al. (2010e), pp. 1–140.

RUFFINI, R., VERESHCHAGIN, G. AND XUE, S.
«Electron-positron pairs in physics and astrophysics: From heavy nuclei to black holes».
Phys. Rep., **487**, pp. 1–140 (2010e).

RUFFINI, R., VITAGLIANO, L. AND XUE, S.S.
«On a separatrix in the gravitational collapse to an overcritical electromagnetic black hole».
Physics Letters B, **573**, pp. 33–38 (2003b).

RUFFINI, R. AND WHEELER, J.A.
«Introducing the black hole.»
Physics Today, **24**, pp. 30–36 (1971).

RUFFINI, R. AND XUE, S.S.
«Dyadosphere formed in gravitational collapse».
In D.S. Lee and W. Lee (eds.), *Relativistic Astrophysics: 5th Sino-Italian Workshop on Relativistic Astrophysics*, volume 1059 of *American Institute of Physics Conference Series*, pp. 72–100 (2008).

RYDE, F.
«The Cooling Behavior of Thermal Pulses in Gamma-Ray Bursts».
ApJ, **614**, pp. 827–846 (2004).

RYDE, F.
«Is Thermal Emission in Gamma-Ray Bursts Ubiquitous?»
ApJ, **625**, pp. L95–L98 (2005).

RYDE, F., AXELSSON, M., ZHANG, B.B., MCGLYNN, S., PE'ER, A., LUNDMAN, C., LARSSON, S., BATTELINO, M., ZHANG, B., BISSALDI, E. ET AL.
«Identification and Properties of the Photospheric Emission in GRB090902B».
ApJ, **709**, pp. L172–L177 (2010).

RYDE, F., BJÖRNSSON, C.I., KANEKO, Y., MÉSZÁROS, P., PREECE, R. AND BATTELINO, M.
≪Gamma-Ray Burst Spectral Correlations: Photospheric and Injection Effects≫.
ApJ, **652**, pp. 1400–1415 (2006).

RYDE, F. AND PE'ER, A.
≪Quasi-blackbody Component and Radiative Efficiency of the Prompt Emission of Gamma-ray Bursts≫.
ApJ, **702**, pp. 1211–1229 (2009).

RYDE, F., PE'ER, A., NYMARK, T., AXELSSON, M., MORETTI, E., LUNDMAN, C., BATTELINO, M., BISSALDI, E., CHIANG, J., JACKSON, M.S. ET AL.
≪Observational evidence of dissipative photospheres in gamma-ray bursts≫.
Monthly Notices of the Royal Astronomical Society, p. 935 (2011).

RYKOFF, E.S., AHARONIAN, F., AKERLOF, C.W., ASHLEY, M.C.B., BARTHELMY, S.D., FLEWELLING, H.A., GEHRELS, N., GÖĞÜŞ, E., GÜVER, T., KIZILOĞLU, Ü. ET AL.
≪Looking Into the Fireball: ROTSE-III and Swift Observations of Early Gamma-ray Burst Afterglows≫.
ApJ, **702**, pp. 489–505 (2009).

SAHU, K.C., LIVIO, M., PETRO, L., MACCHETTO, F.D., VAN PARADIJS, J., KOUVELIOTOU, C., FISHMAN, G.J., MEEGAN, C.A., GROOT, P.J. AND GALAMA, T.
≪The optical counterpart to γ-ray burst grb970228 observed using the hubble space telescope≫.
Nature, **387**, pp. 476–478 (1997).

SAKAMOTO, T., BARBIER, L., BARTHELMY, S., CUMMINGS, J., FENIMORE, E., GEHRELS, N., HULLINGER, D., KRIMM, H., MARKWARDT, C., PALMER, D. ET AL.
≪Grb 060218/sn 2006aj: Swift-bat fluence and peak flux.≫
GCN Circ., **4822** (2006).

SAKAMOTO, T., BARBIER, L., BARTHELMY, S., CUMMINGS, J., HULLINGER, D., FENIMORE, E., GEHRELS, N., KRIMM, H., MARKWARDT, C., PALMER, D. ET AL.
≪GRB 050904 BAT refined analysis of complete data set.≫
GCN Circ., **3938** (2005).

SAKAMOTO, T., NORRIS, J., UKWATTA, T., BARTHELMY, S.D., GEHRELS, N. AND STAMATIKOS, M.
≪Further Swift-BAT analysis of GRB 071227.≫

GCN Circ., **7156**, p. 1 (2007).

SAKAMOTO, T., UKWATTA, T.N. AND BARTHELMY, S.D.
«GRB 090618, Swift-BAT refined spectral analysis.»
GCN Circ., **9534**, p. 1 (2009).

SALPETER, E.E. AND SHAPIRO, S.L.
«Neutrino and photon emission from a dense, high temperature atmosphere».
ApJ, **251**, p. 311 (1981).
ISSN 0004-637X.

SALVATERRA, R., DELLA VALLE, M., CAMPANA, S., CHINCARINI, G., COVINO, S., D'AVANZO, P., FERNÁNDEZ-SOTO, A., GUIDORZI, C., MANNUCCI, F., MARGUTTI, R. ET AL.
«GRB090423 at a redshift of z˜8.1».
Nature, **461**, pp. 1258–1260 (2009).

SARI, R.
«Hydrodynamics of gamma-ray burst afterglow».
ApJ, **489**, p. L37 (1997).

SARI, R.
«The observed size and shape of gamma-ray burst afterglow».
ApJ, **494**, p. L49 (1998).

SARI, R. AND MÉSZÁROS, P.
«Impulsive and Varying Injection in Gamma-Ray Burst Afterglows».
ApJ, **535**, pp. L33–L37 (2000).

SARI, R. AND PIRAN, T.
«Hydrodynamic Timescales and Temporal Structure of Gamma-Ray Bursts».
ApJ, **455**, p. L143 (1995).

SARI, R. AND PIRAN, T.
«Predictions for the Very Early Afterglow and the Optical Flash».
ApJ, **520**, pp. 641–649 (1999).

SARI, R., PIRAN, T. AND HALPERN, J.P.
«Jets in gamma-ray bursts».
ApJ, **519**, pp. L17–L20 (1999).

SARI, R., PIRAN, T. AND NARAYAN, R.
«Spectra and Light Curves of Gamma-Ray Burst Afterglows».
ApJ, **497**, pp. L17–L20 (1998).

SAVAGLIO, S., GLAZEBROOK, K. AND LEBORGNE, D.
«The Galaxy Population Hosting Gamma-Ray Bursts».
ApJ, **691**, pp. 182–211 (2009).

SAXTON, C.J., BARTHELMY, S.D., BAUMGARTNER, W.H., BEARDMORE, A.P., CHESTER, M.M., CUMMINGS, J.R., DE PASQUALE, M., GEHRELS, N., GELBORD, J.M., HOLLAND, S.T. ET AL.
«GRB 101023A: Swift detection of a burst.»
GCN Circ., **11363**, p. 1 (2010).

SAZONOV, S.Y., LUTOVINOV, A.A. AND SUNYAEV, R.A.
«An apparently normal γ-ray burst with an unusually low luminosity».
Nature, **430**, pp. 646–648 (2004a).

SAZONOV, S., LUTOVINOV, A. AND SUNYAEV, R.
Private communication (2004b).

SCHAAB, C., WEBER, F., WEIGEL, M. AND GLENDENNING, N.K.
«Thermal evolution of compact stars».
Nuclear Phys A, **605**, p. 531 (1996).

SCHADY, P.
«GRB090618: Swift/UVOT bright afterglow detection.»
GCN Circ., **9527**, p. 1 (2009).

SCHADY, P., BAUMGARTNER, W.H., BEARDMORE, A.P., CAMPANA, S., CURRAN, P.A., GUIDORZI, C., KENNEA, J.A., MAO, J., MARGUTTI, R., OSBORNE, J.P. ET AL.
«GRB 090618: Swift detection of a bright burst with optical afterglow.»
GCN Circ., **9512** (2009).

SCHAEFER, B.E.
«The Hubble Diagram to Redshift > 6 from 69 Gamma-Ray Bursts».
ApJ, **660**, pp. 16–46 (2007).

SCHAEFER, B.E., PALMER, D., DINGUS, B.L., SCHNEID, E.J., SCHOENFELDER, V., RYAN, J., WINKLER, C., HANLON, L., KIPPEN, R.M. AND CONNORS, A.
«Gamma-Ray–Burst Spectral Shapes from 2 keV to 500 MeV».
ApJ, **492**, p. 696 (1998).

SHARA, M.M., ZUREK, D.R., WILLIAMS, R.E., PRIALNIK, D., GILMOZZI, R. AND MOFFAT, A.F.J.
«HST Imagery of the Non-Expanding, Clumped "Shell" of the Recurrent Nova T Pyxidis».
AJ, **114**, p. 258 (1997).

SHEMI, A.
«Gamma-Ray Bursts from Interaction of Relativistic Flows with Radiation Fields».
MNRAS, **269**, p. 1112 (1994).

SHEMI, A. AND PIRAN, T.
«The appearance of cosmic fireballs».
ApJ, **365**, pp. L55–L58 (1990).

SHTERNIN, P.S., YAKOVLEV, D.G., HEINKE, C.O., HO, W.C.G. AND PATNAUDE, D.J.
«Cooling neutron star in the Cassiopeia A supernova remnant: evidence for superfluidity in the core».
MNRAS, **412**, pp. L108–L112 (2011).

SIRONI, L. AND SPITKOVSKY, A.
«Synthetic Spectra from Particle-In-Cell Simulations of Relativistic Collisionless Shocks».
ApJ, **707**, pp. L92–L96 (2009).

SODERBERG, A.M., BERGER, E., PAGE, K.L., SCHADY, P., PARRENT, J., POOLEY, D., WANG, X.Y., OFEK, E.O., CUCCHIARA, A., RAU, A. ET AL.
«An extremely luminous X-ray outburst at the birth of a supernova».
Nature, **453**, pp. 469–474 (2008).

SODERBERG, A.M., BERGER, E. AND SCHMIDT, B.P.
«Grb060218: optical spectroscopy of grb-sn.»
GCN Circ., **4804** (2006a).

SODERBERG, A.M., KULKARNI, S.R., BERGER, E., FOX, D.W., SAKO, M., FRAIL, D.A., GAL-YAM, A., MOON, D.S., CENKO, S.B., YOST, S.A. ET AL.
«The sub-energetic γ-ray burst grb 031203 as a cosmic analogue to the nearby grb 980425».
Nature, **430**, pp. 648–650 (2004).

SODERBERG, A.M., KULKARNI, S.R., NAKAR, E., BERGER, E., CAMERON, P.B., FOX, D.B., FRAIL, D., GAL-YAM, A., SARI, R., CENKO, S.B. ET AL.
«Relativistic ejecta from x-ray flash xrf 060218 and the rate of cosmic explosions».
Nature, **442**, pp. 1014–1017 (2006b).

SOKOLOV, V.V., CASTRO-TIRADO, A.J., MOSKVITIN, A.S., BARSUKOVA, E.A., KOMAROVA, V.N., BORISOV, N.V., VALEEV, A.F., SOKOLOVA, T.N. AND GORANSKIJ, V.P.
«Grb 130427a:: Bta spectroscopic observations on may 10/11.»
GCN Circ., **14669**, p. 1 (2013).

SOLLERMAN, J., JAUNSEN, A.O., FYNBO, J.P.U., HJORTH, J., JAKOBSSON, P., STRITZINGER, M., FÉRON, C., LAURSEN, P., OVALDSEN, J.E., SELJ, J. ET AL.
«Supernova 2006aj and the associated x-ray flash 060218».
A&A, **454**, pp. 503–509 (2006).

SORIA, R., PIAN, E. AND MAZZALI, P.A.
«A second glance at SN 2002ap and the M 74 field with XMM-Newton».
A&A, **413**, pp. 107–119 (2004).

SPITKOVSKY, A.
«On the Structure of Relativistic Collisionless Shocks in Electron-Ion Plasmas».
ApJ, **673**, pp. L39–L42 (2008a).

SPITKOVSKY, A.
«Particle Acceleration in Relativistic Collisionless Shocks: Fermi Process at Last?»
ApJ, **682**, pp. L5–L8 (2008b).

STAMATIKOS, M., UKWATTA, T.N., SAKAMOTO, T., DHUGA, K.S., TOMA, K., PE'ER, A., MÉSZÁROS, P., BAND, D.L., NORRIS, J.P., BARTHELMY, S.D. ET AL.
«The Correlation of Spectral Lag Evolution with Prompt Optical Emission in GRB 080319B».
In C. Meegan, C. Kouveliotou and N. Gehrels (eds.), *GAMMA-RAY BURST: Sixth Huntsville Symposium*, volume 1133 of *American Institute of Physics Conference Series*, pp. 356–361 (2009).

STERN, B.E. AND POUTANEN, J.
«Gamma-ray bursts from synchrotron self-Compton emission».
MNRAS, **352**, pp. L35–L39 (2004).

STRONG, I.B.
«Cosmic gamma-ray bursts».
In H. Gursky and R. Ruffini (eds.), *Neutron Stars, Black Holes and Binary X-ray Sources*, volume 48 of *Astrophysics and Space Science Library*, pp. 47–58 (1975).

STRONG, I.B. AND KLEBESADEL, R.W.
«Distances to the sources of observed gamma-ray bursts».
Nature, **251**, pp. 396–397 (1974).

STRONG, I.B., KLEBESADEL, R.W. AND EVANS, W.D.
«Observations of gamma-ray bursts».

In P.G. Bergman, E.J. Fenyves and L. Motz (eds.), *Seventh Texas Symposium on Relativistic Astrophysics*, volume 262 of *Annals of the New York Academy of Sciences*, pp. 145–158 (1975).

STRONG, I.B., KLEBESADEL, R.W. AND OLSON, R.A.
«A Preliminary Catalog of Transient Cosmic Gamma-Ray Sources Observed by the VELA Satellites».
ApJ, **188**, p. L1 (1974).

SUGITA, S., YAMAOKA, K., OHNO, M., TASHIRO, M.S., NAKAGAWA, Y.E., URATA, Y., PAL'SHIN, V., GOLENETSKII, S., SAKAMOTO, T., CUMMINGS, J. ET AL.
«Suzaku-WAM, Konus-Wind, and Swift-BAT Observations of Prompt Emission of the High-Redshift GRB 050904».
PASJ, **61**, p. 521 (2009).

TAGLIAFERRI, G., ANTONELLI, L.A., CHINCARINI, G., FERNÁNDEZ-SOTO, A., MALESANI, D., DELLA VALLE, M., D'AVANZO, P., GRAZIAN, A., TESTA, V., CAMPANA, S. ET AL.
«Grb 050904 at redshift 6.3: observations of the oldest cosmic explosion after the big bang».
A&A, **443**, pp. L1–L5 (2005).

TANVIR, N.R., FOX, D.B., LEVAN, A.J., BERGER, E., WIERSEMA, K., FYNBO, J.P.U., CUCCHIARA, A., KRÜHLER, T., GEHRELS, N., BLOOM, J.S. ET AL.
«A γ-ray burst at a redshift of z˜8.2».
Nature, **461**, pp. 1254–1257 (2009).

TANVIR, N.R., ROL, E., LEVAN, A.J., SVENSSON, K., FRUCHTER, A.S., GRANOT, J., O'BRIEN, P.T., WIERSEMA, K., STARLING, R.L.C., JAKOBSSON, P. ET AL.
«Late-time Observations of GRB 080319B: Jet Break, Host Galaxy, and Accompanying Supernova».
ApJ, **725**, pp. 625–632 (2010).

TAVANI, M.
«A Shock Emission Model for Gamma-Ray Bursts. II. Spectral Properties».
ApJ, **466**, p. 768 (1996).

TAVANI, M.
«Euclidean versus non-euclidean gamma-ray bursts».
ApJ, **497**, p. L21 (1998).

TAVANI, M., ARGAN, A., BARBIELLINI, G., BULGARELLI, A., CATTANEO, P., CARAVEO, P., CHEN, A., COSTA, E., DE PARIS, G., DEL MONTE, E. ET AL.
«AGILE and the Gamma-Ray Bursts».

In M. Galassi, D. Palmer and E. Fenimore (eds.), *GAMMA-RAY BURSTS 2007: Proceedings of the Santa Fe Conference*, volume 1000 of *American Institute of Physics Conference Series*, pp. 523–530 (2008).

TAVANI, M., BARBIELLINI, G., ARGAN, A., BOFFELLI, F., BULGARELLI, A., CARAVEO, P., CATTANEO, P.W., CHEN, A.W., COCCO, V., COSTA, E. ET AL.
≪The AGILE Mission≫.
A&A, **502**, pp. 995–1013 (2009).

THOMPSON, C.
≪A Model of Gamma-Ray Bursts≫.
MNRAS, **270**, p. 480 (1994).

TIENGO, A., MEREGHETTI, S., GHISELLINI, G., ROSSI, E., GHIRLANDA, G. AND SCHARTEL, N.
≪The x-ray afterglow of grb 030329≫.
A&A, **409**, pp. 983–987 (2003).

TIENGO, A., MEREGHETTI, S., GHISELLINI, G., TAVECCHIO, F. AND GHIRLANDA, G.
≪Late evolution of the x-ray afterglow of grb 030329≫.
A&A, **423**, pp. 861–865 (2004).

TOMA, K., IOKA, K., SAKAMOTO, T. AND NAKAMURA, T.
≪Low-luminosity grb 060218: A collapsar jet from a neutron star, leaving a magnetar as a remnant?≫
ApJ, **659**, pp. 1420–1430 (2007).

TROJA, E., KING, A.R., O'BRIEN, P.T., LYONS, N. AND CUSUMANO, G.
≪Different progenitors of short hard gamma-ray bursts≫.
MNRAS, **385**, pp. L10–L14 (2008).

TROTTER, A., REICHART, D., HAISLIP, J., LACLUYZE, A., MCLIN, K., COMINSKY, L., BERGER, T., CROMARTIE, H.T., EGGER, R., FOSTER, A. ET AL.
≪GRB 130427A: Ten nights of Skynet/PROMPT/GORT observations≫.
GCN Circ., **14608**, p. 1 (2013a).

TROTTER, A., REICHART, D., HAISLIP, J., LACLUYZE, A., MCLIN, K., COMINSKY, L., SMITH, A., CATON, D., HAWKINS, L., HOLMES, B. ET AL.
≪GRB 130427A: skynet detections of a possible supernova.≫
GCN Circ., **14662**, p. 1 (2013b).

TRÜMPER, J.E.
≪Observations of cooling neutron stars≫.

In A. Baykal, S.K. Yerli, S.C. Inam and S. Grebenev (eds.), *NATO ASIB Proc. 210: The Electromagnetic Spectrum of Neutron Stars*, p. 117 (2005).

TSURUTA, S.
Ph.D. thesis, , Columbia Univ., (1964) (1964).

TSURUTA, S.
≪Thermal properties and detectability of neutron stars. i. cooling and heating of neutron stars.≫
Phys. Rep., **56**, pp. 237–277 (1979).

TSURUTA, S. AND CAMERON, A.G.W.
≪Cooling and detectability of neutron stars≫.
Canadian Journal of Physics, **44**, p. 1863 (1966).

TSURUTA, S., TETER, M.A., TAKATSUKA, T., TATSUMI, T. AND TAMAGAKI, R.
≪Confronting neutron star cooling theories with new observations≫.
ApJ, **571**, pp. L143–L146 (2002).

TUELLER, J., BARBIER, L., BARTHELMY, S., CUMMINGS, J., FENIMORE, E., GEHRELS, N., HULLINGER, D., KOSS, M., KRIMM, H., MARKWARDT, C. ET AL.
≪GRB 060607: Swift-BAT refined analysis.≫
GCN Circ., **5242** (2006).

TUROLLA, R., ZAMPIERI, L., COLPI, M. AND TREVES, A.
≪Spherical accretion onto neutron stars revisited: Are hot solutions possible?≫
ApJ, **426**, p. L35 (1994).
ISSN 0004-637X.

ULANOV, M.V., GOLENETSKII, S.V., FREDERIKS, D.D., MAZETS, R.L.A.E.P., KOKOMOV, A.A. AND PALSHIN, V.D.
≪Fast spectral variability of GRBs with known redshifts≫.
Nuovo Cimento C, **28**, p. 351 (2005).

UPDIKE, A.C., OLIVARES, F.E., GREINER, J. AND KANN, D.A.
≪GRB 110709B: GROND detection of an afterglow candidate.≫
GCN Circ., **12129**, p. 1 (2011).

USOV, V.V.
≪Millisecond pulsars with extremely strong magnetic fields as a cosmological source of gamma-ray bursts≫.
Nature, **357**, pp. 472–474 (1992).

VAN DEN BERGH, S., LI, W. AND FILIPPENKO, A.V.
≪Classifications of the Host Galaxies of Supernovae, Set III≫.
PASP, **117**, pp. 773–782 (2005).

VAN PARADIJS, J., GROOT, P.J., GALAMA, T., KOUVELIOTOU, C., STROM, R.G., TELTING, J., RUTTEN, R.G.M., FISHMAN, G.J., MEEGAN, C.A., PETTINI, M. ET AL.
≪Transient optical emission from the error box of the γ-ray burst of 28 february 1997≫.
Nature, **386**, pp. 686–689 (1997).

VAN PARADIJS, J., KOUVELIOTOU, C. AND WIJERS, R.A.M.J.
≪Gamma-ray burst afterglows≫.
ARAA, **38**, pp. 379–425 (2000).

VAN RIPER, K.A.
≪Magnetic neutron star atmospheres≫.
ApJ, **329**, pp. 339–375 (1988).

VAN RIPER, K.A.
≪Neutron star thermal evolution≫.
ApJSS, **75**, pp. 449–462 (1991).

VAUGHAN, S., GOAD, M.R., BEARDMORE, A.P., O'BRIEN, P.T., OSBORNE, J.P., PAGE, K.L., BARTHELMY, S.D., BURROWS, D.N., CAMPANA, S., CANNIZZO, J.K. ET AL.
≪Swift observations of the x-ray-bright grb 050315≫.
ApJ, **638**, pp. 920–929 (2006).

VILLASENOR, J.S., LAMB, D.Q., RICKER, G.R., ATTEIA, J.L., KAWAI, N., BUTLER, N., NAKAGAWA, Y., JERNIGAN, J.G., BOER, M., CREW, G.B. ET AL.
≪Discovery of the short γ-ray burst grb 050709≫.
Nature, **437**, pp. 855–858 (2005).

VOLNOVA, A., KOROBTSEV, I., KLUNKO, E. AND POZANENKO, A.
≪GRB 130427A: optical observations≫.
GCN Circ., **14645**, p. 1 (2013).

VREESWIJK, P.M., SMETTE, A., MALESANI, D., FYNBO, J.P.U., MILVANG-JENSEN, B., JAKOBSSON, P., JAUNSEN, A.O., OSLO, U. AND LEDOUX, C.
≪VLT/UVES redshift of GRB 080319B.≫
GCN Circ., **7444** (2008).

WANG, X.Y., DAI, Z.G. AND LU, T.
≪Possible geometries of afterglow generation in the gamma-ray burst GRB 990705≫.

A&A, **401**, pp. 593–597 (2003).

WATSON, A.M., BUTLER, N., KUTYREV, A., LEE, W.H., RICHER, M.G., KLEIN, C., FOX, O., PROCHASKA, J.X., BLOOM, J., CUCCHIARA, A. ET AL.
«GRB 130427A: Continued RATIR Optical and NIR Observations».
GCN Circ., **14606**, p. 1 (2013a).

WATSON, A.M., BUTLER, N., KUTYREV, A., LEE, W.H., RICHER, M.G., KLEIN, C., FOX, O., PROCHASKA, J.X., BLOOM, J., CUCCHIARA, A. ET AL.
«GRB 130427A: continued RATIR optical and NIR observations - photometric evidence for a new component.»
GCN Circ., **14666**, p. 1 (2013b).

WATSON, D., HJORTH, J., JAKOBSSON, P., XU, D., FYNBO, J.P.U., SOLLERMAN, J., THÖNE, C.C. AND PEDERSEN, K.
«Are short γ-ray bursts collimated? grb 050709, a flare but no break».
A&A, **454**, pp. L123–L126 (2006).

WATSON, D., HJORTH, J., LEVAN, A., JAKOBSSON, P., O'BRIEN, P.T., OSBORNE, J.P., PEDERSEN, K., REEVES, J.N., TEDDS, J.A., VAUGHAN, S.A. ET AL.
«A very low luminosity x-ray flash: Xmm-newton observations of grb 031203».
ApJ, **605**, pp. L101–L104 (2004).

WAXMAN, E.
«Angular size and emission timescales of relativistic fireballs».
ApJ, **491**, p. L19 (1997).

WIERSEMA, K., SAVAGLIO, S., VREESWIJK, P.M., ELLISON, S.L., LEDOUX, C., YOON, S.C., MØLLER, P., SOLLERMAN, J., FYNBO, J.P.U., PIAN, E. ET AL.
«The nature of the dwarf starforming galaxy associated with grb 060218/sn 2006aj».
A&A, **464**, pp. 529–539 (2007).

WIERSEMA, K., VADUVESCU, O., TANVIR, N., LEVAN, A. AND HARTOOG, O.
«GRB 130427A: host galaxy observations».
GCN Circ., **14617**, p. 1 (2013).

WILLIAMS, J.P., BLITZ, L. AND MCKEE, C.F.
«The Structure and Evolution of Molecular Clouds: from Clumps to Cores to the IMF».
Protostars and Planets IV, pp. 97–+ (2000).

WILLINGALE, R., O'BRIEN, P.T., OSBORNE, J.P., GODET, O., PAGE, K.L., GOAD, M.R., BURROWS, D.N., ZHANG, B., ROL, E., GEHRELS, N. ET AL.
«Testing the standard fireball model of gamma-ray bursts using late x-ray afterglows measured by swift».
ApJ, **662**, pp. 1093–1110 (2007).

WILSON-HODGE, C.A. AND PREECE, R.D.
«GRB 091127: Fermi GBM detection.»
GCN Circ., **10204**, p. 1 (2009).

WOOSLEY, S.E.
«Gamma-ray bursts from stellar mass accretion disks around black holes».
ApJ, **405**, pp. 273–277 (1993).

WOOSLEY, S.E. AND BLOOM, J.S.
«The supernova gamma-ray burst connection».
ARAA, **44**, pp. 507–556 (2006).

WOŹNIAK, P.R., VESTRAND, W.T., PANAITESCU, A.D., WREN, J.A., DAVIS, H.R. AND WHITE, R.R.
«Gamma-Ray Burst at the Extreme: "The Naked-Eye Burst" GRB 080319B».
ApJ, **691**, pp. 495–502 (2009).

XU, D., DE UGARTE POSTIGO, A., KRUEHLER, T., MALESANI, D., LELOUDAS, G., FYNBO, J.P.U., HJORTH, J., SCHULZE, S., JAKOBSSON, P., CANO, Z. ET AL.
«GRB 130427A: excess optical emission consistent with an emerging supernova.»
GCN Circ., **14597**, p. 1 (2013a).

XU, D., DE UGARTE POSTIGO, A., LELOUDAS, G., KRUHLER, T., CANO, Z., HJORTH, J., MALESANI, D., FYNBO, J.P.U., THOENE, C.C., SANCHEZ-RAMIREZ, R. ET AL.
«Discovery of the broad-lined Type Ic SN 2013cq associated with the very energetic GRB 130427A».
ArXiv:1305.6832 (2013b).

XU, D., STARLING, R.L.C., FYNBO, J.P.U., SOLLERMAN, J., YOST, S., WATSON, D., FOLEY, S., O'BRIEN, P.T. AND HJORTH, J.
«In search of progenitors for supernova-less GRBs 060505 and 060614: re-examination of their afterglows».
ArXiv:0812.0979 (2008).

YAKOVLEV, D.G., KAMINKER, A.D., GNEDIN, O.Y. AND HAENSEL, P.
«Neutrino emission from neutron stars».

Physics Reports, **354(1-2)**, pp. 1–155 (2001).
ISSN 03701573.

YAKOVLEV, D.G. AND PETHICK, C.J.
«Neutron star cooling».
ARAA, **42**, pp. 169–210 (2004).

YAMAOKA, K., ENDO, A., ENOTO, T., FUKAZAWA, Y., HARA, R., HANABATA, Y., HONG, S., KAMAE, T., KIRA, C., KODAKA, N. ET AL.
«Design and In-Orbit Performance of the Suzaku Wide-Band All-Sky Monitor».
PASJ, **61**, p. 35 (2009).

YONETOKU, D., MURAKAMI, T., NAKAMURA, T., YAMAZAKI, R., INOUE, A.K. AND IOKA, K.
«Gamma-ray burst formation rate inferred from the spectral peak energy-peak luminosity relation».
ApJ, **609**, pp. 935–951 (2004).

YONETOKU, D., MURAKAMI, T., TSUTSUI, R., NAKAMURA, T., MORIHARA, Y. AND TAKAHASHI, K.
«Possible Origins of Dispersion of the Peak Energy-Brightness Correlations of Gamma-Ray Bursts».
PASJ, **62**, pp. 1495– (2010).

YOSHIDA, A., NAMIKI, M., YONETOKU, D., MURAKAMI, T., OTANI, C., KAWAI, N., UEDA, Y., SHIBATA, R. AND UNO, S.
«A Possible Emission Feature in an X-Ray Afterglow of GRB 970828 as a Radiative Recombination Edge».
ApJ, **557**, pp. L27–L30 (2001).

ZAUDERER, A. AND BERGER, E.
«GRB 110709B / EVLA detection of radio counterpart.»
GCN Circ., **12190**, p. 1 (2011).

ZAUDERER, B.A., BERGER, E., MARGUTTI, R., LEVAN, A.J., OLIVARES E., F., PERLEY, D.A., FONG, W., HORESH, A., UPDIKE, A.C., GREINER, J. ET AL.
«Illuminating the Darkest Gamma-Ray Bursts with Radio Observations».
ApJ, **767**, 161 (2013).

ZDZIARSKI, A.A., SVENSSON, R. AND PACZYNSKI, B.
«Bursts of gamma rays from Compton scattering at cosmological distances».
ApJ, **366**, pp. 343–352 (1991).

ZELDOVICH, Y.B. AND RAIZER, Y.P.
Elements of gasdynamics and the classical theory of shock waves (New York: Academic Press, 1966, edited by Hayes, W.D.; Probstein, Ronald F., 1966).

ZHANG, B., FAN, Y.Z., DYKS, J., KOBAYASHI, S., MÉSZÁROS, P., BURROWS, D.N., NOUSEK, J.A. AND GEHRELS, N.
≪Physical processes shaping gamma-ray burst x-ray afterglow light curves: Theoretical implications from the swift x-ray telescope observations≫.
ApJ, **642**, pp. 354–370 (2006).

ZHANG, B. AND KOBAYASHI, S.
≪Gamma-Ray Burst Early Afterglows: Reverse Shock Emission from an Arbitrarily Magnetized Ejecta≫.
ApJ, **628**, pp. 315–334 (2005).

ZHANG, B. AND MÉSZÁROS, P.
≪Gamma-Ray Burst Afterglow with Continuous Energy Injection: Signature of a Highly Magnetized Millisecond Pulsar≫.
ApJ, **552**, pp. L35–L38 (2001).

ZHANG, B., ZHANG, B.B., LIANG, E.W., GEHRELS, N., BURROWS, D.N. AND MÉSZÁROS, P.
≪Making a short gamma-ray burst from a long one: Implications for the nature of grb 060614≫.
ApJ, **655**, pp. L25–L28 (2007).

ZHANG, B.B., ZHANG, B., LIANG, E.W., FAN, Y.Z., WU, X.F., PE'ER, A., MAXHAM, A., GAO, H. AND DONG, Y.M.
≪A Comprehensive Analysis of Fermi Gamma-ray Burst Data. I. Spectral Components and the Possible Physical Origins of LAT/GBM GRBs≫.
ApJ, **730**, 141 (2011).

ZIAEEPOUR, H., HOLLAND, S.T., BOYD, P.T., PAGE, K., OATES, S., MARKWARDT, C.B., MÉSZÁROS, P., GEHRELS, N., MARSHALL, F.E., CUMMINGS, J. ET AL.
≪GRB 060607A: a gamma-ray burst with bright asynchronous early X-ray and optical emissions≫.
MNRAS, **385**, pp. 453–467 (2008).

ZOU, Y.C., FAN, Y.Z. AND PIRAN, T.
≪A Revised Limit of the Lorentz Factors of Gamma-ray Bursts with Two Emitting Regions≫.
ApJ, **726**, L2 (2011).

ZOU, Y.C. AND PIRAN, T.
≪Lorentz factor constraint from the very early external shock of the gamma-ray burst ejecta≫.

MNRAS, **402**, pp. 1854–1862 (2010).